Narendra Kumar
Sunita Kumbhat

Essentials in Nanoscience & Nanotechnology

WILEY

Table of Contents

- Cover
- Title Page
- Copyright
- Preface
- Acknowledgments
- About the Authors
  - Dr. N. Kumar, Former Director, Defence Laboratory, Jodhpur
  - Dr. S. Kumbhat, Professor, Department of Chemistry, Jai Narain Vyas University, Jodhpur
- Chapter 1: Introduction
  - 1.1 Definitions of Nanoscience and Nanotechnologies
  - 1.2 Uniqueness of the Nanoscale
  - 1.3 Nanoscience in Nature
  - 1.4 Historical Perspective
  - 1.5 Nanomaterials
  - 1.6 Strategies for Synthesis of Nanomaterials
  - 1.7 Properties of Nanomaterials
  - 1.8 Significance of Nanoscience
  - 1.9 Commercial Applications
  - 1.10 Potential Health Hazards and Environmental Risks
  - 1.11 Futuristic Outlook
  - Review Questions
  - References
- Chapter 2: Nanomaterials: General Synthetic Approaches
  - 2.1 Introduction
  - 2.2 Top-Down Approach
  - 2.3 Bottom-Up Approaches
  - Review Questions
  - References
- Chapter 3: Characterization Tools for Nanomaterials
  - 3.1 Introduction
  - 3.2 Imaging Through Electron Microscopy
  - 3.3 Scanning Probe Microscopy (SPM)
  - 3.4 Characterization Through Spectroscopy
  - 3.5 Scattering Techniques
  - Review Questions
  - References
- Chapter 4: Nanomaterials
  - 4.1 Introduction
  - 4.2 Inorganic Nanomaterials
  - 4.3 Organic Nanomaterials
  - 4.4 Biological Nanomaterials
  - 4.5 Nanoporous Materials
  - 4.6 Quantum Dots
  - 4.7 Nanoclusters
  - 4.8 Nanomaterials in Different Configurations
  - Review Questions
  - References
- Chapter 5: Carbon-Based Nanomaterials
  - 5.1 General Introduction
  - 5.2 Fullerene
  - 5.3 Carbon Nanotubes (CNTs)
  - 5.4 Graphene
  - 5.5 Carbon Nano-Onions
  - 5.6 Carbon Nanofibers
  - 5.7 Carbon Black
  - 5.8 Nanodiamond
  - Review Questions
  - References
- Chapter 6: Self-Assembled and Supramolecular Nanomaterials
  - 6.1 Introduction: Self-Assembly
  - 6.2 Historical Perspective of Supramolecular and Self-Assembled Structures
  - 6.3 Fundamental Aspects of Supramolecular Chemistry
  - 6.4 Self-Assembly Via Non-Covalent Interaction
  - 6.5 Synthetic Strategies for Molecular Self-Assembly
  - 6.6 Biological Self-Assembly
  - 6.7 Templated (Non-Molecular) Self-Assembly
  - 6.8 Self-Assembled Supramolecular Nanostructures

- 6.9 Self-Folding Nanostructures
- 6.10 Applications
- Review Questions
- References

Chapter 7: Nanocomposites
- 7.1 Introduction
- 7.2 Ceramic–Matrix Nanocomposites
- 7.3 Metal–Matrix Nanocomposites
- 7.4 Polymer–Matrix Nanocomposites
- 7.5 Nanocoatings
- Review Questions
- References

Chapter 8: Unique Properties
- 8.1 Introduction
- 8.2 Size Effects
- 8.3 Physical Properties
- 8.4 Chemical Properties at Nanoscale
- 8.5 The Concept of Pseudo-Atoms
- Review Questions
- References

Chapter 9: Applications of Nanotechnology
- 9.1 Introduction
- 9.2 Medicine and Healthcare
- 9.3 Drug Development and Drug Delivery System
- 9.4 Information and Computer Technologies
- 9.5 Nanoelectromechanical Systems (NEMS)
- 9.6 Nanotechnologies in Tags
- 9.7 Nanotechnology for Environmental Issues
- 9.8 Energy
- 9.9 Nanotechnology in Enhancing the Fuel Efficiency
- 9.10 Chemical and Biosensors Using Nanomaterials (NMs)
- 9.11 Nanotechnology in Agro Forestry
- 9.12 Defense Applications
- 9.13 Nanotechnology *in Space*
- 9.14 Consumer Goods
- 9.15 Sport Goods
- Review Questions
- References

Chapter 10: Toxicity and Environmental Issues
- 10.1 Introduction
- 10.2 Sources of Nanoparticles and Their Health Effects
- 10.3 Toxicology of Engineered Nanoparticles
- 10.4 Positive Health Effects of Nanoparticles
- 10.5 Environmental Sustainability
- 10.6 Safe Working with Nanomaterials
- 10.7 Nanomaterial Waste Management
- 10.8 Gaps in Knowledge about Health Effects of Engineered Nanoparticles
- 10.9 Government Standards and Materials Safety Data Sheets
- 10.10 Risk Management
- Review Questions
- References

Index

End User License Agreement

List of Illustrations

Chapter 1: Introduction

Figure 1.1 Size comparisons of objects, nanomaterials, and biomolecules.

Figure 1.2 Exponential increases in surface area for cubes ranging from meter to nanosize.

Figure 1.3 Change in optical properties of a semiconductor ranging from bulk to nanosize. Courtesy of Grossman, MIT, USA.

Figure 1.4 Nanotechnology in nature: (a) electron microscopic image of a sensory patch in amphibian ears. http://scinerds.tumblr.com/post/35542105310/stereocilia-stairsteps; (b) peacock feather showing barbules, representing a photonic lattice; (c and d) electron microscopy image of transverse and longitudinal sections of barbules. Zi et al. [2a] © 2003. With permission of National Academy of Sciences, USA.

Figure 1.5 Natural and fabricated antireflective surfaces: (a) schematic of a moth; (b) scanning electron micrograph of antireflective surface of a moth's eye (scale bar = 1 μm); (c) biomimetic replica of a moth eye fabricated with ion- beam etching.

Figure 1.6 (a) Lotus (*Nelumbo nucifera*) plant; (b) spherical water droplet on a nonwettable lotus plant leaf. Blossey [6] © 2003. With permission of Nature Publishing Group. ; (c) self-cleaning: a drop picks up the dirt particles as it rolls off the leaf's surface.

Figure 1.7 Gecko's adhesive system structure: (a) ventral view of a tokay gecko (*Gekko gecko*); (b) sole of the foot showing adhesive lamellae; (c) microstructure: part of a single lamella showing arrays of setae; (d and e) nanostructure: single seta with branched structure at the upper right area, terminating in hundreds of spatular tips. Hansen and Autumn [6], © 2005. With permission of National Academy of Sciences, USA.

Figure 1.8 (a) Lycurgus cups. Courtesy of Trustees of the British Museum. © The Trustees of the British Museum; (b) ancient Maya fresco painting. Reproduced from Sanchez et al. [8] © 2005. With permission of The Royal Society of Chemistry.

Figure 1.9 Richard Feynman.

Figure 1.10 Typical examples showing varied dimensionality in nanomaterials: (a) fullerene; (b) quantum dot; (c) metal cluster; (d) carbon nanotube; (e) metal oxide nanotube; (f) graphene; (g) metal oxide nanobelts; (h) nanodiamond; (i) metal organic frameworks (MOFs).

Chapter 2: Nanomaterials: General Synthetic Approaches

Figure 2.1 "Top-down" and "bottom-up" approaches for the synthesis of nanomaterials.

Figure 2.2 (a) A ball-milling apparatus. Courtesy of PANalytical Inc. (b) Schematic representation of different forms of impact in mechanical ball milling.

Figure 2.3 (a) Set up for etching by electric arc discharge and (b) resultant water stabilization of Au NPs in solution.

Figure 2.4 Setup for laser ablation technique for the synthesis of Fe_2O_3 nanoparticles from iron wire.

Figure 2.5 Soft lithography with polydimethyl siloxane (PDMS) molds.

Figure 2.6 Schematic of nanoimprint lithography process.

Figure 2.7 Nanosphere lithography. (a) Schematic illustration of the NSL process and (b) SEM image of triangular gold nanoprism as a product of nanosphere lithography.

Figure 2.8 Illustration of dip-pen nanolithography.

Figure 2.9 Schematic of ultrasonic spray pyrolysis setup.

Figure 2.10 (a) Schematic of a basic setup for electrospray. Seul-Gi Kim et al. [11] © 2014, With permission of Japan Society of Applied Physics; (b)–(d) three distinct electrospray.

Figure 2.11 Schematics of electrospinning process for nanofiber synthesis.

Figure 2.12 Schematic representation of chemical vapor deposition: (a) thermal and (b) plasma assisted.

Box 2.5 Preparation of Fe_2O_3. Shukla et al. [15] © 2010. With permission of ASPBS.

Figure 2.13 Schematic representation of chemical reduction method for nanosynthesis.

Figure 2.14 Schematic representation different capping agents (a) polymer; (b) organic ligand, and (c) micelle.

Box 2.6 Preparation of Ag NPs by reduction method. Manoth et al. [16] © 2008. With permission of Elsevier.

Figure 2.15 Illustration of the reverse micelle preparation route for hierarchical structuring of TiO_2.

Figure 2.16 Schematic representation of sol–gel process for the synthesis of a variety of nanostructures.

Figure 2.17 (a) Sonochemical reactor; (b) transient cavitation during sonolysis.

Figure 2.18 Scanning electron micrograph (SEM): (a) magnetotactic bacteria (*Magnetospirillum gryphiswaldense*) cell; (b) magnetite crystals observed at the ends of the chain in magnetotactic bacteria.

Figure 2.19 Plant *Curculigo orchioides* (inset shows dried root) root extract used for nanosynthesis and AFM image of resultant silver nanoparticles. Courtesy, Dr. Sushma Dave, VIET, Jodhpur, India.

Figure 2.20 (a)–(c) Molecular biomimetics (I1, inorganic-1; I2, inorganic-2; P1 and P2, inorganic-specific proteins; LP, linker protein; FP, fusion protein).

Figure 2.21 Schematic illustration: (a) Langmuir balance; (b) deposition of a floating monolayer on a solid substrate.

Chapter 3: Characterization Tools for Nanomaterials

Figure 3.1 Electron beam-induced processes and their relative energies.

Figure 3.2 **Schematic of electron gun**: (a) tungsten filament Wehnelt thermionic gun; (b) field emission gun.

Figure 3.3 Electromagnetic lenses.

Figure 3.4 Electron transition path for secondary electron and backscattered electron used in SEM.

Figure 3.5 (**a**, **b**) Principal features of a scanning electron microscope.

Figure 3.6 A secondary electron scintillator–photomultiplier detector.

Figure 3.7 SEM images showing the characteristic depth of field: (a) pollen grains, http://en.wikipedia.org/. ; (b) zinc oxide nanorods arranged as flower.

Figure 3.8 SEM image and EDX spectra. (a) Graphene balls. Adapted from Klajn et al.[12], ©2007 AAAS. (b) Nanoporous material.

Figure 3.9 (a, b) Principal features of a light and transmission electron microscope.

Figure 3.10 TEM image of (a) SnO_2 nanobelts Jiang et al. [14] © 2013. With permission of RSC; (b) CNTs. Wu et al. [15] © 2013. With permission of NPG; (c) graphitized Fe–Co alloy core-shell NPs, (inset, HRTEM image showing Fe–Co core and graphite shell).

Figure 3.11 (a, b) Bright field and dark field modes and the corresponding typical TEM images in bright field and dark field modes.

Figure 3.12 (a–c) TEM images showing the formation of Fe_3O_4 nanocrystals.

Figure 3.13 Essential components of an STM with a close-up view of the tunneling effect between tip of the probe and the surface atoms.

Figure 3.14 (a) Constant current and (b) constant height imaging modes of an STM.

Figure 3.15 STM images of (a) nano-gold on TiO_2. Galhenage et al. [17b], © 2013. With permission of ACS; (b) nano-cobalt on TiO_2 surface Galhenage et al. [17b], © 2013. With permission of ACS; (c) graphene on SiO_2 showing grain boundary. Koepke et al. [19], © 2013. With permission of ACS.

Figure 3.16 Schematic representation of AFM, Courtesy of Keysight Technologies.

Figure 3.17 AFM images showing (a) InAs/GaAs QDs grown on a Ge/Si substrate. Chen et al. [21a], © 2015. With permission of licensee MDPI, Basel, Switzerland; (b) Pt nanoparticles coated with Si nanopillars. Li et al. [21b], © 2015. With permission of NPG; (c) cholesterol–B, SA conjugate. Gehlot et al. [22], © 2013. With permission of NISCAIR, CSIR, New Delhi.

Figure 3.18 (a) AFM image of graphene balls with height bar; (b) cross section along the line indicated in (a). Kumar et al. [13], © 2013. With permission from ASP.

Figure 3.19 Spectrum of various electromagnetic radiations.

Figure 3.20 (a, b) UV–vis spectrum of gold nanoparticles with different geometries: spheres (top), decahedra (middle), and rods (bottom).

Figure 3.21 IR spectra and XRD pattern of pure Fe_3O_4 nanoparticles at: (a) room temperature and after calcination for 2 h at different temperatures; (b) 150 °C; (c) 250 °C; (d) 350 °C; (e) 450 °C; (f) 550 °C.

Figure 3.22 Schematic representation of Raman spectrometer.

Figure 3.23 Energy level diagram showing the states involved in Raman signal.

Figure 3.24 Raman spectra of allotropes of nanocarbon in comparison to amorphous carbon.

Figure 3.25 Working principles of TERS.

Figure 3.26 Schematic electron spectroscopy: (a) X-ray photoelectron spectroscopy; (b) Auger spectroscopy; and (c) X-ray fluorescence spectroscopy.

Figure 3.27 Basic components of XPS/ESCA instrument. https://en.wikipedia.org/wiki/X-ray_photoelectron_spectroscopy.

Figure 3.28 XPS scan survey spectrum for all elements. https://en.wikipedia.org/wiki/X-ray_photoelectron_spectroscopy.

Figure 3.29 C_{1s} XPS of carbon nanomaterials: (a) graphene oxide. Huang [30], © 2012. With permission of RSC; (b) fluorinated SWNTs. Dillon et al. [31], © 2008. With permission of ACS; and (c) fullerene. Arie and Lee [32], © 2009. With permission of Hanyang university, Korea.

Figure 3.30 XPS spectra of TiO_2–WO_3 thin film: (a) survey scan between binding energy 0 and 1200 eV before etching; (b) high-resolution peaks for Ti-2p after etching the film; (c) high-resolution peaks for Ti-2f after etching.

Figure 3.31 AES survey spectrum (upper trace) and differentiated spectrum (lower trace) of an oxidized Fe–Cr–Nb alloy.

Figure 3.32 Schematics: (a) cylindrical mirror analyzer; (b) concentric hemispherical analyzer.

Figure 3.33 Characterization of an Sn–Nb wire by SEM: (a) SEM image; (b) schematic of the elemental distribution; and (c) point analysis giving the percent concentration of Nb and Sn.

Figure 3.34 Process of secondary ion sputtering and the schematic of a dynamical SIMS instrument.

Figure 3.35 Basic features of an XRD spectrometer.

Figure 3.36 A typical XRD pattern of (a) NaCl powder and (b) carbon nanomaterials.

Figure 3.37 (a, b) X-ray diffraction patterns of nanostructured TiO_2 film.

Figure 3.38 Schematic of a typical SAXS setup. www.mrl.ucsb.edu.

Figure 3.39 A typical plots of diffracted intensity versus scattering vector, inset shows centro-symmetric pattern on the 2D detector. www.mrl.ucsb.edu.

Figure 3.40 Basic components and optics for a dynamic light scattering experiment.

Figure 3.41 (a) Electric double layer around a particle; (b) effect of zeta potential on suspension properties.

Figure 3.42 Shift in frequency by a moving particle.

Chapter 4: Nanomaterials

Figure 4.1 Electrostatic and steric stabilization of nanostructure metal colloids.

Figure 4.2 Nanostructured metal colloids obtained via $[BEt_3H-]$ reduction method (including the mean particle sizes in nanometers).

Figure 4.3 Color variation of gold nanoparticles of different sizes.

Figure 4.4 Influence of size, shape, and composition on the light-scattering and resultant colors of silver nanoparticles (quoted nanoparticle sizes are all approximate).

Figure 4.5 TEM image of nano-titanium flower.

Figure 4.6 TEM micrographs of nanocrystals obtained by sulfuric acid hydrolysis of (a) cotton, (b) avicel, and (c–e) tunicate cellulose.

Figure 4.7 Synthesis of a typical dendrimers involving growth (g) and activation (a, a*) steps.

Figure 4.8 Nanometer-scale pores for biotechnology. (a) Single biological pore model of α-hemolysin. http://www.ipt.arc.nasa.gov/carbonnano.html. (b) Electric field-driven entry of a supramolecular entity through a single α-HL channel.

Figure 4.9 (a) Structure and functionality of a nanogear.

Figure 4.10 Types of possible pores in a porous material.

Figure 4.11 Representative zeolite frameworks (with pore openings): (a) zeolite A:3D, 4.2 Å; (b) zeolite Y:3D, 7.4 Å; (c) zeolite L:1D, 7.1 Å; (d) ZSM-5 (silicalite):2D, 5.3 ×5.6 Å, 5.1 ×5.5 Å. Zheng et al. [27] © 2012.With permission of authors.

Figure 4.12 A typical porous texture of a biomass-based activated carbon.

Figure 4.13 A molecular sieve: A metal-organic framework (MOF) MIL-47 loaded with $CuCl_2$.

Figure 4.14 Comparison of band gap energy in a bulk semiconductor, quantum dots, and a molecule. Emission colors in ZnS quantum dots by varying dopants.

Figure 4.15 Schematic of polythiol-coated CdSe-ZnS core–shell quantum dot.

Figure 4.16 Nanocluster from atom/molecule.

Figure 4.17 SEM images of biomimics of natural hierarchical structures: (a) pillared poly(methyl methacrylate) nanofiber.

Figure 4.18 Inorganic nanotube: SEM image of TiO_2 nanotubes.

Figure 4.19 SEM images: (a) SnO_2 nanobelts.

Chapter 5: Carbon-Based Nanomaterials

Figure 5.1 Carbon in different hybridized states: (a) sp^2 with planer geometry as in graphite; (b) sp^3 with tetrahedral geometry as in diamond.

Figure 5.2 Allotropes of carbon nanomaterials in different dimensions.

Figure 5.3 C_{60} fullerene.

Figure 5.4 Possible derivatization of C_{60}: (a) fullerene salts; (b) exohedral adducts; (c) open-cage fullerenes; (d) quasifullerenes; (e) heterofullerenes; (f) endohedral fullerenes.

Figure 5.5 Schematic of arc discharge process.

Figure 5.6 (a–d) Fullerene derivatives.

Figure 5.7 (a–c) Types of carbon nanotubes.

Figure 5.8 Different structural forms of single-wall carbon nanotubes.

Figure 5.9 Transmission electron micrograph (TEM) of MWCNT.

Figure 5.10 Schematic of the arc discharge procedure in liquid nitrogen.

Figure 5.11 SEM images of MWCNTs synthesized: (a) with and (b) without the magnetic field.

Figure 5.12 Schematic of plasma rotating electrode system.

Figure 5.13 (a) Classical laser ablation apparatus used at Rice University; (b) schematic of ultrafast laser evaporation method.

Figure 5.14 Schematic of the apparatus for magnetic purification of CNTs.

Figure 5.15 (a) Planar structure of 2D graphene; Dai et al.[3], © 2012. With permission of Wiley. (b) Graphene shown as chicken net.

Figure 5.16 Band structure of graphene (a) energy bands near the Fermi level in graphene; (b) conic energy bands in the vicinity of the K and K' points; (c) density of states near the Fermi level with Fermi energy EF.

Figure 5.17 Schematic diagram of CVD reactor for preparing graphene.

Figure 5.18 Schematic representation of graphite exfoliation process resulting in graphene.

Figure 5.19 (a) Oxidation of graphite to graphene oxide and reduction to reduced graphene oxide. (b) A proposed reaction pathway for epoxy reduction by hydrazine.

Figure 5.20 Experimental setup for electrochemical synthesis of graphene: (a) electrochemical cell; (b) exfoliation of chemically modified graphene sheets on graphite anode.

Figure 5.21 Isocyanate treatment of GO.

Figure 5.22 Raman spectra of graphene.

Figure 5.23 (a) Optical image graphene flakes showing one, two, three, and four layers; (b) TEM image of graphene showing hexagonal lattice structure with pentagon–heptagon pairs.

Figure 5.24 Carbon nano-onions (a) FESEM image; (b) EDX spectrum; and (c–e) HRTEM images (inset is the corresponding SAED pattern).

Figure 5.25 HRTEM image along with schematic representation of carbon nanofibers with their graphene sheets in "parallel."

Figure 5.26 Pyrolysis furnace for the synthesis of carbon black.

Figure 5.27 Nanodiamond: (a) octahedral model. Krueger [42], © 2008. With permission of RSC; (b) meteoritic diamond with multiple twinning. Daulton et al. [40], © 1996. With permission of Elsevier; (c) triamantane, a diamondoid molecule. Krueger [42], © 2008. With permission of RSC.

Figure 5.28 Formation of nanodiamond at near-ambient conditions via microplasma dissociation of ethanol.

Figure 5.29 Surface functionalization of nanodiamond yields various covalently modified derivatives with different terminal groups for further surface modification.

Figure 5.30 Treating drug-resistant cancer with nanodiamond. Moore et al. [42b], © 2013. Reprinted with permission of John Wiley and Sons.

Chapter 6: Self-Assembled and Supramolecular Nanomaterials

Figure 6.1 Rigid triangular structure self-assembled in combination with macrocycle rings in solution to create a supramolecular organic framework (SOF). Zhang et al. [10], © 2013. With permission of ACS.
Figure 6.2 Schematic illustration of nanoscale self-assembly. vdW attraction and steric repulsion may induce the phase separation of rods and spheres into two closely-packed arrangements (top). Alternatively, when the rods are functionalized with positively charged ligands and the spheres with negatively charged ligands, the particles are expected to organize via electrostatic interactions into a binary lattice (bottom).
Figure 6.3 van der Waals forces driven nanoparticle assemblies: (a) 2D hexagonal close-packed structure of 5 nm Ag-NPs. Harfenist et al. [12], © 1996. With permission of ACS; (b) side-by-side self-organized gold nanorods (15 × 200 nm, aspect ratio >5) leading to continuous ribbons. Sau and Murphy [13], © 2005. With permission of ACS; (c) isotropic self-assembly of gold nanorods (15 × 200 nm, aspect ratio 3.2) Sau and Murphy [13], © 2005. With permission of ACS.
Figure 6.4 TEM image of self-assembly of magnetic nanoparticles formed by strong dipole–dipole interactions: (a) linear chains of 20 nm cobalt-NPs. Thomas [14], © 1966. With permission of AIP; (b) parallel chains of 10 nm .-Fe_2O_3. Lalatonne et al. [15], © 2004. With permission of NPG.
Figure 6.5 STM images of (a) hexagonal close network of trimesic acid on HOPG. Lackinger et al. [17], © 2005. With permission of ACS; and (b) molecular wires of 4-[*trans*-2-(pyrid-4-yl-vinyl)]benzoic acid on Ag(1 1 1) surface. Smith et al. [18], © 2004. With permission of Wiley, VCH-Verlag.
Figure 6.6 Schematic representation of (a) *n*-dodecanethiolate monolayer, self-assembled on an atomically flat gold substrate. Smith et al. [18], © 2004. With permission of Elsevier; (b) dicarboxylic acid derivatives as spacer.
Figure 6.7 (a) Normal capillary bridge forces, (b) lateral capillary forces.
Figure 6.8 Self-assembled 2D (a and b) and 3D (c and d) structures in systems of macroscopic components interacting via capillary interactions.
Figure 6.9 Thermodynamics of self-assembly.
Figure 6.10 Cross-sectional view of SEM image: (a) dried suspension of V_2O_5; (b) polycrystalline silicon templated by 855-nm silica spheres.
Figure 6.11 Nanomotors assembled in ordered arrays: (a–d) Schematic diagrams and snapshot images of a 2 × 2 nanomotor array rotating; (e) overlapped snapshot image of a 1 × 3 nanomotor array.

Chapter 7: Nanocomposites

Figure 7.1 Abalone shell and its structure.
Figure 7.2 Working temperature range for different matrix materials.
Figure 7.3 Types of reinforcements: (a) continuous fibers; (b) whiskers; (c) particulates.
Figure 7.4 (a) Strength and fracture toughness for various Al_2O_3/SiC nanocomposites as a function of SiC volume fraction. Nanocomposites derived from the classical powder route are represented by solid symbols and nanocomposites fabricated from an amorphous Si–C–N powder by open symbols; (b) average matrix grain size (R) as a function of $1/V_f$ of SiC for Al_2O_3/SiC nanocomposites.
Figure 7.5 High magnification SEM images of the 1.5 vol% GPL-Si_3N_4 nanocomposites (arrows illustrate the location of GPL on the fracture surface).
Figure 7.6 Preparation of CNT–metal matrix composites via chemical routes.
Figure 7.7 Common geometries of reinforcement particle and respective surface-to-volume ratios.
Figure 7.8 A simple route for synthesis of polymer–metal oxide nanocomposites [N. Kumar, Unpublished work].
Figure 7.9 Color fluorescence image of (a) QD-poly(lauryl methacrylate) composite rods excited by a UV Hg-lamp (λ_{em} = 365 nm). Lee et al. [22], © 2000. With permission of Wiley-VCH; (b) PVA films containing Au nanorods aligned parallel and perpendicular to the electric field of polarized incoming light (P, represents a polarizer). Pérez-Juste et al. [23], ©2005. With permission of Wiley-VCH.
Figure 7.10 Types of composite derived from interaction between clays and polymers: (a) phase-separated microcomposite; (b) intercalated nanocomposite; and (c) exfoliated nanocomposite.
Figure 7.11 Nylon-6 nanocomposite formed through *in situ* polymerization with ADA–MMT.
Figure 7.12 Carbon nanotube/polymer matrix nanocomposite.
Figure 7.13 SEM micrograph of NiCr–WC coatings with (a) single-layer 60% carbide concentration and (b) double-layer graded coating with outer layer 60% WC over inner layer of 15% WC.

Chapter 8: Unique Properties

Figure 8.1 Schematic representation of tunneling.
Figure 8.2 Relationship between size, energy, and energy of states of nanoparticles.
Figure 8.3 Evolution of the band gap and the density of states as the number of atoms in a system increase.
Figure 8.4 Calculated structures of the fullerene C_{60} (a) and of the Au_{32} (b) nanoclusters, which are both hollow.
Figure 8.5 Size dependence of the dispersion for cubic particles with $n = N^{1/3}$ atoms along an edge.
Figure 8.6 Calculated mean coordination number as a function of inverse radius for magnesium clusters of different symmetries (triangles: icosahedra, squares: decahedra, diamonds: hexagonal close packing).
Figure 8.7 (a) Schematic illustration of the excitation of the dipole surface plasmon oscillation. (b) and (c) Characteristic UV–Vis spectra corresponding to the spherical and rod-shaped Au NPs, respectively.
Figure 8.8 Absorption (a) and Fluorescence (b) spectra of longer gold nanorods (230 nm, upper trace) and shorter gold nanorods (30 nm, lower trace) in aqueous solution. Li et al.[12], © 2005. With permission of RSC.
Figure 8.9 Fluorescence in CdSe–CdS core–shell nanoparticles with a diameter of 1.7 nm (blue); 3.7 nm (green) and ~6 nm (red) giving evidence of the scaling of the semiconductor band gap with particle size. Courtesy of H. Weller, University of Hamburg.
Figure 8.10 The energy levels of valence and conduction bands of core and shell in type I heterostructural QDs.
Figure 8.11 Comparative band gap in (a) metals; (b) insulator; (c) semiconductor.

Figure 8.12 Schematic of the density of states exhibited by bulk metal relative to increasingly smaller nanoclusters. The approximate diameter, nuclearity, and Kubo gap for each size regime are indicated.

Figure 8.13 Voltage endurance characteristics for nanocomposites using 4 μ tip/plane electrodes. (a) Epoxy-TiO_2, (b) XLPE-SiO_2.

Figure 8.14 The different magnetic effects in magnetic nanoparticles shown through spin arrangement in (a) ferromagnet; (b) antiferromagnet D = diameter, D_c = critical diameter; (c) combination of two different ferromagnetic phases; (d) magnetic moments in a superparamagnet; (e) exchange coupling; and (f) pure antiferromagnetic.

Figure 8.15 Calculated electronic orbitals for the core–shell icosahedral cluster $AlPb_{12}^{\pm}$.

Chapter 9: Applications of Nanotechnology

Figure 9.1 Nanobiosensor. (a) Silicon nanowires surface modified with avidin molecules (purple stars), which selectively bind a streptavidin-functionalized molecule or nanoparticle. Courtesy of Raj Mohanty, Boston University, USA. (b) Nano-gold surface immobilized with dengue antigen–BSA conjugate for detection of dengue using SPR technique. Kumbhat et al. [4], ©2010. With permission of Elsevier.

Figure 9.2 Optical image of a flexible paper display containing an LED array (25 × 16). Russo et al. [9], ©2011. With permission of Wiley-VCH Verlag Gmbh and Co.

Figure 9.3 Illustration of (a) barcode and (b) the RFID tag.

Figure 9.4 (a) Solar radiations reaching to earth surface; (b) solar spectrum.

Figure 9.5 Typical sandwich-type dye-sensitized TiO_2 nanocrystal solar cell.

Figure 9.6 Schematic illustration of the structure of (a) quantum dot sensitized solar cell (QDSC) and (b) photoinduced charge transfer processes following a laser pulse excitation. Kamat [16], © 2013. With permission of ACS.

Figure 9.7 Nano-architectures of hybrid solar cell materials. (a) Blend of semiconductor nanoparticles and conducting polymer films; (b) blend of semiconductor nanorods and conducting polymer films; (c) blend of semiconductor nano-tetrapods and conducting polymer films. Courtesy of Liu [17].

Figure 9.8 Thermoelectric devices.

Figure 9.9 (a, b) Nanowires made of piezoelectric materials embedded in shoe sole to generate electricity from mechanical motion such as a human walking or running. http://www.mdpi.com/1424-8220/14/7/12497. Used under CC-BY 3.0. http://creativecommons.org/licenses/by/3.0/.

Figure 9.10 Schematic representation of a fuel cell.

Figure 9.11 Schematic representation of facile cycling of Ti-doped $LiAlH_4$ for high-performance hydrogen storage.

Figure 9.12 Schematic representation of a lithium-ion battery.

Figure 9.13 The complete invisibility system based on metamaterials: (a) Schematic representation of metamaterial showing bending of light. http://www.physics.org. (b) Quantum stealth mock-up using metamaterial. Courtesy of G. Cramer, Hyper Stealth Biotechnology Corp. [27].

Figure 9.14 Space transportation with nanotubes: faster, better, cheaper. [http://www.ipt.arc.nasa.gov/spacetransport.html.]

Figure 9.15 Antibacterial textiles: (a) interaction between bacteria and coating of AgNPs within sol–gel-based silicate material. Hamm et al. [35], © 2012. With permission of ACS; (b) doctor's sterile suit containing nanosilver. http://www.ecouterre.com/.

Figure 9.16 Specific advantages of nanotechnology in sports equipment.

Chapter 10: Toxicity and Environmental Issues

Figure 10.1 Possible pathways of exposure of nanoparticles to human body.

Figure 10.2 Relocation of inhaled NPs after deposition on the alveolar epithelium. Kreyling et al. [6], © 2013. With permission of ACS.

Figure 10.3 Classification of natural and engineered nanoparticles existing in the environments.

Figure 10.4 Indoor air pollution from cooking.

Figure 10.5 Deposition of inhaled particles in the human respiratory tract versus particle diameter.

Figure 10.6 The risk assessment paradigm integrated with life cycle stages of nanomaterials.

List of Tables

Chapter 1: Introduction

Table 1.1 Bio-Inspired Unique Properties

Table 1.2 Milestones Associated with the Evolution of Nanoscience and Nanotechnology

Table 1.3 Characteristics of Nanomaterial and Their Importance

Table 1.4 Size and Shape-Related Attributes and Properties of nanomaterials

Table 1.5 Summary of Some Commercialized Nano-Based Products and Their Specific Applications

Chapter 2: Nanomaterials: General Synthetic Approaches

Table 2.1 Common Techniques for Synthesis of Nanomaterials

Table 2.2 Substrate–Ink Combinations for DPN

Table 2.3 Extracellular Bionanosynthesis of Nanoparticles

Chapter 3: Characterization Tools for Nanomaterials

Table 3.1 Common Investigation Techniques for the Characterization of Nanoparticles

Table 3.2 Fundamental Properties of Electrons

Table 3.3 Electron Wavelength and Velocity at Different Acceleration Voltage

Table 3.4 Comparative Overview of Characteristics of Different Electron Guns

Table 3.5 Characteristic Features of Optical, Electron, and Scanning Probe Microscopes

Table 3.6 Key Attributes of AFM for the Characterization of Nanoparticles

Table 3.7 Radiations Used in Scattering-Based Characterization Techniques

Chapter 4: Nanomaterials

Table 4.1 Important Metallic Nanomaterials

Chapter 5: Carbon-Based Nanomaterials

Table 5.1 A Comparative Account of Different Methods for Synthesis of CNTs

Table 5.2 Potential Applications of Chemically Modified CNTs

Chapter 6: Self-Assembled and Supramolecular Nanomaterials

Table 6.1 Summary of Supramolecular Interactions

Chapter 7: Nanocomposites

Table 7.1 Critical Size of Reinforcement Applicable to Different Properties

Table 7.2 Classification of Nanocomposites and Typical Examples

Table 7.3 Physical and Mechanical Properties of GPL-Si_3N_4 Nanocomposites

Table 7.4 Nanoceramic Metal–Matrix Nanocomposites and Associated Properties

Table 7.5 Potential Application Areas and Unique Properties of CNT-Reinforced Metal Matrix Composites

Table 7.6 Classification and Examples of Clay Minerals

Table 7.7 Potential Application Areas of Polymer–Graphene Nanocomposites

Chapter 8: Unique Properties

Table 8.2 Change in Surface Area on Size Reduction

Chapter 9: Applications of Nanotechnology

Table 9.1 Areas of Application of Nanotechnology

Table 9.2 Nanomaterials for Air Pollution Control

Table 9.3 Nanomaterials Based Commercially Available Batteries

Table 9.4 Chemical Sensors and Biosensors Based on Nanomaterials

Table 9.5 Enhanced Properties of Textile Fibers with Inclusion Nanostructure

Table 9.6 Attributes Nanomaterials in Sports Equipments and Its Associated Benefits

Chapter 10: Toxicity and Environmental Issues

Table 10.1 Measured Concentrations of Nanoparticles Resulting from Various Common Indoor Household Activities

Table 10.2 Expected Toxicological Effects of Engineered Nanoparticles

Table 10.3 Best Practices for a Nanotechnology Laboratory

Essentials in Nanoscience and Nanotechnology

Narendra Kumar
Sunita Kumbhat

WILEY

Copyright © 2016 by John Wiley & Sons, Inc. All rights reserved

Published by John Wiley & Sons, Inc., Hoboken, New Jersey

Published simultaneously in Canada

No part of this publication may be reproduced, stored in a retrieval system, or transmitted in any form or by any means, electronic, mechanical, photocopying, recording, scanning, or otherwise, except as permitted under Section 107 or 108 of the 1976 United States Copyright Act, without either the prior written permission of the Publisher, or authorization through payment of the appropriate per-copy fee to the Copyright Clearance Center, Inc., 222 Rosewood Drive, Danvers, MA 01923, (978) 750-8400, fax (978) 750-4470, or on the web at www.copyright.com. Requests to the Publisher for permission should be addressed to the Permissions Department, John Wiley & Sons, Inc., 111 River Street, Hoboken, NJ 07030, (201) 748-6011, fax (201) 748-6008, or online at http://www.wiley.com/go/permissions.

Limit of Liability/Disclaimer of Warranty: While the publisher and author have used their best efforts in preparing this book, they make no representations or warranties with respect to the accuracy or completeness of the contents of this book and specifically disclaim any implied warranties of merchantability or fitness for a particular purpose. No warranty may be created or extended by sales representatives or written sales materials. The advice and strategies contained herein may not be suitable for your situation. You should consult with a professional where appropriate. Neither the publisher nor author shall be liable for any loss of profit or any other commercial damages, including but not limited to special, incidental, consequential, or other damages.

For general information on our other products and services or for technical support, please contact our Customer Care Department within the United States at (800) 762-2974, outside the United States at (317) 572-3993 or fax (317) 572-4002.

Wiley also publishes its books in a variety of electronic formats. Some content that appears in print may not be available in electronic formats. For more information about Wiley products, visit our web site at www.wiley.com.

Library of Congress Cataloging-in-Publication Data:

Names: Kumar, Narendra (Materials scientist), author. | Kumbhat, Sunita, author.

Title: Essentials in nanoscience and nanotechnology / Narendra Kumar, Sunita Kumbhat.

Description: Hoboken, New Jersey : John Wiley & Sons, Inc. 2016. | Includes bibliographical references and index.

Identifiers: LCCN 2015040306 | ISBN 9781119096115 (cloth)

Subjects: LCSH: Nanotechnology. | Nanoscience.

Classification: LCC T174.7 .K78 2016 | DDC 500–dc23 LC record available at http://lccn.loc.gov/2015040306

Preface

The turn of twenty-first century has witnessed the emergence of three cutting-edge technologies, namely, Information and Communication Technology (ICT), Biotechnology, and Nanotechnology. In 2005, the United Nations Task Force on the Millennium Development Goals touted Nanotechnology as one of three platform technologies that can reduce hunger, promote health, improve water sanitation, develop renewable resources, and improve the environment, and recommended that developing countries should initiate nanotechnology programs at a national level. Inspired by such forecasts, by 2014, over 60 countries followed the United States and established the National Nanotechnology Initiative. These countries range from advanced industrial countries in Europe and Japan to the emerging markets of Russia, China, Brazil, and India.

Physicist Richard Feynman, in his famous speech of 1959, forecasted the development of nanoscience and the punch line “plenty of room at the bottom” became reality by the 1980s when scientists developed techniques and tools to explore and manipulate matter at the atomic scale. The term “nanoscale” defines a size range from 1 to 100 nm, although a scientifically based range goes from the atomic scale (0.2 nm) to 100 nm. The focus on the nanoregime relates to the convenience of some standard definition that can be used to both categorize nanotechnology, nanoscience, and nanoproducts and act as a bridge between quantum mechanical effects and surface area effects.

Nanoscience is not merely about size; it is about the unique physical, chemical, biological, and optical properties that emerge naturally at the nanoscale, whereas nanotechnology is related to the ability to manipulate and engineer such effects. It is a broad new area of science that demolishes boundaries among physics, chemistry, biology, cognitive science, materials science, and engineering at the nanoscale. New technologies, however, are likely to revolutionize the economy and the society only if there is a broader strong National base consisting of trained manpower and infrastructure that allows a new technology to spread and transform to its exciting niche applications, whether civilian or military. To do so, the most important thing is to educate and train the budding manpower at the school and university levels. For that, availability of standard books is necessary, and this book is designed keeping in mind these essential requirements.

Furthermore, keeping in view the unprecedented research and development in the area of nanoscience and nanotechnology and to make the students aware about the latest developments in the field, we have attempted to write this book in a manner as simple as possible while including the latest development in the field. The subject matter of the book, ranging from fundamentals to the latest developments and technological applications, is presented in 10 chapters. The first chapter on introduction gives a historical prospective, provides living examples of nanoscience in nature and artificial nanomaterials, and brings out the likely impact of nanotechnology on human civilization. Chapter 2 describes general synthetic approaches and strategies, while Chapter 3 deals with the characterization of nanomaterials using modern tools and techniques to provide the basic understanding to students who are interested in learning this emerging area. Chapters 4–7 deal with different kinds of nanomaterials such as inorganic, carbon-based nanocomposites, and self-assembled/supramolecular nanostructures, respectively, in terms of their varieties, synthesis, and properties. Following this, Chapters 8 and 9 are devoted to the unique properties and applications of nanotechnology in various disciplines such as information technology, pollution, environment, energy, healthcare, consumer goods, and so on. Finally, the last chapter deals with the toxicological and ethical issues associated with nanotechnology.

We believe this book will generate and promote the basic understanding on the complex and revolutionary disciplines of nanoscience and nanotechnology, which is offered now as a core subject in most of the academic institutions across the globe.

Acknowledgments

Writing a book is always a dedicated effort requiring patience and hidden support of family members, which both the authors have been fortunate to enjoy during the course of writing this book. In this context, Dr. Kumar would like to thank his wife, Mrs. Soma Jain, who supported him at every step and without whom it would have been impossible to accomplish writing this book. She showed immense strength in bearing with little time he could spend with her. Dr. Kumar would like to thank his children and their spouses, Anjali and Vikas; Atul and Parul; Akshaya and Pragati for their support, and his grandchildren Kratyagya, Kritika, and Eshna for always cheering him up. Dr. Kumbhat would like to acknowledge her husband, Air Cmde Jinendra Kumbhat, for being her pillar of strength and standing beside her throughout the course of writing this book. He has been her inspiration and motivation for continuing to improve her knowledge and move her career forward. Dr. Kumbhat would like to thank her children and their spouses, Shruti and Mehul; Kunal and Sonal, who have all been such wonderful and encouraging children.

The authors would like to express their gratitude to a number of distinguished academicians, researchers, and reviewers for their support, discussions, and critical reviews made during the course of writing this book. Dr. Kumar would like to acknowledge the support of students and members of his research group, including Dr. S. R. Vadera, Director, of Defence Laboratory of Jodhpur, Prof. K. Manzoor, Drs Rashi Mathur, A. K. Shukla, M. K. Patra, S. C. Negi, Manoth Mathew, D. R. Sharma, Vivek Kumar Singh, S. Gowda, Vatsana Gupta, Jitendra Singh, and Manoj Dhaka for their ever willing support while Prof. Kumbhat would like to acknowledge the support of Prof. R. P. Singh, Vice Chancellor, of Jai Narain Vyas University, Jodhpur, and her colleagues from the Department of Chemistry for their support in planning and execution of the courses related to nanoscience and nanotechnology. She also acknowledges the ever-willing support of her research students, Drs Urmila Nain, Sushma Dave, Omprakash Khatri, Jaya Jain, Richa Vyas, Kamesh Gangawat, Manjulata Parihar, Rakhee, Kavita, Uravsini Singh, Hema Somani, Ved Prakash, and Menka Khicher.

The authors would like to thank John Wiley & Sons, Inc., for taking up this project and Ms. Anita Lekhwani, Senior Acquisitions Editor, and her team members including Ms. Cecilia Tsai and Ms. Purvi Patel at John Wiley, Hoboken, New Jersey for their consistent interest, timely action in execution of this project, and making the publication of this book a reality.

About the Authors

Dr. N. Kumar, Former Director, Defence Laboratory, Jodhpur

Dr. Narendra Kumar, DRDO fellow, graduated and did his PhD degree in “Organometallic Chemistry” in 1976 from Delhi University. From 1976 to 1981, he served at the National Physical Laboratory, New Delhi, and worked toward the development and application of materials including organometallics, liquid crystals, electrochromics, and electrode materials. He served as a postdoctoral research fellow at Windsor University, Canada, during 1981–1983 and worked in the field of electrochemical synthesis of metallic and organometallic complexes of transition and actinide elements. In 1984, he joined as Scientist at the Defence Laboratory, Jodhpur, and retired from there as its Director in 2012, where he carried out pioneering research work in the development of conducting polymers, liquid loam, nanomaterials, and products based on them for various defence applications. Dr. Kumar has published more than 100 research and review articles in international journals in the areas of Nanoscience, Organometallics, Conducting Polymers, and Electrochemical Synthesis, and also a chapter entitled “Nanotechnology for Sensor and Display Applications” in the *Encyclopedia of Nanoscience and Technology* published by American Scientific Publication, USA. He has 12 patents to his credit and authored one book entitled *Nanotechnology and Nanomaterials in the Treatment of Life Threatening Diseases* published by Elsevier (USA) in 2013. He also served as a visiting Research Associate of CSIR, New Delhi, during 1992–1995 and is a recognized supervisor of J. N. V. University, Jodhpur, for PhD and has guided 6 students for their PhD degrees in the area of nanoscience. He has delivered several invited talks on Conducting Polymers and Nanomaterials in several International and national conferences/seminars, as well as at universities in India, Japan, and the United States.

He received the DRDO Technology Cash Award in 1996 for his pioneering research work on conducting polymers, and DRDO Scientist of the Year award in 2005 from the Prime Minister of India for products based on conducting polymers and nanomaterials for defense applications. He is a recipient of the National MRSI-ICSC Super Conductivity and Materials Science Annual Award for the year 2010 by Materials Research Society of India. Dr. Kumar is a member of various scientific societies including the prestigious American Chemical Society.

Dr. S. Kumbhat, Professor, Department of Chemistry, Jai Narain Vyas University, Jodhpur

Dr. Sunita Kumbhat, Professor and Chemistry Department at J.N.V. University, Jodhpur, has graduated in Chemistry and obtained her PhD degree in the field of Electrochemistry in 1985 from J.N.V. University, Jodhpur. She did postdoctoral research in the fields of Photoelectrochemistry and Sonovoltammetry with Prof. R.G. Compton at Oxford University, UK. Dr. Kumbhat joined the Department of Chemistry, J.N.V. University, as permanent faculty member in 1986, and has been serving as a Professor since 2001 where she has been involved in teaching graduate and postgraduate courses on Analytical Chemistry, Electrochemistry, Sensors, and Nanoscience and supervising PhD students. Her areas of interest are Electrochemistry and Biosensors for Biomedical and Environmental Analysis. She has more than 50 research papers in international journals, three educational films, and one patent to her credit. She has supervised 14 research students for their PhD degrees. Her awards and recognition include Commonwealth Academic Staff Fellowship (1994–1995) at Oxford, UK, National Associate (1997) at BARC, Mumbai, and the INSA–JSPS Visiting Fellowship (2005) at Kyushu University, Fukuoka, Japan. Dr. Kumbhat is associated with various Indian and International scientific societies and is also an assessing member of the National Assessment and Accreditation Council, Bangalore, India.

Chapter 1
Introduction

1.1 Definitions of Nanoscience and Nanotechnologies

Nanoscience is a new discipline concerned with the unique properties associated with nanomaterials, which are assemblies of atoms or molecules on a nanoscale. Nanoscience is actually the study of objects/particles and its phenomena at a very small scale, ranging roughly from 1 to 100 nm. “Nano” refers to a scale of size in the metric system. It is used in scientific units to denote one-billionth of the base unit, approximately 100,000 times smaller than the diameter of a human hair. A nanometer is 10^{-9} m (1 nm = 10^{-9} m), a dimension in the world of atoms and molecules (the size of H atom is 0.24 nm and, for instance, 10 hydrogen atoms lined up measure about 1 nm). Nanoparticles are those particles that contain from 100 to 10,000 atoms. Thus, the particles in size roughly ranging from 1 to 100 nm are the building block of nanomaterials.

Nanomaterials: These materials are created from blocks of nanoparticles, and thus they can be defined as a set of substances where at least one dimension is approximately less than 100 nm. However, organizations in some areas such as environment, health, and consumer protection favor a larger size range from 0.3 to 300 nm to define nanomaterials. This larger size range allows more research and a better understanding of all nanomaterials and also allows to know whether any particular nanomaterial shows concerns for human health or not and in what size range. Nanocarbons such as fullerenes, carbon nanotubes, and graphene are excellent examples of nanomaterials. A comparison of the size of nanomaterials with some natural and biological species is illustrated in Figure 1.1.

Nano-object: Material confined in one, two, or three dimensions at the nanoscale. This includes nanoparticles (all three dimensions in the nanoscale), nanofibers (two dimensions in the nanoscale), and nanoplates (one dimension in the nanoscale). Nanofibers are further divided into nanotubes (hollow nanofiber), nanorods (solid nanofiber), and nanowire (electrically conducting or semiconducting nanofiber). However, the term nano-object is not very popular.

Particle: It is a minute piece of matter with defined physical boundaries. A particle can move as a unit. This general particle definition applies to nano-objects.

Nanoparticle: It is a nano-object with all three external dimensions in the nanoscale. Nanoparticles can have amorphous or crystalline form and their surfaces can act as carriers for liquid droplets or gases.

Nanoparticulate matter: It refers to a collection of nanoparticles, emphasizing their collective behavior.

Agglomerate: It is a group of particles held together by weak forces such as van der Waals forces, some electrostatic forces, and surface tension. It should be noted that agglomerate will usually retain a high surface-to-volume ratio.

Aggregate: It is a group of particles held together by strong forces such as those associated with covalent or metallic bonds. It should be noted that an aggregate may retain a high surface-to-volume ratio.

Nanotechnology is the construction and use of functional structures designed from atomic or molecular scale with at least one characteristic dimension measured in nanometers. Their size allows them to exhibit novel and significantly improved physical, chemical, and biological properties, phenomena, and processes because of their size. Thus, nanotechnology can be defined as research and development that involves measuring and manipulating matter at the atomic, molecular, and supramolecular levels at scales measured in approximately 1–100 nm in at least one dimension.

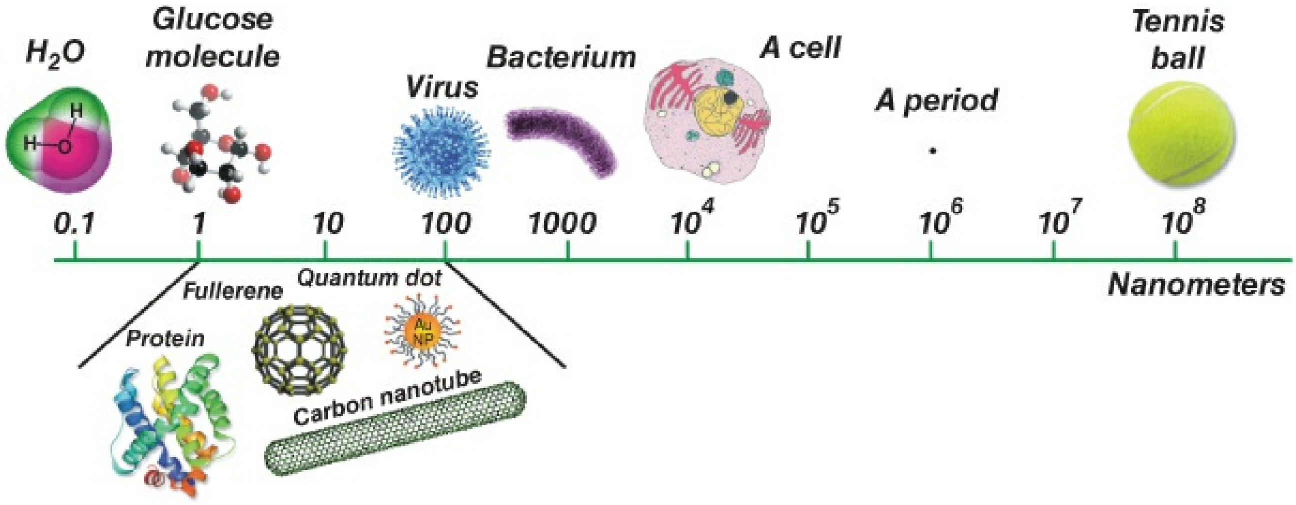

Figure 1.1 Size comparisons of objects, nanomaterials, and biomolecules.

When characteristic structural features are intermediate between isolated atoms and bulk materials in the range of approximately 1–100 nm, the objects often display physical attributes substantially different from those displayed by either atoms or bulk materials. The term “nanotechnology” is by and large used as a reference for both nanoscience and nanotechnology especially in the public domain. We should distinguish between nanoscience and nanotechnology. Nanoscience is a convergence of physics, chemistry, materials science, and biology, which deals with the manipulation and characterization of matter on length scales between the molecular and the micron size. Nanotechnology is an emerging engineering discipline that applies methods from nanoscience to create products.

1.2 Uniqueness of the Nanoscale

At nanoscale, the laws of physics operate in an unfamiliar way because of two important reasons: high surface-to-volume ratio and quantum effect. The key reason for nano-sized regime being special is the dramatic increase in the surface-to-volume ratio. When the size of building blocks gets smaller, the surface area of the material increases by six orders of magnitude, as illustrated in Figure 1.2, while the volume remaining the same. For example, dissecting a 1 m^3 of any material into 1 nm particles increases the total combined surface area from 6 to 60,000,000 m^2, approximately 10 million times larger [1]. Nanomaterials have a wider range of applications such as catalysts, cleanup, and capture of pollution and any other application where chemical reactivity is important such as medicine. This effect occurs at all length scales, but what makes it unique at the nanoscale is that the properties of the material become strongly dependent on the surface of the material since the amount of surface is now at the same level as the amount of bulk. In fact, in some cases such as fullerenes or single-walled nanotubes, the material is entirely the surface.

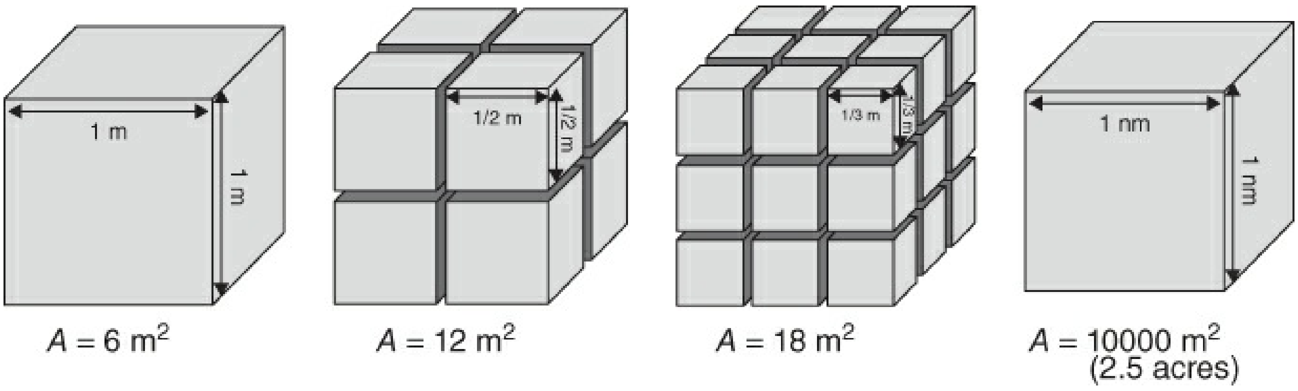

Figure 1.2 Exponential increases in surface area for cubes ranging from meter to nanosize.

Another important attribute of nanoscale materials is the fact that it is possible for the quantum mechanical properties of matter to dominate over bulk properties. One example of this is in the change in the optical properties, for example, in the photoemission, of many semiconductor materials as they “go nano.” Figure 1.3 illustrates how, a material whose optical properties may be considered uninteresting, simply by changing its size to the nanoscale one can control the color of the material [2]. This effect is due to quantum confinement.

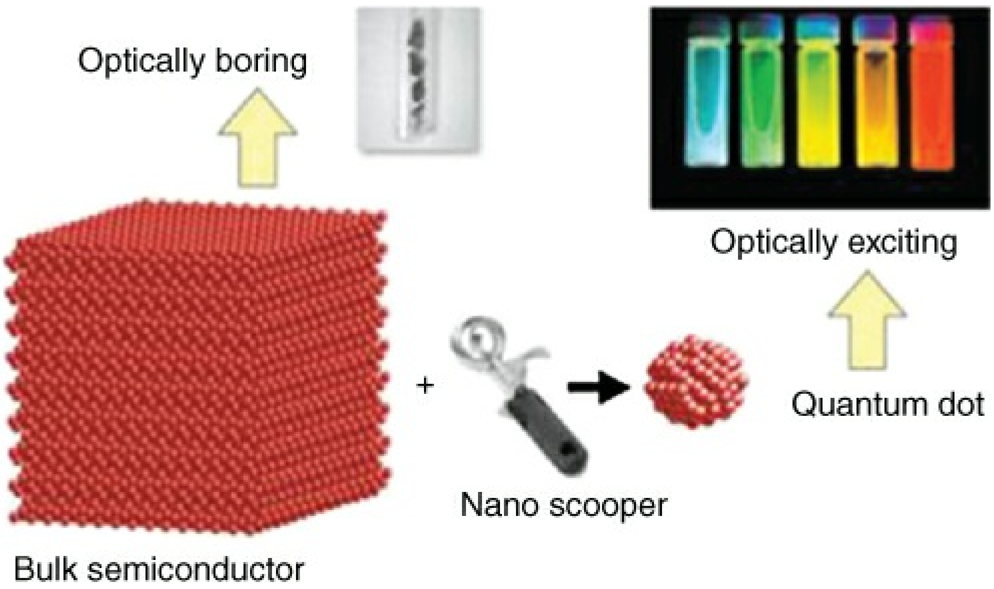

Figure 1.3 Change in optical properties of a semiconductor ranging from bulk to nanosize. Courtesy of Grossman, MIT, USA.

Important consequence of each of these properties is that they offer completely new methods of tuning the properties of materials and devices. Nanotechnology can provide unprecedented understanding about materials and devices and is likely to impact many fields. By using structure at nanoscale as a tunable physical variable, we can greatly expand the range of performance of existing chemicals and materials. Nanoscience and nanotechnology are broad and interdisciplinary areas of research and development activity that have been growing explosively worldwide in the past two decades. Nanoscience has the potential for revolutionizing the methods in which materials and products are created and the range and nature of functionalities that can be accessed; nanotechnology already has a significant commercial impact that will increase exponentially in future.

1.3 Nanoscience in Nature

Nanostructures are plentiful in nature. In the universe, nanoparticles are distributed widely and are considered to be the building blocks in planet formation processes. Indeed, several natural structures including proteins and the DNA diameter of around 2.5 nm, viruses (10–60 nm), and bacteria (30 nm to 10 µm) fit the above definition of nonmaterial, while others are of mineral or environmental origin. For example, these include the fine fraction of desert sand, oil fumes, smog, fumes originating from volcanic activity or from forest fires, and certain atmospheric dusts. Biological systems have built up inorganic–organic nanocomposite structures to improve the mechanical properties or to improve the optical, magnetic, and chemical sensing in living species. As an example, nacre (mother-of-pearl) from the mollusk shell is a biologically formed lamellar ceramic, which exhibits structural robustness despite the brittle nature of its constituents. These systems have evolved and been optimized by evolution over millions of years into sophisticated and complex structures. In natural systems, the bottom-up approach starting from molecules and involving self-organization concepts has been highly successful in building larger structural and functional components. Functional systems are characterized by complex sensing, self-repair, information transmission and storage, and other functions all based on molecular building blocks. Examples of these complex structures for structural purposes are teeth, such as shark teeth, which consist of a composite of biomineralized fluorapatite and organic compounds. These structures result in the unique combination of hardness, fracture toughness, and sharpness. The evolution has worked on much smaller scales too, producing finely honed nanostructures, parts less than a millionth of a meter across, or smaller than 1/20th of the width of a human hair help animals climb, slither, camouflage, flirt, and thrive. Figure 1.4a shows an electron microscopic image of a sensory patch in amphibian ears, which consists of a single bundle of stereo cilia projecting from the epithelium of the papilla, and acts as a nanomechanical cantilevers that measure deflections as small as 3 nm because of sound waves. Many of the shimmering colors in butterfly's wings are produced not with pigments but with nanostructures. The scales on their wings are patterned with nanoscale channels, ridges, and cavities made of chitin, a protein. Unlike pigments, which create color by absorbing some wavelengths of light and reflecting the rest, the nanostructures are shaped so that they physically bend and scatter light in different directions, sending particular colors back to our eyes. This scattering can also make them iridescent (i.e., the color changes with the angle one sees it from. When infrared radiation hits the chitin nanostructures, their shape changes because of expansion, thus changing the colors they display. Figure 1.4b shows glittering colors of peacock feather where barbs project directly from the main feather stem, and barbules (~0.5 mm long) attached to each side of the barb generate the typical “shimmer” of iridescence. Electron microscopy (Figure 1.4c and d) of barbules reveals a highly ordered structure of melanin rods of high refractive index embedded in keratin of lower refractive index with air tube between each square of melanin rods. The whole array of melanin rods, keratin matrix, and air holes comprises a 2D photonic crystal. There is much interest on mimicking these natural wonders with potential applications in optical engineering and communications. Less seriously, photonic crystal pigment-free paints would not fade, fabrics might be more vibrant.

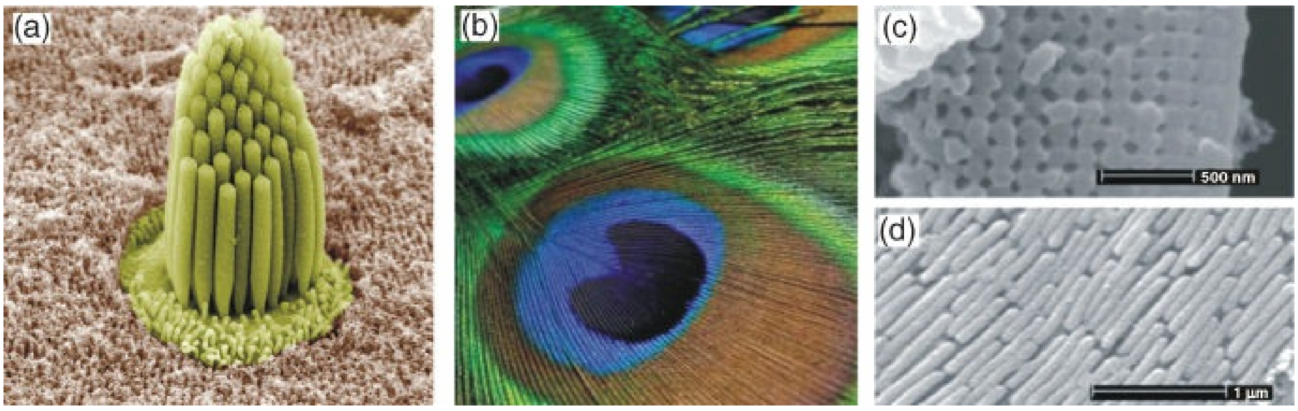

Figure 1.4 Nanotechnology in nature: (a) electron microscopic image of a sensory patch in amphibian ears. http://scinerds.tumblr.com/post/35542105310/stereocilia-stairsteps; (b) peacock feather showing barbules, representing a photonic lattice; (c and d) electron microscopy image of transverse and longitudinal sections of barbules. Zi et al. [2a] © 2003. With permission of National Academy of Sciences, USA.

The compound eye of arthropods uses nanoscale features to enhance their visual sensitivity. An insect's compound eye has about 50–10,000 individual facets, which are studded with an array of nanoscale protuberances called “corneal nipples” (Figure 1.5a and b), each with its own set of optical machinery. These tiny structures of size ranging from 50 to 300 nm cut down the glare that reflects off the insect eye. The nanoscale nipple pattern on moth eyes has inspired new antireflective coatings (Figure 1.5c) for solar cells. The male silk moth can detect, with single-molecule precision, the pheromones of a female moth emitted up to 2 miles away. Spider silks are some of the toughest materials known to man, stronger than steel, and their webs can withstand gusts of wind. The spider's silks get their strength from just nanometers of thin crystal proteins, which are stacked with hydrogen bonds, allowing the silk to stretch and flex under pressure.

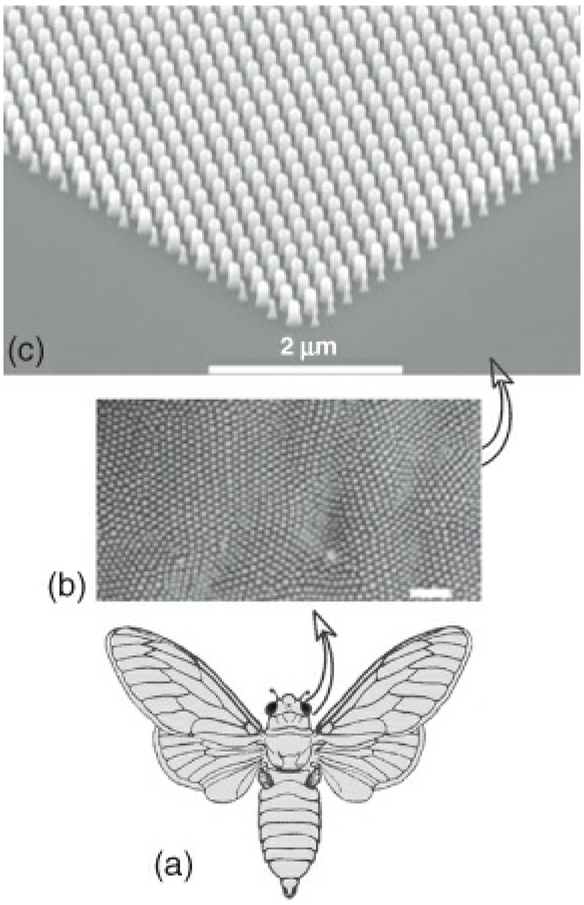

Figure 1.5 Natural and fabricated antireflective surfaces: (a) schematic of a moth; (b) scanning electron micrograph of antireflective surface of a moth's eye (scale bar = 1 µm); (c) biomimetic replica of a moth eye fabricated with ion- beam etching.

Parker & Townley [2c] © 2007. With permission of Nature Publishing Group.

These are only a few of the countless examples of how nature employs nanotechnology in different methods, of course, with the most important technology to us being the human body itself, which contains billions of nanoscale machines! It is both fascinating and humbling to observe that despite all of the phenomenal technological advances in nanoscale synthesis and characterization, in most cases we are still unable to build nanotechnology-based devices that even come close to nature.

1.3.1 Naturally Occurring Nanomaterials

Naturally occurring nanomaterials may originate from one of the following sources:

i. Natural erosion and volcanic activity

Nanoparticles are part of mineral world since they are naturally produced from erosion and volcanic explosions.

ii. Clays

Minerals such as clays are a type of layered nanostructured silicate materials that are characterized by a fine 2D crystal structure. Mica, one among them, is the most studied [3]. In mica, a large number of silicate sheets are held together by relatively strong bonds. On the other hand, montmorillonite, a smectic type of clay, has relatively weak bonds between layers. Each layer consists of two sheets of silica held together by cations such as Li^+, Na^+, K^+, and Ca^{2+}. The presence of the cations is necessary for compensating the overall negative charge of the single layers. The layers are 20–200 nm in diameter laterally and come into aggregates called tactoids, which can be about 1 nm or more thick. The fine nanostructure of clays determines their properties. As an example, the nanostructured clay swells to several times of the original volume, when water is added to it, due the opening of the layered structure by the water molecules that replaces the cations. Clay swelling is a significant factor in soil stability and is taken into account in constructing roads.

iii. Natural colloids

Naturally occurring liquid colloids, such as milk, blood, aerosols (e.g., fog), are some of the examples of natural colloids. In these materials, nanoparticles are dispersed in the medium (liquid or gas) but do not form a solution, rather they form a colloid. All these materials have the characteristic of scattering light and often their color (such as in the case of milk and blood) are due to the scattering of light by the nanoparticles that makes them up.

iv. Mineralized natural materials

Many of the natural materials such as shells, corals, and bones are formed by the self-assembly of calcium carbonate crystals with other natural materials, such as polymers, to form fascinating three-dimensional (3D) architectures. For instance, a shell is grown layer-by-layer coating of protein supported by chitin, a polysaccharide polymer. The proteins act as a nanoassembly mechanism to control the growth of calcium carbonate crystals. Around each crystal remains a honeycomb-like matrix of protein and chitin. This relatively "flexible envelop" is fundamental for the mechanical properties of the shell and mitigate cracking. The size of each crystal is around 100 nm. As a result, the mollusk shell has extraordinary physical properties, namely, strength and resistance to compression.

1.3.2 Nanoscience in Action in Biological World

Two most significant examples of active nanoscience in biological world include the following:

i. Lotus effect

Although the water repellency of lotus had long been recognized, its scientific basis was understood only in 1997 when two botanists Wilhelm Berthelot and Christophe Neinhuis, at the University of Bonn in Germany, examined leaf surfaces of lotus using a scanning electron microscope that resolves structures as small as 1–20 nm [4]. Figure 1.6a shows a nonwettable lotus plant leaf. The self-cleaning property is due to the "**Super hydrophobicity**" of the convex papillae on the surface of leaves, which is coated with wax crystals of nanoscopic dimension of approximately 10–100 nm (Figure 1.6b). Water drop picks up the dirt particles as it rolls off the leaf's surface, showing self-cleaning process (Figure 1.6c). Several other plants such as Nasturtium and cabbages also show lotus effect.

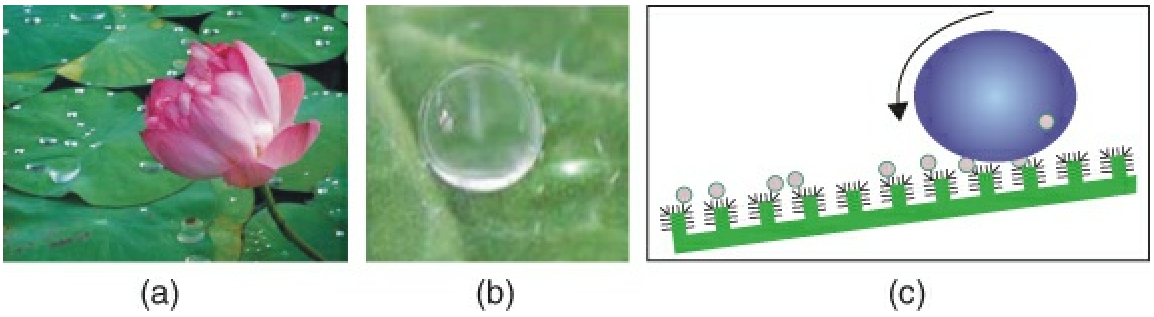

Figure 1.6 (a) Lotus (*Nelumbo nucifera*) plant; (b) spherical water droplet on a nonwettable lotus plant leaf. Blossey [6] © 2003. With permission of Nature Publishing Group. ; (c) self-cleaning: a drop picks up the dirt particles as it rolls off the leaf's surface.

The papilla greatly reduces the contact area of water droplets with it. Every epidermal cell forms a micrometer-scale papilla and has a dense layer of epicuticular waxes superimposed on it. Each of the papillae consists of branch-like nanostructures on the surface, for example, of the lotus leaves, the almost spherical water droplets will not come to rest and simply roll off if the surface is tilted even slightly, which is now usually referred to as the "**Lotus effect**." The self-cleaning effects of the surfaces of the lotus flower have been attributed to the combined micro- and nanostructure, which in combination with hydrophobic groups give the surface a water and dirt-repellent behavior. In the past few years, numerous companies have realized products resembling the surface morphology and chemistry of the lotus flower such as paint, glass surface, and ceramic tiles with dirt-repellent properties.

ii. Geckos Technology

Geckos are one of the few species in the animal kingdom that are known for sticky toes that allow them to climb up walls, even hang upside down on ceiling and at the same time can walk on a leaf; they owe this ability to nanoscale attachment elements. As illustrated in Figure 1.7a–e, on the sole of a gecko's toes there are about a billion tiny adhesive hairs, ~200 nm in both width and length. These hairs put the gecko in direct physical contact with the surface. Spatula-shaped ends on the hairs provide strong adhesion. Industry is researching the evolution of these properties in order to develop artificial dry adhesive systems. Potential applications include reusable adhesive fixtures with the strength of duct tape, which can be removed as easily as a sticky note.

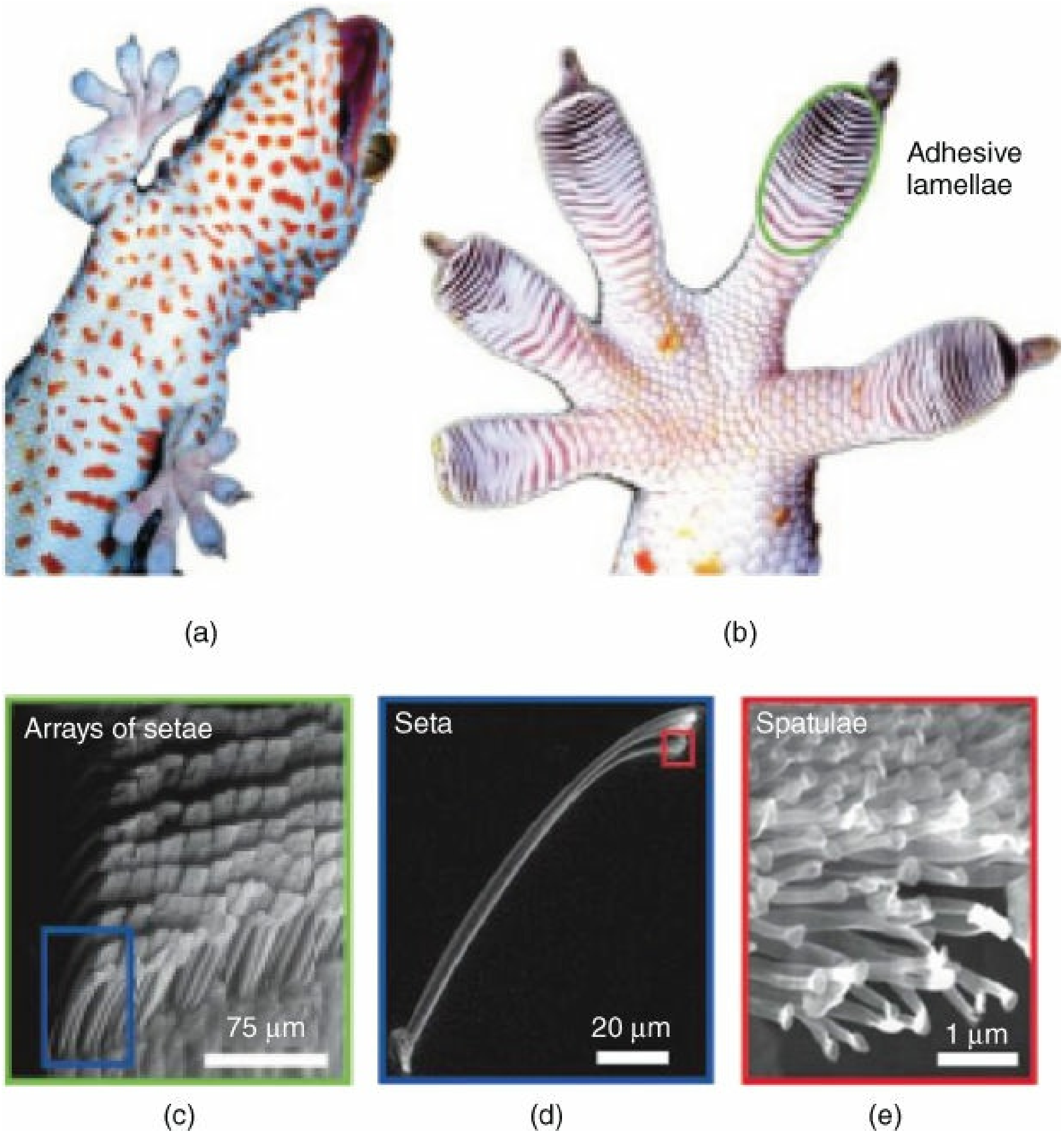

Figure 1.7 Gecko's adhesive system structure: (a) ventral view of a tokay gecko (*Gekko gecko*); (b) sole of the foot showing adhesive lamellae; (c) microstructure: part of a single lamella showing arrays of setae; (d and e) nanostructure: single seta with branched structure at the upper right area, terminating in hundreds of spatular tips. Hansen and Autumn [6], © 2005. With permission of National Academy of Sciences, USA.

Some more examples of naturally occurring materials such as cotton, spider's silk, and opals are also worth mentioning for their nano features and unique properties. Cotton has nanoscale arrangement of cellulose fibers showing high strength, durability, and absorbance. Spider silk showing five time higher strength than that of steel has natural supramolecular organization of fibroin at nanoscale. Precious stone opal consists of spheres of silicon dioxide (150–300 nm diameter) in a hexagonal or cubic close-packed lattice. These ordered silica spheres produce the internal colors by causing the interference and diffraction of light passing through the microstructure of the opal. The realization that nature can provide the model for improved engineering has created a research field called “biomimicking” or bio-inspired material science. It has been possible to process several types of nanostructures inspired from biological nanomaterials, represented in Table 1.1, which provide new technological opportunities and potential for applications.

Table 1.1 Bio-Inspired Unique Properties

Natural System/Materials	Bio-Inspired Properties
Substructure of nacre	Low-density, high-strength composites
Spider silk	High-tensile strength fiber
Wood, ligaments, and bone	High-strength structural material
Eels and nervous system	Electrical conduction
Deep-sea fish and glow worms	Photoemission
Butterfly and bird wings	Photonic crystals
Moth eye	Antireflective
Lotus leaf, human skin, fish scales	Hydrophobic surfaces, self-cleaning
Shark skin	Drag reducing
Gecko's feet	Adhesion
Human brain	Artificial intelligence and computing

1.4 Historical Perspective

Thousands of years bc, people used natural fabrics such as flex, cotton, wool, and silk and processed them into products. What makes these fabrics so special that they developed a network of pores of size 1–20 nm for typical nanoporous materials? Owing to their nanoporous structure, natural fabric possesses high utilitarian properties of absorbing sweat, quickly swelling, and getting dried soon. Since ancient times, people mastered the art of making bread, wine, beer, cheese, and other foodstuffs where fermentation processes at the nanolevel are critical. Romans in the pre-Christian era introduced metals with nanometric dimensions in glass-making: a cup describing the death of King Lycurgus (ca 800 bc) contains nanoparticles of silver and gold [7]; when a light source is placed inside the cup, its color changes from green to red (Figure 1.8a). It was found that it was due to the presence of nano-sized particles of silver (66.2%), gold (31.2%), and copper (2.6%) embedded in the glass. Light absorption and scattering by these nanoparticles determine the different colors. The stained-glass windows of the great medieval cathedrals also contain metallic nanoparticles.

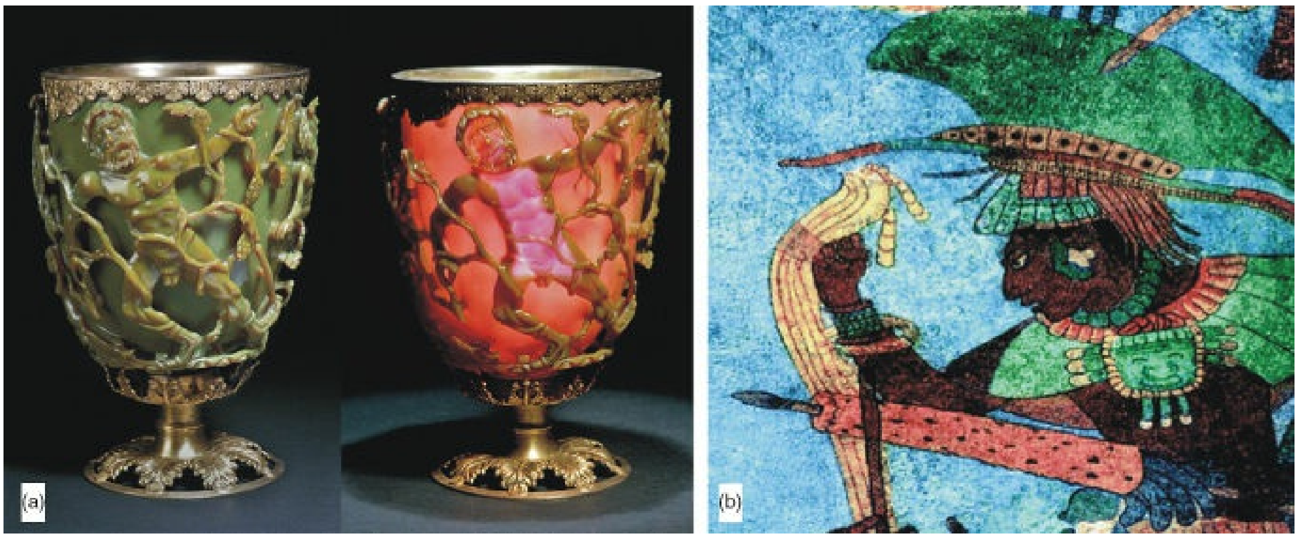

Figure 1.8 (a) Lycurgus cups. Courtesy of Trustees of the British Museum. © The Trustees of the British Museum; (b) ancient Maya fresco painting. Reproduced from Sanchez et al. [8] © 2005. With permission of The Royal Society of Chemistry.

The colors of certain Mayan paintings (Figure 1.8b) also stem from the presence of metallic nanoparticles [8]. Mayan artisans concocting in the eighth century the unique pigment we now know as Maya Blue have endured their lively blue tones for more than 12 centuries of harsh jungle environment. Maya Blue is not an ordinary organic dye nor is it any simple mineral; it is a hybrid organic–inorganic nanocomposite in which the organic dye molecules are protected within palygorskite, a complex natural clay. Art history of India and China is also filled with examples of nanotechnology. Photography, which was developed in the 18th and 19th centuries, provides a more recent example of the use of silver nanoparticles. Nanostructured catalysts have also been investigated for over 70 years. In the early 1940s, precipitated and fumed silica nanoparticles were being manufactured and sold in the United States and Germany as substitutes for ultrafine carbon black for rubber reinforcements. Nano-sized amorphous silica particles have found large-scale applications in many everyday consumer products, ranging from nondiary coffee creamer to automobile tires, optical fibers, and catalyst supports. In addition, the definition of nanoparticles based on size allows us to include colloids and soils that have been used for over a hundred years.

In 1857, Faraday had described the use of colloidal gold in his experiments. In his lecture at Royal Society, Faraday presented a purple color slide, stating that it contained “gold reduced in exceedingly fine particles, which becoming diffused, produced a ruby red fluid. The various preparations of gold, whether ruby, green, violet or blue etc. consist of that substance in a metallic divided state.” Faraday postulated correctly about the physical state of colloids; he also described how a gold colloid would change color (turning blue) on adding salt. Since then, colloidal science has evolved a lot. In the early twentieth century Gustav Mie presented the Mie theory, which is a mathematical treatment of light scattering that describes the relationship between metal colloid size and optical properties of solutions containing them. The Nobel Prize winner for Quantum Electrodynamics, Richard Feynman (Figure 1.9), said, “**Nature has been working at the level of atoms and molecules for millions of years, so why do we not?**” Since his call in a lecture in 1959, nanotechnology has made tremendous progress not only in technical disciplines but also in medicine and pharmaceutics [9]. World began speculating on the possibilities and potential of nanometric materials and on the fact that the manipulation of individual atoms could allow us to create very small structures whose properties would be very different from larger structures with the same composition. Moreover, in an even more radical proposition, he thought that, in principle, it was possible to create “nanoscale” machines through a cascade of billions of factories. According to him, these factories would be progressively smaller scaled versions of machine, hands, and tools. In these speculations, he also suggested that there are various factors that uniquely affect the nanoscale level. Specifically, he suggested that as the scale got smaller and smaller, gravity would become more negligible, while van der Waals attraction and surface tension would become very important. Feynman's talk has been viewed as the first academic talk that dealt with a main tenet of nanotechnology, the direct manipulation of individual atoms (molecular manufacturing). Richard Feynman is considered as the “Father of Nanotechnology,” although he never explicitly mentioned the term “Nanotechnology.”

Figure 1.9 Richard Feynman.

https://commons.wikimedia.org/wiki/Category:Richard_Feynman.

The evolution of integrated chips may also be considered as the part of history of nanotechnology. The first transistor invented in 1947 was a bulk macro-object. To keep with the demand for miniaturization, the dimensions of the transistor have been reduced considerably in the last 30 years. In the year 2002, the nanosize was reached with the achieved size of a single transistor as 90 nm [10]. As on today, a single transistor in an Intel Core 2 Quad Processor is 45 nm. In order to keep pace with Moore's law, transistor would be as small as 9 nm by 2016. However, this dimension is below the fabrication capabilities of last-generation tools used in the microelectronic industry. Numerous novel approaches such as quantum computing and molecular engineering are under investigation to achieve the workable transistor of this size. Material science/engineering is also full with examples of nanomaterials! Often these were produced inadvertently and were not characterized at the nanoscale since the analytic tools were not available. For instance, the process of anodizing was first patented in early 1930s. This represents one of the most important processes used in industry to protect aluminum from corrosion. It consists of depositing a thin protective oxide layer on the aluminum surface. The inventors were not, however, aware that the protective layer is actually a nanomaterial; the anodic layer is composed of hexagonally close-packed channels with diameter ranging from 10 to 250 nm or greater. The first use of the term “nanotechnology” was by Norio Taniguchi in 1974 at the International Conference on Precision Engineering (ICPE). His definition referred to “production technology to get extra high accuracy and ultra-fine dimensions, that is, the preciseness and fineness on the order of 1 nm (nanometer), 10^{-9} m, in length.” The development of nanotechnology has been enabled by the invention of two analytical tools that have revolutionized the imaging (and manipulation) of surfaces at the nanoscale. These are the scanning tunneling microscope (STM) and the atomic force microscope (AFM). The AFM and STM are capable of imaging surfaces at an atomic resolution. Both the instruments were invented by Binning and his coworkers at IBM Zurich. Invention of these versatile tools practically opened the doors of nanoworld to the scientists. With the advent of the STM, scientists were given the tool not only to image surfaces with atomic resolution but also to move individual atoms. The STM is the first step in realizing Feynman's vision of atom-by-atom fabrication. In the 1980s, the basic idea of this definition was explored in much more depth by Eric Drexler, who promoted the technological significance of nanoscale phenomena and devices through speeches and the books, *Engines of Creation: The Coming Era of Nanotechnology* and *Nanosystem: Molecular Machinery, Manufacturing, and Computation* [11] and so the term acquired its current sense. Birth of “Cluster Science” in the late 1980s gave further momentum to the development of nanoscience and nanotechnology. In another development, the studies on the synthesis and properties of metallic and semiconductor nanocrystals led to a fast increasing number of metal and metal oxide nanoparticles and quantum dots. In 2000, the United States National Nanotechnology Initiative (NNI) was founded to coordinate Federal Nanotechnology research and development. In short, the milestones related to the evolution of nanoscience and nanotechnology, from prehistoric to modern era, are given in Table 1.2.

Table 1.2 Milestones Associated with the Evolution of Nanoscience and Nanotechnology

Year	Milestone
Since origin of life	Cell: a magnificent nanomachine
400 bc	Democritus of Abdera gave reasoning about atoms and matter
500 ad	Glazes artisan in Mesopotamia, Mayan paintings
1857	M. Faraday prepared colloidal dispersion of gold that is stable for almost a century before being destroyed during World War II
1931	Electron microscope by Max Knoll and E. Ruska
1959	R. Feynman during an after-dinner talk “There's Plenty of Room at the Bottom” described molecular machines' building with atomic precision
1974	N. Taniguchi used the term “nanotechnology” for fabrication methods below 1 μm
1977	E. Drexler gave, for the first time, the concept of molecular nanotechnology at MIT, USA
1981	G. Binnig and H. Rohrer (IBM) invented scanning tunneling microscope and received Nobel Prize of Physics in **1986**
1985	Fullerene was discovered by R. F. Curl Jr., H. W. Kroto, and R. E. Smelly won Nobel prize of Chemistry in **1996**
1986	**i.** Invention of atomic force microscopy by G. Binning, C. F. Quate, and Ch Gerber (IBM) **ii.** ii. Eric Drexler, *Engines of Creation: The Coming Era of Nanotechnology*, the first book on nanotechnology
1991	Discovery of carbon nanotube (CNT) by S. Iijima
1998	Carbon nanotube transistor by C. Dekkar and coworkers
2000	Discovery of stimulated emission depletion (STED) by S. Hell
2001	Moor's law surpassed by producing world's fastest silicon transistor at Intel Corporation, which switches on and off 1.5 trillion times per second
2004	Discovery of graphene by A. Giem and K. Novoselov and they won Nobel Prize in 2010
2004	Intel launches the Pentium 4 “PRESCOFT” Processor based on 90 nm technology
2006	Discovery of single-molecule microscopy (SMM) by E. Betzig and W. Moerner led to the discovery of nanomicroscopy, surpassing the limits of optical microscopy Based on STED and SMM techniques, super-resolved fluorescence microscopy has emerged to study synapses in Alzheimer's and Huntington's disease, and to gain a better understanding of protein development in embryos, which led to winning the Nobel Prize of Chemistry in **2014** jointly by E. Betzig, S, W. Hell, and W. E. Moerner

1.5 Nanomaterials

Materials are what the world is made of. They are hugely important and hugely interesting. They are also intrinsically complicated. Materials, in general, are comprised of a large number of atoms and molecules and have properties determined by complex, heterogeneous structures. Historically, the heterogeneity of materials plays crucial roles in determining properties that have been determined largely empirically and manipulated through choice of the compositions of starting materials and the conditions of processing.

Nanomaterial means a material that meets at least one of the following criteria:

- Consists of particles with one or more external dimensions in the size range of 1–100 nm for more than 1% of their number.
- Internal/surface structures in one or more dimensions in the size range of 1–100 nm.
- Specific surface-to-volume ratio >60 m^2/cm^3, excluding materials consisting of particles with a size less than 1 nm.

Nanomaterials can be nanoscale in one dimension (e.g., surface films), two dimensions (e.g., strands or fibers), or three dimensions (e.g., precipitates, colloids). They can exist in single, fused, aggregated, or agglomerated forms with spherical, tubular, and irregular shapes.

Nanostructures are the ordered system of one, two, or three dimensions of nanomaterials, assembled with nanometer scale in certain pattern that includes nanosphere, nanotubes, nanorod, nanowire, and nanobelt [12]. Nanostructured materials are classified as zero-, one-, two-, and three-dimensional nanostructures, showing typical examples with varied dimensionality in nanomaterials as in Figure 1.10a–i.

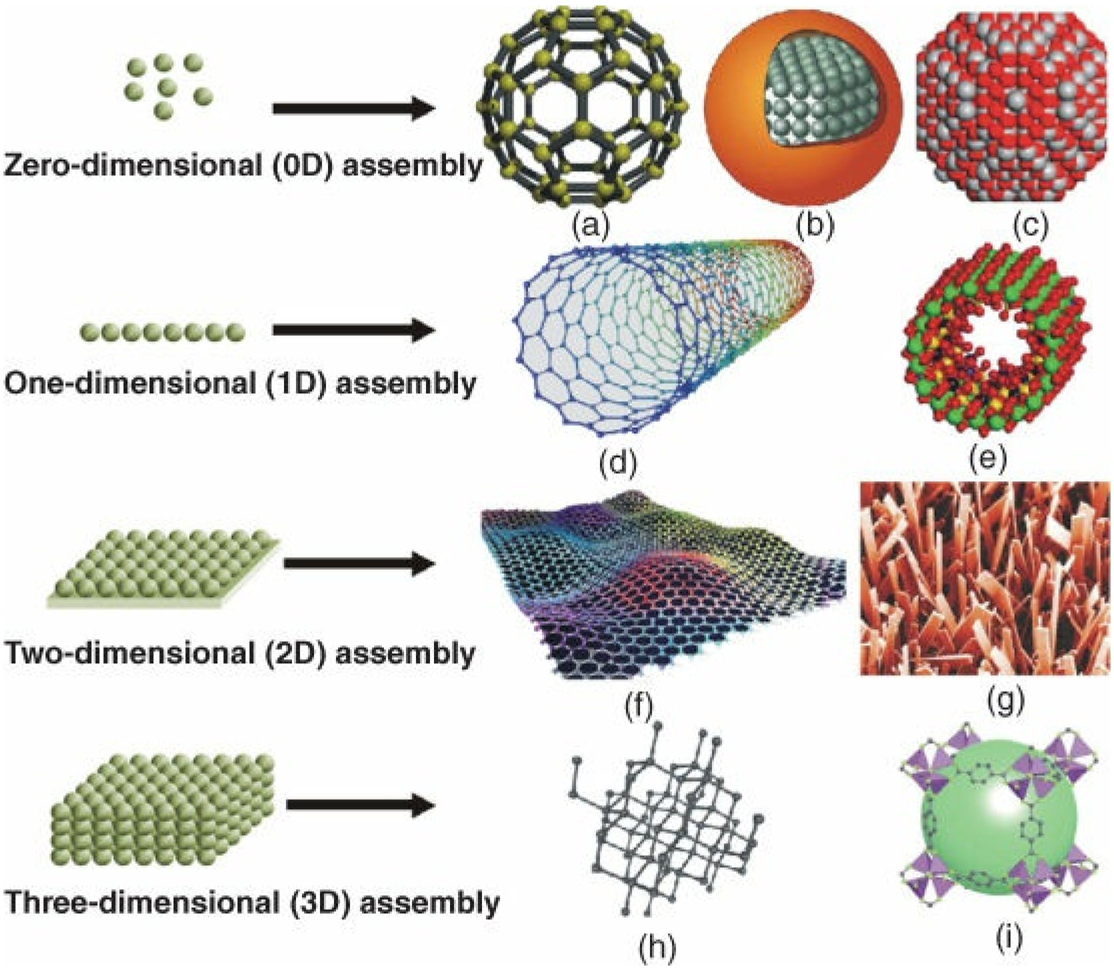
Zero-dimensional (0D) assembly
(a)
(b)
(c)
One-dimensional (1D) assembly
(d)
(e)
Two-dimensional (2D) assembly
(f)
(g)
Three-dimensional (3D) assembly
(h)
(i)

Figure 1.10 Typical examples showing varied dimensionality in nanomaterials: (a) fullerene; (b) quantum dot; (c) metal cluster; (d) carbon nanotube; (e) metal oxide nanotube; (f) graphene; (g) metal oxide nanobelts; (h) nanodiamond; (i) metal organic frameworks (MOFs).

A **nanocrystallite** is generally understood to possess crystalline order in addition to nanoscale size. If one dimension of the 3D nanostructure is at nanoscale, then it is called a **Quantum Well**. If two dimensions of the 3D nanostructure are at nanoscale, then it is called a **Quantum Wire**. If all the three dimensions of the nanostructure are at nanoscale, then it is called a **Quantum Dot**. Nanocrystallites are also called quantum dot. Nanomaterials are of interest because at this scale unique optical, magnetic, electrical, and other properties emerge. These emergent properties have the potential for great impacts in electronics, medicine, and other fields. Nanocarbons such as fullerenes, carbon nanotubes, and graphene are excellent examples of nanomaterials. Nanomaterials are cornerstones of nanoscience and nanotechnology. The creation of functional materials, devices, and systems through control of matter on the nanometer length scale (1–100 nm) is the exploitation of novel phenomena and properties (physical, chemical, biological) at that length scale. The phrase “nanostructured materials” implies two important ideas: (1) at least some of the property determining heterogeneity in materials occurs in the size range of nanostructures (1–100 nm) and (2) these nanostructures might be synthesized and distributed (or organized), at least in part, by design. The idea of “nanostructured materials” thus focuses on four key questions:

i. Why nanostructures are interesting?

ii. How can they be synthesized?

iii. How can they be introduced into materials?

iv. How can the relationships between compositions and structures, and matrices and interfaces control the properties of the resultant materials?

“Materials by design,” pertaining to the last question, have been a goal of material science since its inception. It remains, however, a difficult task because majority of research is still focused to answer the first three questions. All conventional materials such as metals, semiconductors, glass, ceramics, or polymers can in principle be obtained with a nanoscale dimension. The spectrum of nanomaterials ranges from inorganic to organic and from crystalline to amorphous particles, which can be found as single particles, aggregates, powders, or dispersed in a matrix, over colloids, suspensions and emulsion, nanolayers, and nanofilms. Supramolecular structures, such as dendrimers, micelles, or liposomes also belong to the class of nanomaterials.

1.5.1 Nanoparticles

Nanoparticles are solid particles at the intermediate state, that is, between atoms/molecules and macroscopic objects. Nanoparticles constitute of several tens or hundreds of atoms or molecules and can have a variety of sizes and morphologies (amorphous, crystalline, spherical, needles, etc.). The study of nanoparticles relates various scientific fields, for example, chemistry, physics, optics, electronics, magnetism, and mechanism of materials. Some nanoparticles have already reached practical stage. Owning to their small size effect, large surface effect, and quantum tunnel effect, the nanoparticles demonstrate special physical properties and can be widely used in a variety of applications. Some kinds of nanoparticles are available commercially in the form of dry powders or liquid dispersions. The latter is obtained by combining nanoparticles with an aqueous or organic liquid to form a suspension or paste. It may be necessary to use chemical additives (surfactants, dispersants) to obtain a uniform and stable dispersion of particles. With further processing steps, nanostructured powders and dispersions can be used to fabricate coatings, components, or devices that may or may not retain the nanostructure of the particulate raw materials. Industrial scale production of nanoparticulate materials such as carbon black, polymer dispersions, or micronized drugs has been established for a long time. Another important class of nanoparticulate materials is metal oxide nanopowder that includes silica (SiO_2), titania (TiO_2), alumina (Al_2O_3), or iron oxide (Fe_3O_4, Fe_2O_3); compound semiconductors (e.g., cadmium telluride, CdTe or gallium arsenide, GaAs), metals (especially precious metals such as Ag, Au), and alloys are also included in this category that are being commercialized.

1.5.2 Nanowires and Nanotubes

Linear nanostructures such as nanowires, nanotubes, or nanorods can be generated from different material classes, for example, metals, semiconductors, or carbon, by means of several production techniques. Carbon nanotubes are one of the most promising linear nanostructures that can occur in a variety of modifications (e.g., single-, or multiwalled, filled, or surface modified). At present, carbon nanotubes can be produced by CVD methods on a several tons per year scale.

1.5.3 Nanolayers/Nanocoatings

Nanolayers are one of the most important topics within the range of nanotechnology. Through nanoscale engineering of surfaces and layers, a vast range of functionalities and new physical effects (e.g., magnetoelectronic or optical) can be achieved. Furthermore, a nanoscale design of surfaces and layers is often necessary to optimize the interfaces between different material classes (e.g., semiconductor compound on silicon wafers) and to obtain the desired special properties.

1.5.4 Nanoporous Materials

Materials with defined pore sizes in the nanometer range are of special interest for a broad range of commercial applications because of their outstanding properties with regard to thermal insulation, controllable material separation and release, and their applicability as templates or fillers for chemistry and catalysis. One example of nanoporous material is aerogel, which is produced by sol–gel chemistry. A broad range of potential applications of these materials include catalysis, thermal insulation, electrode materials, environmental filters, and membranes as well as controlled release of drug carriers.

1.6 Strategies for Synthesis of Nanomaterials

Preparation of nanoparticles is an important branch of the materials science and engineering. Nanoparticles can be produced by a whole series of chemical, physical, or biological processes, some of which are totally new and innovative, while others have existed for a very long time. Four major processes are employed in synthesizing the new nanoparticles: gaseous phase, vapor deposition, wet chemistry, and grinding. Several of the processes for producing nanoparticles are similar to the existing chemical production processes.

> **i.** The gas phase method includes gas-phase evaporation method (resistance heating, high-frequency induction heating, plasma heating, electron beam heating, laser heating, electric heating evaporation method, vacuum deposition on the surface of flowing oil, and exploding wire method), chemical vapor reaction (heating heat pipe gas reaction, laser-induced chemical vapor reaction, plasma-enhanced chemical vapor reaction), chemical vapor condensation, and sputtering method.
>
> **ii.** Liquid phase method for synthesizing nanoparticles mainly includes precipitation, hydrolysis, spray, solvent thermal method (high temperature and high pressure), solvent evaporation pyrolysis, oxidation–reduction (room temperature and atmospheric pressure), emulsion, radiation-assisted chemical synthesis, and sol–gel processes.
>
> **iii.** Solid phase method includes thermal decomposition, solid-state reaction, spark discharge, stripping, and milling method. Most of these methods result in very fine particles that are more or less agglomerated. The powders are amorphous or crystalline and show a metastable or an unexpected phase, the reasons for which are far from being clear.

Owing to the small sizes, any surface coating of the nanoparticles strongly influences the properties of the particles as a whole. Studies have shown that the crystallization behavior of nanoscale silicon particles is quite different from micron-sized powders or thin films. It was observed that tiny polycrystallites are formed in every nanoparticle, even at moderately high temperatures.

1.7 Properties of Nanomaterials

The interest in nanostructured materials arises from the fact that because of the small size of the building blocks and the high density of interfaces (surfaces, grain, and phase boundaries) and other defects such as pores, new physical and chemical effects are expected or known properties can be improved substantially. The physical and chemical properties of nanostructured materials (such as optical absorption and fluorescence, melting point, catalytic activity, magnetism, electric and thermal conductivity, etc.) differ significantly from the corresponding coarser bulk material. Roughly two types of nanostructure-induced effects can be distinguished:

- The size effect, in particular the quantum size effects, where the normal bulk electronic structure is replaced by a series of discrete electronic levels.
- The surface- or interface-induced effect, which is important because of the enormously increased specific surface in particle systems.

Although the size effect is mainly considered to describe physical properties, the surface- or interface-induced effect plays an eminent role for chemical processing, in particular in connection with heterogeneous catalysis. Experimental evidence of the quantum size effect in small particles has been provided by different methods, while the surface-induced effect could be evidenced by the measurement of thermodynamic properties such as vapor pressure, specific heat, thermal conductivity, and melting point of small metallic particles. Both types of size effects have also been clearly separated in the optical properties of metal cluster composites. Very small semiconductor (<10 nm), or metal particles in glass composites, and semiconductor/polymer composites show interesting quantum effects and nonlinear electrical and optical properties.

These special properties of nanomaterials are mainly due to quantum size confinement in nanoclusters and an extremely large surface-to-volume ratio relative to bulk materials, thus leading to the presence of a high percentage of atoms/molecules lying at reactive boundary surfaces. For example, in a particle with 10 nm diameter only around 20% of all atoms are forming the surface, whereas in a particle of 1 nm diameter this figure can reach more than 90%. The increase in the surface-to-volume ratio results in an increase in the surface energy of the particle, which leads to, for example, a decrease in melting point or an increase in sintering activity. Furthermore, large surface area of particles may significantly raise the level of otherwise kinetically and thermodynamically unfavorable reactions. For instance, even gold, which is a very stable material, becomes reactive when the particle size is small enough. Fundamentally, there are seven key characteristics that contribute to the uniqueness of nanomaterials [13], and these are summarized in Table 1.3. In general, the unique properties of nanomaterials are an outcome of three effects: reduced size, high surface-to-volume ratio, and supramolecular structure arising because of the self-assembly of molecules that are summarized in Table 1.4.

Table 1.3 Characteristics of Nanomaterial and Their Importance

Characteristic	Importance
Size	Key defining criteria for a nanomaterial
Shape	Carbon nanosheets with a flat geodesic (hexagonal) structure show improved performance in epoxy composites versus carbon fibers
Surface charge	Surface charge is as important as size or shape. Can impact adhesion to surfaces and agglomeration characteristics. Nanoparticles are often coated or “capped” with agents such as polymers (PEG) or surfactants to manage the surface charge issues
Surface area	This is a critical parameter as the surface-to-weight ratio for nanomaterials is huge. For example, 1 g of an 8-nm-diameter nanoparticle has a surface area of 32 m^2
	Nanoparticles may have occlusions and cavities on the surface
Surface porosity	Many nanomaterials are characterized with zeolite-type porous surfaces. These engineered surfaces are designed for maximum absorption of a specific coating or to accommodate other molecules with a specific size
Composition	The chemical composition of nanomaterials is critical to ensure the correct stoichiometry being achieved. The purity of nanomaterials, impact of different catalysts used in the synthesis, and presence of possible contaminants need to be assessed along with possible coatings that may have been applied
Structure	Knowledge of the structure at the nanolevel is important. Many nanomaterials are heterogeneous, and information concerning crystal structure and grain boundaries is required

Source: Courtesy of PerkinElmer, Inc.

Table 1.4 Size and Shape-Related Attributes and Properties of nanomaterials

Physical Entity	Functionality
A. Size confinement/reduced size (Quantum dots, wires, rods, wells, fibers) Attributes: • Comparable size of nanoparticles with correlation scale of some physical phenomenon • Characteristic length of some transport process • Abnormal phase state	• Electronic: quantum confinement, molecular electronics • Electrical: tunable dielectric, ferroelectric, dc conductivity, electrical rheology • Optical: nonlinear, luminescence, transmission, selective absorption/reflection/scattering • Magnetic: new magnetic orders such as supermagnetism, paramagnetism, ferromagnetism; GMR, mechanical force transfer (MRF), magnetocaloric effects
B. High surface area (Powders, films, structural elements) Attributes: • Predominance of interfacial phenomenon because of the presence of free bonds, free bonding orbital with affinity for electrons, and occupied bonding orbital with low ionization potential	• Adsorption • Molecular recognition (chemical, biological) • Gas sensing, separation • Mechanical: superplasticity, higher structural strength and toughness, improved elasticity • Electrochemical process • Thermal insulation

C. Supramolecular and self-assembled structure (Nanotubes, fibers, rods, cables, films) Attributes: • Noncovalent and coordination bond • No exchange of electrons between molecules	• Adaptation, evolution, molecular forces holding • nanostructure electronics • Molecular recognition, directed chemical synthesis • Nonlinear optical phenomenon • Thermo-, opto- and electromechanical actuations • High-density ultrafast information processing • Ionic and molecular transport

Source: Patra et al. [15] © 2011. With permission of American Scientific Publisher.

1.8 Significance of Nanoscience

According to much of the information one reads in printed news articles, on websites, and even in many science journals, nanotechnology is projected to hold the key to meet the global energy needs with clean solutions, providing abundant clean water globally, increasing the health and longevity of human life, maximizing the productivity of agriculture, making powerful information technology available everywhere, and even enabling the development of space. Nanotechnology represents an entire scientific and engineering field, and not just a single product or even group of products. As a consequence, there are several areas of nanotechnology with many associated applications. With the increasing understanding on relationship between shape, size, and their physiochemical and biological properties, nanomaterials are considered to be futuristic material for diverse technologies. Current and potential areas of application include transport, manufacturing, biomedicine, sensors, environmental management, information and communications technology, materials, textiles, equipment, cosmetics, skin care, and defense. Although the list is by no means exhaustive, however, emerging application areas are discussed in the following section.

1.9 Commercial Applications

Many nanotech-based products have already been developed and are commercially available. The nanotech industry is poised for rapid growth with many additional nanotech-based products presently in their developmental stage and expected to be commercialized in the near future. The most common commercially exploited nanoparticles in various areas are those of silver, gold, iron metals, oxides of silicon, aluminum, titanium, iron, zinc, and carbon nanomaterials such as carbon nanotubes (CNT) and graphene. These materials are used for their specific and unique chemical, physical, and biological properties together with established technology for their scaled production now. It is also important to note that products are rarely 100% nanotechnology based; nanotechnology will be added to a product and form a part of it. Some of important sectors where nanotechnology-based products are available commercially [15] are given in following sections.

1.9.1 Food Industry

Silver is currently the most common nanoparticle that is used in the food industry. Silver has long been known as an effective antimicrobial agent and in its nanoform can now be easily impregnated invisibly into almost any product to aid in the destruction of bacteria and viruses. This has important applications in the food industry in terms of manufacturing, preserving, and storage. Although the use of nanotechnology directly in food products is limited, however, several food supplements are available that contain nanoparticles as the main active ingredient. The most common nanoparticles used in these supplements comprise silver, gold, copper, or calcium. It is unknown what effect these metals may have on cells and the body as a whole. Refrigerators and food containers are also now available with a silver nanoparticle lining to deter the growth of bacteria and mold. It is not known whether silver nanoparticles can be absorbed by the food while it is being stored and later ingested.

1.9.2 Cosmetics

The fascinating group of nanoparticles known as fullerenes, the C_{60} form, which resemble small “Footballs” of carbon atoms, are being used in cosmetics in the form of face creams to remove other unwanted particles, such as free radicals, which are believed to cause damage to the body and skin. Sun creams are now available with titanium dioxide nanoparticles. The micron-sized particles are used as sunblock, but are white in color and are not used in sun creams that need to be invisible when applied. The nanoparticle form is colorless as the particles are too small to reflect visible light, but still retain their ultraviolet sun-blocking properties that are highly desirable for a sun cream.

1.9.3 Textile

Textile industry is making increasing use of nanomaterials to make them more functional and smart. For example, nanosilver is playing a lead role because of its antimicrobial properties. Clothes can also be treated with nanofilms to make them stain, water and static resistant. These films, which are only a few atoms thick, could be in contact with skin over prolonged periods. Very little information is available what the long-term effect could be, although in the short term most products appear safe as nanotechnology has been used in clothes for several years now.

1.9.4 Medicine

The use of silver nanoparticles for use in medical devices is a hot topic. Nanosilver kills a broad range of harmful microbes and has been shown to be effective against the Methicillin-resistant Staphylococcus aureus (MRSA) superbug and the HIV virus. This could prove beneficial in terms of providing sterile equipment, beds, and wound dressings that limit the spread of harmful bacteria. Nanomedicine is not limited to simple single-element nanoparticles such as silver. More complicated nanoparticles can perform certain tasks such as homing in on cancer cells to destroy them or drug delivery that can send drugs directly into cells. Nanotechnology could also be used to produce new sensors that can detect whether a person has certain types of cancer using only a few drops of blood.

1.9.5 Electrical and Electronic Goods

For the majority of electrical goods, nanotechnology has come from a natural evolution of microtechnology. In order to fit more components into an electronic chip to make it more powerful, the components are made to be smaller. Over the period of time, components that used to be several hundred micrometers are now several hundred nanometers. In this aspect, nanotechnology only represents an arbitrary milestone, as a micron-sized transistor works in the same manner as a nano-sized transistor. Virtually all forms of nanotechnology used in electronics are embedded and are believed to pose a low human health risk and no additional risk to the environment over microtechnology. However, there are many areas that are having a greater impact including quantum computing, nanoelectrical mechanical systems (NEMS), and new display technologies.

Quantum computing uses the quantum mechanical effects available at the nanoscale that gives new methods of performing computational operations. Essentially, some computing tasks that have to be performed sequentially with a standard computer can be performed all at once using a quantum computer. This could dramatically increase the speed of databases, which underpin businesses, and, increasingly, the Internet. NEMS are effectively nano-sized machines that currently perform simple tasks. This type of nanotechnology is currently one of the closest analogies to nano-sized robots, the other type being biological nanomachines that are made from biological molecules. These can produce nano-sized motors and sensors. Applications for NEMS could be very broad, for example, monitoring the environment or even medical nanorobots for targeting cancers or repairing tissues. These examples are still very much in the preliminary or theoretical stage, but once developed could have a huge impact.

Recent display technologies use carbon nanotubes or nano-sized structures to efficiently emit electrons to be used to excite a phosphor display. This type of technology should have the advantage of being lightweight and efficient. Another new display technology is the organic semiconductor film. The term organic is used because the semiconductor material is made of organic or carbon-based polymers. These films may one day be printed off as plastic to provide cheap flexible displays. The nanotechnology element, which lies in the structure of the semiconductor, is not thought to pose any particular new risk over conventional plastics. Some of the commercialized nano-based products and their specific applications are listed in Table 1.5.

Table 1.5 Summary of Some Commercialized Nano-Based Products and Their Specific Applications

Broad Area	Type of Nanomaterials	Specific Application
Environmental protection	Nano zerovalent iron (nZVI)	Remediation of ground and surface waters exposed to chlorinated hydrocarbons
	Nano ZnO, TiO_2, CeO_2	Protection from UV radiations to preserve wood, concrete, and metal surfaces
Food technology	Nano clay	Packaging material to enhance shelf life of food
Energy: conversion,	Pd- and V-doped carbon	More efficient fuel cells by increasing storage capacities and

storage, and distribution	nanotubes	faster hydrogen absorption kinetics
Healthcare	NPs of gold, silver, magnetic oxides, polymers	To achieve better resolution and contrast in MRI and CT-based imaging for diagnosis, therapy and targeted drug delivery
Textiles	Silver nanoparticles	Integrated in dressing and clothing to prevent microbial growth and odor
	Nano TiO_2	Self-cleaning and wrinkle-free clothing
Cosmetics	Nano TiO_2 and nano ZnO	Soaps, sun screen lotion, moisturizers
Defense	CNTs, graphene, metal nano-oxides, nanocomposites	Ballistic protection, kinetic energy penetration, stealth technology
Aerospace	Clay nanoparticles	Fire retardant aircraft interiors
Automotive	CeO_2 NPs	As catalyst to enhance combustion in diesel fuel
Sports equipments	CNTs, carbon nanofiber, nanocomposites	Stronger and flexible golf shafts, tennis racket, racing bicycle components

1.10 Potential Health Hazards and Environmental Risks

It is unclear whether nanoparticles can cause chronic health effects. There are several methods that nanoparticles can enter the body, these include the following: inhalation, ingestion, absorption through the skin, and direct injection for medicinal purposes [16]. The skin is surprisingly permeable to nanomaterials. Carbon nanotubes are strong and can have a similar shape to asbestos fibers; several studies suggest that carbon nanotubes are potentially toxic to humans. Given that nano-sized objects tend to be more toxic than their large-scale form, it would be unwise to allow the unnecessary buildup of nanoparticles within the body until the toxicological effects of that nanoparticle are known however, such studies are still speculative. Concerns are, therefore, being expressed about potential risks to workers, public health, and the environment through manufacture, use, and disposition of these newly developed materials with unique and perhaps unknown properties. Because the scope of the nanotechnology industry is broad and involves many different industrial sectors, an understanding of the associated materials, processes, and applications is critical to ensure responsible industry development in a way that both encourages economic growth and protects public health and the environment. Removing nanoparticles from the environment may also present a significant problem because of their small size. If absorbed, the particles may travel up the food chain to larger animals in a similar process to DDT although there is no evidence either way that this is a valid mechanism. There is still too little research into the potential negative impacts of this technology on the environment. However, some nanoparticles such as copper and silver have been shown to be harmful to aquatic life.

1.11 Futuristic Outlook

Nanoscale materials have been used for decades in applications ranging from window glass and sunglasses to car bumpers and paints. Now, however, the convergence of scientific disciplines (chemistry, biology, electronics, physics, engineering, etc.) is leading to a multiplication of applications in materials manufacturing, computer chips, medical diagnosis and healthcare, energy, biotechnology, space exploration, security, and so on. It is this convergence of science, on the one hand, and growing diversity of applications, on the other hand, that is driving the potential of nanotechnologies. Hence, nanotechnology is expected to have a significant impact on our economy and society within the next 10–15 years, growing its importance over the longer term as further scientific and technology breakthroughs are achieved. In many cases, nanotechnology might only be a minor – but sometimes decisive contribution to the final product. It is believed that by the turn of this decade, the commercial value of products “incorporating nanotechnology” or “manufactured using nanotechnology” may exceed several trillion dollars. Nanomaterials in structures have the potential to significantly reduce production costs and the time of parts assembly, for example, in the automotive, consumer appliance, tooling, and container industries. The potential of significant reductions in weight due to these new materials as they are applied in the transportation industries will have great impact on energy consumption and the environment. Understanding nanoparticle formation is paying dividends in dealing with environmental issues such as atmospheric particulate formation as well. Many fundamental phenomena in energy science, such as electron transfer and exciton diffusion, occur on the nanometer length scale. Thus, the ability to arrange matter, that is, to inexpensive pattern and to develop effective nanostructuring processes, is going to be a vital asset in designing next-generation electronic devices, photovoltaic, and batteries. Size and cost reduction due to advances in the design and manufacture of healthcare-related diagnostic systems have the potential to empower individuals to diagnose and treat diseases in their own homes, decentralizing the healthcare system. Sensors based on nanotechnology are expected to revolutionize healthcare (e.g., via remote patient monitoring); climate control; detection of toxic substances (for environment, defense, and healthcare applications); and energy consumption in homes, consumer appliances, and power tools.

Nanotechnology and synthesis of nanomaterials are going to open new frontiers in the design of catalysts and catalyst technology for the petroleum, chemical, automotive, pharmaceutical, and food industries. The design of catalyst supports commensurating with biological structures can be an important bridge between conventional and enzymatic catalyses. In fact, oxidation catalysis can be performed today more efficiently in a zeolite, “ship-in-a-bottle” catalytic complex than with natural enzymes. This is just one example of an entire array of anticipated future developments.

New discoveries are expected and needed in studies of single objects with nanodimensions ranging in size from single molecules, clusters, and particles to organelles and cells. There is a great scope to learn more about the opportunities for and limits on the synthesis of large, precisely structured objects and clusters. Controlling purity and scale-up of products emanating from such precision syntheses is a major challenge that must and will be tackled in the near future. Many of the important properties of nanostructures depend on obtaining precise building blocks; means of creating and analyzing purity and homogeneity in such products are vitally needed. Furthermore, if production of these materials cannot be done at a sufficiently large scale, this will eventually limit utility in some applications.

Although current microfluidic approaches may be effective for manipulating single objects on the scale of 1 μm or more, new techniques need to be developed for single-object manipulation at smaller scale as well as to do nanomanipulation in three dimensions to guide nanoassemblies in bulk as well as on surfaces. Increasing interactions between nanoscale scientists and system designers are in vogue. An important element of this interaction is toward prototyping methods, an intermediate level of implementation between lab-scale demonstration and mass production. The new nanomaterials are likely to impact not only the performance of the most advanced computational and electronic devices but also objects of daily use familiar to every consumer, such as cars, appliances, films, containers, and cosmetics. The ability to assemble and interconnect nanoparticles and molecules at nanometer dimensions has the potential to develop new types of nanoelectronics circuitry and nanomachinery.

Review Questions

Q1. Define nanoscience and nanotechnology.

Q2. What is so unique about materials at nanoscale?

Q3. Justify that living cell is a nanomachine.

Q4. Give few examples of nano biomaterial that have inspired biomimicking.

Q5. What do you understand by mineralization of natural materials? Illustrate with some examples.

Q6. Give name of scientists whom you think have contributed most in development of nanoscience and nanotechnology.

Q7. Name certain nanomaterials found in nature and outline their specific function.

Q8. Name analytic tools that are considered to have accelerated the growth of nanoscience and nanotechnology.

Q9. Classify the nanomaterials on the basis of their dimension. Give some examples.

Q10. What are nanostructure-induced effects? How do they influence the properties of materials at nanoscale?

Q11. Write a short note on the following characteristics of nanomaterial and their impact on properties: surface charge, surface area, and surface porosity.

Q12. Mention the change in optical, electrical, magnetic, and biological properties when material is brought down to nanoscale.

Q13. Discuss the commercial applications of following nanomaterials: (1) nanoclay; (2) CNTs; (3) silver nanoparticles; and (4) gold nanoparticles.

Q14. What is the commercial market value of nano-based products in 2013 and expected by the year 2025?

Q15. What are the parameters deciding the role of nanomaterials in (1) quantum computing; (2) self-cleaning; (3) antimicrobial action; and (4) nanoelectrical mechanical systems?

Q16. Discuss the properties of TiO_2 NPs to make it suitable for multiple applications.

Q17. What are the deciding factors for applications of nanostructured materials in the automobile industry?

Q18. Which are the sectors likely to be benefitted in future from the advancements in nanotechnology?

Q19. What is the health-risk factors associated with the increasing use of nanoparticles?

Q20. In what way nanotechnology will help in remote health monitoring?

References

1. D. Baxter, T. Maynard, “Nanotechnology: recent developments, risks and opportunities”, *Lloyd's Report,* 2007.

2. (a) J. C. Grossman, “A little bit about nanotechnology”, *Outreach Program*, 2007, MIT.(b). J. Zi, X. D. Yu, Y. Z. Li, X. H. Hu, C. Xu, X. J. Wang, X. H. Liu and R. T. Fu, “Coloration Strategies in Peacock Feathers”, *Proc. Natl. Acad. Sci. U. S. A.*, **100** (2003) 12576–12578.(c). A. R. Parker and H. E. Townley, “Biomimetics of Photonic Nanostructures”, *Nat. Nanotechnol.* **2** (2007) 347–353.

3. A. B. Morgan, “Polymer-Clay Nanocomposites: Design and Application of Multi-functional Materials”, *Mater. Matters*, **2** (2007) 20–23.

4. C. Neinhuis and W. Barthlott, “Characterization and Distribution of Water-Repellent, Self-Cleaning Plant Surfaces”, *Ann. Bot.*, **79** (1997) 667–677.

5. R. Blossey, “Self-Cleaning Surfaces Virtual Realities”, *Nat. Mater.*, **2** (2003) 301–306.

6. W. R. Hansen and K. Autumn, “Evidence for Self-Cleaning in Gecko Setae”, *Proc. Natl. Acad. Sci. U. S. A.*, **102** (2005) 385–389.

7. I. Freestone, N. Meeks, M. Sax and C. Higgitt, “The Lycurgus Cup-A Roman Nanotechnology”, *Gold Bull.*, **40** (2007) 270–277.

8. C. Sanchez, J. Beatriz, P. Belleville and M. Popall, “Applications of Hybrid Organic-Inorganic Nanocomposites”, *J. Mater. Chem.*, **15** (2005) 3559–3592.

9. R. P. Feynman, “There's plenty of room at the bottom”, presentation at the *American Physical Society Conference*, Caltech, California, 1959

10. G. Timp, et al., “The Nano-transistor”, www.electrochem.org/dl/ma/200/pdfs/1233.pdf.

11. (a) K. E. Drexler, *Engines of Creation, “The Coming Era of Nanotechnology”*, Anchor Press, Doubleday, New York, 1986;(b) *Nanosystems: Molecular Machinery, Manufacturing and Computation*, John Wiley & Sons, New York, 1992.

12. P. R. Sajanlal, T. S. Sreeprasad, A. K. Samal and T. Pradeep, “Anisotropic Nanomaterials: Structure, Growth, Assembly, and Functions”, *Nano Rev.*, **2** (5583), (2011) 1–62.

13. A. W. Salamon, P. Courtney and I. Shuttler, *Nanotechnology and Engineered Materials*, GDE Nanotech Publications, 2011.

14. M. K. Patra, K. Manzoor, S. R. Vadra and N. Kumar, “Functional nanomaterials for sensors and display applications”, *Encyclopaedia of Nanoscience and Nanotechnology*, Vol. **14**, Ed. H. S. Nalwa, 2011, pp. 385–435.

15. C. Palmberg, “The Transfer and Commercialization of Nanotechnology: A Comparative Analysis of University and Company Researchers”, *J. Technol. Transf.*, **33** (2008) 631–652.

16. M. R. Gwinn and V. Vallyathan, “Nanoparticles: Health Effects – Pros and Cons”, *Environ. Health Perspect.* **114** (2006): 1818–1825.

Chapter 2
Nanomaterials: General Synthetic Approaches

2.1 Introduction

Nanotechnology has experienced a rapid growth in the past decade, largely owing to the rapid advances in nanosynthesis and nanofabrication techniques employed to synthesize nanoscale material and fabricate nanodevices. Different approaches used in the synthesis of nanomaterials and nanodevices can accommodate solid, liquid, and/or gaseous precursor materials. In general, most of these techniques can be classified as bottom-up and top-down approaches (Figure 2.1) and strategies that have elements of both. **The top-down** approaches start with a bulk material and then break it into smaller pieces using mechanical, chemical, or any other form of energy. The **bottom-up** approach, on the other hand, is to synthesize the nanomaterials from atomic or molecular species via chemical reactions or self-assembly, allowing for the precursor particles to grow in size or gradually assembling the atomic or molecular precursors until desired structure is achieved [1].

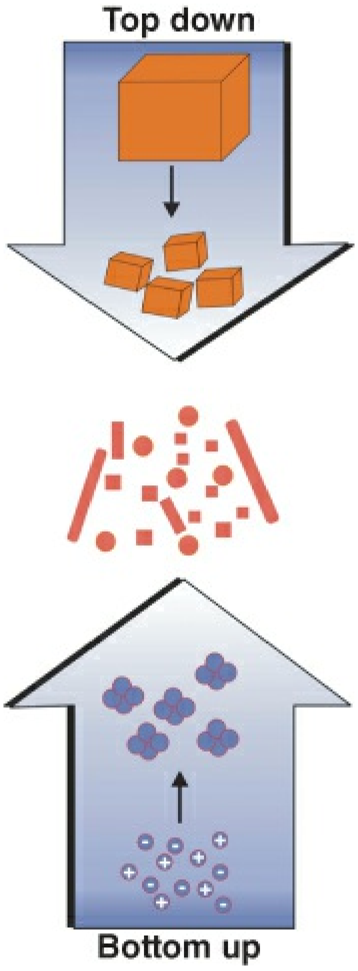

Figure 2.1 “Top-down” and “bottom-up” approaches for the synthesis of nanomaterials.

Both approaches can be performed in the gas or liquid phases, supercritical fluids, the solid state, or under vacuum. The most important aspect of any method lies in its ability to control the particle size, particle shape, size distribution, particle composition, and the degree of particle agglomeration. In both approaches of nanomaterial fabrication, two fundamental requisites are control of fabrication conditions (e.g., energy of electron beam) and control of environmental conditions (e.g., dust, contaminations). Nanotechnologies use highly sophisticated fabrication tools that are mostly operated in a vacuum in clean room laboratories. Liquid- and gas-phase processes are based on the assembly of nanoparticles from single atoms or molecules and, thus, allow good control of particle size, morphology, and sometimes size distribution. Green routes involving plant saps/microbes and biomimetic processes of self-organization and self-assembly have also been suggested for nanosynthesis. Innovations and modifications of fabrication/synthesis procedure are a continuous process that results in innumerable recipes and techniques. Table 2.1 encompasses some of the noted variations of important synthetic procedures although nanomaterial synthesis is maturing with new postulates and procedures that are being introduced on a daily basis.

Table 2.1 Common Techniques for Synthesis of Nanomaterials

Top-Down	Bottom-Up
I. Solid-phase techniques	**III. Vapor-phase techniques**
Milling	**Deposition techniques**
Mechanical	Thermal chemical vapor deposition
Mechanochemical	Plasma-enhanced chemical vapor deposition
Etching	Plasma arching
Wet chemical etching	**Chemical vapor condensation**
Dry etching	Molecular beam epitaxy
Reactive ion etching	Sputtered plasma processing
Plasma etching	**Solution-phase techniques (wet chemical)**
Electro-explosion	Chemical reduction
Sputtering	Precipitation (exchange reaction)
Laser ablation	Sol–gel
Lithography	Solvothermal synthesis
Photolithography	Sonochemical synthesis
Soft lithography	**Self-assembly techniques**
Scanning lithography	Use of templates
Electron-beam lithography	Electrostatic self-assembly
Focused ion-beam lithography	Self-assembled monolayers (SAMs)
Next-generation lithography	Langmuir–Blodgett (LB) formation
Nanoimprint lithography	
Nanosphere lithography	
Colloidal lithography	
Scanning probe lithography	
Dip-pen lithography	

Nanocontact printing Writing atom-by-atom **Aerosol-based techniques:** Electrospraying Flame pyrolysis **II. Liquid-phase techniques** Electrospinning	

2.2 Top-Down Approach

Methods to produce nanoparticles from bulk materials include high-energy ball milling, mechanochemical processing (MCP), electro-explosion, sputtering, and laser ablation. These processes are done in an inert atmosphere or in vacuum. Immediately after processing, nanoparticles are very reactive and can easily form agglomerates. If a reactive gas is present, some additional reactions may occur. This can be used to coat nanoparticles with a material that would prevent further interaction with other particles or the environment. Nanolithography, thin-film deposition, and etching techniques involving progressive removal of material until desired nanomaterial is obtained also belong to top-down category. In the following sections, a more detailed description of the manufacturing techniques from bulk to nano size of the basic nanomaterials is presented.

2.2.1 Mechanical Milling

Mechanical milling is a process that is routinely used in powder metallurgy and mineral processing industries. In this process, mixtures of elemental or prealloyed powders are subjected to grinding under protective atmosphere in an equipment that is capable of high-energy compressive impact forces such as attrition or shaker mills. Figure 2.2a shows a commercial ball milling apparatus and Figure 2.2b reveals different forms of possible impact in mechanical ball milling process. A variety of ball mills have been developed for different purposes including tumbler mills, shaker mills, vibratory mills, and planetary mills. Powders with typical particle diameters of about 50 μm are placed together with a number of hardened steel or tungsten carbide (WC)-coated balls in a sealed container that is shaken or violently agitated. Since the kinetic energy of the balls is a function of their mass and velocity, dense materials are preferable to ceramic balls [2].

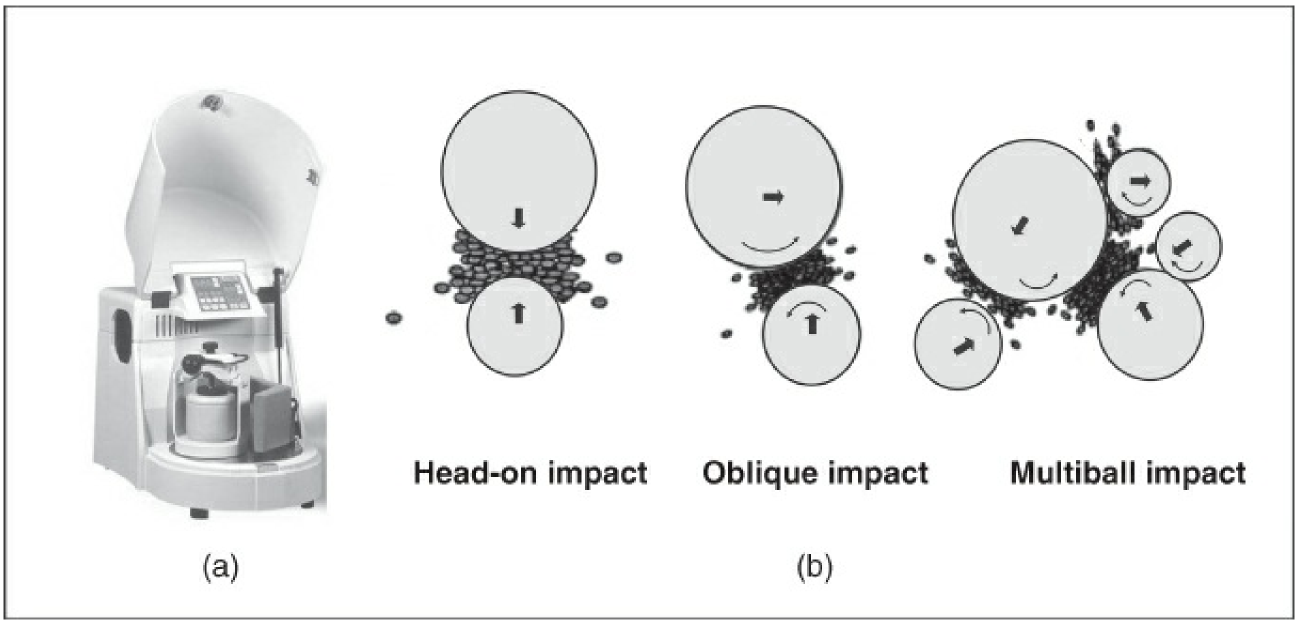

Figure 2.2 (a) A ball-milling apparatus. Courtesy of PANalytical Inc. (b) Schematic representation of different forms of impact in mechanical ball milling.

When a single-phase elemental powder or intermetallic compound powder is milled, the grain size of the powder particles continues to decrease until it reaches a minimum level – in the range of 3–25 nm. For some intermetallic compounds, the powder becomes amorphous beyond this point. For intrinsic brittle powders, such as silicon powder or carbide and oxide powders, the reduction of the grain size is a natural outcome of the transgranular fracturing and cold welding, and the minimum grain size is determined by the grain size that does not allow nucleation and propagation of cracks within grains. The advantage of the mechanical milling process is that the processing temperature is low, so the newly formed grains grow very slowly. Mechanical attrition methods allow the preparation of **alloys and composites**, which cannot be synthesized via conventional casting routes, for example, uniform dispersions of ceramic particles in a metallic matrix and alloys of metals with quite different melting points with the goal of improved strength and corrosion resistance. Mechanical attrition has also gained a lot of attention as a nonequilibrium process resulting in solid-state alloying beyond the equilibrium solubility limit and the formation of amorphous or nanostructured materials for a broad range of alloys, intermetallics, ceramics, and composites. High-energy mechanical milling is a very effective process for synthesizing **metal–ceramic composite** powders as it allows incorporation of the metal and the ceramic phases into each powder particle. A flow chart showing optimized conditions for the production of iron nanoparticles by high-energy ball milling is given in Box 2.1.

Box 2.1 Steps involved in the synthesis of iron nanoparticles by high-energy ball milling.

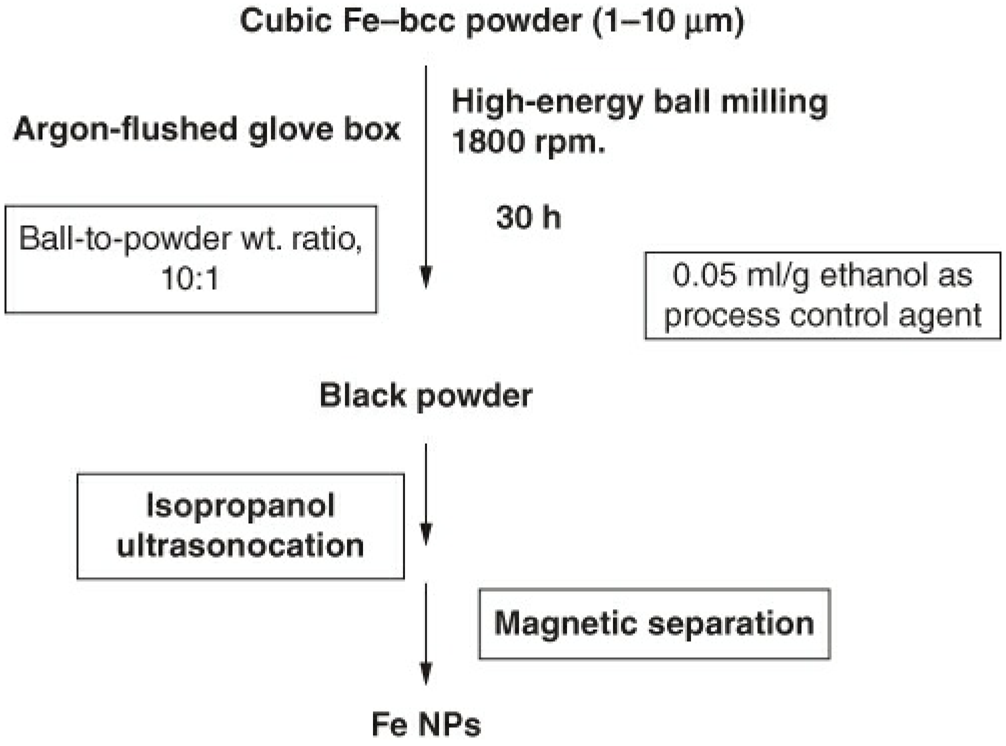
Cubic Fe–bcc powder (1–10 μm)
Argon-flushed glove box
High-energy ball milling
1800 rpm.
30 h
Ball-to-powder wt. ratio, 10:1
0.05 ml/g ethanol as process control agent
Black powder
Isopropanol ultrasonocation
Magnetic separation
Fe NPs

2.2.2 Mechanochemical Processing (MCP)

MCP is a novel, cost-effective method of manufacturing a wide range of nanopowders, wherein a conventional ball mill is used as a low-temperature chemical reactor and not just a grinding tool. The ball milling increases the reaction kinetics in the reacting powder mixture as a result of the intimate mixing and refinement of the grain structure to the nanometer scale, allowing the reaction to occur during the actual milling. Chemical reactions, which usually require high temperatures, are thus activated during milling. This is the key element of the MCP technology. To produce nanoparticles of a specific material, a suitable precursor is chosen. Often a particular product can be produced from a range of precursors, allowing the process to be optimized to use industry standard precursors to reduce cost. Oxides, carbonates, sulfates, chlorides, fluorides, hydroxides, or other compounds are all candidates for use as the precursor material. The chosen precursor is then milled with an appropriate reactant. The resulting product is a single phase nanometer-sized grain in a by-product matrix. After milling, a low-temperature heat treatment is often used to ensure the reaction is complete before the by-product is removed, leaving the pure, nonagglomerated nanopowder, which consists of dispersed nanosized particles of 1–1000 nm in diameter. One simple example is high-energy milling of a mixture of $FeCl_3$ powder and Na pieces induces a reaction between $FeCl_3$ and Na, forming Fe nanoparticles mixed with NaCl. The NaCl can be easily leached out from the powder by using water, and Fe nanopowder is produced.

2.2.3 Electro-Explosion

The process of electro-explosion where an electric power impulse is applied to the wire under argon pressure results in metallic powders in nanoregime. Electro-explosion involves providing a very high current over a very short time through thin metallic wires, in either inert or reactive gas, such that extraordinary temperatures are achieved. The wire is converted into a plasma state, but the plasma is contained and in fact compressed by the very high voltage produced during the pulse. The very high currents heat the wire to 20,000–30,000 °C, where the resistivity of the metal becomes virtually infinite thereby terminating the flow of current [3]. At this point, the electromagnetic field disappears and superheated metal plasma expends with supersonic velocity, creating a shock wave in the ionized gas surrounding the wire. The extremely fast cooling (10^6–10^8 deg/s) rate provides ideal conditions for stabilization of different metastable structures. Few typical examples include the following: a mixture of electro-exploded aluminum and amorphous boron reacts to form aluminum diboride nanoparticles by igniting the pallet with an electric wire; a pallet electro-exploded copper and zinc react at just 200^{o} C to form brass nanoparticles.

2.2.4 Sputtering

Sputtering is a conventional **thin-film deposition** technique, useful for high melting point material also known as sputter deposition. It involves eroding material from a “target” source onto a “substrate,” for example, a silicon wafer. Sputtered atoms ejected into the gas phase are not in their thermodynamic equilibrium state and tend to deposit on all surfaces in the vacuum chamber. A substrate (such as a wafer) placed in the chamber will be coated with a thin film. Sputtering usually uses an argon plasma. The impact of an energetic atom or ion on a surface produces sputtering from the surface as a result of the momentum transfer from the incoming particle. Unlike many other vapor-phase techniques, there is no melting of the materials. Sputtering is performed at low pressure on a cold substrate. The process involves three steps: (1) glow discharge to produce energetic particles, (2) momentum transfer from an indirect energetic projectile to a solid or molten target, and (3) condensation of sputtered species. Sputtering observed to occur below the threshold energy of physical sputtering is often called chemical sputtering. The mechanisms behind such sputtering are not always well understood and may be hard to distinguish from **chemical etching**. At elevated temperatures, chemical sputtering of carbon can be understood to be due to the weakening bonds of the incoming ions in the sample, which then desorbs by thermal activation. The hydrogen-induced sputtering of carbon-based materials observed at low temperatures has been explained by H ions entering between C–C bonds and thus breaking them. A very well-studied example of chemical etching is fluorine etching of silicon.

2.2.5 Etching

Etching refers to removal of material and is one of the common transfer techniques used in microfabrication; however, it has also been used to synthesize nanoparticles. The etching can be achieved through **chemicals**, **plasma**, or by **electric arc-discharge method**. In chemical etching, chemical reacts with substrate material to produce etch profile. Processing gas is selected for chemical etching of substrate materials. Plasma etching also known as reactive ion etching is a dry etching where plasma is used to ionize gas. A negative bias is placed on the substrate to allow for physical etching from positively charged gas species. Unmasked electrochemical or photoelectrochemical etching can also be used to produce regular arrays of shapes within a nanometer range. For example, layers of porous silicon are formed by electrochemically etching the crystalline silicon wafers, employing a mixture of hydrofluoric acid and ethanol as an electrolyte. A combination of lithographically defined patterning with etching is a basis of microelectronics. Regular arrays of the nanometer-sized structures can be produced on a planner substrate by etching.

2.2.5.1 Electric Arc-Discharge Method

dc arc discharge in water is a cheap, effective, rapid, and environmentally friendly process for the production of gold nanoparticles through wet etching. Crucial factors to be optimized and controlled in this method for the production of nanoparticles are as follows: applied working voltage, selected electric current, pulse duration, electrode gap, and temperature of the deionized water. The electric arc-discharge method has been shown to have potential for mass production of nanosized gold nanoparticles [4]. A typical setup and experimental conditions for the production of gold nanoparticles through wet etching employing dc arc-discharge method are given in Figure 2.3a. Under certain specific conditions: electrodes of gold wires of 1 mm diameter, pulse voltage of 70–100 V for 2–3 ms and then maintains a pulse of 20–40 V for around 10 μs, and at that instant an etching current of the order of 4 A can be achieved.

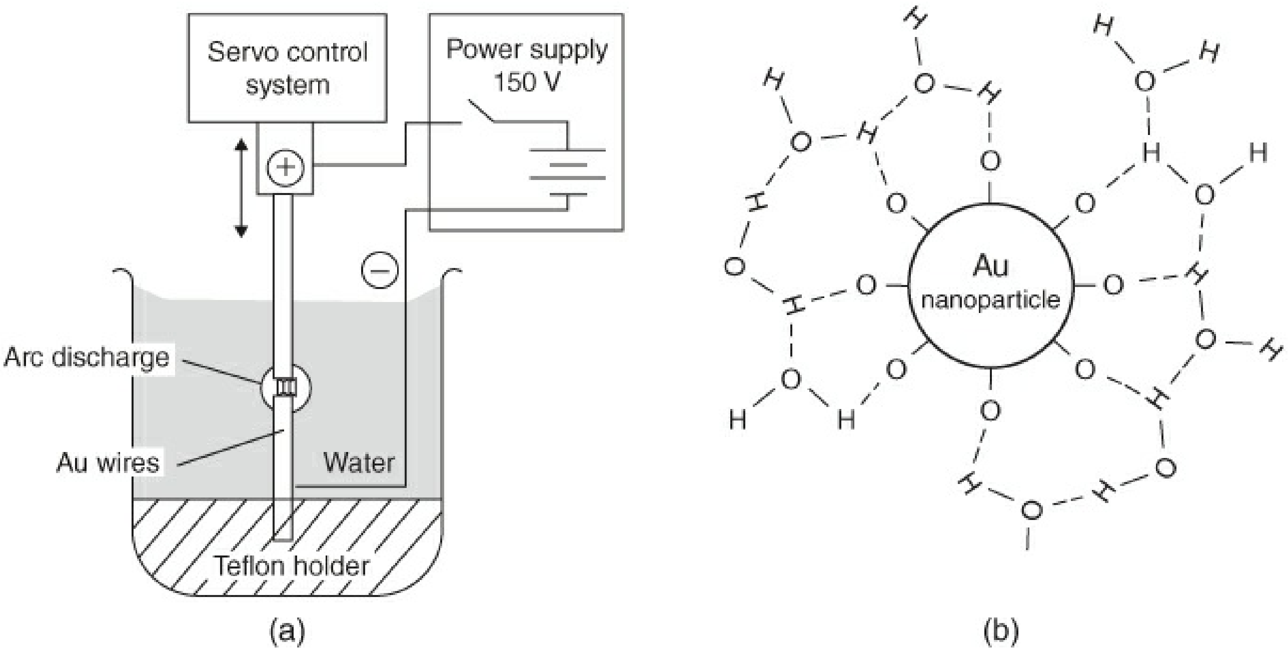

Figure 2.3 (a) Set up for etching by electric arc discharge and (b) resultant water stabilization of Au NPs in solution.

Tien et al. [4] © 2007 IPEM. With permission of Elsevier.

The gold nanoparticles produced by this method are negatively charged as confirmed by zeta potential values. The nanoparticles thus produced could be stabilized by just water molecules. The underlying mechanism of stabilization is that the electrons are injected into the gold nanoparticles by the cathode during arc discharge and negatively charged surfaces of gold nanoparticles are saturated by atomic oxygen, which may result in hydrogen bonding with water molecules in aqueous environment. Without any stabilizers and surfactants, negatively charged gold nanoparticles (Figure 2.3b) surrounded by water molecules can create a stable suspension, such a gold colloid can be heated up to 100 °C without destruction of its structure.

2.2.6 Laser Ablation

Laser ablation is the process of removing material from a solid (or occasionally liquid) surface by irradiating it with a laser beam. At low laser flux, the material is heated by the absorbed laser energy and evaporates or sublimates. At high laser flux, the material is typically converted to plasma. Usually, laser ablation refers to removing material with a pulsed laser, but it is possible to ablate material with a continuous wave laser beam if the laser intensity is high enough. The depth over which the laser energy is absorbed and, thus, the amount of material removed by a single laser pulse depend on the material's optical properties, laser wavelength, and pulse width. The total mass ablated from the target per laser pulse is usually referred to as ablation rate. Laser pulses can vary over a very wide range of duration (milliseconds to femtoseconds) and fluxes and can be precisely controlled. This makes laser ablation a very valuable process in the fabrication of nanostructures.

A broad range of nanoparticulate materials can be obtained by laser ablation [5]. A focused laser beam irradiates on the target (precursor) material and evaporates the target under high vacuum conditions. Atoms and clusters are subsequently being ejected from the target and deposited on to a substrate placed opposite to the target. Laser ablation has been extensively used for the preparation of nanoparticles and particulate films. In a typical example, Figure 2.4 shows the setup for laser ablation technique and conditions for the synthesis of Fe_2O_3 nanoparticles from Fe wire.

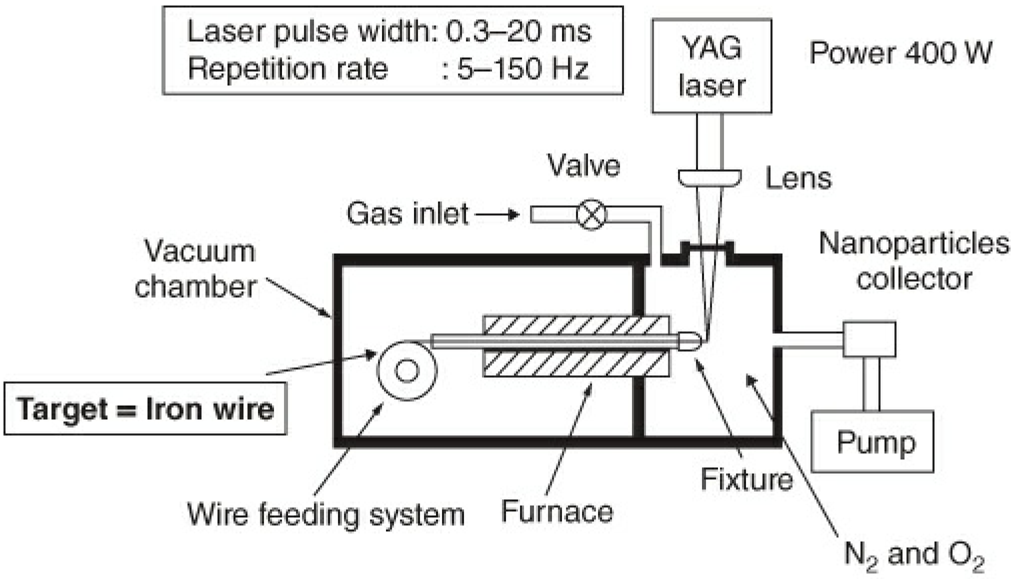

[Figure 2.4](#) Setup for laser ablation technique for the synthesis of Fe_2O_3 nanoparticles from iron wire.

Wang et al. [5] © 2005. With permission of Elsevier.

The distinctive advantage of laser ablation over other deposition techniques is the capability of producing multicomponent materials with a well-controlled stoichiometry. The laser spark atomizer can be used to produce highly mesoporous thick films, and the porosity can be modified by the carrier gas flow rate. ZrO_2 and SnO_2 nanoparticulate thick films were also synthesized successfully using this process with quite identical microstructure. Synthesis of other materials such as lithium, silicon, and carbon has also been carried out by this technique. Laser ablation technique can be complemented by other techniques such as ultrasonication and solution chemistry.

2.2.7 Lithography

Numerous top-down fabrication methods used in nanotechnologies are driven from the fabrication methods used in the semiconductor industry to fabricate integrated circuits (ICs). These methods are collectively called **lithography** and use a light or electron beam to selectively remove microscale structures from a precursor material called resist. Lithographic patterning methods capable of structuring material on a fine scale are referred as microlithography and nanolithography. Typically, features smaller than 10 μm are considered microlithographic, and features smaller than 100 nm are considered nanolithographic. In recent years, there has been a tremendous push to reduce the size of electronic devices and integrate more functions into them, which has been possible because of the advance in lithographic fabrication methods [6–9]. It is possible to obtain single features below 100 nm (the transistors in the latest generation processors are about 45 nm). Conventional lithographic technique includes a series of fabrication steps that share the principle of transferring an image from a **mask** to a receiving **substrate**. A typical lithographic process consists of three successive steps:

i. coating a substrate (Si wafer or glass) with a sensitive polymer layer (the resists),

ii. exposing the resist to light, electrons, or ion beams,

iii. developing the resist image with a suitable chemical (developer), which reveals a positive or a negative image on the substrate depending on the type of resist used (i.e., positive tone or negative tone resist).

However, lithographic techniques can be subdivided into two main groups:

1. Photolithography: Photolithography uses UV, deep UV, extreme UV, or X-ray light source to expose a layer of radiation-sensitive polymer (photoresist) through a mask. The mask is a nearly optically flat glass (or quartz) plate that contains the desired pattern, that is, opaque areas (the pattern, made of an absorber metal) on a UV-transparent background. The image on the mask can be either replicated as it is, placing the mask in physical contact with the resist (contact mode photolithography), or reduced, usually by a factor of 5 or 10, and projected to the resist layer through an optical system (projection-mode photolithography). The resolution of contact-mode lithography is typically 0.5–0.8 μm when UV light (360–460 nm) is used. Higher resolutions cannot be achieved because of the inability to reduce the gap between the mask and the flat substrate below ~1 μm, even when elaborate vacuum systems are used to hold the two parts together. Photolithography is commonly used for fabricating semiconductor microchips and devices of microelectromechanical systems (MEMS).

2. Scanning Lithography: In these methods, software mask is used. Here, a scanning beam irradiates the surface of the resist sequentially, point by point, through a computer-controlled program where the mask pattern is defined. These methods are collectively called scanning lithography. The technique of commercial importance in this category is electron-beam (e-beam) lithography, which is capable of much greater patterning resolution, sometimes as small as a few nanometers. The commercial importance of e-beam lithography is primarily for its use in the manufacturing of photomasks. The main difference between mask and scanning lithography is speed, whereas mask lithography is a parallel, fast technique and scanning lithography is a slow, serial technique. Another important difference is resolution, which, in general terms, is higher for scanning methods. More energetic radiation sources are used to achieve higher resolution. In addition to these well-established conventional lithographic techniques, a large number of promising technologies are being developed, including soft lithography, nanoimprint lithography (NIL), magnetolithography, scanning probe lithography (SPL), and dip-pen lithography (DPN). Some of these new techniques have been used successfully for small-scale commercial and important research applications in the fabrication of micro-/nanoelectronic devices.

2.2.7.1 Soft Lithography

Soft lithography is a name for the number of techniques that fabricate and use a soft mold prepared by casting a liquid polymer precursor against a right master. These methods have been developed specifically for making large-scale micro- and nanostructures with an equipment that is easier to operate as compared to those used in conventional lithography. The master is usually fabricated via a conventional lithographic method. Various polymers (e.g., polyurethanes, epoxides, and polyimides) are used for molding, most commonly is poly(dimethyl siloxane) (PDMS). A PDMS mold is fabricated by pouring its liquid precursor over a lithographically made master (e.g., a photoresist or silicon master), cured to induce cross-linking, and then peeled off from it. The stamp can then be used for printing a desired material to a suitable surface. Figure 2.5 shows the overall principle of soft lithography.

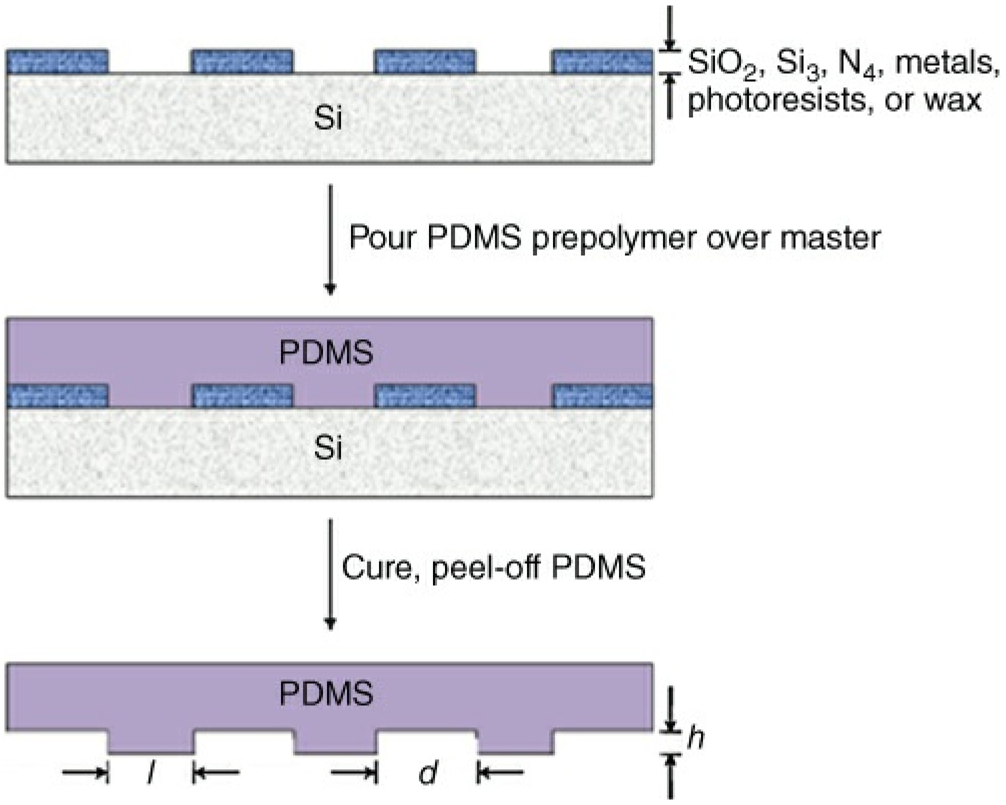
SiO2, Si3, N4, metals, photoresists, or wax
Si
Pour PDMS prepolymer over master
PDMS
Si
Cure, peel-off PDMS
PDMS
h
l
d

Figure 2.5 Soft lithography with polydimethyl siloxane (PDMS) molds.

From Ref. [6].

The resolution of soft lithography is mainly determined by van der Waals interactions, wetting, and kinetic factors such as filling the capillaries on the surface of the master, but not by optical diffraction. This is an important advantage over conventional lithographic techniques. Soft lithography provides access to three-dimensional (3D) and curved structures, tolerates a wide variety of materials, generates well-defined and controllable surface chemistries, and is generally compatible with biological applications. It is also low in cost, experimentally convenient, and has emerged as a technology useful for a number of applications that include cell biology, microfluidics, lab-on-a-chip, microelectromechanical systems, and flexible electronics/photonics. The commonly used soft lithographic techniques are (1) contact printing of alkanethiols and proteins on gold-coated and glass substrates; (2) replica molding for the fabrication of microfluidic devices in PDMS and of nanostructures in polyurethane or epoxy; and (3) solvent-assisted micromolding of nanostructures in poly(methyl methacrylate) (PMMA).

Photolithography versus soft lithography

Photolithography continues as the dominant technology in the fabrication of semiconductor devices and systems that have stringent requirements on the alignment, continuity, isolation, and uniformity in the final patterns. There are, however, many existing and emerging applications for soft lithography that take advantage of (or require) the characteristics of these techniques. For example, soft lithography offers access to a broader range of materials, as well as experimental simplicity and flexibility in forming certain types of test patterns. Procedures involving relatively large features (such as those used in microfluidic devices) can be conducted in an ordinary chemical laboratory and are thus particularly useful to those who do not have routine access to clean room facilities or for applications where the fabrication cost is a serious concern. At the current stage of development, soft lithography still relies on the use of photolithography to generate the master. Once the master is available, most of the fabrication tasks can be continued outside a clean room with the use of only a printing or molding procedure.

2.2.7.2 Nanoimprint Lithography (NIL)

NIL is a revolutionary approach to low-cost and high-throughput nanolithography. NIL in its original version was proposed by Stephen Chou in 1995 as an alternative technique for the embossing of high-resolution patterns in thermoplastic materials. The concept of NIL is to use a hard master with 3D nanostructure to mold another material, which assumes its reverse 3D structure. Since the master has a fine nanostructure, to be successful the process must be done under pressure: a coating must first be placed on the master to avoid catastrophic adhesion to the mold, and then the mold must be heated (above its T_g temperature) in order to be soft enough to completely enter the fine master nanostructure and be effectively replicated. The method is the equivalent of embossing at the nanoscale. NIL is an imprinting process using a mold to create a thickness in contrast to a resist and pattern transfer using anisotropic etching to remove residue resist in compressed areas. The process of NIL is shown in Figure 2.6. NIL patterns a resist by physically deforming the resist shape with a mold (i.e., embossing), rather than modifying the resist chemical structures with radiation as in the case of conventional lithography. This fundamental difference in principles frees NIL from many problems suffered in conventional lithography, such as diffraction limit, scattering, and chemistry. As a result, NIL can achieve ~10 nm structures over large areas with low cost and high throughput, a feat currently unachievable using existing lithography. NIL is believed to impact not only future IC development but also many other disciplines, such as biology, chemistry, medicine, and materials. The main advantages of NIL are as follows:

a. *High-resolution fast process:* Due to the stamping nature of the process, NIL is inherently parallel process and therefore fast. It may take hours, days, or weeks to fabricate the master stamp, but it takes only seconds or minutes to replicate the patterns.

b. *Direct 2.5D patterning:* Different height levels or curved features in the stamp can be replicated.

c. *Direct structuring of functional materials:* After the imprinting step, it is not mandatory to follow the etching step to transfer the pattern into the substrate; in many cases, the structured polymer is the final device.

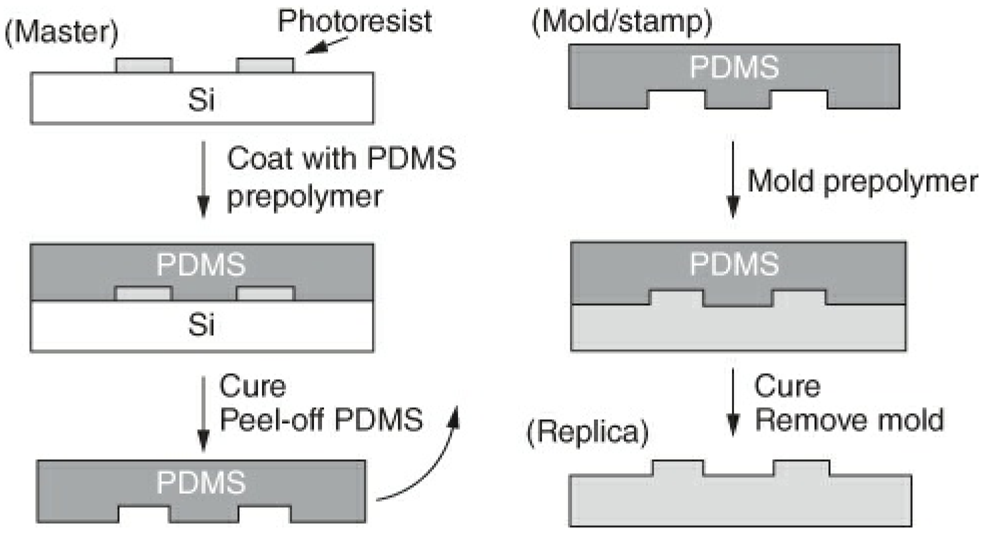

Figure 2.6 Schematic of nanoimprint lithography process.

Hot embossing or **thermal NIL** (using a thermoplastic polymer), **UV-NIL** (utilizing a UV-curing polymer), and **microcontact printing** (μCP) or **nanocontact printing** (nCP), where an ink is transferred from the stamp to the substrate, are three basic variants of the same nanoimprint technique. Each of these three processes appears in a different form in the literature, that is, roller NIL, reversal NIL, and combined photo- and nanoimprint lithograph. The imprint polymer can be droplet dispensed or spin coated. Typically, hot embossing processes require higher pressures than UV-NIL processes with μCP processes using the lowest pressure. μCP is useful for pattering features with the lateral dimension of 500 nm or more. One of the major challenges for μCP has been to achieve the capability to print with high resolution, that is, with the lateral dimension of less than 100 nm. This has been recently achieved by improving the stability of the PDMS, which being soft and highly compressible has a tendency to deform and collapse. One way to improve the stability of the patterns is to affix a backplane to the stamp or to change the chemical formulation of the stamp itself, in order to obtain a harder polymer. With these modifications, it is now possible to print features as small as 50 nm [6, 7]. This printing method, which uses harder stamps, is called nCP.

2.2.7.3 Nanosphere Lithography (NSL)

In nanosphere lithography, an ensemble of nanospheres ordered on a surface are used as a mask. The nanospheres are dispersed in a liquid (i.e., a colloid) and a droplet is placed on the surface and left to dry. Depending on the surface properties (e.g., charge) and media used in the colloid (e.g., presence of electrolytes), the nanosphere will self-assemble in an ordered pattern. In some conditions, a colloidal crystal is obtained and each nanoparticle is surrounded by six other nanospheres. This regular arrangement (which is a 2D colloidal crystal) can be used to create ordered structures on surfaces. In the regular arrangement of nanospheres, there will be an empty space between them, which is regularly repeated in the entire surface. In the simplest method, this space is employed to create relatively flat nanopatterns on the surface. The nanosphere pattern is used as a mask, and a material (e.g., gold, silver) is sputtered on top of it. Once the nanospheres are removed, a regular pattern is left of dot, each shaped as a triangle but with concave sides. Triangular gold nanoprism could be obtained by evaporating gold over the latex nanosphere mask (Figure 2.7a). The gold pattern can also act as growth sites, for example, for the growth of carbon nanotubes or ZnO. Nanosphere lithography has now evolved into a method that allows the fabrication of very complex arrays of nanostructures, including 3D features as shown in Figure 2.7b.

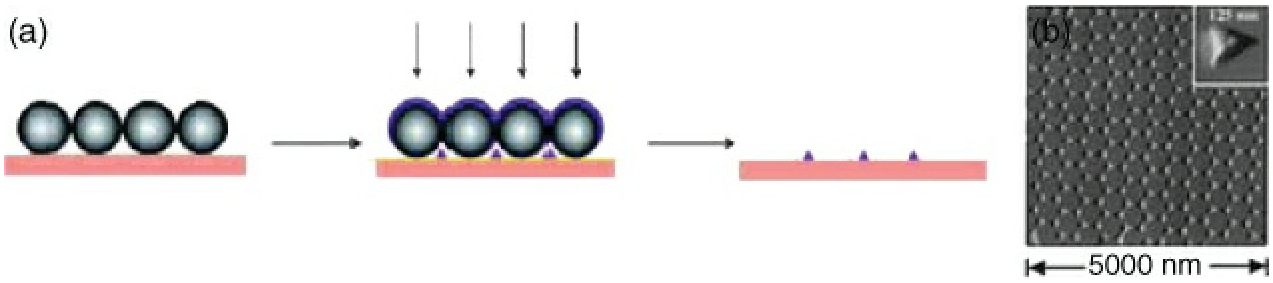

Figure 2.7 Nanosphere lithography. (a) Schematic illustration of the NSL process and (b) SEM image of triangular gold nanoprism as a product of nanosphere lithography.

Liu et al. [8] © 2013. With permission of RSC.

2.2.7.4 Colloidal Lithography

Colloid lithography shares the same principle of nanosphere lithography of using a colloid as a mask for the fabrication of nanostructures on surfaces. In this method, electrostatic forces are employed to obtain short-range ordered arrays of nanospheres on the surface. The electrolyte concentration affects the size of colloidal particles in the formation of the ordered array. The array can then be used to create a number of different nanostructures through various processes such as etching and liftoff. It is interesting to note the different types of nanostructures that can be formed: holes, cones, rings, and sandwiches made of different materials. If the nanostructures are made of metals, then they present a localized surface plasmonic resonance (LSPR) effect that can be used for sensing. These materials are, therefore, under study for various sensing applications, for example, in medical diagnostic devices.

2.2.7.5 Scanning Lithography: e-Beam and Focused Ion-Beam Lithography

Energetic particles such as electrons and ions can be used to pattern appropriate resist films leading to features with nanometer resolution. When using electrons the technology is called **electron-beam (e-beam) lithography**, whereas when using ions the technology is called **focused ion-beam lithography**. In a typical e-beam lithography process, a tightly focused beam of electrons scans across the surface an electron-sensitive resist film such as PMMA. The main advantage of e-beam lithography over photolithography is its high-resolution patterns, with features as small as 50 nm can be routinely generated. The resolution of this technology is mainly determined by the scattering of the electrons in the resist film and the substrate. When using particles with a mass higher than electrons, however, this effect is largely reduced. Focused ion-beam lithography works on the same principle as of e-beam lithography, but ions such as H^+, He^{++}, Li^+, and Be^{++} are used. Both techniques provide a resolution much higher than photolithography but share a main disadvantage of being very slow; therefore, their use is mostly limited to producing photomasks in optical lithography. Finally, a recently established technology uses nanometer scanning probes for patterning resist films and is therefore referred to as SPL. This technology has been extended to the deposition of nanoquantity of material as DPN and has been discussed in the subsequent sections.

2.2.7.6 Scanning Probe Lithography

Scanning probe microscopy (i.e., STM, AFM) uses <50 nm tips to image surfaces with atomic resolution (refer Chapter 6). This ability has opened up opportunities for their use in generating nanostructures and nanodevices. In this form, they are referred to as SPL, which uses the tip of an atomic force microscope (AFM) to selectively remove certain areas on a surface and DPN, which similarly uses the AFM tip to deposit material on a surface with nanometer resolution. Both are direct writing techniques, and their main advantages are high resolution and the ability to generate patterns with arbitrary geometries. Similar to e-beam and ion-beam lithography, SPL and DPN are serial techniques whose main limitation is speed.

Dip-Pen Nanolithography: Scanning probe microscopy (i.e., STM, AFM) uses <50 nm tips to image surfaces with atomic resolution (refer Chapter 3). This ability has opened up opportunities for their use in generating nanostructures and nanodevices. One of the more recent techniques for nCP consists of the direct writing of a molecular ink onto an appropriate substrate via the ultrafine tip of an AFM. Figure 2.8 illustrates the process of DPN for writing nanofeatures of CdS on mica and SiO_2 substrate. The AFM tip is coated with a liquid containing the molecules to be deposited. The use of such a “nanofountain pen” is known as dip-pen nanolithography (DPN), which was first demonstrated by Mirkin and coworkers in the late 1990s. Though the earliest examples of DPN featured alkylthiols as the ink onto Au surfaces, there are now an increasingly large number of other ink/substrate combinations that have been reported for DPN (Table 2.2). Top-down lithographic methods will, of course, continue to be the best for the important specialized task of making planar structures with arbitrary patterns (e.g., circuits). Top-down assembly methods are currently utilized for the interconnection of electronic circuits. A variety of approaches have been demonstrated for the fabrication of nanostructures on solid supports for such plasmonic applications. These include various lithographic methods such as e-beam lithography, nanosphere lithography, and DPN.

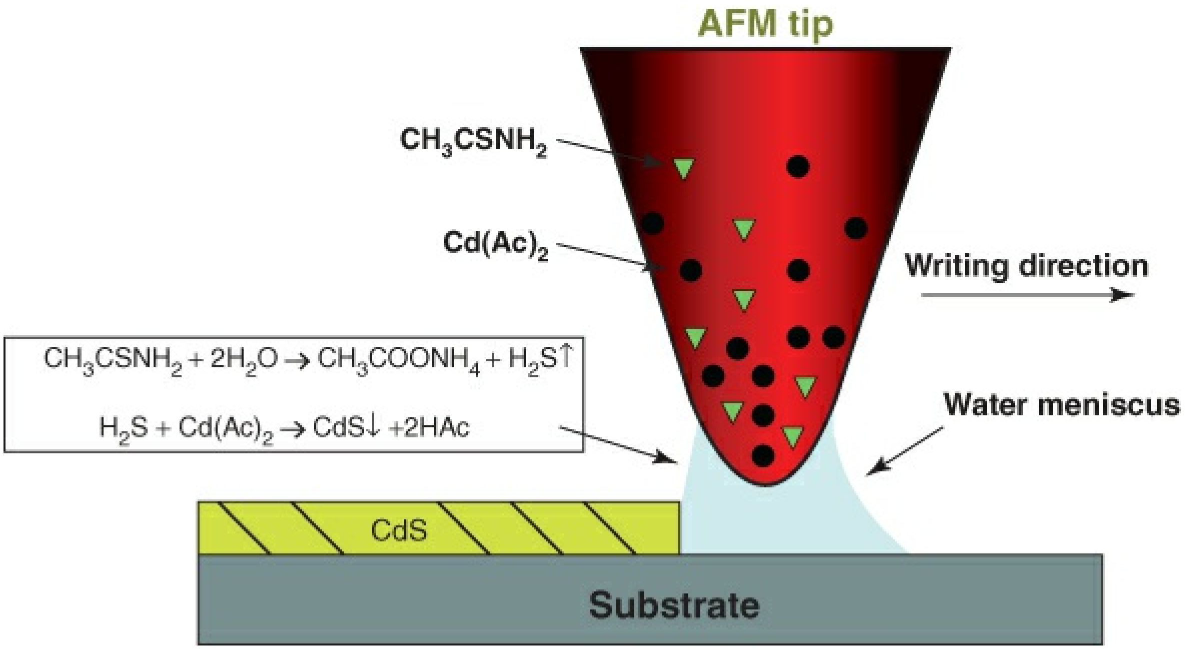
AFM tip
CH_3CSNH_2
$Cd(Ac)_2$
Writing direction
$CH_3CSNH_2 + 2H_2O \rightarrow CH_3COONH_4 + H_2S\uparrow$
$H_2S + Cd(Ac)_2 \rightarrow CdS\downarrow + 2HAc$
Water meniscus
CdS
Substrate

Figure 2.8 Illustration of dip-pen nanolithography.

Ding et al. [9] © 2005. With permission of ACS.

Table 2.2 Substrate–Ink Combinations for DPN

Substrate	Suitable Molecular Ink
Gold (Au)	Alkylthiols, proteins, DNA
Silica (SiO_2)	Silazanes, proteins, conjugated polymers, DNA, thioacetamides, cadmium acetate, colloidal particles
Gallium arsenide (GaAs)	Silazanes
Mica	Thioacetamide, cadmium acetate
Silicon (Si)	Alkynes, alkoxysilanes, metal salts
Germanium (Ge)	Metal salts

2.2.8 Aerosol-Based Techniques

Aerosol-based process is a common method for the industrial production of nanoparticles. Aerosols can be defined as solid or liquid particles in a gas phase, where the particles range from molecules up to 100 μm in size. Aerosol-based techniques involve atomization of a liquid precursor into finely divided submicrometer liquid droplets distributed in the gas medium. Aerosols were used in industrial manufacturing long before the basic science and engineering of the aerosols were understood. For example, carbon black particles used in pigments and reinforced car tires are produced by hydrocarbon combustion; titania pigment for the use in paints and plastic is prepared by the oxidation of titanium tetrachloride; fumed silica and titania are formed from the respective tetrachloride by flame pyrolysis; optical fibers are manufactured by a similar process. Aerosols can be generated by different techniques [10–13] of which the most convenient are flame-assisted ultrasonic methods and electrospray, which are described briefly in the following.

2.2.8.1 Ultrasonic Spray Pyrolysis

Ultrasonic spray pyrolysis may be employed to generate an aerosol from a dilute aqueous metal salt solution, resulting in the production of particles with a narrow size distribution. Figure 2.9 shows a setup for an ultrasonic spray pyrolysis, a technique that is used to synthesize fine powders by aerosol decomposition. Silver nanoparticles are produced by flash pyrolysis of a liquid feed solution of silver nitrate nebulized by an ultrasonic atomizer. Aqueous silver nitrate solution is gravity-fed from a burette to an atomizer, and the atomized spray is discharged into the reaction chamber that is maintained above 650 °C with a tube furnace. Silver nanoparticles are deposited on the substrate placed in the flow path, while the water vapor and off-gases are discharged through an exhaust line. A vacuum pump is used to put the reactor under slight vacuum to discharge the water vapor and exhaust gases to vent.

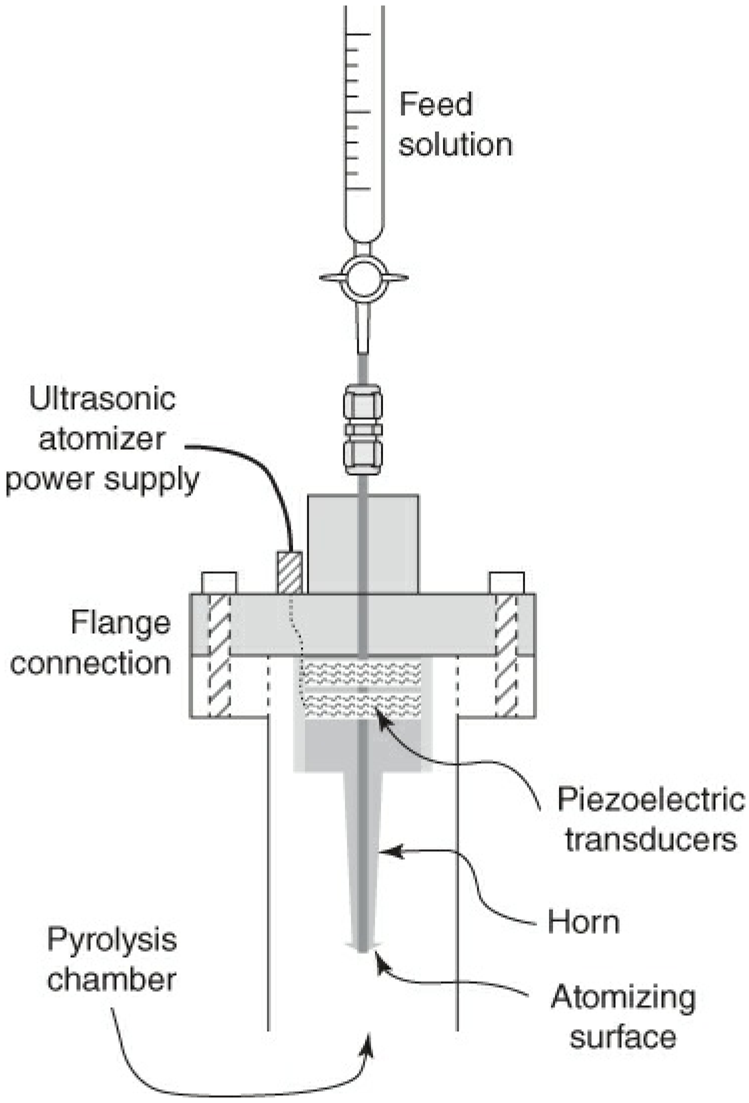

Figure 2.9 Schematic of ultrasonic spray pyrolysis setup.

Pingali et al. [10] © 2005. With permission of AAAR.

2.2.8.2 Electrospray Deposition (ESD) Method

Electrospraying (electrohydrodynamic spraying) is a method of liquid atomization by electrical forces. Spraying solution or suspensions allows the production of fine particles, down to nanometer size. This technique has successfully demonstrated the ability to disperse masses of liquids into very fine mists and has revolutionized the nanotechnology fields in fabricating biomacromolecules without losing their functionalities, metal oxides, polymeric nanoparticles, and so on. While electrospray is a very complicated physical process, which is not fully understood, generally what happens is as follows.

When a sample liquid stored in a thin capillary is supplied with thousands to tens of thousands of voltage relative to counterelectrode, a strong electric field is generated at the tip of the capillary because of the effect of electric field concentration. As the liquid begins to exit from the capillary, it forms a conical shape with the electrically charged ions gathered on its surface. (This is called Taylor cone.) Subsequently, when the electrostatic force becomes stronger than surface tension, the liquid erupts from the tip of the capillary to form a fine jet. Since the jet is highly charged, the liquid immediately turns into fine droplets to generate spray, with each droplet spilt from the next by an electrostatic force. (This is called the Coulomb explosion.) The droplets formed by means of electrospray are tiny. Therefore, the solvent evaporates and dries in a very short period of time, and as a consequence, it forms very fine nanoparticles and fibers. These charged tiny particles are attracted to the counterelectrode by electrostatic force and are deposited in various patterns using electrostatic force. The electrospray deposition (ESD) method facilitates nanostructures in a larger area. Spray substances include solution and dispersion liquid, such as organic/inorganic compounds, biomacromolecules and/or synthetic polymers, and deposit various nanostructures.

The basic setup for electrospraying is shown schematically in Figure 2.10a. Three distinct spray modes are single spray cone mode, multiple spray cone mode, and dripping mode (Figure 2.10b–d), which can be achieved by adjusting the potential difference between two electrodes in the electrospray process. These modes are characterized by the shape of the surface from which the liquid jet originates. These modes have significant effects on droplet size distribution. In the single spray cone mode, only one steady spray cone is observed with the cone axis slightly rotating around the spray nozzle axis; in the multiple spray cone mode, several unstable thin cones are observed revolving around the rim of the spray nozzle; no spray cone, however, is observed in the dripping mode with liquid dripping down at a speed higher than that of natural dripping. It has been observed that under constant processing variables of flow rate, spray solution concentration, and system geometry, the applied voltage differences between two electrodes play key roles in determining the spraying pattern. It has been shown that single spray cone mode is the most desired operating regime for particle fabrication owing to the fact that the single spray cone mode is able to fabricate particles with the most narrow size distribution.

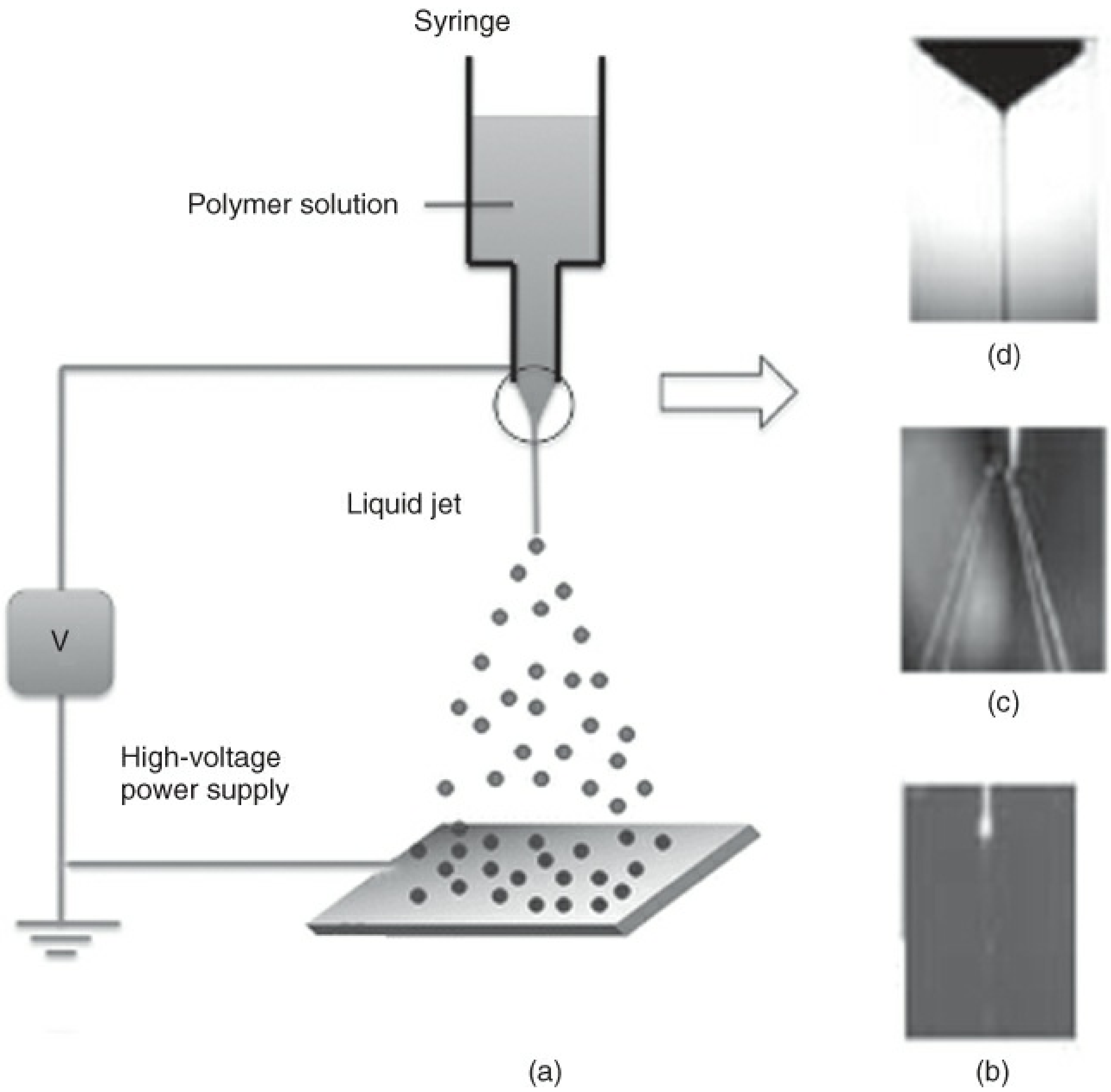

Figure 2.10 (a) Schematic of a basic setup for electrospray. Seul-Gi Kim et al. [11] © 2014, With permission of Japan Society of Applied Physics; (b)–(d) three distinct electrospray.

Deitzel et al. [12]. © 2001. With permission of Elsevier.

ESD technique is profitably used in the formation of different kinds of nanostructured materials, such as nanofibers (formation of fibers using ESD process is now known as electrospinning and is discussed in more details in the next section), thin films, nanocoatings, and nano-/micropatterning. Furthermore, ESD methods can be used to create free-standing protein films. A simple one-step procedure for the production of polyacrylonitrile (PAN) nanoparticles by electrospraying is given in Box 2.2.

Box 2.2 Preparation of polyacrylonitrile (PAN) nanoparticles by electrospraying

About 1–3% (w/w) solution of polyacrylonitrile was prepared in dimethyl formamide (DMF) and kept for 12 h at room temperature. Polymer solution of 1 ml is placed into a syringe connected to a high-voltage source and syringe pump. The horizontal syringe needle and the vertical aluminum foil collector are, respectively, connected to positive and negative electrodes of high-voltage source (220 V, AC input up to 20 kV DC output). The electrical field is formed between the collector and the tip of the syringe tube, the electrospray of the solution resulted in the formation of nanoparticles of PAN.

2.2.9 Electrospinning

It is an emerging technology for the manufacture of nanopolymer fibers based on the principle of spinning the dilute polymer solutions in a high-voltage electric field. It is a process by which a suspended drop of polymer is charged with thousands of volts. At a characteristic voltage, the droplet forms a Taylor cone and a fine jet of polymer releases from the surface in response to the tensile forces generated by the interaction of an applied electric field with the electrical charge carried by the jet. This produces a bundle of polymer fibers. The jet can be directed to a grounded surface and collected as a continuous web of fibers ranging in size from a few micrometers to <100 nm. The process does not require the use of coagulation chemistry or high temperatures to produce solid threads from solution. Electrospinning is a variation of electrospray technique, where the application of high voltage to a polymer solution results in the formation of a cone-jet geometry, which turns into very fine fibers instead of breaking into small droplets as in case of electrospray. Electrospinning shares the characteristics of both electrospraying and conventional solution dry spinning of fibers. The standard laboratory setup for electrospinning consists of a spinneret (typically, a hypodermic syringe needle) connected to a high-voltage (5–50 kV) direct current (dc) power supply, a syringe pump, and a grounded collector as shown in Figure 2.11. A polymer solution, sol–gel, particulate suspension, or melt is loaded into the syringe and this liquid is extruded from the needle tip at a constant rate by a syringe pump. Alternatively, the droplet at the tip of the spinneret can be replenished by feeding from a header tank providing a constant feed pressure. This constant pressure type feed works better for lower viscosity feedstock. Electrospinning process is particularly suited to the production of fibers using large and complex molecules. The technique relies on electrical rather than mechanical forces to form fibers. The charge pulls the polymer solution through the air into a tiny fiber, which is collected on an electrically grounded surface. Modification of the spinneret and/or the type of solution can allow for the creation of fibers with unique structures and properties. Electrospun fibers can adopt a porous or core–shell morphology depending on the type of materials being spun as well as the evaporation rates and miscibility for the solvents involved. For techniques that involve multiple spinning fluids, the general criteria for the creation of fibers depend on the spinnability of the outer solution. This opens up the possibility of creating composite fibers that can function as drug delivery systems or possess the ability to self-heal upon failure.

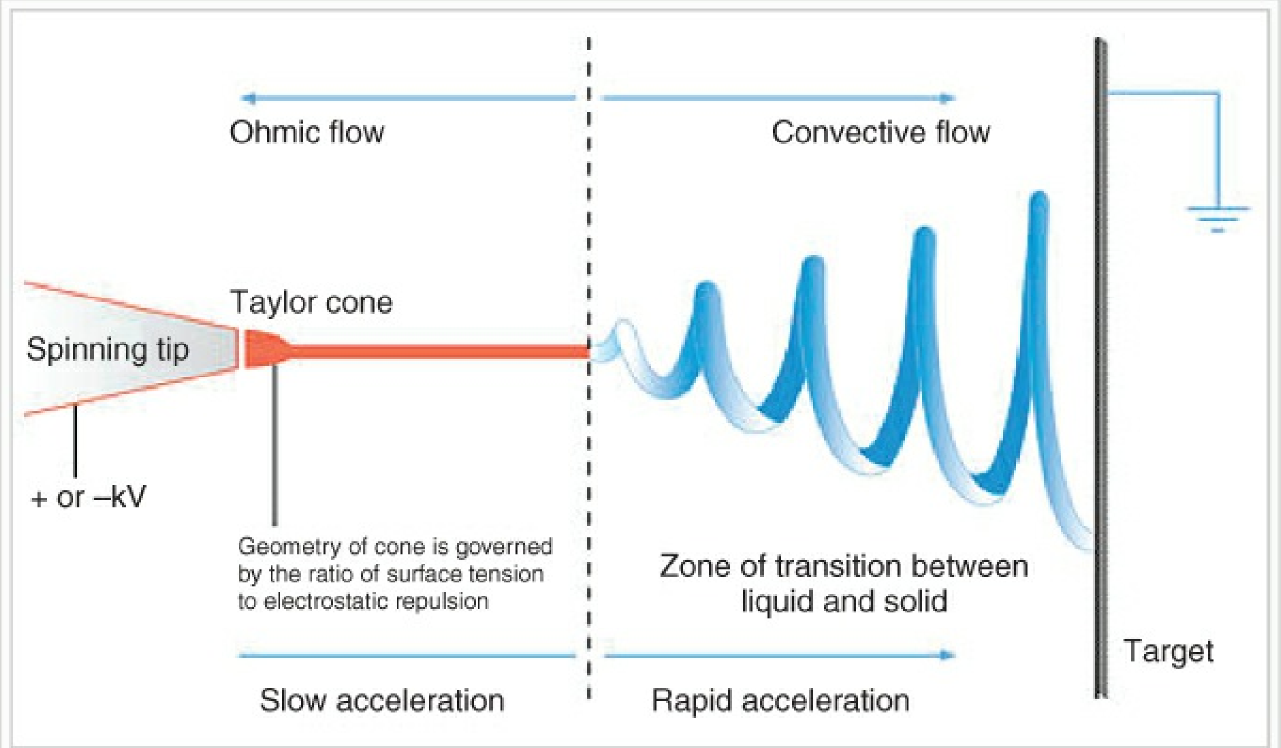
Ohmic flow
Convective flow
Taylor cone
Spinning tip
+ or –kV
Geometry of cone is governed by the ratio of surface tension to electrostatic repulsion
Zone of transition between liquid and solid
Target
Slow acceleration
Rapid acceleration

Figure 2.11 Schematics of electrospinning process for nanofiber synthesis.

Li and Xia [13]. © 2004. With permission of Wiley-VCH.

Synthesis of hierarchical TiO_2 comprising nanorods on nanofibers is a typical example of combined application of electrospinning techniques together with sol–gel and solvothermal processes and is described in Box 2.3. Synthesis of hierarchical TiO_2 nanostructure comprising nanorods on nanofibers has been prepared using a sol–gel route followed by electrospinning and calcination in air at 500 °C. The mat surface of the TiO_2 nanofibers was then exploited as a "seeding ground" to grow TiO_2 nanorods by a solvothermal process in NaOH, resulting in nanorods (diameter ~50–80 nm) evenly distributed on the nanofiber surface (diameter ~100 nm) (see Box 2.3).

Box 2.3 Synthesis of hierarchical TiO_2 nanostructure comprising nanorods on nanofibers

i. Sol–gel of titanium isopropoxide $Ti(iPr)_4$ and polyvinylpyrrolidone (PVP): 13 wt% solution of PVP prepared by dissolving 1.2 g PVP in $DMF/CHCl_3$ solvent mixture (2:1 ratio) and 0.5 g of $Ti(iPr)_4$ is added. The resulting mixture is stirred by the addition of three to five drops of ammonia solution to induce the hydrolysis and condensation of the sol.

ii. A high-voltage power supply was used as a source of electric field with an applied voltage of 20 kV, at a nozzle to collector distance of 20 cm. The sol–gel was supplied through a plastic syringe attached to a capillary tip with a pump rate of 0.30 ml/h. A copper wire originating from the positive electrode (anode) is attached to the needle and a negative electrode (cathode) is attached to a metallic collector covered with an aluminum foil. The resulting fibers are heat-treated to 500 °C in air at 10 °C/min and held at that temperature for 3 h before allowing cooling at 10 °C/min.

iii. Solvothermal synthesis of TiO_2 nanorods on the surface of TiO_2 nanofibers: 0.5 g of TiO_2 nanofibers was added to 15 ml of 4 M NaOH aqueous solution. A 15 ml ethanol solvent is added to this solution followed by heating in a 50-ml Teflon-lined autoclave at 150 °C for 12 h.

2.3 Bottom-Up Approaches

Bottom-up approaches, that is, the production of nanoparticles starting from atoms, are basically the chemical processes based on transformations in gas, liquid, or aerosol form. The popular techniques [14–22] include chemical vapor deposition (CVD), chemical vapor condensation (CVC), plasma or flame spraying synthesis, laser pyrolysis, precipitation, reduction, sol–gel, solvothermal, matrix-mediated (template-assisted) processing, self-assembly, and so on. These chemical processes rely on the availability of “metal-organic” molecules as precursors. Sol–gel processing differs from other chemical processes because of its relatively low processing temperature. This makes the sol–gel process cost-effective and versatile. In spraying processes, the flow of reactants (gas or liquid in the form of aerosols or mixtures of both) is introduced to high-energy flame produced, for example, by plasma spraying equipment or carbon dioxide laser. The reactants decompose and particles are formed in a flame by the homogeneous nucleation and growth. Rapid cooling results in the formation of nanoscale particles.

2.3.1 Chemical Vapor Deposition

The methods of gas-phase synthesis are of increasing interest because they allow an elegant way to control process parameters in order to be able to produce desired size, shape, and chemical composition controlled nanostructures. Multicomponent systems are relatively easy to prepare. Most of the synthesis routes are based on the production of small clusters that can aggregate to form nanoparticles (condensation). Condensation occurs only when the vapor is supersaturated, and in these processes homogeneous nucleation in the gas phase is utilized to form particles. This can be achieved by both physical and chemical methods. The process is often used in the semiconductor industry to produce thin films. In typical CVD, the wafer (substrate) is exposed to one or more volatile precursors, which react and/or decompose on the substrate surface to produce the desired deposit. Frequently, volatile by-products are also produced, which are removed by gas flow through the reaction chamber. Microfabrication processes widely use CVD to deposit materials in various forms including monocrystalline, polycrystalline, amorphous, and epitaxial. These materials include silicon, carbon fiber, carbon nanofibers, filaments, carbon nanotubes, SiO_2, silicon-germanium, tungsten, silicon carbide, silicon nitride, silicon oxynitride, titanium nitride, and various high-κ dielectrics. CVD is also used to produce synthetic diamonds. CVD is commonly used to deposit conformal films. A variety of applications for such films exist. Gallium arsenide is used in some ICs and photovoltaic devices. Amorphous polysilicon is used in photovoltaic devices. Certain carbides and nitrides confer wear-resistance. CVD techniques involve activating a chemical reaction between the substrate surface and a gaseous precursor. CVD is practised in a variety of formats. These processes generally differ in the means by which chemical reactions are initiated. Here, we discuss two important variants, thermal CVD (Figure 2.12a) and plasma-enhanced CVD (PECVD; Figure 2.12b), where activation can be achieved with temperature or with plasma, respectively. The main advantage of CVD is the nondirective aspects of this technology. Plasma allows decreasing the process temperature significantly as compared to that of the thermal CVD process.

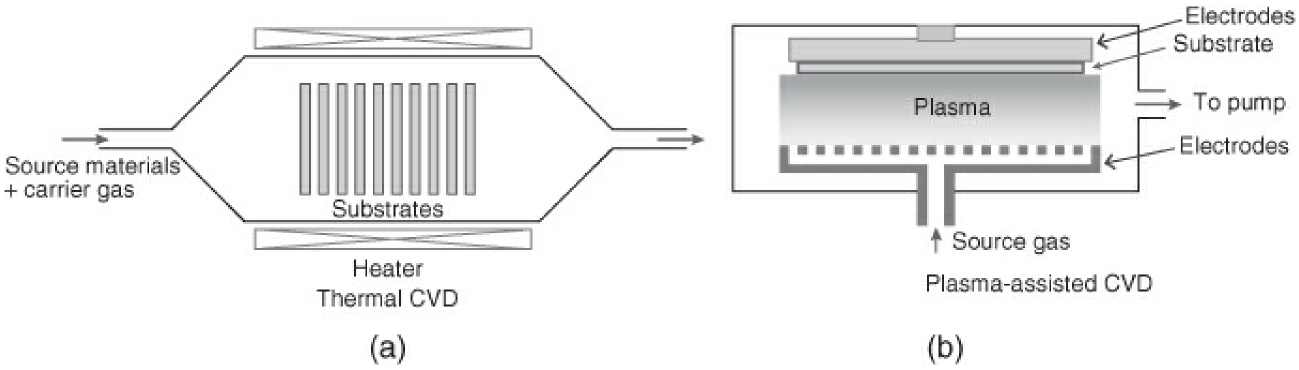

Figure 2.12 Schematic representation of chemical vapor deposition: (a) thermal and (b) plasma assisted.

From Ref. [14].

2.3.1.1 Thermal CVD

The simplest method to produce nanoparticles is by heating the desired material in a heat-resistant crucible.. This method is appropriate only for materials that can sustain a temperature up to 2000 °C. Energy is usually introduced into the precursor by arc heating, electron-beam heating, or Joule heating. The atoms are evaporated into an atmosphere, which is either inert (e.g., He) or reactive (so as to form a compound). To carry out reactive synthesis, materials with very low vapor pressure have to be fed into the furnace in the form of a suitable precursor such as organometallics, which decompose in the furnace to produce a condensable material. The hot atoms of the evaporated matter lose energy by collision with the atoms of the cold gas and undergo condensation into small clusters via homogeneous nucleation. In case a compound is being synthesized, these precursors react in the gas phase and form a compound with the material that is separately injected into the reaction chamber. The clusters would continue to grow if they remain in the supersaturated region. To control their size, they need to be rapidly removed from the supersaturated environment by a carrier gas. The cluster size and its distribution are controlled by only three parameters, that is, the rate of evaporation (energy input), the rate of condensation (energy removal), and the rate of gas flow (cluster removal). A key for the formation of nanoparticles with narrow size distributions is the exact control of the flame in order to obtain a flat flame front. Under these conditions, the thermal history, that is, time and temperature, of each particle formed is identical and results in narrow distributions. However, owing to the oxidative atmosphere in the flame, this synthesis process is limited to the formation of oxides in the reactor zone. Due to its inherent simplicity, it is possible to scale up this process from laboratory (mg/day) to industrial scales (tons/day).

2.3.1.2 Plasma-Enhanced CVD

A **plasma** is a highly energized gaseous state matter where significant fraction of the matter is ionized, and hence it is a conductor of electricity. Although there are free charges in plasma, overall negative and positive charges compensate each other. Therefore, plasmas are electrically neutral, a property that is known as quasineutrality. Plasmas are typically formed by heating and ionizing a gas, stripping electrons away from atoms, thereby enabling the positive and negative charges to move more freely. A candle flame is frequently referred as **partial plasma** because only a small proportion of the gas is ionized, being at a low temperature. Lightning is an example of a plasma present at the Earth's surface. Typically, lightning discharges 30,000 amperes, at up to 100 million volts, and emits light, radio waves, X-rays, and even gamma rays. Plasma temperatures in lightning can approach 28,000 K, and electron densities may exceed 10^{24} m^{-3}.

This technique employs plasma instead of high temperature for the decomposition of the metal-organic precursors. Energy of the plasma is used for particle formation and growth where temperature goes up to 25,000 K; in addition to the use of gases, liquid and solid reactants with low volatility are possible. The reactants evaporate in the plasma zone and are ionized. By introducing the quench gas or cooling via expansion through nozzles, formation of molecules and nucleation are started followed by particle growth in colder reactor zones. High cooling rates in the plasma reactor can be used for the production of metastable phases and nanoscale particles at high concentrations. The hot zone is small and clearly confined. The possible temperatures and cooling rates are much higher than with other gas-phase processes.

The major advantage of the plasma-assisted pyrolysis in contrast to the thermal activation is the low-temperature reaction that reduces the tendency for agglomeration of the primary particles. Additionally, it has been shown that by introducing another precursor into a second reaction zone of the tubular reactor, for example, by splitting the microwave guide tubes, the primary particles can be coated with a second phase. For example, it has been demonstrated that ZrO_2 nanoparticles can be coated by Al_2O_3. In this case, the inner ZrO_2 core is crystalline, while the Al_2O_3 coating is amorphous. The reaction sequence can be reversed with the result that an amorphous Al_2O_3 core is coated with crystalline ZrO_2. While the formation of the primary particles occurs by homogeneous nucleation, it can be easily estimated using gas reaction kinetics that the coating on the primary particles grows heterogeneously and that homogeneous nucleation of nanoparticles originating from the second compound has a very low probability. Following are a few examples of commercially important nanomaterials prepared by CVD.

1. Polysilicon

Polycrystalline silicon is deposited from trichlorosilane ($SiHCl_3$) or silane (SiH_4), using the following reactions:

$$SiH_3Cl \rightarrow Si + H_2 + HCl$$

$$SiH_4 \rightarrow Si + 2H_2$$

This reaction is usually performed in LPCVD systems with either pure silane feedstock or a solution of silane with 70–80% nitrogen. Temperatures between 600 and 650 °C and pressures between 25 and 150 Pa yield a growth rate between 10 and 20 nm per minute. An alternative process uses a hydrogen-based solution. The hydrogen reduces the growth rate, but the temperature is raised to 850 or even 1050 °C to compensate. Polysilicon may be grown directly with doping if gases such as phosphine, arsine, or diborane are added to the CVD chamber. Diborane increases the growth rate, but arsine and phosphine decrease it.

2. Silicon Dioxide (SiO_2)

Silicon dioxide (usually called simply “oxide” in the semiconductor industry) may be deposited by several different processes. Common source gases include silane and oxygen, dichlorosilane ($SiCl_2H_2$) and nitrous oxide (N_2O), or tetraethylorthosilicate (TEOS; $Si(OC_2H_5)_4$). The reactions are as follows:

$$SiH_4 + O_2 \rightarrow SiO_2 + 2H_2$$

$$SiCl_2H_2 + 2N_2O \rightarrow SiO_2 + 2N_2 + 2HCl$$

$$Si(OC_2H_5)_4 \rightarrow SiO_2 + \text{by-products}$$

The choice of source gas depends on the thermal stability of the substrate, for instance, aluminum is sensitive to high temperature. Silane deposits between 300 and 500 °C, dichlorosilane at around 900 °C, and TEOS between 650 and 750 °C, resulting in a layer of *low-temperature oxide* (LTO).

3. Silicon Nitride

Silicon nitride is often used as an insulator and chemical barrier in manufacturing ICs. The following two reactions deposit silicon nitride from the gas phase:

$$3SiH_4 + 4NH_3 \rightarrow Si_3N_4 + 12H_2$$

$$3SiCl_2H_2 + 4NH_3 \rightarrow Si_3N_4 + 6HCl + 6H_2$$

Silicon nitride deposited by LPCVD contains up to 8% hydrogen. It also experiences strong tensile stress, which may crack films thicker than 200 nm. However, it has higher resistivity and dielectric strength than most insulators commonly available in microfabrication (10^{16} Ω cm and 10 MV/cm, respectively). Other reactions that may be used in plasma to deposit SiNH include the following:

$$2SiH_4 + N_2 \rightarrow 2SiNH + 3H_2$$

$$SiH_4 + NH_3 \rightarrow SiNH + 3H_2$$

These films have much less tensile stress, but worse electrical properties (resistivity 10^6–10^{15} Ω cm, and dielectric strength 1–5 MV/cm).

4. Metals

CVD for tungsten is achieved from tungsten hexafluoride (WF_6), which may be deposited in two methods:

$$WF_6 \rightarrow W + 3F_2$$

$$WF_6 + 3H_2 \rightarrow W + 6HF$$

Other metals, notably aluminum and copper, can be deposited by CVD. Until recently, commercially cost-effective CVD for copper did not exist, although volatile sources exist such as Cu $(hfac)_2$. Copper is typically deposited by electroplating.

Aluminum can be deposited from triisobutylaluminum (TIBAL) and the related organoaluminum compounds. CVD for molybdenum, tantalum, titanium, and nickel is widely used. These metals can form useful silicides when deposited onto silicon. Mo, Ta, and Ti are deposited by LPCVD from their pentachlorides. Nickel, molybdenum, and tungsten can be deposited at low temperatures from their carbonyl precursors. In general, for an arbitrary metal M, the chloride deposition reaction is as follows:

$$2MCl_5 + 5H_2 \rightarrow 2M + 10HCl$$

Although the carbonyl decomposition reaction can happen spontaneously under thermal treatment or acoustic cavitation and is as follows:

$$M(CO)_n \rightarrow M + nCO$$

the decomposition of metal carbonyls is often violently precipitated by the moisture or air, where oxygen reacts with the metal precursor to form metal or metal oxide along with carbon dioxide.

Niobium(V) oxide layers can be produced by the thermal decomposition of niobium(V) ethoxide with the loss of diethyl ether according to the equation:

$$2Nb(OC_2H_5)_5 \rightarrow Nb_2O_5 + 5C_2H_5OC_2H_5$$

5. Chalcogenides

Commercially, mercury cadmium telluride is of continuing interest for the detection of infrared radiation. Consisting of an alloy of CdTe and HgTe, this material can be prepared from the dimethyl derivatives of the respective elements.

6. Silicon Carbide

   Synthesis of SiC from rice husks using CVD involves combining silica sand and carbon at high temperature, ranging from 1600 to 2500 °C. Rice hulls consist of silica in hydrated amorphous form and cellulose and yield carbon when thermally decomposed:

   $$\mathrm{SiO_2(amorphous) + 3C(amorphous) \rightarrow SiC + 2CO}$$

   Synthesis conditions are 20 kW, 3 MHz radio frequency (RF) plasma reactor (Ar as plasma generating and powder carrier gas). Particles produced are in the size range from 10 to 20 nm. One can note the advantages that materials with high melting points can be produced in the nanosize range from cheap micron-sized powders and nonoxide materials can be made. However, limitations of this process are broad particle size distributions because of incomplete evaporation of precursors and temperature gradient; high energy consumption; and relatively expensive equipment.

2.3.2 Chemical Vapor Condensation (CVC)

This method is used mainly for metal nanoparticles. A bulk material is heated in vacuum to produce a stream of vaporized and atomized matter, which is directed to a chamber containing either inert or reactive gas atmosphere. Rapid cooling of the metal atoms because of their collision with the gas molecules results in the condensation and formation of nanoparticles. If a reactive gas such as oxygen is used, then metal oxide nanoparticles are produced. The theory of gas-phase condensation for the production of metal nanopowders is well known, having been first reported in 1930. Gas-phase condensation uses a vacuum chamber that consists of a heating element, the metal to be made into nanopowder, powder, collection equipment, and vacuum hardware.

The process utilizes a gas, which is typically inert, at pressures high enough to promote particle formation but low enough to allow the production of spherical particles. Metal is introduced onto a heated element and is rapidly melted. The metal is quickly taken to temperatures far above the melting point. The metal is quickly taken to temperatures far above the melting point but less than the boiling point, so that an adequate vapor pressure is achieved. Gas is continuously introduced into the chamber and removed by the pumps, so the gas flow moves the evaporated metal away from the hot element. As the gas cools the metal vapor, nanometer-sized particles form. These particles are liquid since they are still too hot to be solid. The liquid particles collide and coalesce in a controlled environment so that the particles grow to the specification, remaining spherical and with smooth surfaces. Several variations of gas condensation methods are present such as molecular beam epitaxy (MBE) and sputtered plasma processing.

2.3.2.1 Molecular Beam Epitaxy (MBE)

This is essentially a very sophisticated evaporation method in which molecular beams interact on a heated crystalline substrate under ultrahigh vacuum (UHV) conditions to produce a single crystal film. MBE makes it possible to fabricate crystals of one atomic layer at a time. The growth process is highly controlled to avoid contaminants being introduced during the crystal growth. A range of surface analysis techniques is used to monitor the growth process and ensure purity of the crystal. MBE is presently used in the semiconductor industry, where the performance of the device (e.g., computer chip) depends on precise control of dopants in semiconductors and on the production of extremely thin crystal layers with hyper-abrupt interfaces. MBE is used for the fabrication of numerous important devices such as light-emitting diodes, laser diodes, field-effect transistors, read/write heads for computer drives, and more.

2.3.2.2 Sputtered Plasma Processing

This method is yet again a variation of the gas condensation method excepting the fact that the source material is a sputtering target, and this target is sputtered using rare gases and the constituents are allowed to agglomerate to produce nanomaterial. Both dc and RF sputtering have been used to synthesize nanoparticles. Again reactive sputtering or multitarget sputtering has been used to make alloys and/or oxides, carbides, and nitrides of materials. This method is specifically suitable for the preparation of ultrapure and nonagglomerated nanoparticles of metal. Further cooled under control, they become solid and grow no longer. At this point, the nanoparticles are very reactive, so they are coated with a material that prevents further interaction with other particles (agglomeration) or with other materials.

2.3.3 Plasma Arcing

This is the most common method for fabricating nanotubes. The method uses plasma, which is an ionized gas. A potential difference is placed between two electrodes and the gas ionizes in between the electrodes. A typical arcing device in made of two electrodes, an arc that passes from one electrode to the other. The first electrode (anode) vaporizes as electrons are taken from it by the potential difference. For instance, when a carbon electrode is used, it will be consumed during the reaction producing carbon cations. These positively changed ions pass to the other electrode, pick up electrons, and are deposited to form nanotubes. Plasma arcing can also be used to deposit nanolayers on surfaces rather than making new structures. The deposit can be as little as a few atoms in depth. In this sense, plasma arcing is complementary to CVD. Details are given in Chapter 6.

2.3.4 Wet Chemical Methods

Wet chemical methods are the most exploited bottom-up approach for the synthesis of a variety of nanomaterials. A number of methods included under this category are discussed in following sections.

2.3.4.1 Exchange Reactions

The exchange reactions leading to the precipitation of solids from a solution with metal ions are one of the most common processes for the production of nanomaterials. In supersaturated solutions, particles are formed via homogeneous or heterogeneous nucleation. The growth of particles usually occurs via diffusion or Ostwald ripening. Particle size and particle size distribution, crystallinity, as well as morphology are controlled by applying the reaction kinetics. Important parameters are concentration, temperature, pH of the solution, order of adding the reactants, and mixing processes. The last two parameters make the development of continuous processes and up-scaling difficult. For the production of quantum dots, the formation of nuclei has to be fast and the particle growth slow. For the production of monodisperse particles, all nuclei have to form at about the same time. Metal oxides, metal chalcogenides, and metallic nanoparticles can be produced by using precipitation methods. For the production of metallic nanoparticles, reducing agents are added to the acidic solution of metal salts; metal oxides by adding alkalis to metal salts; metal chalcogenide nanoparticles can be formed by mixing together appropriate reagents, for example, metal sulfides can be produced by purging or *in situ* generation of H_2S to soluble metal salts (halides, sulfates, nitrates, etc.). To avoid the formation of agglomerates during the precipitation process and to produce stable dispersions of nanoparticles, surfactants (especially for high particle concentrations) or electrolytes (especially for diluted suspensions) can be added. Co-precipitation enables the production of nanoparticles containing various elements. In order to avoid inhomogeneity and phase separation, all species have to be precipitated simultaneously. A simple room temperature procedure of colloidal precipitation for the synthesis of highly crystalline and nearly monodisperse chalcogenide and doped ZnS nanoparticles showing vivid luminescent colours (Box 2.4, also refer figure 4.14, Chapter 4). Superparamagnetic iron oxide nanoparticles (SPIONs) can be synthesized from Fe^{3+}/Fe^{2+} salts in the presence of different coating biomaterials such as glycine, gelatin, gum arabic, and a mixture of gelatin and gum arabic using NaOH as precipitating agent (see Box 2.5).

Box 2.4 Synthesis of metal chalcogenides

Chalcogen is added to the metal precursor solution in a hot coordinating solvent.

CdE (E = S, Se or Te) NPs: Chalcogen is added to the Cd precursor (dimethyl Cd, Cd oxide, carbonate, or acetate) in a hot coordinating solvent (e.g., tri-*n*-octylphosphine oxide, TOPO). High temperature is maintained for fast particle nucleation followed by lowering the temperature for slow particle growth.

Doped ZnS NPs: ZnS nanophosphors doped with halides, Cu^+-halides, Cu^+-Al^{3+}, Cu^+-Al^{3+}-Mn^{2+}, or Mn^{2+} can be prepared by the colloidal precipitation method at room temperature.

In a typical synthesis, aqueous copper(II) acetate solution is added to aqueous $ZnSO_4$ solution; to the resulting Zn^{2+}-Cu^{2+} precursor, Na_2SO_3 is added; SO_2 gas generated during this process reduces Cu^{2+} to Cu^+; and followed by the addition of solution of $Mn^{2+}/Al^{3+}/F^-/Cl^-/Br^-/I^-$) and PVP solution. Finally, Na_2S solution is added, leading to the precipitation of doped ZnS nanoparticles.

Box 2.5 Preparation of iron oxide NPs by exchange reaction

In a typical synthesis, a source of iron is prepared by dissolving 0.02 M $FeCl_3$ and 0.01 M Fe_2SO_4 in 250 ml water. Appropriate amount of coating material is added to the source of iron solution. The co-precipitation of SPION was carried out in a reaction with magnetic stirring, by slowly adding 5 M NaOH until obtaining pH 9–10 at room temperature. The resulting solution was kept for 1 h to complete the reaction. Then the precipitate was magnetically separated from the supernatant and washed several times with distilled water, until obtaining pH 7. During each washing step, samples were separated from the supernatant using a permanent magnet. Thoroughly washed magnetic particles were dried at room temperature, yielding a fine powder.

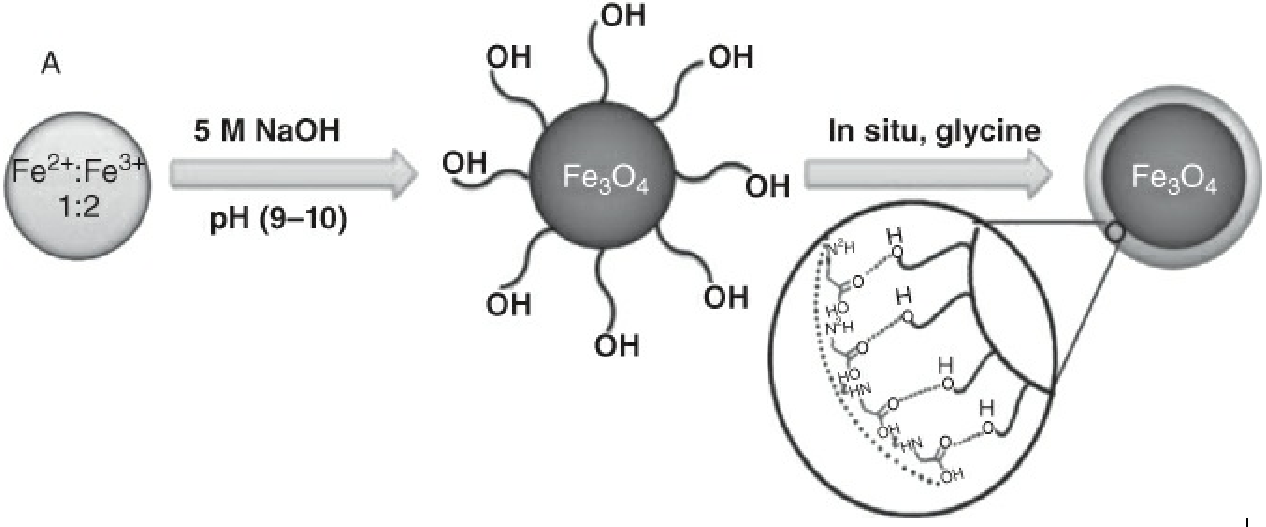

Box 2.5 Preparation of Fe_2O_3. Shukla et al. [15] © 2010. With permission of ASPBS.

2.3.4.2 Chemical Reduction Method

Chemical reduction of metal salts is the most common method for the synthesis of nanoparticles and has the potential to be scaled up even at room temperature. The basic scheme for the synthesis of nanoparticles by chemical reduction method is shown in Figure 2.13.

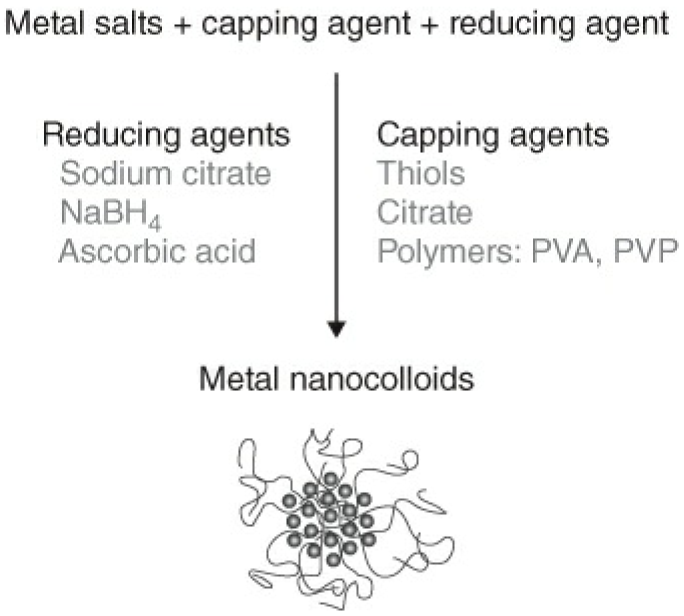

Figure 2.13 Schematic representation of chemical reduction method for nanosynthesis.

Several reducing agents such as ascorbic acid, citric acids, and their salts; alkali hydrides namely $NaBH_4$, $NaB(C_2H_5)_3H$, and $LiB(C_2H_5)_3H$ along with various capping agents such as polymers, for example, polyvinylpyrrolidone; organic ligand, for example, quaternary amines, thiols; and surfactants (Figure 2.14a–c) have been successfully used to prevent aggregation of metal nanoparticles.

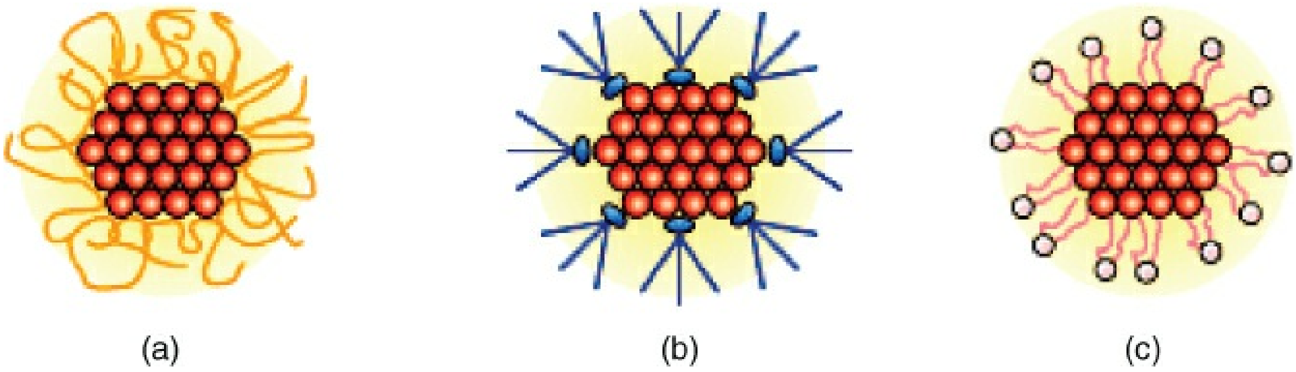

Figure 2.14 Schematic representation different capping agents (a) polymer; (b) organic ligand, and (c) micelle.

A novel method is given here (Box 2.6) for the synthesis of optically clear and stable colloidal solutions of silver nanoparticles at room temperature by chemical reduction of silver ions (silver nitrate) coordinated with dendrimer polymer, polyethyleneimine (PEI) using formaldehyde in aqueous medium. Typical preparations of gold and iron–cobalt nanoparticles are also given in Boxes 2.7 and 2.8, respectively.

Box 2.6 Preparation of silver nanoparticles

In a typical synthesis, 0.85 g of $AgNO_3$ was dissolved in 100 ml of aqueous solution of 0.85 wt% polyethyleneimine (PEI, M_w 600,000–1,000,000) and homogenized by stirring for 2 min. It is followed by the addition of 1 ml of 35% solution of formaldehyde and mixing the resultant solution well. Light yellow color appeared after 2 min, indicating the nucleation and growth of Ag NPs.

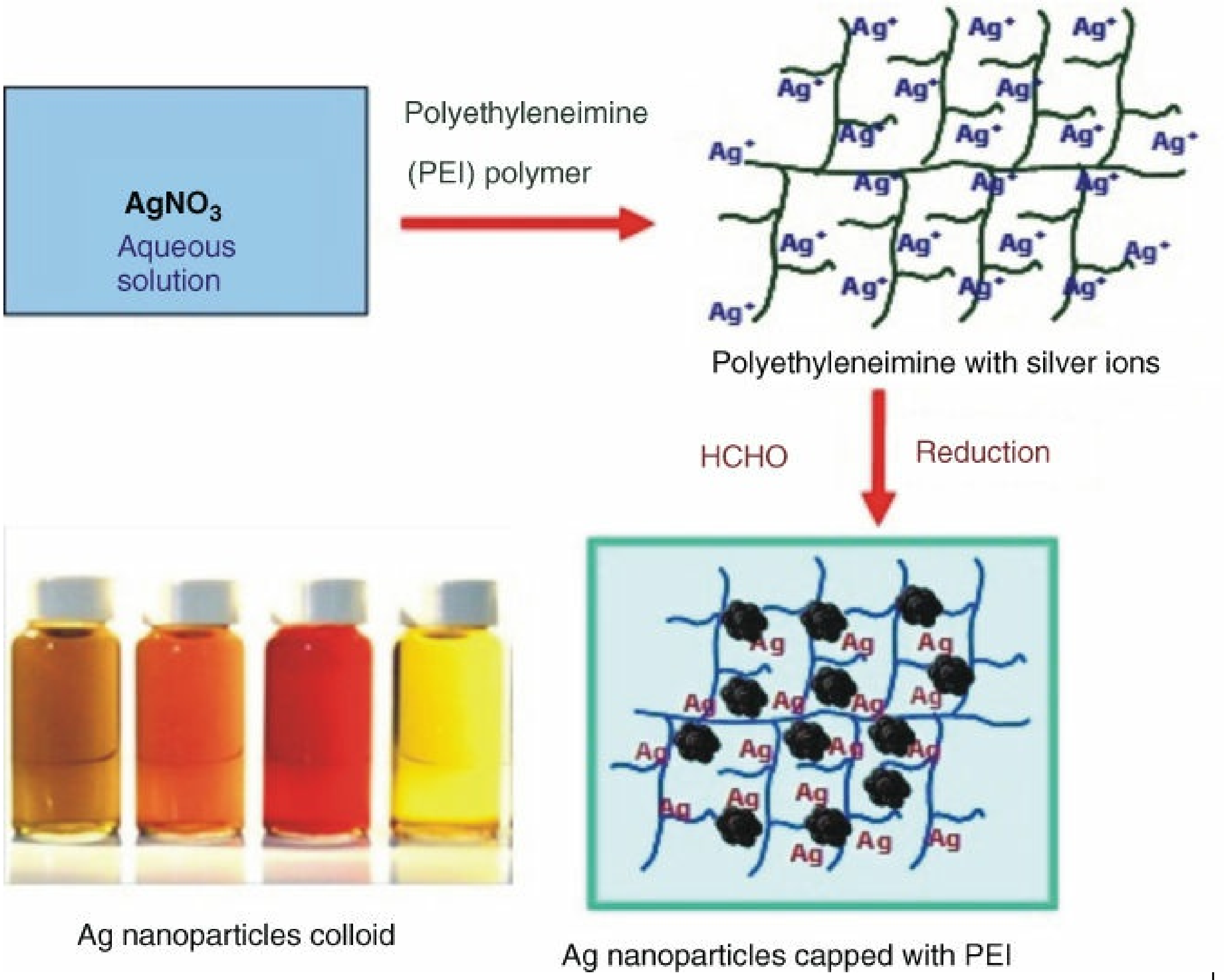

Box 2.6 Preparation of Ag NPs by reduction method. Manoth et al. [16] © 2008. With permission of Elsevier.

Box 2.7 Preparation of gold nanoparticles: Au nanorods

One of the most simple and reproducible methods to synthesize Au nanorods is the seed-mediated growth method. It consists of a two-step process, that is, nucleation and then successive growth of the NPs.

Typical preparation I

I step: A growth solution is prepared by the mild reduction of Au ions ($HAuCl_4$ 0.001 M) with l-ascorbic acid (0.0778 M) in the presence of $AgNO_3$ (0.04 M), which promotes anisotropy and hexadecyltrimethylammonium bromide (CTAB, 0.2 M) and benzyldimethylhexadecylammonium chloride (BDAC, 0.15 M) as surfactants.

II step: The seed solution is prepared afterward by the rapid reduction of the Au precursor with a strong reducing agent ($NaBH_4$, 0.010 M) in the presence of CTAB (0.20 M) as a surfactant.

By introducing some modifications in experimental conditions (e.g., solution temperature, stirring rate, ratio of seed to metal salt), it is possible to obtain a defined aspect ratio of the Au nanorods.

Typical preparation II

1. **Step I:** Aqueous solution of Au ($HAuCl_4$, 0.001 M) is mixed with mercaptosuccinic acid (MSA, 0.005 M in methanol) to give a transparent solution.
2. **Step II:** Freshly prepared aqueous solution of sodium borohydride ($NaBH_4$, 0.010 M) is then added under vigorous stirring conditions. The solution will turn dark brown immediately but remain transparent (which indicates that the nanoparticles have not yet formed) until enough reductant was added till a flocculent dark brown precipitate is generated. The pH of the solution increases gradually with the addition of reactant, and finally the pH of the solution is brought to 8.6. The solvent was removed by decantation after the centrifugation. The precipitate is washed, suspended in ethanol, and dried by rotary evaporation.

Box 2.8 Iron–cobalt nanoparticles

Synthesis of core–shell metal alloy nanoparticles: **first step** involves the synthesis of nanocomposites of mixed metal oxide (FeCo) at the room temperature in the copolymer matrix of aniline formaldehyde, and the **second step** involves the pyrolysis of as-prepared nanocomposite under inert atmosphere [17].

In a typical synthesis, copolymer of aniline and formaldehyde is prepared by adding 10 ml (0.10 M) of aniline to 50 ml of distilled water. To this, 12 ml (0.12 M) of concentrated HCl is added, which results in the formation of water-soluble aniline hydrochloride. To this mixture, 10 ml (0.10 M) of formaldehyde is added. The reaction proceeds through the formation of *p*-aminobenzyl alcohol, followed by the subsequent condensation between the amino and the hydroxyl groups. As this is an exothermic reaction, it is accompanied by the evolution of a large amount of heat, so the solution is kept aside for cooling down to room temperature. Simultaneously, salt solution is prepared by dissolving the metal halide (Fe and Co halides) in 50 ml distilled water. This salt solution is then added to the precooled copolymer solution with constant stirring. This entire mixture is added to 200 ml of 10% sodium hydroxide solution with stirring. It is further stirred for 10 min and then allowed to stand for approximately 45 min to 1 h. This is then filtered under vacuum and washed with distilled water till the filtrate is free of alkali (pH 7–8). This composite is then dried at room temperature to get the nanocomposite of the mixed metal oxide(s) in the powder form.

Furthermore, metal oxide nanocomposite powder is taken in a small quartz holder and placed in quartz reactor tube. Initially, high-purity N_2 (99.99%) is passed in the reactor tube for 5 min to flush off ambient air. The reactor tube containing nanocomposites is then placed in tubular furnace, and temperature was raised at the rate of 10 °C/min. The nanocomposite is heat-treated at 900 °C for 1 h under continuous flow of N_2 gas. Finally, furnace was cooled to room temperature to obtain the desired product. The final product is core–shell graphite-coated FeCo alloy nanoparticles.

2.3.5 Hydrothermal/Solvothermal

This is another solution-based method to prepare a wide range of nanomaterials having diverse shape and size. Hydrothermal and solvothermal methods are very similar in that in both the cases reaction is done in a stainless pressure vessel, known as autoclave. The only difference being that the precursor solution is usually not aqueous in case of solvothermal method. Using the solvothermal route, one gains the benefits of both the sol–gel and hydrothermal routes. Thus, solvothermal synthesis allows for the precise control over the size, shape distribution, and crystallinity of metal oxide nanoparticles or nanostructures. These characteristics can be altered by changing certain experimental parameters, including reaction temperature, reaction time, solvent type, surfactant type, and precursor type. In a typical synthesis, titanium(IV) alkoxide, 10 g, was dissolved in a 70 cm^3 portion of an alcohol in a test tube, which was then set in a 200 cm^3 autoclave. The autoclave was thoroughly purged with nitrogen, heated to desired temperature (523–573 K) at a rate of 2.5 $Kmin^{-1}$, and kept at that temperature for 2 h. After the autoclave treatment, the resulting powders were washed repeatedly with acetone and dried in air.

2.3.6 Reverse Micelle Method

Reverse micelles are water-in-oil droplets stabilized by a surfactant. The surfactant most often used is sodium salt of bis(2-ethylhexyl)sulfosuccinate, usually called Na(AOT). These droplets are displayed randomly and subjected to Brownian motion. They exchange their water content and re-form two distinct micelles. Furthermore, the size of the water-in-oil droplets increases linearly, that is, the micellar concentration decreases, with increasing water content, defined as $w = [H_2O]/[AOT]$. This involves the preparation of two separate micro-emulsions, incorporating the different reactants. Upon mixing, nucleation occurs on the micelle edges as the water inside them becomes supersaturated with reactants. Growth then occurs around this nucleation point, with the arrival of more reactant fed via intermicellar exchange. The reverse micelle permits the synthesis in a very wide range of nanomaterials such as II–VI group semiconductors and metals, with a good control of size and shape. The most widely used approach is shown in Figure 2.15.

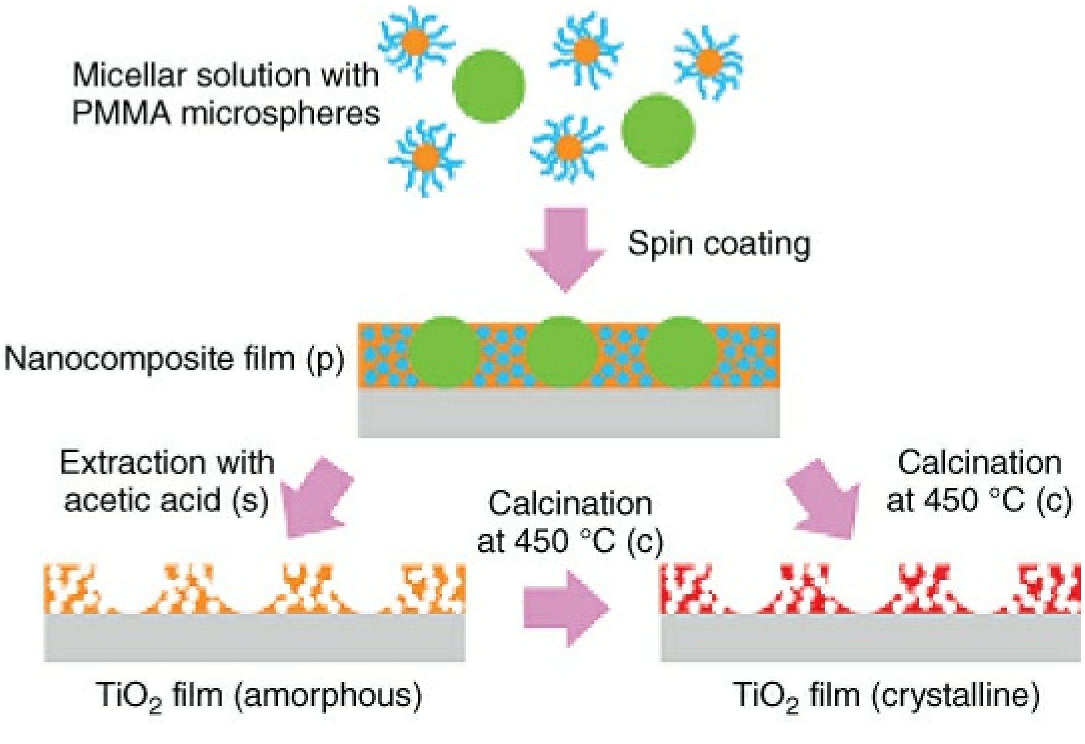
Micellar solution with PMMA microspheres
Spin coating
Nanocomposite film (p)
Extraction with acetic acid (s)
Calcination at 450 °C (c)
Calcination at 450 °C (c)
TiO_2 film (amorphous)
TiO_2 film (crystalline)

Figure 2.15 Illustration of the reverse micelle preparation route for hierarchical structuring of TiO_2.

Kaune et al. [18] ©2009. With permission of ACS.

2.3.7 Sol–Gel Method

A “sol” is a type of colloid in which a dispersed solid phase is mixed in a homogeneous liquid medium. An example of a naturally occurring sol is blood. As the name suggests, the sol–gel process involves the evolution of networks through the formation of a colloidal suspension (sol) and gelation of the sol to form a network in a continuous liquid phase (gel). The first stage in the sol–gel processes is the synthesis of the colloid. The precursors are usually ions of a metal. Metal alkoxide and alkoxysilane are the most popular since they react readily with water (hydrolysis). The most widely used alkoxysilanes are tetramethoxysilane (TMOS) and tetraethoxysilane (TEOS), which form silica gels. Alkoxides such as aluminates, titanates, and borates are also used, often mixed with TMOS or TEOS. In addition, since alkoxides and water are immiscible, a mutual solvent is used such as an alcohol. The sol–gel technique is a long-established industrial process for the generation of colloidal nanoparticles from liquid phase that has been further developed in previous years for the production of advanced nanomaterials and coatings. Sol–gel processes are well adapted for oxide nanoparticles and composites nanopowders synthesis. The main advantages of sol–gel techniques for the preparation of materials are low temperature of processing, versatility, and flexible rheology allowing easy shaping and embedding. They offer unique opportunities for access to organic–inorganic materials.

The sol–gel process involves the evolution of inorganic networks through the formation of a colloidal suspension (**sol**) and gelation of the sol to form a network in a continuous liquid phase (**gel**). The precursors for synthesizing these colloids consist usually of a metal or metalloid element surrounded by various reactive ligands. The starting material is processed to form a dispersible oxide and forms a sol in contact with water or dilute acid. Removal of the liquid from the sol yields the gel, and the sol–gel transition controls the particle size and shape. Calcination of the gel produces the oxide. Sol–gel processing refers to the hydrolysis and condensation of alkoxide-based precursors such as $Si(OEt)_4$ (tetraethyl orthosilicate). The reactions involved in the sol–gel chemistry based on the hydrolysis and condensation of metal alkoxides $M(OR)\boldsymbol{z}$ can be described as follows:

$$\mathrm{MOR} + \mathrm{H_2O} \rightarrow \mathrm{MOH} + \mathrm{ROH}\ (\text{hydrolysis})$$

$$\mathrm{MOH} + \mathrm{ROM} \rightarrow \mathrm{M-O-M} + \mathrm{ROH}\ (\text{condensation})$$

The typical sol–gel process involves four steps.

1. Formation of stable solutions (**sol**) of alkoxide or solvated metal precursor by hydrolysis reaction, in which the –OR group is replaced with an –OH group. The hydrolysis reaction can occur without a catalyst but is more rapid and complete when catalysts (e.g., base NaOH, NH_3 or acid HF,CH_3COOH) are used.

2. After hydrolysis, the sol starts to condense and polymerize (**gel**). This leads to a growth of particles to dimensions of a few nanometers. Gelation resulting from the formation of an oxide- or alcohol- bridged networks by a polycondensation reaction results in a dramatic increase in the viscosity of the solution.

3. **Syneresis**, the aging of the gel during which the polycondensation reactions continue until the gel transforms into a solid mass, is accompanied by the contraction of the gel network and expulsion of the solvent from gel pores. Ostwald ripening (also referred to as coarsening is the phenomenon by which smaller particles are consumed by larger particles during the growth process) and phase transformations may occur concurrently with syneresis. The aging process of gels can exceed 7 days and is critical to the prevention of cracks in gels.

4. **Drying** of the gel, when water and other volatile liquids are removed from the gel network. If the solvent (such as water) is extracted under supercritical or near supercritical conditions, the product is an *aerogel*. Gels are stabilized by dehydration, during which surface-bound M-OH groups are removed. This is usually achieved by **calcining** the monolith at temperatures up to 800 °C.

All the four steps illustrated earlier are affected by the initial conditions for the hydrolysis reaction and the condensation/polymerization. These conditions include pH, temperature and time of reaction, and nature of the catalyst. Figure 2.16 summarizes the different steps involved in sol–gel processes.

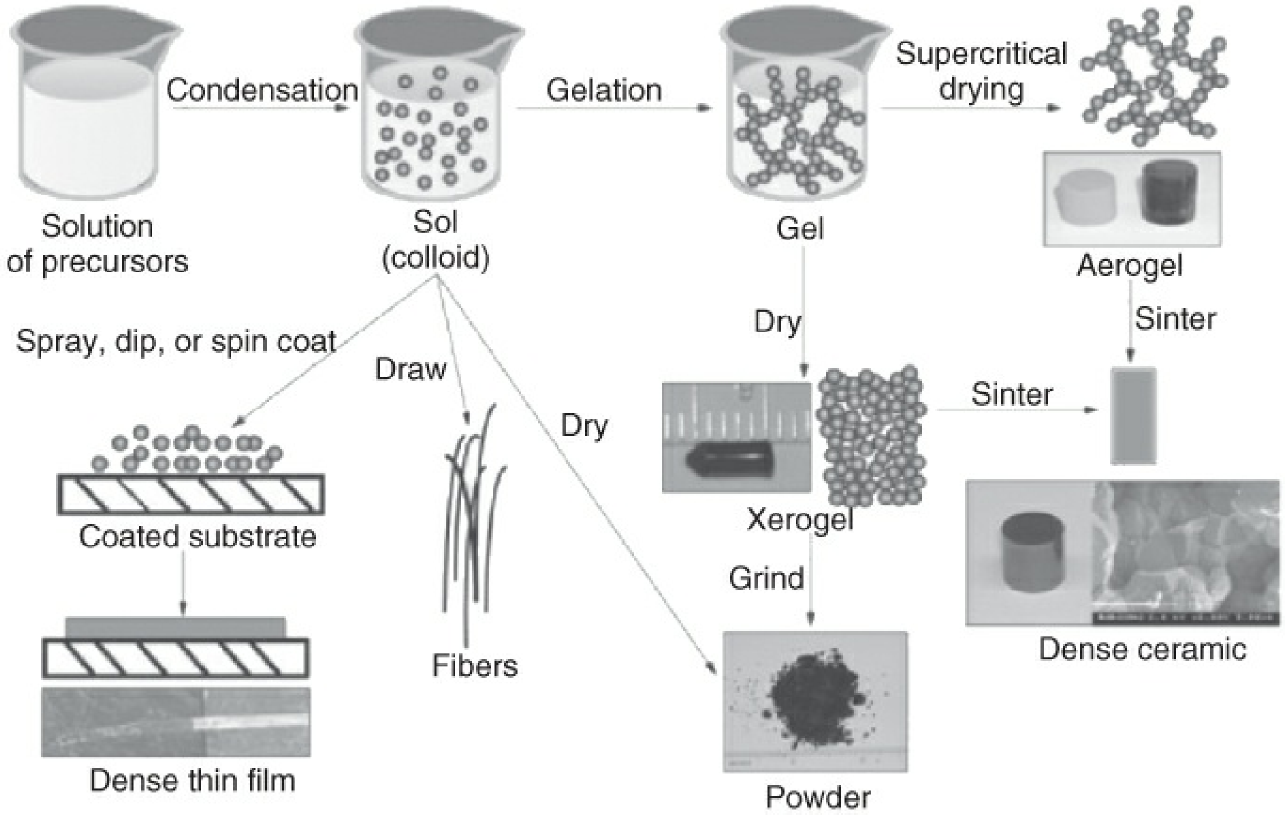

Figure 2.16 Schematic representation of sol–gel process for the synthesis of a variety of nanostructures.

Hench and West [19] © 1990. With permission of ACS.

The sol–gel process is very commonly used to make silica gels. Other types of gels can also be formed: aluminosilicate gels are special because they form tubular structures. One such product is imogolite, which has an external diameter of about 2.5 nm and internal tube diameter of 1.5 nm. These types of nanostructures are known to be good adsorbents for anions such as chloride, chlorate, sulfate, and phosphates. The imogolite structure can be dissolved away with HF. Therefore, these nanostructures can be used for template synthesis: the tube can be filled with atoms and then dissolved away, leaving rows of atoms. Number of strategies based on sol–gel can be adopted to prepare **nanocoatings**. The gel is placed on a surface, a greater bulk–area ratio is obtained. Another strategy is to form an aerogel. These are three-dimensional continuous networks of particles that are trapped at their interstices. Aerogels are characterized by being porous and very light, yet able to withstand 100 times their weight. A versatile way to create ordered surface nanostructures is to perform the sol–gel synthesis in a liquid, which is itself ordered. For example, liquid crystals have a crystalline structure but exist in a liquid phase. Nanostructured silica with controlled pore size, shape, and ordering can be made in this way. The liquid crystalline casting method described earlier can also be used to produce nanostructured metals. This development is very useful for making nanostructured catalytic surfaces, such as platinum or palladium surfaces. Since these metals are very rare and expensive, it is highly advantageous to have surfaces where nearly all metal atoms can take part in the catalytic reaction and not just surface atoms as in conventional solids. The interest in this synthesis method arises due to the possibility of synthesizing nonmetallic inorganic materials such as glasses, glass ceramics, or ceramic materials at very low temperatures compared to that of the high-temperature processes required for melting glass or firing ceramics. The major difficulties to overcome in developing a successful bottom-up approach are controlling the growth of the particles and then stopping the newly formed particles from agglomerating. Other technical issues are ensuring the reactions are complete so that no unwanted reactant is left on the product and completely removing any growth aids that may have been used in the process. Also production rates of nanopowders are very low by this process. The main advantage is one can get monodisperse sizes of nanoparticles by any bottom-up approach.

2.3.8 Sonochemical Method

High-intensity ultrasound can be used for the production of novel materials and provides an unusual route to known materials without bulk high temperatures, high pressures, or long reaction times. Several phenomena are responsible for sonochemistry and specifically the production or modification of nanomaterials during ultrasonic irradiation. The most notable effects are the consequences of acoustic cavitation and can be categorized as primary sonochemistry (gas-phase chemistry occurring inside collapsing bubbles), secondary sonochemistry (solution-phase chemistry occurring outside the bubbles), and physical modifications (caused by high-speed jets or shock waves derived from bubble collapse). Acoustic cavitation (the formation, growth, and implosive collapse of bubbles in a liquid as shown in Figure 2.17a) creates extreme conditions inside the collapsing bubble and serves as the origin of most sonochemical phenomena in liquids or liquid–solid slurries. Nebulization (the creation of mist from ultrasound passing through a liquid and impinging on a liquid–gas interface) is the basis for ultrasonic spray pyrolysis (USP) with subsequent reactions occurring in the heated droplets of the mist. In both cases, we have examples of phase-separated microreactors for sonochemistry; it is a hot gas inside bubbles isolated from one another in a liquid, while for USP it is hot droplets isolated from one another in a gas. Cavitation-induced sonochemistry provides a unique interaction between energy and matter, with hot spots inside the bubbles of ~5000 K, pressure of ~1000 bar, heating and cooling rates of $>10^{10}$ K/s; these extraordinary conditions permit access to a range of chemical reaction space usually not accessible, which allows for the synthesis of a wide variety of unusual nanostructured materials. Complementary to cavitational chemistry, the microdroplet reactors created by USP facilitate the formation of a wide range of nanocomposites. A basic setup for sonochemical reactor is shown in Figure 2.17b.

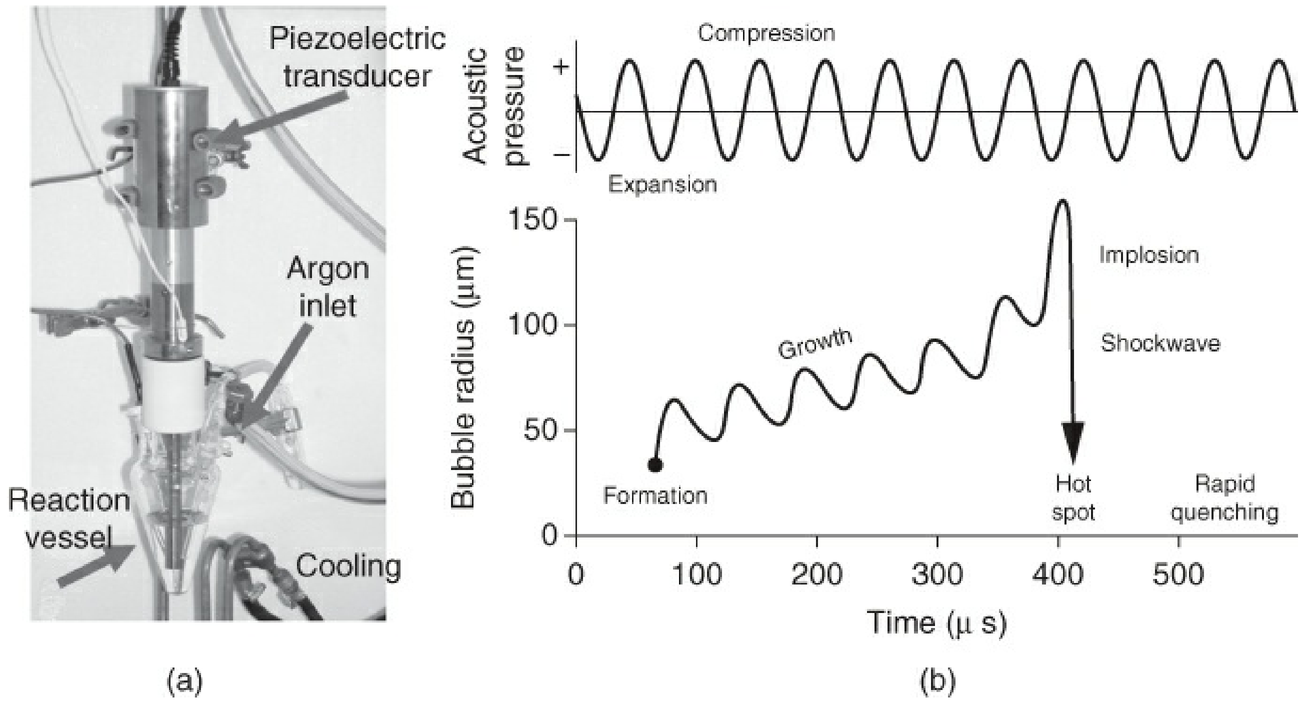

Figure 2.17 (a) Sonochemical reactor; (b) transient cavitation during sonolysis.

Adapted from Xu et al. [20] © 2013, Royal Society of Chemistry.

2.3.8.1 *Synthesis of Inorganic Nanoparticles by Sonolysis*

Molecules can undergo chemical reactions due to the application of powerful ultrasound radiation (20 kHz to 10 MHz). In almost all sonochemical reactions nanomaterials are obtained; they may vary in size, shape, structure, and in their solid phase (amorphous or crystalline) depending on the reaction conditions. Following are the examples of some typical formations of nanometallic powder, metallic colloids, and amorphous alloys. [21].

i. Nanometallic Powder: It can be obtained from sonication of metal carbonyls (e.g., from $Fe(CO)_5$, Ni from $Ni(CO)_4$, Co from $Co(CO)_3NO$, Pd from $Pd(O_2CCH_3)_2$). Sonication of divalent salt of Pd(II) (1.0 mM) solution in polyethylene glycol monostearate solution results in about 5-nm Pd particles with a fairly narrow distribution. Sonication of K_2PdCl_4 or H_2PtCl_6 solution could result in the formation of nano-Pd and nano-Pt particles of size 3.6±0.7 nm Pd under Ar and 2.0±0.3 nm Pt under N_2 stream.

ii. Metal Colloids: Sonication of Au, Pd, Ag in the presence of a surfactant, which largely stabilizes that the colloid have resulted in Fe NPs with 8 nm average size from $Fe(CO)_5$ in the presence of oleic acid; Co NPs stabilized by oleic acid (magnetic fluids); elongated Cu NPs using a zwitterionic surfactant; and Pt NPs (3 nm) from K_2PtCl_6 solution.

iii. Nanometal Alloys: Several examples are available for sonochemical synthesis of metal alloy NPs using a combination of metal salts/complexes as precursor material.

- Amorphous Fe/Co can be synthesized from a mixture of $Fe(CO)_5$ and $Co(CO)_3NO$ in decalin;
- M50 steel powder with extremely high hardness from $Fe(CO)_5$, $(EtxC_6H_{6-x})_2Cr$, $(EtxC_6H_{6-x})_2Mo$, and $V(CO)_6$ in decalin;
- Au/Pd from $NaAuCl_4$ and $PdCl_2$: monodisperse distribution (8 nm) with gold core and Pd shell;
- Ag/Fe_2O_3 from $AgNO_3$ and $Fe(CO)_5$; Fe/Ni/Co from $Fe(CO)_5$, $Ni(CO)_4$, and $Co(CO)_3NO$.

A typical example, preparation of $Fe_{40}Co_{60}$ alloy [22], is given in Box 2.9.

Box 2.9 Sonochemical synthesis of $Fe_{40}Co_{60}$ alloy

In a typical preparation, 2.0 ml $Fe(CO)_5$ (0.15 M) and 1.5 ml $Co(NO)(CO)_3$ (0.15 M) are dissolved in 100 ml diphenylmethane. The sonolysis of the solution is performed for 3 h at 20–30 °C under argon atmosphere by means of an ultrasonic device with a direct immersion titanium horn (working frequency 20 kHz, electric power of generator 600 W, irradiation surface area of the horn 1 cm^2). The black solid product can be separated by centrifugation, washed with pentane inside the N_2-filled glove box, and dried under vacuum at room temperature. The annealing of the solids is performed under an argon flow (99.996%) for 5 h at 600 °C, yielding ~60% $Fe_{40}Co_{60}$ alloy by weight.

2.3.9 Biomimetic Approaches

The limitation of bottom-up approach for nanosynthesis is the lack of a general scheme for the creation and assembly of nanomaterials. On the other hand, through millions of years of evolution, Nature has selected organisms that can create diversified inorganic material structures in nano- or microscale, which is known as biomineralization. Examples include calcification and silification found in diatoms, and the formation of magnetite crystals in magnetotactic bacteria, as shown in Figure 2.18a. These organisms are capable of organizing nanoscale building blocks into large-scale hierarchical structures (Figure 2.18b) to form hard tissues serving different functions such as mechanical support, filtration, light harvesting, gravity sensing, and locomotion. Scientists have long been exploring the approaches and mechanisms adopted by Nature to create functional structures for technical applications, which are usually referred to as biomimetics. Biomimetics refers to applying biological principles for materials formation. Initially, bacteria were used to synthesize nanoparticles and this was later succeeded with the use of fungi, actinomycetes, and more recently plants and specific peptides [23, 24]. Applications of these biological species for bionanosynthesis [25, 26] are summarized in Table 2.3. The number of plant product extracts, predominately medicinal plants, has been used for extracellular synthesis of nanoparticles, Figure 2.19 shows the AFM image of silver nanoparticles synthesized using root extract of *Curculigo orchioides*.

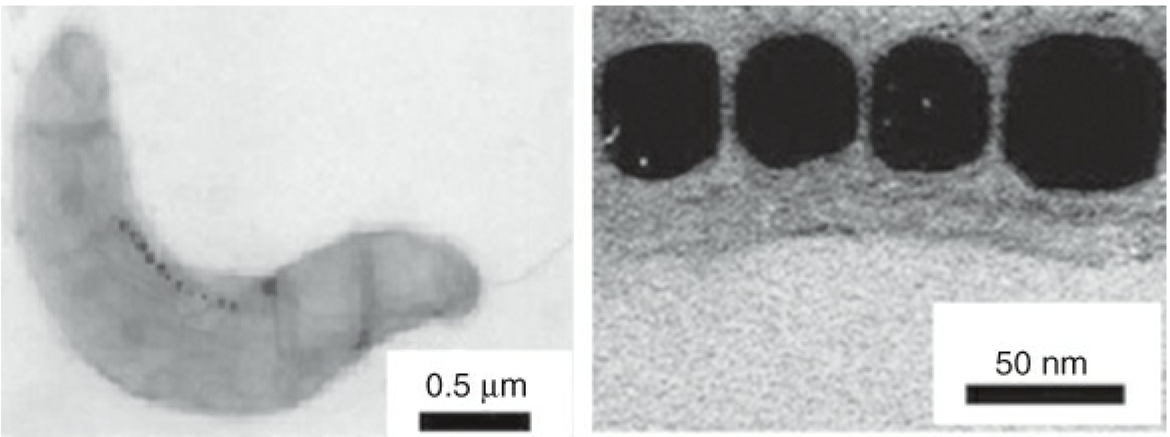

Figure 2.18 Scanning electron micrograph (SEM): (a) magnetotactic bacteria (*Magnetospirillum gryphiswaldense*) cell; (b) magnetite crystals observed at the ends of the chain in magnetotactic bacteria.

Bazylinski and Frankel [23] © 2004. With permission of Nature Publishing Group.

Table 2.3 Extracellular Bionanosynthesis of Nanoparticles

Biological Entity	NPs Synthesized (Size)
Bacteria	
Pseudomonas aeruginosa	Au (15–30 nm)
Rhodopseudomonas capsulata	Au (10–20 nm)
Bacillus megatherium	Au (02–03 nm)
Bacillus subtilis	Ag (05–60 nm)
Bacillus licheniformis	Ag (50 nm)
Enterobacter cloacae	Ag (50–100 nm)
Escherichia coli	Ag (05–25 nm)
Lactobacillus fermentum	Ag (12 nm)
Klebsiella pneumonia	Ag (50 nm)
Proteus mirabilis	Ag (10–20 nm)
Brevibacterium casei	Ag (50 nm)
Actinomycete	
Thermomnospora sp.	Au (08 nm)
Fungi	
Verticillium sp.	Ag (25 nm)
Fusarium semitectum	Ag (10–60 nm)
Fusarium oxysporum	Ag (20–25 nm)
Phanerochaete chrysosporium	Ag (100 nm)
Aspergillus fumigatus	Ag (05–25 nm)
Aspergillus clavatus	Ag (10–25 nm)
Aspergillus flavus	Ag (07–10 nm)
Fusarium solani	Ag (05–35 nm)

Fusarium oxysporum	Au (20–40 nm)
Trichothecium sp.	Au (5–200 nm)
Colletotrichum sp.	Au (20–40 nm)
Algae	
Sargassum wightii	Au (20–40 nm)
Plant leaves extract	
Pelargoncum gravcolens	Au (20–40 nm)
Cymbopogon flexuosus	Au (0.05–2 nm)
Tamarindus indica	Au (20–40 nm)
Coriandrum sativum	Ag, Au (20–26 nm)
Azadirachta indica	Ag, Au, Ag–Au (50–100 nm)
Aloe vera sp.	Ag, Au (15–20 nm)
Piper betle	Ag (03–37 nm)
Medicago sativa	Ag (2–20 nm)
Cinnamomum camphora	Ag (55–80 nm)
Stem/bark/latex	
Cinnamomum zeylanicum	Ag (50–100 nm)
Jatropha curcas	Ag (10–20 nm)
Desmodium triflorum	Ag (05–20 nm)
Pelargoncum gravcolens	Au (8–24 nm)
Fruit extract	
Emblica officinalis	Au (15–20 nm)
Carica papaya	Ag (15 nm)
Root extract	
Pelargoncum graveolens	Au (11–34 nm)
Curculigo orchioides (dave et al)	Ag (20–40 nm)
Plant-derived compound	
Apiin extracted from henna leaf	Ag, Au (20–40 nm)
Phyllanthin from *Phyllantyhus annus*	Ag, Au (10–30 nm)

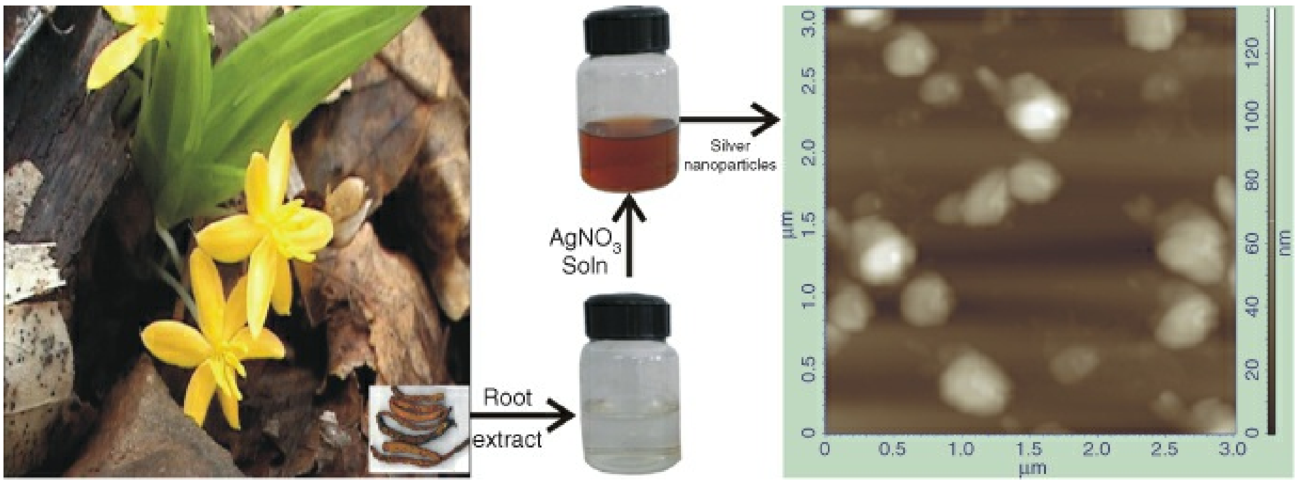

Figure 2.19 Plant *Curculigo orchioides* (inset shows dried root) root extract used for nanosynthesis and AFM image of resultant silver nanoparticles. Courtesy, Dr. Sushma Dave, VIET, Jodhpur, India.

2.3.9.1 Bacteria

Microorganisms are considered as a potential biofactory for the synthesis of nanoparticles such as gold, silver, and cadmium sulfide. Some well-known examples of bacteria synthesizing inorganic materials include magnetotactic bacteria (synthesizing magnetic nanoparticles) and S-layer bacteria that produce gypsum and calcium carbonate layers. The mechanisms involve efflux systems, alteration of solubility, and toxicity via reduction or oxidation, biosorption, bioaccumulation, extracellular complexation or precipitation of metals, and lack of specific metal transport systems, for example, *Pseudomonas stutzeri* AG 259 isolated from silver mines has been shown to produce silver nanoparticles.

2.3.9.2 Actinomycetes

Actinomycetes are microorganisms that share important characteristics of fungi and *Prokaryotes* such as bacteria. Even though they are classified as prokaryotes, they were originally designated as ray fungi. Focus on actinomycetes has primarily centered on their exceptional ability to produce secondary metabolites such as antibiotics that now finds application in biosynthesis of metal nanoparticles.

2.3.9.3 Fungi

Fungi have been widely used for the biosynthesis of nanoparticles. In addition to monodispersity, nanoparticles with well-defined dimensions can be obtained using fungi. Compared to bacteria, fungi could be used as a source for the production of a large amount of nanoparticles. This is due to the fact that fungi secrete a large amount of proteins that directly translate to higher productivity of nanoparticle formation. Instead of fungi culture, isolated proteins from them have also been used successfully in nanoparticles production.

2.3.9.4 Plants

The advantage of using plants for the synthesis of nanoparticles is that they are easily available, safe to handle, and possess a broad variability of metabolites that may aid in reduction. A number of plants have been investigated for their role in the synthesis of nanoparticles (Table 2.3).

While fungi and bacteria require a comparatively longer incubation time for the reduction of metal ions, water-soluble phytochemicals do it in a much lesser time. Therefore, plants are better candidates for the synthesis of nanoparticles when compared to that of bacteria and fungi,. Taking use of plant tissue culture techniques and downstream processing procedures, it is possible to synthesize metallic as well as oxide nanoparticles on an industrial scale once issues such as the metabolic status of the plant are properly addressed.

2.3.9.5 Specific Peptides

A genetically engineered polypeptide for inorganics (GEPI) defines a sequence of amino acids that specifically and selectively binds to an inorganic surface. The surface could be well defined, such as a single crystal or a nanostructure. It might also be rough or totally nondescriptive, such as a powder. In molecular biomimetics, inorganic-binding proteins could potentially be used as (1) linkers for nanoparticle immobilization; (2) functional molecules assembled on specific substrates; and (3) hetero-bifunctional linkers involving two (or more) binding proteins linking several nano-inorganic units as shown schematically in Figure 2.20(a)–(c).

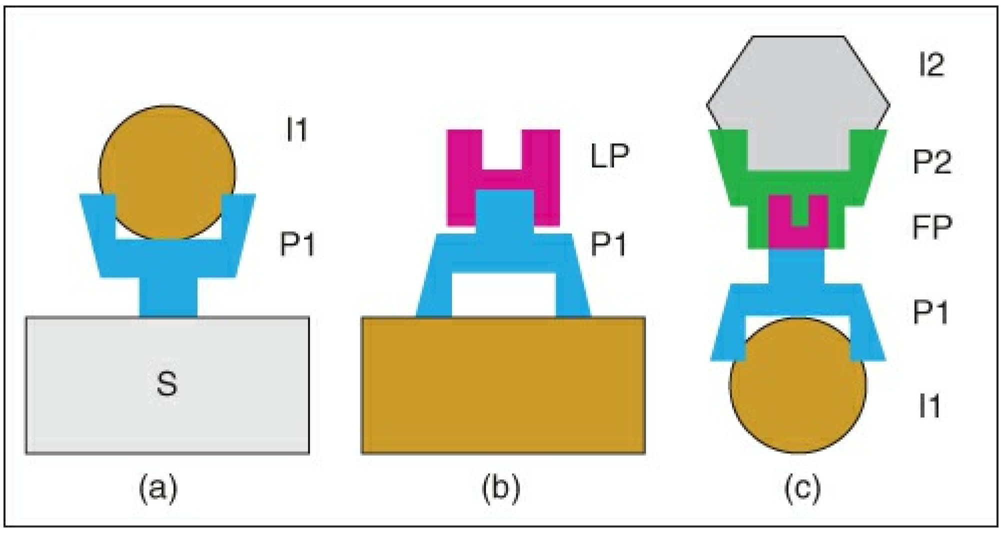

Figure 2.20 (a)–(c) Molecular biomimetics (I1, inorganic-1; I2, inorganic-2; P1 and P2, inorganic-specific proteins; LP, linker protein; FP, fusion protein).

Sarikaya et al. [24] © 2003. With permission of Nature Publishing Group.

Protein bovine serum albumin (BSA) has been used as a scaffold to make Ag and Au nanocrystals (<1 nm) with yellow and red emission, respectively, via a simple, one-pot, solution-phase, green synthetic route (Box 2.10). Controlled binding and assembly of proteins onto inorganics are at the core of biological materials science and engineering with wide-ranging applications such as implants, hard-tissue engineering, genomics, pharmacogenetics, and proteomics. Following the lead of molecular biology, GEPI could be used as a versatile molecular linker and open new avenues in the self-assembly of molecular systems in nanotechnology and nanobiotechnology.

Box 2.10 Bovine Serum Albumin (BSA)-assisted synthesis of Au NPs

In a typical experiment, aqueous $HAuCl_4$ solution (5 ml, 50 mM) is added to BSA solution (10 ml, 3 mg/ml) with vigorous magnetic stirring at room temperature. The mixed solution was vacuumized and kept static under nitrogen protection for 2 h. Then, 0.2 ml of $N_2H_4 \cdot H_2O$ was injected into the vacuumed solution under magnetic stirring. After reaction, the resulting mixed solution was aged under ambient conditions for 24 h.

2.3.10 Molecular Self-Assembly

Nanomaterials can, in principle, be made using both top-down and bottom-up techniques. Self-assembly bridges these two techniques and allows materials to be designed with hierarchical order and complexity that mimics those seen in biological systems. Self-assembly of nanostructured materials holds promise as a low-cost, high-yield technique with a wide range of scientific and technological applications. Nanoparticles of a wide range of materials including a variety of organic and biological compounds as well as inorganic oxides, metals, and semiconductors can be synthesized using chemical self-assembly techniques, which cannot be synthesized by the above-mentioned top-down methods, the most important and obvious of which are molecules. Materials developed by self-assembly are also useful for the following:

- Development of newer methodologies for the synthesis of metal nanoparticles in aqueous medium under ambient conditions without using reducing agents or elevated temperatures.
- Formation of stable supramolecular assembly, by bringing metal nanoparticles close to each other, results in plasmon coupling. This strategy can be effectively utilized for the development of metal nanoparticle-based sensors.
- Supramolecular organization of molecules on surfaces.

Major challenges that lie in the application of organic molecules in electronic devices are (i) precise positioning of organic molecules at predefined locations and the creation of well-defined structures and (ii) interconnecting various functional devices and further integrating into the macroscopic world. Self-assembly approach for nanofabrication addresses many of such requirements and challenges. Detail discussion on these approaches is given in Chapter 6.

2.3.11 Langmuir–Blodgett (LB) Film Formation

The Langmuir–Blodgett films are thin organic films of a thickness of a few nanometers. An organic thin film can be deposited on a solid substrate by various techniques such as thermal evaporation, sputtering, electrodeposition, MBE, adsorption from solution, Langmuir–Blodgett (LB) technique, and self-assembly. The LB technique is one of the most promising techniques for preparing such thin films as it enables (1) the precise control of the monolayer thickness, (2) homogeneous deposition of the monolayer over large areas, and (3) the possibility to make multilayer structures with varying layer composition. An additional advantage of the LB technique is that monolayers can be deposited on almost any kind of solid substrate. Figure 2.21a shows a schematic diagram of an apparatus, known as Langmuir balance, used for depositing LB films. It consists of a Teflon trough to hold the subphase. The trough is thermostated by circulating water in channels placed underneath. The surface area of the trough can be varied by sweeping movable barriers over the surface of the trough. The barrier is made of Delrin, a hydrophilic material, and is heavy enough to prevent any leakage of the monolayer beneath the barrier. The surface pressure and the mean molecular area are continuously monitored during the compression.

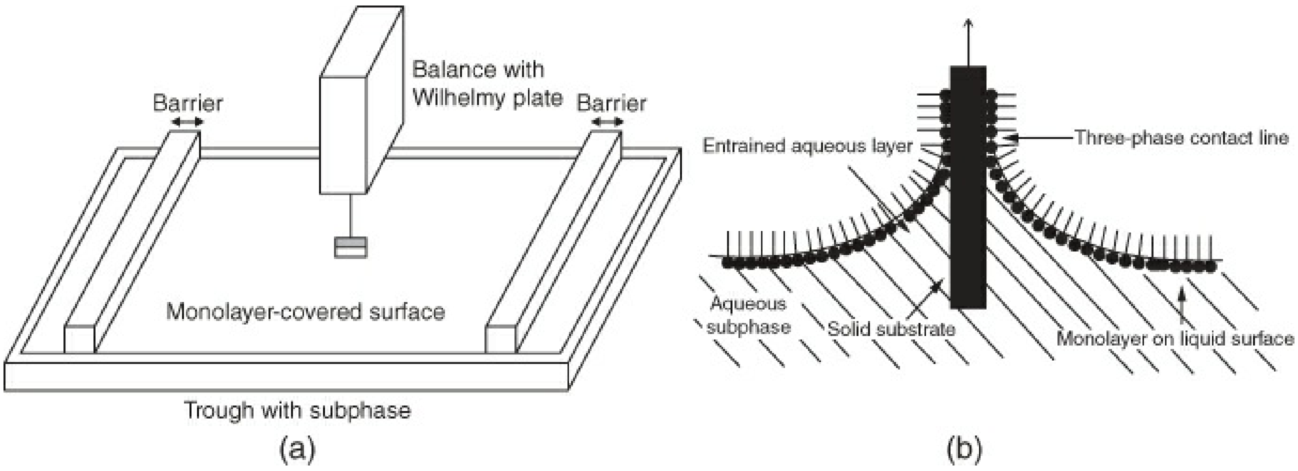

Figure 2.21 Schematic illustration: (a) Langmuir balance; (b) deposition of a floating monolayer on a solid substrate.

With permission, Biolin Scientific. <www.biolinscientific.com/ksvnima>.

The Langmuir film balance can also be used for building up highly organized multilayers of the amphiphiles. This is accomplished by successively dipping a solid substrate up and down through the monolayer while simultaneously keeping the surface pressure constant by a computer-controlled feedback system between the electrobalance measuring the surface pressure and the barrier moving mechanism. Consequently, the floating monolayer is adsorbed to the solid substrate. In this way, multilayer structures of hundreds of layers can be produced. These multilayer structures are commonly called Langmuir–Blodgett or simply LB films. The deposition process is schematically shown in Figure 2.21b. The LB deposition is traditionally carried out in the "solid" phase. The surface pressure is then high enough to ensure sufficient cohesion in the monolayer, for example, the attraction between the molecules in the monolayer is high enough so that the monolayer does not fall apart during transfer to the solid substrate. This also ensures the buildup of homogeneous multilayers. The surface pressure value that gives the best results depends on the nature of the monolayer and is usually established empirically. However, amphiphiles can seldom be successfully deposited at surface pressures lower than 10 mN/m, and at surface pressures above 40 mN/m, collapse and film rigidity often pose problems. When the solid substrate is hydrophilic (glass, SiO_2, etc.), the first layer is deposited by raising the solid substrate from the subphase through the monolayer, whereas if the solid substrate is hydrophobic (HOPG, silanized SiO_2, etc.), the first layer is deposited by lowering the substrate into the subphase through the monolayer. There are several parameters that affect on what type of LB film is produced. These are the nature of the spread film, the subphase composition, and temperature, the surface pressure during the deposition and the deposition speed, the type and nature of the solid substrate, and the time the solid substrate is stored in air or in the subphase between the deposition cycles.

2.3.12 Stabilization and Functionalization of Nanoparticles

Owing to their high reactivity, nanoparticles have a high tendency to build aggregates with respective agglomerates, which could lead to a loss of the desired properties. Therefore, it is often necessary to stabilize the nanoparticles with additional treatments. The commercial success or failure of nanoparticles in a particular application usually depends on the ability to prepare stable dispersions in water or organic fluids with controlled rheology. In turn, the ability to prepare stable nanoparticle dispersions with controlled rheology is enabled by tailoring nanoparticle **coatings**. On the other hand, coating nanoparticles with another material of nanoscale thickness is a simple way to alter the surface properties of nanoparticles. Core–shell structured nanoparticles have been shown to display advanced optical, mechanical, and magnetic properties. One common method to stabilize or modify the reactivity of the nanoparticle is the encapsulation with a molecular or polymeric layer. A thin polymeric shell enables compatibility of the particles with a wide variety of fluids, resins, and polymers. In this way, the nanoparticles retain their original chemical and physical properties, but the coating can be tailored for a wide variety of applications. One example is the Discrete Particle Encapsulation (DPE) method patented by Nanophase Technologies Corporation. Collecting nanoparticles in liquid suspension to prevent agglomeration is another way to ensure the stability of the collected nanoparticle powders. For semiconducting particles, stabilization of the liquid suspension has been demonstrated by the addition of polar solvent; surfactant molecules have been used to stabilize the liquid suspension of metallic nanoparticles.

There are two general methods of stabilizing nanoparticles in aqueous solutions. Firstly by adjusting the pH of the system, the nanoparticle surface charge can be manipulated in such a way that an electrical double layer is generated around the particle. Overlap of two double layers on different nanoparticles causes repulsion and hence stabilization. The magnitude of this repulsive force can be measured via the zeta potential. The second method involves the adsorption of polymers onto the nanoparticles in such a way that the particles are physically prevented from coming close enough for the van der Waals attractive force to dominate. This is termed steric stabilization. A combination of these two mechanisms is called **electrostatic stabilization** and occurs when polyelectrolytes are adsorbed on the nanoparticle surface.

Review Questions

Q1. What do you understand by “top-down” and “bottom-up” approaches for nanosynthesis?

Q2. How MCP method for nanosynthesis is different from mechanical milling?

Q3. What are the basic advantages of electro-expulsion method to produce nanometallic powders?

Q4. Explain the basis of thin-film deposition by sputtering technique.

Q5. What do you understand by reactive-ion etching?

Q6. How can you obtain sputtering of insulating materials?

Q7. Why nanometallic powders produced by electro-expulsion method have greater chemical and metallurgical reactivity?

Q8. What is the main advantage of scanning lithography over photolithography?

Q9. Describe basic principles of electrospinning and its applications in the production of nanofibers.

Q10. How will you differentiate chemical vapor condensation (CVC) and chemical vapor deposition (CVD) techniques for the synthesis of nanoparticles.

Q11. What are the essential parameters required to obtain NPs of nanosized distribution by CVD method?

Q12. What is plasma-enhanced CVD and how it is different from thermal CVD?

Q13. Illustrate versatility of CVD technique giving one example each for the preparation of metals, metal oxide, and silicon carbide nanoparticles.

Q14. How does liquid-phase synthesis differs from gas-phase synthesis for the production of nanoparticles?

Q15. What are the precursors and appropriate solvent systems to obtain (a) metals, (b) alloys, and (c) metal oxides by sonochemical method?

Q16. Nature is known to be the best laboratory to synthesize a variety of nanomaterials. What are the routes it may be following, illustrate with some examples?

Q17. What is self-assembly? How self-assembly approaches are useful in preparing nanostructured materials?

Q18. Distinguish precipitation and sol–gel phenomena. Explain how these techniques are useful for nanosynthesis.

Q19. Enumerate various steps involved in the chemical reduction method for the synthesis of nanomaterials with suitable example.

Q20. How can you obtain stable gold nanoparticles without adding any stabilizers or surfactants?

Q21. Suggest a suitable method for preparing polymer composites.

References

1. O. Masala and R. Seshadri, “Synthesis Routes for Large Volumes of Nanoparticles”, *Ann. Rev. Mater. Res.*, **34** (2004) 41–81.

2. L.S. Wang and R.Y. Hong, “Synthesis, Surface Modification and Characterization of Nanoparticles”, *Advances in Nanocomposites – Synthesis, Characterization and Industrial Applications*, Ed. B. Reddy, InTech, 2011, www.intechopen.com.

3. T. K. Sindhu, R. Sarathi and S. R. Chakravarthy, “Generation and Characterization of Nano Aluminium Powder Obtained Through Wire Explosion Process”, *Bull.Mater. Sci.*, **30** (2007) 187–195.

4. D.C. Tien et al. “Colloidal Silver Fabrication Using the Spark Discharge System and its Antimicrobial Effect, on *Staphylococcus Aureus*”, *Med. Eng. Phys.* **30** (2008), 948–952.

5. Z. Wang, Y. Liu and X. Zen, “One Step Synthesis of Fe_2O_3 Nanoparticles by Laser Ablation”, *Powder Technol.***6** (2006) 65–68.

6. S.W. Kang, “Applications of Soft Lithography for Nano Functional Devices”, *Lithography,* Ed. M. Wang, InTech, 2010, www.intechopen.com.

7. S.Y. Chou, P.R. Krauss, W. Zhang, L. Guo and L. Zhuang,“Sub-10 nm Imprint Lithography and Applications”, *J. Vac. Sci. Technol. B,* **15** (1997) 2897.

8. Y. Liu, J. Goebl and Y. Yin, “Templated Synthesis of Nanostructured Materials”, *Chem. Soc. Rev.*, **42** (2013) 2610–2653.

9. L. Ding, Y. Li, H. Chu, X. Li and J. Liu, “Creating Cadmium Sulphide Nanostructures Using AFM Dip Pen Nanolithography”, *J. Phys. Chem. B,* **109** (2005) 22337–22340.

10. K. C. Pingali, D. A. Rockstraw, and S. Deng, “Silver Nanoparticles from Ultrasonic Spray Pyrolysis of Aqueous Silver Nitrate”, *Aerosol Sci. Technol.*, **39**(10), (2005) 1010–1014.

11. S.G. Kim, J. W. Yang, J. T. Lee and J.Y. Kim, “Highly Conductive PEDOT: PTS Films Interfacially Polymerized Using Electro Spray Deposition and Enhanced by Plasma Doping”, *Jpn. J. Appl. Phys.,* **53**(3), (2014) article id.035501.

12. J. M. Deitzel, J. Kleinmeyer, D. Harris and N. C. Beck Tan, “The Effect of Processing Variables on the Morphology of Electrospun Nanofibers and Textiles”, *Polymer*, **42** (2001) 261–272.

13. D. Li and Y. Xia, “Electrospinning of Nanofibers: Reinventing the Wheel?”, *Adv. Mater.*, **16** (2004) 1151–1170.

14. S. Kei, 2008. http://commons.wikimedia.org/wiki/File:ThermalCVD.PNG and http://commons.wikimedia.org/wiki/File:PlasmaCVD.PNG.

15. A. Shukla, M.K. Patra, M. Manoth, S. Songara, V.K. Singh, S. R. Vadera and N. Kumar, “Preparation and Characterization of Biocompatible and Water-Dispersible Superparamagnetic Iron oxide Nanoparticles (SPIONS)”, *Adv. Sci. Lett.*, **3** (2010) 1–7.

16. M. Manoth, K. Manzoor, M. K. Patra, P. Pandey, S.R. Vadera and N. Kumar, “Dendigraft Polymer-Based Synthesis of Silver Nanoparticles Showing Bright Blue Fluorescence”*, Mater. Res. Bull.*, **44** (2009) 714–717.

17. V. Gupta, M. K. Patra , A. Shukla, L. Saini, S. Songara, R. Jani, S. R. Vadera and N. Kumar, “Synthesis of Core–Shell Iron Nanoparticles from Decomposition of Fe–Sn Nanocomposite and Studies on their Microwave Absorption Properties”, *J. Nanopart. Res.*, **14** (2012) 1271–1280.

18. G. Kaune et al., “Hierarchical Structured Titania Film Prepared by Polymer/Colloidal Templeting”, *Appl. Mater.*, **1** (2009) 2862–2869.

19. L.L. Hench, J. K. West, “The Sol–Gel Process”, *Chem. Rev.*, **90** (1990) 33–72.

20. H. Xu, B. W. Zeiger and K. S. Suslick, “Sonochemical Synthesis of Nanomaterials”, *Chem. Soc. Rev.*, **42** (2013) 2555–2567.

21. V. Sáez and T. J. Mason, “Sonoelectrochemical Synthesis of Nanoparticles”, *Molecules,* **14** (2009) 4284–4299.

22. Q. Li, H. Li, V. G. Pol, I. Bruckental, Y. Koltypin, J. Calderon-Moreno, I. Nowike and A. Gedanken, “Sonochemical Synthesis, Structural and Magnetic Properties of Air-Stable Fe/Co Alloy Nanoparticles”, *New J. Chem.*, **27** (2003) 1194–1199.

23. D.A. Bazylinski and R.B. Frankel, “Magnetosome Formation in Prokaryotes”, *Nat. Rev. Microbiol.* **2** (2004) 217.

24. M. Sarikaya, C. Tamerler, A.K.Y. Jen, K. Schulten, and F. Baneyx , “Molecular Biomimetics: Nanotechnology Through Biology”, *Nat. Mater.*, **2**(2003) 577–585.

25. K. B. Narayan and N. Shakthivel, “Extracellular Biological Synthesis of Gold Particle”, *Colloids in Biotechnology,* Ed. M. Fanun, Surfactant science series volume152, CRC Press, 2011.

26. S. Prabhu and E. K Poulose, “Silver Nanoparticles: Mechanism of Antimicrobial Action, Synthesis, Medical Applications, and Toxicity Effects”, *Int. Nano Lett.*, **2** (2012) 32–42.

Chapter 3
Characterization Tools for Nanomaterials

3.1 Introduction

The fundamentals of nanoscience and nanotechnology lie in the fact that properties of the material change dramatically when their size is reduced to the nanoscale range. Compared to bulk materials, nanomaterials may exhibit changed or additional properties, which are based, for example, on their increased surface-to-volume ratio or quantum physical effects. In order to cope with these modified properties, it seems reasonable to characterize nanomaterials by the following parameters:

- Shape, size of primary particles, aspect ratio
- Degree of aggregation and agglomeration
- Size distribution
- Specific surface
- Surface chemistry (surface charge, functional groups, catalytic activity)
- Crystal structure
- Surface modification (chemical composition, type of modification)

The observation of materials at nanoscale is essential for research and developmental activities in nanoscience and nanotechnology. Characterization and imaging of the nanoscale materials is an emerging and challenging field for scientists and technologists. Nanotechnology has motivated an upsurge in research and developmental activities on invention and innovation of sophisticated nanocharacterization techniques to allow a better control of morphology, size, and dimensions of material in nanorange. Nanostructured materials are subjected to nearly all types of chemical and physical analyses possible. Due to their small sizes, there is a significant focus on tools with high spatial resolution. In fact, the credit of success of nanoscience and nanotechnology largely goes to the development of a variety of advanced instruments that have provided the facility to see the objects at an atomic scale [1, 2]. Invention of revolutionary instruments, namely, Scanning Tunneling Microscope (STM) and Atomic Force Microscope (AFM) in the mid-1980s opened the doors to nanoworld when scientists were able to observe and analyze nanoscale objects, understood their behavior, and imagined the novel ways to manipulate nanomaterials [3–5]. Characterization of nanomaterials is accomplished using a variety of different techniques drawn from interdisciplinary areas. A summary of investigative methods for the characterization of nanoparticles is listed in Table 3.1.

Table 3.1 Common Investigation Techniques for the Characterization of Nanoparticles

Techniques	Characterization Parameters
Dynamic light scattering (DLS)/particle size analyzer	Size and size distribution of nanoparticles suspended in a liquid phase
Zeta potential analyzer	Surface charge of nanoparticles in aqueous solutions or suspensions
Scanning electron microscopy (SEM)	Shape and surface structure
Transmission electron microscopy (TEM)	Size, shape, and morphology (including internal structure), especially useful for biological specimen
Atomic force microscopy (AFM)	Shape and surface morphology of nanoparticles with high lateral and vertical resolutions
Scanning tunneling microscopy (STM)	Surface images with atomic-scale lateral resolution; modification of material at atomic/ molecular/nanometer scale with high precision
Laser scanning confocal microscopy (LSCM)	Noninvasive technique provides information about migration of nanoparticles into bio-barrier; 3D morphology of nanoparticles
Brunauer–Emmett–Teller (BET) technique	Surface area analysis, porosity, and adsorption capability
X-ray diffraction (XRD) technique	Crystal structure, phase, and average particle size
X-ray photoelectron spectroscopy (XPS, ESCA)	Chemical composition (both elemental and chemical states) information on nanoparticle's surface
Fourier transform infrared spectroscopy (FTIR)	Assisted analytical tool for chemical composition
Differential scanning calorimetry (DSC)	Thermal analysis and phase transition studies
High-performance liquid chromatography (HPLC)	Detection, separation, and quantification of nanoparticles/nanomaterials with different particle size

Characterization of physical, chemical, and biological properties on a nanoscale level is an essential prerequisite for commercialization and risk assessment of nanomaterials and to investigate how nanomaterials behave under different chemical and physical conditions; how they move and distribute in different environmental compartments such as water, soil, and air; and how they interact with the biosphere and the human organism. Present chapter gives a concise account of essential analytical imaging and spectroscopic techniques in characterizing the physical and chemical properties of the nanostructured materials, namely, nanoparticles, nanoporous materials, nanostructured surfaces, and so on, with at least one dimension in the nanoscale regime (1–100 nm).

3.2 Imaging Through Electron Microscopy

Optical microscopy is the classical method for obtaining a detailed information about the physical nature of surfaces. The resolution of optical microscopy is limited by diffraction effects to the wavelength of light. An optical microscope uses visible light (i.e., an electromagnetic radiation) and a system of lenses to magnify the images of small samples [1]. For this reason, it is also called a light microscope. Optical microscopes are the oldest and simplest of the microscopes. Resolution, that is, the ability to discriminate between two closely spaced objects, is an important aspect of any microscope. The resolution limit of an optical microscope is imposed by the wavelength of the visible light. As a general rule of thumb, the resolution is about half the wavelength used in the measurement. Visible light has wavelengths between 400 and 700 nm. The resolving power of an optical microscope is around 0.2 µm or 200 nm. Thus, for two objects to be distinguishable, they need to be separated by at least 200 nm. Single objects smaller than this limit are not distinguishable; they are seen as “fuzzy objects.” This is known as the “diffraction limit” of visible light. In order to overcome the limitations set by the diffraction limit of visible light, other microscopes have been designed that use other beams rather than light; they use electron beams to illuminate the sample. Wavelength of electrons is in picometer range, it is natural to expect a resolution of an electron microscope (EM) to the order of picometer. However, this is not the case since electromagnetic lenses also have aberrations, and moreover, it is not possible to get a coherent electron beam. The limitations of imaging using electrons instead of visible light are primarily one cannot see the electron beam, and secondly, electrons do not freely travel through air because there are enough molecules in air to easily absorb an electron beam. Therefore, the electron source, lenses, and sample must all be kept under vacuum. Another limitation is that since electrons are electrically charged, the sample needs to be conductive enough to dissipate this charge. Electron-stimulated microscopic imaging techniques fall into two categories: **electron microscopy** and **scanning probe microscopy (SPM)**. Electron microscope (EM) uses finely focused beam of electrons as the source for illumination of sample and exploits the wave nature of electron to obtain an image. In SPM, a probe of nanometer dimensions is scanned over the surfaced material and the techniques are capable of resolving details of surface down to atomic level and reveal 3D details unlike optical microscope and EM.

Essentially a microscope consist of an illuminating source, a condenser lens to converge the beam on to the sample, an objective lens to magnify the image, and a projector lens to project the image to be photographed or stored. Electron microscope uses finely focused beam of electrons as the source for illumination of sample and exploits the wave nature of electron to obtain an image [6–8]. Electron microscopes have much greater resolving power than light microscopes that use electromagnetic radiation and can obtain much higher magnifications of up to two million times, while the best light microscopes are limited to magnifications of 2000 times. The maximum usable magnification is equal to the resolving power of the eye divided by the resolving power of the instrument. The resolving power of human naked eye is ~250 µm, and therefore, the meaningful minimum magnification with light microscope with a resolving power as 250 nm is to the order of 1000. Theoretically, resolving power of an electron microscope would be 0.0027 nm for electron energy of 50,000 V, reaching a magnification of the order of 10^9. However, this is not achieved due to the aberration of the electromagnetic lenses and complex nature of electron–sample interaction. Another limitation of an optical microscope is its rather poor depth of field because of its large aperture angle, whereas an electron microscope that has a long working distance (the distance between the sample and the final lens) and a small aperture opening results in a very shallow aperture angle and hence it has a good depth of field.

Fundamental properties of an electron are summarized in Table 3.2. Both electron and light microscopes have resolution limitations, imposed by the wavelength of the radiation they use. The greater resolution and magnification of the electron microscope is because the wavelength of an electron (de Broglie wavelength) is much smaller than that of a photon of visible light. The de Broglie wave equation ($\lambda = h/mv$) relates the velocity (v) of electron with its wavelength (λ), where h is Planck's constant. Thus, an electron of charge e and mass m when passes through a potential difference of V volts, it acquires a kinetic energy of $½mv^2 = eV$, giving $v = (2eV/m)^{1/2}$ and $\lambda = h/(2meV)^{1/2}$. However, at high potential, when electron velocity approaches the speed of light (c), relativistic corrections to mass is applied; accordingly, the estimated velocity (v) and the wavelengths (λ) of electrons achieved at different acceleration voltage are included in Table 3.3. The resolution (d) can be expressed as $d = 0.61\lambda/n.\sin\theta$, where n is the refractive index of the medium and θ is the semi-angular aperture of the lens. The quantity ($n.\sin\theta$) is the numerical aperture (NA) of the lens. The theoretical limit of the resolving power of an instrument is determined by the wavelengths of the electron beam used and the numerical aperture of the system. The resolving power R of an instrument is defined as $R = \lambda/2$ NA. The NA (usually ~1.0) is engraved on each objective and condenser lens system and is a measure of electron-gathering ability of the objective and electron-providing ability of the condenser.

Table 3.2 Fundamental Properties of Electrons

Charge (e)	(−) 1.602×10^{-19} C
Rest mass (m_e)	9.109×10^{-31} kg
Rest energy ($m_e c^2$)	511 keV
Kinetic energy (charge × voltage)	1.602×10^{-19} N m (for 1 V potential)
Plank's constant (h)	6.625×10^{-34} N m s
Speed of light in vacuum (c)	2.998×10^8 m/s

Table 3.3 Electron Wavelength and Velocity at Different Acceleration Voltage

V (volts)	λ (nm)	v ($\times 10^{10}$ cm/s)
50,000	0.0055	1.283
100,000	0.0039	1.699
1,000,000	0.0012	2.917

Conceptually, electron microscopes are similar to an optical microscope in the sense that both microscopes use a radiation to visualize a sample: photons in the case of an optical microscope; electrons (i.e., particles) in the case of electron microscopes. Electrons are negatively charged particles within the atom. Unlike light photons, electrons cannot be focused by glass lenses, but electromagnets are capable of guiding and concentrating electrons on to the specimen. Electrons are a type of ionizing radiation, which are capable of removing one of the tightly bound inner-shell electrons from the attractive field of the nucleus and produces many of the secondary signals from the specimen as some of the electrons are transmitted through the sample, get backscattered, or emit secondary electrons that are used in electron microscopy as schematically shown in Figure 3.1.

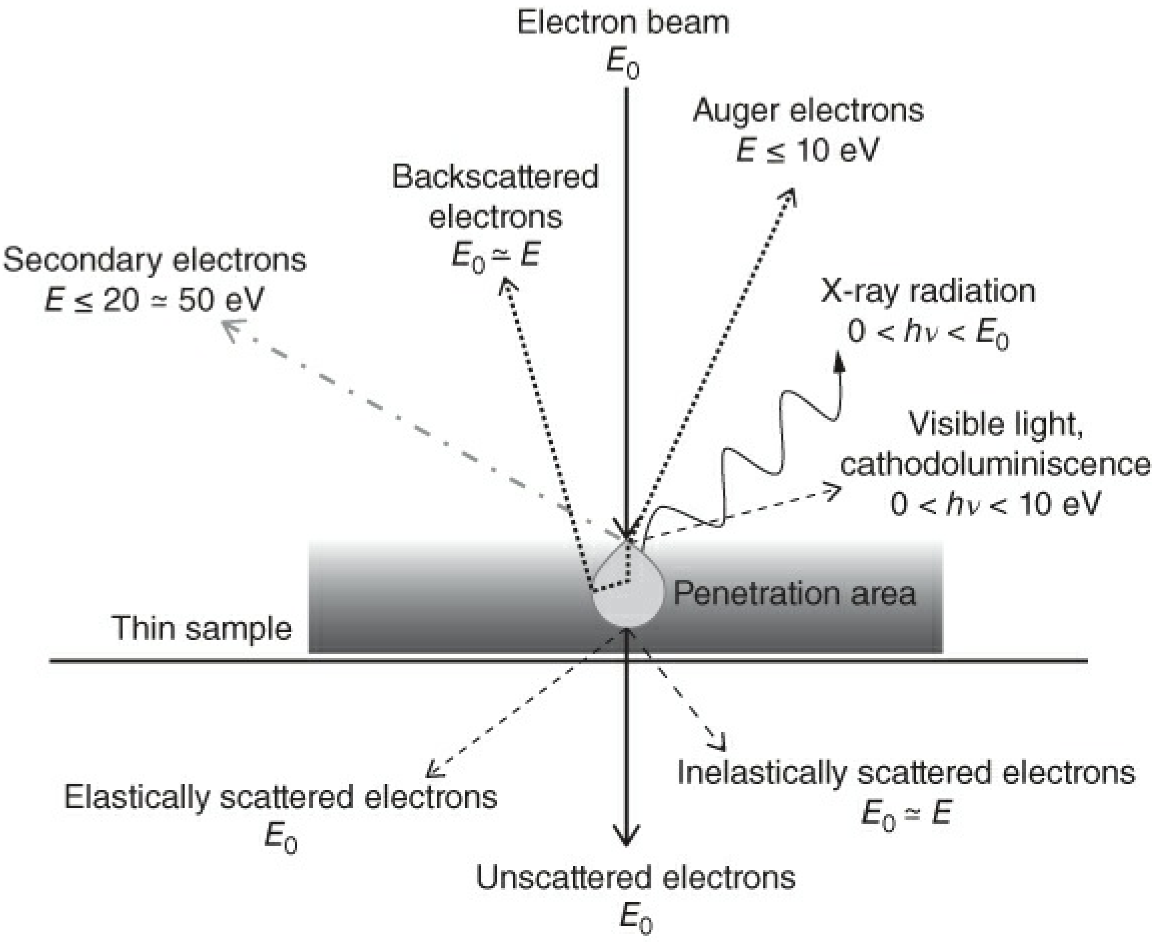

Figure 3.1 Electron beam-induced processes and their relative energies.

i. Sources of electrons

Electron gun: Electron gun provides a stable beam of electrons used in electron microscopy. The most common form of an electron gun is a thermionic emitter, wherein the work function of the metal is overcome by the surface temperature of the filament. Electron guns are of two types:

1. Thermionic gun
2. Field emission gun

The typical **thermionic electron gun** consists of three parts: a tungsten filament, a grid cap (Wehnelt cap) surrounding the filament, and the anode. Figure 3.2a and b shows the schematic of the most common electron gun. It consist of a heated (~2000–2700 K) tungsten filament of 100 µm diameter and bent into a shape of hairpin with a V-shaped tip. The cathodic filament is maintained at a potential of 1–50 kV with respect to anode contained in the gun. The grid cap is biased negatively with respect to the filament. The effect of electric field in the gun is to cause the emitted electrons to converge on a tiny spot called the **crossover** having a diameter d_0. The confined beam of electrons is accelerated to the anode held at ground potential, thus creating an electron beam that streams down the microscope column. The electrons are accelerated to energy between 1 and 30 keV. Cathodes constructed in the form of lanthanum hexaboride (LaB_6) rods are also used in electron guns when greater brightness is desired. LaB_6-based thermionic source is expensive and requires a better vacuum system to prevent oxide formation, which causes the efficiency of the source to deteriorate rapidly. The filament characteristics are given in terms of brightness, as current/area × solid angle (A/cm^2. steradian). The filament gradually evaporates at high operative temperature due to high operative current and reduces the filament life.

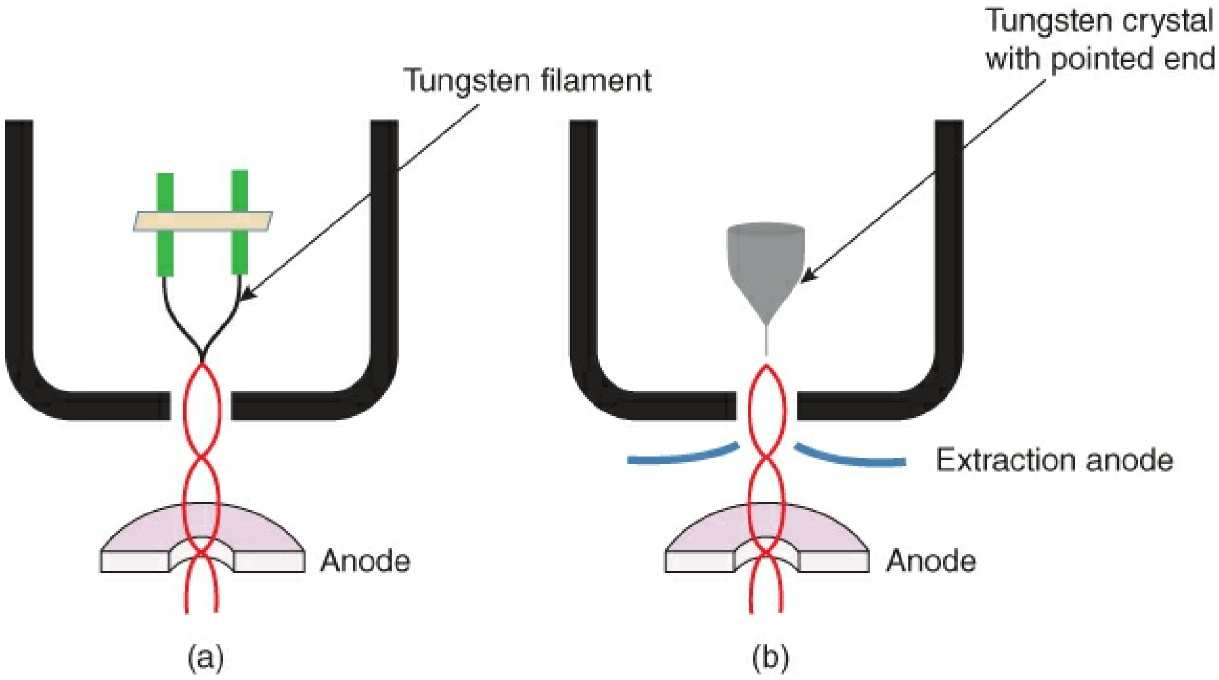

Figure 3.2 Schematic of electron gun: (a) tungsten filament Wehnelt thermionic gun; (b) field emission gun.

Courtesy: NPTEL, IIT-M, India.

Field emission source is a tungsten or carbon cathode shaped up so that it has a very sharp tip (100 nm or less) held at a high potential, the electric field at the tip is so intense (>10^7 V/cm) that electrons are produced by a "tunneling process" in which no thermal energy is required to free the electrons from the potential barrier that usually prevents their emission. Field emission sources provide a beam of electrons that have a much smaller crossover diameter as compared to thermionic sources. These types of sources are fragile and also require better vacuum than thermionic sources; therefore, field emission guns are employed for high-resolution work only. Table 3.4 gives a comparative overview of different electron guns in terms of size, brightness, energy, life, crossover diameter, and vacuum required.

Table 3.4 Comparative Overview of Characteristics of Different Electron Guns

Emission	Thermionic		Field Emission
	W	LaB_6	W/C
Size (nm)	1×10^5	2×10^4	0.2
Brightness (A/cm^2 sr)	10^4–10^5	10^5–10^6	10^7–10^9
Energy spread (eV)	1–5	0.5–3.0	0.2–0.3
Operating lifetime (h)	>20	>100	>300
Vacuum (torr)	10^{-4}–10^{-5}	10^{-6}–10^{-7}	10^{-9}–10^{-10}
Crossover diameter	50 µm	10 µm	10 nm

ii. Electron Optics: In optical microscopy, optical lenses are used where focus is achieved through light refraction, whereas in electron microscopy electromagnetic lenses are used where focus is achieved through Lorentz forces as illustrated in Figure 3.3. Electromagnetic lens consists of a coil of copper wires enclosed in a cylindrically symmetrical iron casing. A current through the coils creates a magnetic field in the bore of the pole pieces. The rotationally symmetric magnetic field is inhomogeneous in such a way that it is weak in the center of the gap and becomes stronger close to the bore. Electrons close to the center are less strongly deflected than those passing the lens far from the axis. The overall effect is that a beam of parallel electrons is focused into a spot (so-called crossover). In a magnetic field, an electron experiences the Lorentz force *F*:

$$\boldsymbol{F} = -e(E + v \times \boldsymbol{B})$$

$$|\boldsymbol{F}| = evB\sin(v, \boldsymbol{B})$$

where *E* and ***B*** represent strength of electric field and magnetic field; *e* and *v* represent the charge and velocity of electrons, respectively. The focusing effect of a magnetic lens, therefore, increases with the magnetic field ***B***, which can be controlled via the current flowing through the coils. As it is described by the vector product, the resulting force ***F*** is perpendicular to ***v*** and ***B***. This leads to a helical trajectory of the electrons and to the magnetic rotation (image is rotated with respect to the object). The degree of rotation depends on the strength of magnetic lens, and the focal length can be altered by changing the strength of the current. Electron microscope contains two types of magnetic lenses: condenser and objective lens system. The magnetic condenser and objective lens system reduce the spot size of electron beam to a diameter of 2–10 nm when it reaches the specimen. The condenser lens system, which consists of one or more lenses, is responsible for the throughput of the electron beam reaching the objective lens; and the objective lens determines the size of the beam hitting the sample surface.

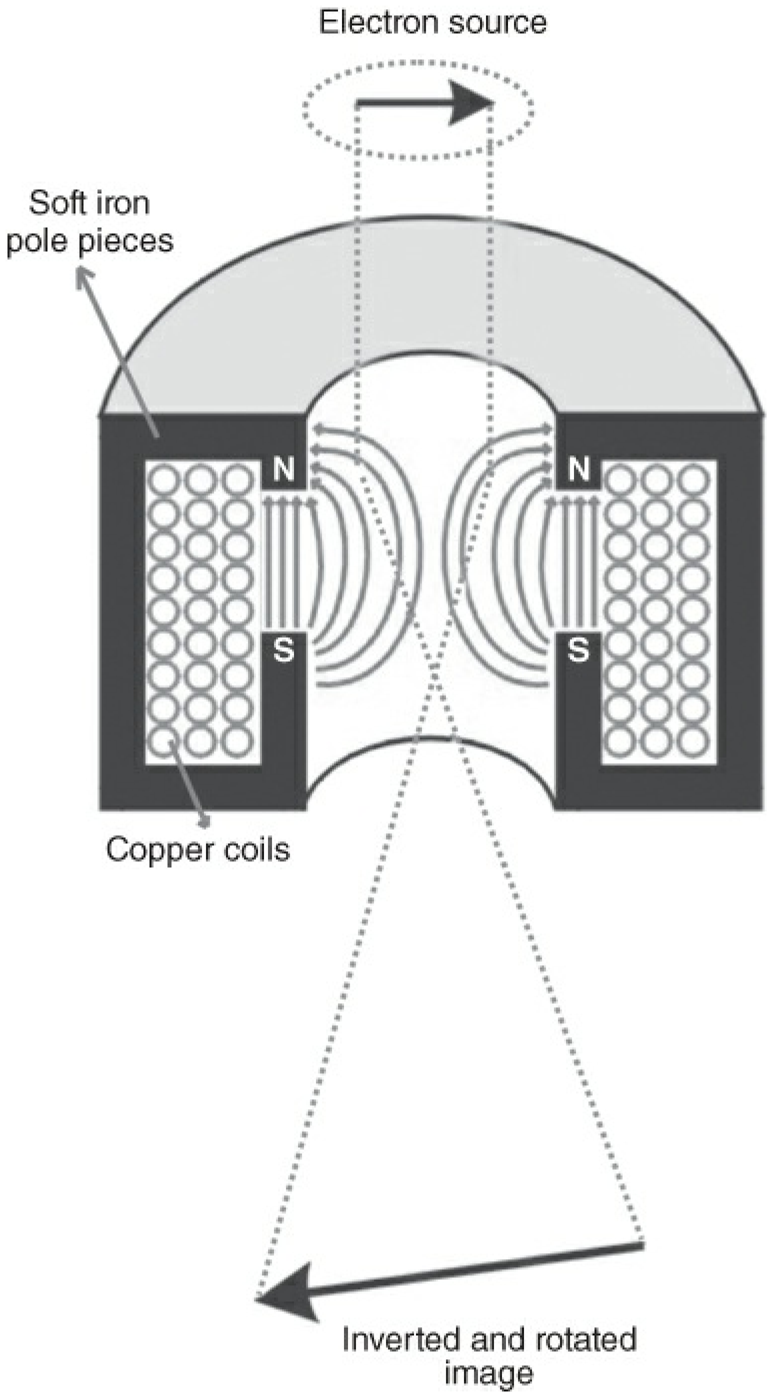

Figure 3.3 Electromagnetic lenses.

Adapted from http://www.microscopy.ethz.ch/lens.htm.

There are two modes of a microscope: a **scanning mode**, when a probe beam is scanned over the surface and image is created point by point, and a **transmission mode**, where probe beam passes through the specimen and differentially refracted and absorbed and image is created. Accordingly, there are two important types of electron microscopes: **scanning electron microscope (SEM)** and **transmission electron microscope (TEM)**. Although scanning and transmission electron microscopy methods have many similarities, both methods use electron as the source for illumination, however, differing in many other aspects [9]. In TEM, the electron beam passes through the sample specimen whereas in SEM, the electron beam scans over the surface. Scanning electron microscopy can be thought of as providing images of external morphology, similar to those accessed by the human eye. In contrast, transmission electron microscopy probes the internal structure of solids and gives us information about microstructural detail that is inaccessible to the eye.

3.2.1 Scanning Electron Microscope (SEM)

A SEM is a tool for seeing the otherwise invisible world of microspace (1 μm = 10^{-6} m) and nanospace (1 nm = 10^{-9} m). By using a focused high-energy beam of electrons, the SEM reveals levels of detail and complexity inaccessible by light microscopy. SEMs can magnify an object from about 10 times up to 300,000 times. A scale bar is often provided on an SEM image; from this, the actual size of structures in the image can be calculated. As the images are created without light waves, they are black and white. Very high-resolution images of the dimensions of 1–5 nm can be obtained. The surface structure of polymer composites, fracture surfaces, nanofibers, nanoparticles, and nanocoating can be imaged through SEM with great clarity. In tissue engineering, the SEM images are the prime characterization technique for viewing, cell development and growth, scaffold construction, and so on. The SEM provides the competent user with an advantage over the light microscope (LM) in three key areas:

1. *Resolution at high magnification*. Resolution can be defined as the least distance between two closely opposed points, at which they may be recognized as two separate entities. The best resolution possible in an LM is about 200 nm, whereas a typical SEM has a resolution of better than 10 nm (typically 5 nm).
2. *Depth of field*. It is the height of a specimen that appears in focus of an image – more than 300 times the depth of field compared to the LM. This means that great topographical detail can be obtained. The 3D appearance of the specimen image is the most valuable feature of the SEM. This is because such images, even at low magnifications, with much more information can be obtained about a specimen than is available using the LM.
3. *Microanalysis*. It is the analysis of sample composition that includes information about chemical composition. In addition, crystallographic, magnetic, and electrical characteristics are also possible with modern instrumentation.

Basic principle: When a finely focused beam of electrons impinges on the surface of the solid sample and interacts with the atom of sample, several signals in the form of backscattered electrons, secondary electrons, Auger electrons, and characteristic X-rays are generated from the surface, which contains information about surface topography and composition of specimen. Figure 3.4a and b shows signals used in SEM, which are generated by electron beam–sample interactions. The interactions of a solid with an electron beam can be divided into two categories: *elastic* interactions that affect the trajectories of the electrons in the beam without altering their energies significantly, and *inelastic* interactions that result in transfer of a part of all of the energy of the electrons to the solid. The excited solid then emits secondary electrons, Auger electrons, X-ray, and sometimes longer wavelength photons.

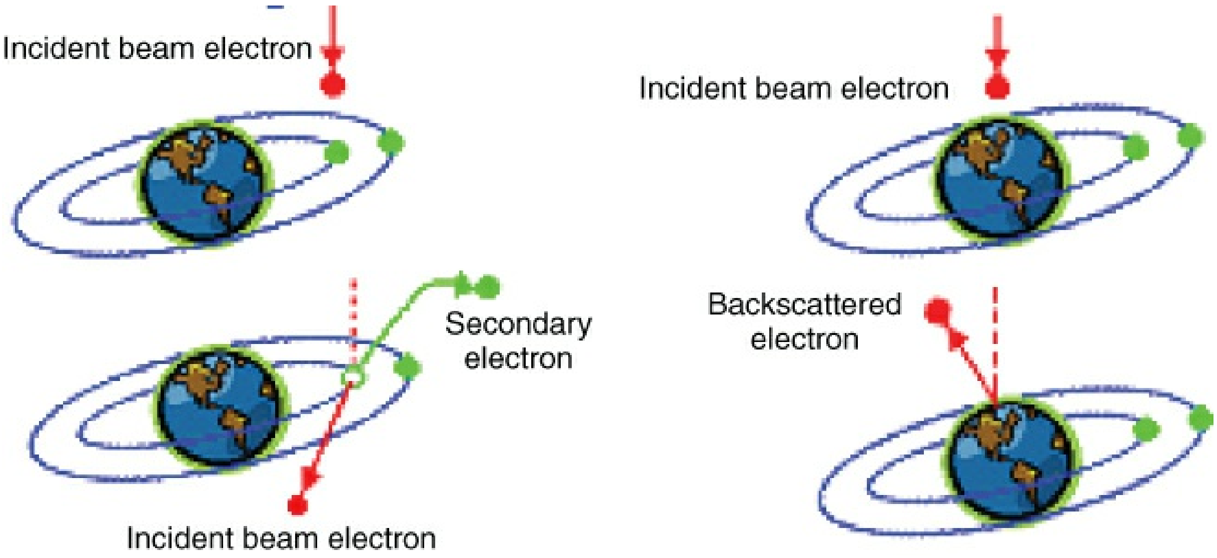

Figure 3.4 Electron transition path for secondary electron and backscattered electron used in SEM.

In a typical SEM, a source of electrons is focused into a beam, with a fine spot size of ~5 nm, having energy ranging from a few hundred electron volts to 50 keV, that is rastered over the surface of the specimen by deflection coils. As the electron strikes and penetrate the surface, a number of interactions occur, which result in the emission of electrons and photons from the sample, and the SEM images are produced by collecting the emitted electrons on a cathode ray tube (CRT). Basic components of a SEM are shown in detail in Figure 3.5a and b.

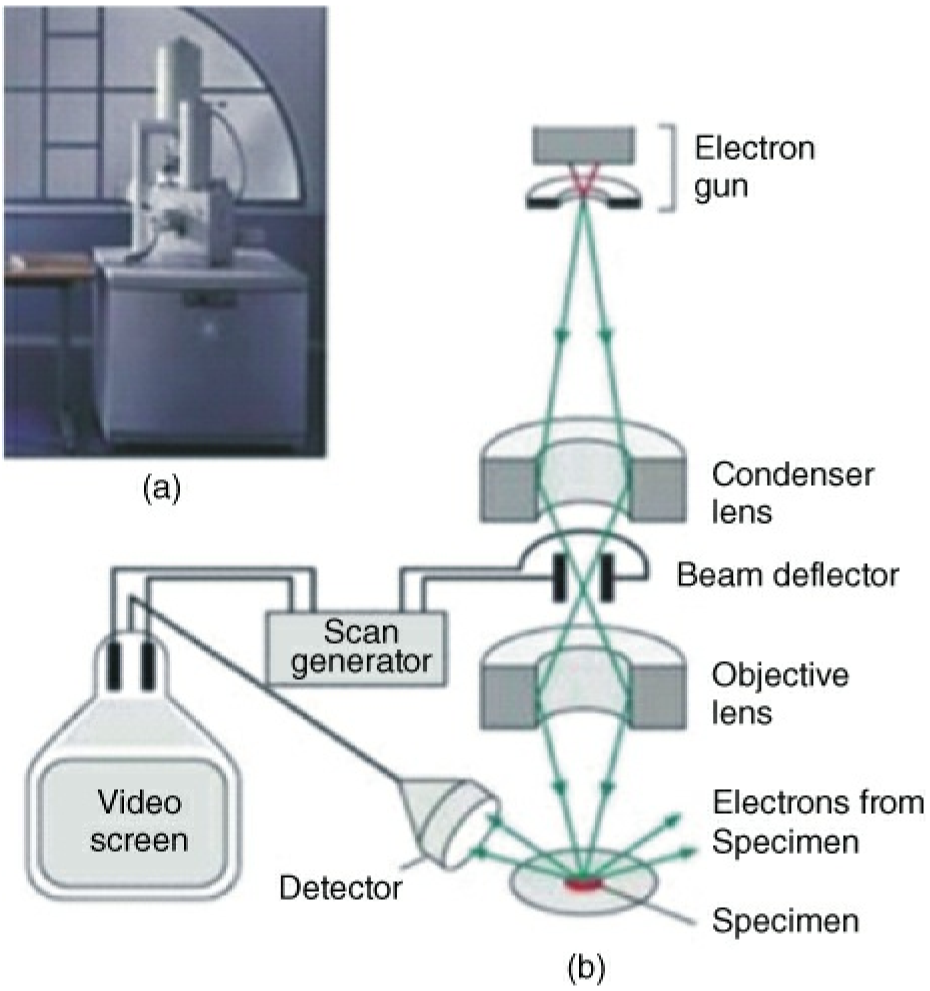

Figure 3.5 (**a**, **b**) Principal features of a scanning electron microscope.

Alberts et al. [9], © 2002. With permission of Garland Publishing Inc.

Various SEM techniques are differentiated on the basis of what is subsequently detected and imaged. The principle images produced in the SEM are of three types: secondary electron images, backscattered electron images, and elemental X-ray maps. A high-energy primary electron interacting with an atom results in either inelastic scattering (deflecting the electrons with loss of energy) with atomic electrons or elastic scattering (deflecting the electrons with no loss of energy) with the atomic nucleus. In an inelastic collision with an electron, the primary electron transfers a part of its energy to the other electron. When the energy transferred is large enough, the other electron will emit from the sample. If the emitted electron has the energy of less than 50 eV, it is referred to as **secondary electron**. Backscattered electrons are the high-energy electrons that are elastically scattered and essentially possess the same energy as the incident or primary electrons. The number of secondary electrons is generally one-half to one-fifth or less the number of backscattered electrons. Secondary electrons are produced as a result of interactions between energetic beam electrons and weakly bound conduction electrons in the solid, which leads to ejection of the conduction band electrons with a few electron volts of energy. Secondary electrons are produced from a depth of only 50–500 Å and exit in a beam that is slightly larger in diameter than the incident beam. Beam of backscattered electrons has a much larger diameter than the incident beam. The diameter of backscattered beam is one of the factors limiting the resolution of an electron microscope. The probability of backscattering increases with the atomic number of the sample material. Although backscattering images cannot be used for elemental identification, useful contrast can develop between regions of the specimen that differ widely in atomic number *Z*.

Instrumentation: In a typical SEM, the electron beam passes through pairs of scanning coils or pairs of deflector plates in the electron column to the final lens, which deflects the beam horizontally and vertically so that it scans in a raster manner over a rectangular area of sample surface. Electronic devices are used to detect and amplify the signals and display them as an image on a CRT in which the raster scanning is synchronized with that of the microscope. Therefore, the image displayed is the distribution map of the intensity of the signal being emitted from the scanned area of the specimen. The typical laboratory SEM has three components:

1. the microscope column, including the electron gun at the top, the column, through which the electron beam travels, the sample chamber at the base, detectors for signals of interest and output display device
2. the computer that drives the microscope, with the additional bench controls
3. ancillary equipment for composition analyses

Furthermore, infrastructure requirements includes vacuum system, cooling system, vibration free floor, room free of ambient magnetic and electric fields. SEMs always have at least one detector, usually a secondary electron detector. Mostly additional detectors are also there in SEMs. The specific capabilities of a particular instrument are critically dependent on which detectors it accommodates.

Scanning the sample specimen with SEM: Scanning with an SEM is accomplished by the two pairs of electromagnetic coils located within the objective lens (see Figure 3.4); one pair deflects the beam in the *x*-direction across the sample, and the other pair deflects it in the *y* direction. Scanning is controlled by applying an electrical signal to one pair of scan coils, such that the electron beam strikes the sample to one side of the center axis of the lens system. By varying the electrical signal to this pair of coils (i.e., the *x*-coils) as a function of time, the electron beam is moved in a straight line across the sample and then returned to its original position. After completion of the line scan, the other set of coils (*y* coils in this case) is used to deflect the beam slightly, and the scanning of the beam using the *x* coils is repeated. Thus, by rapidly moving the beam, the entire sample surface can be irradiated with the electron beam. The signals to the scan coils can be either analog or digital. Digital scanning has the advantage of very reproducible movement and location of the electron beam. The signal from the sample can be encoded and stored in digital form along with digital representation of the *x* and *y* positions of the beam.

Samples and sample holder: The specimen for SEM should be conductive for the electron beam to scan the surface and that the electrons have a path to ground for conventional imaging. Examining nonconducting materials particularly polymers and biological material may present other difficulties, such as thermal degradation, radiation damage, and sample volatility in the high vacuum. Nonconductive solid specimen is generally coated with a layer of conductive material by low-vacuum sputter coating or high-vacuum evaporation.

Sample chambers are designed for rapid changing of samples. Large-capacity vacuum pumps are used to hasten the switch from ambient pressure to ~10^{-4} torr or less for conventional SEMs. The sample holder, or stage, in most instruments is capable of holding samples many centimeters on an edge. Furthermore, the stage can be moved in the *x*-, *y*-, and *z*-directions, and it can be rotated about each axis. As a consequence, the surfaces of most samples can be viewed from almost any perspective. Environmental SEMs use much higher pressures in the sample chamber and allow for variations in temperature and gas composition.

Detector: In SEM, two types of electrons come out of the sample: secondary electrons having energies of a few electron volts and the backscattered electrons with higher energies. The most common detectors in SEM are scintillation detectors. The detector consists of a doped glass or plastic target that emits a cascade of visible photon when struck by an electron. Photons are conducted by a light pipe to a photomultiplier tube that is housed outside the high-vacuum region of the instrument. Typical gains with scintillation detectors are 10^5–10^6.

A scintillator–photomultiplier detector based on the Everhart–Thornley design is shown in Figure 3.6. It is used to detect the secondary electrons emitted from the specimen. Low-energy secondary electrons (trajectories shown by dashed lines) are collected by applying a suitable bias (from −50 to +300 V) to the Faraday grid. These electrons are further accelerated in order to give them sufficient energy to scintillate the phosphor that is highly efficient at converting the energy contained in the electrons into ultraviolet (UV) light photons (4000 Å). The response time of phosphor is fast and permits high-resolution scanning. Semiconductor detector consisting of flat wafer of a semiconductor is also used in electron microscopy. When high-energy electrons strike the detector, electron–hole pairs are produced that result in an increase in conductivity. Current gains with typical semiconductor detector are 10^3–10^4. The X-rays produced in the SEM are usually detected and measured with energy dispersive system. Characteristic X-rays are used for qualitative and quantitative information about the sample.

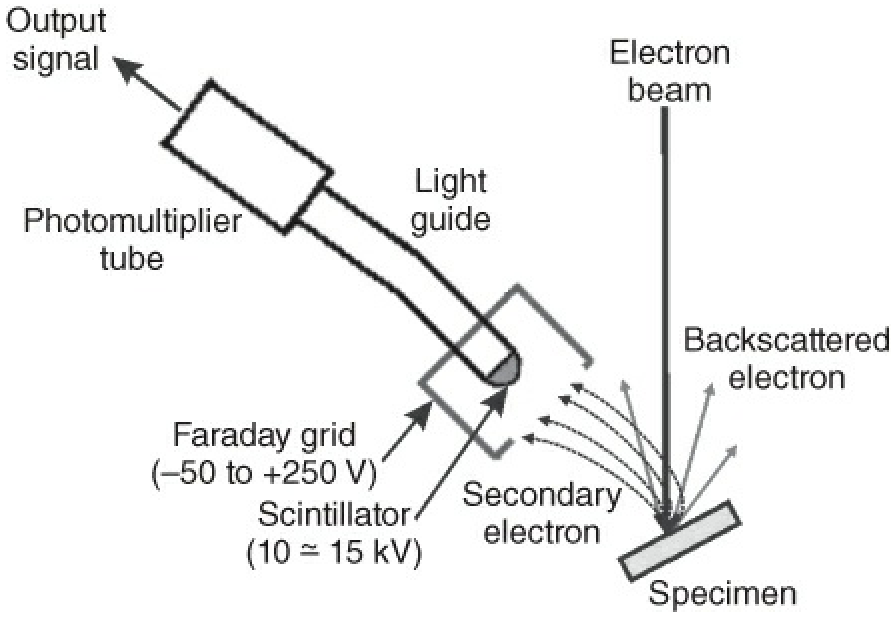

Figure 3.6 A secondary electron scintillator–photomultiplier detector.

Adapted from Potts, [10] © 1987, Springer Science.

Applications: SEM is one of the most widely used techniques used in the characterization of nanomaterials and nanostructures. SEM shows detailed 3D images with a resolution of few nanometers and at much higher magnification (up to ×300,000) as compared to light microscope (up to ×10,000). However images are black and white as they are created without light waves. SEM not only produces topographical information, it also provides the information on chemical composition near the surface. The surface structure of polymers, nanocomposites, fracture surfaces, nanofibers, nanoparticles, and nanocoatings can be imaged through SEM with great clarity. The SEM technique is used to view dispersion of nanoparticles and synthetic nanostructures such as carbon nanotubes, nanoclays, nanofillers, and nanocomposites. SEM image is the prime characterization technique in biomedical, environmental, textile, tissue engineering, cell culture and cell development, and scaffold construction. Figure 3.7a and b depicts SEM images showing the characteristic depth of field in natural pollen grains and laboratory-prepared zinc oxide nanorods arranged as flower. Bulk samples can be observed and larger sample area can be viewed by SEM, photo-like images are generated with high resolution; however, the limitations of SEM are that sample must have surface electrical conductivity. A nonconductive sample needs to be coated by conductive layers. Specialized SEM developed to cater for nonconductive samples in their natural states.

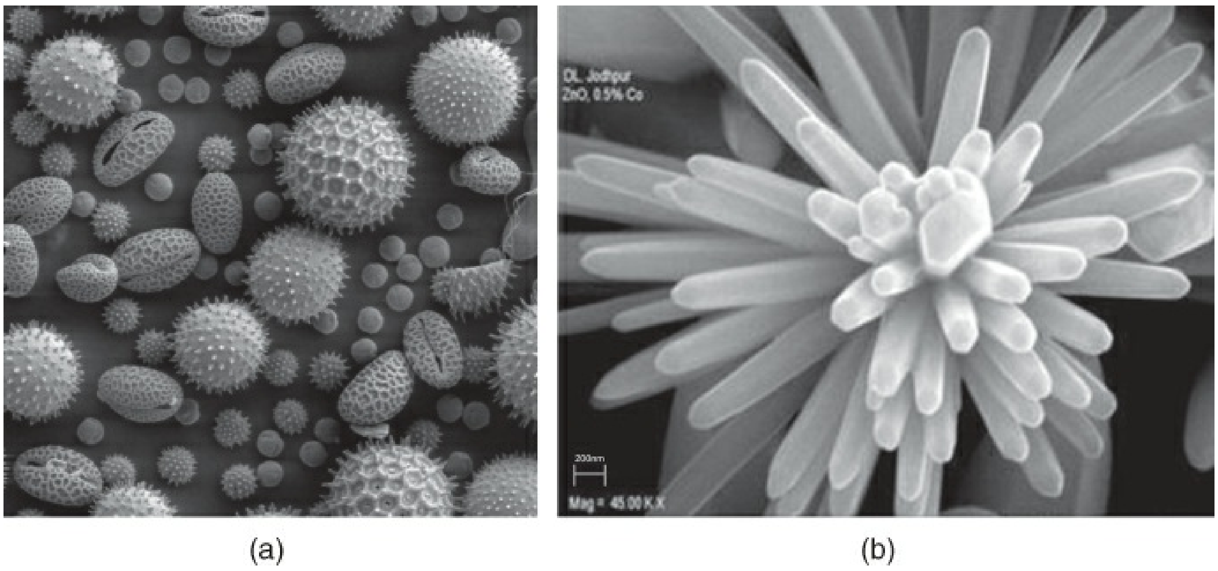

Figure 3.7 SEM images showing the characteristic depth of field: (a) pollen grains, http://en.wikipedia.org/. ; (b) zinc oxide nanorods arranged as flower.

Patra et al. [11], © 2009. With permission of Trans Tech. Publication, Switzerland.

Backscattered electrons from sample are also used to form an image. Secondary electrons can prevent from reaching the detector by applying a small negative bias on the transducer housing. BES images are often used in analytical SEM along with X-ray spectrum to get an idea about the chemical composition of the sample. For the purpose of chemical analysis, many modern SEMs also have X-ray detectors that allow qualitative and quantitative determinations to be made by means of X-ray fluorescence. An additional electron interaction in the SEM is that the primary electron collides with and ejects a core electron from an atom in the sample. The excited atom will decay to its ground state by emitting either a characteristic X-ray photon or an Auger electron, both of which have been used for chemical characterization under X-ray photoelectron spectroscopy (XPS) and Auger spectroscopy, respectively (refer Sections 3.4.4 and 3.4.5). Combining with chemical analysis capabilities, SEM not only provides the image of the morphology and microstructures of bulk and nanostructured materials and devices, but can also provide detailed information about chemical composition and distribution.

The versatility of the SEM and electron microprobe for the study of solids arises from the wide variety of signals generated when the electron beam interacts with the solid. In basic scanning electron microscopy instruments, the primary detection mode is the imaging of secondary electrons. X-rays are the second most common imaging mode for an SEM and are used to identify the elemental composition of the sample (X-rays being the characteristic) and the technique is called as energy dispersive X-ray (EDX).

Energy dispersive X-ray analysis (EDX): EDX Analysis used in conjunction with SEM is a technique to analyze near-surface elements and their proportion at different position, thus obtaining an overall mapping of the sample. Under SEM conditions when electron beam strikes the surface of a conducting sample, the energy of beam (typically in the range 10–20 keV) causes the emission of the characteristic X-rays (see Figure 3.1). The energy of X-rays emitted depends on the material under examination. The X-rays are generated in a region about 2 μm in depth, and thus EDX is not truly a surface technique. By moving the electron beam across the material, an image of each element in the sample can be obtained. Figure 3.8a and b shows SEM image and the corresponding EDX spectra of graphene balls and a nanoporous material made from 3:1 Au:Ag, revealing the qualitative and quantitative understanding of the sample under study.

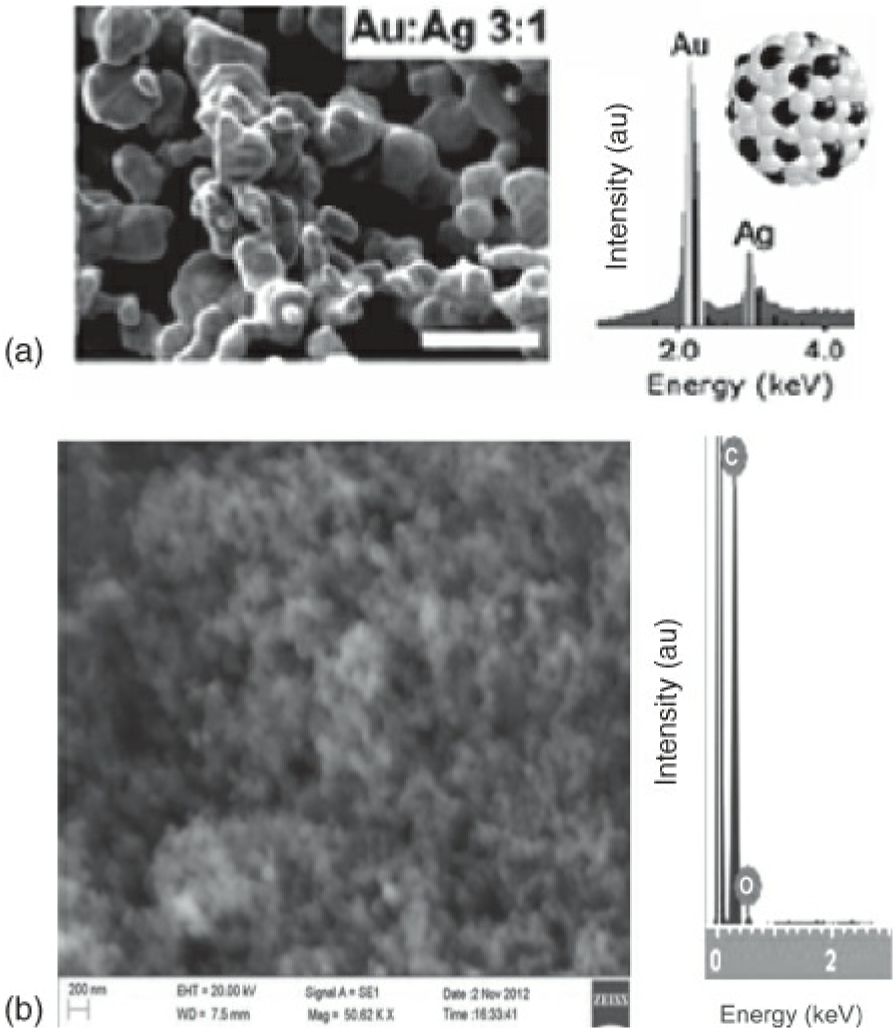

Figure 3.8 SEM image and EDX spectra. (a) Graphene balls. Adapted from Klajn et al.[12], ©2007 AAAS. (b) Nanoporous material.

Kumar et al. [13], ©2013. With permission of ASP.

Presence of heavy metal ions such as Au and Ag nanoparticles on the surface can easily be identified using EDX techniques. Elements of low atomic number are difficult to detect by EDX; however, FESEM and the corresponding EDX spectrum may overcome this limitation [12]. Environmental SEM (ESEM) and field emission gun SEM (FESEM) operates at low voltage–high vacuum and at low vacuum–high voltage conditions, respectively. Wet, oily, volatile, and nonconductive specimen in their natural state can be examined. Conductive coating that mask valuable information is not required. Both secondary and backscattered electrons may be detected with an ESEM. Everhart–Thornley detector cannot be used because the high bias voltage of scintillator would cause electrical breakdown at high pressure instead, gas-phase secondary electron detectors, which make use of cascade amplification, are employed.

3.2.2 Transmission Electron Microscope (TEM)

The TEM is actually the first electron microscope to be developed by Knoll and Ruska in the 1930s, where the electrons were focused on a thin specimen and the electrons transmitted through the specimen are detected. Basic features of a light microscope and TEM are illustrated in Figure 3.9a and b, which shows its similarity with optical microscopy.

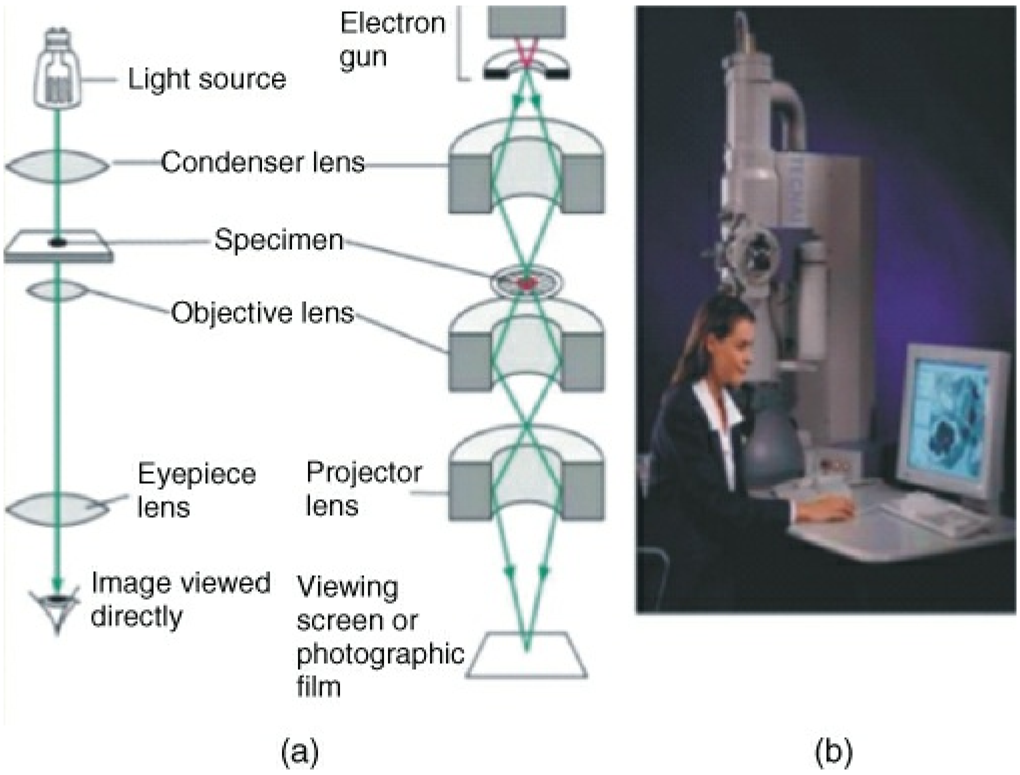

Figure 3.9 (a, b) Principal features of a light and transmission electron microscope.

Alberts et al. [9], © 2002. With permission of Garland Publishing Inc.

A beam of electrons is transmitted through an ultrathin specimen (<200 nm); upon interaction of transmitted electrons with the specimen, image is formed, magnified, and focused onto an image device such as a fluorescent screen or a layer of photographic film, or to be detected by a camera. The microscope is kept under high vacuum to insure unimpeded travel of electrons to and by the specimen. Electron beam is focused through a series of electromagnetic lenses on to the specimen. The greatest advantages that TEM offers are the high magnification (×1000,000) and its ability to provide both image and diffraction information from a single sample. Interaction of electrons transmitted through the specimen results in scattering that can be elastic (no energy change) or inelastic (energy change), refer to Figure 3.1. Elastic scattering can be coherent or incoherent. Well-arranged atoms in a crystalline substance result in coherent scattering, giving spot patterns. Inelastic processes give characteristic absorption or emission specific to the compound/elements/chemical structure. In TEM, one can switch between imaging the sample and viewing its diffraction pattern by changing the strength of the intermediate lens.

Basic principle: In TEM, electrons are accelerated from 100 keV to 1 MeV, projected onto a thin specimen by means of the condenser lens system, and penetrate the sample thickness either unscattered or scattered. The scattering processes experienced by electrons during their passage through the specimen determine the kind of information obtained. Elastic scattering involves no energy loss and gives rise to diffraction patterns. Inelastic interactions between primary electrons and sample electrons at heterogeneities such as grain boundaries, dislocations, second-phase particles, defects, density variations, and so on, cause complex absorption and scattering effects, leading to a spatial variation in the intensity of the transmitted electrons. The high magnification and resolution of all TEM is a result of the effective electron wavelengths (λ), given by the de Broglie relationship and the resolution (d). In order to maximize the resolving power, λ must be decreased and the refractive index of the medium, n, or the semi-angular aperture of the lens, θ, must be increased. In case of TEM, $n = 1$ (vacuum), sine $\theta = 10^{-2}$, and λ is of the order of 0.005 nm, and thus, the resolution $d = 0.3$ nm. The higher the operating voltage of a TEM instrument, the greater is the lateral spatial resolution (e.g., at 400 kV, the resolution is <0.2 nm) and has an additional advantage of greater electron penetration, allowing to work with thicker samples.

TEM image: The contrast in a TEM image is not similar to that in a light microscope. In a TEM, the crystalline sample interacts with the electron beam mostly by diffraction. The intensity of the diffraction depends on the orientation of the plane of the atoms in a crystal relative to the electron beam; at certain angles the electron beam is diffracted strongly from the axis of the incoming beam, while at other angles the beam is largely transmitted. Typical TEM images of some nanomaterials [14–16] are shown in Figure 3.10a–c.

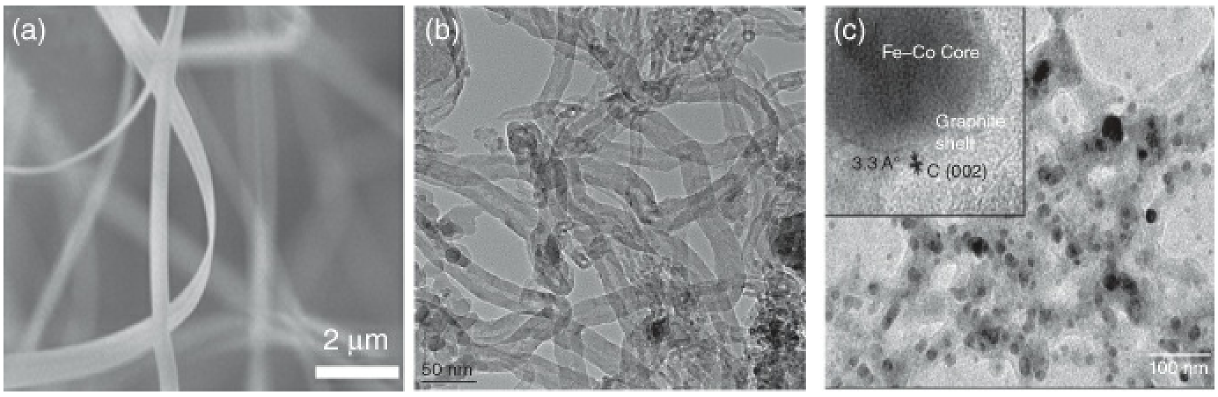

Figure 3.10 TEM image of (a) SnO_2 nanobelts Jiang et al. [14] © 2013. With permission of RSC; (b) CNTs. Wu et al. [15] © 2013. With permission of NPG; (c) graphitized Fe–Co alloy core-shell NPs, (inset, HRTEM image showing Fe–Co core and graphite shell).

Gupta, et al. [16], © 2014. With permission of ASP.

There are two main mechanisms of contrast in an image, the transmitted and scattered beams that can be recombined at the image plane, thus preserving their amplitude and phases. This results in phase contrast image of the object. The amplitude contrast image can be obtained by eliminating the diffracted beams. This is achieved by placing suitable apertures below the back focal plane of the objective lens either by using a movable aperture or by shifting the incident beam, keeping the aperture constant as shown in Figure 3.11a and b. The image using transmitted beam is called the “bright field image,” image obtained from diffracted beam is called as ‘dark field image’.

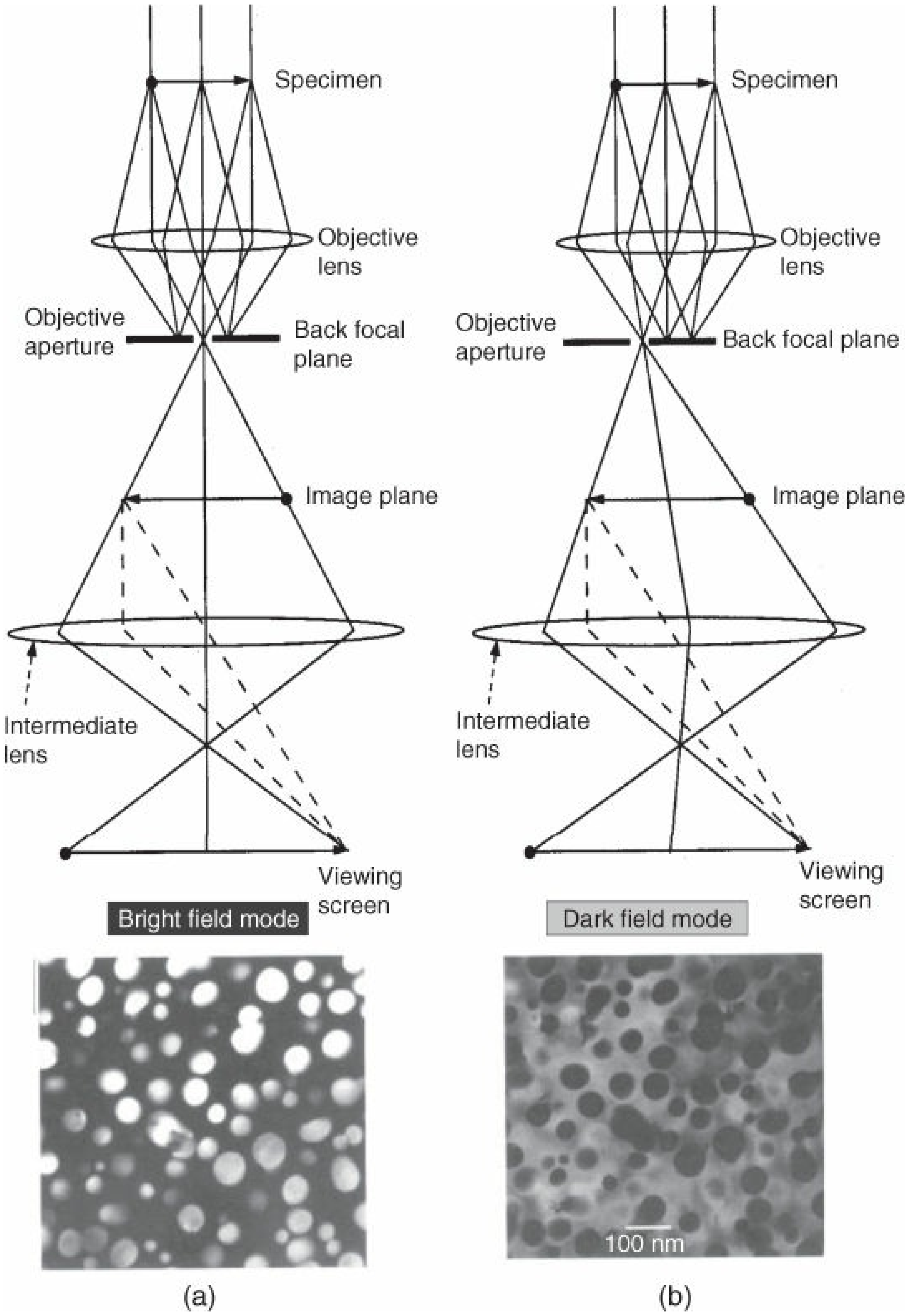

Figure 3.11 (a, b) Bright field and dark field modes and the corresponding typical TEM images in bright field and dark field modes.

Modern TEMs are equipped with specimen holders that allow tilting the specimen to a range of angles in order to obtain specific diffraction conditions. This produces a variation in the electron intensity that reveals information on the crystal structure. The technique of bright field imaging is particularly sensitive to the extended crystal lattice defects. Limitation of TEM lies in its limited depth resolution. Electron scattering information in a TEM image originates from a 3D sample, but is projected onto a 2D detector. Therefore, the structural information along the electron beam direction is superimposed at the image plane.

Sample preparation: The most difficult aspect of the TEM technique is in the preparation of samples. The specimen for TEM must be prepared as a thin film/foil so that an electron beam can penetrate and be able to withstand the vacuum present inside the instrument. Nanopowders and nanotubes can be quickly produced by the deposition of a dilute sample containing the specimen onto the support grid. The biological specimens are, however, inherently unstable under vacuum and thus have to be fixed usually in glutaraldehyde and paraformaldehyde, dehydrated, and stabilized in resins before they can be placed in a vacuum. Polymeric nanocomposites and biological samples are cut into thin films/slices (<100 nm) using ultramicrotome with a diamond knife at the cryogenic condition (in liquid nitrogen). These sections are electron transparent, and specimen contrast is enhanced using metal stains such as lead citrate, uranyl acetate, and phosphotungstic acid.

Applications: TEM is widely used in materials science and biological sciences. TEM images reveal the distribution and dispersion of nanoparticles in nanocomposites and nanocoatings and the extent of exfoliation, intercalation, and orientation of nanoparticles. Monitoring the morphology and the extent of dispersion or intercalation/exfoliation of nanoparticulates is very crucial for the synthesis of nanocomposites. Figure 3.12a–c) shows different stages for the synthesis of Fe_3O_4 nanocrystals.

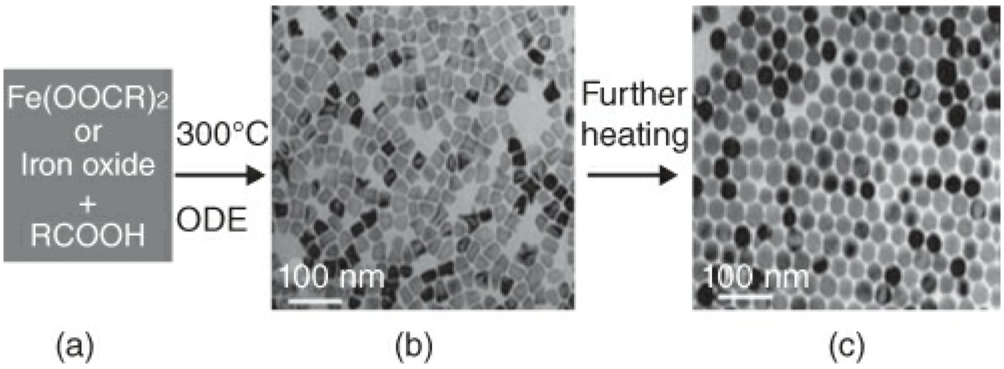

Figure 3.12 (a–c) TEM images showing the formation of Fe_3O_4 nanocrystals.

Jana et al. [17(a)] © 2004. With permission of ACS.

In addition to the capability of structural characterization and chemical analyses, TEM has also been explored for other applications in nanotechnology. Examples include the determination of melting points of nanocrystals, in which an electron beam is used to heat up the nanocrystals and the melting points are determined by the disappearance of electron diffraction. Another example is the measurement of mechanical and electrical properties of individual nanowires and nanotubes. This technique allows a one-to-one correlation between the structure and properties of the nanowires.

TEM has been used extensively for the study of subcellular structures and has now moved on to the resolution at the molecular level. When the chemical fixation methods described earlier are replaced through cryofixation and stabilization, tissue artifacts caused by traditional sample processing are reduced. The electron microscope can also be used to study organelle and virus structure using the method of negative staining. TEM has begun to be used in the analyses of biological macromolecules such as proteins (enzymes) and viruses on the molecular level. Recently, strong demands for TEM observation of 3D structures of biological macromolecules in the hydrated state (the native state in living bodies) at atomic resolution have been made. However, there are two difficult problems in using the TEM for these purposes. First, the path of the electron beam must be in vacuum, therefore, the specimen to be observed must also be kept in vacuum. Second, damage of the specimen due to electron-beam irradiation is large and must be reduced considerably. A method for overcoming these difficulties and for observing the specimen at the atomic resolution while keeping it in the hydrated state is Cryo-TEM, the so-called ice-embedding method for preparing a frozen specimen. Cryo-TEM method has been used for demonstrating the nonpenetration of titania nanoparticles into the human dermis. Laser scanning confocal microscope (LSCM) provides the facility for noninvasive investigation of migration of nanoparticles across the bio-barrier and reveals the 3D morphology of nanoparticles.

High-resolution transmission electron microscopy (HRTEM): HRTEM is one of the most essential tools of nanoscience having resolving powers in the vicinity of 1 Å, where individual atoms and crystalline defects can be imaged. The microscope is kept under high vacuum to ensure unimpeded travel of electrons to and by the specimen. The electrons pass by the specimen on to a phosphor screen for visualization. External structures of microbes can be viewed at a high magnification using the method of scanning electron microscopy. The specimen is stabilized through either chemical or cryofixation, covered through a layer of conductive material carbon or gold/platinum, and the specimen is scanned with an electron beam. The electrons are either reflected or passed by the specimen and a digital image is created from the composite data, thus creating 3D structures. This technique has been a further establishment for the examination of specimens at low vacuum and ambient conditions. Typical HRTEM images of carbon nano-onions can be seen in Figure 5.27.

3.3 Scanning Probe Microscopy (SPM)

SPMs are capable of resolving details of surfaces down at the atomic level. The first example of this type of microscope, the STM was described in 1982. Unlike optical and electron microscopes, SPMs reveal details not only on the lateral *x*- and *y*-axes of a sample but also on the *z*-axis, which is perpendicular to the surface. The resolution of SPMs can be as low as 0.1 nm (1 Å) in the *x*- and *y*-axes (resolution in the *z*-dimension is even better than 0.1 nm) as compared to the resolution of a typical electron microscope. SPMs allow seeing surface structures with unprecedented resolution, as a consequence, novel ideas emerge in research and development of novel products. Both electron microscopy (SEM, TEM) and SPM are significant in nanocharacterization; however, the basic attributes in their operation vis-à-vis optical microscopy are summarized in Table 3.5.

Table 3.5 Characteristic Features of Optical, Electron, and Scanning Probe Microscopes

Features	Optical Microscope	Electron Microscope	Scanning Probe Microscope
Operation	Air, liquid	TEM: Vacuum	STM: Vacuum
		SEM: Vacuum	AFM: Air, liquid dispersion, solid dispersion
Imaging radiations	Visible light	SEM: Secondary electrons Backscattering electrons	STM: Quantum tunneling
		TEM: Transmitted electrons	AFM: nN force between cantilever tip and surface
Wavelength of interacting radiations	400–700 nm	0.01–0.006 nm (vary with accelerating voltage)	N/A
Operating voltage	N/A	SEM: < 20–40 kV	STM: < 1 V
		TEM: 40 kV~1 MV	
Sample type	Not completely transparent	SEM: Conducting/non conducting	STM: Conducting, surface height < 10 mm
		TEM: Vacuum-compatible thin film	AFM: Conducting/nonconducting
Lateral resolution	1 μm	SEM: 1–5 nm	AFM: 2–10 nm
		TEM: 0.1 nm	STM: 0.1 nm
Vertical resolution	–	–	AFM: 0.1 nm STM: 0.01 nm
Magnification	~10^3	SEM: ~10^5 TEM: ~10^6	AFM: ~10^6 STM: ~10^9
Contrast	Absorption reflection	SEM: Inclination effect, shadowing, edge contrast	STM: Variations in charge/ electron density
		TEM: Scattering, diffraction	AFM: Variation in the interaction strength between surface and cantilever tip
Working mode		TEM: Bright field and dark field	AFM: Contact and tapping
			STM: Constant current and constant height

SPM provides images of surfaces by scanning the surface line by line with a probe. Scanning works very similar to the way the blind reads Braille, line by line, by moving a finger over buds on the paper. Both are based on scanning the surface of the sample in a raster pattern with a very sharp tip that moves up and down along the *z*-axis along the surface topography. This movement is measured and translated into an image with details on an atomic size scale. Scanning tunneling microscopy, atomic force microscopy, scanning electrochemical microscope, and numerous variations of these techniques fall under the category of SPM. All these techniques work on different principles, but the most significant common feature is to produce a highly magnified image of the surface or bulk of the sample. Two types of SPMs that are most widely used in nanoscience and nanotechnology are the STM and AFM. The basic principle, methodology, and applications of these techniques are described in subsequent sections.

3.3.1 Scanning Tunneling Microscope (STM)

In 1981, Binning and his coworkers [3] introduced a totally new concept of imaging based on measuring the tunneling current, and the device is named as STM. The invention of the STM earned Binning and his coworker Heinrich Rohrer (at IBM Zürich) the Nobel Prize in Physics in 1986. This device was found to be capable of resolving features on an atomic scale on the surface of a conducting solid specimen. They used a small metal tip placed at a minute distance from a conducting surface: when the metal tip and the conducting surface are placed very close to each other, but not actually touching, a bias between the two can allow electrons to tunnel through the vacuum between them creating tunnelling current, which is a function of the electron density on the surface. Electron density is the probability of finding an electron in a particular place. There is high electron density around the atoms and bonds in molecules. Variations in current as the probe passes over the surface are translated into an image. This type of microscope is called the STM [18].

The STM can create detailed 3D images of a sample with an atomic resolution. In real sense, the resolution is so high (0.2 nm = 2×10^{-10} m) that it is possible to see and distinguish the individual atoms on the surface. The STM has proved to be a powerful tool in nanoscience and nanotechnology and is being used for industrial and fundamental research to obtain images at an atomic scale of metal and semiconducting surfaces. It provides a 3D profile of the surface roughness; it allows observing surface defects and determining the size and conformation of molecules and aggregates. Another astonishing property of the STM is that it can be used to manipulate individual atoms, trigger chemical reactions, and perform electronic spectroscopy. STM instrument is found to be capable of resolving features on an atomic scale on the surface of a conducting solid. The lateral resolution of STM is of the order of 0.1 nm and depth resolution is of the order of 0.01 nm. With this resolution, individual atoms within materials can be routinely imaged and manipulated. The STM can be used not only in ultrahigh vacuum but also in air, water, and various other liquid or gas ambient, and at temperatures ranging from near zero Kelvin to a few hundred degrees Celsius.

> **Basic principle:** STM relies on two physical principles: quantum tunneling of electrons across a potential barrier and the piezoelectric effect. The STM is based on the concept of quantum mechanical tunneling, which occurs when a small bias voltage (millivolt to 3 V) is applied between a sharp tip and conducting sample and the tip is within a few nanometers of the surface. The resulting **tunneling current** is a function of tip position,

applied voltage, and the local density of states (LDOS) of the sample. The magnitude of tunneling current I_t is given by

$$I_t = Ve^{-Cd}$$

where V is the bias voltage, C is a constant, and d is the distance between the probe and the surface. Information is acquired by monitoring the current as the tip's position scans across the surface and is usually displayed in image form. When a voltage bias is applied and the tip is brought close to the sample by coarse sample-to-tip control, which is turned off when the tip and sample are sufficiently close. At close range, fine control of the tip in all three dimensions when near the sample is typically piezoelectric, maintaining tip–sample separation d, typically in the 4–7 Å (0.4–0.7 nm) range, which is the equilibrium position between attractive ($3 < d < 10$ Å) and repulsive ($d < 3$ Å) interactions. In this situation, the voltage bias will cause electrons to tunnel between the tip and sample, creating a current that can be measured. Once tunneling is established, the tip's bias and position with respect to the sample can be varied and data are obtained from the resulting changes in current.

The essential components of an STM are shown in Figure 3.13. The components of an STM include scanning tip, piezoelectric controlled height and x, y scanner, coarse sample-to-tip control, vibration isolation system, and computer. The scanning waveforms, applied on the x- and y-piezo, make the tip raster scan on the sample surface. A bias voltage is applied between the sample and the tip to induce a tunneling current. The z-piezo is controlled by a feedback system to maintain the tunneling current constant. The voltage on the z-piezo represents the local height of the topography. A probe tip is attached to a piezo-drive, which consists of three mutually perpendicular piezoelectric transducers: x-piezo, y-piezo, and z-piezo. Upon applying a voltage, a piezoelectric transducer expands or contracts. By applying a saw tooth voltage on the x-piezo and a voltage ramp on the y-piezo, the tip scans on the x, y plane. Using the coarse positioner and the z-piezo, the tip and the sample are brought to within a fraction of a nanometer to each other. The electron wave functions in the tip overlap electron wave functions in the sample surface. A finite tunneling conductance is generated. By applying a bias voltage between the tip and the sample, a tunneling current is generated. To ensure stable operation, vibration isolation is essential.

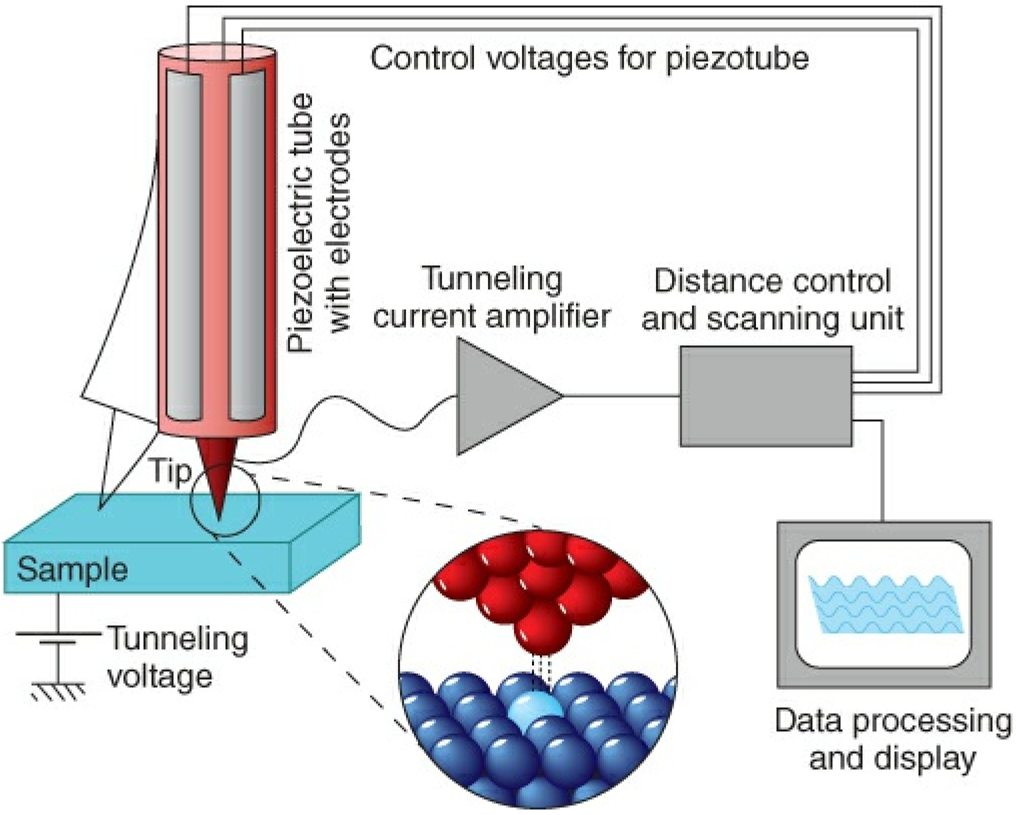
Control voltages for piezotube
Piezoelectric tube with electrodes
Tunneling current amplifier
Distance control and scanning unit
Tip
Sample
Tunneling voltage
Data processing and display

Figure 3.13 Essential components of an STM with a close-up view of the tunneling effect between tip of the probe and the surface atoms.

http://en.wikipedia.org/wiki/Scanning_tunneling_microscope.

Tips: The probe of an STM is a very thin needle called the "tip" that is so small that it ends in just a few atoms. The tip is made up of a conducting material (e.g., metal, typically tungsten or Pt–Ir alloy). The precise movement of the tip is controlled by a piezomotor. The tip of an STM is about 3 mm long and should be located very close to the surface to be scanned. In practice, the distance between the end of the tip and the surface must be less than 0.1 nm, without the tip actually hitting the surface. One of the fundamental elements of the STM is the tip of the probe that scans the surface, which must be sharpened to a very fine tip. The fabrication of sharper probes allows better resolution of surface features. Ultimately, a probe tip sharpened to one atom would provide the best resolution.

Modes of STM: In principle, the STM can be operated in two modes, first the **constant height mode**, in which the tip position is kept constant in the z-direction while the tunneling current is monitored. In **constant current mode**, the tunneling current is kept constant while the z-position of the tip changes to keep d constant as shown in Figure 3.14a, and the z-position of the tip is monitored. The up-and-down motion of the tip reflects the topography of the surface. Most STM operates at constant current mode. In constant current mode, the contrast on the image is due to variations in charge density. Second is the **constant height mode**, in which both the voltage and height are held constant while the current changes to keep the voltage from changing; this leads to an image made of current changes over the surface, which can be related to charge density (Figure 3.14b). The benefit of using a constant height mode is that it is faster, as the piezoelectric movements require more time to register the height change in constant current mode. All images produced by STM are grayscale, with color optionally added in postprocessing in order to visually emphasize important features.

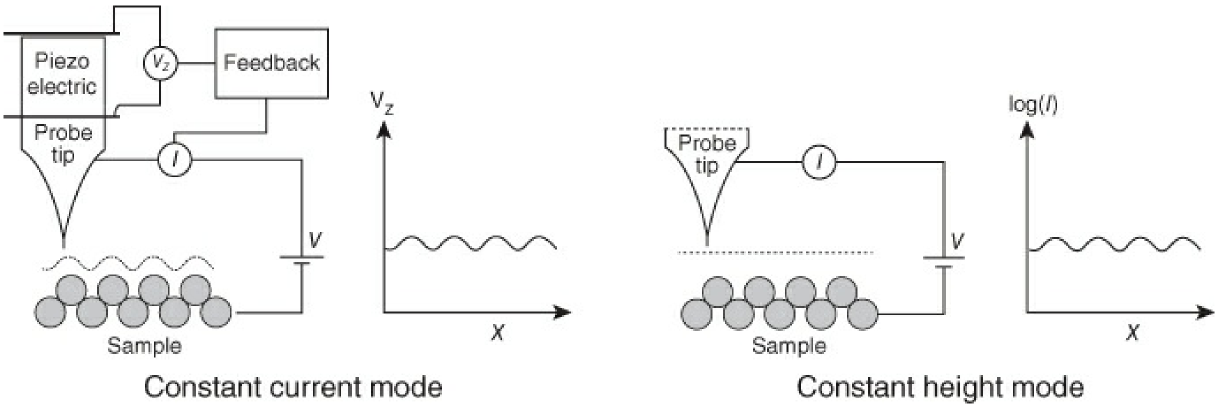

Figure 3.14 (a) Constant current and (b) constant height imaging modes of an STM.

Creating images with STM: When a conducting tip is brought very near to a metallic or semiconducting surface, at a distance of about 0.1 nm, it can induce the formation of a tunnel current between the tip and the surface: a bias between the two atoms (tip and surface) can allow electrons to tunnel through the vacuum between them and induce the formation of a current. Variations in current as the probe passes over the surface are translated into an image. As the conducting tip of an STM scans over a conducting or semiconducting surface, a "tunnel current" is formed, which arises from electrons jumping from the surface to tip of the STM probe. The probability of this happening depends largely on the distance between the surface and tip; thus, the size of the current depends on this distance. Small changes in the distance between the probe tip and the substrate surface translate into large changes in tunnel current. Thanks to this phenomenon, atomic scale resolution by STM is possible in the *x*-, *y*-, and *z*-directions. With the STM, surfaces can be scanned by moving the tip in steps of 0.1 nm (10^{-10} m), thus providing a very accurate representation of the surface. For the technique to work, it is necessary that a tunnel flow is induced as the tip scans over the surface. Thus, the surface must be conductive to some extent. To scan a surface which in itself is not electrically conductive, one can coat it with a very thin layer of conductive material, such as gold. STM is successfully used to detect and characterize materials such as carbon nanotubes (single- and multiwalled), graphene, intriguing chalcogenides, and so on. Some of the STM images of nanostructures as shown here; Figure 3.15a–c shows some representative STM images of nano-gold on TiO_2, nano-cobalt on TiO_2 surface, and graphene grown on SiO_2 showing grain boundary. The instrument has also been used to move single metal atom, nanotubes, or molecules on smooth surfaces with high precision.

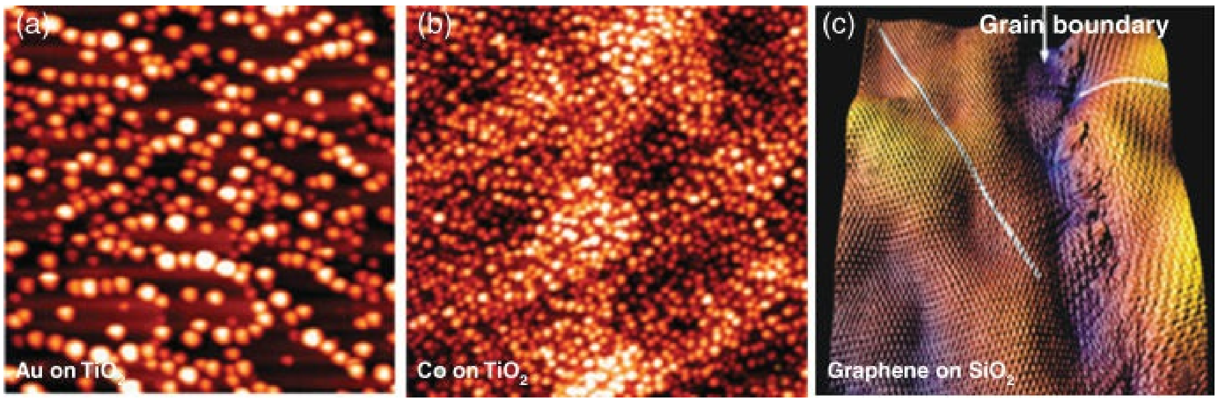

Figure 3.15 STM images of (a) nano-gold on TiO_2. Galhenage et al. [17b], © 2013. With permission of ACS; (b) nano-cobalt on TiO_2 surface Galhenage et al. [17b], © 2013. With permission of ACS; (c) graphene on SiO_2 showing grain boundary. Koepke et al. [19], © 2013. With permission of ACS.

Scanning transmission electron microscopy (STEM): A scanning transmission electron microscope is a TEM that works in the scanning mode as an SEM. An electron beam is focused to a small spot and scanned across the specimen exactly as done in SEM. A STEM allows detecting the transmitted as well as secondary and backscattered electrons. This mode of electron microscope provides spatially resolved information about the specimen.

3.3.2 Atomic Force Microscope (AFM)

AFM, another SPM technique, was developed in 1985, also by Binning and coworkers at IBM Zürich [4]. AFM does not measure the tunnel current, but measures the forces between tip and surface, and therefore does not require the surface to be conductive. The atomic force microscopy was developed specifically to overcome the intrinsic limitations of the scanning tunneling microscopy, which was not suitable for imaging surfaces coated with biological entities such as DNA or proteins. The AFM operates in air and not under a vacuum [[20]]. AFM is a nondestructive technique with a very high 3D spatial resolution. It offers the capability of 3D visualization and both qualitative and quantitative information on many physical properties including size, morphology, surface texture, and roughness. Statistical information, including size, surface area, and volume distributions, can be determined as well. A wide range of particle sizes can be characterized in the same scan from 1 nm to 8 μm. In addition, the AFM can characterize nanoparticles in multiple media including ambient air, controlled environments, and even liquid dispersions.

Basic principle: In atomic force microscopy, a sharp tip that is mounted on a cantilever is moved along the surface to be measured and the changes of voltage in term of height are recorded. These height changes can be caused by particles lying on the surface but can also be a measure of the roughness of the surface itself. In its most basic setup, the instrument works similar to a record player, with the tip being the needle and the record the surface to be measured. In the simplest of setups, the bend in the cantilever is kept constant and the instrument measures how much the cantilever needs to be moved up and down to achieve constant bending. The force acting between the cantilever and the sample surface causes minute deflections on the cantilever, which are detected by optical means. Figure 3.16 shows schematically the most common method of detecting the deflections of the cantilever holding the tip. A laser beam is reflected off a spot on the cantilever to a segmented photodiode that detects the motion of the probe. The output from the photodiode then controls the force applied to the tip so that it remains constant. Optical control system in AFM is analogous to the tunneling current system in the STM. The movement system is a tubular piezoelectric device that moves the sample in the *x*-, *y*-, and *z*-directions under the tip. The signal from laser beam detector is then fed back into the sample piezoelectric transducer, which causes the sample to move up and down, maintaining a constant force between the tip and the sample.

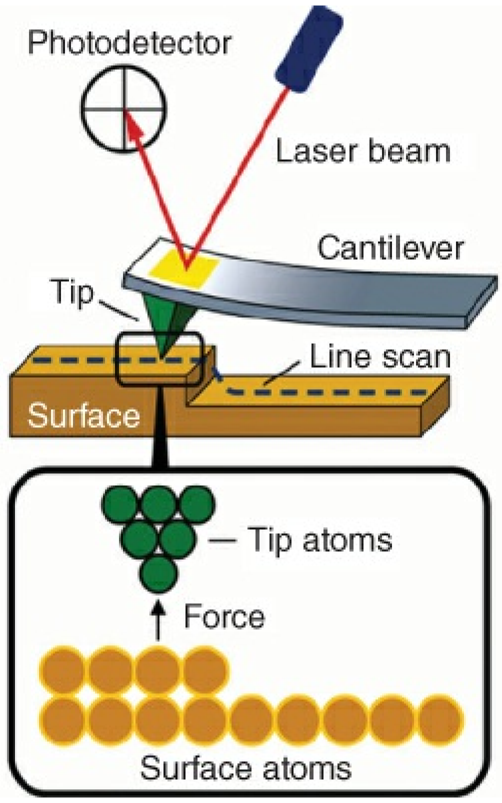

Figure 3.16 Schematic representation of AFM, Courtesy of Keysight Technologies.

AFM images are not only influenced by the substrate surface but also depend on the physical characteristics of the cantilever and tip. In early AFMs, cantilevers were cut from metal foil and tips were made from crushed diamond particles, glued manually to the cantilever. This method has been replaced by producing integral semiconductor cantilever–tip assemblies that are produced by etching single chip of silicon, silicon oxide, or silicon nitride. The most common cantilever–tip assemblies in use today are micromachined from monolithic silicon. The cantilever and tips are remarkably small, ideally, a single atom at the tip apex.

AFM modes: Three modes are commonly used in AFMs: contact mode, noncontact mode, and tapping mode. Contact mode is also called as static mode, whereas other two modes are called dynamic modes. **Contact mode** is the most common mode as the AFM probe tip is very sharp with a radius of curvature of the order of 10 nm, and if the surface under analysis is soft, the probe can penetrate it with the risk of damaging it and degrading the spatial resolution of the resulting micrograph. To overcome this limitation, instruments working in **noncontact mode** and **tapping mode** have been developed. In these systems, the probe is not simply dragged onto the surface but oscillated vertically with respect to the surface while it is scanned, thereby significantly reduces the damage that can be induced by the probe and allows imaging of soft, compressible samples such as biomolecules and cells.

In tapping mode, the cantilever is driven to oscillate up and down at or near its resonance frequency by a small piezoelectric element mounted in the AFM tip holder similar to noncontact mode. However, the amplitude of this oscillation is greater than 10 nm, typically 100–200 nm. The interaction of forces acting on the cantilever when the tip comes close to the surface, such as van der Waals forces, dipole–dipole interactions, and electrostatic forces, causes the amplitude of this oscillation to decrease as the tip gets closer to the sample. An electronic servo uses the piezoelectric actuator to control the height of the cantilever above the sample. The servo adjusts the height to maintain a set of cantilever oscillation amplitude as the cantilever is scanned over the sample. A tapping AFM image is therefore produced by imaging the force of the intermittent contacts of the tip with the sample surface.

In noncontact atomic force microscopy mode, the tip of the cantilever does not contact the sample surface. The cantilever is instead oscillated at either its resonant frequency (frequency modulation) or just above (amplitude modulation) where the amplitude of oscillation is typically a few nanometers (<10 nm) down to a few picometers. The van der Waals forces, which are strongest from 1 to 10 nm above the surface, or any other long-range force that extends above the surface acts to decrease the resonance frequency of the cantilever. This decrease in resonant frequency combined with the feedback loop system maintains a constant oscillation amplitude or frequency by adjusting the average tip-to-sample distance. Measuring the tip-to-sample distance at each (x, y) data point allows the scanning software to construct a topographic image of the sample surface. However, the tip of an AFM can be used deliberately to “scratch” and remove some molecules from a surface or to use the tip to write with an “ink.” Both are “writing” methods in the sense that they allow creating nanostructures on a surface with any geometry. This technique is called dip-pen nanolithography (DPN) and is discussed in Chapter 2.

Sample preparation: Nanoparticles typically fall into one of two categories when it comes to sample preparation. The first category is nanoparticles rigidly attached to a solid structure. The second category is nanoparticles with weak adhesion to the substrate, such as dispersions of nanoparticles in liquid or dry media. A good example of the first category is nanoparticles embedded in a solid matrix, as in the case of nanocomposites or nanoprecipitates. In such cases, typically a cross section of the composite material is scanned to determine such properties as average particle size and spatial distribution. Examples of nanoparticles in the second category are quantum dots, diesel soot particles, carbon black, and colloidal suspensions. Sample preparation for the second category of nanoparticles involves the stable attachment of particles onto the substrate. Because the AFM works by scanning a mechanical probe across the sample surface, any structure being imaged must have greater affinity to the flat surface than to probe tip. When nanoparticles do accidentally attach to the probe, the resulting images typically show reduced resolution. Streaking will occur in the images if nanoparticles are not rigidly attached to the flat surface while scanning in the contact mode. To avoid such artifacts, close contact mode (near contact) or CFM (crystal sensing) is strongly recommended for such samples. In certain cases, it is necessary to affix nanoparticles to a sticky substrate within liquid or dry media. A cheap and easy way to do this is the use of double-sided sticky tape or other similar methods commonly used by microscopists. More refined techniques include the use of mica, “Tacky Dot” slides, and TempFix.

Applications

Qualitative analysis: Using the AFM, individual particles and groups of particles can be resolved. Microscope images can be critical when troubleshooting quality control issues. The AFM offers visualization in three dimensions. Resolution in the vertical or the z-axis is limited by the vibration environment of the instrument, whereas resolution in the horizontal or the x–y axis is limited by the diameter of tip utilized for scanning. Typically, AFM instruments have vertical resolutions of less than 0.1 nm and the x–y resolutions of around 1 nm. In material sensing mode, the AFM can distinguish between different materials, providing spatial distribution information on composite materials with otherwise uninformative topographies. Figure 3.17a shows the typical AFM image of a nanomaterial. The in-homogeneity in the material can be seen on a topographically flat organic film (Figure 3.17b), similarly, dispersion of nanoparticulate matter in nanocomposites (Figure 3.17c) can be visualized by AFM imaging.

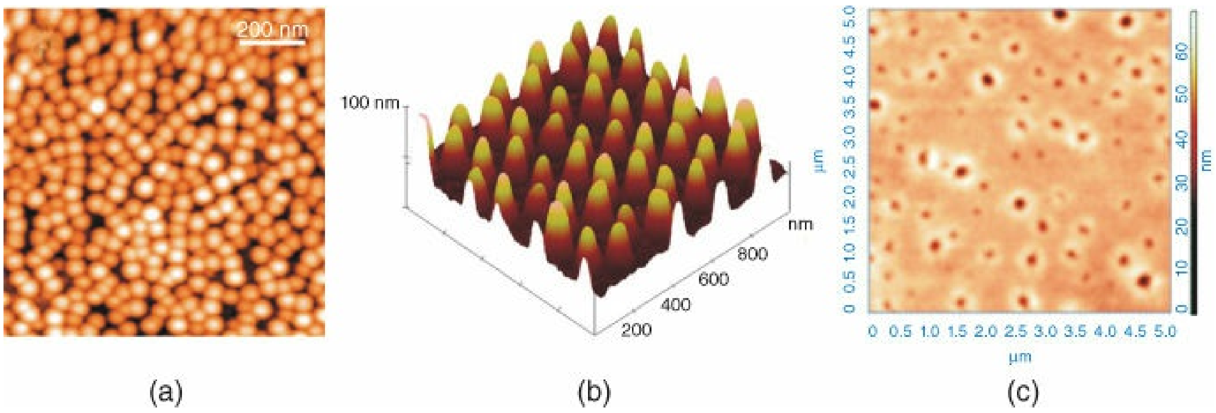

Figure 3.17 AFM images showing (a) InAs/GaAs QDs grown on a Ge/Si substrate. Chen et al. [21a], © 2015. With permission of licensee MDPI, Basel, Switzerland; (b) Pt nanoparticles coated with Si nanopillars. Li et al. [21b], © 2015. With permission of NPG; (c) cholesterol–B, SA conjugate. Gehlot et al. [22], © 2013. With permission of NISCAIR, CSIR, New Delhi.

Quantitative analysis: Software-based image processing of AFM data can generate quantitative information from individual nanoparticles and between groups of nanoparticles. For individual particles, the size information (length, width, and height) and other physical properties (such as morphology and surface texture) can be measured. Statistics on groups of particles can also be measured through image analysis and data processing. Commonly desired ensemble statistics include particle counts, particle size distribution, surface area distribution, and volume distribution. With knowledge of the material density, the mass distribution can be easily calculated. Image processing of an AFM image is shown in Figure 3.18a and b.

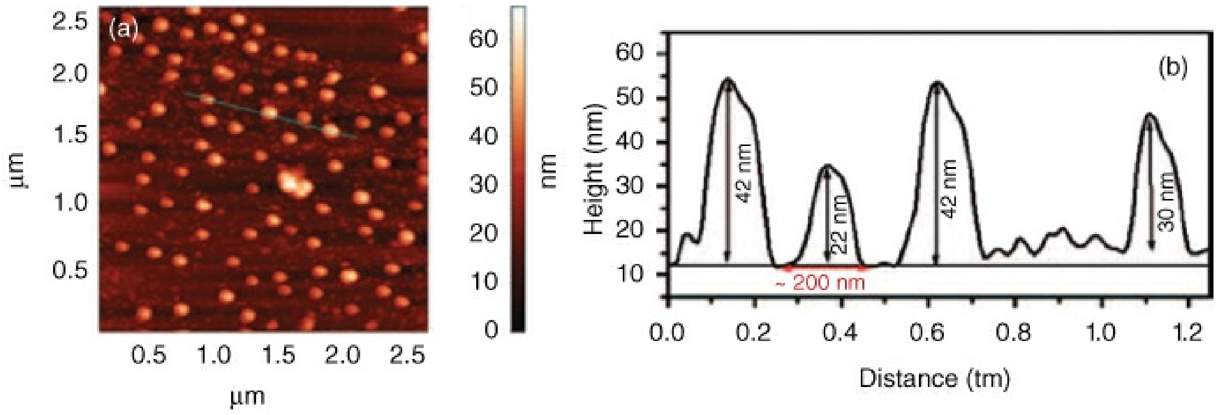

Figure 3.18 (a) AFM image of graphene balls with height bar; (b) cross section along the line indicated in (a). Kumar et al. [13], © 2013. With permission from ASP.

In general, the scan of AFM for sample size ranges up to 80 µm, and size of the particles in the range 1 nm to 8 µm can be imaged. Dry particles can be scanned both in ambient air and in controlled environments, such as nitrogen or argon gas. Liquid dispersions of particles can also be scanned, provided that the dispersant is not corrosive to the probe tip and can be anchored to the substrate. Particles dispersed in a solid matrix can also be analyzed by topographical or material sensing scans of cross sections of the composite material. Such a technique is useful for investigating spatial nanocomposites. The key attributes of AFM are included in Table 3.6.

Table 3.6 Key Attributes of AFM for the Characterization of Nanoparticles

Qualitative Analysis	3D visualization and material sensing
Quantitative Analysis	Size, morphology and surface texture/roughness parameters
Statistical Information	Particle size counting, size distribution, surface area, volume, and mass distribution

3.4 Characterization Through Spectroscopy

Spectroscopy is defined as the branch of science that deals with interaction of matter with electromagnetic (EM) radiations. Absorption, transmission, and scattering of various electromagnetic radiations are used as spectroscopic characterization methods. Depending on the wavelength of the electromagnetic radiations used and the intensity of interaction, a lot of information regarding identity, chemical composition, chemical structure, size, surface, and morphological characteristics can be inferred. Figure 3.19 summarizes the spectrum of electromagnetic radiation, and methods based on radiation specified in the box are mostly known for the characterization of material. The following section briefly describes the spectroscopic methods that are most relevant in the characterization of nanoparticles and nanosurfaces [23–25].

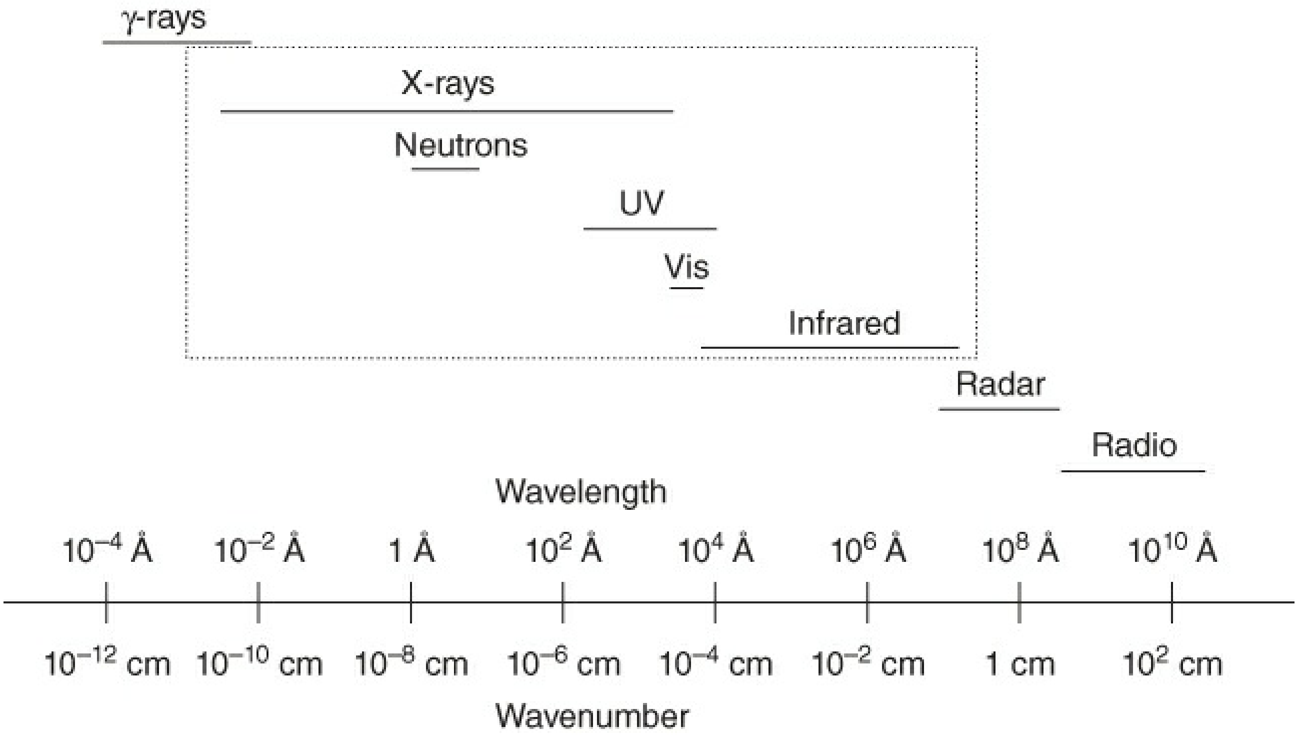

Figure 3.19 Spectrum of various electromagnetic radiations.

Different forms of radiation such as X-rays, neutrons, electrons, laser light, and so on, are used for scattering purposes to characterize materials in the solid state. The small-angle neutron and X-ray scattering methods (SANS, SAXS) probe size scales from the near atomic to the near micron. Light scattering methods (SLS, DLS) complement these techniques by focusing on the micron length scale. Other methods such as wide-angle neutron scattering and wide-angle X-ray scattering (WANS, WAXS) and low-energy electron diffraction (LEED) probe very local (atomic) structures.

3.4.1 UV–Visible Plasmon Absorption and Emission

The absorption of light in the UV and visible (vis) spectra is an effective spectroscopic method for detecting specific chemical bonds in small molecules and in macromolecules. The UV–vis absorption spectrophotometer instrument uses a Xenon pulse lamp, which provides a wide wavelength range (from 190 to 1100 nm) and a dual silicon diode detector. A holographic grating is used to scan the wavelength. The reference radiation beam in the spectrophotometer travels from the light source to the detector without interacting with the sample. The sample radiation beam interacts with the sample exposing it to the UV light of continuously changing wave length. When the emitted wavelength corresponds to the energy level, which promotes an electron to a higher molecular orbital, energy is absorbed. The detector records the intensity of absorption versus wavelength (absorption spectrum), and the wavelength at which the sample absorbs maximum (i.e., λ_{max}) is the characteristic of the analyte.

Localized surface plasmon resonance (LSPR): Metal nanoparticles, in particular gold and silver, are characterized by a plasmon resonance absorption that gives rise to intensely colored solutions. The absorption band is due to electrons confined at the particle surface that collectively oscillate at a specific frequency, commonly referred to as the surface plasmon resonance frequency. To give some examples, the plasmon band of 20 nm silver (Ag) particle is centered at 395 nm, resulting in a yellow solution, while 20 nm gold (Au) particle absorbs at 520 nm resulting in a red solution. The plasmon absorption effect occurs for particles up to approximately 50 nm in diameter and scales with particle volume. Absorption can be in the visible and UV area of the spectrum. Particles can be visualized by absorbance in solution at nanomolar and picomolar concentrations.

Plasmon resonance light scattering: In larger metal nanoparticles (>30 nm), another effect, light scattering, is observed. When illuminated with white light, metal nanoparticles in the size range 50–120 nm diameter scatter light of a specific color at the surface plasmon resonance frequency. This effect is called plasmon resonance light scattering. As in the case of plasmon absorbance, light scattering scales with particle volume, but the scattered light can be detected at much lower concentrations than absorbed light. For example, light scattered by a solution of 80-nm-diameter gold particles is detectable down to 5 fM concentration (fM = 10^{-15} M). For this reason, metal nanoparticles are interesting materials for use in techniques that rely on labeling (such as microarray technology).

Applications: The plasmon resonance in metals such as gold and silver is responsible for their unique optical properties. Such nanoparticles scatter light elastically with remarkable efficiency because of the collective resonance of the conduction electrons in the metal known as surface plasmon resonance. The peak wave length, magnitude, and spectral bandwidth of plasmon resonance associated with a nanoparticle are dependent on the size, shape, and material composition of the particle and its local environment. The absorption spectrum of metal nanoparticles shifts to longer wavelengths with increasing particle size. The position and shape of the plasmon absorption of silver nanoclusters are strongly dependent on the particle size, dielectric medium, and surface adsorbed species.

The truncated triangular silver nanoparticles with [1 1 1] lattice plane as the basal plane displayed the strongest biocidal action compared to spherical, rod shaped, or with $AgNO_3$ (as Ag^+). This shape of silver nanoparticles can be identified by observing the absorption spectra (Figure 3.20a and b); the peak shifts as per the particle shape – triangular appear mostly red, pentagon as green, and the spherical as blue.

UV–vis absorption spectroscopy for macromolecules: The UV–vis absorption spectroscopy method is used extensively in biology to detect the presence and relative amount of DNA or proteins. For example, this technique is sensitive to the π-bonding in the amine bases of DNA. The π-bonding absorption line occurs at a wavelength around 260 nm for the various nucleotides. The UV–vis absorption technique is also sensitive to the presence of two amino acids forming the proteins: tryptophan and tyrosine. The absorption signal from proteins (around the 280-nm absorption line) is 40 times smaller than that from DNA (around the 260-nm absorption line) for comparable concentrations.

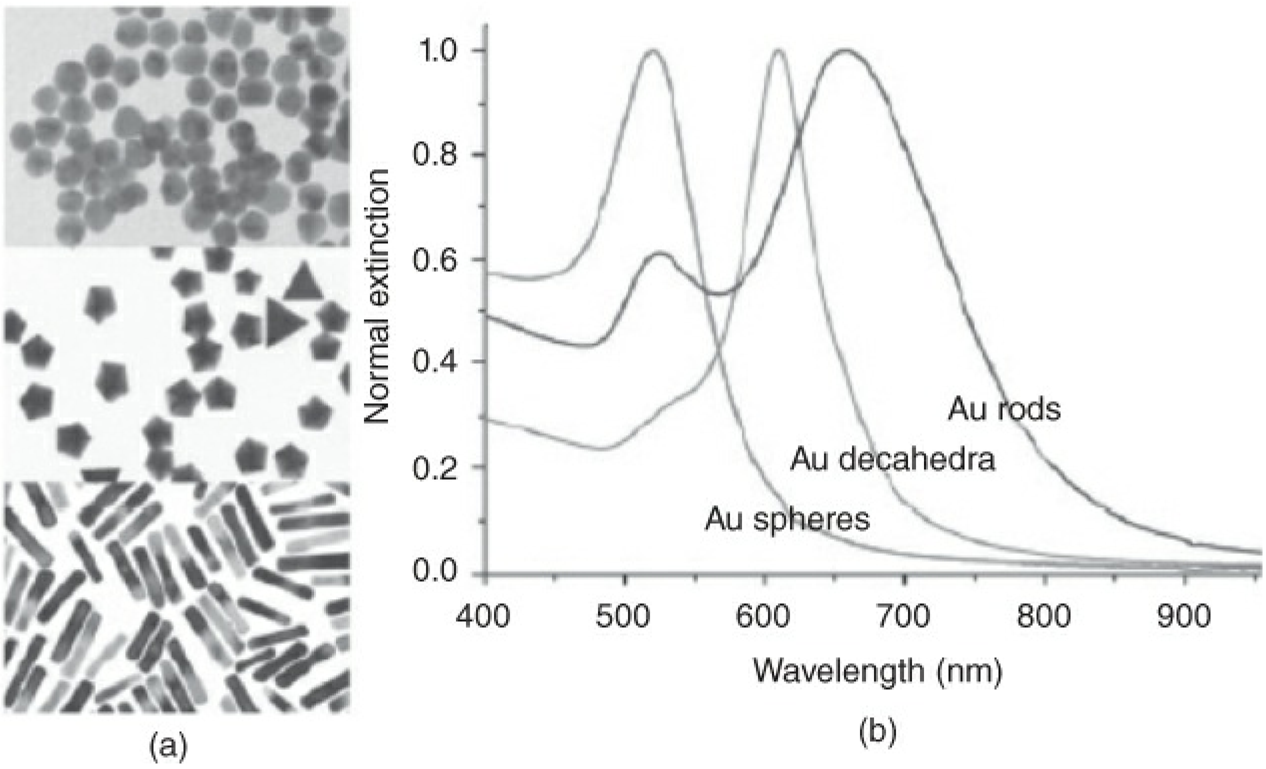

Figure 3.20 (a, b) UV–vis spectrum of gold nanoparticles with different geometries: spheres (top), decahedra (middle), and rods (bottom).

Sepulueda et al. [26], ©2009. With permission of Elsevier.

3.4.2 Vibrational Spectroscopies: FTIR and Raman Spectroscopy

Vibrational spectroscopies comprise Fourier transform infrared (FTIR) spectroscopy and Raman spectroscopy (RS). These two methods are used to investigate the structure of molecules. Both methods can be performed on dry powders or on liquid suspensions. The vibrational states probed by Raman spectroscopy are similar to those involved in infrared spectroscopy. However, the two vibrational spectroscopic techniques are complementary, in that vibrations that are strong in an infrared spectrum (those involving strong dipole moments) are typically weak in a Raman spectrum. Likewise, nonpolar functional group vibrations that give very strong Raman bands usually result in weak infrared signals. For example, stretching vibrations of hydroxyl, amine, and carbonyl groups are usually very strong in an FTIR spectrum but weak in a Raman spectrum. The stretching vibrations of carbon double and triple bonds and the symmetric vibrations of aromatic groups give a very strong Raman signal. Infrared spectroscopy and Raman spectroscopy are used as complementary techniques because each method looks at different aspects of a given sample. While IR is sensitive to functional groups and to highly polar bonds, Raman is more sensitive to backbone structures and symmetric bonds. Using both techniques provides twice the information about the vibrational structure than can be obtained by using either of them separately. These two techniques are discussed below with reference to their operational principle and applications in nanoscience and nanotechnology.

3.4.2.1 Fourier Transform Infrared Spectroscopy

FTIR spectroscopy is an absorption/transmission method used to probe chemical bonds and their crowding environment in molecular systems. From the IR spectrum, one can observe the absorption and emission due to the molecular vibration and rotation in the electromagnetic wave infrared region (15,000 ~ 10 cm^{-1}). The IR spectrum reveals the unknown composition qualitatively according to the characteristic frequency of the bands and determines the content of component in a sample (quantification) according to band intensity. It can also reveal the molecular structure (such as functional group, bond), identify isomer, and determine structures of compounds. This method can be used to measure samples in the gaseous, liquid, and solid states. Modern FTIR instruments are effective at measuring different classes of molecular substances in a short amount of time. FTIR bands for the stretching modes of some common bonds are as follows:

$$3700\text{–}2500\ \text{cm}^{-1}\ \text{for H} - (\text{C, N, O, or S})\ \text{stretching}$$

$$2300\text{–}2000\ \text{cm}^{-1}\ \text{for C} \equiv (\text{C or N})\ \text{stretching}$$

$$1900\text{–}1500\ \text{cm}^{-1}\ \text{for C}{=}(\text{C, N, or O})\ \text{stretching}$$

$$800\text{–}1300\ \text{cm}^{-1}\ \text{for C} - (\text{C, N, or O})\ \text{stretching}$$

The FTIR technique can distinguish between symmetric and antisymmetric bond stretching. The interaction among molecules can also be understood by anatomizing the band change. Since most organic molecules have single bonds, the region below 1500 cm^{-1} can become quite complex. The “fingerprint zone” (1300~400 cm^{-1}) reveals extremely sensitive changes in the molecular structure that provides a reliable determination to analyze unknown composition and structure.

FTIR is well adapted for organic compounds and is extensively used for the characterization of carbon nanoparticles for the detection of fullerenes or polycyclic aromatic hydrogenated (PAH) species. For FTIR, the absorption spectra can be deduced from transmission measurements through a KBr pellet with entrapped nanoparticles or directly on nanoparticles in a reflection mode measurement (DRIFT).

IR spectroscopy can be used to determine the crystallization and grain sizes in ceramic powders, for example, Si/C/N composites, where the spectra of the nanostructured powders differ significantly from the coarser bulk material.

IR spectroscopy may help in the identification of phase transfer that sometimes XRD cannot differentiate. For example, upon calcination, pure Fe_3O_4 nanoparticles transform into γ-Fe_2O_3 and α-Fe_2O_3. To reveal the difference in IR spectra of magnetite samples calcined at different temperatures (Figure 3.21), one can find the absorption peak of Fe–O in Fe_3O_4 at 571.1 cm^{-1}, which splits into two peaks at 632.9 and 563.4 cm^{-1}, respectively, after calcined at 150 °C for 2 h which are associated with Fe–O bond, are the characteristic peaks of γ-Fe_2O_3. Due to extreme similarity in crystal structure of the two phases, XRD is not sensitive enough to differentiate between Fe_3O_4 and γ-Fe_2O_3. Afterwards, the peak at 632.9 cm^{-1} becomes increasingly weaker and disappears, while another new peak at 463.1 cm^{-1} becomes stronger at 550 °C. The two absorption peaks at 532.5 cm^{-1} and 463.1 cm^{-1} can be assigned to the Fe–O absorption in hematite (α-Fe_2O_3). Therefore, one can get that 550 °C is the minimal temperature for the complete transformation from magnetite (Fe_3O_4) to hematite (α-Fe_2O_3), consistent with the results of the analyses of XRD and magnetic properties.

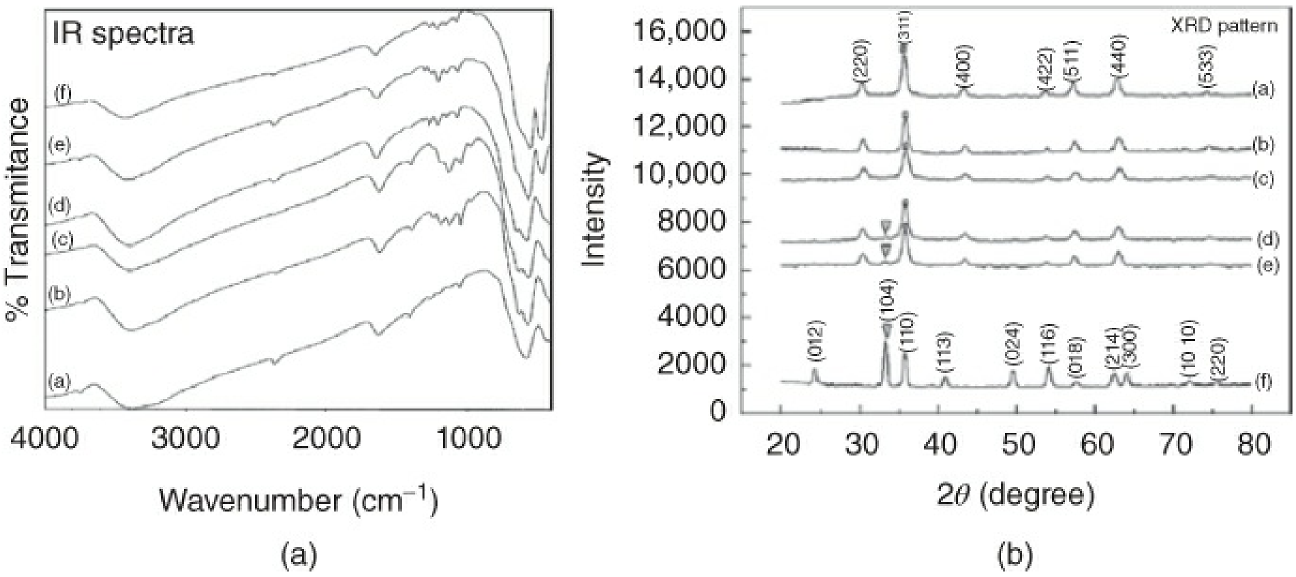

Figure 3.21 IR spectra and XRD pattern of pure Fe_3O_4 nanoparticles at: (a) room temperature and after calcination for 2 h at different temperatures; (b) 150 °C; (c) 250 °C; (d) 350 °C; (e) 450 °C; (f) 550 °C.

Li et al. [27], ©2009. With permission of Elsevier.

3.4.2.2 Raman Spectroscopy

Usually when light is scattered from an atom or molecule, it has the same energy (frequency) and wavelength as the incident light (Rayleigh scattering). This is an elastic scattering. However, a small fraction of the scattered light (approximately 1 in 10 million photons) is scattered by an excitation, with the scattered photons having energy (frequency) different from the frequency of the incident photons. This is known as **Raman effect**, the phenomenon first observed by C. V. Raman in 1928, who was awarded the Nobel Prize in 1930.

Raman spectroscopy, based on Raman effect, is used to study vibrational, rotational, and other low-frequency modes in a system of condensed matter physics and chemistry. It is based on inelastic scattering (Raman scattering) of monochromatic light usually from laser in the visible, near infrared, or near UV range. The laser light interacts with phonons or other excitations in the system, resulting in the energy of the laser photons being shifted up or down. The shift in the energy gives information about the phonon model in the system. All collective vibrations that occur in crystals can be viewed as the superposition of plane waves that virtually propagate to infinity. These plane waves, the so-called normal modes of vibration, are commonly modeled by quasiparticles called **phonons**.

The first ever Raman “instrument” was constructed in 1928 by Sir C. V. Raman where monochromatized sunlight was used as a light source and a human eye as a detector modified using arc lamps and photographic plates soon became very popular up until the 1950s. Since these early days, Raman instrumentation has evolved markedly. Modern instrumentation typically consists of a laser, Rayleigh filter, a few lenses, a spectrograph, and a detector (typically a CCD or ICCD). Raman spectrometers as shown schematically in Figure 3.22: a laser light excites the sample, light is scattered in all directions, and some of this light is directed to the detector, which records the Raman spectrum. Raman spectrum shows light at its original laser frequency (Rayleigh) and the spectral features that are unique to the sample.

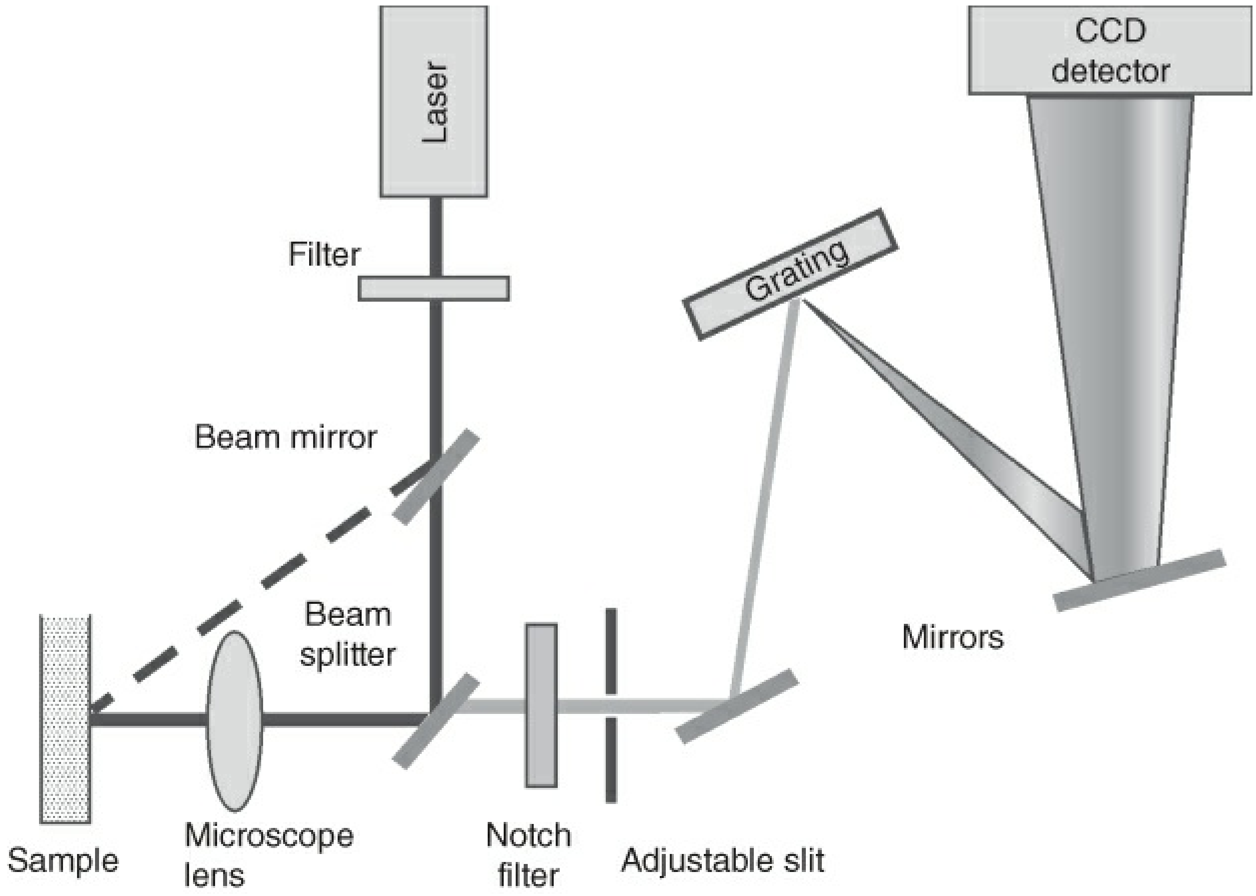

Figure 3.22 Schematic representation of Raman spectrometer.

Operational principle: In Raman spectroscopy, it is the shift in wavelength of the inelastically scattered radiation that provides the chemical and structural information. Raman-shifted photons can be of either higher or lower energy, depending on the vibrational state of the molecule under study. A simplified energy diagram that illustrates these concepts is shown on the right. Stokes radiation occurs at lower energy (longer wavelength) than the Rayleigh radiation, and anti-Stokes radiation has greater energy. The energy increase or decrease is related to the vibrational energy levels in the ground electronic state of the molecule, and as such, the observed Raman shift of the Stokes and anti-Stokes features is a direct measure of the vibrational energies of the molecule. A schematic Raman spectrum may appear as shown in Figure 3.22. The spontaneous Raman effect, which is a form of light scattering a photon, excites the molecule from the ground state to a virtual energy state. When the molecule relaxes, it emits a photon and it returns to a different rotational or vibrational state. The difference in energy between the original state and this new state leads to a shift in the emitted photon's frequency away from the excitation wavelength. The Raman effect, which is a light-scattering phenomenon, should not be confused with absorption (as with fluorescence) where the molecule is excited to a discrete (not virtual) energy level. If the final vibrational state of the molecule is more energetic than the initial state, the emitted photon will be shifted to a lower frequency for the total energy of the system to remain balanced. This shift in frequency is designated as a **Stokes shift**. If the final vibrational state is less energetic than the initial state, then the emitted photon will be shifted to a higher frequency, and this is designated as an **anti-Stokes shift**. Accordingly, the signal strength due to Stokes shift is higher than that of anti-Stokes shifts. Figure 3.23 shows the energy level diagram of the states involved in Raman signal; the line thickness is roughly proportional to the signal strength from the different transitions.

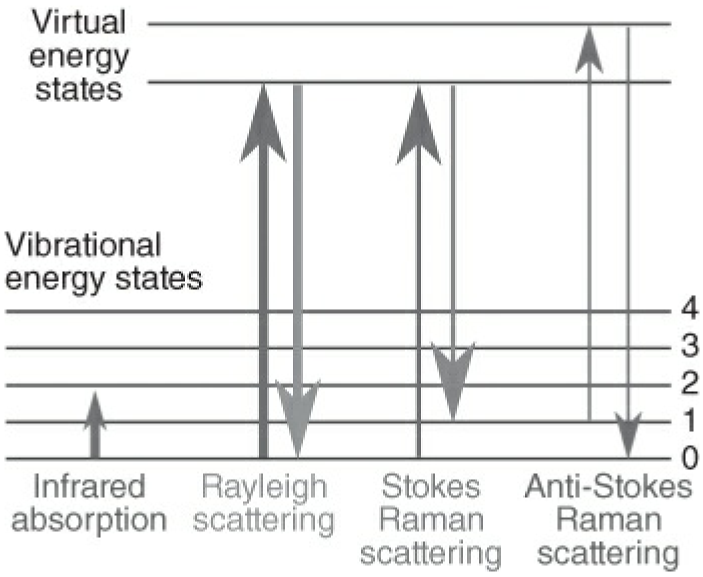

Figure 3.23 Energy level diagram showing the states involved in Raman signal.

The energy of the scattered radiation is less than the incident radiation for the Stokes line and the energy of the scattered radiation is more than the incident radiation for the anti-Stokes line. The energy increase or decrease from the excitation is related to the vibrational energy spacing in the ground electronic state of the molecule, and therefore the wavenumber of the Stokes and anti-Stokes lines is a direct measure of the vibrational energies of the molecule. The pattern of shifted frequencies is determined by the rotational and vibrational states of the sample. This dependence on the polarizability differs from infrared spectroscopy where the interaction between the molecule and light is determined by the dipole moment; this contrasting feature allows one to analyze transitions by Raman spectroscopy that might not be IR active. Spectral wavelength and shift in the Raman spectrum can be determined by the following formula (3.1):

$$\Delta w = \left(\frac{1}{\lambda_0} - \frac{1}{\lambda_1}\right), \tag{3.1}$$

where Δw is the Raman shift expressed in wave number (cm^{-1}), λ_0 is the excitation wavelength, and λ_1 is the Raman spectrum wavelength. Raman shifts are typically reported in wave numbers (inverse of wave length units), as this value is directly related to energy.

Applications of Raman spectroscopy (RS): Raman spectroscopy is commonly used in chemistry, since vibrational information is specific to the chemical bonds and symmetry of molecules. Therefore, it provides a fingerprint (range 500–2000 cm^{-1}) by which the molecule can be identified. Raman spectroscopy provides key information about the structure of molecules. The position and intensity of features in the spectrum reflect the molecular structure and can be used to determine the chemical identity of the sample. Spectra may also show subtle changes depending on the crystalline form. With the extensive spectral libraries that are now available, it is very straightforward to identify compounds by spectral library searching. In addition, Raman spectroscopy can be used to observe other low-frequency excitations of a solid, such as plasmons and superconducting gap excitations.

Characterizing carbon materials with Raman spectroscopy: Raman spectroscopy is shown to characterize and differentiate between two different carbon nanostructures such as fullerene, carbon nanotubes, and graphene (Figure 3.24). It is indeed one of the few techniques sensitive to the full range of structural states present in this class of materials, from perfectly crystalline to amorphous. The common crystalline phases of carbon yield very simple spectra: diamond (sp^3 hybridization) peaks at 1332 cm^{-1} (single mode of T$_2$g symmetry) whereas graphite (sp^2 hybridization) has doubly degenerate E$_2$g modes at 42 and 1582 cm^{-1}. The latter is referred to as G band and corresponds to vibrations in the graphene planes (which crystalline quality can be measured by the width of G band), whereas the former corresponds to weak interplanar van der Waals interactions (the reason for its low energy). Two additional modes appear whenever flaws are created, grain size is reduced, or graphene planes are curved. These modes are called D and D′ (the letter stands for “disorder”). D′ results from the splitting of G band and peaks around 1620 cm^{-1}, at the value where the dispersion curve of graphite is the flattest.

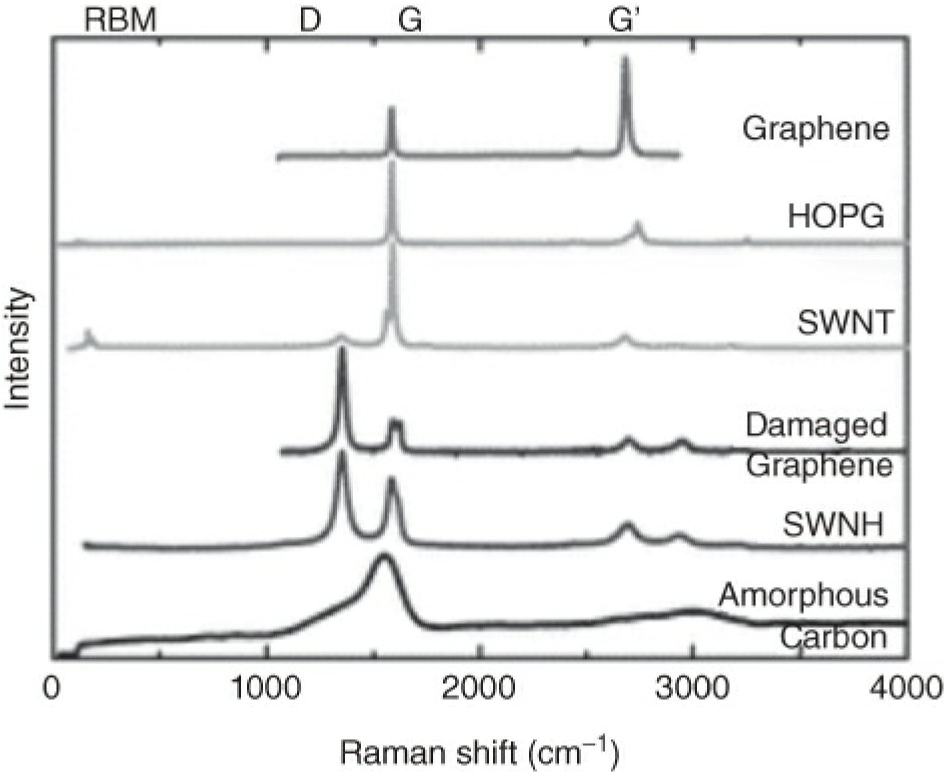

Figure 3.24 Raman spectra of allotropes of nanocarbon in comparison to amorphous carbon.

Dresselhaus, et al. [28], ©2010. With permission of ACS.

Extended application of Raman spectroscopy: For quite a long time, Raman spectroscopic technique was mainly devoted to fundamental research, but instrumental progress (laser miniaturization, CCD detection, notch filters, and data processing software) has rendered it as a general characterization method. Not only can it provide basic phase identification but subtle spectra alterations can be used to assess nanoscale structural changes and characterize micromechanical behavior. Consequently, RS has proved to be a unique tool for probing or mapping nanophase dispersed in a matrix (e.g., pigments in a ceramic glaze, precipitates in a fiber coating, surface-formed nanophase (corrosion mechanisms) and solid-state devices. Some specific features can even be used to study a charge transfer, a film orientation, the size of clusters trapped in nanocavities, Grüneisen parameter, configurational order (e.g., the proportion of trans–gauche chains in poly(ethyleneterephthalate) PET) or intercalation, interfacial, and polymerization reactions.

Raman spectroscopy being noninvasive offers several advantages for microscopic analysis. For example, the specimens need not be fixed or sectioned; spectra can be collected from a very small volume (<1 μm in diameter) for the identification of species present therein. Water does not generally interfere with Raman spectral analysis, thus making it suitable for the microscopic examination of minerals, materials (polymers and ceramics), cells, proteins, and forensic trace evidence. In *direct imaging*, the whole field of view is examined for scattering over a small range of wavenumbers (Raman shifts). For instance, a wavenumber characteristic for cholesterol could be used to record the distribution of cholesterol within a cell culture.

Dispersive Raman microscopy is ideal for the analysis of very small samples. Since spatial resolution is diffraction limited, the short excitation laser wavelengths used for dispersive Raman are optimal for analyzing small sample features. With 532 nm excitation, a modern Raman microscope can achieve submicron spatial resolution. The analysis of small defects in the polymer films used in liquid crystal displays is a typical application

3.4.3 Raman Spectroscopy Based Imaging

Raman spectroscopy is a promising technique for the identification and analysis of molecules in a sample without any labeling or modification. For imaging applications, several variations of Raman spectroscopy with enhanced sensitivity have been developed. Raman spectroscopy-based imaging includes the following: coherent anti-Stokes Raman spectroscopy (**CARS**), primarily used for imaging the C–H bond in lipids; surface-enhanced Raman spectroscopy (**SERS**), where a variety of nanoparticles can be used as contrast agents; and tip-enhanced Raman spectroscopy (**TERS**) to improve the spatial resolution of Raman microscopy or to acquire very specific information (resonance Raman).

Over the last several years, Raman spectroscopy imaging has advanced significantly and many critical proof-of-principle experiments have been successfully carried out. Since Raman scattering spectra provide information about intracellular molecular distributions, metabolism, and chemical reactions, Raman microscopy has been widely utilized for bioimaging and biofunctional analysis. It is expected that imaging with Raman spectroscopy will continue to be a dynamic research field over the next decade.

3.4.3.1 Surface-Enhanced Raman Spectroscopy (SERS)

The Raman scattering from a compound (or ion) adsorbed on or even within a few Angstroms of a structured metal surface can be 10^3–10^6 times greater than in a solution. This surface-enhanced Raman scattering is strongest on silver, but is observable on gold and copper as well. At practical excitation wavelengths, enhancement on other metals is not so important. SERS arises as a result of two mechanisms: (1) enhanced electromagnetic field produced at the surface of the metal, and (2) enhancement by the formation of a charge–transfer complex between the surface and analyte molecule. When the wavelength of the incident light is close to the plasma wavelength of the metal, conduction electrons in the metal surface are excited into an extended surface electronic excited state called a surface plasmon resonance. Molecules adsorbed or in close proximity to the surface experience an exceptionally large electromagnetic field. Vibrational modes normal to the surface are most strongly enhanced. The electronic transitions of many charge-transfer complexes are in the visible range so that resonance enhancement occurs. Molecules with lone-pair electrons or π-clouds show the strongest SERS. The effect was first discovered with pyridine. Other aromatic nitrogen or oxygen-containing compounds, such as aromatic amines or phenols, are strongly SERS active. The effect can also been seen with other electron-rich functionalities such as carboxylic acids. The intensity of the surface plasmon resonance is dependent on many factors including the wavelength of the incident light and the morphology of the metal surface. The wavelength should match the plasma wavelength of the metal. This is about 382 nm for a 5 μm silver particle, but can be as high as 600 nm for larger ellipsoidal silver particles. The plasma wavelength is toward the right of 650 nm for copper and gold, the other two metals show SERS at wavelengths in the 350–1000 nm region. The best morphology for surface plasmon resonance excitation is a small (<100 nm) particle or an atomically rough surface. SERS is commonly employed to study monolayers of materials adsorbed on metals, including electrodes. Other popular surfaces include colloids, metal films on dielectric substrates, and, recently, arrays of metal particles bound to metal or dielectric colloids through short linkages. SERS allows easy observation of Raman spectra from solution concentrations in micromolar range. The superb multiplexing capability of SERS-based Raman imaging can be extremely powerful in future research where different agents can be attached to different Raman tags to enable the interrogation of multiple biological events simultaneously in living subjects.

The SERS effect can induce a signal enhancement of more than 100 times. The SERS signal depends on the characteristics of the nanosubstrate: the size, shape, orientation, and composition of the surface nanoroughness. Advancement in SERS technology allows detection at the attomole (10^{-18} M) level and detection of a single molecule. Integration of scanning near-field optical microscopy (SNOM) and Raman for acquiring Raman images via an SNOM tip is suited for very strong Raman scatterers or surface-enhanced Raman spectroscopy (SERS) experiments because of the low light levels.

3.4.3.2 Tip-Enhanced Raman Spectroscopy (TERS)

TERS can be applied to obtain a lateral resolution far below the diffraction limit. In a typical TERS experiment, a gold- or silver-coated AFM tip is utilized as a nanostructure to create signal enhancement on the surface of a sample after focusing the excitation laser on the apex of a tip (Figure 3.25), and the tip is brought very close to the surface. The tip radius is in the range 10–20 nm and defines the lateral resolution of an AFM measurement. The lateral resolution is based on the size of the hot spot in a TERS experiment, and one can expect a resolution in the 20–50 nm range for Raman spectroscopy and imaging measurements.

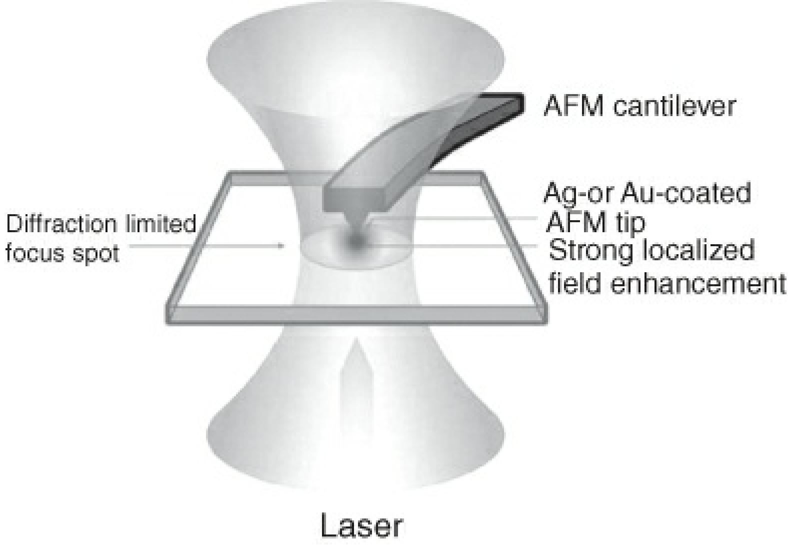
AFM cantilever
Ag-or Au-coated AFM tip
Strong localized field enhancement
Diffraction limited focus spot
Laser

Figure 3.25 Working principles of TERS.

Courtesy: Gordon, University of California, Santa Barbara.

The application possibilities range from obtaining single Raman spectra in TERS mode to nanoscale Raman imaging. TERS seems to be ideal for chemical imaging at a resolution beyond the diffraction limit. However, various challenges must be taken into consideration to establish this method as a standard and routine analysis technique.

3.4.3.3 Confocal Raman Imaging

Confocal microscopy is an optical imaging technique that employs a point light source (laser), which is directed onto the sample. The same objective usually collects the reflected (fluorescence) light, which is focused into a pinhole in front of the detector. This is made to make sure that only light from the image focal plane reaches the detector, which considerably increases image contrast; resolution can also be increased with appropriate selection of pinhole size. Unique filters are utilized to restrain the reflected laser light while allowing the Raman scattered light to be detected with a combination of charge couple devices (CCD) camera and spectrometer. In order to acquire an image, thousands of spectra are obtained in an extremely short time with less than 100 ms integration time per spectrum.

In confocal Raman imaging, the use of a spectroscopic electron multiplying charge couple devices (EMCCD) as the detector can considerably reduce the acquisition time down to a few milliseconds per spectrum, while enhancing sensitivity. However, since the Raman scattering cross section is small and the excitation power is restricted to a few milliwatts, it becomes challenging to enhance the overall sensitivity of a confocal Raman system. Choosing an appropriate detector with the highest sensitivity is very important.

An EMCCD is a standard back-illuminated CCD with an extra readout register, which is driven with a higher clock voltage than a normal CCD readout register. Owing to this high clock voltage, an electron multiplication via impact ionization is obtained by amplifying the signal up to 1000 times. With this arrangement, it is possible to increase the signal higher than the readout noise so that the signal-to-noise ratio is always restricted by the Poisson noise of the signal, even if an extremely fast readout amplifier is employed. For instance, a 1600 × 200 pixel EMCCD with a 2.5-MHz readout amplifier can be read out in just 2.3 ms. For higher signals, wherein the intensity of signal is not readout limited, the excess noise factor of the EM process reduces the EMCCD's signal-to-noise ratio to less than that of a standard CCD. In such cases, the EM register can be switched off and the “normal” readout register is utilized.

3.4.4 X-Ray Photoelectron Spectroscopy (XPS)

Electron spectroscopy is mainly used to identify the chemical compositions of the sample. Depending on the source of excitation and the product being detected, there are a variety of spectroscopic techniques including AES, XPS, and EDX. XPS, also called electron spectroscopy for chemical analysis (ESCA), was pioneered by the Swedish physicist K. Siegbahn, who subsequently received the 1981 Noble Prize in Physics for his work. XPS enables the determination of the surface chemistry and the way in which that chemistry changes in the surface and near-surface region. XPS provides quantitative elemental and chemical information with extremely high surface specificity (from outer 10 nm of the sample). Depth profiling extends the technique measuring this film layers. XPS is ideal for comprehensively and quantitatively characterizing the composition and chemical bonding states at surfaces and interfaces. XPS is a method used to determine the elemental composition of a material's surface; however, it can be further applied to determine the chemical or electronic state of these elements [29]. One of the most important applications of XPS has been the identification of oxidation states of elements in inorganic compounds.

The photoelectric effect is the ejection of electrons from the surface of a material upon exposure to electromagnetic radiation of sufficient energy (Figure 3.26a–c). Electrons emitted have characteristic kinetic energies proportional to the energy of the radiation,

$$\mathrm{KE} = h\nu - E_b - \varphi \tag{3.2}$$

where KE is the kinetic energy of the electron, h is the Planck's constant, v is the frequency of the incident radiation, E_b is the ionization, or binding, energy, and . is the work function. The work function is a constant which is dependent on the spectrometer.

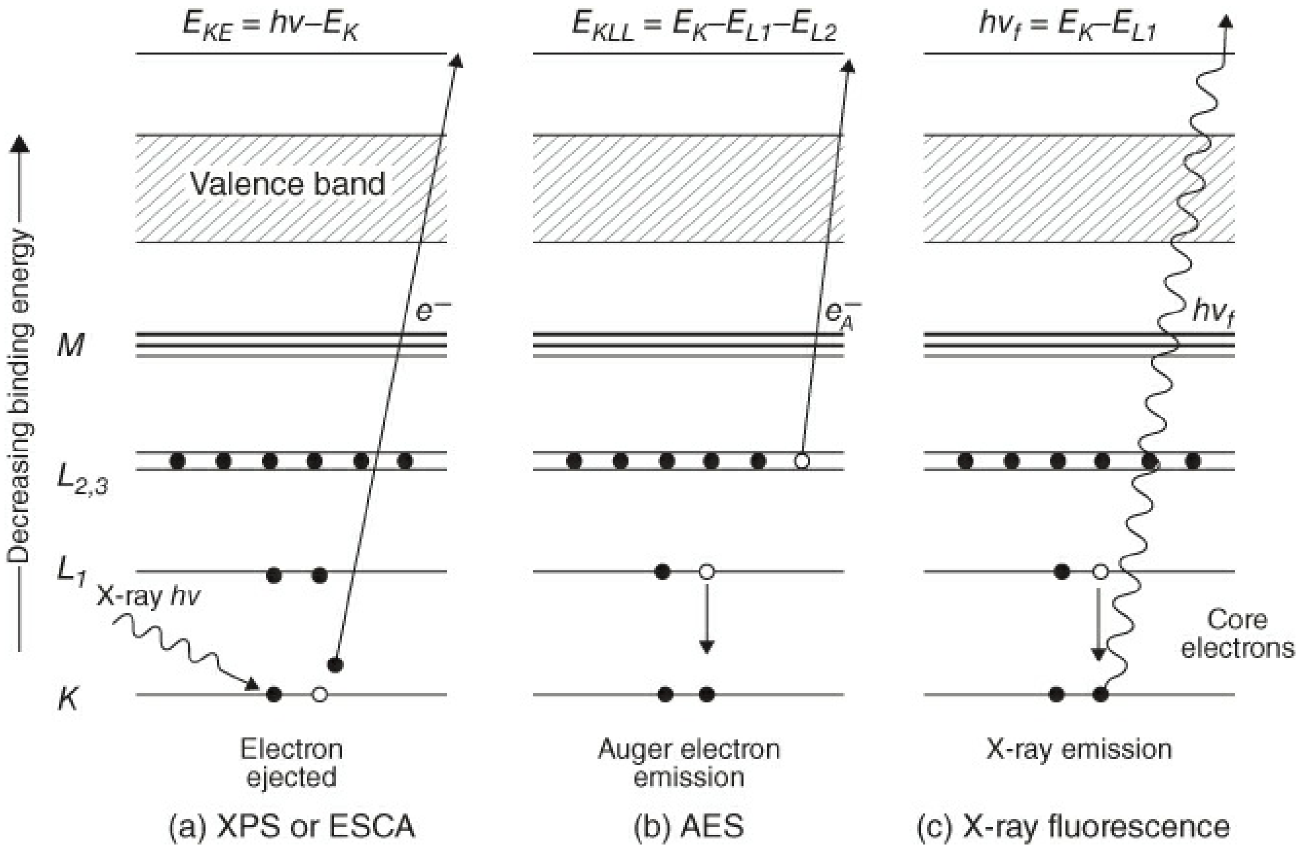

Figure 3.26 Schematic electron spectroscopy: (a) X-ray photoelectron spectroscopy; (b) Auger spectroscopy; and (c) X-ray fluorescence spectroscopy.

In photoelectron spectroscopy, high-energy radiation is used to expel core electrons from a sample. The kinetic energies of the resulting core electrons are measured. Using the equation with the kinetic energy and known frequency of radiation, the binding energy of the ejected electron may be determined. By Koopman's theorem, which states that ionization energy is equivalent to the negative of the orbital energy, the energy of the orbital from which the electron originated is determined. These orbital energies are characteristic of the element and its state. Figure 3.26a–c is a schematic representation of the physical process involved in various electron spectroscopic techniques. As shown in the illustration, one of the photons of a monochromatic X-ray beam of known energy hv displaces an electron e^- from a K-orbital of energy E_b. The process can be represented as

$$A + hv \rightarrow A^{+*} + e^- \qquad \textbf{3.3}$$

where A can be an atom, a molecule, or an ion and A^{+*} is an electronically excited ion with one positive charge greater than that of A.

Various methods are available to determine the value of v. The binding energy of an electron is the characteristic of the atom and orbital that emits the electron. XPS/ESCA provides a means of qualitative identification of the elements present on the surface of solids. Electron spectroscopy records the kinetic energy of emitted electrons, the spectrum thus consists of a plot of the number of emitted electrons, or the power of the electron beam, as a function of the energy (or the frequency or wavelength) of the emitted electrons.

Instrumentation: Electron spectrometers essentially have components whose functions are analogous to those encountered in optical spectroscopic instruments. These components include (1) a source; (2) a sample holder; (3) an analyzer, which has the same function as a monochromator; (4) a detector; and (5) a signal processor and readout. Figure 3.27 shows a typical arrangement of these components. Electron spectrometers generally required elaborate vacuum systems to reduce the pressure in all of the components to as low as 10^{-8}–10^{-10} torr.

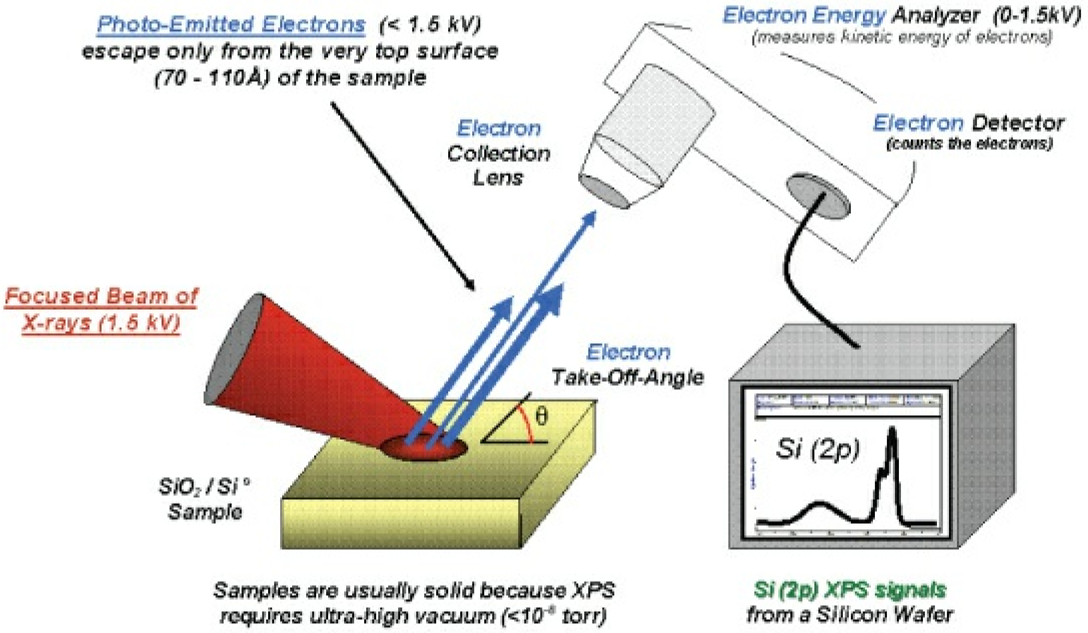
Photo-Emitted Electrons (< 1.5 kV)
escape only from the very top surface
(70 - 110Å) of the sample
Electron Energy Analyzer (0-1.5kV)
(measures kinetic energy of electrons)
Electron Collection Lens
Electron Detector
(counts the electrons)
Focused Beam of X-rays (1.5 kV)
Electron Take-Off-Angle
θ
SiO_2 / Si°
Sample
Si (2p)
Samples are usually solid because XPS requires ultra-high vacuum (<10^{-8} torr)
Si (2p) XPS signals from a Silicon Wafer

Figure 3.27 Basic components of XPS/ESCA instrument. https://en.wikipedia.org/wiki/X-ray_photoelectron_spectroscopy.

Source: The X-ray sources for XPS spectrometers are X-ray tubes equipped with magnesium or aluminum targets and suitable filters. Monochromatic aluminum ($h\nu$ = 1486.6 eV) or magnesium ($h\nu$ = 1253.6 eV) K_α X-rays are used to eject core electrons from the sample. The *K*∝ lines for these two elements have considerably narrower bandwidths (0.8–09 eV) than those encountered with higher atomic number targets; narrow bands are desirable because they lead to enhanced resolution. Nonmonochromatic sources typically illuminate a spot of a few centimeters in diameter. Relatively sophisticated XPS instruments employ a crystal monochromator to provide an X-ray beam having a bandwidth of about 0.3 eV.

Sample holders: Solid samples are mounted in a fixed position as close as possible to the photon or electron source and the entrance slit of the spectrometer.

Detector: The photoelectrons ejected from the material are detected and their energies measured. Ultrahigh vacuum conditions are used in order to minimize gas collisions interfering with the electrons before they reach the detector. The detector consists of collection lens and the electron energy analyzer, which disperses the emitted electrons according to their kinetic energy. The lens system usually allows a wide collection angle (−30°) for high efficiency.

In some angle-resolved experiments, an aperture reduces the angles collected. Such experiments are used in depth-profiling studies. Typically, photoelectron experiments are carried out in constant analyzer energy mode, in which electrons are accelerated or retarded by the lens system to some user-defined energy as they pass through the analyzer (the pass energy, *E*). Often, pass energies of 5–25 eV will give high-resolution spectra, and 100–200 eV pass energies are used for survey scans. The signal intensity decreases as the pass energy decreases. Most energy analyzers are of the type as illustrated in Figure 3.29, where the electron beam is deflected by the electrostatic field of a hemispherical capacitor. The electrons thus travel in a curved path from the lens to the multichannel transducer. The radius of curvature depends on the kinetic energy of the electrons and the magnitude of the electrostatic field. An entire spectrum is obtained by varying the field so as to focus electrons of various kinetic energies on the transducer. Most modern electron spectrometers are based on solid-state channel electron multipliers, which consist of tubes of glass that have been doped with lead or vanadium. When a potential difference of several kilovolts is applied across these materials, a cascade or pulse of 10^6–10^8 electrons is produced for each incident electron.

Data collection: X-ray photoelectron (XP) spectra provide the relative frequencies of binding energies of electrons detected, measured in electron volts (eV). Detectors have accuracies on the order of ±0.1 eV. The binding energies are used to identify the elements to which the peaks correspond. XPS data are given in a plot of intensity versus binding energy. Intensity may be measured in counts per unit time (such as counts per second, denoted c/s). Often, intensity is reported as arbitrary units, since only relative intensities provide relevant information. Comparing the areas under the peaks gives relative percentages of the elements detected in the sample. Initially, a survey XP spectrum (Figure 3.28) is obtained, which shows all of the detectable elements present in the sample. Elements with low detection limit of the spectrometer may be missed with the survey scan, which may be obtained by repeating a high-resolution spectrum. High-resolution scans of a peak can also be used to distinguish among species of the same element.

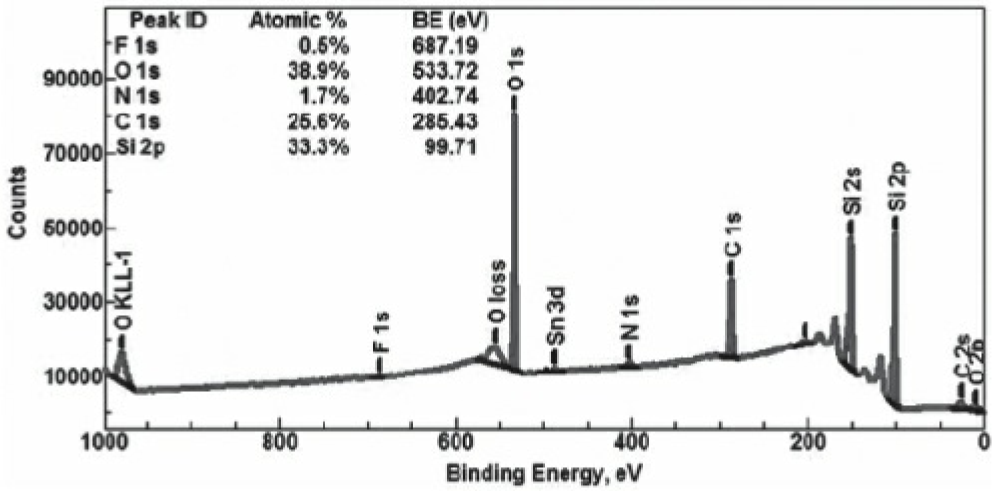

Figure 3.28 XPS scan survey spectrum for all elements. https://en.wikipedia.org/wiki/X-ray_photoelectron_spectroscopy.

The photoelectrons produced in XPS are incapable of passing through more than perhaps 1–5 nm of a solid. Thus, the most important applications of electron spectroscopy, such as X-ray microprobe spectroscopy, are for the accumulation of information about surfaces. Examples of some of its uses include identification of active sites and poisons on catalytic surfaces, determination of surface contaminants on semiconductors, analysis of the composition of human skin, and study of oxide surface layers on metals and alloys. It is also evident that the method has a substantial potential in the elucidation of chemical structure. Information from XPS spectra is comparable to that from nuclear magnetic resonance (NMR) or IR spectroscopy. The ability of XPS to distinguish among oxidation states of an element in noteworthy.

Both hydrogen and helium cannot be detected using XPS. For this reason, XPS can provide only relative, rather than absolute, ratios of elements in a sample. Also, elements with relatively low atomic percentages close to that of the detection limit or low detection by XPS may not be seen in the spectrum. Furthermore, each peak represents a distribution of observed binding energies of ejected electrons based on the depth of the atom from which they originate, as well as the state of the atom. Electrons from atoms deeper in the sample must travel through the above layers before being liberated and detected, which reduces their kinetic energies and thus increases their apparent binding energies. The width of the peaks in the spectrum consequently depends on the thickness of the sample and the depth to which the XPS can detect; therefore, the values obtained vary slightly depending on the depth of the atom. Additionally, the depth to which XPS can analyze depends on the element being detected. High-resolution scans of a peak can be used to distinguish among species of the same element. However, the identification of different species is discretionary. Computer programs are used to deconvolute the elemental peak. The peaks may then be assigned to a particular species, but the peaks may not correspond with the species in the sample.

Application of XPS to characterize nanomaterials: XPS is a facile and effective method for determining the elemental composition of a material's surface. As a quantitative method, it gives the relative ratios of detectable elements on the surface of the material. Additional analysis can be done to further elucidate the surface structure. Despite the aforementioned limitations, XPS is a powerful surface technique that can be used to accurately detect the presence and relative quantities of elements in a sample. This is particularly useful for carbon nanomaterials, in which surface structure and composition greatly influence the properties of the material. There is great research interest in modifying carbon nanomaterials to modulate their properties for use in many different applications. Hybridization, bonding, functionalities, and reaction progress are among the characteristics that can be inferred using XPS. The application of XPS to carbon nanomaterials provides much information about the material, particularly the allotropic forms, which are most important for the properties and uses of carbon nanomaterials.

Carbon nanomaterials: The effect of structure on the position of XPS peaks for carbon in three different allotropic forms of carbon nanomaterials, namely, graphene, CNTs, and fullerene, is illustrated in Figure 3.29. In each case, the peaks correspond to the 1s electron of the carbon atom; however, the shift in binding energies can be rationalized by taking into account the influence of the various functional groups on the effective nuclear charge experienced by the 1s core electron. For example, presence of nitrogen in graphene (Figure 3.29a), attached fluorine atoms to carbon of CNTs (Figure 3.29b), causes a shift toward higher binding energy. The effective nuclear charge felt by the carbon 1s electron in the later is a maximum, as is the binding energy owing to the electron-withdrawing capability of fluorine. Figure 3.29c shows an XPS of fullerene film without (b) and with (a) plasma excitation during the deposition process.

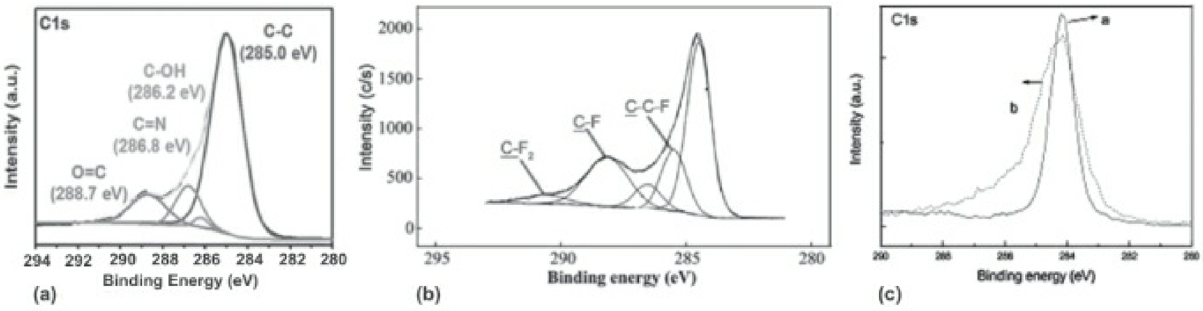

Figure 3.29 C_{1s} XPS of carbon nanomaterials: (a) graphene oxide. Huang [30], © 2012. With permission of RSC; (b) fluorinated SWNTs. Dillon et al. [31], © 2008. With permission of ACS; and (c) fullerene. Arie and Lee [32], © 2009. With permission of Hanyang university, Korea.

Nanometal/Metal Oxides: XPS is quite useful to characterize the ionic state of metal ions and chemical composition of nanometal oxides. For example, XPS spectra of TiO_2–WO_3 thin film (Figure 3.30a) obtained from survey scans on the surface of the co-evaporated film between binding energies 0 and 1200 eV. As expected elements of C, O, Ti, and W were detected along with the impurities of K and P. From high-resolution spectra (Figure 3.30b), the core levels of Ti-$2p_{1/2}$ and Ti-$2p_{3/2}$ are found at binding energies of 465.6 eV and 459 eV, respectively, with a peak separation of 6.6 eV. Figure 3.30c shows the core level of W-$4f_{5/2}$ (38.2 eV) and W-$4f_{7/2}$ (36 eV) obtained from high-resolution measurements and the two peaks are separated by 2.2 eV. The binding energy Ti-$2p_{3/2}$ peak (459 eV) corresponds to the fully oxidized Ti^{+4} in titanium dioxide showing that the Ti in the metal oxide film can be assigned to the TiO_2 and the binding energy of W-$4f_{7/2}$ (36 eV) is in agreement with the corresponding characteristic binding energy of W-4f (35.8 eV) in tungsten trioxide film. The peak position of O 1 s was at 531 eV but this value is shifted, for example, by 1.1 eV when compared with the core level of O 1 s (529.9 eV) of the anatase TiO_2 film. This can be due to the nanocrystalline nature of the mixed oxide thin film that may cause a shift of the core levels.

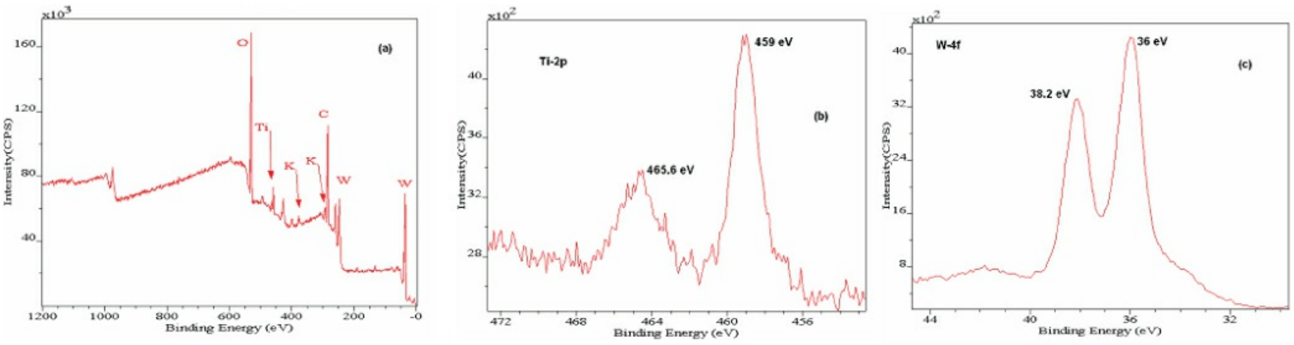

Figure 3.30 XPS spectra of TiO_2–WO_3 thin film: (a) survey scan between binding energy 0 and 1200 eV before etching; (b) high-resolution peaks for Ti-2p after etching the film; (c) high-resolution peaks for Ti-2f after etching.

Tesfamichael et al. [33], © 2006. With permission of Elsevier.

Depth profiling of nanostructures is of high importance both technologically and fundamentally. Therefore, many different methods (destructive and nondestructive) have been developed for the determination of the depth distribution of atoms. Each of the depth-profiling techniques has its own advantages and disadvantages. However, in many cases, nondestructive techniques are preferred; these include ARXPS and XPS peak-shape analysis. The former together with parallel factor analysis is suitable for giving an overall understanding of chemistry and morphology with depth. It works very well for flat surfaces but it fails for rough or nanostructured surfaces because of the shadowing effect. In the latter method, shadowing effects can be avoided because only a single spectrum is used in the analysis, and this may be taken at near normal emission angle. It is a rather robust means of determining atom depth distributions on the nanoscale both for large-area XPS analysis and for imaging. Traditional XPS analysis relies on XPS peak intensity, assuming that the concentration in the surface region is proportional to the XPS peak intensity. The XPS peak-shape method is nondestructive and, therefore, also allows one to study the change in surface composition during surface treatment as, for example, in chemical reactions and gradual annealing. It has been applied in the study of a wide range of systems and physical phenomenon including growth mechanisms and nanostructures of metal/metal, metal/metal oxide, films, and so on.

3.4.5 Auger Electron Spectroscopy

Auger electron spectroscopy (AES) is one of the most commonly employed surface analysis techniques. It uses the energy of emitted electrons to identify the element present in a sample, similar to XPS. The main difference is that XPS uses an X-ray beam to eject an electron while AES uses an electron beam to eject an electron. In AES, the sample depth is dependent on the escape energy of the electrons. It is not a function of the excitation source as in XPS. In AES, the collection depth is limited to 1–5 nm due to the small escape depth of electrons, which permits the analysis of the first 2–10 atomic layers. In addition, a typical analysis spot size is roughly 10 nm. A representative AES spectrum illustrating the number of emitted electrons, *N*, as a function of kinetic energy, *E*, in direct form (gray) and in differentiated form (black) is shown in Figure 3.31.

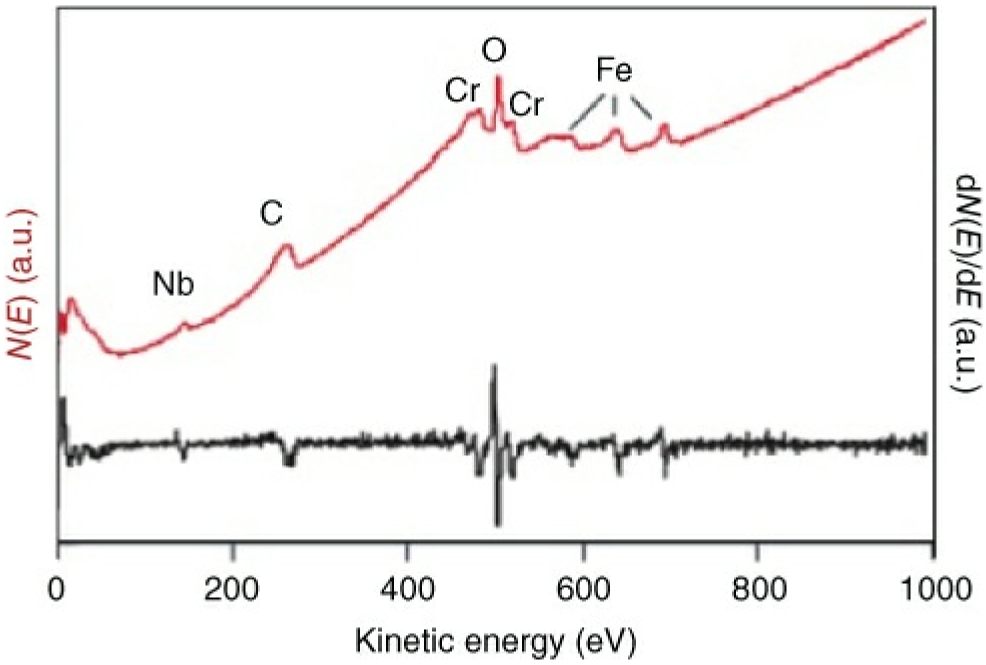

Figure 3.31 AES survey spectrum (upper trace) and differentiated spectrum (lower trace) of an oxidized Fe–Cr–Nb alloy.

Vickerman [29], © 2011. With permission of Wiley-VCH, Weinheim.

Similar to XPS, AES measures the kinetic energy (E_k) of an electron to determine its binding energy (E_b). The binding energy is inversely proportional to the kinetic energy and can be found from Equation 3.4, where hv is the energy of the incident photon and ΔΦ is the difference in work function between the sample and the detector material.

$$E_b = hv - E_k + \Delta\Phi \tag{3.4}$$

Since the E_b is dependent on the element and the electronic environment of the nucleus, AES can be used to distinguish elements and their oxidation states. For instance, the energy required to remove an electron from Fe^{3+} is more than in Fe^{0}. Therefore, the Fe^{3+} peak will have a lower E_k than the Fe^{0} peak, effectively distinguishing the oxidation states.

Auger process: An Auger electron comes from a cascade of events. First, an electron beam comes in with sufficient energy to eject a core electron creating a vacancy. Typical energies of the primary electrons range from 3 to 30 keV. A secondary electron (imaging electron) of higher energy drops down to fill the vacancy (B) and emits sufficient energy to eject a tertiary electron (Auger electron) from a higher shell (C) as shown in Figure 3.26. The shells from which the electrons move from the lowest energy to the highest energy are described as the K-shell, L-shell, and M-shell. This nomenclature is related to quantum numbers. Explicitly, the K-shell represents the 1 s orbital, the L-shell represents the 2s and 2p orbitals, and the M-shell represents the 3s, 3p, and 3d orbitals. The cascade of events typically begins with the ionization of a K-shell electron, followed by the movement of an L-shell electron into the K-shell vacancy. Then, either an L-shell electron or M-shell electron is ejected. It depends on the element, which peak is prevalent but often both peaks will be present. The peak seen in the spectrum is labeled according to the shells involved in the movement of the electrons. For example, an electron ejected from a gold atom could be labeled as Au KLL or Au KLM. The intensity of the peak depends on the amount of material present, while the peak position is element dependent. Auger transitions characteristic of each elements can be found in the literature [29].

Instrumentation: Important elements of an Auger spectrometer include a vacuum system, an electron source, and a detector. AES must be performed at pressures less than 10^{-3} Pascal (Pa) to keep residual gases from adsorbing to the sample surface. This can be achieved using an ultrahigh vacuum system with pressures from 10^{-8} to 10^{-9} Pa. Typical electron sources include tungsten filaments with an electron beam diameter of 3–5 μm, LaB_6 electron sources with a beam diameter of less than 40 nm, and Schottky barrier filaments with a 20-nm beam diameter and high beam current density. Two common detectors are the cylindrical mirror analyzer and the concentric hemispherical analyzer discussed earlier. Notably, concentric hemispherical analyzers typically have better energy resolution.

Cylindrical mirror analyzer and concentric hemispherical analyzer: A cylindrical mirror analyzer (CMA) composed of an electron gun, two cylinders, and an electron detector (Figure 3.32a). The operation of a CMA involves an electron gun being directed at the sample. An ejected electron then enters the space between the inner and outer cylinders (IC and OC). The inner cylinder is at ground potential, while the outer cylinder's potential is proportional to the kinetic energy of the electron. Due to its negative potential, the outer cylinder deflects the electron toward the electron detector. Only electrons within the solid angle cone are detected. The resulting signal is proportional to the number of electrons detected as a function of kinetic energy. A concentric hemispherical **analyzer** (CHA) contains three parts, that is, a retarding and focusing input lens assembly; an inner and outer hemisphere (IH and OH); and an electron detector as illustrated in Figure 3.32b. Electrons ejected from the surface enter the input lens, which focuses the electrons and retards their energy for better resolution. Electrons then enter the hemispheres through an entrance slit. A potential difference is applied on the hemispheres so that only electrons with a small range of energy differences reach the exit. Finally, an electron detector analyzes the electron.

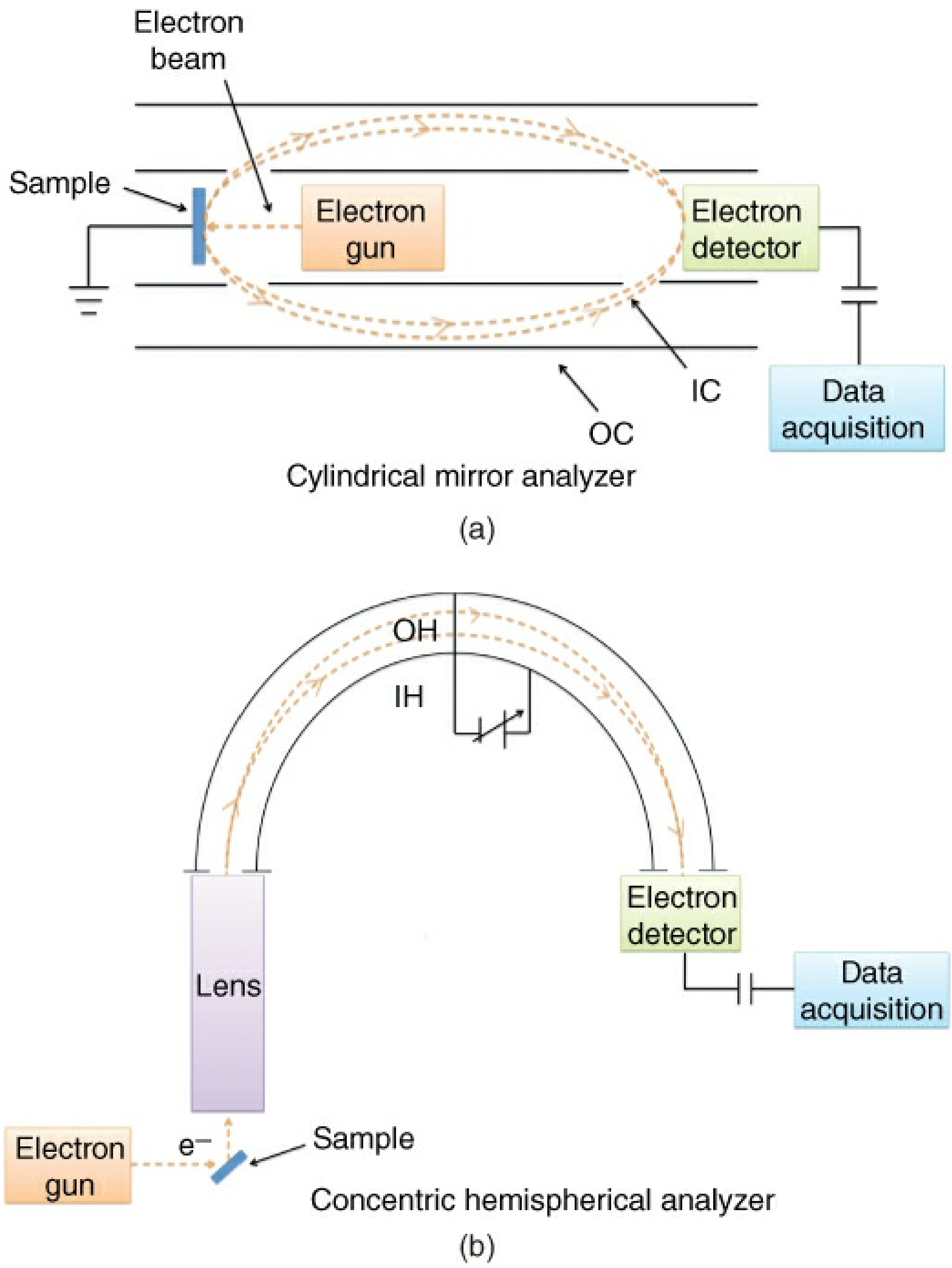

Figure 3.32 Schematics: (a) cylindrical mirror analyzer; (b) concentric hemispherical analyzer.

Vickerman [29], © 2011. With permission of Wiley-VCH, Weinheim.

Applications: AES is an excellent complementary technique to SEM in that AES can provide elemental maps with significantly better spatial resolution and surface sensitivity than SEM/EDS. The typical information depth for Auger is in the range of 30–60 Å (3–6 nm), with a spatial resolution in the 10 nm range. AES is in widespread use owing to its ability to analyze small spot sizes with diameters from 5 µm down to 10 nm depending on the electron gun. For instance, AES is commonly employed to study film growth and surface chemical composition, as well as grain boundaries in metals and ceramics. It is also used for quality control surface analyses in integrated circuit production lines due to short acquisition times. Moreover, AES is used for areas that require high spatial resolution, which XPS cannot achieve. AES can also be used in conjunction with TEM and SEM to obtain a comprehensive understanding of microscale materials, both chemically and structurally. As an example of combining techniques to investigate microscale materials, the characterization of a single wire from an Sn–Nb multiwire alloy is shown. Figure 3.33a is an SEM image of the singular wire and Figure 3.33b depicts the distribution of Nb and Sn within the wire, while Figure 3.33c gives a point analysis along the length of the wire to determine the percent concentrations of Nb and Sn.

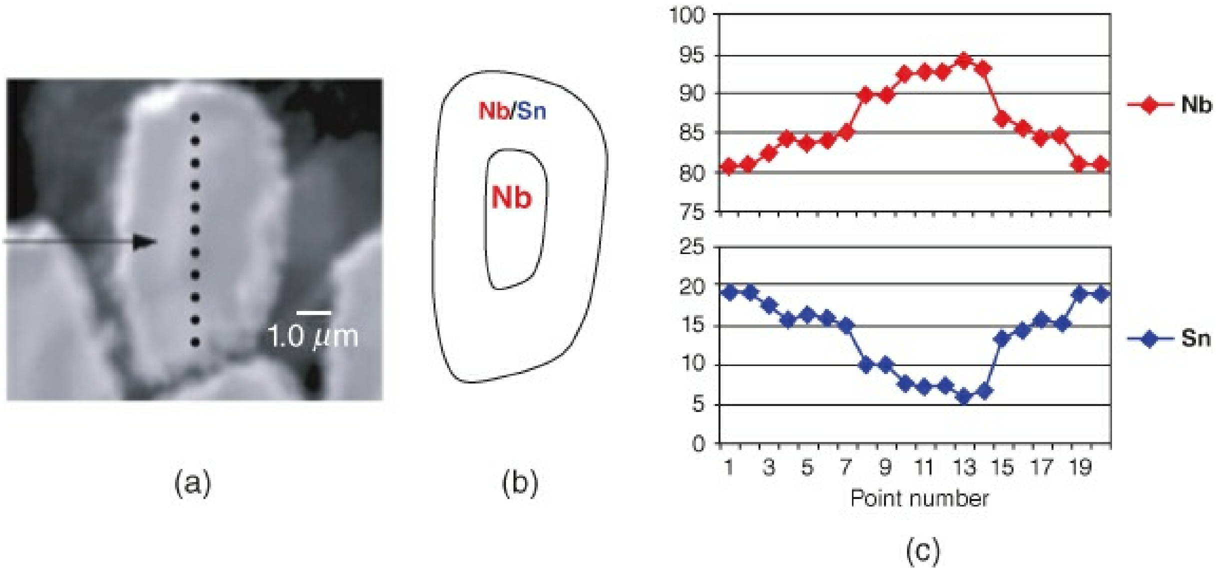

Figure 3.33 Characterization of an Sn–Nb wire by SEM: (a) SEM image; (b) schematic of the elemental distribution; and (c) point analysis giving the percent concentration of Nb and Sn.

Vickerman [29], © 2011. With permission of Wiley-VCH, Weinheim.

AES is widely used for depth profiling. It allows the elemental distributions of layered samples of 0.2–1 μm thick to be characterized beyond the escape depth limit of an electron. Varying the incident and collection angles, the primary beam energy controls the analysis depth. In general, the depth resolution decreases with the square root of the sample thickness. Notably, in AES, it is possible to simultaneously sputter and collect Auger data for depth profiling. The sputtering time indicates the depth and the intensity indicates elemental concentrations. Since the sputtering process does not affect the ejection of the Auger electron, helium or argon ions can be used to sputter the surface and create the trench, while collecting Auger data at the same time. The depth profile does not have the problem of diffusion of hydrocarbons into the trenches. Thus, AES is better for depth profiles of reactive metals (e.g., gold or any metal or semiconductor). Yet, care should be taken because sputtering can mix up different elements, changing the sample composition.

Limitations: Although AES is a very valuable surface analysis technique, there are certain limitations as well. AES is a three-electron process, elements with less than three electrons cannot be analyzed. Therefore, hydrogen and helium cannot be detected. Nonetheless, detection is better for lighter elements with fewer transitions. The numerous transition peaks in heavier elements can cause peak overlap, as can the increased peak width of higher energy transitions. Detection limits of AES include 0.1–1% of a monolayer, 10^{-16}–10^{-15} g of material, and 10^{12}–10^{13} atoms/cm^2. Another limitation is sample destruction. Although focusing of the electron beam can improve resolution, the high-energy electrons can destroy the sample. To limit destruction, beam current densities of greater than 1 mA/cm^2 should be used. Furthermore, charging of the electron beam on insulating samples can deteriorate the sample and result in high-energy peak shifts or the appearance of large peaks.

3.4.6 Secondary Ion Mass Spectrometry (SIMS)

The ion-beam detecting techniques are classified as secondary ion mass spectrometry (SIMS), ion-scattering spectroscopy, Rutherford backscattering spectroscopy, and laser–microprobe mass spectrometry. The origins of SIMS can be traced back to the early part of the last century and the discharge tube experiments of J. J. Thomson, who was the first person to investigate the effects of positive ions on a metal plate. The first SIMS analytical instruments were built in the late 1940s by Herzog and coworkers, and SIMS was used in the 1960s to analyze the spatial and isotopic distribution of all the elements from hydrogen to uranium present in samples of moon rock brought back to earth.

In an SIMS analysis, the sample is bombarded with a beam of charged particles with energies in the 1–25 keV range. These incoming particles are called primary ions. The primary ions deposit energy into the surface layers. Around the impact site and to the depth of ~3 nm, many bonds are broken and there is much random displacement and movement of atoms. This region is called the collision cascade. Collisions that result in translational energy being directed back to the surface layer lead to the ejection of material. This process is termed sputtering of the surface (Figure 3.34). Thus, SIMS is based on the sputtering of atomic layers from the surface of a sample by a primary ion beam.

Instrumentation: A basic SIMS instrument essentially has (1) a primary beam source (usually O^{2+}, O^-, Cs^+, Ar^+, Ga^+, or neutrals) to supply the bombarding species; (2) a target or sample that must be solid and stable in a vacuum; (3) a method of collecting the ejected secondary ions; (4) a mass analyzer to isolate the ion of interest (quadrupole, magnetic sector, double-focusing magnetic sector, or time of flight); and (5) an ion detection system to record the magnitude of the secondary ion signal such as photographic plate, Faraday cup, electron multiplier or a CCD camera, and a image plate.

The primary ion impact triggers a cascade of atomic collisions leading to atom, molecule fragments, and ion ejection. The secondary ions are characteristic of the composition of the analyzed area. They are separated according to their mass, and an image containing quantitative information is formed for a selected mass. SIMS reveals elemental and isotopic surface composition. It is one of the most powerful and versatile analytical techniques for semiconductor characterization with detection limits for some elements in the 10^{14}–10^{15} cm^{-3} range if there is very little background interference signal. Lateral resolution of conventional SIMS is typically 100 μm but can be as small as 0.5 μm with depth resolution of 5–10 nm. Cesium (for negatively charged secondary ions) and oxygen (for positively charged secondary ions) are commonly used excitation ions. Other nonreactive primary ions such as Ga or Bi, widely used in liquid–metal ion sources in focused ion beam systems with lateral resolutions below 100 nm, yield 100–1000 times lower signal intensities for elements.

SIMS is the most highly developed technique of the mass spectrometric surface methods, with several manufacturers offering instruments for these techniques. SIMS has proven useful for determining both the atomic and the molecular composition of solid surfaces. There are basically three variations of the SIMS experiment: **static SIMS** is used for elemental analysis of sub-monolayers on surfaces. In this mode, the surface integrity is maintained during the timescale of the experiment; **dynamic SIMS** is used to obtain compositional information as a function of depth below the surface, which takes advantage of the destructive nature of SIMS to obtain information on various layers of materials, and **imaging SIMS**, also called scanning SIMS, is used to provide spatial images of surfaces.

Applications to nanomaterials: Ion beams can be used in a variety of ways to obtain information about the nature of nanoparticles. One of the primary uses of TOF-SIMS is to extract molecular information about the functional groups and, possibly, molecular orientation of molecular coatings on particle surfaces. During SIMS, measurements, primary ion beams with energies between 3 and 20 keV are incident on the surface, and the ions removed (sputtered) from the surface are detected. Surface selectivity arises from the depth of the region where the sputtered ions arise. Using cluster ion beams has enhanced the surface sensitivity and, for some materials, minimized the region of damage, allowing sputter depth profiles of organic layers. To extract surface molecular information, SIMS is used in a “static” mode that involves a low density and low total dose of ions so that the surface damage and alteration are minimized. Both atomic and molecular secondary ions are used to extract the surface information. Similar to the electron spectroscopy, SIMS is useful for obtaining information about surface layers, functional groups added to the surface, and contamination. Two differences between the electron spectroscopy and SIMS are (1) the high sensitivity (HS) of time-of-flight SIMS (TOF-SIMS) to many trace elements and functional groups and (2) the changes (damage) induced to the surface due to ion sputtering. The functional group sensitivity has been usefully applied in many ways. For example, TOF-SIMS has been used to examine peptides conjugated to Au nanoparticles as part of a protein kinase assay and to examine a multilayer, plasma-produced organic coating deposited on alumina nanoparticles. For relatively large nanoparticles produced during welding, SIMS with sputter profiling has been used to examine the complex layers that form on the particles. Unlike XPS, which often infers chemistry indirectly from binding energy shifts, SIMS has the advantage of measuring molecular fragments directly.

In addition to understanding surface coatings or functional groups, SIMS has proven to be equally useful for examining the basic composition of nanoparticles, both as they are being processed inside the TOF-SIMS vacuum system and after they have been introduced into the vacuum system for analysis. *In situ* thermo-TOF-SIMS was used to examine the thermal decomposition of zinc acetate dehydrate during nanoparticle formation within an SIMS system. SIMS, in combination with TEM and *in situ* optical transmission spectroscopy, has been used to study the composition and plasmon resonance of unique ZrN nanoparticles produced by laser ablation/evaporation and adiabatic expansion from zirconium nitride powder targets. TOF-SIMS has also been used to characterize the composition and oxidation state of spark-generated nanoparticles made from pairs of Ir–Ir and Ir–C electrodes. From detailed analysis of the SIMS data, it was also possible to obtain information about particle size.

As SIMS depends on the sputtering process, it inherently damages a nanostructured material under study, and this must be taken into consideration. Although many nanomaterials and nanoparticles have been successfully examined using SIMS, it is now established that nanoparticles sputter at different rates than flat surfaces or films. Recent work shows that in several circumstances, nanoparticles melt or evaporate after direct or grazing impact from many types of primary ions. Thus, it has been demonstrated that SIMS can be a useful and important tool for characterization of nanomaterials, but appropriate consideration should be given to potential implications of enhanced sputter rates or sample melting.

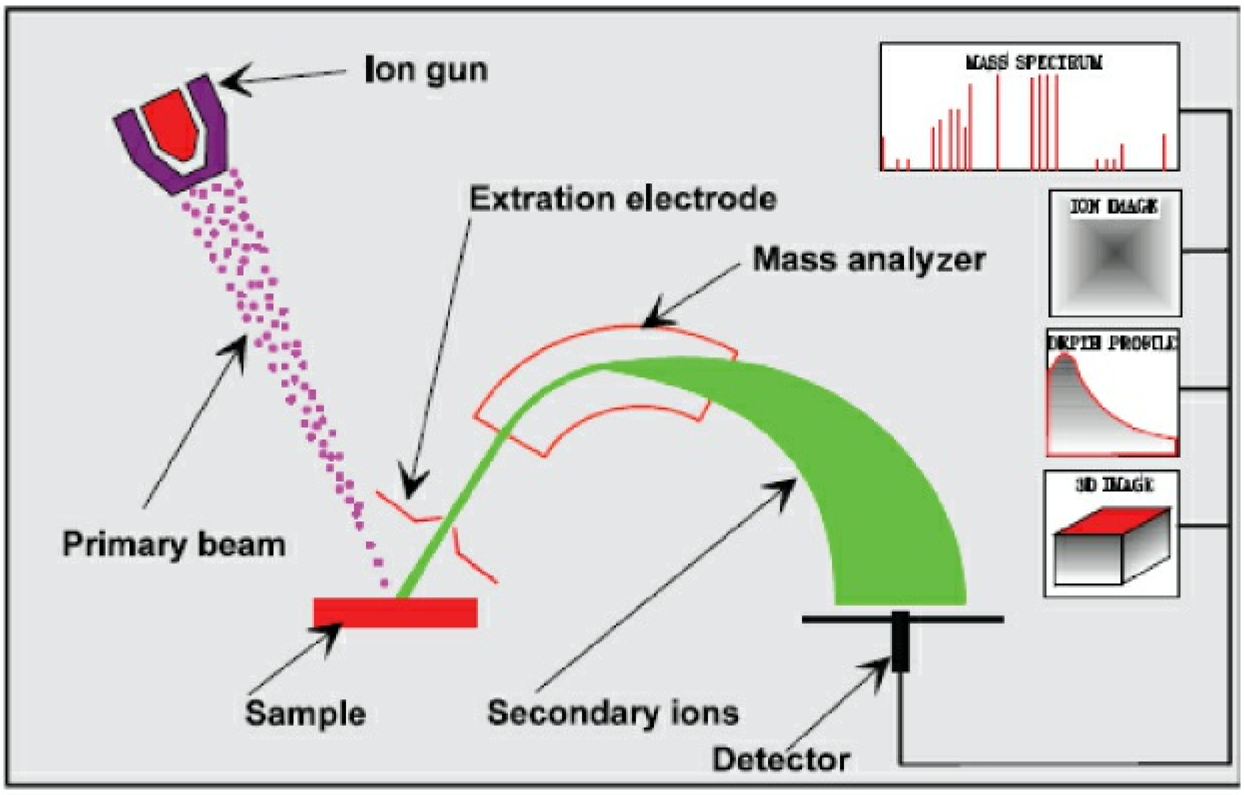

Figure 3.34 Process of secondary ion sputtering and the schematic of a dynamical SIMS instrument. http://en.wikipedia.org/wiki/Secondary_ion_mass_spectrometry.

3.5 Scattering Techniques

Many forms of radiation are used for scattering purposes, namely, X-rays, neutrons, electrons, and laser light, each have different characteristics, accordingly the number of different scattering-based nanocharacterization techniques are available (Table 3.7). The small-angle neutron scattering (SANS) and small angle X-ray scattering (SAXS) methods probe the size of object scales from the near atomic to the near micron. Dynamic light scattering (DLS) methods complement these techniques by focusing on the micron length scale. Other methods such as wide-angle neutron scattering method (WANS), wide angle X-ray scattering (WAXS), and LEED probe the local atomic structures. A brief description of scattering techniques based on X-ray scattering-based techniques is given in following sections.

Table 3.7 Radiations Used in Scattering-Based Characterization Techniques

Scattering Techniques	Type of Radiation (Wavelength, λ)	Sample Thickness	Limitations
SAXS, WAXS	X-rays (0.1–5 Å)	<1 mm	Absorption
SANS, WANS	Neutrons (1–15 Å)	1–2 mm	Low fluxes
LEED	Electrons (0.1 Å)	100 µm	Low penetration
SLS, DLS	Laser light (1 µm)	1–5 mm	Scattering from dust

3.5.1 X-Ray Diffraction Methods

X-rays are short wavelength (~10^{-5}–100 Å) electromagnetic radiations produced by the deceleration of high-energy electrons by electronic transitions involving electrons in the inner orbitals of atoms. X-ray methods involve exciting a sample either with a beam of high-energy electrons (creating X-rays) or by exposure of primary beam of X-rays (generating secondary beam of X-rays). X-rays can be also generated by bombarding a sample with alpha particles. The energy of emitted X-rays is equal to the difference between the binding energies of the electrons involved in the transition. X-ray spectroscopy, similar to optical spectroscopy, is based on the measurement of emission, absorption fluorescence, scattering, and diffraction of electromagnetic radiations [34].

Since X-ray wavelengths are in the same order as the sizes of nanostructures, X-ray diffraction is an important characterization tool. X-ray diffractograms hold a wealth of structural information about the nanomaterials and fundamental features such as (1) the crystallite size, (2) size distribution, (3) the defect structure/distribution, (4) texture, and (5) micro and macro strain.

The two principal tools for describing the microstructure of nanostructured materials are electrons and X-ray probes. TEM and electron diffraction images provide local information about the primary nanostructure. X-ray diffraction (XRD) provides complementary information about the nanostructure by showing the average coherence length as a function of direction. X-ray diffraction results are averaged over a large volume giving an overall view of the nanostructure. XRD and neutron diffraction are complementary methods used to obtain a contrast effect on the diffracted beam. Indeed, diffracted intensities are modulated by weighting factors, which differ between X-ray and neutron due to the difference in the nature of interaction. X-ray crystallography, X-ray powder diffraction (XRD), small angle X-ray scattering are all based on elastic scattering. The X-ray powder diffraction is most widely used for the identification of unknown crystalline materials (e.g., minerals, inorganic compounds). Determination of unknown solids is critical to studies in geology, environmental science, material science, engineering, and biology.

3.5.1.1 Wide-Angle X-Ray Diffraction (XRD)

The fundamental equation on which XRD is based is Bragg's law, which links lattice spacing with the observed angles of constructive interferences when X-ray scatter from a crystalline material. For nanomaterials, measurements are made on powders containing a very large number of randomly oriented particles. Thus, diffraction rings or halos are seen at various angles with respect to the incoming beam, each originating from a subset of particles oriented correctly to satisfy the Bragg equation, and the corresponding technique is known as the **powder method** or **Debye–Scherrer method**. Analysis of the position and intensity of the peaks in the powder diffraction pattern allows the identification and quantification of the phase composition of the sample.

According to **Bragg's law**, when a narrow beam of radiation of wavelength λ strikes the crystal surface at incident angle θ, scattering occurs as a consequence of interaction of the radiation with a regular array of atoms (scatterers). When distance $2d \sin \theta$ is equal to $n\lambda$, where n is an integer, and d is the interplanar distance of crystal, then the crystal will appear to reflect the X-radiation. The conditions for constructive interference of the beam at angle θ are given by 3.5

$$n\lambda = 2d \sin \theta \qquad \textbf{3.5}$$

Thus, among scattering, diffraction takes place when the distance between the scattering centers are of the same order of magnitude as the wavelength ($n\lambda$) of the radiation. Bragg's equation is of fundamental importance. The X-rays appear to be reflected from the crystal only if the angle of incidence satisfies the condition that $\sin \theta = n\lambda/2d$. In this case, a part of the incoming beam is deflected by an angle 2θ, producing a *reflection* spot in the diffraction pattern. At all other angles, destructive interferences occur. X-rays are used to produce the diffraction pattern because their wavelength λ is typically the same order of magnitude (1–100 Å) as the spacing d between planes in the crystal. Another fundamental equation applied to XRD analysis is the **Debye–Scherrer equation**, which relates the broadening of XRD peaks to the (average) finite size of the individual diffracting domains. This finite size can correspond with the crystals within a solid, but it can also correspond with the individual (monocrystalline) particles in an agglomerated or aggregated nanomaterials. The Scherrer equation can be written as Equation 3.6:

$$\tau = \frac{K\lambda}{\beta \cos \theta} \qquad \textbf{3.6}$$

where τ is the average size of the ordered (crystalline) domains, which may be smaller or equal to the grain size, K is a dimensionless shape factor, with a value close to unity. The shape factor has a typical value of about 0.9, but varies with the actual shape of the crystallite; λ is the X-ray wavelength; β represent the line broadening, that is, full width at half the maximum intensity (FWHM); and θ is the Bragg angle. The Scherrer equation provides a powerful and relatively simple way of determining the average particle size of a nanomaterial, but not the size distribution. The technique is more reliable for the particles in the 1–100 nm size range since the peak broadening is much more pronounced for smaller particles; bulk material results in sharp and narrow peaks. The method is limited to particles that are crystalline; average size of particles is inversely proportional to the FWHM. For amorphous or very poorly crystalline particles, Fourier transform technique can be used in principle to determine the average particle size; however, they may not be very accurate.

> **Instrumentation:** Many XRD systems are available commercially, mostly offering the powder diffraction technique and being provided with software for peak shape analysis and deduction of average crystallite size. X-ray diffractometer consist of three basic elements: an X-ray tube, a sample holder, and an X-ray detector.
>
> X-rays are generated in a CRT by heating a filament to produce electrons, accelerating the electrons toward a

target by applying a voltage, and bombarding the target material with electrons. When electrons have sufficient energy to dislodge inner-shell electrons of the target material, characteristic X-ray spectra are produced. These spectra consist of several components, the most common being K_α and K_β. The specific wavelengths are characteristic of the target material (Cu, Fe, Mo, Cr). Filtering, by foils or crystal monochromator, is required to produce monochromatic X-rays needed for diffraction. Copper is the most common target material for single-crystal diffraction, with CuK_α radiation = 1.5418 Å.

These X-rays are collimated and directed onto the sample. As the sample and detector are rotated, the intensity of the reflected X-rays is recorded. When the geometry of the incident X-rays impinging the sample satisfies the Bragg equation, constructive interference occurs and a peak in intensity occurs. A detector records and processes this X-ray signal and converts the signal to a count rate, which is then output to a device such as a printer or computer monitor.

The geometry of an X-ray diffractometer is such that the sample rotates in the path of the collimated X-ray beam at an angle θ while the X-ray detector is mounted on an arm to collect the diffracted X-rays and rotates at an angle of 2θ. The instrument used to maintain the angle and rotate the sample is termed a *goniometer*. For typical powder patterns, data are collected at 2θ from ~5° to 70°, angles that are preset in the X-ray scan. Figure 3.35 shows typical features of a basic XRD spectrometer.

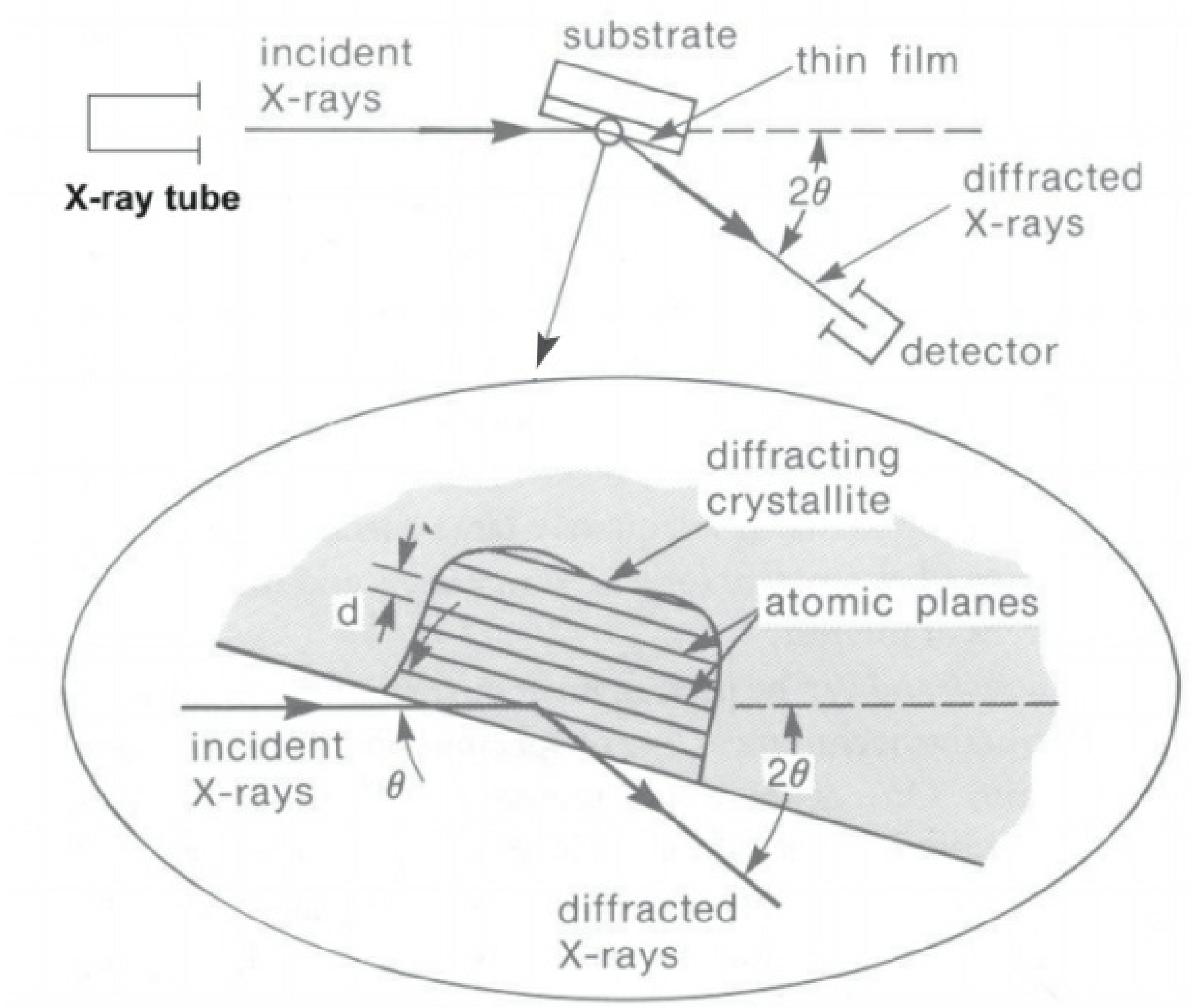

Figure 3.35 Basic features of an XRD spectrometer.

XRD spectra: X-ray powder diffraction method is unique in that it is the only analytical method that is capable of providing qualitative and quantitative information about the compounds presents in a solid sample. X-ray diffraction pattern is unique for each crystalline substance, and chemical identity is assumed by matching the diffraction pattern of an authentic sample. Figure 3.36a and b shows a typical powder diffractogram of NaCl, peak positions occur where the X-ray beam has been diffracted by the crystal lattice. The unique set of d-spacing derived from this pattern can be used to “fingerprint” the minerals.

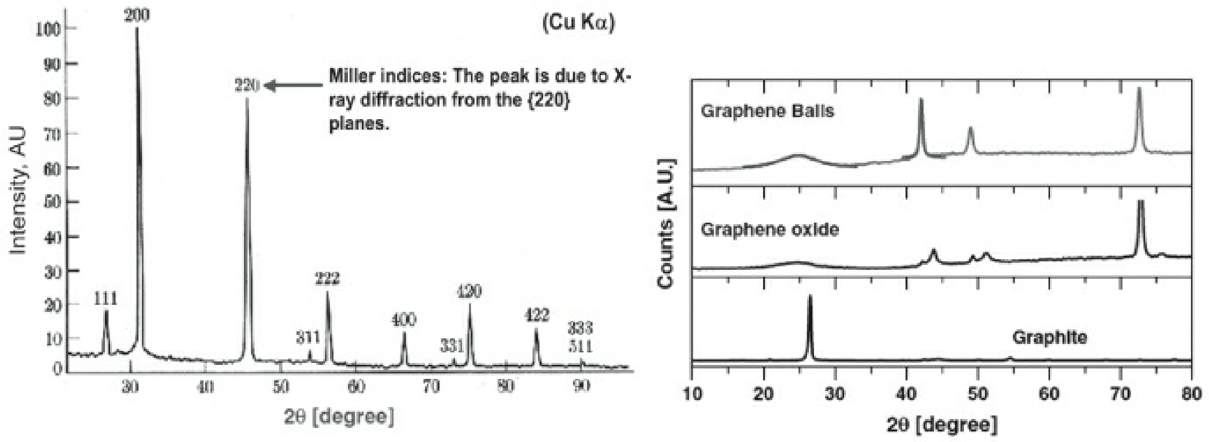

Figure 3.36 A typical XRD pattern of (a) NaCl powder and (b) carbon nanomaterials.

Kumar et al. [13], © 2013. With permission of ASP.

X-ray powder diffraction method is unique in that it is the only analytical method that is capable of providing qualitative and quantitative information about the compounds presents in a solid sample. X-ray powder diffraction methods are based on the fact that an X-ray diffraction pattern is unique for each crystalline substance, and chemical identity is assumed by matching the diffraction pattern of an authentic sample. Figure 3.37a and b shows X-ray diffraction patterns of nanostructured titanium oxide film on different phases, namely anatase and rutile phases. Various carbon nanomaterials can also be distinguished by their characteristic peaks in their XRD spectra.

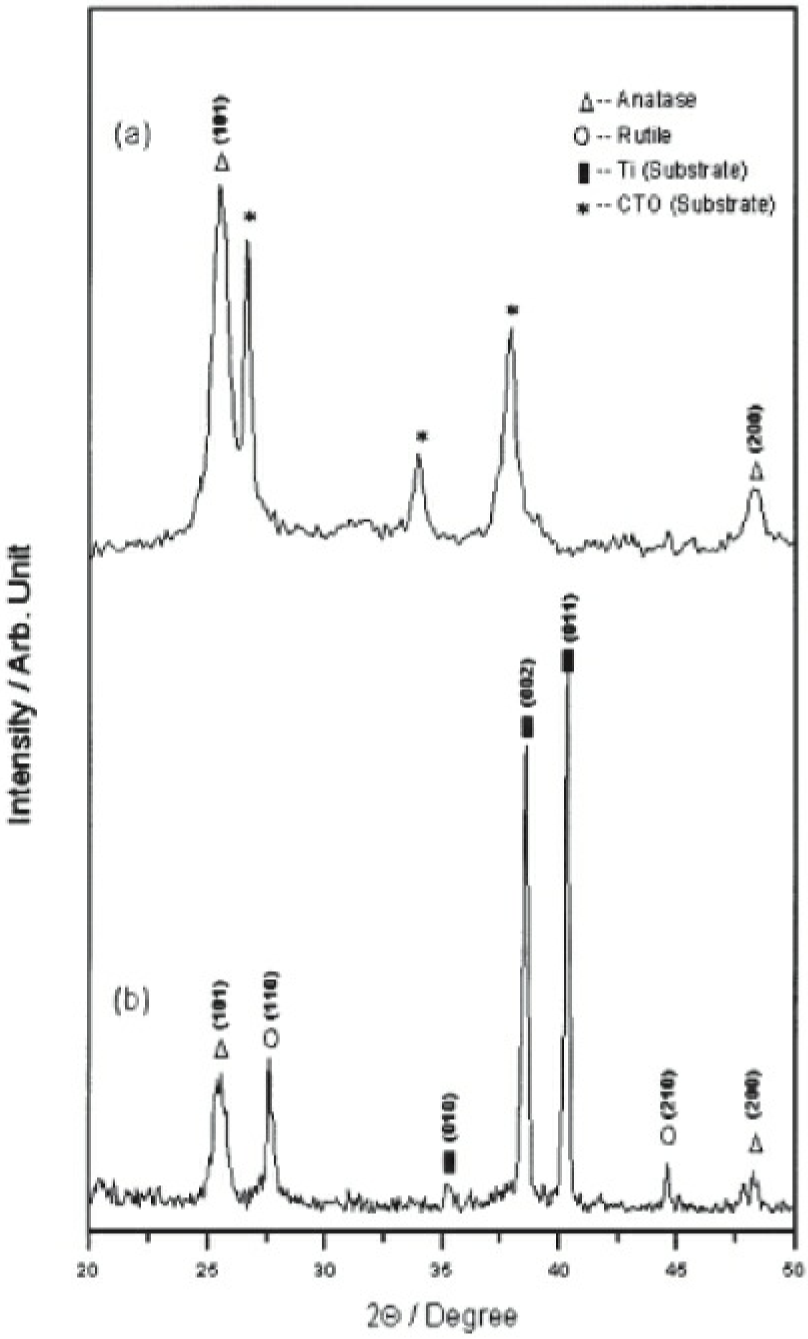

Figure 3.37 (a, b) X-ray diffraction patterns of nanostructured TiO_2 film.

Shrivastava et al. [35], © 2005. With permission of Indian Academy of Sciences.

3.5.1.2 Small-Angle X-Ray Scattering (SAXS)

Small-angle X-ray scattering (SAXS) is a small-angle scattering (SAS) technique where the elastic scattering of X-rays (wavelength 0.1–0.2 nm) by a sample, which has inhomogeneities in the nanometer range, is recorded at very low angles (typically 0.1–10°). This angular range contains information about the shape and size of macromolecules, characteristic distances of partially ordered materials, pore sizes, and other data. To satisfy Bragg's law, θ must change as d changes, for example, θ decreases as d increases, thus making SAXS to be capable of delivering structural information of macromolecules between 5 and 25 nm, of repeat distances in partially ordered systems of up to 150 nm. SAXS is ideally suited for the study of ordered systems with large repeat distances, such as liquid crystalline mesophases, complex fluids, and nano- to mesoporous materials. In addition, the elastic scattering of X-rays that can be observed at small and very small angles gives information about the shape and size of macromolecules.

Instrumentation: The SAXS instrument consists of an X-ray source, a pinhole or a slit collimation system, a sample environment, a scattering vessel, and a 2D detector. The X-ray source is either a laboratory source such as a Kratky or a rotating anode (whereby X-rays are produced when charged particles hit a Cu or a Mo target), or a synchrotron facility (whereby X-rays are produced by accelerated particles moving in a magnetic field). Synchrotron light provides a higher X-ray flux. The pinhole collimation is preferred but is characterized by low flux-on-sample. Slit collimation yields higher fluxes but produces slit-smeared data. For example, most laboratory X-ray sources use slit collimation, whereas most synchrotron sources use pinhole collimation. The CuK_α line is characterized by a source wavelength of 1.54 Å. Schematic of a typical SAXS setup is shown in Figure 3.38.

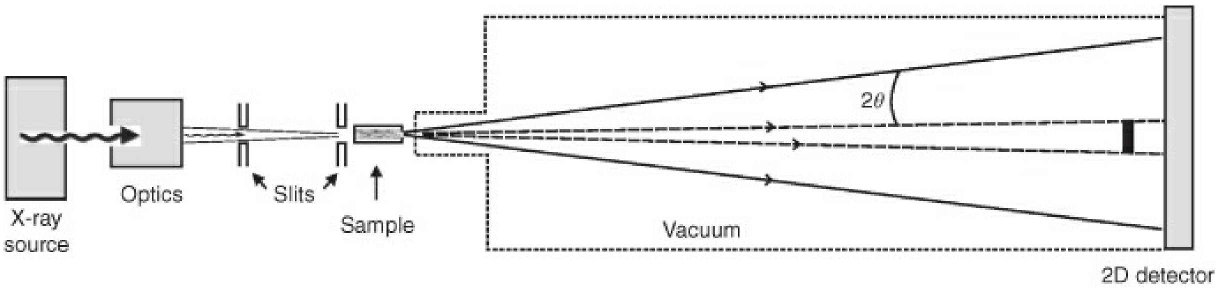

Figure 3.38 Schematic of a typical SAXS setup. www.mrl.ucsb.edu.

Measurements: SAXS measures the size of particle based on scattering of X-rays at the particle surface. Light passing through a medium that is not completely homogeneous is forced to deviate from the straight line. Scattering angle, that is, the degree of deviation from straight line, depends on the wave length of light and the size of the particle on which it is scattered. X-rays that have wavelengths in the range of 0.1 nm and 1 nm are scattered by particles in the range between 1 nm and 100 nm. The intensity of scattered radiation is measured in dependence of the scattering angle. This intensity pattern can give information of the particle size distribution as well as the shape of the particles. Size and shape of the particles are obtained via fitting of the measured scattering curve (scattering intensity vs. scattering angle). Unoriented samples yield a centro-symmetric pattern on the 2D detector, which is radially averaged to give the typical plots of diffracted intensity versus scattering vector q ($=4\pi \sin\theta/\lambda$) (Figure 3.39).

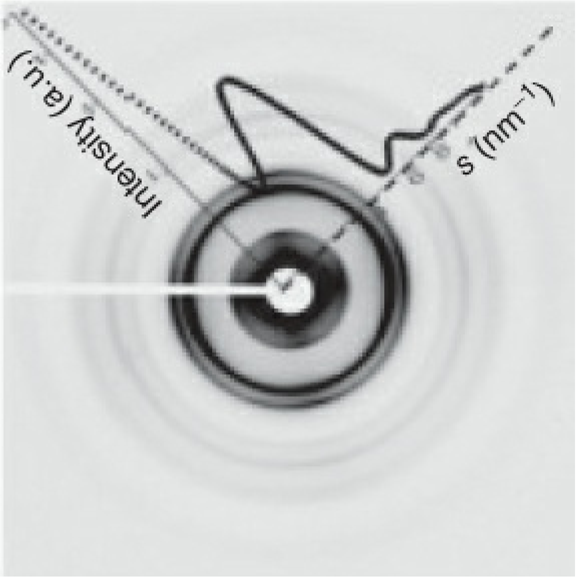

Figure 3.39 A typical plots of diffracted intensity versus scattering vector, inset shows centro-symmetric pattern on the 2D detector. www.mrl.ucsb.edu.

Different algorithms are used for calculations from particle size distribution from raw SAXS data. For relatively monodispersed samples, oscillations are observed in the scattering curve. The periodicity is directly related to the mean particle diameter. By fitting the curve, number, volume, and intensity, weighted mean diameter can be obtained.

Application of SAXS: SAXS is used for the determination of the microscale or nanoscale structure of particle systems in terms of such parameters as averaged particle sizes, shapes, distribution, and surface-to-volume ratio. SAXS can be applied to any two-phase system where the phases have different density. In such a system, SAXS measures a phase with the smaller volume fraction. This means that in suspension, but not to powders, the volume fraction has to be below a few percent to avoid particle–particle interactions. Not only particles but also the structures of ordered systems such as lamellae and fractal-like materials can be studied. The method is accurate, nondestructive, and usually requires only a minimum of sample preparation. Applications are very broad and include colloids of all types, metals, cement, oil, polymers, plastics, proteins, foods, and pharmaceuticals and can be found in research as well as in quality control.

In the case of biological macromolecules such as proteins, the advantage of SAXS versus crystallography is that a crystalline sample is not needed.

3.5.2 Dynamic Light Scattering (DLS)

Dynamic light scattering (DLS) is an important tool for characterizing the size of nanoparticles in solution. Although there are several techniques for the measurement of particle size and its distribution (PSD) such as sieve analysis, optical counting method, electroresistance counting methods, sedimentation techniques, laser diffraction method, acoustic spectroscopy, however, DLS is mostly used for nanoparticle size and its distribution.

Basic components and optics for a DLS experiment are illustrated schematically in Figure 3.40. DLS measures the light scattered from a laser that passes through a colloidal solution, and by analyzing the modulation of the scattered light intensity as a function of time, the hydrodynamic size of particles and particle agglomerates can be determined. Larger particles will diffuse slower than smaller particles and the DLS instrument measures the time dependence of the scattered light to generate a correlation function that can be mathematically linked to a particle size. DLS is a valuable tool for determining and measuring the agglomeration state of nanoparticles as a function of time or suspending solution. When DLS sizing data are compared to transmission electron microscopy images, the aggregation state of the particles can be determined. In an unagglomerated suspension, the DLS-measured diameter will be similar or slightly larger than the TEM size. If the particles are agglomerated, the DLS measurement is often much larger than the TEM size and can have a high polydispersity index (large variability in the particle size).

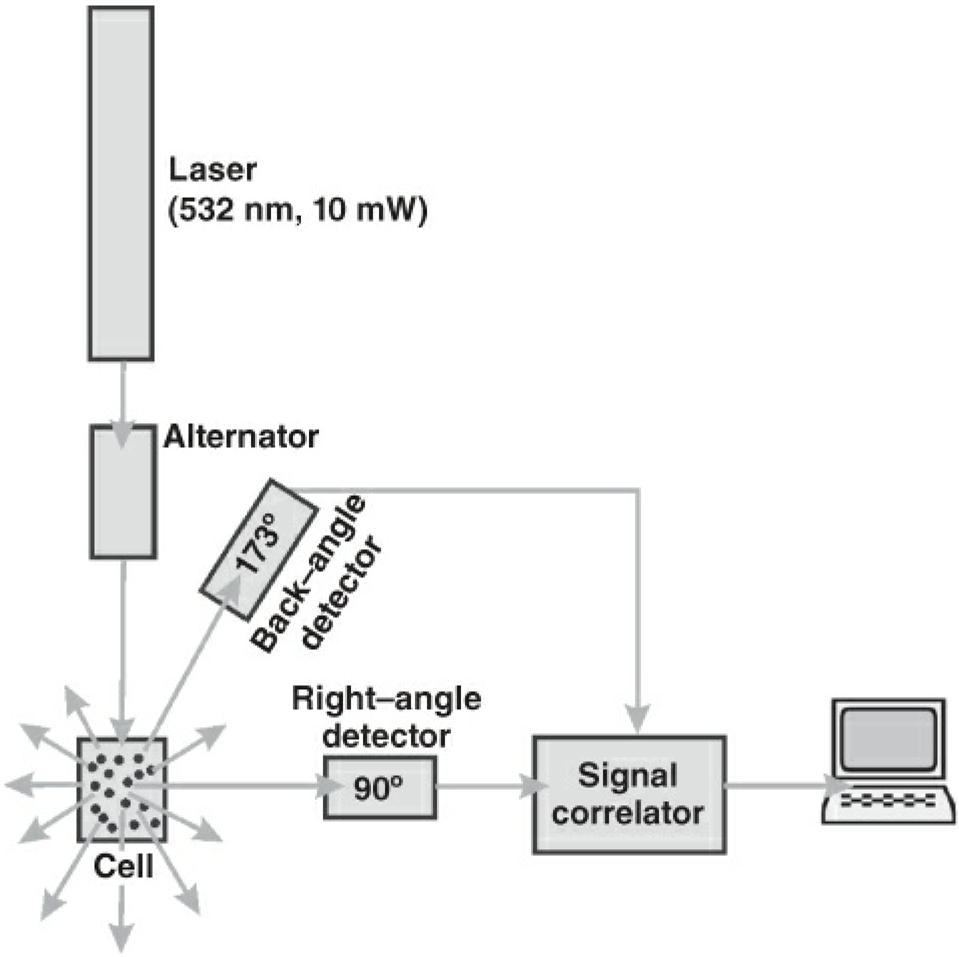

Figure 3.40 Basic components and optics for a dynamic light scattering experiment,

Dynamic light scattering (DLS) measuring the hydrodynamic radius (D_h) of a particle determines how fast a particle moves in a suspension through Brownian motion. To measure this, DLS using a laser beam, when passes through a suspension, is scattered by the nanoparticles. The Brownian motion of the particles causes fluctuations in the intensity of scattered light around a mean value. When light hits small particles (below 250 nm), the light scatters in all directions, that is, Rayleigh scattering; when light source is a laser (a monochromatic and coherent source of light), then a time-dependent fluctuations in the scattering intensity is observed. This is due to the fact that the small molecules undergo a diffusive Brownian motion when in solution and the distance between the scatterers in the solution is constantly changing with time. This scattered light then undergoes either constructive or destructive interference by the surrounding particles, and within this intensity fluctuation, information is contained about the timescale of movement of the scatterers. In most DLS instruments, the autocorrelation function of the fluctuations is recorded as a function of time. Size of the particles can be obtained, for example, by fitting the autocorrelation function to an exponential decay function that delivers an average diffusion coefficient (D_t) for the particles. The diffusion coefficient can be used to calculate an average radii of the particles via the Stoke–Einstein relationship, given as in Equation 3.7

$$D_h = k_B T / 6\pi\eta D_t \tag{3.7}$$

where D_h is the hydrodynamic radius of particle, T is the sample temperature in absolute units, k_B is the Boltzmann constant, and η is the sample viscosity. DLS can thus be used to determine the size distribution profile of small particles in suspension including nanoparticles.

Dynamic light scattering is used to characterize the size of various particles including proteins, polymers, micelles, carbohydrates, and nanoparticles. If the system is monodisperse, the mean effective diameter of the particles can be determined. This measurement depends on the size of the particle core, the size of surface structures, the particle concentration, and the type of ions in the medium. Sample preparation is critical in DLS experiment. Sample is prepared either by filtration or centrifugation to remove dust and artifacts from the solution. Since DLS essentially measures fluctuations in scattered light intensity due to diffusing particles, the diffusion coefficient of the particles can be determined. DLS software of commercial instruments typically displays the particle population at different diameters. If the system is monodisperse, then there should only be one population, whereas a polydisperse system would show multiple particle populations. If there is more than one size population present in a sample, then **CONTIN analysis** must be applied. For more than two populations, CONTIN analysis at several scattering angles is required. Stability studies can be done conveniently using DLS. Periodical DLS measurements of a sample can show whether the particles aggregate over time by seeing whether the hydrodynamic radius of the particle increases. If particles aggregate, there will be a larger population of particles with a larger radius.

Advantages of Dynamic Light Scattering Method

DLS method for characterizing size of nanomaterials offers several advantages, such as accuracy in determining the hydrodynamic size of monodisperse samples, and capabilities of measuring diluted samples, analyzing samples in a wide range of concentrations, and detecting small amounts of higher molecular weight species, along with reproducible measurement in much less time (in minutes) at comparatively low cost for a material in a relatively small size range (1 nm–3 µm). However, the functions of DLS are impacted by several factors such as difficulty in correlating size fractions with a particular composition when certain amounts of aggregates or dust particles are present, interfering in the scattering intensity.

Limitations of Dynamic Light Scattering Method

1. DLS, in its standardized form, does not produce particle size distribution.
2. DLS results are strongly biased in the presence of a small fraction of large particles, hence the average particle size determined by DLS may be misleading.
3. DLS does not distinguish between constituent particles, aggregates, and agglomerates.
4. Moreover dynamic light scattering is performed in liquids, which further limits its use for the analysis of particles not dispersed in liquids.

3.5.3 Zeta Potential Analysis

Zeta potential is a scientific term for electrokinetic potential in colloidal systems, usually denoted using the Greek letter zeta (ζ), hence ***ζ-potential***. In a colloidal solution, around each particle, an electrical double layer exists: an inner region (**stern layer**) where the ions are strongly bound and an outer (**diffuse layer**) region where ions are less firmly associated. Within this diffuse layer is a notional boundary within which the particle acts as a single entity, the potential at this boundary is the **zeta potential** (Figure 3.41a). From a theoretical viewpoint, the zeta potential is the electric potential in the interfacial double layer (DL) at the location of the slipping plane versus a point in the bulk fluid away from the interface. The magnitude of zeta potential gives an indication of the potential stability of the colloidal system. A value of 25 mV (positive or negative) can be taken as the arbitrary value that separates low-charged surfaces from high-charged surfaces. The significance of zeta potential is that its value can be related to the stability of colloidal dispersions. The zeta potential indicates the degree of repulsion between adjacent, similarly charged particles in dispersion. For molecules and particles that are small enough, a high zeta potential will confer stability, that is, the solution or dispersion will resist aggregation. When the potential is low, attraction exceeds repulsion and the dispersion will break and flocculate. So colloids with high zeta potential (negative or positive) are electrically stabilized while colloids with low zeta potentials (< ±5 mV) tend to aggregate due to van der Waal interparticle attractions while > ±40 mV is considered to be highly stable [36–38].

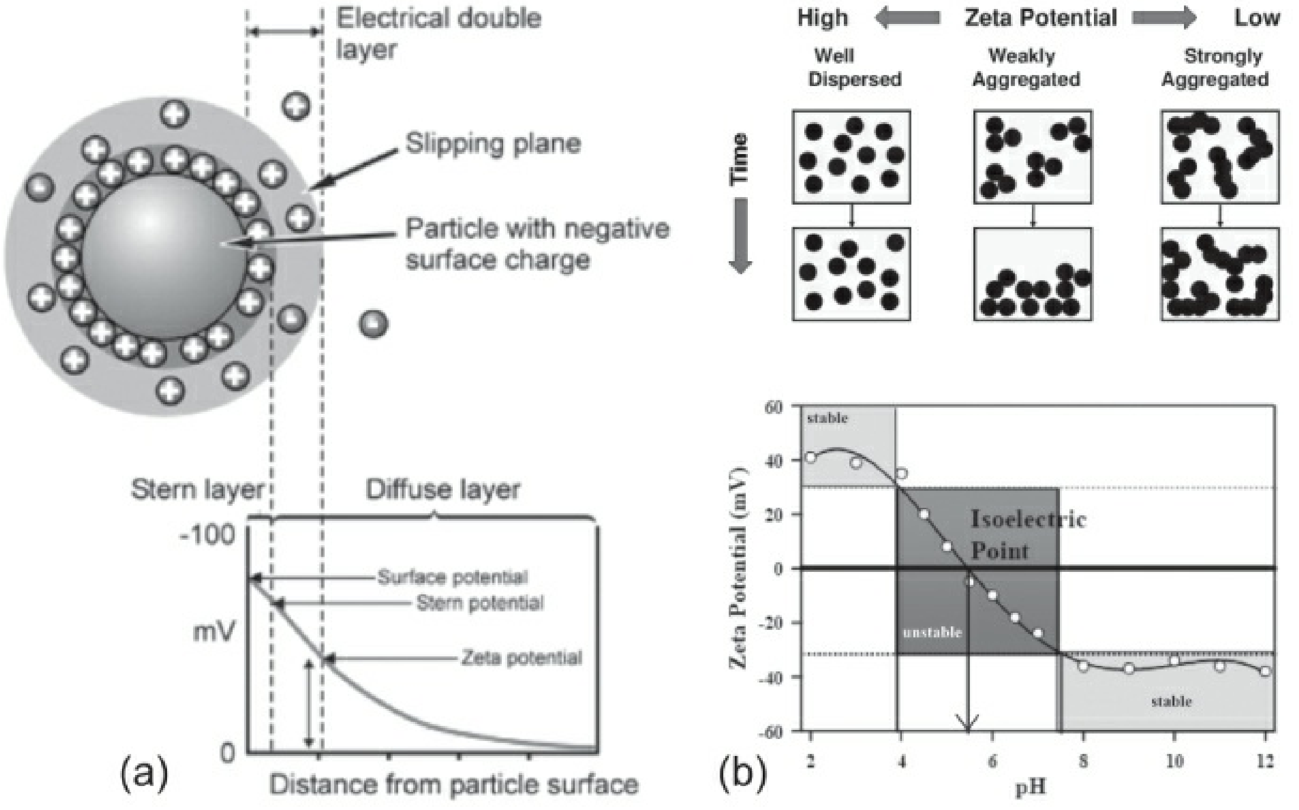

Figure 3.41 (a) Electric double layer around a particle; (b) effect of zeta potential on suspension properties.

From Ref. [36].

3.5.3.1 Surface Charge of Nanoparticles

The surface charge of nanoparticles in solution (colloids) can be determined by zeta potential analysis. Nanoparticles have a surface charge that attracts a thin layer of ions of opposite charge to the nanoparticle surface. This double layer of ions travels with the nanoparticle as it diffuses throughout the solution. Therefore, zeta potential, the electric potential at the boundary of the double layer, is an important tool for understanding the state of the nanoparticle surface and predicting the long-term stability of the nanoparticle. Zeta potential analysis is quite useful in understanding the surface modification of the nanoparticles.

Zeta potential is sensitive to environmental changes including pH and ionic strength. Therefore, care must be exercised in preparing sample for zeta potential measurement. Sample must be monodisperse in particulate free, polar solvent (e.g., high purity water) and concentration is high enough to effectively scatter 633 nm light. Overall salt concentrations must be low (conductivities <1 mS/cm) since movement of the conductive ions can lead to electrode polarization and degradation. Measurement of the zeta potential of a particle dispersion as a function of pH and concentration of additives may help in formulating condition for a product with maximum stability as illustrated in Figure 3.41b.

3.5.3.2 Measurement of Zeta Potential

The zeta potential instrument measures the phase change in the light scattered by particles moving under the influence of an applied electric field, a phenomenon known as **electrophoresis**. The phase change is proportional to the electrophoretic mobility (velocity) of the particles from which the zeta potential can be calculated. Zeta potential is related to electrophoretic mobility by Henry equation:

$$U_E = \frac{2\varepsilon Z f(K_a)}{3\eta}$$

where U_E = electrophoretic mobility; Z = zeta potential, . = dielectric constant, η = viscosity, and $f(K_a)$ is the Henrys function; K_a represents the ratio of particle radius (a) to the double layer thickness ($1/K$, the Debye length). Unit of K is the reciprocal of length. In nonpolar media $f(K_a)$ is ~1.0 and in polar media it is ~1.5.

Electrophoretic light Scattering (**ELS**) technique simultaneously measures the velocities of many charged particles in liquid. A sample cell with two gold electrodes is used, where the movement of particles under the influence of the applied electric field (up to 200 V) is captured by the instrument. Among the methods of evaluating zeta potential, the technique of ELS is most commonly used; however, it suffers electro-osmotic effect that reduces precision and reproducibility of the measurement.

Laser Doppler Electrophoresis is another technique to measure the movement of charged particles in an electric field that utilizes well-known Doppler effect. A pair of mutually coherent laser beams were derived from a single source, following similar path lengths; one of the beam passes through the dispersion is called **scattering beam** and the other beam routed around the cell is called as **reference beam**. When particle is stationary, the scattered light has same frequency (F_1) as that of incident radiation (F_1), whereas there is a shift in frequency of light scattered from a moving particle from F_1 to F_2 (Figure 3.42). The shift in frequency of light is measured by optical mixing or interferometric technique. The scattered light is combined with reference beam to create intensity variations, which are carried to the detector.

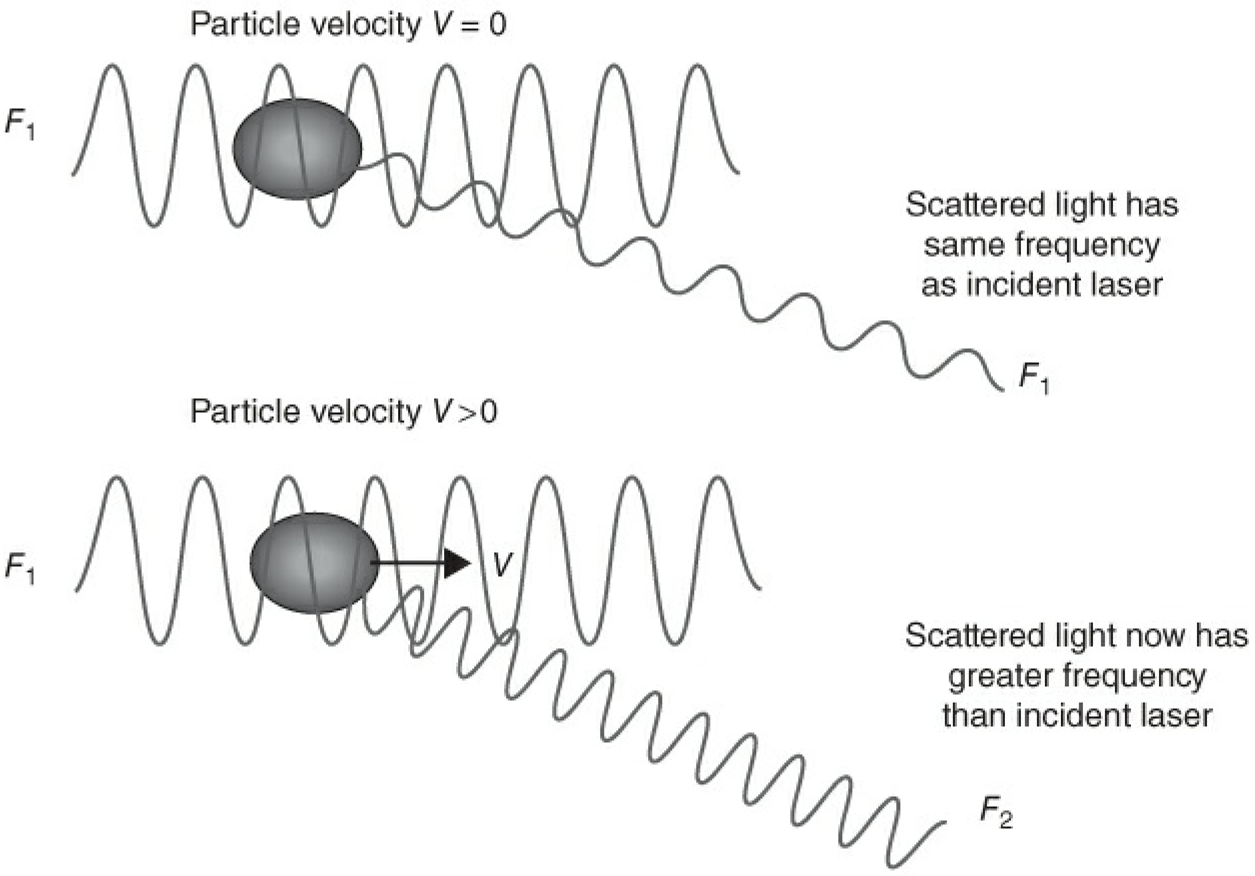
Particle velocity $V = 0$
F_1
Scattered light has same frequency as incident laser
F_1
Particle velocity $V > 0$
F_1
V
Scattered light now has greater frequency than incident laser
F_2

Figure 3.42 Shift in frequency by a moving particle.

Finally, characterization of nanostructured material is best accomplished by the combination of various imaging and spectroscopic and scattering techniques.

Review Questions

Q1. Name the suitable techniques for the characterization of nanoparticles with reference to the following parameters: (1) particle size, shape, and their distribution; (2) chemical composition; (3) porosity and surface area; (4) surface morphology; (5) thermal characteristics.

Q2. What is the basic difference between microscopy and spectroscopy?

Q3. How does the electron microscopy different from optical microscopy?

Q4. Which all signals may generate upon interaction of electron beam with matter and how are they being utilized in the characterization of nanomaterials?

Q5. Illustrate basic difference between scanning mode and transmission mode of electron microscopy with the help of schematic diagrams.

Q6. Illustrate the basic principles of the techniques discovered in the late 1980s led to revolutionary development in nanoscience and nanotechnology.

Q7. What are the basic components of scanning electron microscope and their respective functions?

Q8. How does energy-dispersive X-rays are being used in the elemental analysis of nanomaterials?

Q9. What is tunneling current? Discuss the operating modes of STM.

Q10. What is the basic difference between STM and AFM? Which of the two methods can be used for manipulation at anatomic level in the designed synthesis of nanomaterials?

Q11. Discuss the basic principles and unique capabilities of atomic force microscopy. Illustrate the answer with examples.

Q12. What is Raman effect? How Raman scattering differ from Rayleigh scattering.

Q13. Give a schematic diagram to illustrate the principle of Raman scattering.

Q14. How does Raman spectroscopy is used to differentiate different carbon-based nanomaterial such as CNT, graphene, and graphene oxide as compared to graphite?

Q15. How Raman spectroscopy is being used for imaging of nanostructured materials? Discuss different types of imaging base on Raman spectroscopy.

Q16. What do you understand by confocal Raman imaging? Discuss advantages of confocal Raman imaging over imaging by charge couple device (CCD).

Q17. Give the range of scattering angle for wide-angle and small-angle XRDs?

Q18. Discuss different forms of wide-angle X-ray scattering?

Q19. How will you determine size of particles using XRD techniques?

Q20. How will you differentiate crystallinity of a given material from XRD pattern?

Q21. What do you understand by hydrodynamic radius? How dynamic light scattering technique is useful in characterizing the nanoparticles?

References

1. B. Hammouda, “Physical Characterization Methods”, http://www.ncnr.nist.gov/staff/hammouda/physical_characterization_methods.pdf.

2. P. S. Hale, L. M. Maddox, J. G. Shapter, N. H. Voelcker, M. J. Ford and E. R. Waclawik, “Growth Kinetics and Modeling of ZnO Nanoparticles”, *J. Chem. Educ.* **82** (5), (2005) 775–778.

3. G. H. Binning, H. Roher, Ch. Gerber and E. Weibel, “A*tomic Resolut*i**on** Images of Conducting Surfaces”, *Phys. Rev. Lett.* **49** (1982) 57–61.

4. A. G. H. Binning and C. F. Quate, “ Atomic Resolution Images on Conducting/N**on**- conducting Surfaces”, *Phys. Rev. Lett.* **56** (1986) 930–933.

5. L. Mu and R. L. Sprando, “**Ap**plication of Nanotechnology in Cosmeti**cs**”, *Pharm. Res.* **27** (2010) 1746–1749.

6. M. Ruhle, F. Phillipp, A. Seeger and J. Heydenreich, Ed., “High-Voltage and High-Resolution Electron Microscopy”, *Ultramicroscopy*, **56** (1994) 1–3.

7. M. Sarikaya, H. K. Wickramasinghe and M. Isaacson, Ed., “Determining Nanoscale Physical Properties of Materials by Microscopy and Spectroscopy”, *Mater. Res. Soc. Symp. Proc.*, **332** (1995) , Materials Research Society, Pittsburgh.

8. S. Horiuchi, *Fundamentals of High Resolution Transmission Electron Microscopy*, North Holland, Amsterdam, 1994.

9. B. Alberts, A. Johnson, J. Lewis, M. Raff, K. Roberts and P. Walter, *Molecular Biology of the Cell.* 4th Edition, Garland Science, New York, 2002.

10. P. J. Potts, *A Handbook of Silicate Rock Analysis*, Springer Science, 1987.

11. M. K. Patra, A. Padhye, M. Manoth, G. S. Gowd, V. K. Singh, S. R. Vadera and N. Kumar, “Growth and Studies of S^{2-} Doped ZnO Nanorods by Solution Growth Technique”, *Adv. Mater. Res.*, **67** (2009) 239–243.

12. R. Klajn, K.J. M. Bishop and M. Fialkowski et al., “Plastic and Moldable Metals by Self Assembly of Sticky Nanoparticle Aggregates” *Science*, **316** (5822), (2007) 261.

13. N. Kumar, A. Shukla, J. Singh, M. K. Patra, P. Ghosal and S. R. Vadera, “Simple Route for Synthesis of Multilayer Graphene Nanoballs by Flame Combustion of Edible Oil”, *Graphene*, **1** (2013) 1–5.

14. C. Jiang, Y. Han, S. Liu and Z. Zhang. “A General Approach to Functional Metal Oxide Nanobelts: Thermal Decomposition of Precursors and Interface Diffusion Growth Mechanism”, *Cryst. Engg. Comm.* **16**(6), (2013) 6924.

15. C. Wu, Z. Wang, P. T. Williams and J. Huang, “Renewable Hydrogen and Carbon Nanotubes from Biodiesel Waste Glycerol”, *Sci. Rep.*, **3** (2013).

16. V. Gupta, M. K. Patra, A. Shukla, L. Saini, S. Songara, R. Jani, S. R. Vadera and N. Kumar, “Synthesis and Investigations on Microwave Absorption Properties of Core–Shell FeCo(C) Alloy Nanoparticles” *Sci. Adv. Mater.*, **6** (2014) 1–7.

17. (a) N. R. Jana, Y. Chen and X. Peng, “Size and Shape Controlled Magnetic (Cr, Mn, Fe, Cu, Ni) Oxide Nano Crystals via a Simple and General Approach”, *Chem. Mater.*, **60** (2004) 3931–3938.(b) P. Randima, H. Y. Galhenage and A. Samuel et al., “Understanding the Nucleation and Growth of Metals on TiO$_2$:Co Compared to Au, Ni, and Pt”, *J. Phys. Chem. C*, **117** (2013) 7191–7201.

18. A. Stroscio and W. J. Keiser, *Scanning Tunneling Microscopy*, Academic Press, 1993.

19. J. C. Koepke, J. D. Wood, D. Estrada, Z._Y. Ong, K. T. He, E. Pop and J. W. Lyding, “Atomic Scale Evidence for Potential Barriers and Strong Carrier Scattering at Graphene Grain Boundaries: a STM Study”, *ACS Nano*, **7** (2013) 75.

20. F. J. Giessibl, “Advances in Atomic Force Microscopy”, *Rev. Mod. Phys.* **75** (3), (2003) 949–983.

21. (a) S. Chen, M. Tang, J. Wu, Q. Jiang, V. G. Dorogan, M. Benamara, Y. I. Mazur, G. J. Salamo, A. Seeds and H. Liu, “Long Wavelength InAs/GaAs Quantum-Dot Light Emitting Sources Monolithically Grown on Si Substrate”, *Photonics*, **2** (2015) 646–658.(b) W. Li, S. Wang, M. Hu, S. He, P. Ge, J. Wang, Y. Y. Guo and L. Zhaowei, “Enhancement of Electroluminescence from Embedded Si Quantum Dots/SiO$_2$ Multilayers Film by Localized-Surface-Plasmon and Surface Roughening”, *Sci. Rep.* **5** (2015) Article number: 11881.

22. R. Gehlot, K. Sharma, M. Mathew and S. Kumbhat, “Surface Plasmon Resonance Based Biosensor for Label Free Detection of Cholesterol”, *Indian J. Chem.,* **47A** (12), (2008) 1804–1808.

23. L. S. Wang and R. Y. Hong, *Synthesis, Surface Modification and Characterisation of Nanoparticles*, InTech Open, 2011.

24. B. Reddy Ed., *Advances in Nanocomposites: Synthesis, Characterization and Industrial Applications*, InTech Open, 2011.

25. W. Luther Ed., *Industrial Application of Nanomaterials-Chances and Risks, Technology Analysis*, Future Technologies Division of VDI Technologiezentrum GmbH, 2004.

26. B. Sepulveda Martinez, P. C. Angelomé, L.M. Lechuga and L. M. Liz-Marzán, “LSPR-Based Nanobiosensors”, *Nano Today*, **4** (2009) 244–351.

27. J. H. Li, R. Y. Hong, H. Z. Li, Y. Zheng, J. Ding and D. G. Wei, “Simple Synthesis and Magnetic Properties of Fe$_3$O$_4$-BaS O$_4$ Multi-Core-Shell Particles”, *Mater. Chem. Phys.*, **113** (2009) 140–144.

28. M. S. Dresselhaus, A. Jorio, M. Hofmann, G. Dresselhaus and R. Saito, “Perspectives on Carbon Nanotubes and Graphene Raman Spectroscopy”, *Nano Lett.*, **10** (3), (2010) 751–758.

29. J. C. Vickerman Ed., *Surface Analysis: The Principal Techniques*, 2nd Edition, Wiley-VCH, Weinheim, 2011.

30. H. Huang, Y. Xia, X. Tao, J. Du, J. Fang, Y. Gan and W. Zhang, “Highly efficient electrolytic exfoliation of graphite into graphene sheets based on Li ions intercalation–expansion–microexplosion mechanism”, *J. Mater. Chem.*, **22** (2012) 10452–10456.

31. E. P. Dillon, C. A. Crouse and A. R. Barron, “Synthesis, Characterization, and Carbon Dioxide Adsorption of Covalently Attached Polyethyleneimine-Functionalized Single-Wall Carbon Nanotubes”, *ACS Nano,* **2** (2008) 156–164.

32. A. A. Arie and J. K. Lee, “Fullerene Coated Silicon Electrodes Prepared by a Plasma-Assisted Evaporation Technique for the Anodes of Lithium Secondary Batteries”, *J. Ceram. Proc. Res.*, **10** (2009) 614–617.

33. T. Tesfamichael, N. Motta, T. Bostrom and J. M. Bell, “Development of Porous Metal Oxide Thin Films by Co-evaporation”, *Appl. Surf. Sci.* **253** (2006) 4853–4859.

34. T. Pradeep, *Nano: The Essentials*, Tata McGraw Hill, New Delhi, 2007.

35. O. N. Shrivastava, A. Shrivastava, D. Dash, D. P. Singh, R. M. Yadav,P. R. Mishra and J. Singh, “Synthesis, Characterizations and Applications of Some Nanomaterials (TiO_2 and SiC Nanostructured Films, Organized CNT Structures, ZnO Structures and CNT-Blood Platelet Clusters)”, *PRAMANA-J. Phys.*, **65** (2005) 581–592.

36. D. Fairhurst, “An Overview of the Zeta Potential Part 3: Uses and Applications”, *Am. Pharm. Rev.* Featured articles, *Posted*: June 13, 2013.

37. W. B. Russel, D.A. Saville and W. R. Schowalter, *Colloidal Dispersions*, Cambridge University Press, 1992.

38. R. J. Hunter, *Foundations of Colloid Science*, Oxford University Press, 1989.

39. Zeta Potential Using Laser Doppler Electrophoresis – www.malvern.com.

Chapter 4
Nanomaterials

4.1 Introduction

Nanomaterials (also called nanoparticles or nanopowders) are increasingly becoming part of our daily lives. Their novel properties, which are not apparent in larger forms of the same material, have led to their desirability and exploitation in a wide range of applications. Nanomaterials can be defined as substances that are intentionally produced, manufactured, or engineered to have specific properties and one or more dimensions typically between 1 and 100 nm. “Nanomaterials” also means a natural, incidental, or manufactured material containing particles in an unbound state or as an aggregate or agglomerate, where one or more external dimensions are in the size range 1–100 nm. The “particle” is a minute piece of matter with defined physical boundaries: “agglomerate” is a collection of weakly bound particles or aggregates where the resulting external surface area is similar to the sum of the surface areas of the individual components; and “aggregate” is a particle comprising strongly bound or fused particles. Nanomaterials cover a range of materials such as inorganic metal and metal oxide nanomaterials, carbon-based nanomaterials, and polymeric particulate materials in a variety of forms. Nanomaterials are generally classified based on their dimensionality, morphology, composition, uniformity, and agglomeration. On the basis of dimensionality, they can be broadly separated into the following four categories:

- 0D nanomaterials with diameter in nanoscale, for example, spheres, clusters.
- 1D nanomaterials with one dimension in the nanoscale, for example, thin films, plates, surface coatings.
- 2D nanomaterials with two dimensions in the nanoscale, for example, nanotubes, nanofibers, nanowire, nanorods.
- 3D nanomaterials with all three dimensions in nanoscale, for example, nanocrystallites.

In terms of chemical composition, nanomaterials can be organic, inorganic, or biological in nature. Inorganic nanostructures include metals, alloys, metal oxide and semimetal oxides, semiconductor quantum dots, and carbon structures (nanotubes, graphene, and fullerenes). Organic structures include polymer nanoparticles and dendrimers. Obviously, none of these classifications can be considered complete in itself. One must take into consideration the fact that the majority of the nanostructures are synthesized using organic substances necessary for stabilizing and functionalization of inorganic nanoparticles; therefore, nanomaterials are usually hybrid in nature.

4.2 Inorganic Nanomaterials

4.2.1 Metals and Alloys

Industrially metallic particles are of great importance. Therefore, an understanding of their properties at the levels of small clusters to bulk materials is essential. Nanoscale colloidal metals are of interest in many disciplines. Methods for their preparation and chemical applications are of primary focus of chemists. Colloidal gold metal, originally called gold sols, generated interest because of their intensive colors, which enabled them to be used as pigments for glass or ceramics [1]. Nanoparticulate metal colloids are generally defined as isolable particles between 1 and 50 nm in size that are prevented from agglomerating by protecting shells. Depending on the protection shell used, they can be re-dispersed in water ("hydrosols") or organic solvents ("organo sols"). The number of potential applications for these colloidal particles is growing rapidly because of the unique electronic structure of the nanosized metal particles and their extremely large surface areas. A considerable body of knowledge has been gained about these materials throughout the last few decades.

Nanostructured metal colloids can be obtained by both the so-called top-down and bottom-up methods. A typical "top-down" method, for example, involves the mechanical grinding of bulk metals and the subsequent stabilization of the resulting nanosized metal particles by the addition of colloidal protecting agents. The "bottom-up" methods of wet chemical nanoparticles preparation rely on the chemical reduction of metal salts, electrochemical pathways, or controlled decomposition of metastable organometallic compounds. A large variety of stabilizers, for example, donor ligands, polymers, and surfactants, are used to control the growth of the primarily formed nanoclusters and to prevent them from agglomerating. The chemical reduction of transition metal salts in the presence of stabilizing agents to generate zerovalent metal colloids in aqueous or organic media was first published in 1857 by Faraday [2], and this approach has become one of the most common and powerful synthetic methods in this field.

The metal salt is reduced to give zerovalent metal atoms in the embryonic stage of nucleation. These can collide in solution with further metal ions, metal atoms, or clusters to form an irreversible "seed" of stable metal nuclei. Depending on the difference of the redox potentials between the metal salt and the reducing agent applied, and the strength of the metal–metal bonds, the diameter of the "seed" nuclei can be well below 1 nm. Nanostructured colloidal metals require protective agents for stabilization and to prevent agglomeration. The two basic modes of stabilization [3] that have been distinguished are electrostatic and steric (Figure 4.1). Electrostatic stabilization involves the columbic repulsion between the particles caused by the electrical double layer formed by ions adsorbed at the particle surface (e.g., sodium citrate) and the corresponding counter-ions. As an example, gold sols are prepared by the reduction of $[AuCl^{4-}]$ with sodium citrate. By coordinating sterically demanding organic molecules that act as protective shields on the metallic surface, steric stabilization is achieved. In this way, nanometallic cores are separated from each other, and agglomeration is prevented.

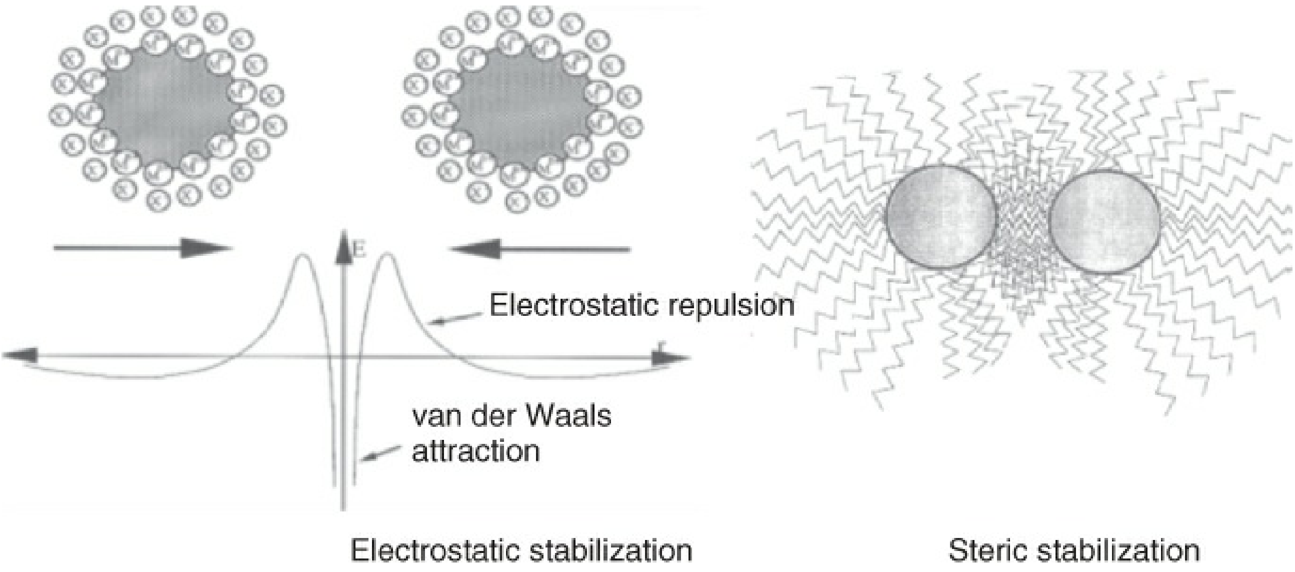

Figure 4.1 Electrostatic and steric stabilization of nanostructure metal colloids.

Bradley [3], © 1994. With permission of VCH, Weinheim.

The main classes of protective groups are polymers and block copolymers; P, N, S donors (e.g., phosphines, amines, thioethers); solvents such as THF, THF/MeOH, or propylene carbonate; long-chain alcohols; surfactants; and organometallics. In general, lipophilic protective agents give metal colloids that are soluble in organic media ("organosols") while hydrophilic agents yield water-soluble colloids ("hydrosols"). In Pd organosols stabilized by tetraalkylammonium halides, the metal core is protected by a monolayer of the surfactant coat. Metal hydrosols, in contrast, are stabilized by zwitterionic surfactants that are able to self-aggregate and are enclosed in organic double layers. Wet chemical reduction procedures have been used predominately to combine practically all transition metals with different types of stabilizers and the whole range of chemical reducing agents. Some of the commonly used reducing agents for preparing nanometals are discussed as follows:

Reduction using diborane: Clusters of Au_{55} are formed when a stream of B_2H_6 is carefully introduced into Au^{3+} ion solution. Bimetallic nanoclusters can also be synthesized by this method. The phosphine ligands may be exchanged by sislesquioxanes in the Au_{55} nanoclusters quantitatively, which causes important changes in the physical and chemical behavior of the gold clusters.

Reduction using alcohols: The method is widely applicable to the preparation of colloidal precious metals stabilized by organic polymers such as poly(vinylpyrrolidone) (PVP), poly(vinyl alcohol) (PVA), and poly(methyl vinyl ether). Alcohols containing a hydrogen atom are oxidized to the corresponding carbonyl compound (e.g., methanol to formaldehyde) during the metal salt reduction. Monodisperse ruthenium nanoparticles in the 1–6 nm size range could be prepared by the reduction of $RuCl_3$ in liquid polyol [4]. The method can also be used for preparing bimetallic nanoparticles via co-reduction of mixed ions.

Reduction using hydrogen: Hydrogen is used as an efficient reducing agent for the preparation of electrostatically stabilized metal sols and of polymer-stabilized hydrosols of Pd, Pt, Rh, and Ir.

Reduction employing tetraalkylammonium hydrotriorganoborates: This method offer a wide range of applications in wet chemical reduction of transition metal salts [5], where the reducing agent serves dual purpose of being reducing agent $[BEt_3H^-]$ as well as stabilizing agent $[NR_4^+]$. The surface-active NR_4^+ salts are formed immediately at the reduction center at high local concentration and prevent particle aggregation (Eq. 4.1).

$$MX_v + NR_4(BEt_3H) \rightarrow M_{colloid} + vNR_4X + vBEt_3 + \frac{v}{2}H_2\uparrow \qquad 4.1$$

Trialkylboron is recovered unchanged from the reaction, and there are no borides contaminating the products. It has been observed that the chain length of the alkyl group in the tetraalkylammonium ion plays a critical role in the stabilization of various metal colloids. Figure 4.2 summarizes nanometals stabilized by tetrahydrofuran (THF), tetraalkylammonium ion (NR_4^+) as well as without any stabilizer.

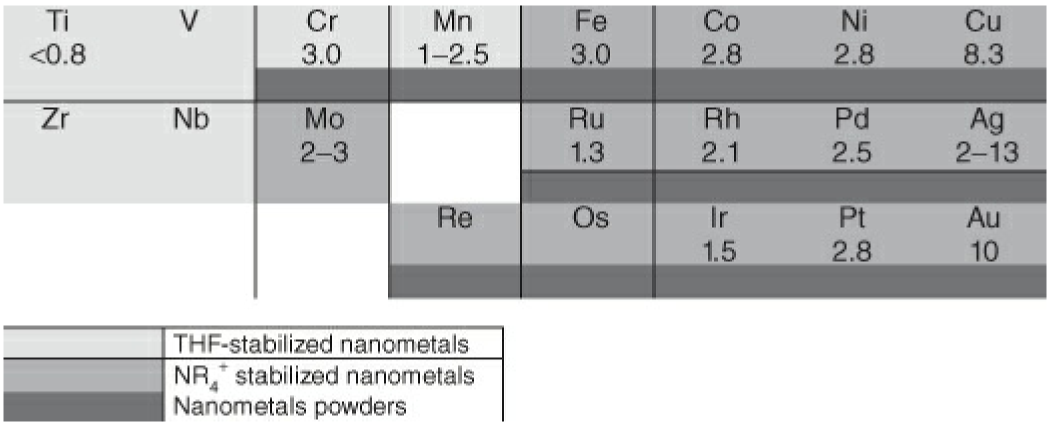

Figure 4.2 Nanostructured metal colloids obtained via [BEt_3H^-] reduction method (including the mean particle sizes in nanometers).

Vnnemann et al. [5], © 1996. With permission of Elsevier.

The advantages of reduction method employing tetraalkylammonium hydrotriorganoborates may be summarized as follows:

- The method is generally applicable to salts of metals in groups 4–11 of periodic table.
- It yields extraordinarily stable metal colloids that are easy to isolate as dry powders.
- The particle size distribution is nearly monodisperse.
- Bimetallic colloids are easily accessible by co-reduction of different metal salts.
- The synthesis is suitable for bulk preparations and easy to scale up.

Miscellaneous reducing agents: Colloidal Pt in water can be obtained using CO, formic acid/sodium formate, formaldehyde, or benzaldehyde as reductant. Silanes have been found to be effective for the reductive preparation of Pt sols. Tetrakis(hydroxymethyl) phosphonium chloride (THPC) has been successfully introduced as a reducing agent, which allows the size and morphology-selective synthesis of Ag, Cu, Pt, and Au nanoparticles from their corresponding metal salts. Furthermore, hydrazine, hydroxylamine, and electrons trapped in, for example, K^+ $[(crown)_2K]^-$, have also been successfully applied as reducing agent. In addition, BH^{4-} has been found to be a powerful and valuable reagent for the salt reduction method; however, transition metal borides are often found along with the nanometallic particles.

Nanometals have an enormous potential for applications in electronics, construction, power transformation, energy storage, telecommunications, information technology, medicine, catalysis, and environment protection, with high possible impact in the areas of technology related to energy, health, and materials. The most exploited properties of nanopowders are based on common phenomena at nanoscale such as high specific surface area, soft magnetic properties, and new deformation mechanisms. Metallic nanomaterials included in Table 4.1 are most promising for a variety of applications: some of them are discussed here.

Table 4.1 Important Metallic Nanomaterials

Metallic Nanomaterials	Examples
Metals and alloys	Ti, Ti–Al, Ti–transition metals (Fe, Ni, Cu) alloy; Fe–transition metal (Co, Ni, Cr, Cu, Zr) alloy; Fe–Cu–Nb–Si–B alloy; Al, Al–transition metal (Fe, Ni, Ti, Zr) alloy; Mg, Mg–Ni alloy; Mg–Al alloy
Powder of Nobel nanometals	Ag, Au, Pt, Pd

Gold (Au)

Colloidal gold, due to their nanosized dimensions, has increasingly received considerable attention in nanotechnological advancement and development. Depending on the particle size, shape, and agglomeration, gold colloids can be red, violet, or blue, Figure 4.3, exhibiting interesting optical properties [6].

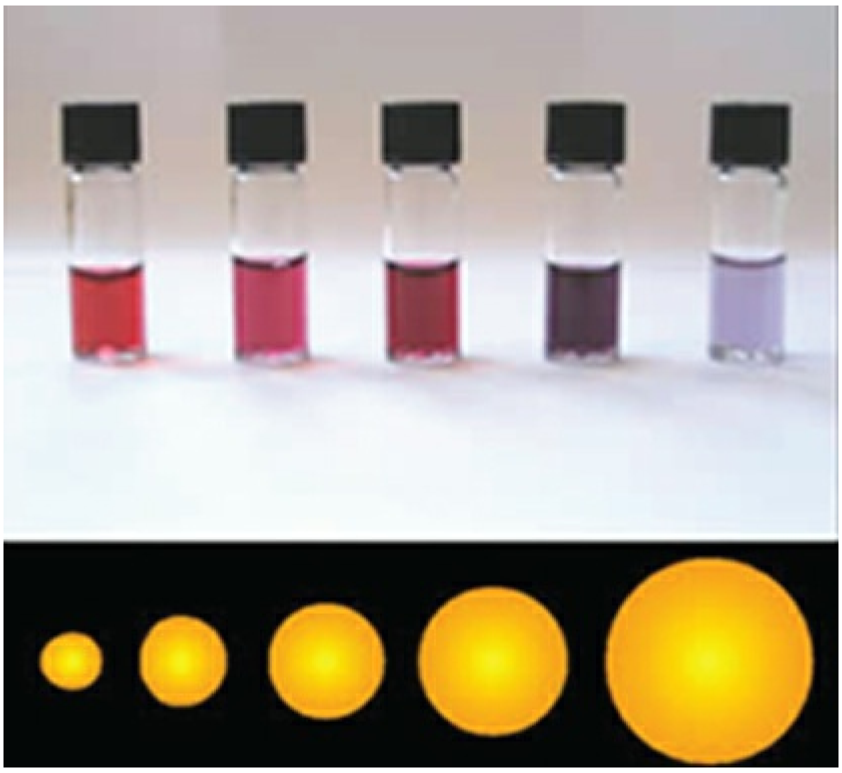

Figure 4.3 Color variation of gold nanoparticles of different sizes.

http://www.webexhibits.org/causesofcolor/credits.html.

Typically, colloidal gold nanoparticles are prepared by the treatment of $HAuCl_4$ with a reducing agent, namely, $NaBH_4$. It can also be obtained by the treatment of $HAuCl_4$ with Ag metal (Eq. 4.2).

$$3Ag(s) + HAuCl_4(aq) \rightarrow Au(s) + 3AgCl(aq) + HCl(aq) \tag{4.2}$$

Furthermore, for catalysis purposes, the incipient wetness impregnation is unsuitable to produce well-dispersed gold catalysts. In order to obtain high activity, the catalyst must be prepared via co-precipitation or deposition precipitation.

Gold nanoparticles are mostly used in medical applications, in particular for *in vitro* diagnostics. Other applications include catalysts, optics, solar cells, inks for printable electronics, sensors, and surface coatings. Gold colloids also find applications in areas of Histochemistry and Cytochemistry, where they are used as electron-dense labeling agents. Moreover, due to high thermal and electrical conductivity, gold NPs also find application in electronics.

Gold is also widely used in biocatalysis and catalysis. Nano-gold has been widely used to construct biosensors due to its excellent ability to immobilize biomolecules such as proteins, enzymes, and antibodies while maintaining the biocatalytic activities of those biomolecules. Supported gold catalysts provide a high catalytic activity in numerous reactions such as the reduction of nitrogen oxide and oxidation of CO and the epoxidation of propene at low temperatures. Reactive molecules such as CO and H_2 do not adsorb on the surface of gold. However, this behavior dramatically changes when gold is dispersed as nanosized particles on certain metal oxides including TiO_2.

Silver (Ag)

Nanosized silver was first produced in 1880. It was used for a long time in photographic film applications. Today, nano-silver is mostly used in antimicrobial applications where a high release of silver ions is needed to kill the bacteria. Silver nanoparticles are synthesized either by using traditional Creighton methods, where the $AgNO_3$ is reduced with $NaBH_4$, or through nontraditional methods such as photoreduction and electrolysis of Ag salt solution. Similar to nAu, the optical properties of nAg can be systematically manipulated by adjusting the size, composition, and shape (Figure 4.4).

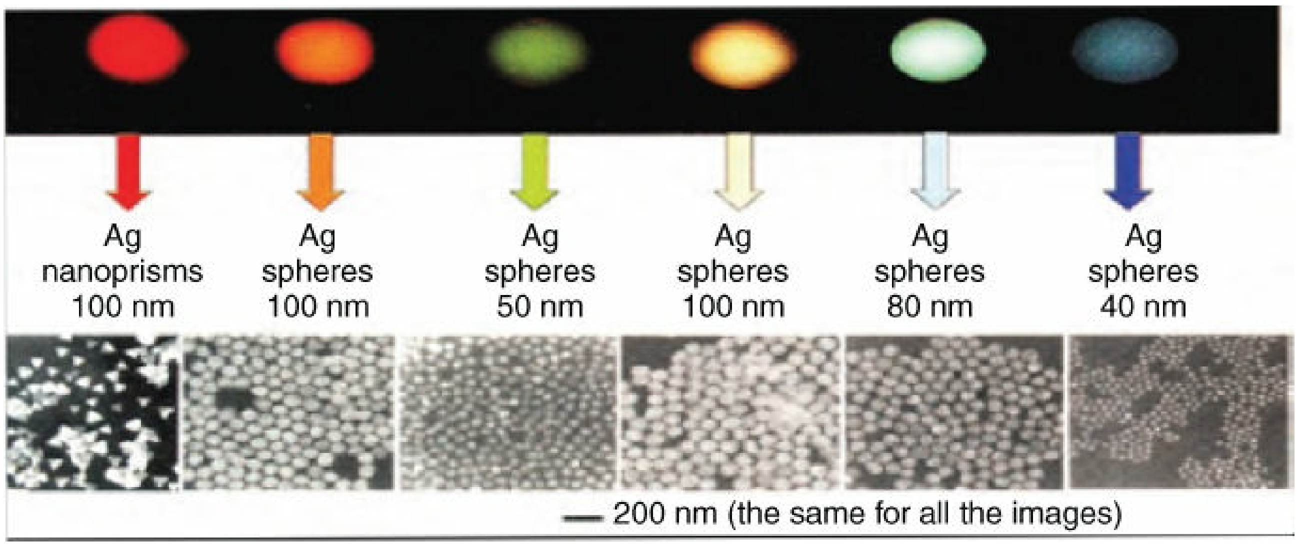

Figure 4.4 Influence of size, shape, and composition on the light-scattering and resultant colors of silver nanoparticles (quoted nanoparticle sizes are all approximate).

Mirkin [7], © 2005. With permission of Wiley-VCH.

Antimicrobial uses of nano-silver include antimicrobial textiles for hospitals, wound plasters, and anti-odor sportswear, bed mattresses, socks, or inner wears. There are also reported uses in toys, household appliances such as refrigerators and washing machines, cosmetics, containers for contact lenses, nontextile antimicrobial coatings, inks for inkjet printers, printable electronics, catalysts, photovoltaic, displays, and fuel cells.

Copper

Copper nanopowders are used in electronics and, to a small degree, in inks. For nanostructured metal growth, the simple reduction of metal salts (usually via $NaBH_4$, H_2, or hydrazine as reducing agents) in presence of a stabilizing agent is amenable for mild, solution-phase growth, for example, Equation 4.3 for Cu metal [8]. In theory, any metal with a larger standard reduction potential (E^0) than the reducing agent (e.g., −0.481 V for borohydride ion) is a candidate for reduction to its metallic form. This includes most of the first-row transition metal ions, and many others from the main group/transition metal series. However, it should be noted that solution pH and side reactions (e.g., metal ions being converted to borides by BH_4^- rather than reduction) often provide a barrier toward successful metal-ion reduction.

$$Cu^{2+} + 2Cl^- + 6H_2O + 2NaBH_4 \rightarrow Cu^0 + 2NaCl + 7H_2 + 2B(OH)_3 \quad \textbf{4.3}$$

Iron

Fe NPs are mostly used in magnetic recording tapes, waste water, and land remediation [9]. Nano-zerovalent iron (nZVI) can be synthesized in a variety of pathways such as the reduction and precipitation of ZVI from an aqueous iron salt solutions using sodium borohydride; reduction of iron oxides, or hydroxides by hydrogen. nZVI may react with oxygen/water and get oxidized to ferrous ions (Fe^{2+}), where the electrons released are available to reduce other compounds (Eqs 4.4 and 4.5)

$$2Fe^0(s) + O_2(aq) + 4H^+(aq) \rightarrow 2Fe^{2+}(aq) + 2H_2O(l) \quad \textbf{4.4}$$

$$Fe^0(s) + 2H_2O(aq) \rightarrow Fe^{2+}(aq) + H_2(g) + 2OH^-(aq) \quad \textbf{4.5}$$

nZVI is highly reducing and generates reactive oxygen species (ROS) through Fenton chemistry. Nano-iron-based magnetic alloys are used for efficient energy transmission due to small size of the grains compared to the magnetic domain size.

Platinum and Palladium Alloy Nanoparticles

These are mostly used in electronics (production of multilayer ceramic capacitors, MLCC). Other uses include catalysis (including combustion exhaust purification) and energy technologies. Uses in data storage and healthcare field have also been reported.

Others

Titanium nanoparticles are a material of choice for medical implants. Figure 4.5 shows a TEM image of nano-titanium assembled as flower. Nano-titanium- and **Nano–aluminum**-based alloys are increasingly used as lightweight alloy in aerospace and automotive sector due to their superior mechanical properties for structural applications. **Nano-magnesium** and its alloys are used for hydrogen storage. **Rhodium nanoparticles** are reported to be used in catalysis. Other metal nanoparticles, for example, nickel, cobalt, aluminum, zinc, manganese, molybdenum, tungsten, lanthanum, and lithium are used in electronics. Coatings based on metallic NPs are used for improving tribological properties such as higher wear resistance, less friction, better corrosion resistance, and sustainable production process.

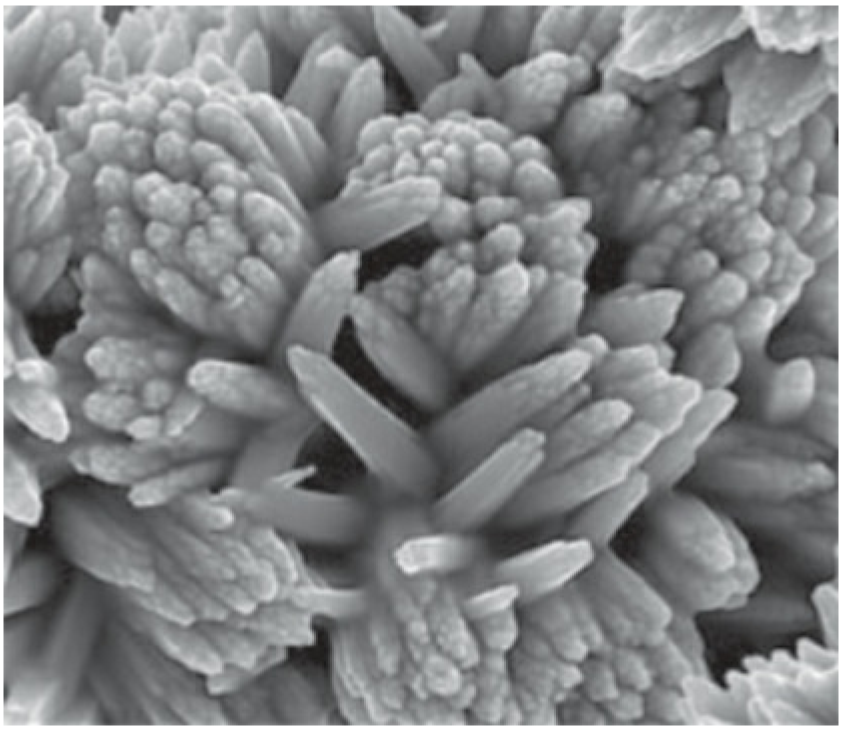

Figure 4.5 TEM image of nano-titanium flower.

Ghosh et al. [10], © 2008. With permission of ACS.

4.2.2 Metal Oxides of Transition and Non-transition Elements

Nanoparticles of transition and non-transition metal oxides [11–14] are among the very important class of nanomaterials, discussed here from the point of view of unique properties and applications in diverse areas.

Silicon Dioxide (SiO_2)

The various forms of synthetic amorphous silica are precipitated silica, silica gels, colloidal silica (or silica sols), and fumed (or pyrogenic silica). Most forms are either used as stable dispersions of nonagglomerated SiO_2 particles (colloidal silica) or as agglomerated or aggregated particles (other forms of silica). Colloidal silica is stabilized dispersions of nonagglomerated, mostly spherical, SiO_2 particles. Their main uses are in paper industry (e.g., providing antislip properties; retention aids and in coatings of inkjet paper; better handling of recycled paper); chemical mechanical planarization (CMP) slurries (e.g., polishing agent for Si wafers used to produce computer chips); coatings, paints, inks, and adhesives (increasing strength, scratch, and abrasion resistance); precision metal casting and refractory (e.g., molds for casting around wax originals); food industry (e.g., as an aid for clarifying wine, beer, fruit juices); bulk plastics and composites; photography; metal surface treatment; catalysis; textile; leather; and building industry (e.g., thermal and acoustic insulation).

Precipitated Silica

It is made up of primary particles in the size range of around 5–100 nm, which are aggregated and agglomerated in the final product. The biggest use of precipitated silica is for the reinforcement of elastomer products, primarily automotive tires, footwear, rubber articles, and cable sheathing. In tires, formulations using precipitated silica reduce rolling resistance, improve traction under slippery conditions, and improve fuel efficiency. Precipitated silica is also used in batteries; as antiblocking agent in thermoplastic films; as carrier silica for liquids and semiliquids and anticaking agent in food powders, in healthcare products such as toothpastes, detergents, and cosmetics; as matting agents in paints and varnishes; in the paper industry as advanced fillers in newsprint paper and in special coated papers for inkjet and direct thermal printing to enhance ink absorption; and in agricultural products.

Synthetic Silica Gels

These are products of the polymerization process of fine colloidal silica. They have a similar structure as precipitated silica, the difference being that the cross-linked silica particle networks form a nanoporous structure that is finer than the porous structure of the aggregated particles in precipitated silica. Silica gels are sold in various types of gels (hydrogel, aerogel, xerogel, etc.). They are used in many food and health products (e.g., to selectively remove certain proteins and polyphenols that precipitate upon chilling). They are used in food industry as an anticaking agent, a carrier for vitamins and a tableting aid in pharmaceuticals. They are also used in cosmetics such as face powders, as flow conditioner, and for oil absorption. Silica gels also serve as drying agents, protecting a wide variety of products during shipment and storage.

Pyrogenic (Fumed) Silica

It is manufactured by high-temperature hydrolysis process. It consists of agglomerated and aggregated primary silica particles. The latter particles are of size typically between 5 and 100 nm. The aggregates, which are fused and chemically bonded primary particles, typically are of size between 100 and 350 nm. The aggregates in turn form agglomerates typically in the range from 150 nm up to the several hundreds of nanometers. Pyrogenic or fumed silica is used in silicone rubber applications, as a reinforcement and thixotropic agent in plastics, gel coats, sealants and adhesives, cosmetics, and toothpastes; in coatings and printing inks; as a free flow, antistatic agent in animal feedstuffs and hygroscopic powders; and as a carrier for active ingredients. It is also used as an antifoaming agent in the manufacture of paper, decaffeinated coffee and tea, poultry and sea food processing, and oil refining.

Titanium Dioxide (TiO_2)

Titanium dioxide powder exists in both bulk and nanoform, as well as in various crystalline modifications, including rutile and anatase. In its bulk form, it has been used extensively as white pigment showing maximum reflectivity at a particle size of ~300 nm. Titanium dioxide is also an effective UV filter. The nanoform (~50 nm) is transparent, which provides an esthetic advantage for uses in sunscreens (mostly rutile). Nanoform TiO_2 in the anatase modification also has specific electrical and photocatalytic as well as antimicrobial properties. The nanoform of anatase is reported to be more reactive than the bulk form. There are various methods available for the production of small $nTiO_2$ but the sol–gel method has been widely used since it is deemed relatively inexpensive. Unfortunately, the sol–gel derived material is amorphous in nature and often requires a further treatment to induce crystallization. Elevated treatment temperatures (higher than 350 °C) are often necessary to expedite the transition from the amorphous material to the crystalline anatase phase, but such high temperatures result in increased size of the nanoparticles and subsequently a decrease in the surface area. Apart from sunscreens, the UV filtering property of TiO_2 is also used in coatings for plastics and metals, varnishes for wood preservation, in textile fibers, and in packaging films. Another main use is catalysts (e.g., decomposing NOx into nitrates or N_2). The photocatalytic and antimicrobial properties are used in "self-cleaning" products (e.g., windows, cement, tiles, and textiles for use in hospitals) and air purification systems. Use of tribological coatings prevents deposits in engines and enhances fuel efficiency. TiO_2 nanoparticles are also used to increase scratch resistance of coatings and in the production of electronic components and dental impressions. TiO_2 can also be used in dye-sensitized solar cells to produce electricity, although efficiency is currently lower than traditional silicon solar cells.

Zinc Oxide (ZnO)

Similar to titanium dioxide, zinc oxide powder exists in bulk and in nanoform. Its nanoform is colorless and it is an effective UV filter with a different spectrum than titanium dioxide. It also has antimicrobial properties (though less strong than TiO_2) and can be used as an active agent in self-cleaning products. Several methods of synthesizing ZnO nanocrystals have been developed including thermal transport and condensation template and surfactant-assisted liquid methods. Although these methods are relatively inexpensive and generate products that are pure and homogeneous but are limited in a number of ways. For example, the removal of the homogeneously mixed template is always a challenging task. However, hydrothermal synthesis has proven to be a facile method for the synthesis of nZnO. The use of microwave-assisted hydrothermal is also an alternative option that offers many advantages such as low cost, short reaction time, high purity, and large-scale production. Studies have shown that the morphology of nanoparticles of nZnO may be influenced by factors such as synthesis method and temperature. The hydrothermal synthesis of nZnO using hydrothermal synthesis is carried out in the presence of a strong alkaline solution such as NaOH or KOH.

According to SRI, the global market for nanoform zinc oxide is several thousand tons per year. Major uses are as a UV filter in cosmetics (where it competes with bulk zinc oxide but has the advantage of being transparent), in varnishes (as a UV filter and self-cleaning agent), ceramics, and electronics. Nanoform zinc oxide is also used in rubber, improving toughness, increasing abrasion resistance (e.g., reducing wear loss in tires), and preventing UV and bacterial degradation. In this way, the life time of rubber products can be prolonged. An emerging use is zinc oxide nanowires for UV nanolasers. Uses are also reported in liquid crystal displays and solar cells.

Aluminum Oxide (Al_2O_3)

Aluminum oxide nanoparticles are widely used as fillers in polymers and tires and to increase scratch and abrasion resistance in coatings. Nanoform Al_2O_3 powders and dispersions are used *inter alia* in scratch- and abrasion-resistant coatings (e.g., for cutting and grinding tools, automobile exteriors, safety glasses and scratch-resistant windows for barcode scanners, flooring), as abrasive particles in slurries for polishing semiconductor and precision optical components, in the coating of light bulbs and fluorescent tubes, as a flame retardant, as fillers for polymers and tires, in coatings of high-quality inkjet papers, in catalysts including the support structure in automobile catalytic converters, in refractory materials, and as ceramic filtration membranes. Nanoform alumina can also be used for the manufacture of transparent ceramic bodies for high-pressure lamps.

Aluminum Hydroxides and Aluminum-Oxo Hydroxides

Different forms of aluminum hydroxide (e.g., bayerite and gibbsite) and aluminum-Oxo hydroxide (e.g., boehmite and diaspore) particles in nanoform are available. Aluminum hydroxide $Al(OH)_3$ in powder form is used as a flame retardant and as filler in carpets, rubbers, plastics, and foamed plastics. Moreover, it is used in toothpaste and cosmetics. Aluminum-Oxo hydroxides are often used in the dye and plastics industries as thickeners and fillers and as agents that reduce adhesiveness and increase scratch resistance. In addition, they also serve to enhance the color saturation of paints and varnishes.

Iron Oxides: Diiron Trioxide (Ferric Oxide, Hematite, Fe_2O_3)

There are several types of nano-iron oxide, the most common ones are hematite (ferric oxide, Fe_2O_3) and magnetite (ferro-ferric oxide, Fe_3O_4). Nanosized ferric oxide are commonly used in pigment applications (e.g., in automotive industry or in cosmetics), offering clean shades of a number of colors but with high transparency while still offering protection from UV light. Magnetite particles have been used for a long time for data storage in magnetic tapes and hard drives. Another use of magnetite nanoparticles is ferro-fluids, which are stable colloidal suspensions of magnetic nanoparticles in a liquid carrier. Ferro-fluids are used in electronic components such as loudspeakers and hard disks (preventing dirt particles from entering the hard drive), or in shock absorbers in the automotive industry. Other emerging applications of nano-iron oxides are in medicine. After selectively attaching nanoparticles to tumor cells, those cells can selectively be destroyed by applying electromagnetic energy. Drugs and diagnostic agents attached to magnetic nanoparticles could selectively be transported to targets in the body. Other uses of iron oxide nanoparticles include polishing media, catalysts, components in fuel cells, oxygen sensors, ceramics and optoelectronic devices, and soil and groundwater remediation and water treatment.

Cerium Dioxide (CeO_2)

Ceria (CeO_2) is a rare-earth oxide with specific optical properties. Nanostructured nonstoichiometric CeO_{2-x} films are used for applications in optical, electro-optical, microelectronic, and optoelectronic devices. Nanoform ceria is used *inter alia* as a polishing material for glass surfaces and silicon wafers to finish photomasks and disk drives, as an anticorrosion material, for example, in exterior architectural paint, steel and other metal plates, and in fuel cells. Another major application is as a catalytic diesel fuel additive, decreasing toxic diesel emissions and increasing fuel efficiency.

Zirconium Dioxide (ZrO_2)

Ceramic materials made by sintering nanoform zirconia (ZrO_2) powder have a number of unique properties, including some forms with very high fracture toughness. The most significant application of ZrO_2 is in optical connectors, followed by fuel cells, lithium-ion batteries, catalysts, and ceramic membranes. Other developing applications are in structural and electronic ceramics, dental fillings, prostheses, fluorescent lighting, polishing agent, and so on.

Mixed Metal Oxide Nanomaterials

Indium tin oxide (ITO) is a semiconducting material used as thin-film material for the production of transparent electrodes in liquid crystal displays, touch screens, organic LEDs, thin-film solar cells, semiconducting sensors, and so on. Due to its IR-radiation reflectivity, it is often used as thermal insulation coating on window glass. Its antistatic properties make it additionally suitable for packing and storage of sensitive electronic components. The high price and increased global demand of ITO has intensified the research for its alternatives. Antimony tin oxides (ATO) have similar IR-radiation reflecting properties and considered as alternative to ITO.

Other Oxygen-Containing Inorganic Nanomaterials

Other oxygen-containing inorganic nanomaterials include barium titanate, barium sulphate, strontium titanate, and strontium carbonate. Barium titanate powders are the dominating raw material for the production of ceramic dielectric layers in low-temperature MLCC. Nano-calcium carbonate also exists, although most of the fine-ground calcium carbonate is generally in a particle size above 100 nm. Ultrafine calcium carbonate is used as advanced filler in sealants and in plastic for window frames. Fine-ground calcium carbonates are widely used as fillers in paper, plastics, paints, coatings, adhesive, and sealants. They are also used as a food additive.

4.2.3 Non-oxide Inorganic Nanomaterials

Nonoxide inorganic nanomaterials include aluminum nitride, silicon nitride, titanium nitride, titanium carbonitride, tungsten carbide, and tungsten sulfide [15, 16]. Aluminum nitride is used in the electronic industry in various particle sizes, including nanosize regime. Titanium nitride powders with a particle size from nano- to micrometers are used as additive in the production of wear-resistant sintered materials. Furthermore, it is added to plastics, particularly to polyethylterephthalate (PET). TiN nanoparticles improve the thermal properties of the material and allow increasing the production output of PET bottles. Tungsten carbide nanoparticles are used mainly for hardening the surfaces of cutting tools to improve wear and temperature resistance. Tungsten carbide nanoparticles are at the threshold to large-scale production. Molybdenum and tungsten sulfide nanoparticles seem to be a promising lubricant for harsh conditions.

4.3 Organic Nanomaterials

The organic nanoworld is predominated by polymers. Nanopolymeric materials can be obtained in the form of particles, tubes, fibers, films, and branched structures known as dendrimers. A brief description of these materials [17–19] and their potential application area are given in following sections.

4.3.1 Polymeric Nanoparticles

Polymer nanoparticles are nanoscale polymeric units such as polyacylbenzene polydiene (PAB-PD) nanoparticles. They are used in drug-delivery systems or as filler material in polymer/metal/ceramic nanocomposites. Polymer nanotubes, nanowires, and nanorods have potential applications in electronic, magnetic, optical, optoelectronic, and micromechanical devices. One of the promising polymeric nanotubes is polyaniline (PANI) nanotubes, which show good conductivity and may be used in conductive fabrics. Polyglycidylmethacrylate (PGMA) fibers are utilized in making smart fabrics and are called as “smart fibers,” as they can change their properties depending on the environmental conditions. Textiles based on PGMA fibers may switch between contradictory properties such as hydrophobic and hydrophilic; conductive and nonconductive; acidic and basic; or may switch to different colors.

4.3.2 Polymeric Nanofilms

Polyalkylthiophene, polystyrene-polyethylene oxide (PS-PEO), poly(methyl methacrylate) (PMMA, the acrylic glass) are reported to form polymeric nanoscale thin films. They are mainly used as coatings in the biomedical applications. There are also other nanofilms, for example, based on styrene-ethylene-butylene-styrene (SEBS), polyacrylonitrile nanostructures (PAN) are found in semiconductors, solar cells, sensors, and membranes in filters. Their electrical properties are based on a variable and controllable band gap for semiconductor use.

4.3.3 Nanocellulose

Cellulose is the most abundant natural biopolymer on earth, which is renewable, biodegradable, as well as nontoxic. It is a carbohydrate polymer made up of repeating d-glucopyranose units and consists of three hydroxyl groups per anhydroglucose unit (AGU), giving the cellulose molecule a high degree of functionality. The knowledge of the molecular structure of cellulose is of prime importance as it explains the characteristic properties of cellulose, such as hydrophilicity, chirality, biodegradability, and high functionality. As a renewable material, cellulose and its derivatives have been widely studied, focusing on their biological, chemical, as well as mechanical properties. The materials based on cellulose and its derivatives have been used for more than 150 years in a wide variety of applications, such as food, paper production, biomaterials, and pharmaceuticals.

Nanocrystalline cellulose (NCC) obtained from acid hydrolysis of cellulose fibers has been realized as a new class of nanomaterials. Compared to cellulose fibers, NCC possesses many advantages, such as nanoscale dimension, high specific strength and modulus, high surface area, and unique optical properties. These amazing physicochemical properties and wide application prospects have attracted significant interest from both research scientists and industrialists. Nanocellulosic materials can be used as a reinforcement material in composites and for medical implants. NCC derived from acid hydrolysis of native cellulose possesses different morphologies depending on the origin and hydrolysis conditions. NCCs are rigid rod-like crystals with a diameter in the range of 10–20 nm and lengths of a few hundred nanometers.

NCC materials, for example, crystallites from tunicates and green algae have lengths in the range of a few micrometers and crystallites from wood and cotton have lengths of the order of a few hundred nanometers, while some spherical shape NCCs were also produced during the acid treatment (Figure 4.6). Therefore, the relative degree of crystallinity and the geometrical aspect ratio, that is, the length-to-diameter (L/d), are very important parameters controlling the properties of NCC-based materials. An important characteristic of NCCs, when prepared in sulfuric acid, is that they possess negative charges on their surface due to the formation of sulfate ester groups during acid treatment, which enhances their stability in aqueous solutions. NCC derived from acid hydrolysis using various forest product sources can disperse in water due to their negative-charged surfaces. At low concentration, NCC particles are randomly oriented in aqueous suspension as an isotropic phase, and when the concentration reaches a critical value, they form a chiral nematic ordering, where NCC suspensions transform from an isotropic to an anisotropic chiral nematic liquid crystalline phase. As the concentration increased further, aqueous NCC suspensions showed a shear birefringence phenomenon. NCC suspensions exhibited negative diamagnetic susceptibility anisotropy as they dried under the influence of a magnetic field.

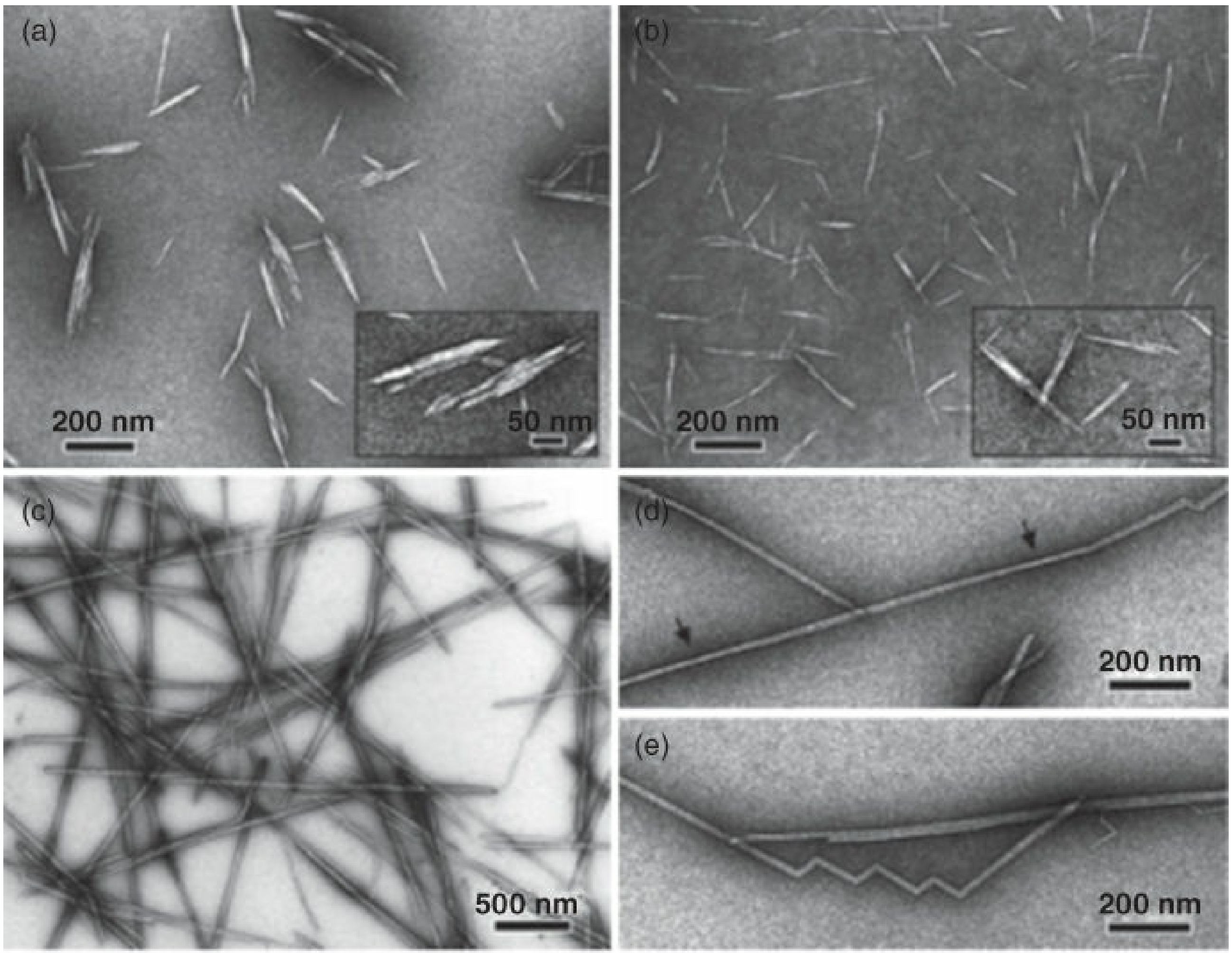

Figure 4.6 TEM micrographs of nanocrystals obtained by sulfuric acid hydrolysis of (a) cotton, (b) avicel, and (c–e) tunicate cellulose.

Hafraoui et al. [20], ©2008. With permission of ACS.

Synthesis: Both the bottom-up and top-down processes are applicable to the production of cellulose nanofibers. In the bottom-up method, techniques such as electrospinning can be used where nanofiber is spun from cellulose solution, which initially may also contain solid nanoparticles. The top-down method uses physical or chemical refining, biorefining, or combinations of these methods, consisting the removal of plant cell constituents other than cellulose, such as pectin, hemicellulose, lignin, and minerals. Moreover, the appropriate treatment of cellulose fibers can increase the availability of hydroxyl groups, change the degree of crystallinity, develop the inner surface, and break hydrogen bonds, which increase the reactivity of cellulose. Conducting the process under appropriate conditions can lead to the separation of cellulose fibers in macro- and microfibrils. Microfibrils in cellulose are composed of elongated crystalline areas separated by amorphous regions. It is assumed that the amorphous regions may act as structural defects of the material, which are responsible for the lateral division of microfibrils into nanocrystals during the hydrolysis of cellulose. Cellulosic materials intended for use as nanofillers in composites are usually subjected to hydrolysis by strong acids such as sulfuric or hydrochloric acid, which causes a selective degradation of amorphous regions of cellulose and, consequently, the splitting of microfibril beams. As a result of cellulose hydrolysis, the disintegration of its hierarchical structure takes place to form crystalline nanofibers or nanocrystals, usually referred to in the literature as nanowhiskers. The morphology of the nanocrystals obtained depends on the source of cellulose and hydrolysis conditions used, such as acid concentration, the ratio of acid to cellulose, temperature, and reaction time. Since nanofibers can be produced from polymers that do not always fall within the concept of classical fiber forming polymers, it is anticipated that the scope of use of these nanoproducts may be far beyond the use of standard fibers, microfibers, or fibrous materials.

Applications: As a result of their distinctive properties, NCC has the potential of becoming an important class of renewable nanomaterials, which could find many useful applications. The main application of NCC is for the reinforcement of polymeric matrix in nanocomposites materials. The use of NCC as reinforcing fillers in poly(styrene-*co*-butyl acrylate) (poly(S-*co*-BuA))-based nanocomposites was reported in the 1990s. . Since then, numerous nanocomposite materials have been reported by incorporating NCC into a wide range of polymeric matrices. The properties of these cellulosic nanocomposites depend on the types and characteristics of NCC and polymeric matrices (which could be both natural and synthetic polymers). Chemical functionalization of NCC improves its dispensability in organic solvents, and this greatly expands its potential applications in various sectors.

Many applications in diverse fields have been proposed and explored, ranging from iridescent pigments to bimolecular NMR contrast agents. In addition, NCC may be used in security paper based on the solidified liquid crystals property. It is believed that NCC may be used in lithium battery products as a mechanical reinforcing agent for low-thickness polymer electrolytes.

Cellulose nanofibers derived from plant biomass are a particularly desirable group of nanoproducts. The almost unlimited availability of the raw material, its biodegradability, and biocompatibility with the animated world make a lot of laboratories conduct research on the development of nanofiber manufacturing technologies. Some of the areas in which the use of cellulose nanofiber is expected are medicine (drug carriers, surgical materials, prostheses, dressings), cosmetics (creams and nutritional ingredients, tampons, masks), the environment (sensors, filters, nanofilters, absorbers), energy (electric cells, hydrogen storage), chemistry (catalysts with high efficiency, ultralight materials and composites), electronics (computers, shields for electromagnetic radiation, electronic equipment), textiles (clothing and functional products), and defense (special-purpose clothing, face masks).

4.3.4 Biodegradable Polymer Nanoparticles

Organic nanoparticles mostly consisting of insoluble polymers are biodegradable. These polymer nanoparticles are used for drug delivery with diffusion-controlled delayed dissolution or drug solution flow control mechanisms. Polymers used for controlled drug release include the well-known poly(esters); several examples include polylactic acid (PLA), polyglycolic acid (PGA), copolymer of PLA and PGA (PLGA); 3,9-diethylidene-2,4,8,10 tetraoxaspiro[5,5]undecane (DETOSU)-based poly(ortho esters); sebacic acid (SA), *p*-(carboxyphenoxy)propane (CPP) and *p*-(carboxyphenoxy)hexane (CPH)-based poly(anhydrides); poly(amino acids) such as poly(lactic acid-*co*-lysine) (PLAL);

and finally phosphorous-containing polymers. Polymeric nanoparticle drug-delivery systems have been shown to encapsulate a variety of therapeutic compounds. Biodegradable polymer nanoparticles, consisting of polylactic acid (PLA), polyglycolic acid (PGA), or a copolymer of PLA and PGA, have been investigated for the delivery of proteins and genes, vaccines, and anticancer drugs. However, due to copolymer crystallization, aggregation, low biodegradation rate, or poor flexibility, the application of polymer nanoparticles is limited. In order to prevent the aggregation of PLGA particles, anionic, cationic, nonionic, and zwitterionic (amphoteric) polymers are often used as stabilizers.

4.3.5 Dendrimers

The highly branched and symmetrical molecules known as dendrimers are the most recently recognized members of the polymer family because of their unique branched topologies, which confer them with properties that differ substantially from those of counterpart linear polymers that are tree-shaped molecular structures similar to polymers. Synthesis of dendrimers was first reported in 1978 by Vögtle [21a]. They are 3D globular, monodisperse, highly branched polymers prepared in a series of repetitive reactions from simple branched monomer units emitted from a central core with an exterior corrugated surfacing whose size and shape can be precisely controlled. Dendrimers are fabricated from monomers using either convergent or divergent step growth polymerization (Figure 4.7). Dendrimer's unique architecture enhances their ability to exhibit high functional structures, and subsequently, a wide range of dendrimers of different structural classes are synthesized using divergent (built from the central core to the periphery) or convergent (built from the periphery toward the central core) strategies – using repeat units ranging from pure hydrocarbons to peptides, or coordination compounds. They are characterized by a high specific surface and, when dispersed, by a nonlinear mass–viscosity relation. The well-defined structure, monodispersity of size, surface functionalization capability, and stability are properties of dendrimers that make them attractive drug-carrier candidates. Drug molecules can be incorporated into dendrimers via either complexation or encapsulation. Dendrimers are being investigated for both drug and gene delivery, for instance, as carrier for penicillin and in anticancer therapy. Other dendrimers' applications include catalysis and molecular encapsulation for light harvesting. Thus, major applications of dendrimers include pharmaceuticals, light-emitting diodes and lasers, catalyst carrier crystals, cross-linking agents in radiation-curable surface-coating resin, semipermeable membranes, polymer additives, and biotechnological applications.

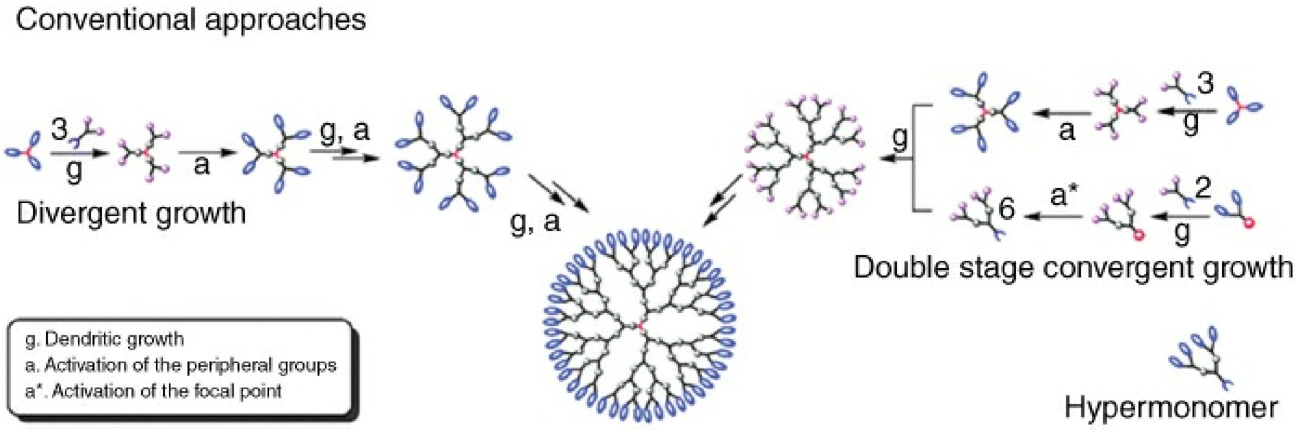
Conventional approaches
3
g
a
g, a
Divergent growth
g, a
g
a
3
g
a*
6
2
g
Double stage convergent growth
g. Dendritic growth
a. Activation of the peripheral groups
a*. Activation of the focal point
Hypermonomer

Figure 4.7 Synthesis of a typical dendrimers involving growth (g) and activation (a, a*) steps.

Walter and Malkoch [21b], © 2012. With permission of RSC.

4.4 Biological Nanomaterials

The biological nanomaterials are materials of biological origin that are used for nanotechnological applications, whereas the term biomaterials has often been used to describe the materials of nonbiological origin used in medical applications as biocompatible materials [22]. In biology, practically all materials can be considered as nanomaterials in one way or another, for example, enzymes have well-defined structures at the nanometer level and work as nanomachines. Inorganic nanomaterials, such as alumina, can be used as implants; this may be called biomaterials, but are not as biological nanomaterials. Several examples of biological nanomaterials exist in the groups of proteins and nucleic acids and also, for example, lipids do constitute parts of nanomaterials. Bacterial or animal cells are typically in the micrometer range and are not included as nanomaterials, however. In some cases, it may be convenient to add categories such as “viruses” that can contain components of all three previously mentioned groups. In bionanomaterials, there are two common features that are prominent and exploited: self-assembling properties and specific molecular recognition property.

Some of the emerging application areas of biological nanomaterials include the following:

- Producing a self-assembled protein microarray useful in rapid diagnostic applications.
- Manufacture of film or controlling cholesteric pitch of nanoparticle, by using self-assembled biological molecule that has been modified to possess amino acid oligomer capable of specific binding to semiconductor material.
- Forming spatially organized nanostructures by applying an external perturbation with preset magnitude on localized regions of smooth thin film of bistable or multistable molecules and forming nanostructure by self-organization of molecules.
- Screening peptides that bind to nanographite structures such as carbon nanohorns for producing various functional materials applicable in, for example, nanobiotechnology, comprises oxidation, biotinylation, and immobilization.
- Detecting a conformational change or binding event in a targeted molecule by combining a magnetically active nucleus sensor with a targeted molecule and recording the detectable signal upon the conformational change or binding event.

4.4.1 Categories

Biological nanomaterials can be broadly classified into following six groups:

a. *Protein-Based Nanomaterials*

Most of the examples in this category are dealing with 2D crystallization and 3D self-assembly of proteins and peptides making into lattices. Such 3D constructions can be used as structural or functional elements such as molecular sieves or to be used for drug delivery. The self-assembling protein or peptide can be inserted by a functionality, for example, binding activity for a semiconducting material or an antigenic determinant for immunization purposes. Advantages of protein- and peptide-based nanomaterials are their homogeneity over organic and inorganic materials producing structures with predictable geometry and stoichiometry.

A variety of protein based biological nano materials are available [23a,b] in various forms including:

- 2D protein structures: S-layer protein, Hydrophobins and Chaperones
- Self-assembled peptides: Peptides can form different types of nanostructures such as nanopillars, nanocrystals, nanorods, nanowires, nanotubes, nanofilaments, nanofibers, nanoshells and nanocontainers. Nanocontainers are template forming peptides used for formation of silicon particle and metallic nanowire
- Functional protein units: bacteriorhodopsin
- Nanopores: A single biological pore model of α-Hemolysin (α-HL) and electric field driven entry of an individual DNA molecule through α-Hemolysin channel used in biotechnology are shown in figure 4.8.
- Proteins for specific molecular recognition: antibodies, single chain antibodies
- Conformation switching proteins: periplasmic carbohydrate binding protein, calmodulin
- Protein based biological molecular machines includes actin network, kinesin motors, myosin motors (figure 4.9a). ATP synthase motors with benzyne molecules bonded as teeth to ATP synthase is shown in figure 4.9b.

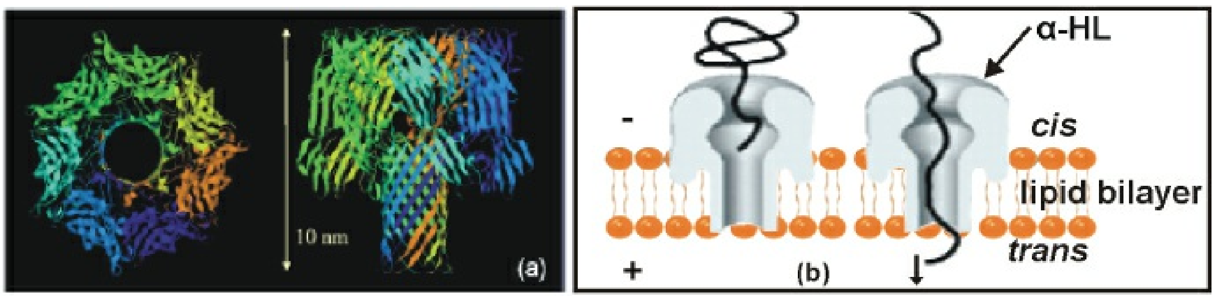

Figure 4.8 Nanometer-scale pores for biotechnology. (a) Single biological pore model of α-hemolysin. http://www.ipt.arc.nasa.gov/carbonnano.html. (b) Electric field-driven entry of a supramolecular entity through a single α-HL channel.

Ying et al. [23b], ©2013. With permission of NPG.

b. *Nucleic Acids* Nucleic acid molecules can be used to form nanoscale devices, for example, resistors, capacitors, inducers, transistors, wires, switches, memory devices, and nanoscale containers for drug or other materials. Also nanoscale filters and molecular sieves can be constructed.

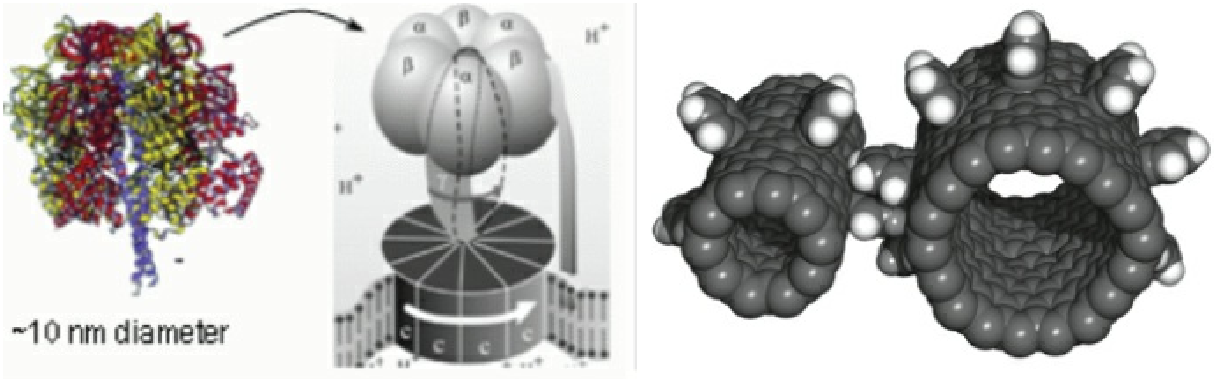

(a)

(b)

Figure 4.9 (a) Structure and functionality of a nanogear.

www.science.doe.gov/bes/scale of things.html; (b) benzyne molecules bonded as teeth to ATP synthase. http://www.ipt.arc.nasa.gov/carbonnano.html.

DNA molecules may be used in various forms, namely,

- 2D DNA lattices
- 3D cages and networks
- Hybrid structures of DNA and protein
- DNA templates: nanowire
- Nanomechanical DNA device

In many ways, life is like a computer. An organism's genome is the software that tells the cellular and molecular machinery (the hardware) what to do. But instead of electronic circuitry, life relies on biochemical circuitry, a complex network of reactions and pathways that enable organisms to function. DNA can function as a template for a variety of structures. DNA template nanocircuitry represents the most complex biochemical circuit ever created from scratch, fabricated with DNA-based devices in a test tube that is analogous to the electronic transistors on a computer chip [24]. The test tube circuit made of DNA-based logic gates can calculate the square root of numbers up to 15, using DNA replication and sequence binding to conduct computations. It is excruciatingly slow, a calculation can take up to 10 h; however, the real breakthrough is in how this system enable control of a chemical systems.

c. *Nanocarbohydrates* Nanocarbohydrate of animal origin: crystalline cellulose, for example, olectin is used for molecular recognition.

d. *Small Molecules* Virus particles, structured materials with virus as the core component.

e. *Lipids* Nanocontainers, liposomes consisting of lipid bilayers, act as support or template for self-assembly. The 3D assemblies of lipids can be used to deliver biomolecules across cell membranes.

f. *Bionanocomposites* Examples of some of the important bionanocomposites, which are known to exist in animal systems, include magnetsomes, ferritin, and Ca-biomolecules composites. Biomolecules can be peptides, proteins, DNA, lipids, or combinations of them, for example, single-stranded DNA can be used as a tag to immobilize peptides and proteins in an ordered array format to oligonucleotide-coated immobilization surfaces. These surfaces can be 2D surfaces or 3D particles or beads made of various materials, for example, glass, silica, polymers, and metals. Site-directed, ordered immobilization is advantageous in biosensors, micro-/nanoarrays, biochips, and nanocomposite materials, which can be used in applications such as detection and quantification of genes, diagnostics of various compounds, assaying protein–target interactions, proteomics, drug development, and screening or using of catalytic enzymes. Immobilized biomolecules can be used to modify the properties of the surface or to introduce a functionality, for example, binding activity.

4.4.2 Potential Applications

One of the main trends for biological molecules is the use of molecular self-assembled structures as a means to manufacture various nanodevices. There are a multitude of biological nanomaterials considered for bioanalytical applications. Most of the applications are related to health and medical areas. Typical examples include arrays (chips) for large-scale DNA or protein screening. Drug delivery is another much studied example. Various self-assembled peptide structures can be designed to release compounds under specific conditions.

The use of biomolecules in the energy sector has so far been rather limited. Although there are, in principle, possibilities for applications such as using biological light-harvesting complexes for solar energy capture, the formats are so far not very compatible. If such applications were to be realized, it is very likely that they would rely heavily on biological nanomaterials. Lately, there has been focus on fuel cells for using chemical redox reactions for the production of electricity. Some success has been reported for such devices that include biomolecules. In this case, it can be seen that performance of such devices might get a boost by nanostructured biomaterials.

In the material sector, the self-assembling properties of the biomolecules are utilized. Examples include biological arrays for the formation of 2D organization of semiconductor nanoparticles. Self-assembly is seen as a route to designing materials with tailored properties, such as responsive materials. The biological recognition of various molecules (such as the antibody–antigen interaction) can be used to build nanomaterials with specific permeation selectivity. Several of the biological materials that have interesting properties are nanostructured composite materials obtained through biomineralization. Examples of materials that are being mimicked include bone, tooth, and mollusk shells.

Biological molecular machines are being mimicked to achieve devices for mechanical action. Bimolecular motors are envisioned to be able to be the part of materials in roles such as molecular assembly lines, construction of nanonetworks, or part of adaptive materials. Some of the possibilities of biological molecular machines that are being pointed out are based on proteins.

4.5 Nanoporous Materials

A solid material that contains cavities, channels, or interstices can be regarded as porous. Nanoporous materials [25, 26] are of great interest in various applications, ranging from catalysis, adsorption, sensing, energy storage, and electronics owing to their high surface area, tunable pore size, adjustable framework, and surface properties. The specific surface area can reach values of up to several thousand square meters per gram, depending on the material. The behavior and performance of such materials can be determined by many characteristics such as surface area, porosity, and pore size distribution. Physical properties such as density, thermal conductivity, and strength are dependent on the pore structure of the solid. Porosity influences the chemical reactivity of solid and the physical interaction of solids with gases and liquids. Porous materials of high surface area are of great importance especially as catalyst, catalyst supports, thermal insulators, sensors, filters, electrodes, and burner materials. The science and technology of porous materials has progressed steadily and is expanding in many new directions with respect to processing methods and applications. Many synthetic pathways have been reported for the synthesis of porous materials with either a disordered pore system or an ordered pore system with various structures, which can meet the demands of the target application. Nanoporous ceramic materials are synthesized by various methods such as polymer sponge method, foam method, leaching, sintering of particles having a range of sizes, emulsion templating, gel casting, injection molding, sol–gel process, and heat treatment of a ceramic precursor containing carbon-rich compound.

Classification of pores: Based on the accessibility of an external fluid, pores can be classified into closed pores, open pores, and blind (Figure 4.10). Closed pores are totally isolated from their neighbors and surface of the particle. They influence macroscopic properties such as bulk density, mechanical strength, and thermal conductivity; however, they are inactive in processes such as fluid flow and adsorption of gases. Pores which have a continuous channel of communications with external surface of the body are called open pores, and those with one closed end are blind or saccate pores.

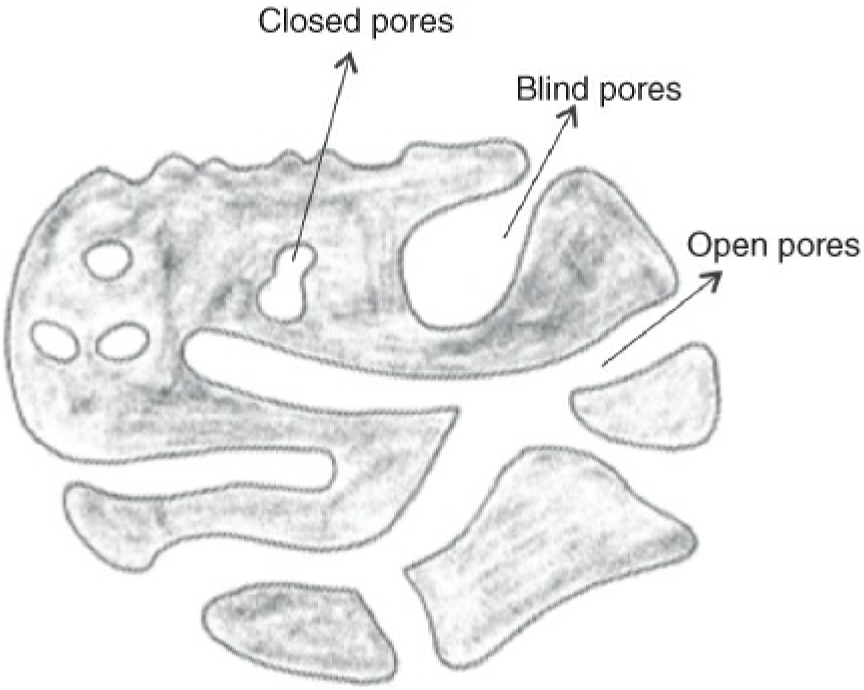

Figure 4.10 Types of possible pores in a porous material.

Based on the pore size, IUPAC classified porous materials into microporous (0–2 nm), mesoporous (2–50 nm) and macroporous (>50 nm). Synthesis, development, and application of nanoporous materials are exclusively focused on the microscale and mesoscale because the adsorptive ability contributed by macropores is negligible. Microporous materials are generally used for gaseous applications while mesoporous materials are usually used in aqueous-based media because gaseous molecules (CO_2, methane, and hydrogen) are smaller in size compared to aqueous-based species (heavy metals and organics). Zeolites, which represents the largest group of microporous materials, are crystalline inorganic polymers based on a 3D tetrahedral arrangement of SiO_4 and AlO_4 (aluminosilicate) connected through their oxygen atoms. Some of the best-known mineral zeolites are clinoptilolite, chabazite, phillipsite, mordenite, and analcite. Figure 4.11a–d shows the framework structure of the four commonly used zeolites: zeolite A, zeolite Y, zeolite L, and ZSM-5. Owing to their ion-exchange properties, as well as adsorption and reactions of molecules within its cages, zeolites have found use in numerous applications in catalysis and separations and are one of the most used nanoporous materials in the world today.

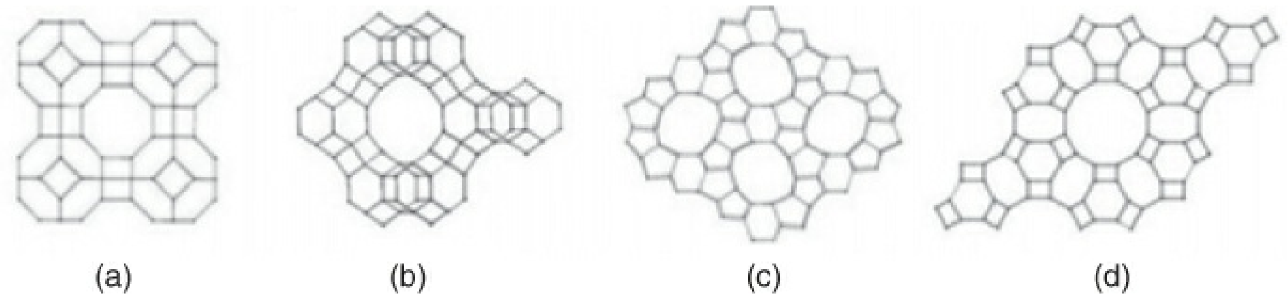

Figure 4.11 Representative zeolite frameworks (with pore openings): (a) zeolite A:3D, 4.2 Å; (b) zeolite Y:3D, 7.4 Å; (c) zeolite L:1D, 7.1 Å; (d) ZSM-5 (silicalite):2D, 5.3 ×5.6 Å, 5.1 ×5.5 Å. Zheng et al. [27] © 2012.With permission of authors.

Activated carbon (AC): A well-established nanoporous material, which is basically an amorphous organic material with an extensive network of micro- and mesopores. The conventional precursor of AC is coal, although biomass sources such as wood and agricultural wastes are being increasingly used as substitutes. AC is typically produced via a two-step process, namely, charring to produce black carbon and subsequent physical (thermal) and/or chemical activation to produce pores [28]. A typical porous texture of a biomass-based AC is shown in Figure 4.12.

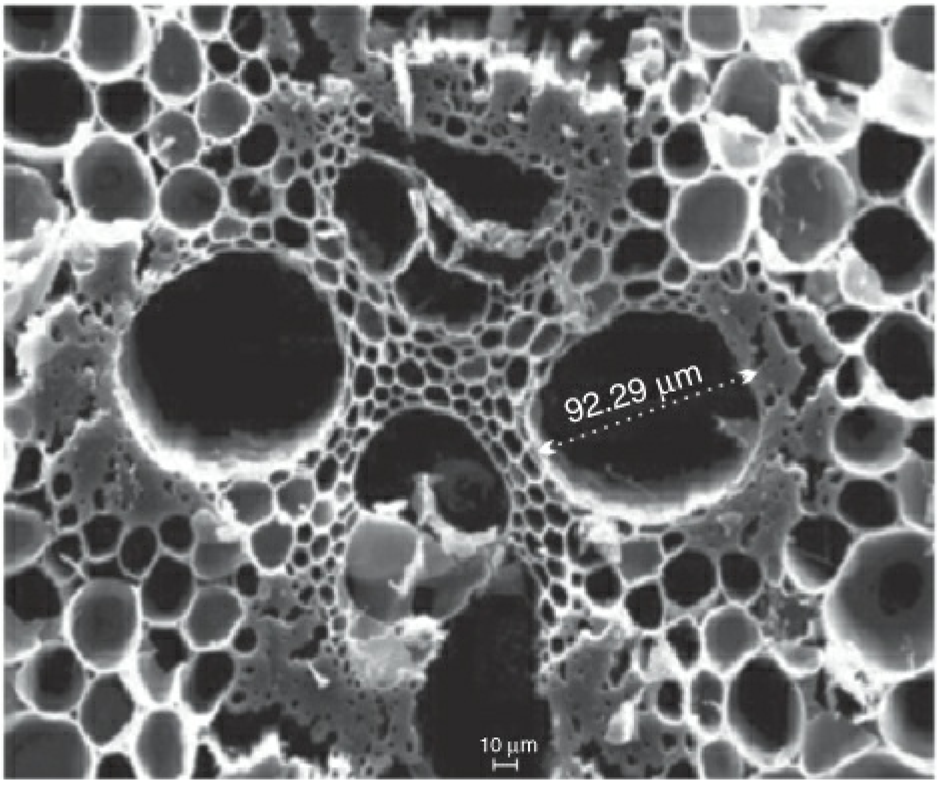

Figure 4.12 A typical porous texture of a biomass-based activated carbon.

Weber et al. [28], ©2013. With permission of Elsevier.

In addition to zeolite and activated carbon, there are a plenty of novel synthetic nanoporous materials that, in the future, may be used prominently alongside the aforementioned adsorbents. One such novel synthetic nanoporous material is the Mobil Crystalline Material number 41 (MCM-41), first reported in 1992. This is basically an inorganic, hexagonal mesoporous material initially synthesized to be applied as a catalyst support. Porous coordination polymers built from metal ions connected by organic linkers referred to as metal-organic frameworks (MOFs), and molecular frameworks consisting of light elements (carbon, boron, hydrogen, and oxygen) referred to as covalent organic frameworks (COFs), are more recent additions to the ranks of ordered porous materials. MOFs are highly diversified materials composed of metal atoms (ions) linked together by multifunctional organic ligands. The controllable length of organic linker and the variation of metal oxide allow for tailoring the functionality, pore volume, and size over a wide atomic-scale range. In contrast to the spherical or slit-shaped pores usually observed in carbon and zeolite materials, MOFs incorporate crystallographically well-defined pores including squared, rectangular, triangular, and window-connected cages. Therefore, MOFs provide a wealth of opportunities for engineering new functional materials with tunable properties. Figure 4.13 shows a molecular sieve composed of MOF MIL-47 loaded with $CuCl_2$, representing remarkable adsorption capacity for benzothiophene because of the presence of Cu^I ions derived from $Cu^{II\cdot}$ ions and porous MIL-47 [29]. The Cu^I ions were obtained by reduction of Cu^{II} with V^{III} ions in MIL-47. The modified MOF could be successfully used for the desulfurization of a liquid fuel.

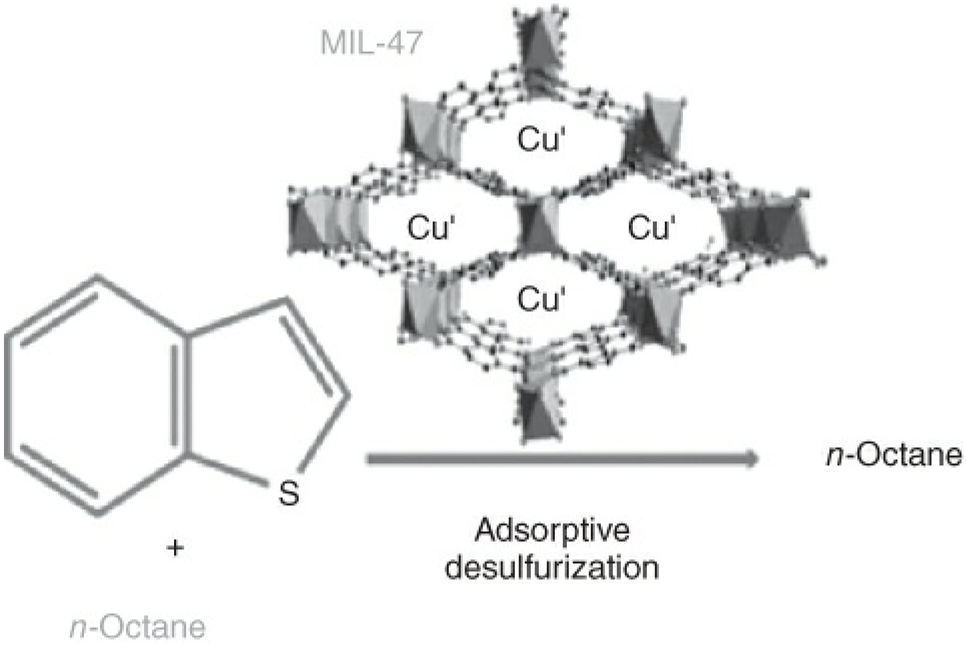

Figure 4.13 A molecular sieve: A metal-organic framework (MOF) MIL-47 loaded with $CuCl_2$.

Khan and Jhung [29], © 2012. With permission of Wiley.

4.6 Quantum Dots

Quantum dots, discovered in 1980, are tiny particles or nanocrystals of a semiconducting material with diameters in the range of 2–10 nm (10–50 atoms). Quantum dots display unique electronic properties, intermediate between those of bulk semiconductors and discrete molecules, which are partly the result of the unusually high surface-to-volume ratios for these particles [30]. The most apparent result of this is fluorescence, wherein the nanocrystals can produce distinctive colors determined by the size of the particles.

Due to their small size, the electrons in quantum dots are confined in a small space (quantum box), and when the radii of the semiconductor nanocrystal is smaller than the exciton Bohr radius (exciton Bohr radius is the average distance between the electron in the conduction band and the hole it leaves behind in the valence band), there is quantization of the energy levels according to Pauli's exclusion principle. The discrete, quantized energy levels of quantum dots relate them more closely to a molecule rather than bulk materials and have resulted in quantum dots being nicknamed “artificial atoms” [31]. Progress in semiconductor technology has enabled the fabrication of structures so small that they can contain just one mobile electron. By varying controllably the number of electrons in these “artificial atoms” and measuring the energy required to add successive electrons, one can conduct atomic physics experiments in a regime that is inaccessible to experiments on real atoms. Generally, as the size of the crystal decreases, the difference in energy between the highest valence band and the lowest conduction band increases. More energy is then needed to excite the dot, and concurrently, more energy is released when the crystal returns to its ground state, resulting in a color shift from red to blue in the emitted light. As a result of this phenomenon, quantum dots can emit any color of light from the same material simply by changing the size of quantum dot. Additionally, it is possible to control over the band gap of the nanocrystals by changing the composition of semiconductors; therefore, emission color of quantum dots can also be tuned by changing dopant during synthesis [32] as shown in Figure 4.14b.

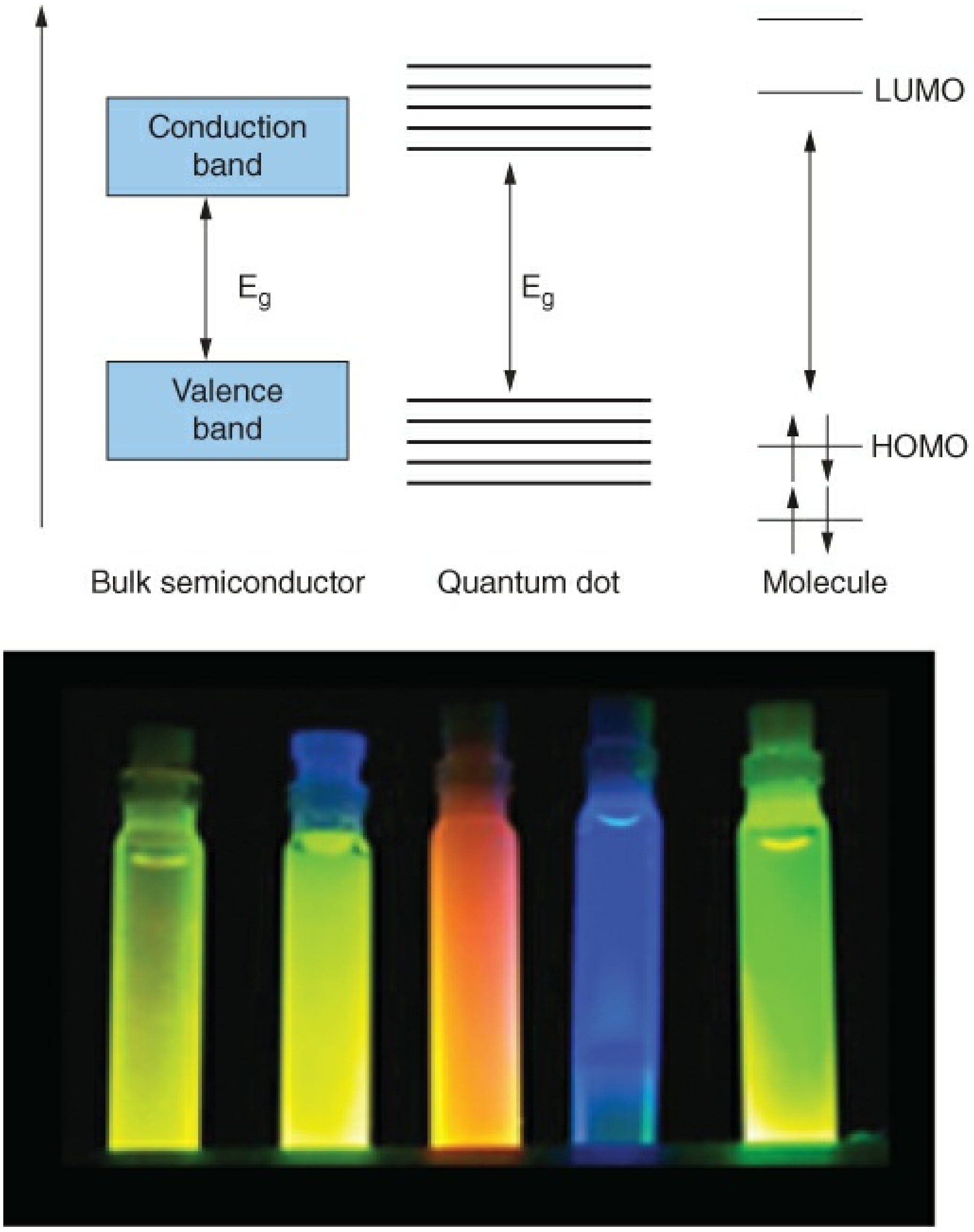

Figure 4.14 Comparison of band gap energy in a bulk semiconductor, quantum dots, and a molecule. Emission colors in ZnS quantum dots by varying dopants.

Manzoor et al. [32], © 2007. With permission of ASP.

Quantum dots can be classified as core, core–shell, and alloyed quantum dot.

Core-type quantum dots are single component materials with uniform internal compositions, such as chalcogenides (selenides or sulfides) of metals such as cadmium or zinc, for example, ZnS, CdS, or CdSe. The photoluminescence and electroluminescence properties of core-type nanocrystals can be fine-tuned by simply changing the crystallite size.

Core–shell quantum dots (CSQDs) are nanomaterials with small regions of one material embedded in another with a wider band gap, for example, CdSe in the core and ZnS as shell. Coating quantum dots with shells improves the quantum yield by passivating nonradiative recombination sites and also makes them more robust to processing conditions for various applications. Further coating of core–shell QDs with hydrophilic polymers (Figure 4.15) makes them water soluble and biocompatible for various medical applications [33].

Alloyed quantum dots are formed by alloying together two semiconductors with different band gap energies and exhibit interesting properties distinct not only from the properties of their bulk counterparts but also from those of their parent semiconductors. Thus, alloyed nanocrystals possess novel and additional composition-tunable properties aside from the properties that emerge due to quantum confinement effects.

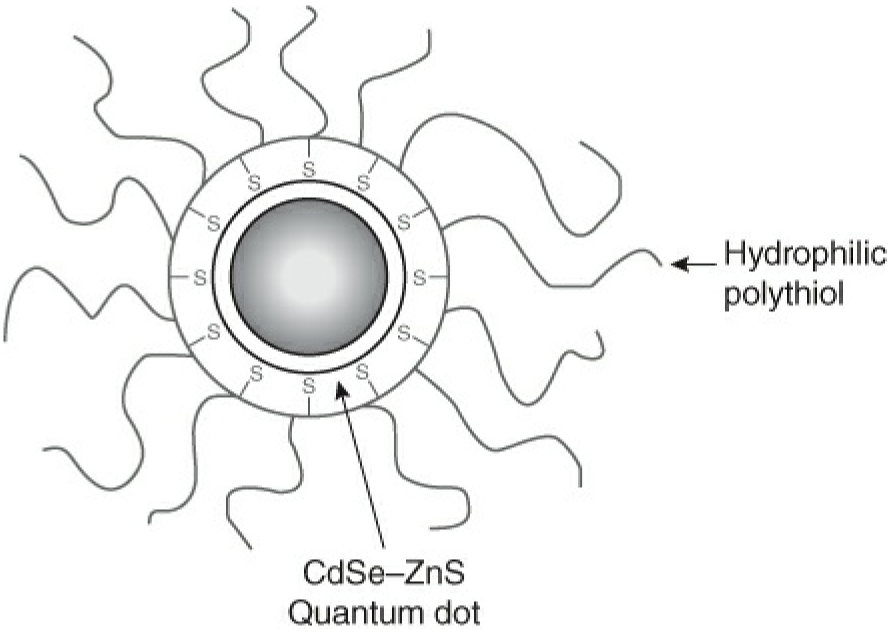

Figure 4.15 Schematic of polythiol-coated CdSe-ZnS core–shell quantum dot.

Yildiz et al.[33], ©2009. With permission of ACS.

Several methods for the fabrication of quantum dots, namely, molecular beam epitaxial (MBE), electron beam lithography and MBE, metal-organic chemical vapor deposition (MOCVD), and colloidal synthesis are in practice. Each method has its own advantages. Semiconductor quantum dots can be tuned and adjusted for many applications, including optics, medicine, and quantum computation. Quantum dots are used in biolabeling, anti-counterfeiting applications to create special inks, dyes and paints, light displays, and chemical sensing. In addition, quantum dots have found applications in composites, solar cells (Grtzel type), and fluorescent biological labels (e.g., to trace a biological molecule), which use both the small particle size and tunable energy levels. Recent advances in chemistry have resulted in the preparation of monolayer-protected, high-quality, monodisperse, crystalline quantum dots as small as 2 nm in diameter, which can be conveniently treated and processed as a typical chemical reagent.

4.7 Nanoclusters

Nanoclusters are agglomerates of a finite number of atoms or molecules, from a few to thousands, forming a bridge between small molecules and crystalline materials (Figure 4.16), representing an intermediate stage between single atoms/molecules and bulk materials [34]. The evolution of their properties and structures can be traced as a function of size, and quantum effects unique to finite systems can be observed. The subunits of nanoclusters can be atoms of a single element, molecules, or even combinations of atoms of several elements in subunits with equal stoichiometries (alloys, etc.), for example, Na_n, $(SF_6)_n$, $(H_2O)_n$, $(Cu_3Au)_n$, $(ClCH_3C_6H_3CO_2H)_n$, $(TiO_2)_n$. The greatest difference arises from the fact that molecules have functionality that directly depends on the interpositioning of their atoms, whereas the properties of nanoclusters are solely guided by the number of subunits they contain. In general, the physical properties of materials are dependent on the dimensions of the material in question; their properties (e.g., conductivity, elasticity) are scalable with respect to the amount of atoms in the material. In scalable size-regime, the properties of nanoclusters vary greatly with every addition or subtraction of an atom, whereas in nonscalable size-regime, every atom counts for its properties. Usually, the crystal structure of a large nanocluster is the same as the bulk structure of the material, with somewhat different lattice parameters (in general, clusters are slightly contracted as compared to bulk); however, some exceptions do occur.

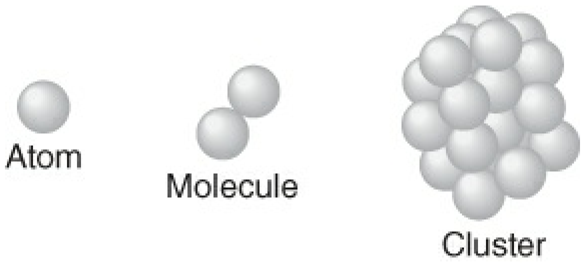

Figure 4.16 Nanocluster from atom/molecule.

Structural magic numbers occur when an exact amount of atoms is needed for a specific structure. Even smaller clusters can be amorphous-like (spherical, etc.), although a general tendency of the clusters is to form structures where the total surface energy (and internal energy) is minimized – the exact structure then depends on the surface energies related to the specific crystal facets of the material.

Structural magic numbers affect the formation and abundance of larger clusters, whereas for the case of smaller clusters the combined electronic structure of all the atoms is of greater importance. For instance, in a Pb_n cluster spectrum, clusters with $n = 7$ or 10 are more abundant than others. When the ionization potentials of sodium clusters are plotted as a function of the number of atoms in the clusters, peaks are observed at clusters having two and eight atoms. This can be compared to the high ionization potentials observed, for example, in rare-gas atoms, where electrons are removed from filled orbital.

Electronic magic numbers are observed for clusters (although most apparent for small clusters, these magic numbers can be noticed even for very large clusters – up to several thousands of atoms). The jellium model has successfully been used in the theoretical modeling of nanoclusters. The jellium model envisions a cluster of atoms as a single large atom, where the distribution of ionic cores is replaced by a constant positive background, the so-called “jellium density,” and only valence electrons are treated explicitly. It can be seen from the jellium model, the electronic structure of a cluster varies from that of single atom, but it also varies greatly from that of a bulk material. When a bulk lattice is formed, the discrete energy levels of the atoms are smudged out into energy bands. For example, valence bands and conduction bands exist in semiconductors and metals. As particles shrink in size, there is a dramatic increase in energy band as well as in discrete energy levels, and thus the continuous density of states in bulk is replaced with a set of discrete energy levels.

Properties of Clusters

Optical. In semiconductors, the band gap will be increased as cluster size is decreased – a blue shift in the absorption spectrum of the semiconductor (good for tailoring lasers). Individual energy levels and energy level separations are also dependent on the size of the clusters, which therefore affect the energies needed for the transitions of electrons to excited states. Clusters of different sizes will therefore have different absorption spectra – and hence different colors.

Magnetic properties. Interesting magnetic properties have also been observed in small clusters. In a cluster, the magnetic moment of each atom will interact with the moments of the other atoms, and can force all the moments to align in one direction with respect to some symmetry axis of the cluster – the cluster will have a net magnetic moment, it will be magnetized. As cluster size decreases, it becomes easier for them to exhibit ferromagnetic behavior. In some cases, even clusters made up of nonmagnetic atoms can have a net magnetic moment. For instance, rhenium clusters show a pronounced increase in their magnetic moment when they contain less than 20 atoms. For clusters with less than 15 atoms, these moments are fairly large.

Reactivity. Since the electronic structure of nanoclusters depends on their size, their ability to react with other species should also depend on size. This has important applications for the design of catalytic agents. Reactivity is highly dependent on the electronic structure, leading to large variations in the reactivity of clusters even with sizes differing by only single atoms. In general, however, the reactivity of all nanoclusters is high as compared to that of bulk due to their higher surface-to-volume ratio. For example, gold nanoclusters are highly reactive if compared to the fairly inert bulk material.

Melting temperatures. Another effect caused by a high surface-to-volume ratio in clusters is a substantially lower melting temperature as compared to bulk materials. Unusual phenomena such as negative heat capacities have also been observed in clusters (at the melting temperature, an increase in the internal energy of Na^+_{147} by 1 eV leads to a decrease in temperature by about 10 K).

Preparation

Initial vaporization of atoms from a bulk target is the essential step for obtaining nanoclusters. In principle, there are three different physical methods for obtaining nanoclusters.

Energetic vaporization. It is the simplest of all cluster production methods where clusters are produced as a result of the ejection of a large number of atoms, at high energies, from the bulk material.

Seeded supersonic nozzle sources. The sources where the material is vaporized in a hot oven are mixed with (or “seeded” in) an inert carrier gas, by pressurizing the oven with the inert gas.

Gas-aggregation cluster sources. The sources where the material is vaporized (e.g., by magnetron sputtering) and are introduced into a flow of cold inert gas. This causes the vapor to become highly supersaturated. Pressures in the aggregation chamber are necessarily high in order to cause initial cluster growth.

Applications

The applications of physically manufactured nanoclusters generally rely on the use of nanoclusters beams and the deposition of clusters on surfaces with the help of these. The inherent properties of “free” clusters are therefore seldom used, as this forced interaction with a substrate of some sort, which slightly alters the cluster properties, is almost always necessary.

The use of beams and deposition of clusters, however, opens new possibilities as the range of energy and mass deposition in cluster beams greatly differs from that of conventional ion beams and atomic or molecular beams. The resulting features produced with cluster beams generally rely on the energy at which the clusters are deposited.

4.8 Nanomaterials in Different Configurations

Following the discovery of CNTs by Iijima in 1991, there has been a great interest in the synthesis and characterization of 1D nanostructured materials in different forms such as fibers, rods, belts, wires, and tubes, owing to their distinct attributes such as their unique geometry and possible quantum confinement effects; the dependence of the electrical and thermal transport or mechanical properties on dimensionality; better transport phenomena as compared to 0D and 2D systems; a wide variety of morphologies leading to novel technological applications including the electronic interconnect units, solar cells, photonics, thermoelectric, electromechanical, and fluidic nanoscale devices and magnetic data storage. Some of the significant morphologies are discussed in following sections.

4.8.1 Nanofibers

Nanofibers, in particular, are of great interest because of their long length scales, resulting in very high aspect ratios and the high degree of possible orientation. Nanofibers are slightly larger in diameter than the typical nanomaterial definition, though still invisible to the naked eye, size ranges between 50 and 300 nm in diameter. Nanofibers are generally prepared using drawing with a micropipette, template synthesis, phase separation, chemical vapor deposition (CVD), melt blowing, and electrospinning [35]. Of the aforementioned techniques, electrospinning is the most versatile and simplest method of preparing such nanofibers. It is also potentially scalable and requires little equipment. Polymers in the solution and melt form, as well as nonpolymeric materials such as ceramics and metals, can be fabricated into nanofibers via electrospinning (see Chapter 2).

An assortment of natural polymers, such as the proteins, collagen, elastin, and silk fibroin, has been electrospun. In addition, a wide variety of synthetic polymers such as polystyrene (PS), polycaprolactone (PCL), poly(methyl methacrylate) (PMMA), and poly(vinyl alcohol) (PVA) have been electrospun from solution. Melt electrospinning requires that a heating system surround the reservoir and, despite its advantages of improved cost effectiveness and environmental safety due to the absence of solvents in the process, is generally more challenging. Polyethylene and polypropylene are two polymers that have been successfully fabricated from the melt. Ceramic fibers such as TiO_2 have been fabricated from a sol of ceramic precursor and a host polymer such as polyvinylpyrrolidone (PVP). Metallic fibers, such as copper fibers, have also been generated by electrospinning a metal acetate or nitrate solution with a host polymer, followed by degradation of the host polymer and reduction.

Nanofibers can be aligned electrostatically or biochemically. Figure 4.17 shows an SEM image of aligned nanofibers showing biomimics of natural hierarchical structures.

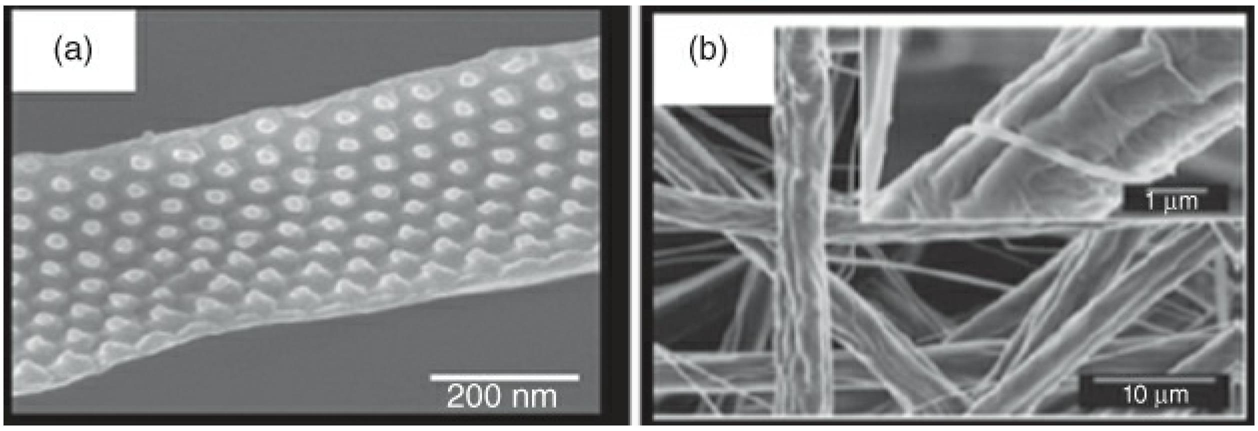

Figure 4.17 SEM images of biomimics of natural hierarchical structures: (a) pillared poly(methyl methacrylate) nanofiber.

Chen et al. [36], © 2012. With permission of ACS; (b) nylon-6 and polystyrene nanofiber. Li et al. [37] © 2009. With permission of ACS.

4.8.2 Nanowires

Nanowires distinguish themselves from other nanomaterials by their unique one-dimensionality (1D). 1D systems exhibit peculiar electronic structures including density of states singularities, molecule-like states over large distances, and spin–charge separation associated with a Luttinger liquid [38]. Nanowires are similar to nanofibers albeit considerably smaller in diameter, of the order of 4 nm. Practically, nanowires could become crucial elements for new nanoscale devices owing to their unique properties. After all, 1D is the smallest dimension for efficient transport of electrons and optical excitations, which qualifies nanowires as interconnections for nanoscale devices. The anisotropy of nanowires renders them more difficult to assemble than spherical nanoparticles into a large structure of any dimensionality, be it a horizontal or a vertical array. Post assembly strategy has been used to obtain horizontal nanowire arrays via solvent flow through microfluidic channels and by the Langmuir–Blodgett deposition, whereas it is difficult to apply to vertical nanowires arrays. Yet vertical nanowire arrays display many desirable characteristics for device integrations, such as enhanced capacity and rate capability in lithium-ion batteries and improved light coupling and electron lifetime in dye-sensitized solar cells. Traditionally, vertical nanowire arrays were fabricated by the use of templates such as membranes of anodic aluminum oxide (AAO) and track-etched polycarbonate. In recent years, a variety of inorganic nanowires have been synthesized and characterized. Thus, nanowires of elements, oxides, nitrides, carbides, and chalcogenides have been generated by employing various strategies.

One of the crucial factors in the synthesis of nanowires is the control of composition, size, and crystallinity. Among the methods employed, some are based on vapor-phase techniques, while others are solution techniques. Compared to physical methods such as nanolithography and other patterning techniques, chemical methods have been more versatile and effective in the synthesis of these nanowires. Thus, techniques involving CVD, precursor decomposition, as well as solvothermal, hydrothermal, and carbothermal methods have been widely employed.

The unique setting of nanowires aligned on a conducting substrate have facilitated the studies on properties and applications of these novel materials in field emission, gas sensors, dye-sensitized solar cells/photoelectrochemical devices, field effect transistors, and so on.

4.8.3 Nanotubes

Nanotubes constitute an exciting class of 1D nanomaterials of which CNTs are recognized widely as materials of importance (refer Chapter 5). The possibility of having inorganic nanotubes was realized by Tenne et al. in 1992 with the synthesis of tungsten disulfide nanotubes just after the discovery of CNTs [39]. Since then nanotubes of several inorganic materials, that is, metals, metal oxides, metal chalcogenides, nitrides, have been reported. Typical inorganic nanotube materials are 2D layered solids such as tungsten(IV) sulfide (WS_2), molybdenum disulfide (MoS_2), and tin(IV) sulfide (SnS_2)WS_2 and SnS_2/tin(II) sulfide (SnS). Traditional ceramics such as titanium dioxide (TiO_2) and zinc oxide (ZnO) also form inorganic nanotubes. More recent nanotube and nanowire materials are transition metal/chalcogen/halogenide

(TMCH), described by the formula $TM_6C_yH_z$, where TM is transition metal (molybdenum, tungsten, tantalum, niobium), C is chalcogen (sulfur, selenium, tellurium), H is halogen (iodine), and the composition is given by $8.2 < (y + z) < 10$. TMCH tubes can have a sub-nanometer diameter, lengths tunable from hundreds of nanometers to tens of microns and show excellent depressiveness owing to extremely weak mechanical coupling between the tubes. Figure 4.18 shows SEM image of TiO_2 nanotubes obtained by the calcination of poly(vinyl alcohol) titanium tetraisopropoxide (PVA-TTIP) hybrid nanofibers [40].

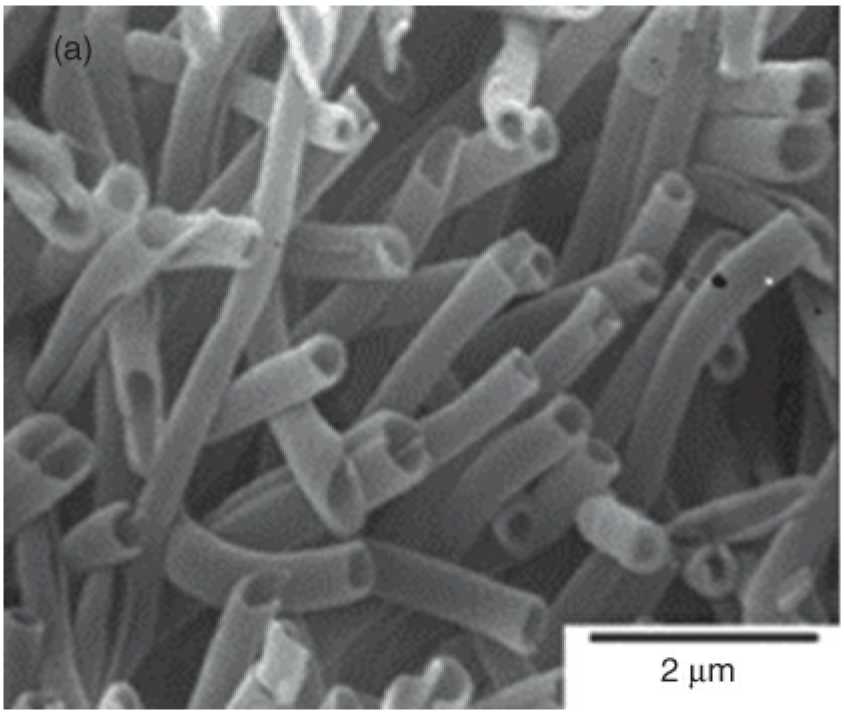

Figure 4.18 Inorganic nanotube: SEM image of TiO_2 nanotubes.

Nakane et al. [40], © 2007. With permission of Springer.

Synthesis of Inorganic Nanotubes

The synthesis of anisotropic metastable materials such as nanotubes is particularly challenging. One approach is the use of templates that force the product into anisotropic morphology. Additionally, templates are favorable in applications and investigations that require a homogeneous and monodisperse product in order to avoid tedious and expensive postreaction separation procedures [41]. Template method can be of two types, that is, template inside or template outside.

Template inside – CNTs as template:

Use of CNTs as template is well-developed for the synthesis of metal chalcogenide nanotubes (MS_2NTs) and metal oxide nanotubes (MOxNTs).

Metal chalcogenides: The basic principle of this template synthesis is to coat CNTs with MS_2 (M = Nb, Mo, W, etc.) layer. The CNTs are suspended in a suitable precursor solution. Drying leads to a uniform coating with the precursor material that is subsequently sulfurized with H_2S at elevated temperatures. Variation of the reaction parameters allows single or multilayer coating; the template can be removed with HF resulting in hollow MS_2 NTs.

Metal oxide nanotubes: Sol–gel chemistry is widely used in the synthesis of metal oxide nanotubes, a good example being that of silica and TiO_2. Oxide gels in the presence of surfactants or suitable templates form nanotubes. For example, by coating CNTs with oxide gels and then burning off the carbon, one obtains nanotubes and nanowires of a variety of metal oxides including ZrO_2, SiO_2, and MoO_3.

Template outside – membranes and inverse micelle technique: One main disadvantage of an inner template is the lack of controllability of the diameter of the resulting nanotubes. Therefore, outer templates are preferred to achieve (nearly)-monodisperse sizes of the nanomaterials. As an example, Al_2O_3 membrane with uniform holes, prepared by an anodization process, can be used to synthesize MoS_2-NTs by decomposition of $(NH_4)_2MoS_4$ and $(NH_4)_2Mo_3S_{13}$. In this method, the product is formed within the pores of the Al_2O_3 membrane leading to nanotubes with a nearly monodisperse diameter distribution. On the one hand, this method allows a high yield production of nanotubes. Sol–gel synthesis of oxide nanotubes is also possible in the pores of alumina membranes.

Non-template Method: Anatase-type TiO_2 nanotubes are also formed by calcination of poly(vinyl alcohol)-Ti alkoxide hybrid precursor nanofibers in air. The outer and inner diameters of the TiO_2 nanotubes calcined at 500 °C for 5 h were ca. 440 nm and ca. 270 nm, respectively.

Properties

Metal oxide nanotubes have properties quite different from those of CNTs. They can be made more hydrophilic than carbon and can load nearly 50% of their weight with water. Controlling dimensions of nanostructures is critical because properties such as electronic band gap largely depend on dimensions. Dimension control has proven difficult in CNTs, but control is possible with different chemical process conditions across a broad range of metal oxide materials according to researchers. Inorganic nanotubes are heavier than CNTs and not as strong under tensile stress, but they are particularly strong under compression, leading to potential applications in impact resistant applications such as bullet-proof vests. Metal oxide nanotubes show superior catalytic properties as compared to their respective nanoparticles. For example, the photocatalysis of the TiO_2 nanotubes is reported to be better than that of commercially available anatase-type TiO_2 nanoparticles. Inorganic nanotubes are most likely the best conductor of electricity on a nanoscale level. Their thermal conductivity is comparable to that of the diamond along the tube axis. Mechanically they are the stiffest, strongest, and toughest fiber that can ever exist. Strong van der Waals attraction in nanotubes leads to spontaneous roping of many nanotubes, leading to self-assembled structure that may prove to be important in many applications.

Applications

Nanodevices based on 1D nanomaterials are thought for the next-generation electronic and photoelectronic systems having small size, faster transport speed, higher efficiency, and less energy consumption. A high-speed photodetector for visible and near-infrared light based on individual WS_2 nanotubes has been prepared in laboratory. Since inorganic nanotubes are hollow and can be filled with another material, they can be used to preserve or guide it to a desired location or generate new properties in the filler material, which is confined within a nanometer-scale diameter. To this goal, inorganic nanotube hybrids were made by filling WS_2 nanotubes with molten lead, antimony, or bismuth iodide salt by a capillary wetting process, resulting in $PbI_2@WS_2$, $SbI_3@WS_2$, or $BiI_3@WS_2$ core–shell nanotubes.

4.8.4 Nanobelts

Nanobelts are a class of nanostructure often viewed as a type of nanowire, usually made from semiconducting metal oxides (such as SnO_2, ZnO, In_2O_3, or CdO, or selenides such as CdSe). Nanobelts form ribbon-like structures with widths of 30–300 nm, thicknesses of 10–30 nm, and lengths in the millimeter range. They are chemically pure and structurally uniform single crystals, possessing rectangular cross sections, clean edges, and smooth surfaces. By virtue of their unique geometry (Figure 4.19a), nanobelts have enormous surface areas per unit mass and most of the material is at the surface; much research has been conducted on the use of nanobelts as gas sensors [42, 43]. When gases are adsorbed onto the nanobelts surface, the electron depletion or accumulation behavior becomes pronounced (as is the effect on the current flowing along the nanobelts) allowing them to act in a manner similar to field emission transistors (FETs). Furthermore, their small size helps in greatly reducing power consumption as compared to macroscale sensors. Research has shown this behavior to be the basis for effective nanobelt gas sensors, and similar sensors have been made for nerve gas detection, ethanol sensing, and hydrogen sensing. Nanobelts represent a unique way to manipulate light at the microscopic scale. They join smaller nanoparticles such as gold nanorods and nanoshells that can be tuned to absorb light strongly at certain wavelengths and then steer the light around or emit it in specific directions. The effect is due to surface plasmons, which occur when free electrons in a metal or doped dielectric interact strongly with light. When prompted by a laser, the sun or other energy source, they oscillate like ripples on a pond and re-emit energy as either light or heat. Nanobelts are unique because the plasmonic waves occur across their width, not along their length. Nanobelts scatter light at a particular wavelength (or color), depending on the aspect ratio of their cross sections – width divided by height. This makes them highly tunable. Nanobelts possess essentially similar properties to nanowires; they can exhibit FET behavior and have functionalizable surfaces, thus making sensor development strategies for nanowires also available to nanobelts.

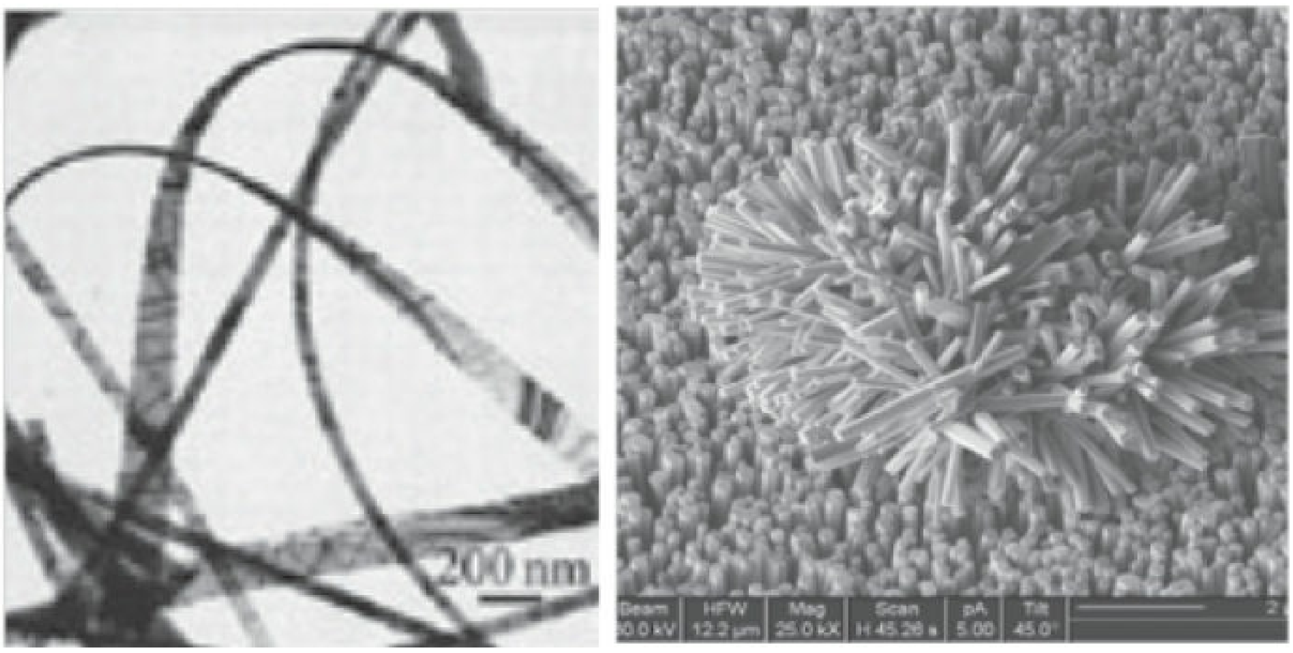

Figure 4.19 SEM images: (a) SnO_2 nanobelts.

Fields et al. [42], © 2006. With permission of AIP.; (b) ZnO nanorods grown in aqueous solution. Courtesy of Y. Lei, University of Connecticut, USA.

4.8.5 Nanorods

Nanorods are solid nanostructures morphologically similar to nanowires but with aspect ratios of approximately 3 : 5. Figure 4.19b shows an image of ZnO nanorods grown from aqueous solution. They are formed from a variety of materials including metals, semiconducting oxides, diamonds, and organic materials. Aggregated diamond nanorods produced from fullerenes are the hardest material so far discovered. Nanorods show characteristic size-dependent properties with the greatest effects observed in the 1–10-nm size range. This is due to the large surface area-to-volume ratio of nanoparticles, which increases surface free energy to a point that is comparable to their lattice energy. Nanorods have the capacity for large variations in composition. In recent years, there has been an escalation in the development of techniques for synthesis of multicomponent nanorods and subsequent surface functionalization. Multifunctional nanoparticles exhibit characteristic electronic, optical, and catalytic properties significantly different from those of their individual constituent metals.

Nanorods are produced by a number of techniques, including a vapor–liquid–solid approach; mechanical alloying; direct chemical synthesis using ligands for shape control; plasma arc discharge; laser ablation; and catalytic decomposition. A novel nanostructure fabrication technique is introduced in the production of nanorods called glancing angle deposition (GLAD). GLAD is a physical vapor deposition technique in which the substrate is rotated in the polar and azimuthal directions by two stepper motors programmed by a computer [44]. The experimental results have demonstrated that the GLAD technique offers several strategic advantages compared to other nanofabrication technique, the structures of the nanorods can be well designed and controlled by computer programming, a feature that cannot be achieved by any other fabrication technique.

Nanorods are under considerable investigation for applications in the area of gas sensors; video displays; computer components; nanoelectronics and nano-optoelectronic components; MEMS devices; and solar energy conversion. One of the factors in their investigation is that both the size and shape can be controlled by the use of additives during synthesis so that scaling as well as basic properties can be studied, and flexibility is available for component integration. By functionalizing the nanorods, amphiphilic entities that can self-assemble and form a convex curvature can be created – a capability of importance in nanoelectronics and biomedical applications. A biosensor for heavy metals is based on hydrothermally grown ZnO nanorod/nanotube and metal-binding peptides, where ZnO acts as an FET and heavy metal binding with a peptide causes an electrical signal change, which can be measured and correlated to the concentration of heavy metals. A gold nanorod sensor for mercury is able to determine mercury in tap water samples at the parts-per-trillion level. The selectivity and sensitivity result from the amalgamation of mercury and gold, and the entire sensing procedure takes less than 10 min, with no sample separation and/or sample pre-concentration requirements. The particular morphology of nanorods also leads to properties that may have unusual, niche applications. For example, the light emitted from or scattered off of gold nanorods is strongly polarized along the rod length axis, an excellent property for an ideal orientation probe. A novel, tapered form of nanorod, known as "**nanorice**," has shown to have potential to be the most sensitive surface plasmon resonance nanosensors [44].

Review Questions

Q1. What are the important criteria for a material to qualify as nanomaterials?

Q2. How will you classify nanomaterials based on structure and dimensions?

Q3. How nanomaterials can be stabilized to prevent their aggregation?

Q4. Discuss the most common synthetic route to prepare metallic nanoparticles?

Q5. Give examples of metals that show different color on varying their size.

Q6. Give significance of nano-oxides of transition metals and nontransition metals.

Q7. Discuss important characteristics and significance of inorganic nanotubes.

Q8. Discuss various nonoxidic inorganic nanomaterials.

Q9. Discuss different types of organic nanomaterials and their significance.

Q10. What is the significance of cellulose and how can it be converted into nanocrystalline cellulose?

Q11. Give potential application of nanocrystalline cellulose.

Q12. What are dendrimers? How do they differ from a polymer in general?

Q13. Justify the statement “In biology, practically all materials can be considered as nanomaterials in one way or another.”

Q14. What is the importance of nucleic acids in nanoelectronics?

Q15. Name the bionanocomposites known to exist in animal system.

Q16. What are nanoporous materials? Give some examples of naturally occurring nanoporous materials and their application?

Q17. What are metal-organic framework (MOF) materials? Give examples.

Q18. Define quantum dots. How band gap of QDs affects luminescent properties?

Q19. What is the basic difference between atom/molecule and nanocluster?

Q20. What is the difference between electronic magic numbers and structural magic numbers?

Q21. Discuss some important properties shown by nanocluster materials.

Q22. What are the basic similarities and difference between nanofiber, nanorods, nanowires, and nanotubes?

Q23. Discuss important characteristics and significance of nanobelts.

Q24. Discuss important characteristics and significance of nanobelts.

References

1. R. Sardar, A. M. Funston, P. Mulvaney and R.W. Murray, “Gold Nanoparticle: Past, Present, and Future”, *Langmuir*, **25** (2009) 13840–13851.

2. M. Faraday, “The Bakerian Lecture: Experimental Relations of Gold (and Other Metals) to Light”, *Philos. Trans.Roy. Soc. London*, **147** (1857) 36.

3. J. S. Bradley, *Clusters and Colloids*, Ed. G. Schmid, VCH, Weinheim, 1994, pp. 469–473.

4. G. Viau, R. Brayner, L. Poul, N. Chakroune, E. Lacaze, F. Fiévet-Vincent and F. Fiévet, “Ruthenium Nanoparticles: Size, Shape, and Self-Assemblies”, *Chem. Mater.*, **15** (2003) 486–494.

5. H. B. Vnnemann, G. Braun, W. Brijoux, et al., “Nanoscale Colloidal Metals and Alloys Stabilized by Solvents and Surfactants. Preparation and Use as Catalyst Precursors”, *J. Organomet. Chem.* **520** (1996) 143–162.

6. http://en.wikipedia.org/wiki/Colloidal_gold.

7. C.A. Mirkin, “Beginning of a Small Revolution”, *Small*, **1** (2004) 14–16.

8. N.A. Dhas, C.P. Raj and A. Gedanken, “Synthesis, Characterization, and Properties of Metallic Copper Nanoparticles”, *Chem. Mater.*, **10** (1998) 1446–1452.

9. R. Panţuru, G. Jinescu, E. Panţuru, et al., “Synthesis and Characterization of Zerovalent Iron Intended to be Used for Decontamination of Radioactive Water”, *U.P.B. Sci. Bull., Series C*, **72** (4) (2010) 207–218.

10. D. Ghosh, S. Pradhan, W. Chen and S. Chen, “Titanium Nanoparticles Stabilized by Ti-C Covalent Bonds”, *Chem. Mater.* **20** (2008) 1248–1250.

11. M. Fernández-Garcia and J. A. Rodriguez, “Metal oxide nanoparticles”, *Nanomaterials: Inorganic and Bioinorganic Perspectives, Encyclopedia of Inorganic Chemistry*, Wiley VCH, 2009.

12. H.S. Seok, H. Y. Hyun, H. H. Chang, D. K. Seung, H. L. Seok and B. Y. Jun, “Metal-Oxide-Semiconductor Field Effect Transistor Humidity Sensor Using Surface Conductance”, *Appl. Phys. Lett.*, **100** (2012) 101603.

13. H. Iida, K.Takayanagi, T. Nakanishi, T. Osaka, “Synthesis of Fe_3O_4 Nanoparticles with Various Sizes and Magnetic Properties by Controlled Hydrolysis”, *J. Colloid Interface Sci.*, **314** (2007) 274–280.

14. H. Giesche, “Synthesis of Monodispersed Silica Powders - 2. Controlled Growth Reaction and Continuous Production Process”, *J. Eur. Ceram. Soc.* **14** (1994) 205–214.

15. P. A. Ajibade and J. Z. Mbese, “Synthesis and Characterization of Metal Sulfides Nanoparticles/Poly(methyl methacrylate) Nanocomposites”, *Int. J. Polym. Sci.*, **8** Article ID 752394 (2014).

16. C. Giordano, C. Erpen, W. Yao et al., “Metal Nitride and Metal Carbide Nanoparticles by a Soft Urea Pathway”, *Chem. Mater.*, **21** (2009) 5136–5144.

17. K. Li, and B. Liu, “Polymer-Encapsulated Organic Nanoparticles for Fluorescence and Photoacoustic Imaging”, *Chem. Soc. Rev.*, **43** (2014) 6570–6597.

18. R. W. J. Scott, O. M. Wilson and R. M. Crooks, “Synthesis, Characterization, and Applications of Dendrimers-Encapsulated Nanoparticles”, *J. Phys. Chem. B*, **109** (2005) 692–704.

19. J. Prasad Rao, Kurt E. “Geckeler, Polymer Nanoparticles: Preparation Techniques and Size-Control Parameters”, *Prog. Polym. Sci.*, 2011, **36**, 887–913.

20. S. E. Hafraoui, Y. Nishiyama, J. L. Putaux, L. Heux, F. Dubreuil and C. Rochas, “The Shape and Size Distribution of Crystalline Nanoparticles Prepared by Acid Hydrolysis of Native Cellulose”, *Biomacromolecules*, **9** (2008) 57–65.

21. (a) E. Buhleier, W. Wehner, F. Vögtle, ““Cascade”- and “Nonskid-Chain-like” Syntheses of Molecular Cavity Topologies”, *Synthesis*, **2** (1978) 155–158.(b) M. V. Walter and M. Malkoch, “Simplifying the Synthesis of Dendrimers: Accelerated Approaches”, *Chem. Soc. Rev.*, **41** (2012) 4593–4609.

22. W. J. Stark, “Nanoparticles in Biological Systems”, *Angew. Chem. Int. Ed.*, **50** (2011) 1242–1258.

23. (a) J. J. Kasianowicz, E. Brandin, D. Branton and D.W. Deamer, “Characterization of Individual Polynucleotide Molecules Using a Membrane Channel”, *Proc. Natl. Acad. Sci.* **93** (1996) 13770–13773.(b) Y.-L. Ying, Junji Zhang,Fu-Na Meng, Chan Cao, Xuyang Yao, Itamar Willner, H. Tian and Y.-T. Long, “A stimuli-Responsive Nanopore Based on a Photoresponsive Host-Guest System”, *Sci. Rep.*,**3**(2013)Article number:1662.

24. B. L. Qian and E. Winfree, “Scaling Up Digital Circuit Computation with DNA Strand Displacement Cascades”, *Science*, **332** (2011) 1196–1201.

25. N. Z. Logar and V. Kaucic, “Nanoporous Materials: From Catalysis Hydrogen Storage to Wastewater Treatment”, *Acta Chim. Slov.*, **53** (2006) 117–135.

26. R. Babarao and J. Jiang, “Molecular Computations of Adsorption in Nanoporous Materials”, Chapter 4, *Adsorption and Phase Behaviour in Nanochannels and Nanotubes*, Eds. L. J. Dunne and G. Manos, Springer, 2010.

27. Y. Zheng, X. Li and P. K. Dutta, “Exploitation of Unique Properties of Zeolites in the Development of Gas Sensors”, *Sensors* **12** (2012) 5170–5194.

28. J. Beau W. Weber, P. Corbett, K. T. Semple, U. Ogbonnaya, W. S. Teel, C. A. Masiello, Q. J. Fisher, J. J. Valenza II, Y. Q. Song and Q. Hui, “An NMR Study of Porous Rock and Biochar Containing Organic Material”, *Micropor. Mesopor. Mat.*, **178** (2013) 94–98.

29. N. A. Khan and S. H. Jhung, “Remarkable Adsorption Capacity of $CuCl_2$-Loaded Porous Vanadium Benzenedicarboxylate for Benzothiophene”, *Angew. Chem. Int. Ed.* **51**(5), (2012) 1198–1201.

30. M. A. Kastner, “Artificial Atoms” *Phys. Today*, **46**(1),(1993) 24–31.

31. R. C. Ashoori, “Electrons in Artificial Atoms”, *Nature*, **379**, (1996) 413–419.

32. K. Manzoor, V. Aditya, S. R. Vadera, N. Kumar, T. R. N. Kutty, “A Single-Source Solid-Precursor Method for Making Eco-Friendly Doped Semiconductor Nanoparticles Emitting Multi-Color Luminescence”, *J. Nanosci. Nanotechnol.*, **7** (2007) 463–73.

33. I. Yildiz, B. McCaughan, S. F. Cruickshank, J. F. Callan and F. M. Raymo, “Biocompatible CdSe–ZnS Core–Shell Quantum Dots Coated with Hydrophilic Polythiols,” *Langmuir*, **25**(2009) 7090–7096.

34. F. Baletto and R. Ferrando, “Structural Properties of Nanoclusters: Energetic, Thermodynamic, and Kinetic Effects”, *Rev. Mod. Phys.*, **77** (2005) 371–434.

35. Z. Huang, Y.-Z. Zhang M. Kotaki, S. Ramakrishna, “A Review on Polymer Nanofibers by Electrospinning and their Applications in Nanocomposites”, *Compos. Sci. Technol.*, **63** (2003) 2223–2253.

36. J.T. Chen, W.L. Chen and P.W. Fan, “Hierarchical Structures by Wetting Porous Templates with Electrospun Polymer Fibers”, *ACS Macro Lett.* **1**(2012) 41–46.

37. X. Li, B. Ding, J. Lin, J. Yu and G. Sun, “Enhanced Mechanical Properties of Superhydrophobic Microfibrous Polystyrene Mats via Polyamide 6 Nanofibers”, *J. Phys. Chem. C*, **113** (2009) 20425–20457.

38. F. D. M. Haldane, “Luttinger Liquid Theory' of One-Dimensional Quantum Fluids”, *J. Phys. C: Solid State Phys.* **14** (1981) 2585–2609.

39. R. Tenne, L. Margulis, M. Genut and G. Hodes, “Polyhedral and Cylindrical Structures of WS2”, *Nature*, **360** (1992) 444–445.

40. K. Nakane, N. Shimada, T. Ogihara, N. Ogata and S. Yamaguchi, “Formation of TiO_2 Nanotube by Thermal Decomposition of Poly(vinyl alcohol)-Titanium Alkoxide Hybrid Nanofiber”, *J. Mater. Sci.*, **42** (2007) 4031–4035.

41. C. N. R. Rao and A. Govindaraj, “Synthesis of Inorganic Nanotubes”, *Adv. Mater.*, **21**(2009) 4208–4233.

42. L.L. Fields, J. P. Zheng, Y. Cheng and P. Xiong, “Room-Temperature Low-Power Hydrogen Sensor Based on a Single Tin Dioxide Nanobelt”, *App. Phys. Lett.*, **88** (2006) 263102-1–263102-3.

43. E. G. Comini, G. Faglia, Z. Sberveglieri, Z. L. Pan and X. Wang, “Stable and Highly Sensitive Gas Sensors Based on Semiconducting Oxide Nanobelts”, *App. Phys. Lett.*, **81** (2002) 1869–1871.

44. C. Patzig, T. Karabacak, B. Fuhrmann and B. Rauschenbach, “Glancing Angle Sputter Deposited Nanostructures on Rotating Substrates: Experiments and Simulations”, *J. App. Phys.* **104** (2008) 094318-1–094318-9.

Chapter 5
Carbon-Based Nanomaterials

5.1 General Introduction

Carbon is the third most abundant element in the universe after hydrogen and oxygen, respectively. Carbon arguably is the most fascinating element in the periodic table having the ability to bind itself and to nearly all elements. Carbon is the base material for DNA and thus provides the basis for life on earth. Carbon can exist in several different forms. The most common form of carbon is graphite, which consists of stacked sheets of carbon with a hexagonal structure. Under extreme high pressure, carbon forms diamond, which is a metastable form of carbon. Carbon having an electron configuration 1s^2, 2s^2, 2p^2 forms a great variety of crystalline and disordered structures because it can exist in three different hybridizations sp^3, sp^2, and sp^1. The specific hybridization of carbon and its bonding to the surrounding atoms determine which allotrope carbon will assume [1, 2]. Carbon with sp^3 hybridization forms a tetrahedral lattice giving rise to diamond, and with sp^2 hybridization it forms graphite, arranged in hexagonal sheets (Figure 5.1a and b). Diamond and graphite have been known since ancient times. The word diamond comes from the ancient Greek word, “adamas” meaning “impossible to break.”

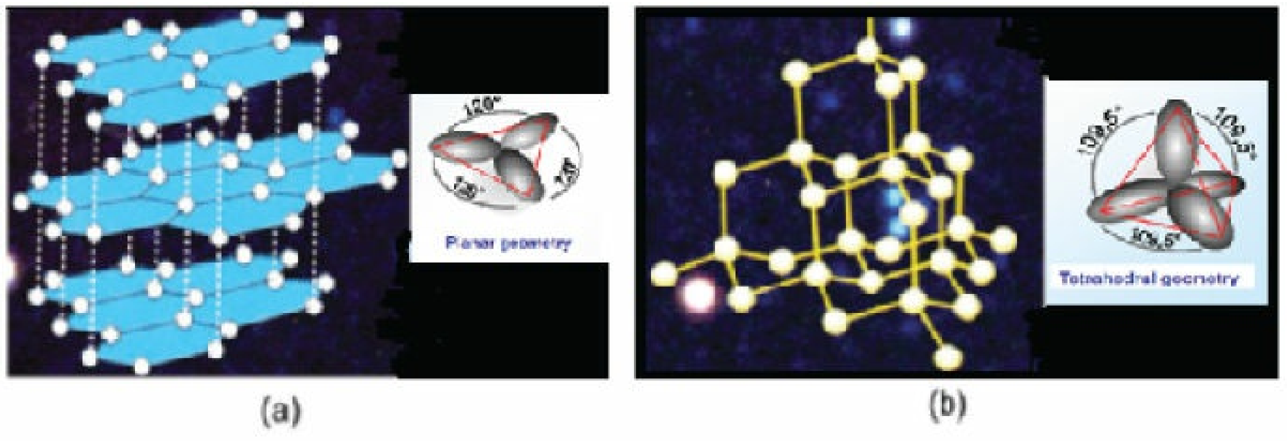

Figure 5.1 Carbon in different hybridized states: (a) sp^2 with planer geometry as in graphite; (b) sp^3 with tetrahedral geometry as in diamond.

Dai et al. [3], © 2012. With permission of Wiley-VCH.

Carbon is important for many technological applications, ranging from drugs to synthetic materials. This role is a consequence of carbon's ability to bind to itself and to nearly all elements in almost limitless variety. The resulting structural diversity of organic compounds and molecules is accompanied by a broad range of chemical and physical properties. The tools of modern synthetic chemistry allow the tailored design of these properties by the controlled combination of structural and functional building blocks in new target systems.

5.1.1 Carbon Nanomaterials: Synthetic Carbon Allotropes (SCAs)

Conceptually, many other ways to construct carbon allotropes are possible by altering the periodic binding motif in networks consisting of sp^3, sp^2, and sp^1 hybridized carbon atoms. As a consequence of the expected remarkable physical properties of these elusive carbon allotropes, it has been appealing, for some time, to develop concepts for their preparation in macroscopic quantities. However, diamond and graphite represented the only known allotropes of carbon for a long time. This situation changed in 1985 with the discovery of **fullerenes**, which were observed for the first time by Kroto et al. [4]. Serendipitous discovery of fullerenes marked the beginning of an era of synthetic carbon allotropes (SCAs) or better known as **carbon nanomaterials**. The new members added to this family include the **carbon nanotubes** (**CNTs**) in 1991 by Iijima [5] and the rediscovery of **graphene** in 2004 by Geim and coworkers [6]. These new carbon allotropes are bonded by sp^2 carbon atoms. Keeping in mind the numerous possible carbon modifications and the number of ongoing investigations, the list has certainly not yet completed.

What makes **carbon nanomaterials** so attractive for chemists, physicists, and materials scientists is not only the sheer multitude of esthetically pleasing structures but, even more so, their outstanding and in many cases unprecedented properties [7]. They consist of fully conjugated π-electron systems and can be considered as topologically confined objects in zero, one, or two dimensions, respectively (Figure 5.2).

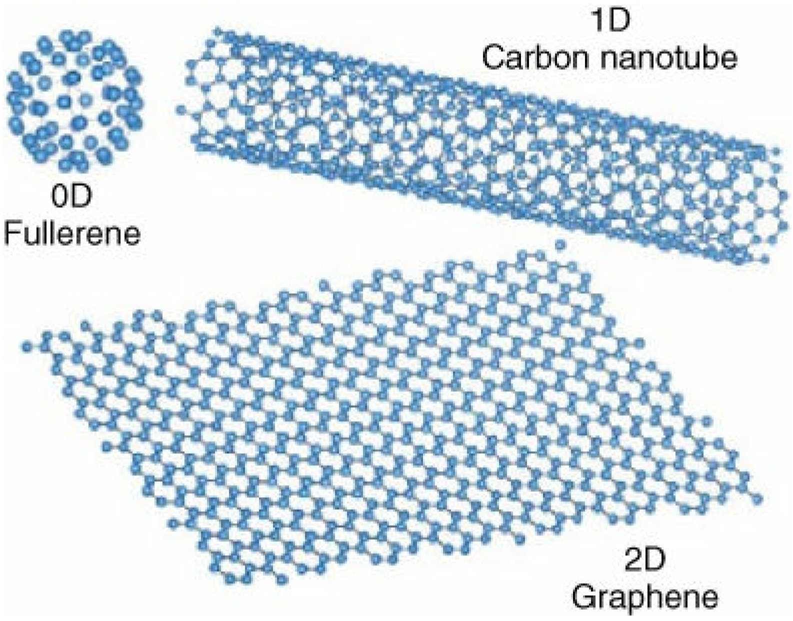

Figure 5.2 Allotropes of carbon nanomaterials in different dimensions.

Wan et al. [7], © 2012. With permission of ACS.

These extended electron reservoirs yield pronounced redox activity and high electron mobility. At the same time, SCAs are characterized by stability under ambient conditions. Carbon nanomaterials currently represent one of the most promising material families with enormous potential for high-performance applications in the fields of nanoelectronics, optoelectronics, hydrogen storage, sensors, and reinforcements of polymers based on their unprecedented electronic, optical, mechanical, and chemical properties. At the same time, they are ideal targets for the investigation of fundamental chemical and physical questions such as shape- and charge-dependent binding and release of molecules, charge transport in confined spaces, and superior sensing of supramolecular interactions down to the single molecule regime. Indeed, metallic CNTs and graphene are the first representatives of stable organic metals, where no further activation by doping or charge transfer is required.

Chemical functionalization of SCAs is certainly a key for the systematic development of SCA technology, since covalent and noncovalent derivatization allows for (1) increasing tuning and adjusting the solubility, dispensability, and processability both on aqueous and organic media; (2) modifying and tailoring electronic, optical, and mechanical properties; (3) separation and isolation of specific types (e.g., tube chiralities and helicities); and (4) construction of ordered 2D and 3D superstructures. Moreover, the investigation of the chemical behavior and reactivity of SCAs itself represent an exciting research subject on its own right.

In principle, the physical and chemical properties of fullerenes, CNTs, and graphene are related to each other, although their levels of development vary considerably [8, 9]. Although the chemistry of fullerenes has already achieved a rather mature state and numerous derivatives have been synthesized and characterized in detail, functionalization of graphene is of current research interest. CNT chemistry keeps an intermediate position. Compared to the various types of CNTs (broad variation of helicities, single walled, multiwall), graphene is a much more uniform material and this facilitates the development of its chemistry considerably. In contrast to the fullerenes and CNTs, which exhibit exo- and endofaces, covalent attacks to graphene are possible from both sides of the plane. Appealing synthetic targets are, *inter alia*, graphene and its alkyl-, aryl-, and fluoro derivatives, which represent the first prototypes of 2D polymers, dye-functionalized graphene for the photoinduced H_2 generation, and polymer-functionalized graphene as stable building block for the construction of electroactive composite materials. Many protocols that have been efficiently used for the functionalization of fullerenes, and CNTs are expected to be transferred successfully for the chemical derivatization of graphene. New C-allotropes are of fundamental interest and opens the door to unprecedented materials applications.

The applications for these new nanostructures are immense. Although no practical application for Bucky balls have been developed yet, scientists are extremely excited about the potential uses of CNTs. These structures have a diameter between 1 and 10 nm (about 1000 times thinner than a human hair!), yet are 50 times stronger than steel [10]. CNTs are also structurally perfect, and this property gives rise to a whole host of other unique properties, such as unique electrical properties and high thermal conductivity. Carbon-based nanomaterials are produced and used in many industrial sectors. These materials include CNTs, fullerenes, carbon nanofibers, carbon black, and carbon-onions. Arc discharge, chemical vapor deposition (CVD), and laser ablation are major methods for fabrication of these materials (except carbon black), and by changing fabrication conditions, the properties of carbon-based nanomaterials can be changed. In CVD, just changing chamber conditions can change the types of carbon materials deposited on the substrate. For example, changing of reaction temperature, input gas concentration, or pressure alters the types and properties of CNTs.

5.2 Fullerene

As is the case with numerous, important scientific discoveries, fullerenes were accidentally discovered. In 1985, Kroto and Smalley found strange results in mass spectra of evaporated carbon samples [4]. Herewith, fullerenes were discovered and their stability in the gas phase was proven. The search for other fullerenes had started. The fullerenes, of which the smallest stable and most prominent is C_{60}, are molecular carbon allotropes. C_{60} consists of a spherical network of 60 structurally equivalent sp^2 hybridized carbon atoms in the shape of a football (or, a soccer ball or, more technically, an I_h-symmetrical truncated icosahedron) composed of 12 pentagons and 20 hexagons (Figure 5.3). The C_{60} fullerene (Buckminsterfullerene or Bucky ball) is the representative and approximately 0.7 nm in diameter. In the fullerene structure, all C sites are equivalent and the bond lengths are 0.14 nm for the double bond and 0.146 nm for the single bond.

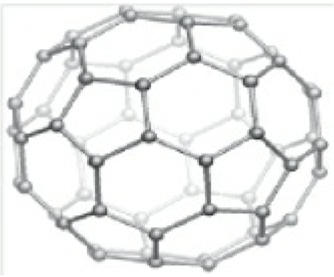

Figure 5.3 C_{60} fullerene.

Dai et al. [3], © 2012. With permission of Wiley-VCH.

Following the isolation and structural determination of C_{60}, the first successful preparation of 0D fullerenes in macroscale quantities was reported after 5 years. This involved the evaporation and re-condensation of graphite using an arc discharge method to produce C_{60}. Now, fullerenes can be prepared on the tonnage scale. Many representatives of higher fullerenes that have been isolated and characterized are as follows: D_{5h}-C_{70}, chiral D_2-C_{76}, D_{6h}-C_{84}, and D_{5h}-C_{90} [10]. Furthermore, a lot of chemistry has been performed on fullerenes to create fullerene salts, open-cage fullerenes, and quasifullerenes (Figure 5.4a–f).

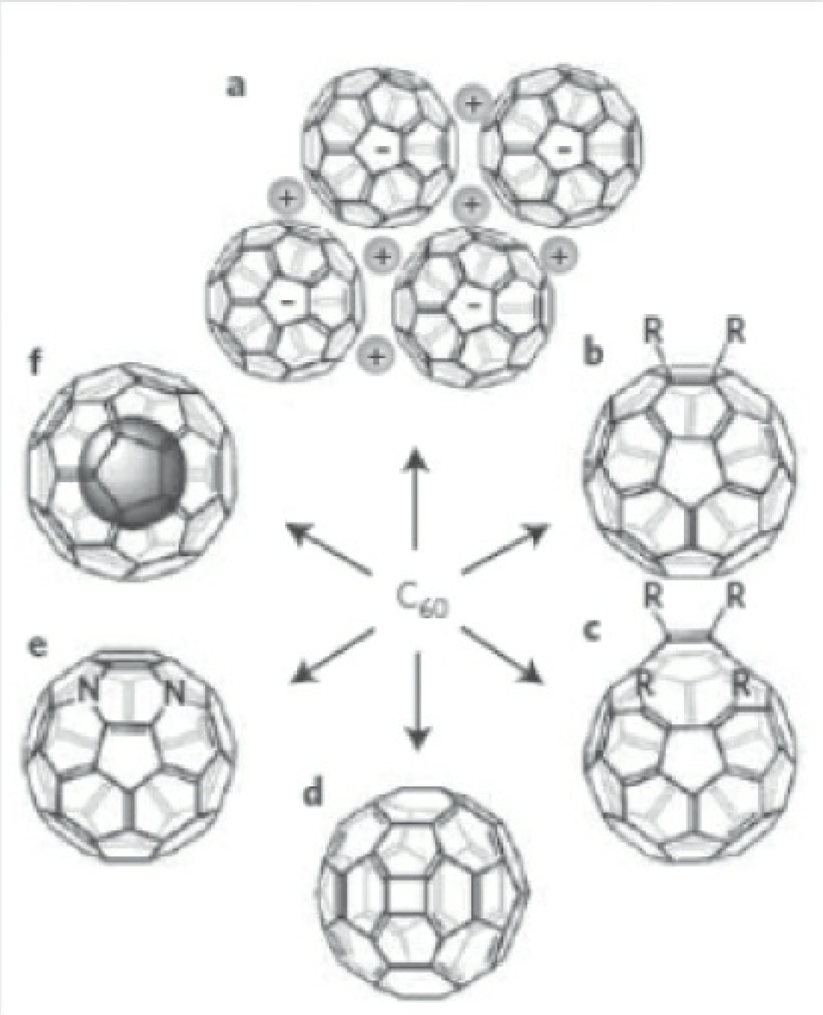

Figure 5.4 Possible derivatization of C_{60}: (a) fullerene salts; (b) exohedral adducts; (c) open-cage fullerenes; (d) quasifullerenes; (e) heterofullerenes; (f) endohedral fullerenes.

Hirsch [10], © 2010. With permission of NPG.

The quasifullerenes are spherical closed structures composed of pentagons and hexagons combined with rings of other sizes. Another family of fullerenes, namely **endohedral fullerenes**, incorporates guest atoms or molecules inside the carbon framework. Examples of endohedral fullerenes include $La@C_{82}$ and $Sc_{3N}@C_{80}$ and, most recently, the first endohedral fullerene containing an I_h-symmetrical C_{60} cage, $Li@C_{60}$, was structurally characterized. Fullerenes are produced using an electric arc discharge as well as by CVD technique [11]. A setup for electric arc discharge for the preparation of fullerene is shown in Figure 5.5. During arc discharge process for the production of fullerenes, reaction gas must be free from hydrogen.

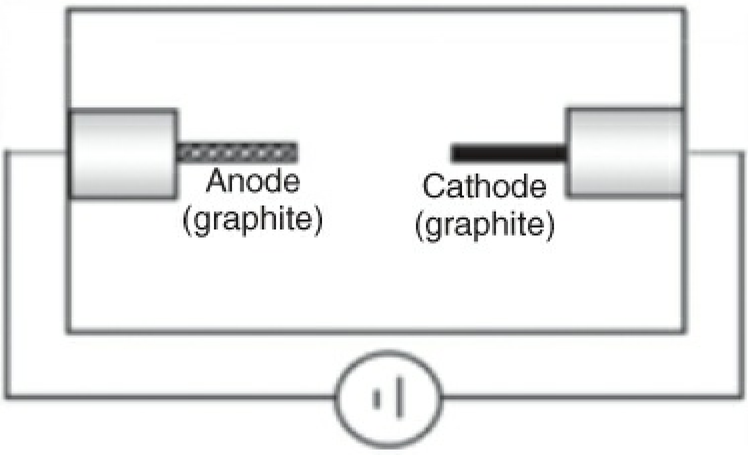

Figure 5.5 Schematic of arc discharge process.

Kratschmer et al. [11], © 1990. With permission of NPG.

5.2.1 Properties of Fullerene

Fullerenes are large, closed-cage, carbon clusters and have several special properties that were not found in any other compound before. Fullerenes are nontoxic and soluble in many organic solvents. Functionalization of fullerenes further enhances its solubility. Spherical curvature in fullerene molecules, however, produces angle strain that allows fullerenes to undergo characteristic reactions of addition to double bonds (hybridization turns from sp^2 to sp^3), thus forming a large number of derivatives known as fullerides. C_{60} fullerene in organic solvents exhibits five stages of reversible oxidation/reduction, thereby making it as either electrophiles or nucleophiles. This characteristic conjugation leads to the pronounced redox activity and imparts outstanding electronic properties. Furthermore, chemical functionalization enables a dramatic increase in the solubility of fullerenes, in any solvent, which is required for their development as new materials or as bioactive redox drugs. Further, chemical functionalization also provides the possibility of combining the unique properties of fullerenes with those of other compounds. Figure 5.6 shows some of the fullerene derivatives with outstanding biological properties. Exohedral addition reactions to the conjugated π-system (Figure 5.4b) represent the most important functionalization methods realized so far. The driving force for exohedral additions is the reduction of strain energy stored in the spherical carbon framework. Additions usually occur regioselectively at fusions of two six-membered rings because, in contrast to the neighboring [5,6]-bonds, these [6,6]-bonds are shorter and have more double-bond character.

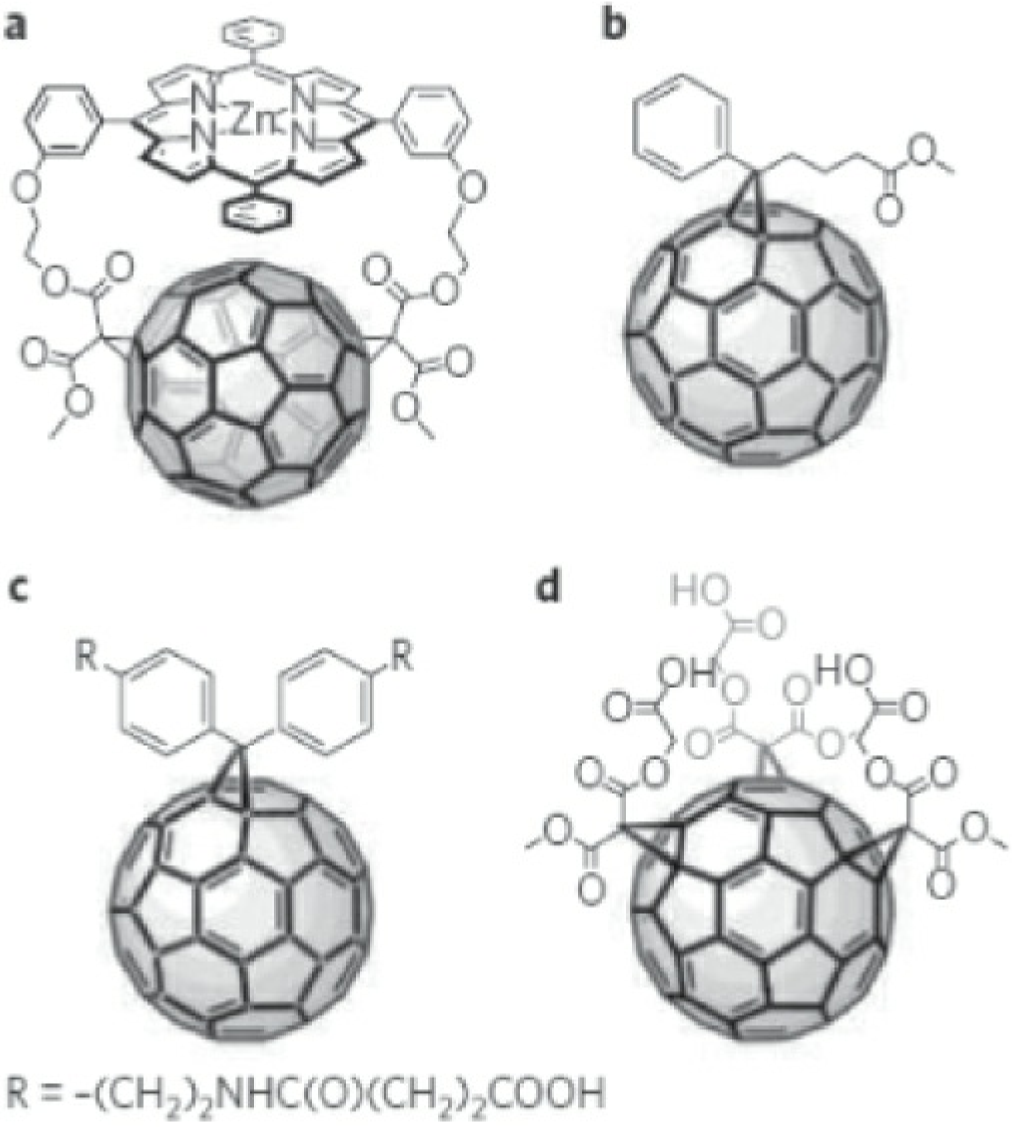

Figure 5.6 (a–d) Fullerene derivatives.

Hirsch [10], © 2010. With permission of NPG.

Over the past couple of decades, thousands of well-characterized adducts of C_{60} and other fullerenes have been synthesized for their remarkable properties. For example, the exohedral covalent binding of organic donor molecules such as porphyrins (Figure 5.6a) has attracted a lot of attention to simulate natural photosynthesis or to transform light into chemical energy. Donor–acceptor dyads undergo photoinduced electron transfer from the porphyrins donor to the fullerene acceptor and serve as ideal model compounds for organic solar cells. Indeed, no other class of compound surpasses fullerenes as electron acceptors in photovoltaic devices. Phenyl-C_{61}-butyric acid methyl ester (PCBM), structure shown in Figure 5.6b, serve as an *n*-type semiconductor in very inexpensive and comparatively efficient plastic solar cells (bulk heterojunction solar cells). Structures shown in Figure 5.6c and d are water-soluble fullerene adducts and exhibit remarkable biological properties with regard to anti-HIV activity and metal-free superoxide dismutation, respectively. The latter is a principal mechanism for efficient neuroprotection. Further applications of fullerene adducts in materials science include the fields of nonlinear optics and liquid crystals. Other types of fullerene derivative show unprecedented properties: for example, salts, such as K_3C_{60} and tetrakis(dimethylamino)ethylene (TDAE)-C_{60} are superconductors and ferromagnets, respectively. Cluster-opened fullerenes have been prepared that can be filled with small molecules, such as hydrogen, and subsequently reclosed to form $H_2@C_{60}$. This opens the door to a whole world of new endohedral derivatives. The substitution of carbon atoms with heteroatoms such as nitrogen realized in the heterofullerene $(C_{59}N)_2$ (Figure 5.4e) allows for further variation of the electronic properties of the fullerene core.

5.2.2 Application Potentials of Fullerene

Fullerenes in general form an interesting class of compounds that surely will be used in future technologies and applications [12]. Fullerenes packed, in fcc structure, can be intercalated with alkali and alkaline earth metal atoms, which provide electrons to the conduction band (from semiconducting to metallic behavior). K-doped fullerene (K_3C_{60}) revealed superconductivity behavior at 18 K. Physical and chemical properties may be tuned via the addition of element and molecular species into the fullerene lattice ($C_{59}N$), within the cage (N at center of C_{60}), or coating the surface of fullerene with transition metals, thereby forming a variety of new fullerenes. Fullerene and its derivatives are considered potential candidates for a number of applications, which includes the following:

i. Hydrogenation of fullerene produces hydrides. The reaction is reversible and can be catalyzed with metals at low pressure.

ii. Fullerene catalyzes the conversion of methane into hydrocarbons and prevents coking reaction.

iii. Fullerene-based capacitors can be used as sensors to detect H_2S in N_2 and water in isopropanol at ppm levels.

iv. Fullerene can be transformed to diamond at high pressure at room temperature and can also be used as a diamond nucleation center during CVD.

v. Fullerenes are used to strengthening, hardening, and improving the electrical conductivity of alloys.

vi. Fullerene derivatives find several application in biomedical fields such as inhibition of human HIV replication; biological antioxidant (radical sponge); binding specific antibiotics to the structure of resistant bacteria and even target certain types of cancer cells such as melanoma; and light-activated antimicrobial agents.

5.3 Carbon Nanotubes (CNTs)

Carbon nanotubes can be described as a rolled-up tubular shell of graphene sheet, one-atom-thick layer, which is made of benzene-type hexagonal rings of carbon atoms. The tubular shell is thus mainly made of hexagonal rings (in a sheet) of carbon atoms, whereas the ends are capped by half-dome-shaped half-fullerene molecules. Due to their special 1D form, they have interesting physical properties such as they have metallic or semiconducting electrical conductivity depending on the chirality of the carbon atoms in the tube. Nanotubes have a large geometric aspect ratio and they are the first nanocavities.

5.3.1 Classification of CNTs

Carbon nanotubes are classified as single-walled carbon nanotubes (SWCNTs) and multiwalled carbon nanotubes (MWCNTs) as shown in Figure 5.7a–c. The SWCNTs may bundle into a rope of SWCNTs. MWCNTs are nanotubes with more than one graphene cylinder nested one into another. Typical MWCNTs have an inner diameter of 1–3 nm and an outer diameter of approximately 10 nm with the interlayer separation of ~0.34 nm.

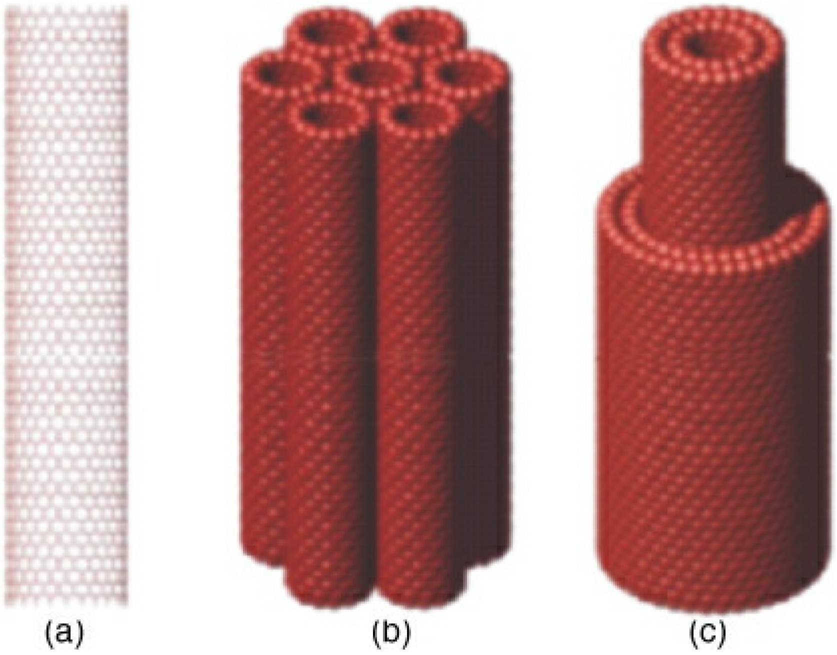

Figure 5.7 (a–c) Types of carbon nanotubes.

Courtesy of Dr. S. Musso, MIT, USA.

Most SWCNTs have a diameter close to 1 nm, with a tube length that can be many millions of times longer. CNTs can also be classified on the basis of structures [13] as follows: armchair, zigzag, and chiral nanotubes, depending on how the 2D graphene sheet is “rolled up” (Figure 5.8).

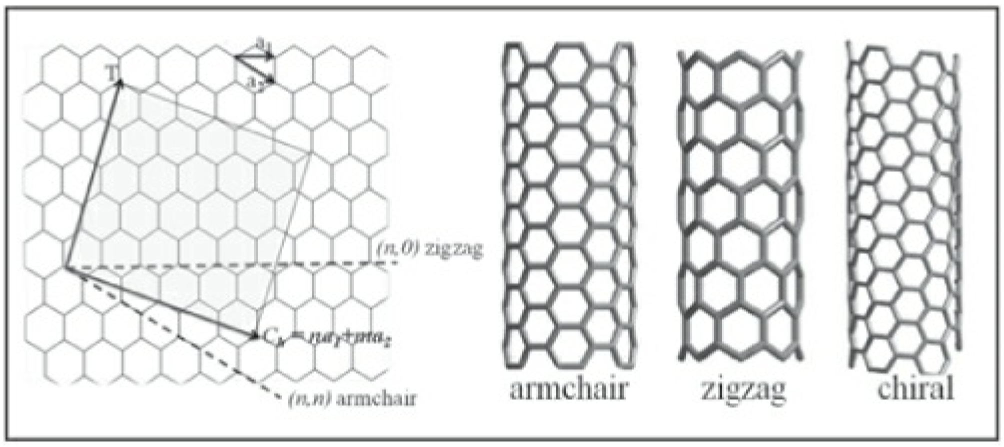

Figure 5.8 Different structural forms of single-wall carbon nanotubes.

Saito et al.[13], © 1992. With permission of AIP Publishing LIC.

The way the graphene sheet is wrapped is represented by a pair of indices (*n*, *m*). The integers *n* and *m* denote the number of unit vectors along two directions in the honeycomb crystal lattice of graphene. The diameter (*d*) of an ideal nanotube can be calculated from its (*n*, *m*) indices as follows (5.1), where $a = 0.246$ nm.

$$d = \frac{a}{\pi}\sqrt{(n^2 + nm + m^2)} \tag{5.1}$$

In zigzag SWCNTs, the zigzag pattern is around the circumference and $m = 0$; in chiral SWCNTs, the twisting of hexagons is around tubule body; and in armchair SWCNTs, the chair-like pattern is around circumference and $n = \text{m}$. To discriminate between different types of CNTs, the chiral angle and vector play an important role in determining the important properties of nanotubes. Armchair nanotubes are formed when $n = \text{m}$ and the chiral angle is 30°. Zigzag nanotubes are formed when either *n* or *m* is zero and the chiral angle is 0°. All other nanotubes, with chiral angles intermediate between 0° and 30°, are known as chiral nanotubes. The name chiral means handedness and indicates that the tubes may twist in either direction. The geometry of the chiral SWCNT lies between that of the armchair and zigzag SWCNTs. The chiral form is believed to be the most commonly occurring SWCNT.

The properties of nanotubes are also determined by their diameter, which depends on *n* and *m*. A nanotube is usually characterized by its diameter *d* and the chiral angle θ ($0 \le |\theta| \le 30°$). The integers (*n*, *m*) determine *d* and θ. Furthermore, *n* and *m* also determine the conducting behavior of nanotubes; if $(n - m) \ne 3\times$ integer, it is semiconducting behavior, whereas when $(n - m) = 3\times$ integer, it is a metallic conducting behavior. MWCNTs are nanotubes with more than one graphene cylinder nested one into another. Typical sizes for MWCNTs are an inner diameter of 1–3 nm and an outer diameter of approximately 10 nm. The spacing of intershell by using image of TEM with high resolution; spacing found to vary from 0.34, augmenting with the diameter of tube diminishing. The biggest spacing for the smallest diameter is allocated in the high curve, following in a distasteful force augmented, linked to the diameter diminished by the shells of CNTs. The value of 0.34 nm spacing in the bulk graphite crystal is approximately that of the CNTs. However, a closer study revealed that the mean value of the interlayer spacing is 0.3444 ± 0.001 nm; the values in CNTs are larger, by a few percent, than those in the bulk graphite crystal. According to theoretical calculations, the distance between two layers is d = 3.39 Å, slightly bigger than in graphite. Based on TEM images, the interlayer separation of d = 3.4 Å is commonly reported for MWCNT.

5.3.2 Synthesis of CNTs

Several methods are used to synthesize CNTs such as arc discharge, CVD, and laser ablation [14–18]. Commercial supplies are currently available worldwide from small laboratory scale to mass production scale. However, to use CNTs, pretreatment such as purification and/or surface modification of the CNTs is necessary.

5.3.2.1 Arc Discharge Technique

The carbon arc discharge method, initially used for producing C_{60} fullerenes, is the most common and perhaps easiest way to produce CNTs as it is rather simple to undertake. However, it is a technique that produces a mixture of components and requires separating nanotubes from the soot and the catalytic metals present in the crude product. This method creates nanotubes through arc vaporization of two carbon rods placed end to end, separated by approximately 1 mm, in an enclosure that is usually filled with inert gas (helium, argon) at low pressure (between 50 and 700 mbar). Recent investigations have shown that it is also possible to create nanotubes with the arc method in liquid nitrogen. A direct current of 50–100 A driven by approximately 20 V creates a high-temperature discharge between the two electrodes. The discharge vaporizes one of the carbon rods and forms a small rod-shaped deposit on the other rod. Producing nanotubes in high yield depends on the uniformity of the plasma arc and the temperature of the deposit form on the carbon electrode. Insight into the growth mechanism is increasing, and measurements have shown that different diameter distributions have been found depending on the mixture of helium and argon. These mixtures have different diffusion coefficients and thermal conductivities. These properties affect the speed with which the carbon and catalyst molecules diffuse and cool. This implies that single-layer tubules nucleate and grow on metal particles in different sizes depending on the quenching rate in the plasma and this suggests that temperature and carbon and metal catalyst densities affect the diameter distribution of nanotubes. Depending on the exact technique, it is possible to selectively grow SWCNTs or MWCNTs. For example, employing arc discharge method, a pure graphite anode gives a high proportion of MWCNTs whereas when a graphite anode is doped with Ni/Co, SWCNTs is the major product. TEM image of double-walled CNT (DWCNT) and multiwalled CNT (MWCNTs) are shown in Figure 5.9.

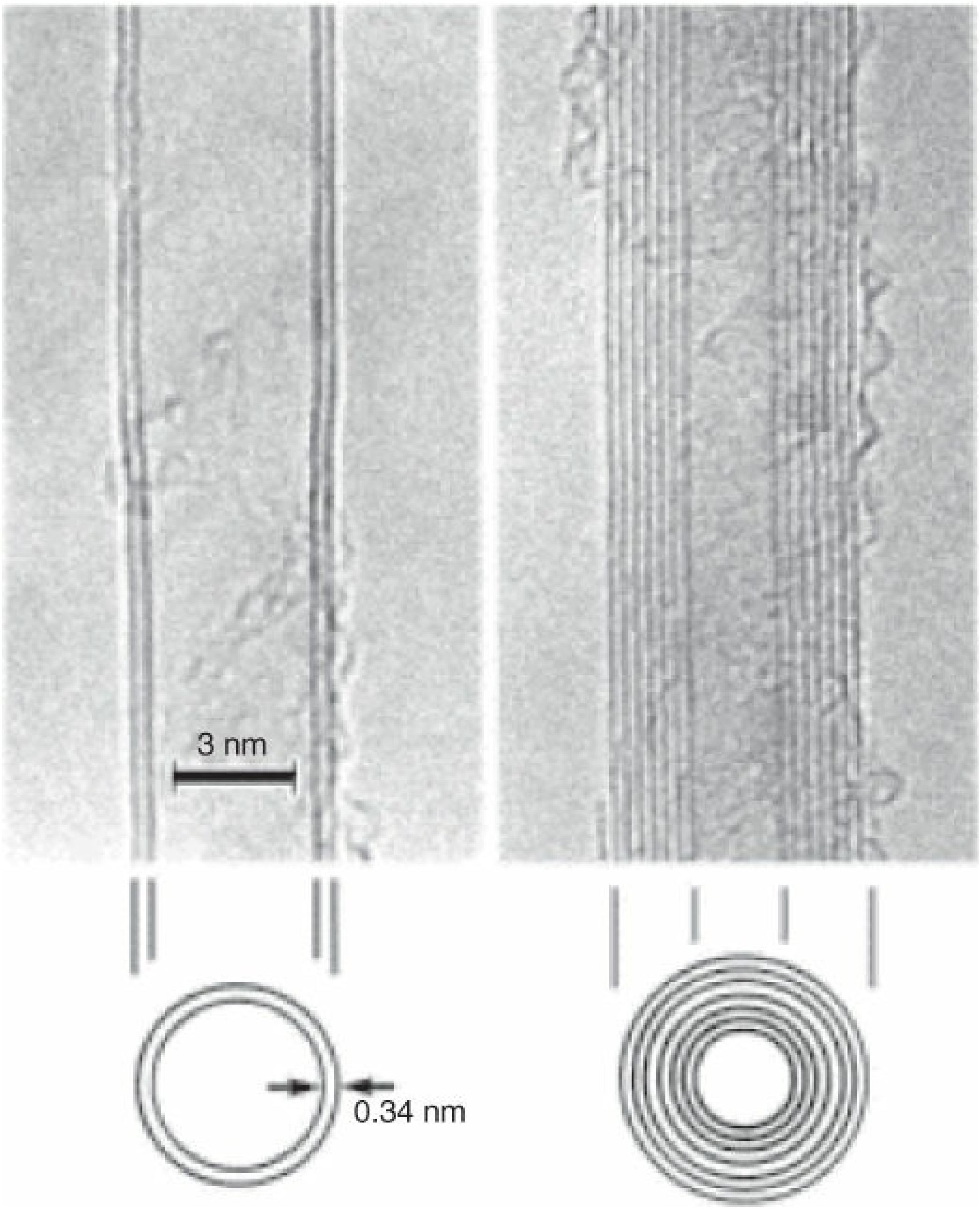

Figure 5.9 Transmission electron micrograph (TEM) of MWCNT.

Iijima [5], © 1991. Reproduced with permission of NPG.

I. Synthesis of SWCNT

If SWCNTs are preferable, the anode has to be doped with metal catalyst, such as Fe, Co, Ni, Y, or Mo. The quantity and quality of the nanotubes obtained depend on various parameters such as the metal concentration, inert gas pressure, kind of gas, the current, and system geometry. Usually, the diameter of the SWCNTs is in the range of 1.2–1.4 nm. A couple of ways to improve the process of arc discharge are stated as follows:

a. Synthesis in inert gas

The most common problems with SWCNT synthesis are that the product contains a lot of metal catalyst, SWCNTs have defects, and purification is hard to perform. On the other hand, an advantage is that the diameter can be slightly controlled by changing thermal transfer and diffusion, and hence condensation of atomic carbon and metals between the plasma and the vicinity of the cathode can control nanotube diameter in the arc process. This was shown in an experiment in which different mixtures of inert gases were used. It appeared that argon, with a lower thermal conductivity and diffusion coefficient, gave SWCNTs with a smaller diameter of approximately 1.2 nm. A linear fit of the average nanotube diameter showed a 0.2 nm diameter decrease per 10% increase in argon:helium ratio, when nickel/yttrium was used (C/Ni/Y is 94.8:4.2:1) as catalyst.

b. Optical plasma control

A second way is the adjustment of ACD in order to obtain strong visible vortices around the cathode. This enhances anode vaporization, which improves the formation of nanotubes. Combined with controlling the argon/helium mixture, one can simultaneously control the macroscopic and microscopic parameters of the nanotubes formed. With a nickel and yttrium catalyst (C/Ni/Y is 94.8:4.2:1), the optimum nanotube yield was found at a pressure of 660 mbar for pure helium and 100 mbar for pure argon. The nanotube diameter ranges from 1.27 to 1.37 nm.

c. Catalyst

Knowing that CVD could give SWCNTs with a diameter of 0.6–1.2 nm, same catalyst could be used in arc discharge as used in CVD. Not all of the catalysts used appeared to result in nanotubes for both methods. Using a mixture of Co and Mo in high concentrations as catalyst resulted in CNTs of smaller diameter than usual size gained from arc discharge (1.2–1.4 nm). The synthesized nanotubes are cleaner and less defective compared with those synthesized by conventional methods.

II. Synthesis of MWCNT

If both electrodes are graphite, the main product will be MWCNTs. However, along with MWCNTs, a lot of side products, namely, fullerenes, amorphous carbon, and some graphite sheets are also formed. Purifying the MWCNTs results in the loss of structure and disorders the walls.

a. Synthesis in liquid nitrogen

A first viable route to highly crystalline MWCNTs is the arc discharge method in liquid nitrogen. With this route as shown in Figure 5.10, mass production is also possible. For this option, low pressures and expansive inert gases such as helium or argon are needed. The content of the MWCNTs can be as high as 70% of the reaction product free of nitrogen [15].

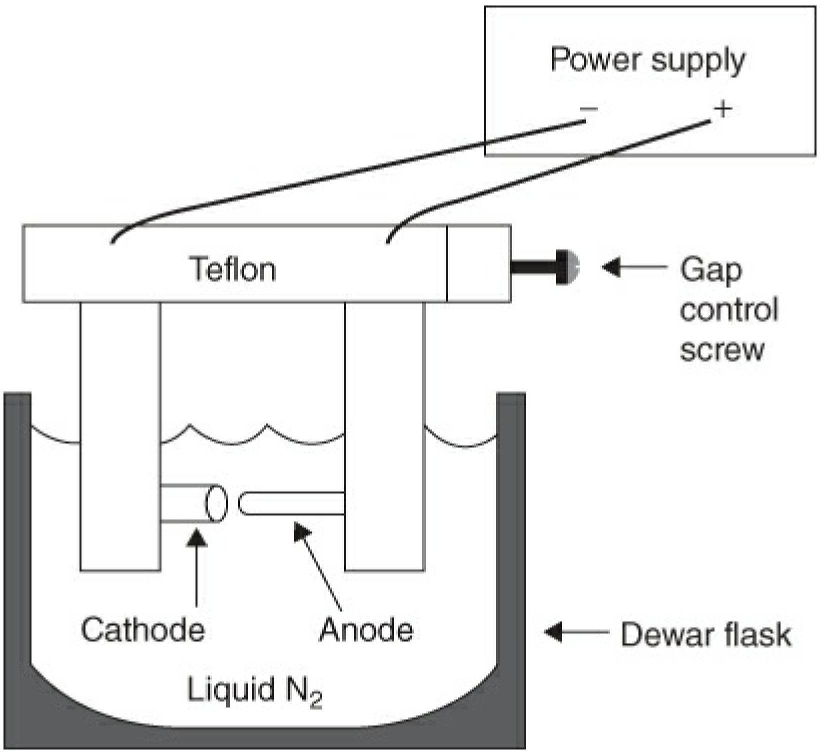

Figure 5.10 Schematic of the arc discharge procedure in liquid nitrogen.

Jung et al. [15], © 2003. With permission of Springer-Verlag.

b. Magnetic field synthesis

Synthesis of MWCNTs in a magnetic field gives defect-free MWCNTs of high purity, which can be used as nanosized electric wires for device fabrication. In this method, the arc discharge synthesis is controlled by a magnetic field around the arc plasma. Extremely pure graphite rods (purity > 99.999%) were used as electrodes. Highly pure MWCNTs (purity > 95%) were obtained without further purification as is revealed from SEM image given in Figure 5.11a and b.

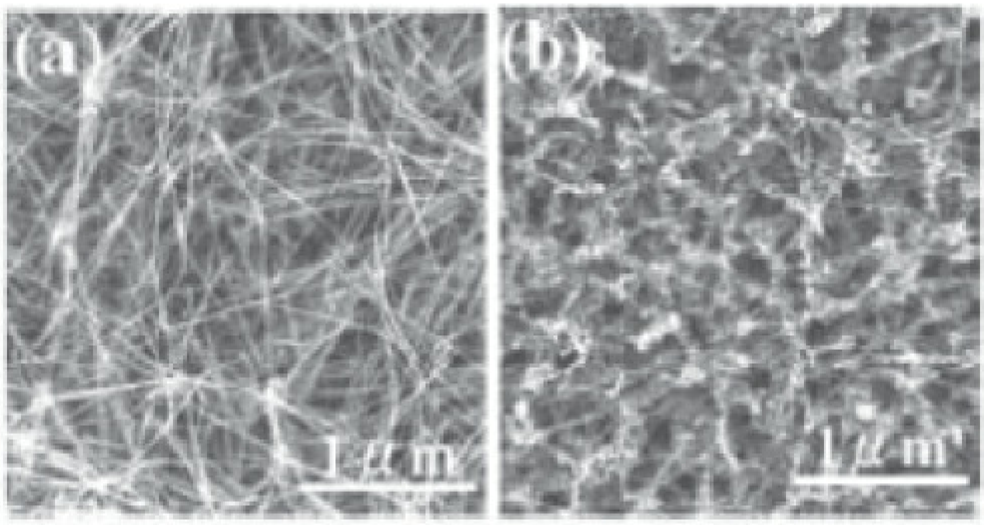

Figure 5.11 SEM images of MWCNTs synthesized: (a) with and (b) without the magnetic field.

Anazawa et al. [16], © 2002. With permission of AIP Publishing LLC.

c. Plasma rotating arc discharge

A second possibly economical route to mass production of MWCNTs is synthesis by plasma rotating arc discharge technique. The centrifugal force caused by the rotation generates turbulence and accelerates the carbon vapor perpendicular to the anode (Figure 5.12). In addition, the rotation distributes the microdischarges uniformly and generates stable plasma. Consequently, it increases the plasma volume and raises the plasma temperature. At a rotation speed of 5000 rpm, a yield of 60% was found at a formation temperature of 1025 °C without the use of a catalyst. The yield increases up to 90% after purification if the rotation speed is increased and the temperature is raised to 1150 °C.

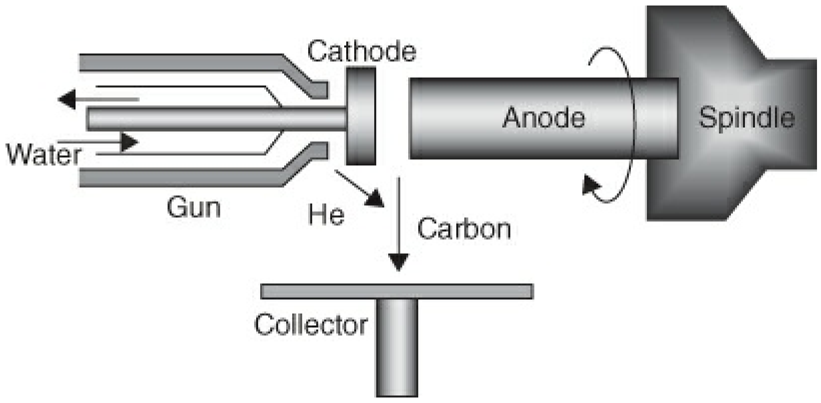

Figure 5.12 Schematic of plasma rotating electrode system.

Lee et al. [17], © 2002. With permission of Elsevier.

5.3.2.2 Laser Ablation

In 1995, Smalley's group at Rice University reported the synthesis of CNTs by laser vaporization. The laser vaporization apparatus used by Smalley's group is shown in Figure 5.13a and b, a detailed schematic of reaction chamber for ultrafast laser (FEL, the free electron laser).

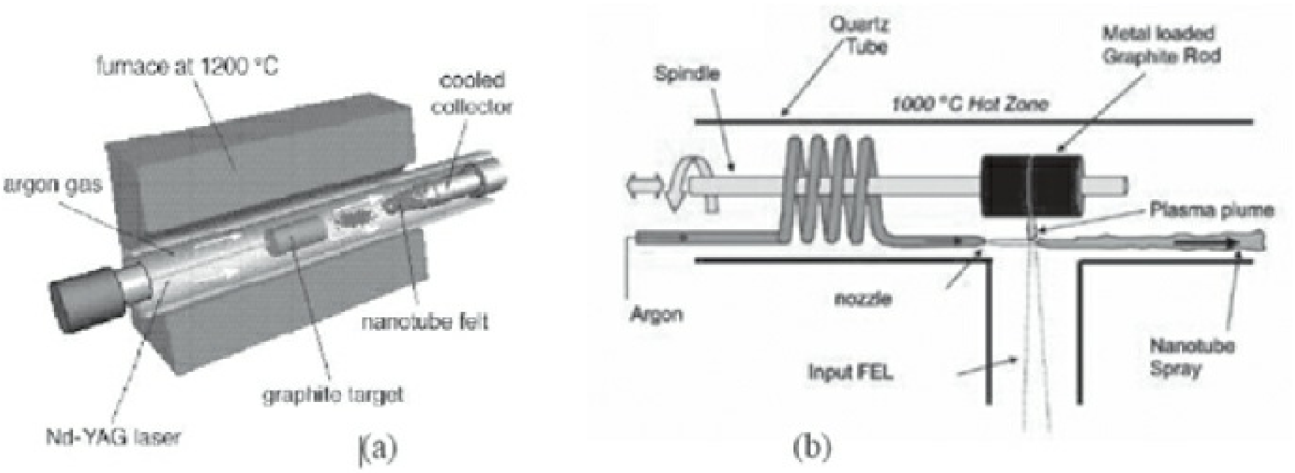

Figure 5.13 (a) Classical laser ablation apparatus used at Rice University; (b) schematic of ultrafast laser evaporation method.

Guo et al. [18], © 1995. With permission of Elsevier.

Laser ablation is almost similar to arc discharge since the optimum background gas and catalyst mix is the same as in the arc discharge process. This might be due to very similar reaction conditions needed, and the reactions probably occur with the same mechanism. A pulsed or continuous laser is used to vaporize a graphite target in an oven at 1200 °C. The main difference between continuous and pulsed laser is that the pulsed laser demands a much higher light intensity (100 kW/cm compared with 12 kW/cm). The oven is filled with helium or argon gas in order to keep the pressure at 500 Torr. A very hot vapor plume forms, then expands, and then cools rapidly. As the vaporized species cool, small carbon molecules and atoms quickly condense to form larger clusters, possibly including fullerenes. The catalysts also begin to condense, but more slowly at first, and attach to carbon clusters and prevent their closing into cage structures. Catalysts may even open-cage structures when they attach to them. From these initial clusters, tubular molecules grow into single-wall CNTs until the catalyst particles become too large, or until conditions have cooled sufficiently that carbon no longer can diffuse through or over the surface of the catalyst particles. It is also possible that the particles become so much coated with a carbon layer that they cannot absorb more and the nanotube stops growing. The SWCNTs formed in this case are bundled together by van der Waals forces.

There are some striking, but not exact similarities, in the comparison of the spectral emission of excited species in laser ablation of a composite graphite target with that of laser-irradiated C_{60} vapor. This suggests that fullerenes are also produced by laser ablation of catalyst-filled graphite, as is the case when no catalysts are included in the target. However, subsequent laser pulses excite fullerenes to emit CO_2 that adsorbs on catalyst particles and facilitates SWCNT growth. Table 5.1 summarizes the comparative details including advantages and disadvantages of arc discharge, CVD, and laser ablation methods to synthesize CNTs.

Table 5.1 A Comparative Account of Different Methods for Synthesis of CNTs

Technique	Procedure	Typical Yield, %	Typical Product		Advantages	Disadvantages
			SWCNT	MWCNT		
Arc discharge method	Connect two graphite rods to a power supply, place them a few millimeters apart. At 100 amp, carbon vaporizes and forms hot plasma	30–90	Short tubes, 0.6–1.4 nm diameter	Short tubes with inner diameter of 1–3 nm and outer diameter of approximately 10 nm	Inexpensive and open-air method for the production of SWCNT, MWCNT	Nanotubes tend to be short with random sizes and directions; often needs a purification step
Chemical vapor deposition	Place substrate in oven, heat to 873 K, and slowly add a carbon-bearing gas such as methane. As gas decomposes, it frees up carbon atoms, which recombine in the form of CNTs	20–100	Long tubes, 0.6–4 nm diameter	Long tubes with diameter ranging from 10 to 240 nm	A simple process, suitable for industrial production; long length, diameter controllable	Yield predominately MWCNTs and often riddled with defects
Laser ablation	Blast graphite with intense laser pulses; use the laser pulses rather than electricity to generate carbon gas from which the CNTs form; try various conditions until hit on one that produces prodigious amounts of SWCNTs	Up to 70	Long bundles of tubes (5–20 microns), with individual diameter of 1–2 nm	MWCNT synthesis is possible	Primarily SWCNTs, with good diameter control and few defects. The reaction product is quite pure	Comparatively costly technique due to expensive lasers and high power requirement

5.3.3 Functionalization of CNTs

Functionalization is a surface treatment that brings functional groups at the surface of nanofilters/nanoparticles. The filler functionalization brings about favorable interactions between the functional groups and the polymer matrix. This is particularly important for fillers having strong tendency toward agglomeration as, for instance, CNTs. The enhanced filler–matrix interactions facilitate the dispersion of the filler in the polymer matrix and strengthen the interfacial bonding, leading to better reinforcement effects. The filler functionalization often leads to restricted chain mobility at the vicinity of the filler surface and, sometimes, to enhanced glass-transition temperature.

The functionalization might also accomplish changes in the chemical structure and physical properties of the fillers [19]. The electrical conductivity and the outstanding mechanical properties of CNTs can be mainly explained in terms of the graphite-like structure of the walls of these materials. The sp^2-hybridized carbon atoms in conjugated C=C bonds, in analogy to those described for graphite, enable the electron delocalization. Therefore, chemical reactions involving the cleavage of the C=C can lead to decreased electrical conductivity. Moreover, functionalization method imputing higher amounts of energy, such as milling in liquid ammonia, can cause the shortening of the CNTs. The functionalization methods can be classified in four main groups:

> ***Strong oxidation:*** The main goal of this procedure is the introduction is the introduction of carboxylic acids and other carbonyl compounds at the surface of the CNTs. As a result the structural quality of the CNTs is worsened. This method is mostly suitable when an optimal reinforcement effect is primarily required.
>
> ***Cycloaddition reactions:*** In this method, the C=C bonds of the CNTs react with dienes or tetrazines. Although this procedure is not as drastic as the oxidation-based reaction, still C=C bonds are broken due to the chemical reactions, therefore changes in the electrical conductivity might take place.
>
> ***Radical-based reactions:*** Although milder than the other reactions, this method is based on the cleavage of C=C by radical, which are generated *in situ* during the functionalization process.
>
> ***Mild oxi-reduction reactions***: In these procedures, the C=C bonds are broken through reduction with metals followed by another functionalization step. This method has high selectivity, and the functionalized CNTs exhibit a remarkable dispensability. The main disadvantage of such methods is their complexity due to the use of air-sensitive and moisture-sensitive chemical, which is the most significant drawback for the breakthrough of this method.

On the other hand, the use of surfactants, aromatic hydrocarbons (pyrenes), conjugated polymers, aromatic polyimide biomacromolecules, cytosine, thiophene, as modifiers of CNTs has emerged as convenient method for the surface modification of CNTs. This method is often reported as noncovalent functionalization and often facilitates significantly the CNT dispersion in polymeric matrices and solvents. The main advantage of this method is that no cleavage of C=C is necessary, so the electrical, thermal, and mechanical properties of the CNTs are not necessarily affected. Since the epoxy resin is normally cured with an amine hardener, the chemical properties of the functionalized CNTs should be tailored for the chemical reactions involved during the curing process. Therefore, the introduction of amine groups at the surface of the CNTs seems to be a plausible method for improving the epoxy dispersion in the epoxy as well as the filler adhesion to this polymer matrix.

5.3.4 Purification of CNTs

Purification of CNTs is a big challenge in realizing their application. The as-produced SWCNT soot contains a lot of impurities. The main impurities in the soot are graphite (wrapped up) sheets, amorphous carbon, metal catalyst, and the smaller fullerenes. These impurities will interfere with most of the desired properties of the SWCNTs. Also in the fundamental research, it is preferred to obtain SWCNTs as pure as possible. In order to understand the measurements better, the SWCNT samples also have to be as homogeneous as possible. The common industrial techniques use strong oxidation and acid-refluxing techniques, which have an effect on the structure of the tubes [20]. Basically, these techniques can be divided into two main streams: structure selective and size-selective separations. The first one will separate the SWCNTs from the impurities; the second one will give a more homogeneous diameter or size distribution. The purification techniques include oxidation, acid treatment, annealing, ultrasonication, microfiltration, ferromagnetic separation and cutting, functionalization and chromatography techniques. Some of the common of the purification methods are summarized as follows:

Oxidation: Oxidative treatment of the SWCNTs is a good way to remove carbonaceous impurities or to clear the metal surface. The main disadvantages of oxidation are that along with impurities, the SWCNTs are oxidized. Luckily the damage to SWCNTs is less than the damage to the impurities. These impurities have relatively more defects or a more open structure. Another reason why impurity oxidation is preferred is that these impurities are most commonly attached to the metal catalyst, which also acts as oxidizing catalyst. In total, the efficiency and the yield of the procedure are highly dependable on a lot of factors, such as metal content, oxidation time, environment, oxidizing agent, and temperature. There are a couple of examples to prepare metal-free SWCNTs. The first one is (mild) oxidation in a wet environment with soluble oxidizing agents, such as H_2O_2 and H_2SO_4. These will only oxidize the defects and will clear the surface of the metal.

Acid treatment: In general, the acid treatment will remove the metal catalyst. First of all, the surface of the metal must be exposed by oxidation or sonication. The metal catalyst is then exposed to acid and solvated. The SWCNTs remain in suspended form. When using a treatment in HNO_3, the acid only has an effect on the metal catalyst. It has no effect on the SWCNTs and other carbon particles. If a treatment in HCl is used, the acid has also a little effect on the SWCNTs and other carbon particles. The mild acid treatment (4 M HCl reflux) is basically the same as the HNO_3 reflux, but here the metal has to be totally exposed to above oxidative techniques is microwave heating. The microwaves will heat up the metal and the acid to solvate it.

Annealing: Annealing at high temperatures (873–1873 K) leads to the formation of defects due to rearrangement of nanotubes. The high temperature also causes the graphitic carbon and the short fullerenes to pyrolyze. When using high-temperature vacuum treatment (1873 K), the metal gets melted and can be removed.

Ultrasonication: In this technique, particles are separated due to ultrasonic vibrations. Agglomerates of different nanoparticles will be forced to vibrate and will become more dispersed. The separation of the particles is highly dependable on the surfactant, solvent, and reagent used. The solvent influences the stability of the dispersed tubes in the system. In poor solvents, the SWCNTs are more stable if they are still attached to the metal. But in some solvents, such as alcohols, monodispersed particles are relatively stable. When an acid is used, the purity of the SWCNTs depends on the exposure time. When the tubes are exposed to the acid for a short time, only the metal solvates, but for a longer exposure time, the tubes will also be chemically cut.

Magnetic purification: In this method, ferromagnetic (catalytic) particles are mechanically removed from their graphitic shells. The SWCNTs suspension is mixed with inorganic nanoparticles (mainly ZrO_2 or $CaCO_3$) in an ultrasonic bath to remove the ferromagnetic particles [21]. Then, the particles are trapped with permanent magnetic poles. After a subsequent chemical treatment, a high-purity SWCNT material will be obtained. Figure 5.14 shows a schematic diagram of the apparatus for magnetic purification. This process does not require large equipment and enables the production of laboratory-sized quantities of SWCNTs containing no magnetic impurities.

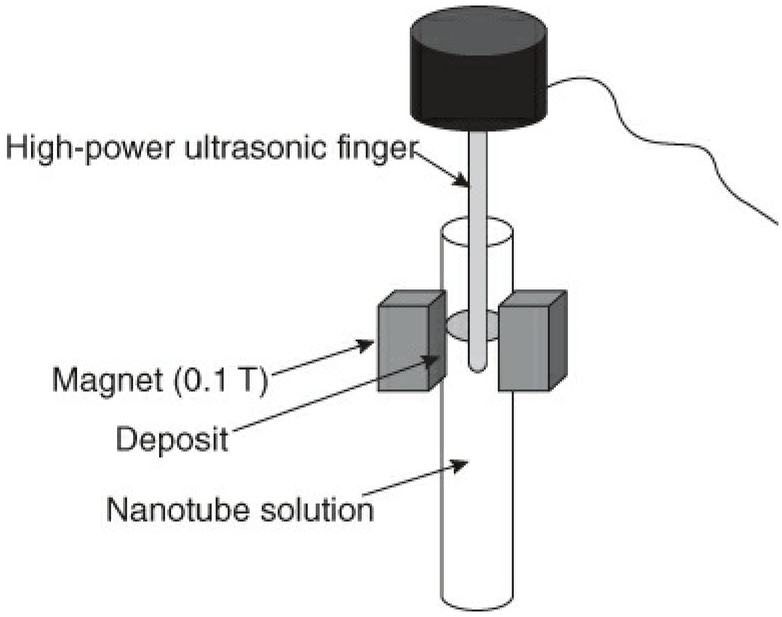

Figure 5.14 Schematic of the apparatus for magnetic purification of CNTs.

Le et al. [21], © 2002. With permission of ACS.

5.3.5 Special Properties of Carbon Nanotubes

Based on the rolling direction, CNTs can be semiconductors or conductors. CNTs show extraordinary mechanical, electrical, and thermal properties because of their C–C covalent bonding and seamless hexagonal network architecture. Electronic, molecular, and structural properties of CNTs are determined to a large extent by their nearly 1D structure. The most important properties of carbon nanomaterials and their molecular background [22] are discussed as follows:

The chemical reactivity: The chemical reactivity of a CNT is, compared with a graphene sheet, enhanced as a direct result of the curvature of the CNT surface. CNT reactivity is directly related to the π orbital difference caused by an increased curvature. Therefore, a difference must be made between the sidewall and the end caps of a nanotube. For the same reason, a smaller nanotube diameter results in increased reactivity. Covalent chemical modification of either sidewalls or end caps has shown to be possible. For example, the solubility of CNTs in different solvents can be controlled this way. However, direct investigation of chemical modifications on nanotube behavior is difficult as the crude nanotube samples are still not pure enough.

Electrical conductivity: Depending on their chiral vector, CNTs with a small diameter are either semiconducting or metallic. The differences in conducting properties are caused by the molecular structure that results in a different band structure and thus a different band gap. The differences in conductivity can easily be derived from the graphene sheet properties. It is shown in Figure 5.8 that a (n, m) nanotube is semiconducting if $n - m \neq 3\times$ integer whereas shows metallic conductivity when $n = m$ or $n - m = 3\times$ integer, where n and m are defining coordinates of the nanotube. The resistance to conduction is determined by quantum mechanical aspects and was proved to be independent of the nanotube length.

Optical activity: Theoretical studies have revealed that the optical activity of chiral nanotubes disappears if the nanotubes become larger. Therefore, it is expected that other physical properties are influenced by these parameters too. Use of the optical activity might result in optical devices in which CNTs play an important role.

Mechanical strength: CNTs have a very large Young modulus in their axial direction. The nanotube as a whole is very flexible because of the great length. Therefore, these compounds are potentially suitable for applications in composite materials that need anisotropic properties.

5.3.6 Applications

CNTs are the most intensively researched nanomaterials and have great potential for numerous applications [22, 23]. CNTs are used in the plastics industry for composite materials, the electronics industry for display or conductive transparent films, the semiconductor industry for transistor channels, the energy industry for batteries or solar cells, and the biohealth industry for sensors. Small additions of nanomaterials such as CNTs can greatly improve structural properties of composite materials. Due to their electrical conductivity, CNTs also have application for the manufacture of low-cost solar cells, electronics, and antistatic composite materials. Some of the potential applications of chemically modified CNTs with covalently bonded moieties are summarized in Table 5.2.

Table 5.2 Potential Applications of Chemically Modified CNTs

Application Area	Function
Electronic devices, for example, nanodiodes	Local modification of the electronic band structure
Biochemical/chemical sensors	Selective recognition of analyte
Catalyst supports	Anchoring of molecules/metal nanoparticles
Mechanically reinforced composites	Chemical coupling with a matrix
Chemically sensitive tips for scanning probe microscopy	Selective chemical interaction with surfaces
Field emission	Reduction of work function for electrons at the tube ends
Nanofiltration	Control of passage of molecules/ions through stearic effects or coulombic interactions
Artificial muscles	Mechanical stabilization of nanotube films through covalent cross-linking
Controlled drug release	Biocompatibility; recognition of biological fingerprints
Pharmacology	Enzymatic inhibition/blocking of ionic channels in the cell membrane
Directed cell growth on surfaces	Specific interaction with cell surfaces

5.4 Graphene

Graphene, the youngest allotropes of elemental carbon, is a one-atom-thick sheet of sp^2-bonded carbon atoms in a hexagonal arrangement as in chicken net (Figure 5.15). Graphene is at the cutting-edge of materials science and condensed matter physics research [24, 25]. It is the thinnest known material in the world and conceptually a basic build block for constructing many other carbon materials. It can be rolled into 1D CNTs and stacked into 3D graphite. With the addition of pentagons, it can be wrapped into a spherical fullerene. In one sense, it is the mother of all graphitic materials.

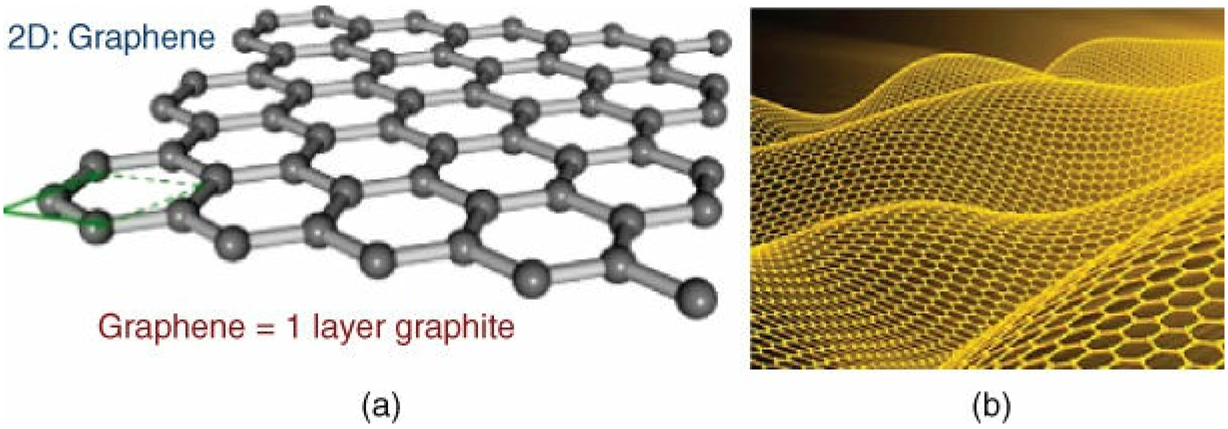

Figure 5.15 (a) Planar structure of 2D graphene; Dai et al.[3], © 2012. With permission of Wiley. (b) Graphene shown as chicken net.

Katsnelson and Novoselov [24] © 2007. With permission of Elsevier.

From the viewpoint of its electronic properties, graphene is a zero-gap semiconductor with unique electronic properties originating from the fact that charge carriers in graphene are described by a Dirac-like equation, rather than the usual Schrödinger equation. As a consequence of its perfect crystal structure, low-energy quasiparticles in it obey a linear dispersion relation, similar to massless relativistic particles. This essential characteristic of a gapless semiconductor has led to many observations of peculiar electronic properties including ballistic transport, pseudospin chirality based on the “Berry phase,” a room-temperature half-integer “chiral” quantum Hall effect, and conductivity without charge carriers, which make it a promising choice for future electronic materials, both as a device and as an interconnect [26]. For example, graphene has the fastest electron mobility of ~15,000 cm^2/(V cm) or 10^6 Ω cm (lower than Ag), a superhigh mobility of temperature-independent charge carriers of 200,000 cm^2/(V s) (200 times higher than Si), and an effective Fermi velocity of 10^6 m/s at room temperature, similar to the speed of light. More importantly, graphene possesses not only unique electronic properties but also excellent mechanical, optical, thermal, and electrochemical properties that are superior to other carbon allotropes such as graphite, diamond, fullerene, and CNTs. Single-layer graphene has excellent mechanical properties with a Young's modulus of 1.0 TPa and a stiffness of 130 GPa, optical transmittance of ~97.7% (absorbing 2.3% of white light), and superior thermal conductivity of 5000 W/(m K) (about 100 times that of Cu). It also has a high theoretical specific surface area of 2620 m^2/g, extreme electrical conductivity, and good flexibility. Due to its unique properties, it is speculated that in many applications graphene will outperform CNTs, graphite, metals, and semiconductors where it is used as an individual material or as a component in a hybrid or composite material.

5.4.1 Electronic Structure of Graphene

The electronic structure of graphene is rather different from usual 3D materials [26]. Its Fermi surface is characterized by six double cones, as shown in Figure 5.16. In intrinsic (undoped) graphene, the Fermi level is situated at the connection points of these cones. Since the density of states of the material is zero at that point, the electrical conductivity of intrinsic graphene is quite low and is of the order of the conductance quantum $\sigma \sim e^2/h$; the exact prefactor is still debated. The Fermi level can, however, be changed by an electric field so that the material becomes either n-doped (with electrons) or p-doped (with holes) depending on the polarity of the applied field. Graphene can also be doped by adsorbing, for example, water or ammonia on its surface. The electrical conductivity for doped graphene is quite high and may even be higher than that of copper at even room temperature. The black line in Figure 5.16 represents the Fermi energy for an undoped graphene crystal. The energy, E, for the excitations in graphene as a function of the wave numbers, k_x and k_y, in the x and y directions. The black line represents the Fermi energy for an undoped graphene crystal. Close to the Fermi level the energy spectrum is characterized by six double cones where dispersion relation for electrons and holes is linear. Since the effective masses are given by the curvature of the energy bands, this corresponds to zero effective mass. The equation describing the excitations in graphene is formally identical to the Dirac equation for massless fermions, which travel at a constant speed. The connection points of the cones are therefore called Dirac points. This gives rise to interesting analogies between graphene and particle physics, which are valid for energies up to approximately 1 eV, where the dispersion relation starts to be nonlinear. One result of this special dispersion relation is that the quantum Hall effect becomes unusual in graphene.

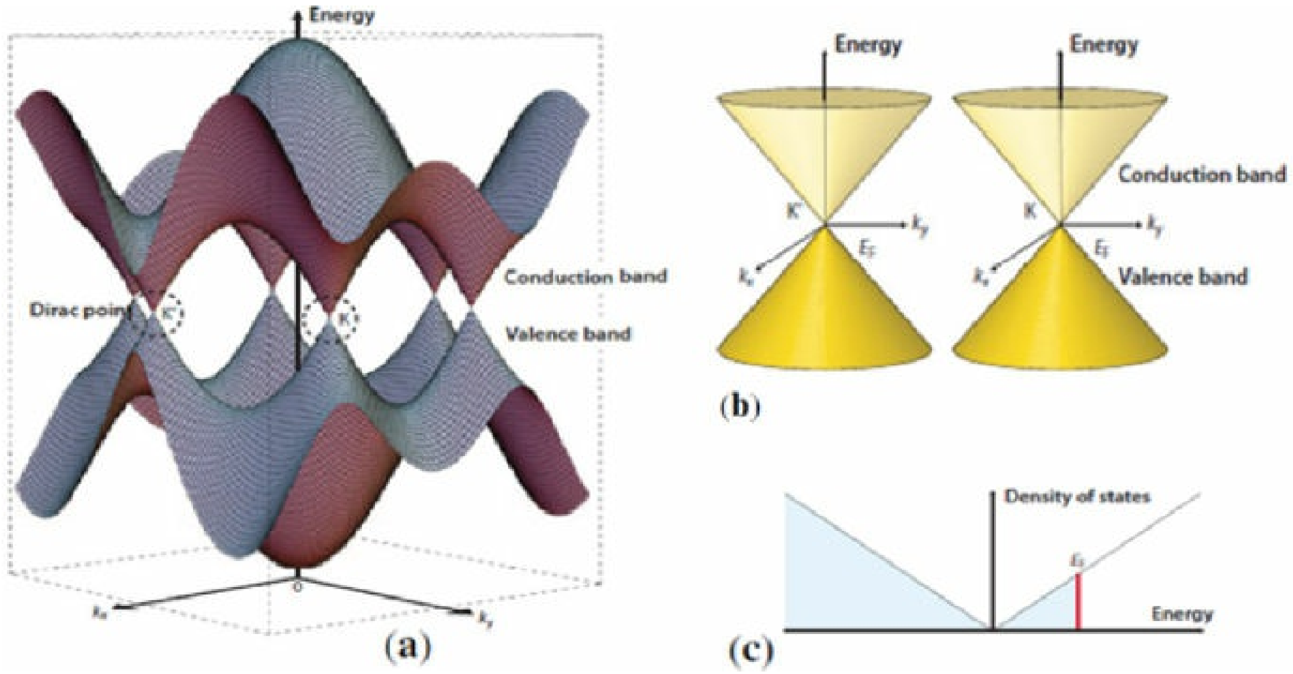

Figure 5.16 Band structure of graphene (a) energy bands near the Fermi level in graphene; (b) conic energy bands in the vicinity of the K and K' points; (c) density of states near the Fermi level with Fermi energy EF.

Ando [26], © 2009. With permission of NPG.

5.4.1.1 Band Structure

Band structure of graphene shows the π-bands that are responsible for charge carrier transport. In contrast to semiconductors, which possess a parabolic dispersion relation, graphene exhibits a linear dependence of the electron energy on the wave vector. Figure 5.16a shows **e**nergy bands near the Fermi level in graphene. The first Brillouin zone of graphene is illustrated in the horizontal plane and labeled with some points of interest. The conduction and valence bands crossing at points K and K′ are the two nonequivalent corners of the zone, also known as the Dirac points. Figure 5.16b shows the conic energy bands in the vicinity of the K and K′ points and the density of states near the Fermi level with Fermi energy EF are seen in Figure 5.16c.

Graphene differs extremely from conventional 2D electron gas systems created in semiconductor heterostructures. The reason is the linear dispersion relation $E(\boldsymbol{k})$ of the charge carriers in the vicinity of the K-point of the hexagonal Brillion zone, where the bonding π-band meets the antibonding π*-band. The band structure thus has the form of a double cone, which formally is equivalent to the dispersion relation of rest-massless particles. The symmetry of the lattice requires a two-component wave function, similar to particles known from relativistic quantum mechanics. The charge carriers and their behavior are described by Dirac equation for massless fermions. This has several interesting consequences. An example is the unusual Landau level spectrum when the system is subject to a magnetic field and results in new half-integer quantum Hall effect. Other interesting properties of charge carriers in graphene are their scattering and interference phenomena. Graphene thus provides new and interesting physics to study both experimentally and theoretically.

5.4.2 Unique Properties of Graphene

A concise account of unique and technologically significant properties of graphene [26, 27] is given here.

Charge carrier mobility: One of the interesting properties of graphene is its high charge carrier mobility, ranging between 10,000 and 200,000 VS/cm^2, which is independent of temperature. Further, carrier concentration of $n = 2 \times 10^{11}$ have been reported. These numbers translate into ballistic transport in the micrometer range. Graphene is thus a candidate for high-frequency electronic devices. But other applications such as ultrasensitive gas detectors, spintronics, or quantum computing are also under investigation.

Density of graphene: The unit hexagonal cell of graphene contains two carbon atoms and has an area of 0.052 nm^2. We can thus calculate its density as being 0.77 mg/m^2. A hypothetical hammock measuring 1 m^2 made from graphene would thus weigh 0.77 mg.

Optical transparency of graphene: Graphene is almost transparent; it absorbs only 2.3% of the light intensity, independent of the wavelength in the optical domain. This number is given by $\pi\alpha$, where α is the fine structure constant. Thus, suspended graphene does not have any color.

Strength of graphene: As yet, graphene appears to be one of the strongest materials ever tested. Measurements have shown that graphene has a breaking strength 200 times greater than steel, with a tensile strength of 130 GPa (19,000,000 psi). Graphene has a breaking strength of 42 N/m. Steel has a breaking strength in the range of 250–1200 MPa = $0.25 - 1.2 \times 10^9$ N/m^2.

Electrical conductivity of graphene: The sheet conductivity of a 2D material is given by $\sigma = en\mu$. The mobility is theoretically limited to $\mu = 200{,}000$ cm^2/(V s) by acoustic phonons at a carrier density of $n = 10^{12}$ cm^{-2}. The 2D sheet resistivity, also called the resistance per square, is then 31 Ω. Our fictional hammock measuring 1 m^2 would thus have a resistance of 31 Ω. Using the layer thickness, we get a bulk conductivity of $0.96 \times 10^6\ \Omega^{-1}\ \text{cm}^{-1}$ for graphene. This is somewhat higher than the conductivity of copper, which is $0.60 \times 10^6\ \Omega^{-1}\ \text{cm}^{-1}$.

Thermal conductivity: The thermal conductivity of graphene is dominated by phonons and has been measured to be approximately 5000 W/(m K). Copper at room temperature has a thermal conductivity of 401 W/(m K). Thus, graphene conducts heat 10 times better than copper.

5.4.3 Synthesis

There are four main methods of interest to synthesize graphene, namely exfoliation of graphite, CVD, chemical, and electrochemical synthesis route [27–30] and are discussed in following sections. Surface modifications to functionalize the graphene oxide have also been included in this section.

5.4.3.1 Exfoliation and Cleavage

The relevant properties of graphene are highly dependent on the exfoliation of the graphite down to single graphene sheet in the matrices. The key challenge in synthesis and processing of graphene sheets in bulk quantity is to prevent aggregation. Unless well separated from each other, graphene tends to form irreversible agglomerates or even restack to form graphite through van der Waals interactions. Various exfoliation approaches are discussed as follows.

a. Mechanical exfoliation in solutions

Mechanical exfoliation is a simple peeling process where a commercially available highly oriented pyrolytic graphite (HOPG) sheet is dry etched in oxygen plasma to many 5 μm deep mesa. The mesa is then stuck onto a photoresist and peeled off layers by a scotch tape. The thin flakes left on the photoresist are washed off in acetone and transferred to a silicon wafer. It was found that these thin flakes were composed of monolayer or a few layers of graphene. On the other hand, although chemical oxidation of graphite and the subsequent exfoliation provide a large amount of graphite oxide monolayer, the invasive chemical treatment inevitably generates structural defects as revealed by Raman spectroscopic studies. These structural defects disrupt the electronic structure of graphene and make it to be semiconducting. Therefore, physical exfoliation approaches are desirable where it is required to maintain the graphene structure. Graphite can also be exfoliated in *N*-methyl pyrrolidone to produce defect-free monolayer graphene. The disadvantage of this process, however, is the high cost and the high boiling point of the solvent. Exfoliation of graphite in water in the presence of surfactants such as sodium dodecylbenzenesulfonate, SDBS, has also been reported to produce graphene. The graphene monolayers are stabilized against aggregation by a relatively large potential barrier caused by the Coulomb repulsion between surfactant-coated sheets.

b. Intercalation of small molecules followed by mechanical exfoliation

Agglomeration in graphite can be reduced appreciably by incorporating small molecules between the layers of graphite or by noncovalently attaching molecules or polymers onto the sheets, generating graphite intercalation compounds (GICs). In GICs, the graphite layers remains unaltered with guest molecules located in the interlayer galleries. When the layers of graphite interact with the guest molecules by charge transfer, the in-plane electrical conductivity generally increases, but when the molecules form covalent bonds with the graphite layers as in fluorides or oxides the conductivity decreases as the conjugated sp^2 system is disrupted. Acetic acid, acetic acid anhydride, concentrated sulfuric acid, and hydrogen peroxide are the examples of few ultrasonic solvents. Among all those, concentrated sulfuric acid had been proved to be the best ultrasonic solvent to provide optimum condition for preparing the expandable graphite (EG) with ultrasound irradiation. Such sulfuric acid intercalated graphite compound consisted of layers of hexagonal carbon structure within which H_2SO_4 was intercalated. EG could be prepared by oxidation with either a chemical reagent or electrochemically in the intercalating acid. Graphite could expand up to a hundred times in volume at high temperature due to the thermal expansion of the evolved gases trapped between the graphene sheets. So it was reasonably assumed that oxidants and other molecules could enter in the interlayer space of EG more easily compared to natural graphite.

5.4.3.2 Chemical Vapor Deposition

In principle, CVD for obtaining graphene can be achieved in the following three different ways:

a. Thermal decomposition

During the process of thermal decomposition of hydrocarbons on transition metals, graphene growth occurs due to the precipitation of graphite from hydrocarbon species within the Ni film. The Ni film and the carbon atoms form a solid solution, resulting in an ultrathin graphene film (1–~10 layers) over the Ni surface [27]. This method allows the transfer of the produced film to alternative substrates, in our case a polycarbonate (PC), by wet-etching the Ni film. This results in a free-standing PC/graphene membrane that exhibits outstanding optical transparency and electrical conductivity. The ability to grow single and few-layer graphene with CVD is an important advantage. This technique can potentially enable the simple growth of graphene at particular locations and with desired geometries by controlling the catalyst morphology and position. The schematic of experimental setup is shown in Figure 5.17. An interesting feature of the CVD approach to synthesize graphene is the possibility for substitutional doping by introducing other gases, such as NH_3, during the growth. The nitrogen atoms can be doped into graphene as “pyridinic,” “graphitic,” and “pyrrolic” forms. These nitrogen-doped graphene (N-graphene) layers have demonstrated interesting properties.

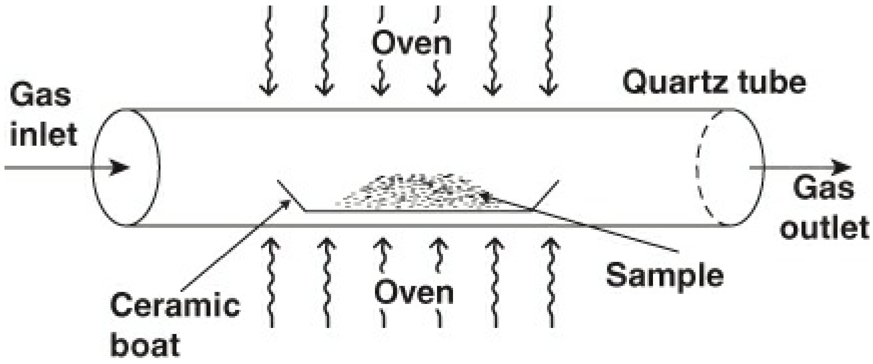

Figure 5.17 Schematic diagram of CVD reactor for preparing graphene.

b. Plasma-enhanced CVD

Plasma-enhanced chemical vapor deposition (PECVD) offers another route of graphene synthesis at a lower temperature compared to thermal CVD. Thick graphite structures were observed during the fabrication of “‘nanostructured graphite-like carbon’” using a dc discharge PECVD. The first report of the production of a monolayer and a few layers of graphene by PECVD involved a radio-frequency PECVD system to synthesize graphene on a various substrate where graphene sheets were produced from a gas mixture of 5–100% CH_4 in H_2 (total pressure 12 Pa), at 900 W power, and at 680 °C substrate temperature. The advantages of the plasma deposition include very short deposition time (<5 min) and a lower growth temperatures of 650 °C compared to the thermal CVD approach (1000 °C).

c. Thermal decomposition of SiC and other substrates

Producing graphene through ultrahigh vacuum (UHV) annealing of SiC surface has been an attractive approach especially for semiconductor industry because the products are obtained on SiC substrates and requires no transfer before processing devices. When SiC substrate is heated under UHV, silicon atoms sublimate from the substrate. The removal of Si leaves surface carbon atoms to rearrange into graphene layers. The thickness of graphene layers depends on the annealing time and temperature. The formation of “few-layer graphene” (FLG) typically requires few minutes annealing of the SiC surface at temperature around 1200 °C. More recently, vapor-phase annealing has been used to produce FLG on SiC. At the expense of a higher temperature (typically 400 °C above UHV temperature), this method leads to the formation of FLG on SiC with improved thickness homogeneity.

5.4.3.3 Chemically Derived Graphene

Chemically derived method essentially consists of oxidation of graphite flakes to graphite oxide (GO) via one of three principal methods developed by Brodie, Hummers, and Staudenmeier. Out of these Hummer's method is most common method; a typical preparation method is given in Box 5.1. The mechanism of the overall process to obtain graphene from graphite including oxidation of graphite, exfoliation, and reduction is shown in Figure 5.18.

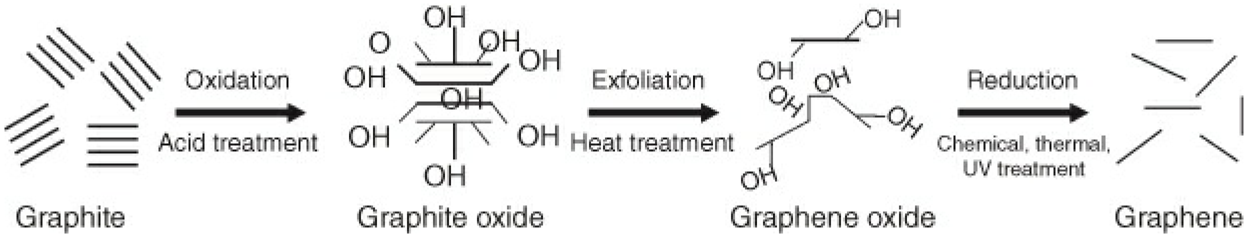

Figure 5.18 Schematic representation of graphite exfoliation process resulting in graphene.

Box 5.1 Hummer's method

A 10 g of graphite powder is dispersed in 230 ml of cold concentrated solution of sulphuric acid, and 30 g of potassium permanganate ($KMnO_4$) is added gradually with continuous stirring and simultaneously cooling the aqueous suspension so that the temperature does not exceed 293 K. The system is then kept at 30–40 °C for 30 min followed by slow addition of deionized water (230 ml). The addition of water causes a rapid increase in the solution temperature. As a precautionary measure, the temperature should be kept between 80 and 100 °C. Gradually the color of the solution becomes brownish yellow. Then, the suspension is stirred for 30 min at 90 °C by sealing the heat in the suspension. Now, 50 ml of hydrogen peroxide in 200 ml of distilled water is rapidly added. The solution is subjected to washing for around seven times with distilled water, then washed with 5% HCl for three times and subsequently with acetone (three times), and air-dried overnight at 65 °C (338 K). The graphite oxide (GO) thus obtained is converted to graphene oxide by its thermal exfoliation at ≥150 °C.

Compared to pristine graphite, GO is heavily oxygenated bearing hydroxyl and epoxy groups on sp^3 hybridized carbon on the basal plane, in addition to carbonyl and carboxyl groups located at the sheet edges on sp^2 hybridized carbon. Hence, GO is highly hydrophilic and readily exfoliated in water, yielding stable dispersion consisting mostly of single-layered sheets (graphene oxide). GO consists of graphene sheets decorated mostly with epoxide and hydroxyl groups. Rapid heating of GO results in its expansion and delamination caused by rapid evaporation of the intercalated water and evolution of gases from pyrolysis of the oxygen-containing functional groups. Such thermal treatment has recently been suggested to be capable of producing individual functionalized graphene sheets.

Graphene oxide on reduction gives graphene by one of the following methods:

a. Chemical reduction of graphene oxide

One of the processes of reduction of graphene oxide is by the addition of hydrazine as a reducing agent (Figure 5.19a and b). The process involves addition of hydrazine to a suspension of graphene oxide in deionized water. An anionic water-soluble polymer can be used during the reduction process, giving rise to stable aqueous dispersion which on ultrasonication for 30 minutes followed by drying at 100 °C results in reduced graphene oxide (RGO) [31].

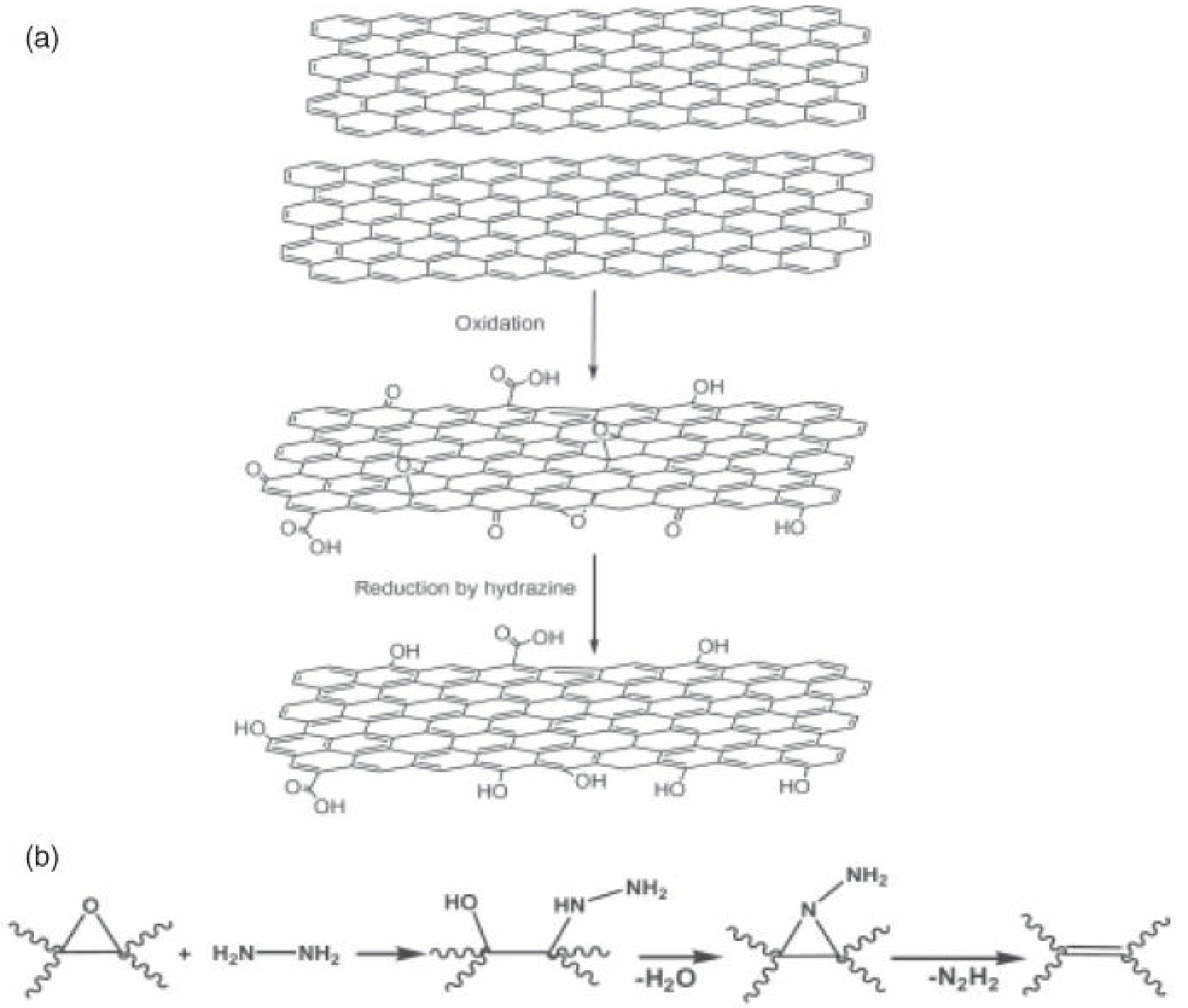

Figure 5.19 (a) Oxidation of graphite to graphene oxide and reduction to reduced graphene oxide. (b) A proposed reaction pathway for epoxy reduction by hydrazine.

Stankovich et al. [31], © 2007. With permission of Elsevier.

Another possible route to reduce GO is by using sodium borohydride ($NaBH_4$) in aqueous solution where sodium borohydride is more effective than hydrazine as a reductants of graphene oxide although it can be slowly hydrolyzed by water. The $NaBH_4$ treatment eliminates all the parent oxygen-containing groups, and the resultant solid becomes IR inactive like pure graphite. Other chemical reduction routes including using hydroquinone, gaseous hydrogen (after thermal expansion), and strongly alkaline solutions have also been investigated. Thermal reduction is another approach to RGO that utilizes the heat treatment to remove the oxide functional groups from graphene oxide surfaces. Recently, a simple one-step, solvothermal reduction method is reported to produce RGO dispersion in organic solvent. The solvothermal-RGO layers remained in a stable dispersion after the reaction. This approach provides a simple, low-temperature method to produce RGO.

b. Ultrasonication

Ultrasonication of graphite oxide, followed by filtration and drying, has proved to be a far better choice of obtaining graphene oxide from graphite oxide and graphene from graphene oxide followed by heat treatment at 500 °C for a period of 1 h. Firstly, the graphite oxide is dispersed in distilled water and subjected to ultrasonication in a sonicator for a period of 1 h, eventually after that graphene oxide can be acquired. Secondly, if some amount of heat is applied, around 500 °C to the ultrasonically obtained graphene oxide, then graphene particles can be obtained.

c. Thermal method: one-step heat treatment and two-step heat treatment

In order to obtain graphene thin films, very low concentration of oxygen-containing functional groups were produced by the reduction of graphene oxide nanosheets (prepared by using a chemical exfoliation) in a reducing environment and using two different heat treatment procedures (called one-step and two-step heat treatment procedures). The two-step method requires low temperatures of near about 500 °C, whereas in a one-step reducing procedure high temperature of 1000 °C is required for the formation of graphene thin films. It is also to be noted that the heating environment around the sample must be devoid of oxygen and can be replaced by Nobel gases such as argon or argon–hydrogen environment in the ratio of 4:1.

5.4.3.4 Electrochemical Synthesis

Electrochemical synthesis of graphene sheets is a one-step method and can be classified as a subcategory of chemical method described earlier. In this case, two high-purity graphite rods are used as electrodes. In the electrochemical cell, they are immersed in the electrolyte bath composed of ionic liquid and water. The schematic of the electrochemical cell is shown in Figure 5.20a and b. Static potential is applied to the two electrodes. Under these conditions, the anode is corroding and a black precipitate is gradually appearing in the reactor. After electrolysis, stable graphene dispersion is obtained. The supernatant can be directly filtered to form a graphene paper, or washed and dried to obtain bulk powders of graphene. The as-prepared graphene nanosheets are stable in aqueous solution, ready to be isolated as monolayer or multilayer graphene sheets.

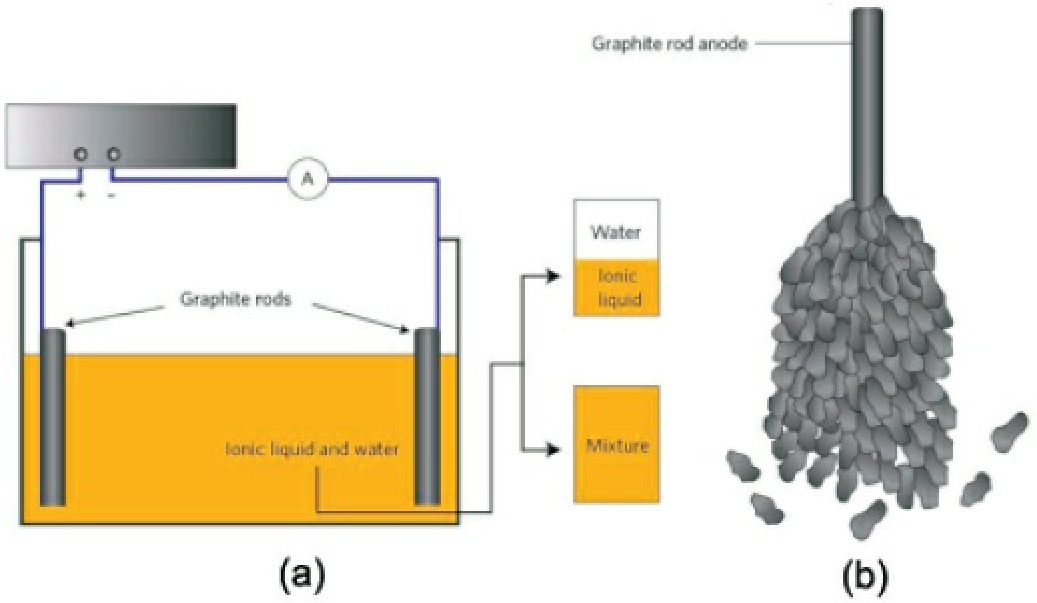

Figure 5.20 Experimental setup for electrochemical synthesis of graphene: (a) electrochemical cell; (b) exfoliation of chemically modified graphene sheets on graphite anode.

Liu et al. [32], © 2008. With permission of John Wiley.

5.4.3.5 Surface Modification of Graphene Oxide

The surface modifications to functionalize of graphene oxide can be achieved by two approaches, that is, covalent bonding and noncovalent bonding [32]. In covalent functionalization, oxygen functional groups on graphene oxide surfaces, including carboxylic acid groups, at the edge and epoxy/hydroxyl groups on the basal plane can be utilized to change the surface functionality of graphene oxide. Graphene oxide had been treated with organic isocyanates to give a number of chemically modified GO. Treatment of isocyanates reduces the hydrophilicity of graphene oxide by forming amide and carbamate esters from the carboxyl and hydroxyl groups of graphene oxide, respectively. The subsequent addition of nucleophilic species, such as amines or alcohols, produced covalently attached functional groups on graphene oxide via the formation of amides or esters. Figure 5.21 shows isocyanate treatment of GO where organic isocyanate reacts with the hydroxyl and carboxyl groups of the graphene oxide sheets. The resultant amine-functionalized graphene oxide has demonstrated various applications in optoelectronics, drug-delivery materials, biodevices, and polymer composites. The attachment of hydrophobic long, aliphatic amine groups on hydrophilic graphene oxide improved the dispensability of modified graphene oxide in organic solvents, while porphyrin-functionalized primary amines and fullerene-functionalized secondary amines introduced interesting nonlinear optical properties. The amine groups and hydroxyl groups on the basal plane of graphene oxide have also been used to attach polymers through either grafting-onto or grafting-from approaches. To grow a polymer from graphene oxide, an atom transfer radical polymerization (ATRP) initiator was attached to graphene surfaces. In addition to the carboxylic acid groups, the epoxy groups on graphene oxide can be used to attach different functional groups through a ring-opening reaction.

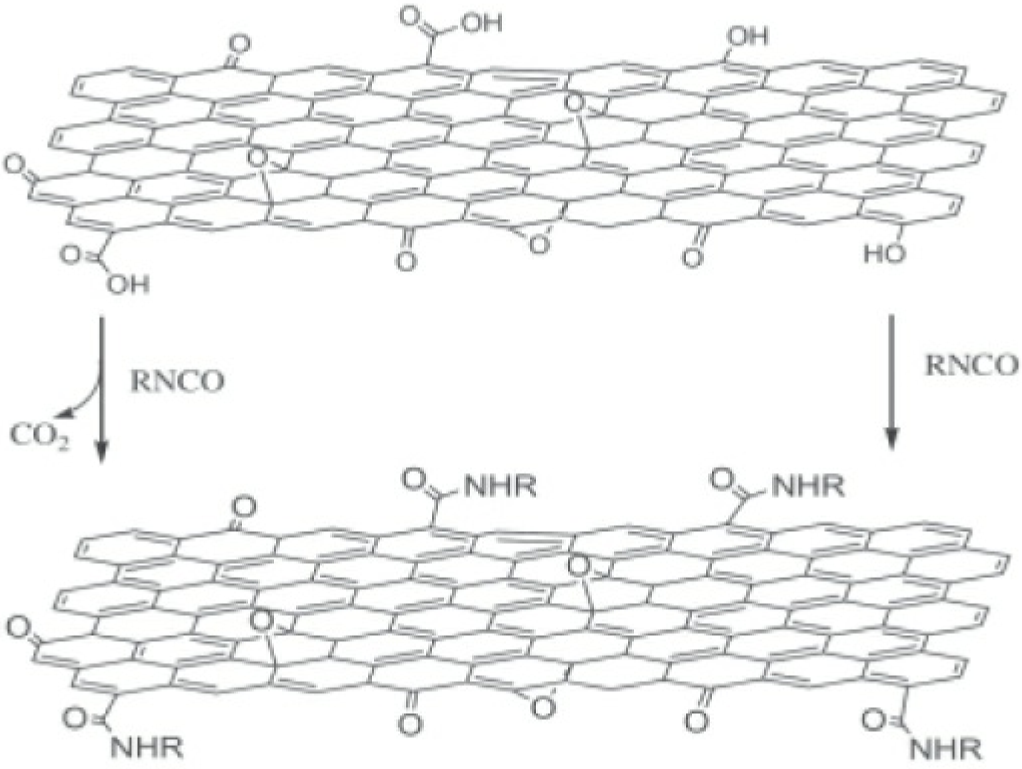

Figure 5.21 Isocyanate treatment of GO.

Stankovich et al. [33], © 2006. With permission of Elsevier.

The noncovalent functionalization of graphene oxide utilizes the weak interactions (i.e., p–p interaction, van der Waals interactions, and electrostatic interaction) between the graphene oxide and target molecules. The sp^2 network on graphene oxide provides p–p interactions with conjugated polymers and aromatic compounds that can stabilize RGO resulted from chemical reduction and produce functional composite materials. During the chemical reduction of graphene oxide, RGO nanosheets are stabilized via the p–p interaction between aromatic molecules and RGO nanosheets. Aromatic molecules have large aromatic plane and can anchor onto the RGO surface without disturbing its electronic conjugation, providing stability for RGO. Dye-labeled DNA has also been used to functionalize graphene oxide to detect proteins and DNA. In the presence of a target, the binding between the dye-labeled DNA and target molecule will alter the conformation of dye-labeled DNA and disturb the interaction between the dye-labeled DNA and graphene oxide. Such interactions will release the dye-labeled DNA from the graphene oxide, restoring of dye fluorescence.

5.4.4 Characterization of Graphene

Many modern spectroscopic, microscopic, and imaging techniques are being used to characterize graphene. We discuss here some of the important techniques with a particular emphasis on the identification of graphene.

5.4.4.1 Raman Spectroscopy

Raman spectroscopy is an important characterization tool used to probe the phonon spectrum of graphene [34]. Raman spectroscopy of graphene can be used to determine the number of graphene layers and stacking order as well as density of defects and impurities. The three most prominent peaks in the Raman spectrum of graphene and other graphitic materials are the G band at ~1580 cm^{-1}, the 2D band at ~2680 cm^{-1}, and the disorder-induced D band at ~1350 cm^{-1} as shown in Figure 5.22. The G band results from in-plane vibration of sp^2 carbon atoms and is the most prominent feature of most graphitic materials. This resonance corresponds to the in-plane optical phonons at the Γ point. The 2D band arises as a result of a two phonon resonance process, involving phonons near the K-point, and is very prominent in graphene as compared to bulk graphite. The D band is induced by defects in the graphene lattice (corresponding to the in-plane optical phonons near the K-point) and is not seen in highly ordered graphene layers. The intensity ratio of the G and D bands can be used to characterize the number of defects in a graphene sample. The line shape of the 2D peak, as well as its intensity relative to the G peak, can be used to characterize the number of layers of graphene present. Single-layer graphene is characterized by a very sharp, symmetric, Lorentzian 2D peak with intensity greater than twice the G peak. As the number of layers increases, the 2D peak becomes broader, less symmetric, and decreases in intensity.

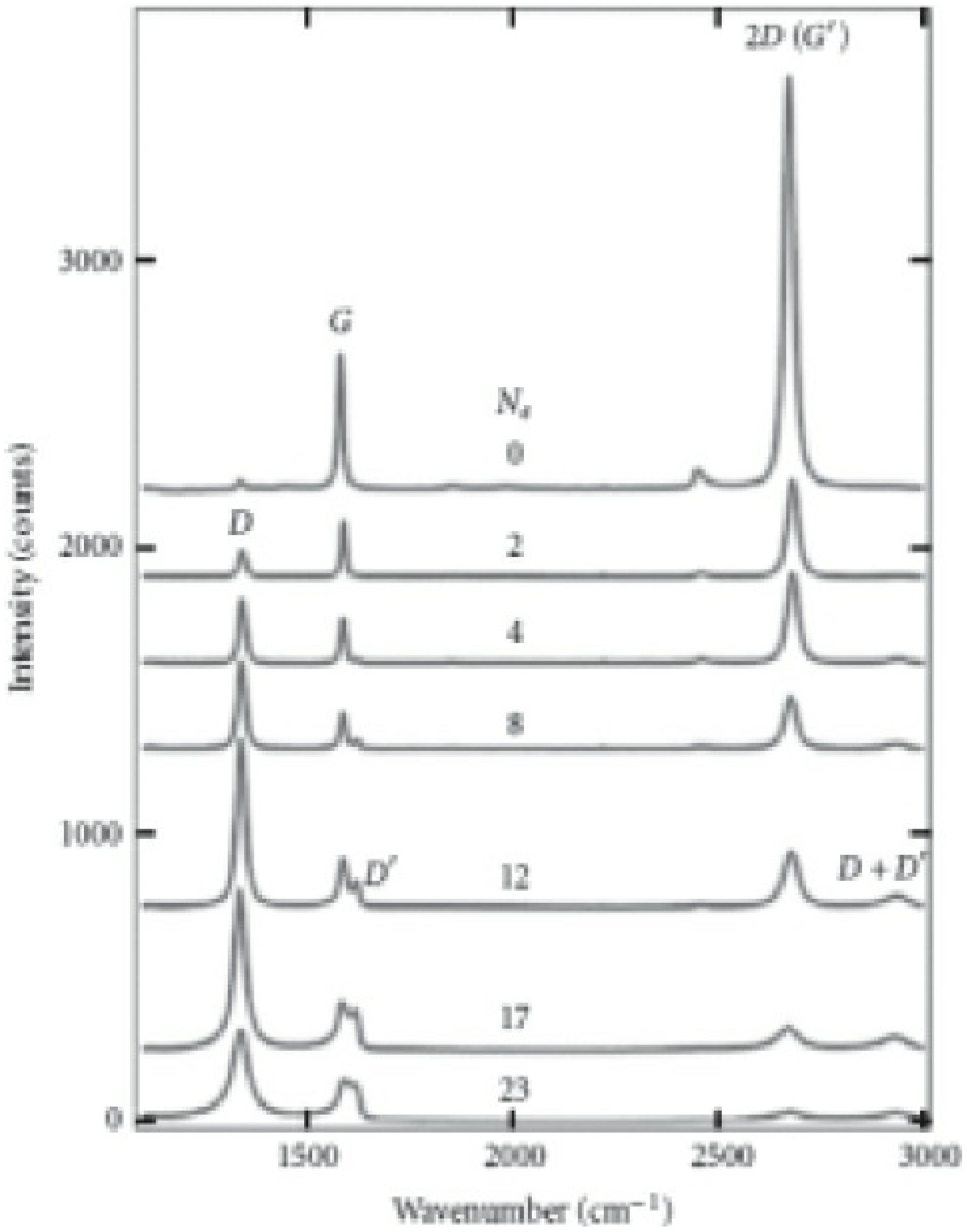

Figure 5.22 Raman spectra of graphene.

5.4.4.2 Optical Microscopy

Monolayer graphene becomes visible on SiO_2 using an optical microscope. The contrast depends on the thickness of SiO_2, the wavelength of light used, and the angle of illumination. This feature of graphene is useful for the quick identification of few- to single-layer graphene sheets and is very important for mechanical exfoliation. Figure 5.23a shows the optical contrast of one, two, three, and four layers of exfoliated graphene on a 285-nm thick SiO_2-on-Si substrate.

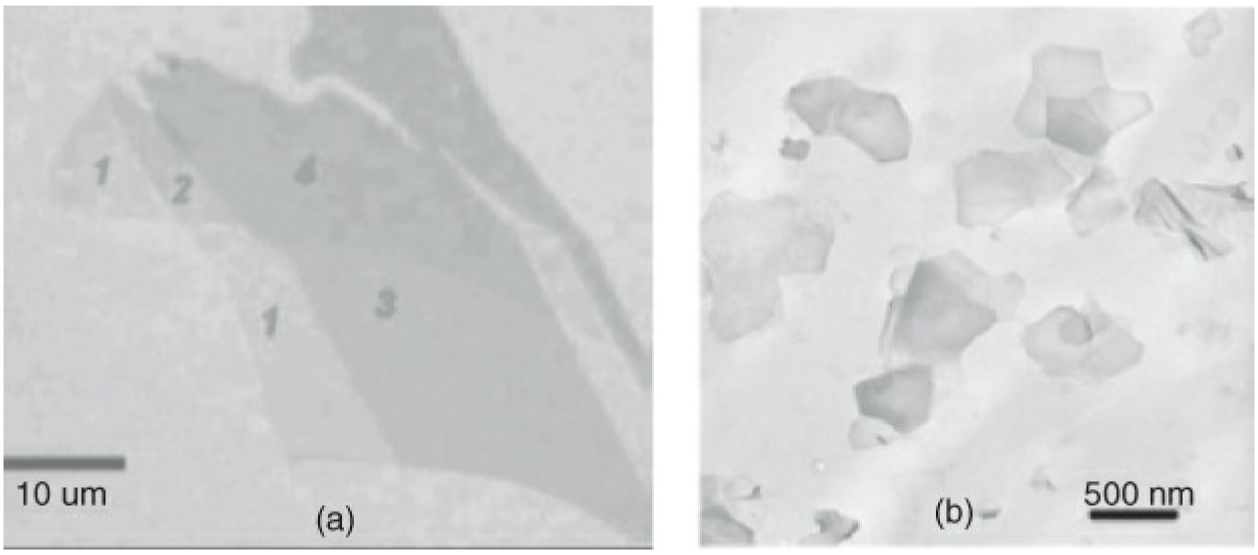

Figure 5.23 (a) Optical image graphene flakes showing one, two, three, and four layers; (b) TEM image of graphene showing hexagonal lattice structure with pentagon–heptagon pairs.

Ni et al. [35], © 2007. With permission of ACS.

5.4.4.3 Electron Microscopy

Transmission electron microscopy has been used to image single-layer graphene suspended on a microfabricated scaffold. It was found that single-layer graphene displayed long-range crystalline order despite the lack of a supporting substrate. Suspended graphene was found to have considerable surface roughness with out-of-plane deformations of up to 1 nm. Aberration-corrected annular dark-field scanning transmission electron microscopy (ADF-STEM) was used in order to image CVD-grown graphene suspended on a TEM grid. Observing a TEM image of graphene obtained by electrochemical method, it is found that along the grain boundaries, hexagonal lattice structure breaks down and the grains are “stitched together” with pentagon–heptagon pairs as seen in Figure 5.23b.

5.4.5 Applications

Graphene, a one-atom-thick sheet of sp^2-hybridized, hexagonally arranged carbon atoms, has triggered tremendous interest due to its high electron mobility, superb mechanical flexibility, and unique optical characteristics. Graphene-based applications such as transparent electrodes, solar cells, and ultrafast photodetectors, and phototransistors have been recently demonstrated [34–36]. The linear dispersion of graphene and the absence of a band gap, along with its unusual doping properties, make it a material of extraordinary potential for optoelectronic device applications. Graphene has a number of properties that makes it interesting for several different applications. It is an ultimately thin, mechanically very strong, transparent, and flexible conductor. Its conductivity can be modified over a large range either by chemical doping or by an electric field. The mobility of graphene is very high, which makes the material very interesting for electronic high-frequency applications. Recently, it has become possible to fabricate large sheets of graphene. Using near-industrial methods, sheets with a width of 70 cm have been produced. Since graphene is a transparent conductor, it can be used in applications such as touch screens, light panels, and solar cells, where it can replace the rather fragile and expensive indium tin oxide (ITO). Flexible electronics and gas sensors are other potential applications. The quantum Hall effect in graphene could also possibly contribute to an even more accurate resistance standard in metrology. Graphene is not only lighter, stronger, harder, and more flexible than steel, it is also a recyclable and sustainably manufacturable product that is ecofriendly and cost-effective in that would allow the development of lighter and stronger cars and planes that use less fuel. Large aerospace companies such as Boeing have already started to replace metals with carbon fibers and carbon-based materials, and graphene paper with its incomparable mechanical properties would be the next material for them to explore.

5.5 Carbon Nano-Onions

Carbon nano-onions (CNOs), a fullerene-related material having concentric graphitic shells, represent another new allotropic nanophase of carbon materials. It is essentially a multiwall fullerene since center shell is a C_{60} molecule. CNOs have already been shown to offer a variety of potential applications such as solid lubrication, electromagnetic shielding, fuel cells, heterogeneous catalysis, gas and energy storage, and electro-optical devices owing to their outstanding chemical and physical properties. According to a recent study, CNOs can also be used to produce ultrahigh power micrometer-sized supercapacitors due to their accessible external surface area for ion adsorption.

Since the first observation of the onion-like structure by Ugarte in 1992, who obtained them by intense electron irradiation of carbon soot, several methods have been reported to prepare CNOs, for example, by irradiating carbon material consisting of different carbon nanostructures (fullerenes, nanotubes, amorphous carbon), high-temperature annealing of diamond nanoparticles under vacuum, high-dose carbon-ion implantation into copper and silver, and arc discharge between two graphite rods immersed in water. In addition, CVD was also considered as a viable method to synthesize CNOs. Other methods to synthesize CNOs include laser irradiation, shock compression, and high-energy ball milling. However, most of the methods above-mentioned require high-energy input, and CNOs are sometimes of low yield or just as a by-product. For applications such as fuel-cell electrodes, large quantities (kilograms) of the material are desired. Therefore, how to economically synthesize CNOs in a large scale is of great importance for their wide applications. Recently, a simple, efficient, and economical route has been reported for large-scale preparation of CNOs with uniform morphology and size [37] via reaction between CaC_2 and $CuCl_2{\cdot}2H_2O$ at 600 °C. A typical procedure is included in Box 5.2. The morphology of as-obtained CNO products observed by FESEM is shown in Figure 5.24a. The product comprises numerous quasispheres of about 30 nm in diameter; no other nanocarbon structures such as CNTs are detected. Figure 5.24b is the EDX spectrum taken from the spheres, from which there is no detectable metal catalyst (Cu) or other impurities except for C and a little O resulting from absorption, indicating the high purity of the spheres. The examination by HRTEM (Figure 5.24c–e) demonstrates that the spheres have an onion-like structure. The interplanar spacing of 0.34 nm corresponds to that of the (0 0 2) plane of graphite. The short-range order or turbostratic graphite structure gives rise to concentric graphite layers around a hollow and irregular core about 5 nm in diameter. The corresponding selected area electron diffraction (SAED) pattern (inset of Figure 5.24d) reveals the poor graphitization of the CNOs. It is worthwhile to note that Cu-encapsulating CNOs can hardly be observed in the product even by careful TEM examination.

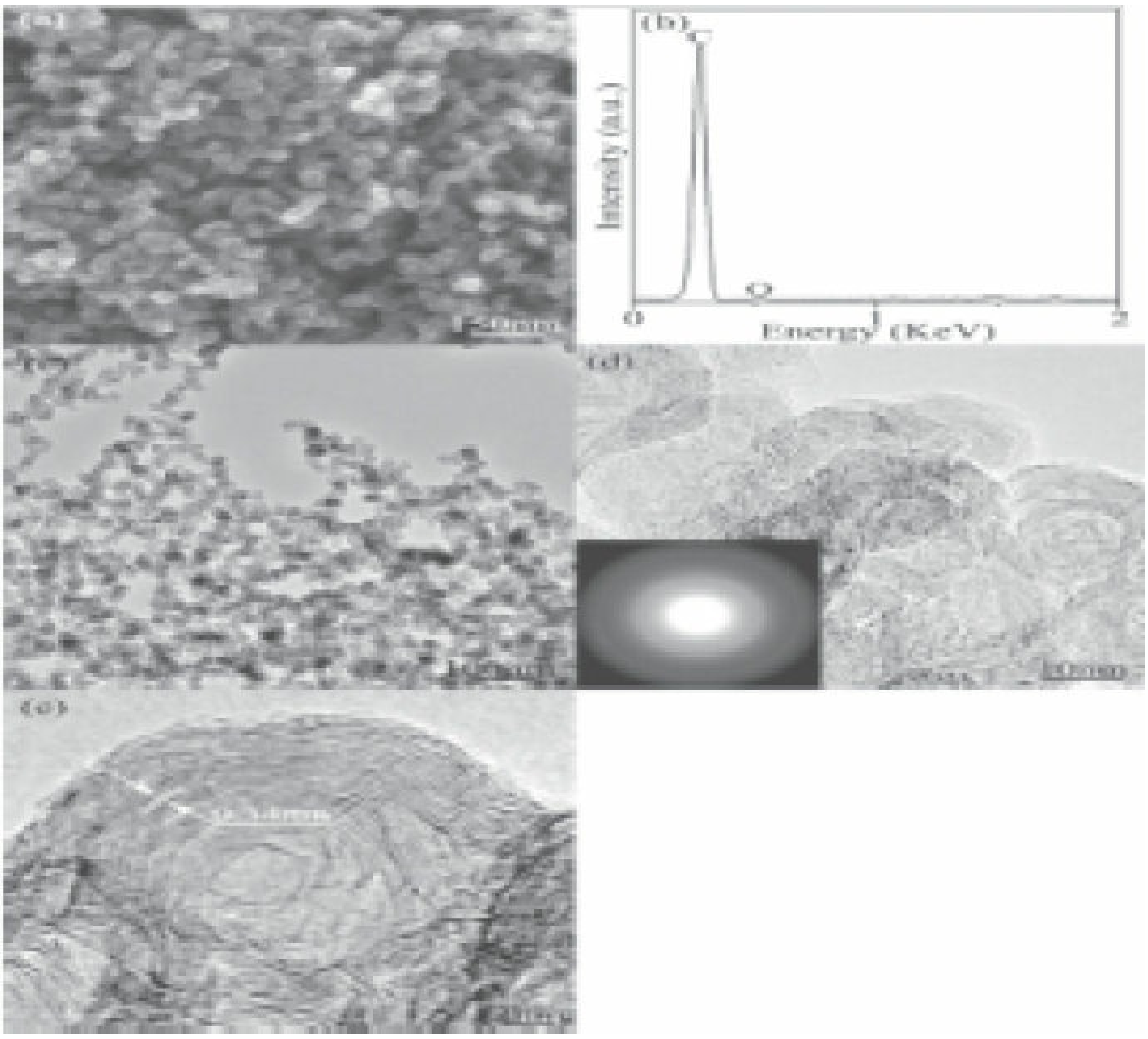

Figure 5.24 Carbon nano-onions (a) FESEM image; (b) EDX spectrum; and (c–e) HRTEM images (inset is the corresponding SAED pattern).

Han et al. [37], © 2011. With permission of ACS.

Box 5.2 Preparation of CNOs

In a typical procedure, 10 g (0.059 mol) $CuCl_2 \cdot 2H_2O$ and 3.2 g (0.05 mol) CaC_2 were put into a stainless steel autoclave of 30 ml capacity. The amount of $CuCl_2 \cdot 2H_2O$ was slightly in excess to ensure the complete reaction of CaC_2. The autoclave containing the raw materials was sealed tightly and heated in an electric oven to 600 °C and maintained for 10 h at this temperature. When the autoclave was cooled naturally to an ambient temperature, the products in the autoclave were collected and primarily washed several times with a mixed solution of ammonia ($NH_3 \cdot 3H_2O$) and carbon tetrachloride (CCl_4) to remove the by-product copper and then rinsed successively with dilute hydrochloric acid and deionized water until all soluble materials were removed. After drying at 60 °C for 10 h, black powders were ultimately obtained. The irradiation of convergent electron beam onto carbon blacks leads to remarkable improvements in the crystallinity of the primary particles and at the same time to disintegration of agglutinate structures.

In spite of the characteristic structure equivalent to MWCNTs with zero length, carbon nano-onions have never been isolated in macroscopic amounts, impeding physical or chemical characterization of bulk or dispersion properties. However, their atomistic structures are well investigated by calculation, and their bulk forms have often been observed under electron microscopes. All the shells in an onion structure are akin irrespective of its size. In this regard, a mixture of nano-onions having a size distribution is similar to homologous mixtures of hydrocarbons such as kerosene and gasoline. Nanofractionation of the particles according to diameter is a challenging subject. There will be a number of potential applications worth examining, once carbon nano-onions are isolated. While some have made a “sour grapes” like explanation that bunched agglutinates of carbon blacks are favorable for reinforcing rubber by tangling well with the polymer backbones, it is also likely that nanodispersion of primary particles provides even a better effect due to the incomparably larger total surface area. The unique structures composed of nested fullerenes will give rise to novel properties suitable for solid-state optical limiter, solar heat storage, or in general as the substitute of graphite micropowder.

5.6 Carbon Nanofibers

Nanofibers consist of the graphite sheet completely arranged in various orientations [38]. One of the most outstanding features of these structures is the presence of plenty of sides, which in turn make sites available for chemical or physical interaction, especially adsorption. Carbon nanofibers can be obtained in size ranging from 5 to several hundred microns on length and between 100 and 300 nm in diameter. From electronic microscopy studies, it is possible to define sequence of the events leading to the formation of carbon nanofibers.

Surface studies have revealed that certain faces prefer precipitation of the carbon in the form of the graphite. The choice of the catalyst, the relation of the hydrocarbon/hydrogen reactant mixture, and reaction conditions control the morphological qualities, the degree from crystallinity, and the orientation of the precipitated graphite crystallites with regard to the fiber axis. The space between graphite layers is 0.34 nm. This spacing can be increased by introducing selected groups between the layers, a process known as intercalation, thereby generating new types of sophisticated molecular sieves. Such unique structural conformations found in carbon nanofibers open up numerous possibilities in the fabrication of new materials. It is possible to make nanofibers, which will consist completely of plates of graphite, that is, show double structure depending on crystallographic to orientation of catalyst faces, which exist in the metal–carbon interface. Over the past few years, many researchers have performed a very comprehensive evaluation of the potential of a number of metals and bimetallic as catalysts for the production of carbon nanostructures; nickel- and iron-based alloys are among the most effective catalysts for the reaction. The “herringbone structures” of the carbon nanofiber are frequently found when alloy catalysts are used in the nanofiber process. It is possible to tailor this arrangement and obtain two further conformations where graphite platelets aligned in directions parallel and perpendicular to the fiber axis [38]. A more detailed appreciation of these structures can be seen from the respective 3D models, where the darker geometric shapes represent the metal catalyst particles responsible for generating these conformations. The metal catalyst particles (<0.4%) can be easily removed by acid treatment, thus producing high-purity graphite nanofibers (Figure 5.25).

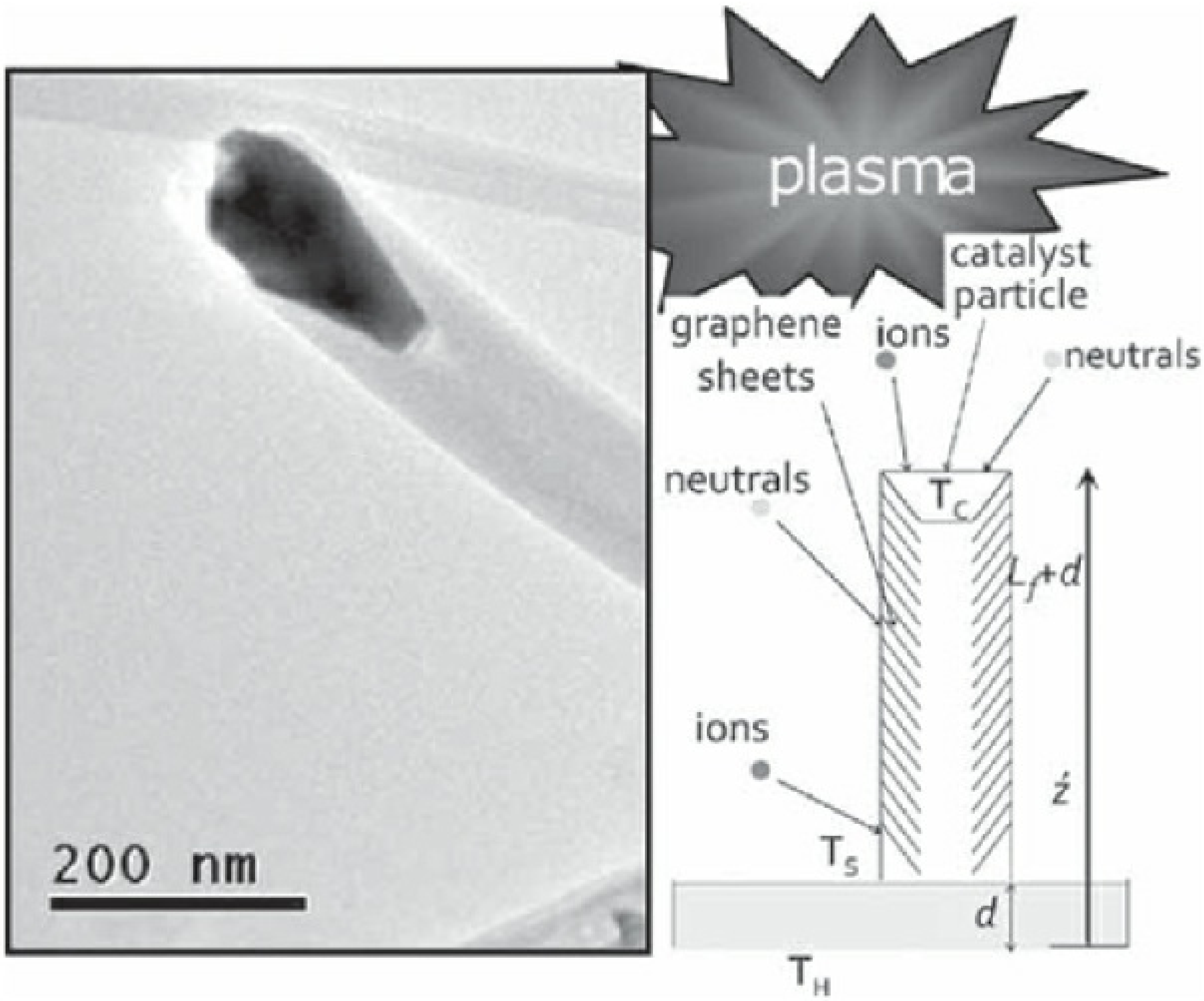

Figure 5.25 HRTEM image along with schematic representation of carbon nanofibers with their graphene sheets in “parallel.”

Mehdipour et al. [38], © 2011. Reprinted with permission of John Wiley and Sons.

5.7 Carbon Black

Carbon black is pure elemental carbon in the form of colloidal particles. It is produced by incomplete combustion or thermal decomposition of gaseous or liquid hydrocarbon under controlled conditions. The furnace black and thermal black processes are used to make carbon black, but the furnace black process is the most common commercial process. The average particle size of carbon black is of a few nanometers. The primary use of carbon black is in rubber products (approximately 90%), mainly tires and other automotive rubber products such as hoses, gaskets, and coated tubes. About 9% of carbon black is used for pigment in toners and inks, and the remaining 1% is used as an ingredient in hundreds of diverse applications. Much smaller amounts of carbon black are used in the manufacture of dry-cell batteries. Essentially carbon blacks are the pure soot and are produced by the pyrolysis of carbonaceous industrial waste [39]. The pyrolysis furnace, the core of the whole process, is a huge empty tube of several dozen meters in length, ca. 2 m in diameter, and made of heat-resistant bricks as illustrated in Figure 5.26. Classically, process produces chemically pure carbon that turned out to be a sort of fullerene. Coal gas or natural gas is mixed with air and the mixed gas introduced from one end of the tube, compression-ignited, and the high-temperature flame (1800–2000 °C in the highest case) thus generated is blown at a supersonic flow toward the other end. A little downstream, carbon-containing industrial waste such as oil cokes or residual oil, fluidized by preheating at 200–300 °C, is sprayed into the high-temperature current of flame to produce soot through cracking. When the soot thus produced grew to a desired size, water is sprayed in further downstream to extinguish combustion and suspend the cracking processes, and the soot is gathered after cooling by passing through a long vertical pipe. With the knowledge on the formation mechanism and on the structure of primary as well as secondary particles of carbon blacks, their potential applications can be derived.

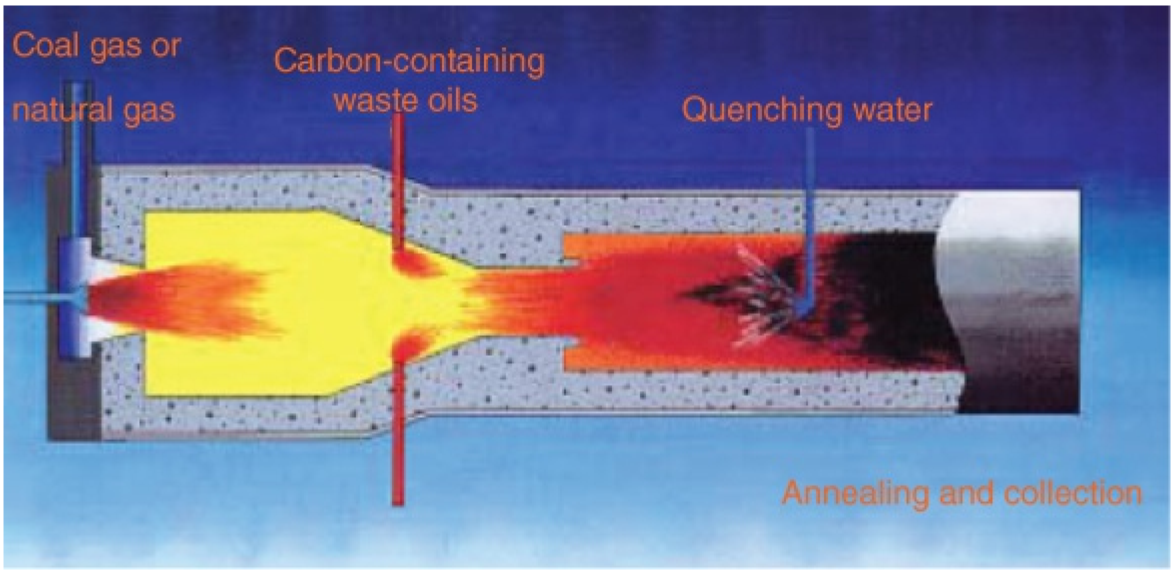

Figure 5.26 Pyrolysis furnace for the synthesis of carbon black.

Ozawa and Ōsawa [39], © 2006. With permission of Elsevier:Dordrecht.

5.7.1 Crystallinity

The biggest defect of carbon blacks of industrial carbon source is low crystallinity. How can the degree of crystallization be improved? Heating has been the traditional step to increase the crystallinity of poorly crystalline or amorphous carbons. The process is also called graphitization because graphite was the goal of the highest crystalline carbon. Now that fullerenes are recognized as another crystalline form of carbon, which attains stability due to the closed structure and favorable disposition of pentagonal defects, a new strategy can be formulated to increase the crystallinity of nongraphitizing carbon so as to convert carbon black into the most stable isomer of the corresponding fullerene analog on heating above 3000 °C. The results of heating sharply contrasts with those of electron-beam irradiation, wherein agglutination are destroyed and primary particles are crystallized into nano-onions without any void. Annealing of carbon black at high temperature is much slower process than irradiation of high-current electron beam to give different products. Clearly the polyhedral particles with pentagonal defects are aligned vertically to absorb uneven interlayer steric energy. Interactions are more stable than the carbon nano-onion where interlayer steric energy is absorbed by skeletal deformations to a sphere. The fate of deformed outer layers is unclear under these two different modes of annealing; the slow heating probably crystallized the outermost layers as well, which should then become more resistant against destruction. On the contrary, rapid absorption of high-density electron beam at the surface of agglutinate must have led to destruction rather than crystallization. Only the high-density electron beam is mentioned, but high-energy beams of atoms such as proton and carbon should give similar but more pronounced effects compared to the former. The success of isolating carbon nano-onions or any other form of multishell fullerenes from carbon black is of concern since it is rather difficult to keep them dispersed in nanosize form.

5.7.2 Homogeneity and Uniformity

Even though the structural homogeneity of carbon blacks is almost perfect, the structure itself is of low crystallinity. Furthermore, the nanostructure of carbon black is not uniform, consisting of highly defective primary particles and deformed outer layers on the surface of agglutinates. The unique structures composed of nested fullerenes present in carbon black will give rise to novel properties suitable for solid-state optical limiter, solar heat storage, or in general as the substitute of graphite micropowder.

5.8 Nanodiamond

Diamond is a true gift of nature and is well known as the hardest natural material. The properties of diamond and its practical and technological applications have been extensively investigated for centuries. Elemental carbon has been known since prehistory, and diamond is likely to have been mined in India already 2000 years ago. But its utilization could date as far back as 6000 years ago, as suggested by recent archaeological discoveries of diamond utensils in China. It is widely used in the jewelry and abrasion industries. Unlike graphite, diamond is a semiconductor similar to silicon and gallium arsenide, which is the dominant material in the electronics industry and used in lasers and other optical devices.

In the last two decades, a “new” form of diamond has attracted much attention [40,41,42a]: **nanometer-sized diamond** particles (Figure 5.27a and b). Such particles were formed even before the solar system and have been found in primitive meteorites, protoplanetary nebulae, interplanetary dust, and in several earth sediments dated around 13,000 years bc. The study of the origin and formation of nanodiamond particles in and from outer space may shed light on several problems, including the understanding of possible impacts of meteorites (carbonaceous chondrites) with our planet. On the other hand, the study of the relative stability of **diamondoid** (hydrocarbon molecules with a diamond structure, terminated by hydrogen atoms shown in Figure 5.27c), is helpful to assess the ultimate depth of crude-oil preservation on earth. The first diamondoid (adamantane) was identified in crude oil in 1933, but it is only a few years ago that higher molecules (with 22 C atoms or more) were recovered from oil.

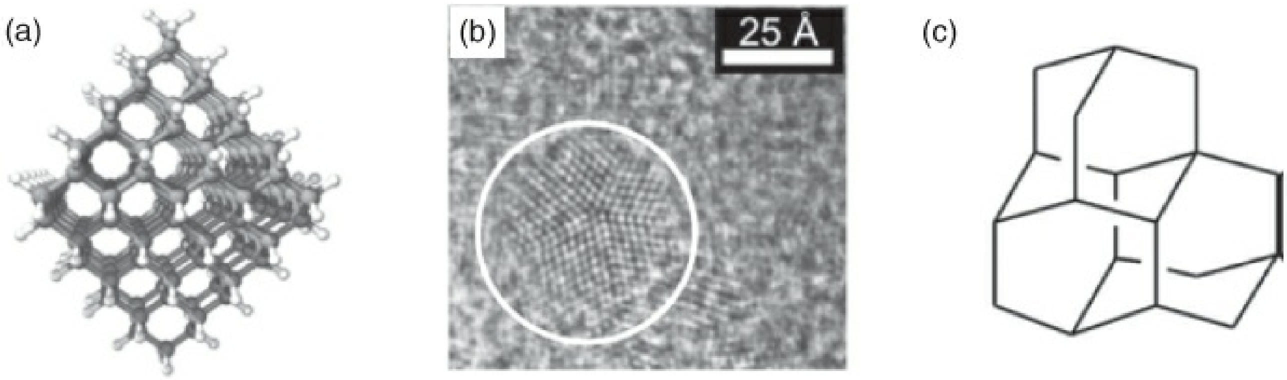

Figure 5.27 Nanodiamond: (a) octahedral model. Krueger [42], © 2008. With permission of RSC; (b) meteoritic diamond with multiple twinning. Daulton et al. [40], © 1996. With permission of Elsevier; (c) triamantane, a diamondoid molecule. Krueger [42], © 2008. With permission of RSC.

5.8.1 Synthesis of Nanodiamond

There are several methods for the synthesis of nanodiamonds (ND). They can be synthesized by the detonation technique, laser ablation, high-energy ball milling of high pressure high temperature (HPHT), CVD, autoclave synthesis from supercritical fluids, and ion irradiation of graphite and ultrasound cavitations. Out of all these methods listed, the first three are used commercially for the synthesis of NDs.

a. ***Detonation Technique***

Currently, nanodiamonds are made by detonating an explosive in a reactor vessel to provide heat and pressure. The nanodiamonds synthesized by the detonation technique are often termed as the ultradispersed diamonds (UDD). The nanodiamond can be synthesized by the detonating mixture of TNT, that is, trinitrotoluene ($C_6H_5N_3O_6$) and hexogen ($C_6H_6N_6O_6$), that is, RDX and from the remaining soot of the explosion.

The detonation takes place in the closed chamber filled with water (ice) as coolant or inert gas. The diamond yield after detonation crucially depends on the synthesis condition and especially on the heat capacity of the cooling medium in the detonation chamber (water, air, CO_2). The higher the cooling capacity, the larger the diamonds yield (which can reach 90%). The diamond particles are then removed and purified from contaminating elements massed around them. The process is quick and cheap, but the nanodiamonds aggregate and are of varying size and purity.

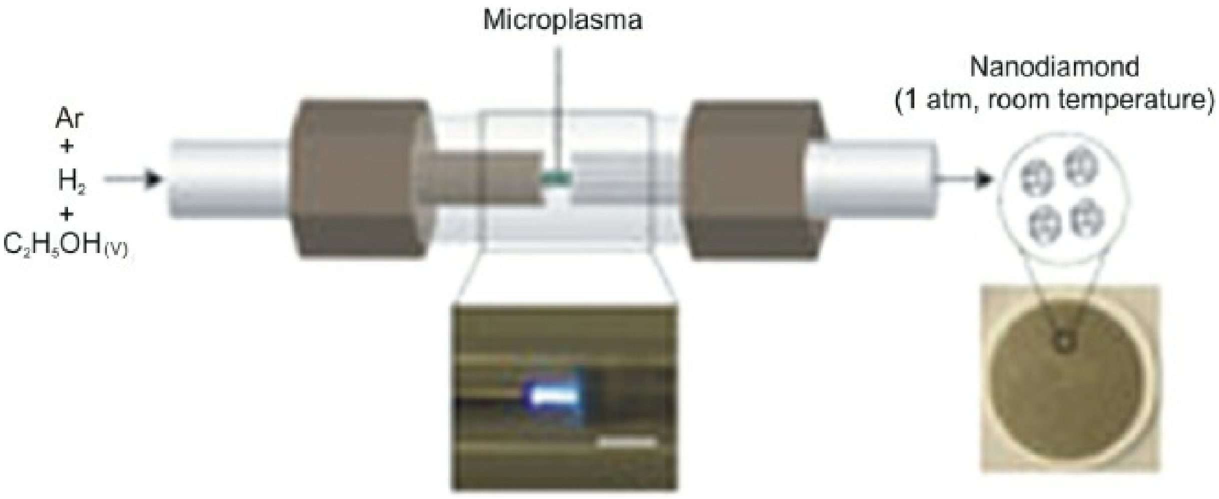

Figure 5.28 Formation of nanodiamond at near-ambient conditions via microplasma dissociation of ethanol.

Kumar et al. [41], © 2014. With permission of NPG.

b. ***Chemical Vapor Deposition*** CVD technique under some conditions generates high-quality diamond films. The deposited film is no longer a microcrystal assembly, but a smooth film of much smaller diamond particles. A typical CVD method involves the injection of a mixture of methane and hydrogen gas in a plasma reactor. The diamond film, with variable morphologies, is deposited on a silicon substrate. CVD-deposited diamond films are distinguished into three categories: microcrystalline diamonds (0.5–10 mm), nanocrystalline diamonds (50–100 nm), and **ultrananocrystalline diamonds (UNCD**) (2–5 nm). Diamond particles of 50 nm diameter are formed by applying a negative dc bias voltage during the first minutes of the deposition from a mixture of 4% CH_4 in H_2. The nanometric diamonds appear to represent the first stage of diamond growth, as long deposition times show them coalesce to form a microcrystalline diamond film. Nanocrystalline diamond crystals with a typical size of 50–100 nm are produced by hollow cathode arc plasma CVD or by direct current glow discharge-assisted CVD, among many other experiments. Replacing the majority of hydrogen by argon (typical 1% hydrogen) in the plasma yields the deposition of a smooth film of nanoparticles of only a few nanometers in size. The procedure has been perfected over the years and now UCND films are used for several applications. For example, for MEMS, diamond nanocrystals can also be synthesized from a suspension of graphite in organic liquid at atmospheric pressure and room temperature using ultrasonic cavitation. The yield is approximately 10%. An alternative synthesis technique is irradiation of graphite by high-energy laser pulses. The structure and particle size of the obtained diamond is rather similar to that obtained in explosion. In particular, many particles exhibit multiple twinning.

c. *Microplasma Method* It usually requires high pressures and high temperatures to convert graphite to diamond or a combination of hydrogen gas and a heated substrate to grow diamond rather than graphite. Recently, the fact idea that at nanoscale, surface energy makes diamond more stable than graphite has been used to make nanodiamond on a lab bench at atmospheric pressure and near room temperature directly from a gas; it require no surface to grow on. In this method, microplasma dissociates ethanol vapor. The resulting nanodiamond particles are collected and dispersed in solution. Electron microscope image reveals nanosized diamond particles (Figure 5.28). Some of the common physico-chemical properties of nanodiamonds are briefly discussed here.

5.8.2 Properties

The nanodiamonds have a diamond cubic lattice, thus the name “nanodiamond.” Nanodiamonds have become a focus of extensive study due to advances in synthesis techniques, such as CVD and detonation synthesis. It has been shown that nanodiamonds can coexist along with bucky-diamonds (carbon-onions), when annealed at high temperatures or treated by electron-beam radiation. Here, the outer surfaces of the diamond nanocrystals undergo a graphitization process, forming a carbon-onion structure, as a transition from sp^3 to sp^2 type bonds occurs. This graphitization process, which occurs due to dangling bonds appearing at the diamond's outer surfaces, was observed both experimentally and theoretically. The same studies have also shown that hydrogenation of the nanodiamond surfaces may prevent such graphitization by the elimination of the dangling bonds, thus stabilizing the crystal structure.

Recently, chemical doping of nanodiamonds has been studied extensively aiming to control their physical properties and enable the design of nanoscale diamond-based semiconductors and fluorescent biomarkers with the desired physical properties. Apart from chemical doping, several experimental studies have addressed the issues of surface functionalization exploring the possibility to enhance solubility in polar organic solvents and reduce aggregation of the nanoparticles in physiological conditions, as well as to create platforms for catalysis and linkage to organic and bioorganic materials material as shown in Figure 5.29. Precise control over surface chemistry requires a sample of purified nanodiamond with only one kind of functional group attached to its surface. Nanodiamond terminated with carboxylic groups (ND-COOH) is a common starting material.

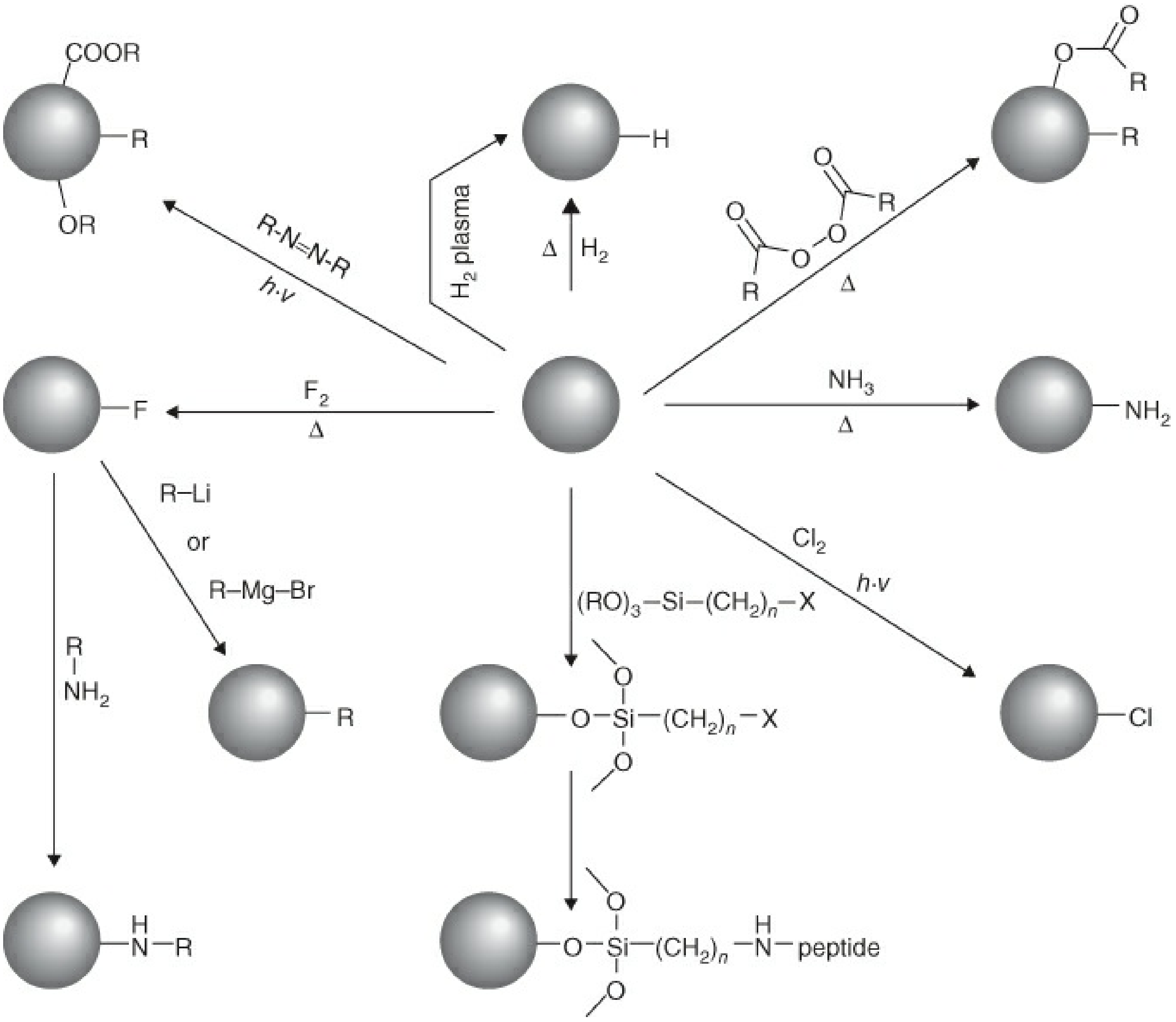

Figure 5.29 Surface functionalization of nanodiamond yields various covalently modified derivatives with different terminal groups for further surface modification.

Krueger [42], © 2008 With permission of Royal Society of Chemistry.

Hardness: The hardness of the diamond is about 50 times more than that of the titanium and stainless steel. The hardness of diamond makes its useful in cutting tools and implants.

Thermal stability: Diamond can withstand very high temperatures.

Chemical inertness: Alloy of Ti_6Al_4V coated with ND films show that the diamond films have a very good chemical resistance to the corrosive liquids.

Adsorption: NDs also have exceptional adsorptive properties they can adsorb water up to four times their own weight. Each carbon atom on the surface of ND has at least one free electron, which may bind to elements such H, O, or N. This makes NDs an excellent adsorbent for amino acids, proteins, platelets, and DNA.

Optical properties: Presence of a nitrogen atom next to a vacancy in nanodiamond known as Nitrogen-vacancy (NV) centers leads to useful fluorescence properties. Nanodiamonds emit bright fluorescence at 550–800 nm from nitrogen-vacancy centers produced by high-energy ion-beam irradiation and subsequent thermal annealing. The emission, together with no cytotoxicity and easiness of surface functionalization, makes nanosized diamonds a promising fluorescent probe for single-particle tracking in heterogeneous environment as well as can be used as biomarkers and biolabels.

Biocompatibility: Nanodiamonds with size of 2–10 nm are not toxic to a variety of cells through mitochondrial function and luminescent ATP production assays. It was found that morphology of cells remain unaffected with incubation with NDs. Moreover, it has excellent optical properties to be used as biolabel or biomarker. Chemical modification of diamond surface is essential for diamond to be applied as potential biosensor or biochip or a substrate to immobilize biological molecules.

5.8.3 Applications

In addition to geological and astrophysical interest, nanometer-sized diamonds have attracted the interest of the nanoscience and nanotechnology communities, for the potential application of nanodiamond films as bright, low-voltage (cold) cathodes and light emitters and of diamondoids as electron emitters. The exceptional hardness, fracture strength, and inertness of ultrananocrystalline diamond films, together with their smooth surface, make them unique materials for miniaturized mechanical systems and devices (MEMS). Such devices include cantilevers and gears, and nanodiamond MEM devices have already been successfully produced. The electrochemical properties of diamond make it an interesting material for sensing applications in sensor arrays and “lab-on-a-chip.”

Nanodiamond powder has been adopted for many industrial uses such as for polishing, coating, lubricant additives, and catalysts due to its excellent thermal and chemical stability combined with the superhard nature. Due to the properties of nontoxicity and high biocompatibility, it has also attracted considerable attention on some new applications, especially in the biomedical fields, such as imaging, diagnostics, and drug or gene delivery [43]. Figure 5.30 illustrates effective use of cancer treatment drug by forming a nanodiamond-drug composite The success of nanodiamond materials in biomedical applications stems from the fact that many small molecules such as proteins, antibodies, therapeutics, and nucleic acids can bind electrostatically to the surface of nanodiamonds, making it an ideal candidate for use in drug delivery and surgical implants.

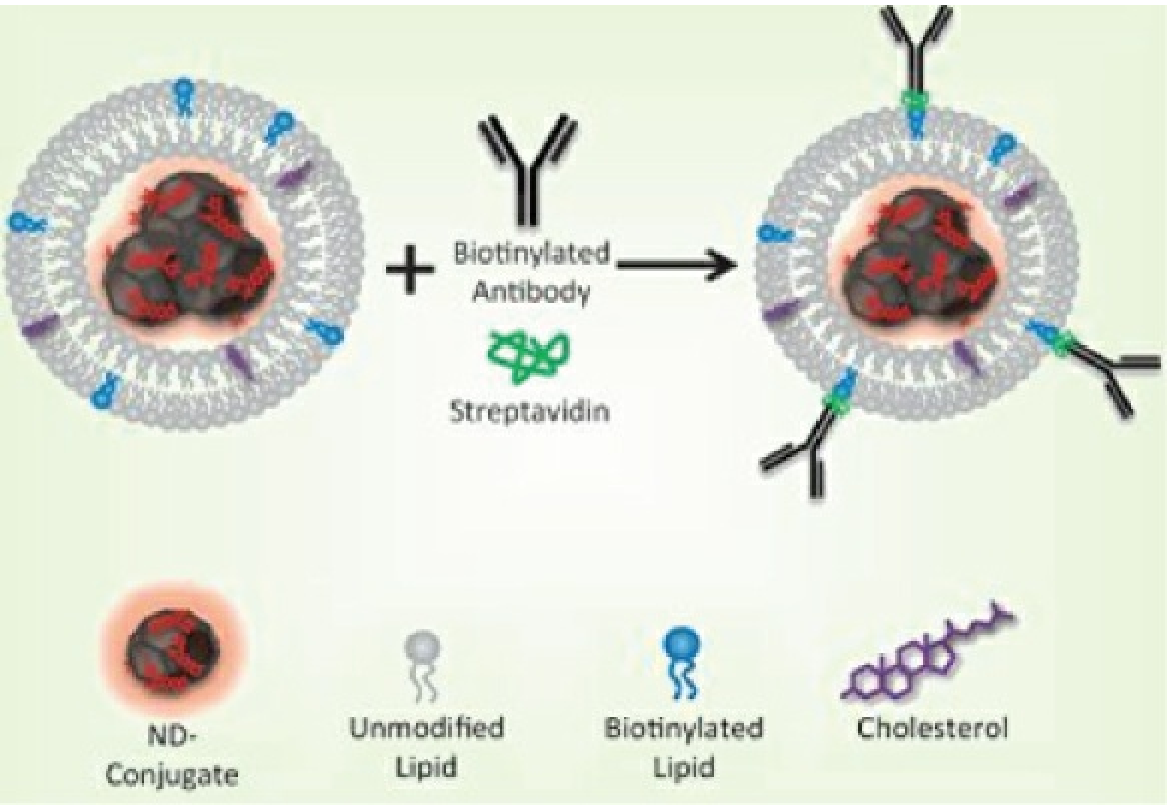

Figure 5.30 Treating drug-resistant cancer with nanodiamond. Moore et al. [42b], © 2013. Reprinted with permission of John Wiley and Sons.

Review Questions

Q1. What makes carbon as unique element? Discuss some of its key attributes.

Q2. Name natural and synthetic allotropes of carbon.

Q3. Mention the development of different synthetic allotropes of carbon in a chronological order along with the names of inventors.

Q4. Why it is necessary to functionalize fullerenes and how it is achieved?

Q5. How does spherical structure of fullerene facilitate its addition reaction? Give some examples.

Q6. Give applications of functionalized CNTs.

Q7. Why is it important to purify CNTs? Give some methods to purify them.

Q8. What are the parameters responsible for giving rise the metallic or semiconductor properties in CNTs.

Q9. What are the basic differences between single-wall and multiwall carbon nanotubes and how the properties differ in these two types.

Q10. How are the following pairs different in their structure: graphite and graphene; graphene and carbon nanotubes; carbon-onion and fullerenes?

Q11. Which functional group differentiates graphite oxide from graphene oxide?

Q12. What makes exfoliation of graphite oxide easy to obtain graphene oxide?

Q13. Discuss electronic and band structures of graphene.

Q14. Give unique properties of graphene.

Q15. Discuss physical and chemical routes to synthesize graphene.

Q16. What makes graphene to be seen by naked eye?

Q17. How are the carbon-onion different from fullerenes?

Q18. How is CNT different from carbon nanofiber?

Q19. How can you improve the crystallinity of carbon black?

Q20. What are the advantages of using carbon black in synthesis of nanoallotropes of carbon?

Q21. How Raman spectroscopy is useful in distinguishing the graphite, graphene, fullerene, and carbon nanotubes?

References

1. H. Marsh, *Introduction to Carbon Science*, Butterworths, London, 1989.

2. *Carbon Nanotechnology: Recent Developments in Chemistry, Physics, Material Science and Device applications*, L. Dai, Ed., Elsevier, 2006.

3. L. Dai, D. W. Chang, J.-B. Baek and W. Lu, “Carbon Nanomaterials for Advanced Energy Conversions and Storage”, *Small*, **8** (2012) 1130–1166.

4. H. W. Kroto, J. R. Heath, S. C. O'Brien, R. F. Curl and R. E. Smalley, “C-60: Buckminister Fullerene”, *Nature* **318** (1985) 162–163.

5. S. Iijima, “Helical Microtubules of Graphitic Carbon”, *Nature* 1991, **354**, 56–58.

6. K. S. Novoselov, A. K. Geim and S. V. Morozov et al., “Electric Field in Atomically Thin Carbon Films,”*Science*, **306** (5696) (2004) 666–669.

7. X. Wan, Y. Huang and Y. Chen, “Focusing on Energy and Optoelectronic Applications: A Journey for Graphene and Graphene Oxide at Large Scale”, *Acc. Chem. Res.*, **45** (2012) 598–607.

8. http://en.wikipedia.org/wiki/allotropes of carbon.

9. M.-F. Yu, O. Lourie, M. J. Dyer, K. Moloni, T. F. Kelly and R. S. Ruoff, “Strength and Breaking Mechanism of Multiwalled Carbon Nanotubes Under Tensil Load”, *Science*, **287** (5453) (2000) 637–640.

10. A. Hirsch, “The Era of Carbon Allotropes”, *Nat. Mater.*, **9** (2010) 868.

11. W. Krätschmer, L. D. Lamb, K. Fostiropoulos and D. R. Huffman, “Solid C-60: A New Form of Carbon”, *Nature*, **347** (1990) 354–58.

12. M. D. Diener, Fullerenes for Photovoltaic and Bioscience Applications, http://www.sigmaaldrich.com.

13. R. Saito, M. Fujita, G. Dresselhaus and M. S Dresselhaus, “Electronic Structure of Chiral Graphene Tubules”, *Appl. Phys. Lett.*, **60** (1992) 2204–2206.

14. A. Szabó, C. Perri, A. Csató, G. Giordano, D. Vuono and J. B. Nagy, “Synthesis Methods of Carbon Nanotubes and Related Materials”, *Materials*, **3** (2010) 3092–3140.

15. S. H. Jung, M. R. Kim, S. H. Jeong S. U. Kim, O. J. Lee and K. H. Lee, et al. “High Yield Synthesis of Multiwall Carbon Nanotubes by Arc Discharge in Liquid Nitrogen”, *Appl. Phys. Mater. Sci. Process.*, **76** (2003) 285–286.

16. K. Anazawa, K. Shimotani, C. Manabe, H. Watanabe and M. Shimizu, “High Purity CNT Synthesis Method by an Arc Discharging in Magnetic Field”, *Appl. Phys. Lett.*, **81**(4) (2002) 739–741.

17. S. J. Lee, H. K. Baikb, J. Yooc and J. H. Hanc, “Large Scale Synthesis of Carbon Nanotubes by Plasma Rotating Arc Discharge Technique”, *Diam. Relat. Mater.*,**11** (2002) 914–917.

18. T. Guo, P. Nikolaev, A. Thess, D.T. Colbert and R. E. Smally, “Catalytic Growth of Single Walled Nanotubes by Laser Vaporization”, *Chem. Phys. Lett.*, **243** (1995) 49–54.

19. H. Kuzmany, A. Kukovecz, F. Simon, M. Holzweber, C. Kramberger and T. Pichler, “Functionalization of Carbon Nanotubes”, *Synth. Met.* **141** (2004) 113–122.

20. P.-X. Hou, C. Liu and H.-M. Cheng, “Purification of Carbon Nanotubes” *Carbon*, **46** (2008) 2003–2025.

21. T.N. Le, K. Hernadi and E. Ljubovic et al. “Mechanical Purification of Single Walled CNT Bundles from Catalytically Particles”, *Nano Lett.* **2** (2002) 1349–1352.

22. V. N. Popov, “Carbon Nanotubes: Properties and Application”, *Mat. Sci. Eng. R.* **43** (2004) 61–102.

23. M. F. L., De Volder, S. H. Tawfick, R. H. Baughman and A. J. Hart, “Carbon Nanotubes: Present and Future Commercial Applications”, *Science*, **339** (1), (2013), 535–539.

24. M.I. Katsnelson and K.S. Novoselov, “Graphene: New Bridge Between Condensed Matter Physics and Quantum Electrodynamics”, *J. Solid State Commun.*, **143** (2007).

25. J. Meyer, A. K. Geim, M. I. Katsnelson, K. S. Novoselov, T. J. Booth and S. Roth, “The Structure of Suspended Graphene Sheets”, *Nature* **446** (7131), (2007) 60–63.

26. T. Ando, “The Electronic Properties of Graphene and CNTs”, *NPG Asia Mater.*, **1**(1), (2009) 17–21.

27. U. Kosidlo, M. A. Ruiz de Larramendi, F. Tonner, H. J. Park, C. Glanz, V. Skakalova, S. Roth and I. Kolaric, “Production methods of graphene and resulting material properties”, www.ipa.fraunhofer.de. 23.11.09.

28. A. Reina, X. Jia, J. Ho, D. Nezich, H. Son, V. Bulovic, M. S. Dresselhaus and J. Kong, “Large Area, Few-Layer Graphene Films on arbitrary Substrates by Chemical Vapor Deposition”, *Nano Lett.*, **9** (2009) 30–35.

29. G. Wang et al., “Highly Efficient and Large-Scale Synthesis of Graphene by Electrolytic Exfoliation”, *Carbon* **47** (2009) 3242–3246.

30. M. Hakimi and P. Alimard, “Synthesis and Applications in Biotechnology – A Review”, *World Appl. Program.*, **2**(6) (2012) 377–388.

31. S. Stankovich, D. A. Dikin, R. D. Piner, K. A. Kohlhaas, A. Kleinhammes, Y. Jia, Y. Wu, S. T. Nguyen and R. S. Ruoff, “Synthesis of Graphene-Based Nanosheets via Chemical Reduction of Exfoliated Graphite Oxide”, *Carbon*, **45** (7), (2007) 1558–1565.

32. N. Liu, F. Luo, H. Wu and Y. Liu, “One-Step Ionic-Liquid-Assisted Electrochemical Synthesis of Ionic-Liquid-Functionalized Graphene Sheets Directly From Graphite”, *Adv. Funct. Mater.* **18** (2008) 1518–1525.

33. S. Stankovich, R. Piner, S. T. Nguyen and R. S. Ruoff, “Synthesis and Exfoliation of Isocyanate-Treated Graphene Oxide Nanoplatelets,” *Carbon*, **44** (2006), 3342–3347.

34. I. Chidres, L. A. Jauregui, M. Foxe, J. Tian, R. Jalilian, I. Jovanovic and Y.P. Chen, “Effect of Plasma Etching on Graphene,” *New J. Phys.*, **13** (2011) 025008.

35. Z. H. Ni, H. M. Wang, J. Kasim, H. M. Fan, T. Yu, Y. H. Wu, Y. P. Feng and Z. X. Shen, “Graphene Thickness Determination Using Reflectance Measurement”, *Nano Lett.*, **7** (2007) 2758.

36. A. V. Klekachev, A. Nourbakhsh, I. Asselberghs, A. L. Stesmans, M. M. Heyns and S. De Gendt, “Graphene Transistors and Photodetectors”, *Electrochem. Soc. Interf.* Spring 2013.

37. F. D. Han, B. Yao and Y.J. Bai, “Preparation of Carbon Nano-Onions and their application as anode materials for rechargeable Lithium-Ion Batteries”. *J. Phys. Chem. C*, **115** (2011) 8923–8927.

38. H. Mehdipour, K. Ostrikov, A. E. Rider and Z. Han, “Heating and Plasma Sheath Effects in Low-Temperature, Plasma-Assisted Growth of Carbon Nanofibers”, *Plasma Processes Polym.*, **8**(5)(2011) 386–400.

39. M. Ozawa and E. Ōsawa, “Carbon black as the source materials for carbon nanotechnology”, Chapter 6, *Carbon Nanotechnology Recent Developments in Chemistry, Physics, Materials Science and Device Applications*, Ed. L. Dai, Elsevier, 2006.

40. T. L. Daulton, D.D. Eisenhour and T. J. Bernatowicz, et al., “Genesis of Presolar Diamond: Comparative High-Resolution Transmission Electron Microscopy Study of Meteroritic and Terrestrial Nanodiamonds”, *Geochim. Cosmo Chim. Acta*, **60** (23), (1996) 4853–4872.

41. A. Kumar, P. A. Lin, A. Xue, B. Hao, Y. K. Yap and R. M. Sankaran, “Formation of Nanodiamonds at Near-Ambient Conditions via Microplasma Dissociation of Ethanol Vapour”, *Nat. Commun.* **4** (2014) *Article number:* 2618

42. A. Krueger, “The Structure and Reactivity of Nanodiamonds”, *J. Materials Chem.*, **18** (2008) 1485.

43. (a) T. J. Merkel and De Simone, “Dodging Drug Resistant Cancer with Diamonds”, *Sci. Transl. Med.* **3** (2011) 58.(b) L. Moore, E. Kai-Hua Chow, E. Osawa, J. M. Bishop and D. Ho, “Diamond-Lipid Hybrids Enhance Chemotherapeutic Tolerance and Mediate Tumor Regression”, *Adv. Mater.* **12;25** (26), (2013) 3532–3541.

Chapter 6
Self-Assembled and Supramolecular Nanomaterials

6.1 Introduction: Self-Assembly

Self-assembly is defined as the spontaneous organization of individual components into an ordered structure without human intervention. A great part of current advances in nanoscience and nanotechnology is based on self-assembly process, a mechanism by which disordered small building units spontaneously arrange into large, ordered phases. For example, self-assembly steers the growth of molecular crystals and molecular monolayers, is responsible for the folding of proteins, and affects the morphology of lipid bilayers and colloidal particles. Thus, the importance of self-assembly manifests itself not only in the advances in materials science but also through its role in biology, life science, and the physics and chemistry of soft matter. Further examples for the successful use of self-assembly as a bottom-up approach for engineering at very small dimensions include the fabrication of nanoscopic structures such as quantum dots, photonic band gap materials, and the design of hybrid organic–inorganic materials. Supramolecular chemistry at surfaces, that is, the association of molecules through rather weak noncovalent bonds, is yet another case where molecular self-assembly is decisive [1, 2]. Self-assembly is scientifically interesting and technologically important for the following reasons set out.

> **i.** It is centrally important in life. The cell contains an astonishing range of complex structures such as lipid membranes, folded proteins, structured nucleic acids, protein aggregates, molecular machines, and many others that form by self-assembly.
>
> **ii.** Self-assembly provides routes to a range of materials with regular structures: molecular crystals, liquid crystals, and semicrystalline and phase-separated polymers. Self-assembly also occurs widely in systems of components larger than molecules, and there is a great potential for its use in materials and condensed matter science.
>
> **iii.** Self-assembly seems to offer one of the most general strategies now available for generating nanostructures. Thus, self-assembly is important in a range of fields: chemistry, physics, biology, materials science, nanoscience, and manufacturing. There is an exciting opportunity for self-assembly to develop through the interchange of concepts and techniques among these fields.

Engineering principles for micro- and nanofabrication can be learned by understanding molecular self-assembly phenomena in nature. As a matter of fact, most of the advancements in nanoscience draw inspiration from biology. The biological structures from the simplest and small RNA molecule, to functional organelles such as ribosomes or flagellar nanomotors, to viruses and complete cells are all self-assembled structures [3]. In a living system, a cell can be treated as "an ensemble of functional nanostructures, enclosed in a molecule- and ion-selective, semi-permeable membrane, which replicates itself." Furthermore, organisms themselves can be considered as a collection of self-assembled materials: lipid bilayers, the extracellular matrix, tendon and connective tissue, skin, spider silk, cotton fiber, wood, and bone are all self-assembled biological materials, with an internal hierarchically ordered structure from the molecular to the macroscopic scale. Self-assembly offers endless opportunities and has a significant future in a long list of potential applications: micro-/optoelectronics, catalysis, energy/magnetic storage, biotechnology, and novel materials that adapt according to their environment, to name a few.

6.1.1 Supramolecular Chemistry

The "chemistry beyond the molecule," involves the study of interactions among molecules rather than within the molecules. Traditional molecular chemistry involves the strong covalent bonds formed by the sharing or exchange of electrons between the atoms within a molecular system. In supramolecular chemistry, molecules are used as building blocks that provide excellent possibilities for the design of complex architectures [4]. Herein, molecular building blocks are assembled together with relatively weak noncovalent interactions, such as hydrogen bonding, π–π stacking, electrostatic, and hydrophilic–hydrophobic interactions, and van der Waals forces. Strength and examples of supramolecular structures formed by such noncovalent interactions are given in Table 6.1.

Table 6.1 Summary of Supramolecular Interactions

Interactions	Strength (kJ/mol)	Example
Ion–ion	20–300	Tetrabutylammonium chloride
Ion–dipole	50–200	Sodium [15]crown-5
Dipole–dipole	5–50	Acetone
Hydrogen bonding	4–120	Water
Cation-π electrons	5–80	K^+ in benzene
$\pi - \pi$	0–50	DNA
van der Waals	<5, variable depends on surface area	Packing in molecular crystals
Hydrophobic	Related to solvent–solvent interaction energy	Inclusion compounds of cyclodextrin

Source: Albrecht [4], © 2007. With permission of Springer-Verlag.

In fact, nature has utilized these interactions for the creation of well-defined and esthetically appealing architectures that can perform specific functions. Biological systems are often the inspiration for supramolecular research. Nature uses supramolecular chemistry to form the double-helix of DNA or to fold proteins. Using nature as a source of inspiration, over the years scientists have mastered the principles of supramolecular chemistry for the demonstration of many important concepts such as molecular and nanomaterials self-assembly, folding, molecular recognition, host–guest chemistry, mechanically interlocked molecular architectures, and dynamic covalent chemistry. Many of the synthetic schemes reported for the preparation of nanoparticles utilize supramolecular approaches involving electrostatic or covalent interactions of the capping agent, which stabilizes the nanoparticles, for example, the citrate capped metal nanoparticles are stabilized by an electrical double layer of citrate and chloride ions. The columbic repulsions between the particles, which decay exponentially with increasing interparticle separation, further reduce agglomeration of nanoparticles. Polymer and dendrimers capped nanoparticles are stabilized through the steric interactions. The ability of thiol groups to form self-assembled monolayer (SAM) on metallic surfaces has been effectively utilized for the preparation of thiolate-stabilized Au/Ag nanoparticles.

6.2 Historical Perspective of Supramolecular and Self-Assembled Structures

The existence of intermolecular forces was first postulated by Johannes Diderik van der Waals in 1873. However, it was Nobel Laureate Hermann Emil Fischer who for the first time introduced the concept of supramolecular chemistry in 1890. Fischer suggested that enzyme–substrate interactions take the form of a "lock and key," pre-empting the concepts of molecular recognition and host-guest chemistry [5]. In the early twentieth century, noncovalent bonds were understood gradually in more detail, with the hydrogen bond being described by Latimer and Rodebush in 1920. The use of these principles led to an increasing understanding of protein structure and other biological processes. For instance, the important breakthrough that allowed the elucidation of the double helical structure of DNA occurred when it was realized that there are two separate strands of nucleotides connected through hydrogen bonds. The use of noncovalent bonds is essential to replication because they allow the strands to be separated and used to template new double-stranded DNA. Concomitantly, chemists began to recognize and study synthetic structures based on noncovalent interactions, such as micelles and microemulsion. Eventually, chemists were able to take these concepts and apply them to synthetic systems. The breakthrough came in the 1960s with the synthesis of the crown ethers by Pedersen [6]. Following this work, other researchers such as Donald J. Cram, Jean-Marie Lehn, and Fritz Vogtle became active in synthesizing shape- and ion-selective receptors, and throughout the 1980s research in the area gathered a rapid pace with concepts such as mechanically interlocked molecular architectures. The importance of supramolecular chemistry was recognized by the award of 1987 Nobel Prize for Chemistry to Donald J. Cram, Jean-Marie Lehn, and Charles J. Pedersen for their pioneering work in this area [7]. The development of selective "host–guest" complexes in particular, in which a host molecule recognizes and selectively binds a certain guest, was cited as an important contribution.

In the 1990s, supramolecular chemistry [8, 9] became even more advanced, with researchers such as James Fraser Stoddart developing molecular machinery and highly complex self-assembled structures and developing sensors and methods of electronic and biological interfacing by Itamar Willner. During this period, electrochemical and photochemical motifs became integrated into supramolecular systems in order to increase functionality. Research and development on synthetic self-replicating system and work on molecular information processing devices began during this period. The emerging science of nanotechnology also had a strong influence on the subject, with building blocks such as fullerenes, nanoparticles, and dendrimers becoming involved in synthetic systems.

6.3 Fundamental Aspects of Supramolecular Chemistry

Broadly, self-assembly can be classified as static self-assembly and dynamic self-assembly. In **static** self-assembly, the ordered state is formed as the system approaches equilibrium, reducing its free energy, whereas in **dynamic** self-assembly, patterns of pre-existing components are organized by specific local interactions. Associated disciplines describe the dynamic self-assembled patterns as “self-organized” and not as “self-assembled.” Notwithstanding the huge interest aroused by dynamic interactions, particularly in biological self-assembled systems, most applicative research is still focused on the structures of the static type. Advanced materials such as 2D and 3D nanostructured materials and devices using chemical approaches typically include both molecular self-assembly through weak noncovalent interactions and directed assembly of molecules via strong chemical bonds with solid surfaces. Both of these assembly techniques particularly those of organic molecules on solid surfaces form an important basis for a wide spectrum of promising applications, including molecular electronic devices, biomolecular recognition chips, tribology, corrosion inhibition, and 3D nanopatterning. The focus on self-assembly as a strategy for synthesis has been confined largely to molecules because chemists are professionally concerned with manipulating the structure of matter at the molecular scale. The expanding contact of chemistry with biology and materials science and the direction of technology toward nanometer- and micrometer-scale structures, however, have begun to broaden this focus to include matter at scales larger than the molecular. There are now three ranges of sizes of components for which self-assembly is important: molecular, nanoscale (colloids, nanowires and nanospheres, and the related structures), and mesoscopic to macroscopic (objects with dimensions from microns to centimeters). The rules for self-assembly in each of these ranges are similar but not identical. The concepts of self-assembly historically have come from studying molecular processes. The success of self-assembly in a molecular system is determined by five characteristics of the system.

i. Components: A self-assembling system consists of a group of molecules or segments of a macromolecule that interact with each other. These molecules or molecular segments may be the same or different. Their interaction leads from some less ordered state (a solution, disordered aggregate, or random coil) to a final state (a crystal or folded macromolecule) that is more ordered.

ii. Interactions: Self-assembly occurs when molecules interact with one another through a balance of attractive and repulsive interactions. These interactions are generally weak (i.e., comparable to thermal energies) and noncovalent (van der Waals and Coulomb interactions, hydrophobic interactions, and hydrogen bonds), but relatively weak covalent bonds (coordination bonds) are recognized increasingly as appropriate for self-assembly. Complementarity in shapes among the self-assembling components is also crucial.

iii. Reversibility: For self-assembly to generate ordered structures, the association either must be reversible or must allow the components to adjust their positions within an aggregate once it has formed. The strength of the bonds between the components, therefore, must be comparable to the forces tending to disrupt them. For molecules, the forces are generated by thermal motion. Processes in which collision between molecules leads to irreversible sticking generate glasses, not crystals.

iv. Environment: Usually, the self-assembly of molecules is carried out in solution or at an interface to allow the required motion of the components. The interaction of the components with their environment can strongly influence the course of the process.

v. Mass transport and agitation: For self-assembly to occur, the molecules must be mobile. In solution, thermal motion provides the major part of the motion required to bring the molecules in contact.

6.3.1 Molecular Self-Assembly

Molecular self-assembly is the construction of systems without guidance or management from an outside source (other than to provide a suitable environment). The molecules are directed to assemble through noncovalent interactions. Self-assembly may be subdivided into intermolecular self-assembly (to form a supramolecular assembly) and intramolecular self-assembly (or folding as demonstrated by foldamers and polypeptides). Molecular self-assembly also allows the construction of larger structures such as micelles, membranes, vesicles, and liquid crystals and is important to crystal engineering.

6.3.2 Molecular Recognition and Complexation

Molecular recognition is the specific binding of a guest molecule to a complementary host molecule to form a host–guest complex. Often, the definition of which species is the “host” and which is the “guest” is arbitrary. The molecules are able to identify each other using noncovalent interactions. Key applications of this field are the construction of molecular sensors and catalysis.

6.3.3 Mechanically Interlocked Molecular Architectures

Mechanically interlocked molecular architectures consist of molecules that are linked only as a consequence of their topology. Some noncovalent interactions may exist between the different components (often those that were utilized in the construction of the system), but covalent bonds do not. Supramolecular chemistry and template-directed synthesis, in particular, are key to the efficient synthesis of the compounds. Examples of mechanically interlocked molecular architectures include catenanes, rotaxanes, molecular knots, and molecular borromean rings.

6.3.4 Supramolecular Organic Frameworks (SOFs)

Among the supramolecular structures metal-organic frameworks (MOFs) are commanding much of the attention because of their appetite for greenhouse gases, but a new player has joined the field – supramolecular organic frameworks (SOFs). The first 2D SOFs that self-assemble in solution is an important breakthrough that holds implications for sensing and separation technologies, energy sciences, and, perhaps most importantly, biomimetics [10]. Solution-based processing of SOFs offers several advantages in that it allows for mass production and reduced manufacturing costs, is an important step for transferring materials to a dry state without losing their structural integrity, and also allows for biorelated applications such as biomimetic sensing, where the framework structure is advantageous for the capturing of guest molecules and the amplification of chemical signals. The self-assembly of well-defined 2D polymeric supramolecular systems in solution has been a challenge because such polymers tend to precipitate out of solution, making them difficult to manipulate and characterize. To meet this challenge, a combination of self-assembling tripods and macrocycle rings is used to form a porous framework with honeycomb periodicity, similar to that of an MOF, but this remains rigid in solution (Figure 6.1). Equipping the tripods with bulky hydrophilic groups that resist stacking preserved the solubility and single-layer 2D architecture of the framework.

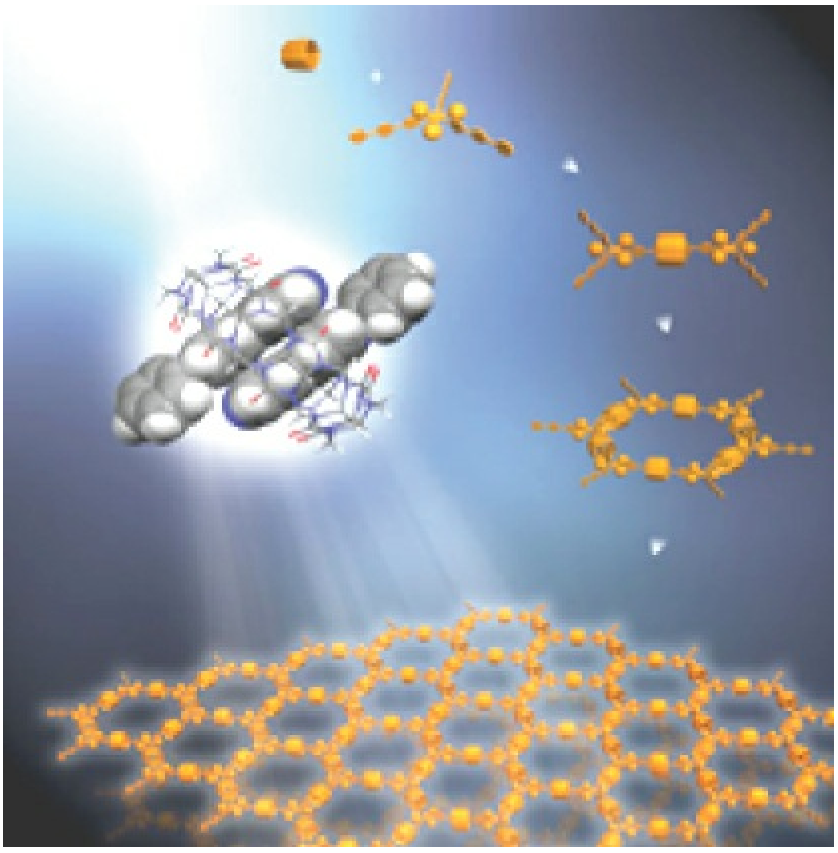

Figure 6.1 Rigid triangular structure self-assembled in combination with macrocycle rings in solution to create a supramolecular organic framework (SOF). Zhang et al. [10], © 2013. With permission of ACS.

6.3.5 Biomimetic

Many synthetic supramolecular systems are designed to copy functions of biological systems. These biomimetic architectures can be used to learn about both the biological model and the synthetic implementation. Examples include photoelectrochemical systems, catalytic systems, protein design, and self-replication.

6.3.6 Imprinting

Molecular imprinting describes a process by which a host is constructed from small molecules using a suitable molecular species as a template. After construction, the template is removed leaving only the host. The template for host construction may be subtly different from the guest that the finished host binds. In its simplest form, imprinting utilizes only **steric interactions**, but more complex systems also incorporate **hydrogen bonding** and other interactions to improve binding strength and specificity.

6.3.7 Molecular Machines

Molecular machines are molecules or molecular assemblies that can perform functions such as linear or rotational movement, switching, and entrapment. These devices exist at the boundary between supramolecular chemistry and nanotechnology, and prototypes have been demonstrated using supramolecular concepts.

6.4 Self-Assembly Via Non-Covalent Interaction

Most of the expected applications of nanotechnology are based not on individual nano-objects rather on assemblies in which these nano-objects interact with one another and organize themselves in a purposeful manner. The challenge to nanoscience is to develop efficient and robust ways of assembling nano components. Self-assembly is the most promising candidate for this task [11]. As an illustrative example, nanoscale self-assembly of individual particles into higher-order structures (Figure 6.2) shows that in addition to “body” forces between the material particles (e.g. Vander Wall or magnetic interactions), the interactions between nanoscale spheres and rods are to be tuned through appropriate surface functionalization.

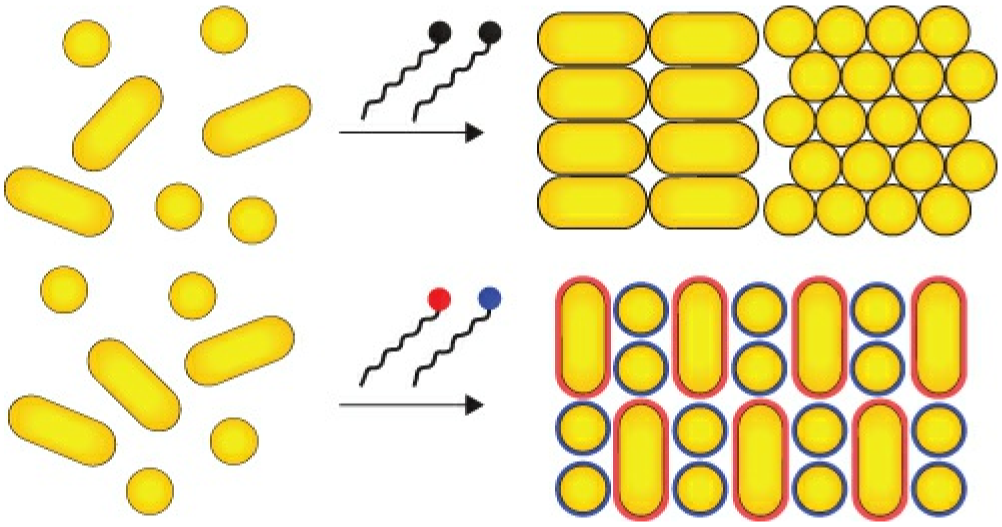

Figure 6.2 Schematic illustration of nanoscale self-assembly. vdW attraction and steric repulsion may induce the phase separation of rods and spheres into two closely-packed arrangements (top). Alternatively, when the rods are functionalized with positively charged ligands and the spheres with negatively charged ligands, the particles are expected to organize via electrostatic interactions into a binary lattice (bottom).

Bishop et al. [11], © 2009. With permission of Wiley-VCH Verlag GmbH & Co. KGaA, Weinheim.

Interactions between nanoscale components differ substantially from the molecular interactions from which they derive. Ability of a given interaction to induce self-assembly depends on its magnitude and length scale. Furthermore, the range of an interaction relative to the size of interacting particles can determine whether or not these particles will assemble into an ordered structure or into an amorphous phase. Common attractive interactions (e.g. vdW forces) act appreciably over molecular dimensions. In order to apply these forces in self-assembly, it is necessary to use nanoscopic components (~2–30 nm) at few to tens of times larger than molecular length scale (3–10 Å).

6.4.1 Long-Range Forces in Self-Assembly

Self-assembly occurs when molecules interact with each other through a balance of attractive and repulsive interactions. These interactions are generally weak (i.e., in terms of thermal energies) and noncovalent (van der Waals and Coulomb interactions, hydrophobic interactions, and hydrogen bonds) but relatively weak covalent bonds (coordination bonds), electrostatic, and magnetic interactions are recognized increasingly as appropriate for self-assembly. In addition, complementarity in shapes (Lego chemistry) among the self-assembling components is also crucial.

a. ***van der Waals (vdW)*** van der Waals interactions originate from the electromagnetic fluctuations due to the incessant movements of positive and negative charges within all types of atoms, molecules, and bulk materials. They are therefore present between any two material bodies, usually acting in an attractive manner to bring the bodies together. The magnitude of these attractive interactions can be considerable –few to hundreds of times greater than kT – between even nanoscopic components. Because of this, van der Waals forces are often considered an untoward effect, causing the undesired precipitation of nanoparticles from solution. Through the use of stabilizing ligands or appropriate solvents, however, van der Waals interactions can be controlled to provide a useful tool to guide self-assembly processes [12, 13]. Some examples of self-assembled nanostructures are illustrated in Figure 6.3a–c. In each of these examples, the specific molecular interactions give rise to significant and often specific interparticle potentials between much larger components and enable their spontaneous organization into a variety of ordered structures.

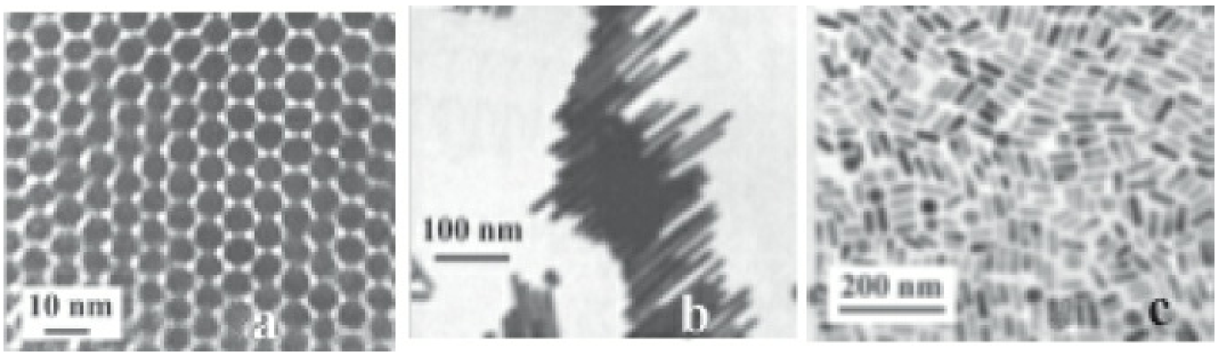

Figure 6.3 van der Waals forces driven nanoparticle assemblies: (a) 2D hexagonal close-packed structure of 5 nm Ag-NPs. Harfenist et al. [12], © 1996. With permission of ACS; (b) side-by-side self-organized gold nanorods (15 × 200 nm, aspect ratio >5) leading to continuous ribbons. Sau and Murphy [13], © 2005. With permission of ACS; (c) isotropic self-assembly of gold nanorods (15 × 200 nm, aspect ratio 3.2) Sau and Murphy [13], © 2005. With permission of ACS.

b. ***Electrostatic Interaction*** Almost as ubiquitous as van der Waals forces, electrostatic interaction provides a basis for the formation of ionic, colloidal, and even macroparticle crystals and have recently been applied at the nanoscale to form a variety of unique structures such as diamond-like NP crystals and robust monolayer or multilayer surface coatings. Unlike van der Waals interactions, which are primarily attractive in nature, electrostatic interactions can be either attractive (between like-charged particles) or repulsive (between oppositely charged particles) and even directional, as in the case of particles with asymmetric surface charge distributions or permanent electric polarization. Furthermore, the magnitude and length scale of these electrostatic interactions can be tuned controllably through the choice of solvent (e.g., dielectric constant) as well as the concentration and chemical nature (e.g., size and valence) of the surrounding counter-ions. Due to these unique attributes, electrostatic interactions are useful both for stabilizing particles in solution and for guiding their self-assembly into binary superstructures. It is to be emphasized that the electrostatic charge on a nanoscale particle is predominately a surface effect, for example, through the adsorption or desorption of ionic species. Therefore, it does not preclude the presence of additional interparticle forces acting between the particles' volumes. In addition to van der Waals forces, other “body” forces arise between materials with a permanent electric or magnetic polarization. However, despite of several interesting examples of electrically polarized particles (e.g., CdSe particles or other semiconductors), these forces are typically weak and subject to screening in electrolyte solutions.

c. *Magnetic Interaction*

Self-assembly due to magnetic interaction in nanoparticles is sought in high-density storage of data and magnetic energy, magnetic separations, drug delivery, and hyperthermia treatments, as well as in magnetic relaxation switches for sensing biological interactions between proteins, DNA, and viruses. When magnetic nanoparticles self-assemble, they tend to align their magnetic moments in the direction of the local magnetic field due to neighboring particles or applied fields. This gives rise to a specific directionality of interaction, enabling magnetic NPs to form micron-sized, one-dimensional chains/wires or rings as shown in Figure 6.4a and b. More recently, these NPs have also been shown to form 2D aggregates and even 3D superlattices. Controlling these self-assembly processes requires the understanding of the relationship between the magnetic properties and other particle characteristics such as size or shape.

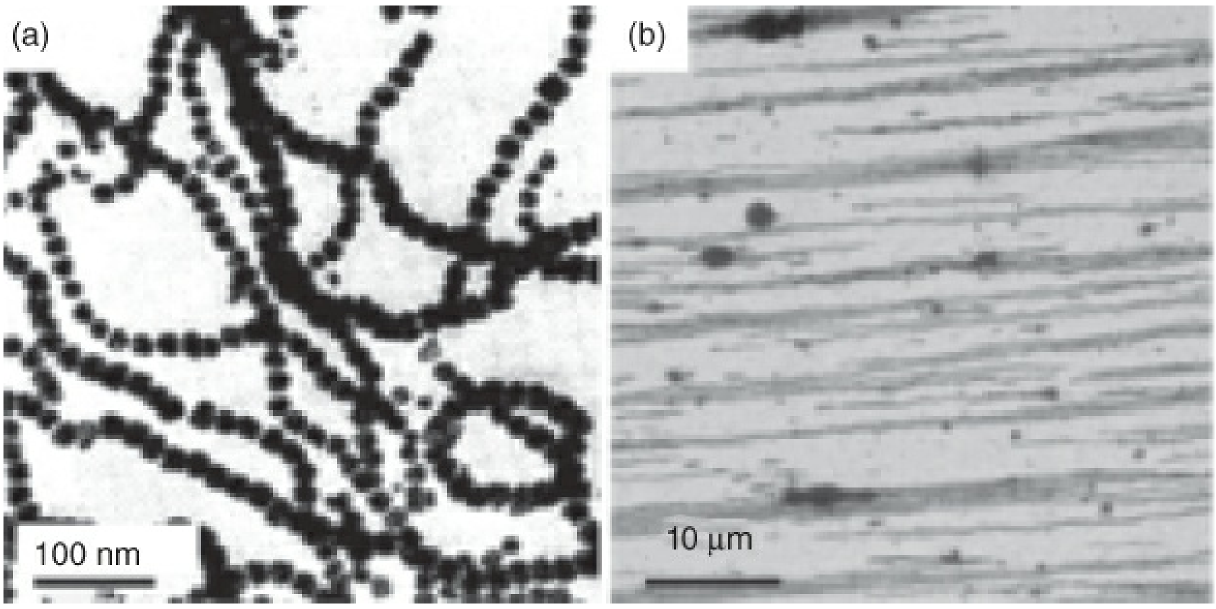

Figure 6.4 TEM image of self-assembly of magnetic nanoparticles formed by strong dipole–dipole interactions: (a) linear chains of 20 nm cobalt-NPs. Thomas [14], © 1966. With permission of AIP; (b) parallel chains of 10 nm .-Fe_2O_3. Lalatonne et al. [15], © 2004. With permission of NPG.

So far, it was tactically assumed that the magnetic dipole–dipole interactions were the sole forces responsible for particle assembly. In reality, magnetic interactions always compete with van der Waals forces (and possibly other types of forces), which become increasingly important with decreasing particle size. Thus, the van der Waals interaction scales linearly with the particle's radius, while the magnetic interaction scales with its volume. It follows that for sufficiently small particles and/or surface separations, van der Waals interactions are expected to be the dominant contributions to the total interparticle potential. For example, in the absence of an external field, the experimentally observed aggregation of 10-nm maghemite (.-Fe_2O_3) nanoparticles can be attributed predominantly to van der Waals rather than magnetic forces. Only with the help of the strong external magnetic fields (~0.6 T), the magnetic forces dominate self-assembly of such particles.

6.4.2 Short-Range Forces in Self-Assembly

At the molecular scale, one finds a variety of short-range attractive forces, including covalent bonds, dipolar interactions, hydrogen bonding, donor–acceptor interactions, and so on – used to build complex molecules, crystals, and supramolecular architectures. Such interactions may also be employed at the nanoscale by decorating the surfaces of nanoscale components with various chemical functionalities. For instance, hydrogen bonds organize nanorods into linear chains; divalent “linkers” such as DNA bring particles together selectively and reversibly; and dipole–dipole interactions between photoisomerizable surface groups enable rapid assembly and disassembly of ordered nanoparticle structures.

There are four different molecular surface forces useful in nanoscale self-assembly: molecular dipole interactions, hydrogen bonding, DNA base–pair interactions, and reversible cross-linking interactions. In addition, entropic and solvent effects also play important role in self-assembly.

a. *Molecular Dipole Interactions* Molecules with a permanent electric dipole moment interact with each other via dipole–dipole interactions analogous to those between magnetic particles. In general, these molecular dipole interactions are only relevant to low-dielectric solvents; however, in water, the charges (not the dipoles) are needed to induce significant electrostatic interactions. Even in low-dielectric solvents, however, the dipole–dipole interactions are too weak to drive their alignment into the minimal energy inline configuration, and it is more appropriate to model them as thermally averaged interactions between freely rotating dipoles. Although individual molecular dipole interactions have a small magnitude, these can become strong enough to induce self-assembly when several of them are tethered onto a particle's surface with density. Clearly, when acting in concert, these molecular dipole interactions have the strength to induce self-assembly.

b. *Hydrogen Bonding*

Similar to dipolar interactions, hydrogen bonds are largely electrostatic in nature, whereby a proton mediates the attraction of two larger atoms with partial negative charges. In addition to their widespread use in supramolecular systems, these molecular interactions have also been applied to the self-assembly of larger nanoscale building blocks such as nanoparticles and nanorods. Magnitudes of individual hydrogen bonds range from 10 to 40 kJ/mol and depend strongly on the solvent conditions. In general, the free energy of hydrogen bond formation is significantly weaker in protic solvents (e.g., water, alcohols), in which molecule–solvent bonds are possible. At the nanoscale, hydrogen bonding has been shown to induce the aggregation of metal nanoparticles functionalized with hydrogen bonding ligands (e.g., $HS–C_6H_4–X$ on gold where X is OH, COOH, NH_2) where the degree of aggregation and ordering depends on the strength of the individual hydrogen bonds formed [16]. For example, very strong bonds between divalent hydrogen bonding molecules tethered to Au-NPs induce rapid formation of fibrous NP gels characteristic of strong, short-ranged potentials. Hydrogen bonding can also be used in a more controlled manner by site-selective functionalization of the particles or by pH-responsive hydrogen bonding moieties. The first approach has been used to create end-to-end assembles of gold nanorods mediated by hydrogen bonding functionalities tethered selectively to the ends of the rods. When these groups are also acidic (e.g., carboxylic), the interactions are dependent on the pH of the surrounding solution, exhibiting strong hydrogen bond interactions at low pH and repulsive electrostatic interactions at high pH. In this way, nanorods assemble end-to-end at low pH and disassemble at high pH; in between, however, the balance between hydrogen bond attraction and electrostatic repulsion gives way to side-to-side assemblies governed predominantly by van der Waals interactions. These relative simple examples illustrate the potential of using various interparticle interactions simultaneously to achieve a desired self-assembled nanostructure.

Hydrogen bonding is particularly important in biological systems where many protein structures in water are held together by hydrogen bonds. Of course, the existence of life as we know it depends on hydrogen bonds, which stabilize H_2O in the liquid form. In proteins, intramolecular hydrogen bonds between NH groups and $C_{1/4}O$ groups that are four residues apart underpin the formation of a helix structure. On the other hand, hydrogen bonds between neighboring peptide chains lead to sheet formation. Similarly, collagen fibers contain triple-helical proteins held together by hydrogen bonding. The folding pattern of proteins is also based on the intramolecular hydrogen bonding. The smaller the number of hydrogen bonds in the folded protein, the higher is its free energy and lower is the stability. The reason that nature exploits hydrogen bonds in this way is because of the strength of this bond. Hydrogen bonds (ca. 20 kJ/mol) are weaker than covalent bonds (ca. 500 kJ/mol), so that superstructures can self-assemble without the need of chemical reactions to occur, but nevertheless the bonds are strong enough to hold the structures together once formed.

c. *DNA Base Pair Interactions* An important type of hydrogen bond interaction is between complementary DNA base pairs (adenine with thymine; guanine with cytosine). These interactions are highly specific such that short DNA strands bind strongly only with complementary strands. Furthermore, by modulating the temperature below and above the melting temperature (typically, T_m ~ 40–80°C for oligomers of ~20 bases in a solution with 50 mM cations), the interactions may be turned "on" and "off," respectively, enabling precise control over the magnitude of the attraction. These features make DNA-mediated interactions highly desirable for the self-assembly of nanoscale components. This approach was first realized using gold nanoparticles covered with noncomplementary DNA strands, which self-assemble upon the addition of a complementary DNA "linker." In a similar work, the directionality of DNA was exploited whereby Au-NPs attached to either the 3′ or 5′ terminus of complementary strands hybridize into head-to-tail or head-to-head dimers. DNA-based self-assembly has enabled the formation of complex assemblies such as nanoscale circuits from metals and conductive polymers; ordered arrays of nanorods and proteins; as well as nanoparticle chains, rings, spirals, and, appropriately, double helices. In the context of templated self-assembly, surfaces patterned with DNA (using an AFM tip) enable to create arbitrary 2D superstructures through the selective deposition of nanoscale objects bearing complementary DNA sequences.

d. *Cross-Linking Interactions* Nanoparticles are also known to get self-assembled by the binding of divalent "linker" molecules dissolved in the surrounding medium, for example, Au-NPs cross-linked by alkane dithiols. Regardless of the specific nature of the linker molecule, the magnitude of cross-linking depends on the concentration of linkers in solution and on the energy of the bonds formed during cross-linking. In practice, such cross-linking interactions have been used to build 3D NP crystals, NP supra-spheres ranging in size from 30 to 300 nm, and even molecule-like clusters of asymmetric Au-Fe_3O_4 NPs.

Entropic Effects in Self-Assembly

All the interactions described so far have their origins in the static or transient electromagnetic forces between atoms and molecules, working together to create various interparticle potentials between nanoscale components. Yet, even in the absence of attractive potential, self-assembly is still possible due to the so-called depletion forces or confinement effects. Common to these phenomena is the role of entropy, which can give rise to both attractive and repulsive interactions between components in dilute systems or provide a driving force for order in concentrated systems. In general, entropic ordering effects always favor the formation of order structures from of monodisperse particles at sufficiently high volume fractions provided that the system remains ergodic. This ergodic criterion may be difficult to achieve at the highest volume fractions; however, nanoscale systems are particularly well suited for this challenge, as they rapidly sample their accessible phase space. These effects are often encountered in nanoparticle systems during the evaporation of the surrounding solvent. Further evaporation of the solvent ultimately "freezes" the particles in a close-packed geometry, for which the system is no longer ergodic but retains the order induced by entropic crystallization. In addition, a host of different microscopic and microscopic structures such as opals, fractals, mixed structures, and other forms based in NPs are observed as a result of the balance between electrostatic forces; surface tension; entropy; topography; substrate affinity; and, most importantly, the size, shape, and concentration of the particles.

Solvent Effect

In self-assembly process, it is important to understand the various interactions between NPs, substrates, and solvents, which lead to the patterns formed. There are several competing interactions/forces between particles that control the self-assembly behavior such as Brownian motion, electrostatic interaction and repulsion such as van der Waals attraction, steric repulsion, and capillary force, among others. Since a common method for initiating aggregation of NPs is to evaporate their solvent, the drying kinetics, substrate roughness, solvent wetting/dewetting, hydrodynamic effects, and self-diffusion of the NPs on the substrate also play important role in self-assembly process leading to unusual nonequilibrium structures. Furthermore, the evaporation rate of the solvent affects particle–particle interaction since the relatively weak attraction between NPs, which are efficiently screened in dilute solution, becomes noticeable as the solvent evaporates, initiating the assembly of slowly evolving structures. The quality of assembly is also determined by factors such as the solvent evaporation rate, the ionic strength, the surfactant concentration, and the particle size and shape distribution. For the self-assembly of anisotropic shaped NPs such as nanorod (NR), nanowire (NW), and nanodisks (ND), the situation becomes even more complex.

6.4.3 Self-Assembly in Soft Materials

Self-assembly, particularly in soft materials such as colloids, liquid crystals, and so on, relies on the fact that the energy dissipated by fluctuations in the position and the orientation of the molecules or particles, which are the result of Brownian motion, is comparable to the thermal energy. Thermal energy has a dramatic influence on soft materials at the nanoscale as weak noncovalent bonds are broken and sometimes re-formed. This process enables the system to reach thermodynamic equilibrium, which is often a nonuniform state. Because of the relatively weak interactions between molecules, transitions between different structures can readily be driven by changes in conditions, for example, temperature or pH value. Such external triggers that induce phase transitions could lead to a host of responsive materials or coupled with an appropriate source of energy to nanomechanical systems. There is a diversity of phase transitions between different structures in soft materials. Self-assembly bridges these diverse transitions, and provides a strategy that makes possible the patterning (in a broad sense) of nanostructures made by bottom-up synthesis; it can also use patterns generated by top-down fabrication to guide the ordering of nanostructures made by bottom-up methods. This capability of self-assembly to make ordered arrays of nanostructures is, in essence, nothing new. Crystallization of molecular or atomic species (whether it is the phase transition of liquid water into solid ice, or of liquid silicon into semiconductor-grade silicon crystal) is an example of self-assembly, as are the formation of surfactants in soap bubbles, the crystallization of viruses for X-ray structure determination, and the ordering of liquid crystals in displays.

6.4.4 Advantages of Self-Assembly

Self-assembly has a number of advantages as a strategy: first, it carries out many of the most difficult steps in nanofabrication – those involving atomic-level modification of structure – using the very highly developed techniques of synthetic chemistry. Second, it draws from the enormous wealth of examples in biology for inspiration: self-assembly is one of the most important strategies used in biology for the development of complex, functional structures. Third, it can incorporate biological structures directly as components in the final systems. Fourth, because it requires that the target structures be the thermodynamically most stable ones open to the system, it tends to produce structures that are relatively defect-free and self-healing. Furthermore, there are several general areas where self-assembly seems to be the best method (by whatever standard may be practicality, cost, order, dimensionality) for building functional materials with nanodimensional structural regularities. Following are some of such advantages described briefly.

a. *Components Too Small for Top-Down* Self-assembly provides the only approach to nanostructured materials that simply cannot be fabricated by current top-down methods. Although top-down methods are versatile and can fabricate astonishingly small structures, there are many types of structures that they cannot fabricate the most important and obvious of which are molecules. The ability of scanning probe devices to arrange atoms on surfaces is a demonstration of the power of these devices, but it is a methodology that is limited in its practicality and in the complexity of the systems that it can make. Self-assembly is, thus, an essential part of the generation of materials starting from their atomic or molecular components. Top-down lithographic methods, of course, continue to be the best for the specialized task of making planar structures with arbitrary patterns (e.g., circuits).

b. *Too Many Components for Conventional Placement* Self-assembly is a parallel process and usually involves very large number of components. Robotic pick-and-place methods for placement are limited by the fact that they are serial. Although the process can be accelerated by using a number of robotic devices in parallel (e.g., the multiple scanning probe heads), they cannot approach the number of molecules in a test tube. For numerous small components, self-assembly is still the best approach, whereas for unsymmetrical patterns with relatively large components, for example, microelectronic circuits, top-down fabrication remain the method of choice.

c. *Too Many Dimensions* The technologies for making nanometer-scale structures by current lithographic methods are largely restricted to planar or quasiplanar geometries. An array of trenches carved into silicon by reactive-ion etching is formally a 3D structure, but its method of production precludes more complex 3D structures without elaborate stacking and registration. Self-assembly is not limited to planar surfaces and may work better in 3D than in 2D in some cases. Crystallization is a good example of 3D self-assembly. In crystallization, each atom benefits from bonding interactions with all of its neighboring atoms. While there are some materials that form stable 2D structures (e.g., self- assembled monolayers), the majority of materials form solids in three dimensions because of energy minimization through interactions with neighbors.

d. *Cost* Since self-assembly is a parallel process and it does not involve robotic or other devices to impose order on nanostructures, it will probably, when applicable, ultimately always have an advantage in cost over other methods of fabrication.

6.4.5 Challenges in Self-Assembly

Self-assembly also poses a number of substantial intellectual challenges. The brief summary of these challenges is that we do not yet know how to do it and cannot even mimic those processes known to occur in biological systems at other than quite elementary levels. Although there are countless examples of self-assembly all around us – from molecular crystals to mammals – the basic rules that govern these assemblies are not understood in useful detail, and self-assembling processes cannot, in general, be designed and carried out “to order.” Many of the ideas that are crucial to the development of this area – “molecular shape,” the interplay between enthalpy and entropy, the nature of noncovalent forces that connect the particles in self-assembled molecular aggregates – are simply not yet under the control of investigators. In addition, there are issues of function in self-assembled aggregates that need solution. The most promising avenues for self-assembly are presently those based on organic compounds, and organic compounds, as a group (although with exceptions), are electrical insulators; thus, many ideas for information processing and electrical/mechanical transduction will require either fundamental redesign in going from the macroscopic systems presently used to self-assembled systems, or the development of new types of organic molecules that show appropriate properties.

6.5 Synthetic Strategies for Molecular Self-Assembly

The synthesis of self-assembled nanoscale materials and devices is determined by various surface chemistries involved on the nanoscale. These assemblies originate from interfacial noncovalent interactions and/or surface chemical reactions at the molecular or atomic scale. The surface chemistry involved in these techniques and applications is termed **nanoscale surface chemistry**.

Molecular synthesis is a technology that chemists use to make molecules by forming covalent bonds between atoms. Molecular self-assembly is a process in which molecules (or parts of molecules) spontaneously form ordered aggregates and involve no human intervention; the interactions involved usually are noncovalent. In molecular self-assembly, the molecular structure determines the structure of the assembly. Synthesis makes molecules; self-assembly makes ordered ensembles of molecules (or ordered forms of macromolecules). The structures generated in molecular self-assembly are usually in equilibrium states (or at least in metastable states). The novelty of self-assembly is in the focus on the formation of matter structured rationally at scales less than 100 nm, and the realization that the only practical method of achieving these structures is to have the components assemble themselves spontaneously. Molecular self-assembly can be achieved by using following three common approaches:

- Self-assembly through physiosorption (patterned organic monolayers)
- Self-assembly through chemisorption
- Self-assembly through metal ion–ligand interactions.

6.5.1 Physiosorption (Patterned Organic Monolayers)

Physiosorption of molecules involves formation of patterned monolayers through self-assembly. Molecules are adsorbed onto the surface through relatively weak van der Waals interactions and probable electronic interactions of the adsorbate with the surface. The overall structure and stability of the molecular assembly is determined by various intermolecular interactions such as hydrogen bonding, coordinate bonding, host–guest interactions, and so on [16, 17]. For example, trimesic acid and structurally related compounds form hexagonal networks (rosette structures) through hydrogen bonding on Cu(1 1 1) and graphite surfaces (Figure 6.5a). Similarly, 4-[*trans*-2-(pyrid-4-yl-vinyl)]benzoic acid forms molecular wires through the head-to-tail hydrogen bonding between pyridyl and benzoic acid moieties (Figure 6.5b).

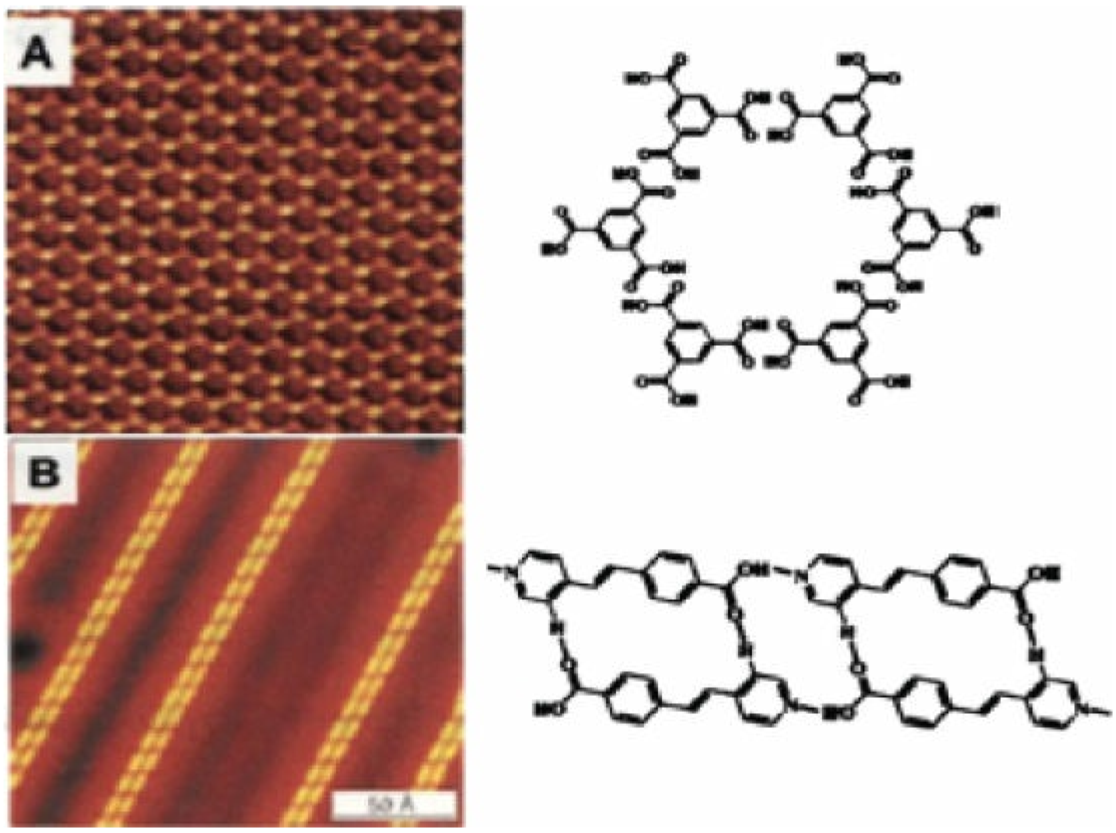

Figure 6.5 STM images of (a) hexagonal close network of trimesic acid on HOPG. Lackinger et al. [17], © 2005. With permission of ACS; and (b) molecular wires of 4-[*trans*-2-(pyrid-4-yl-vinyl)]benzoic acid on Ag(1 1 1) surface. Smith et al. [18], © 2004. With permission of Wiley, VCH-Verlag.

6.5.2 Chemisorption

The chemisorption of surfactants, with electron-rich head groups (e.g., S, O, N), on transition metals such as copper and gold is one of the widely used methods for self-assembly of molecules on surfaces. The assembly takes place through the polar covalent or ionic bond interactions between the surfaces and head group and further strengthened through favorable lateral interactions between adjacent molecules. The chemisorption of thiol groups on Au(1 1 1) surface is the most widely investigated system due to its strong coordinating ability with the metal [18]. A schematic representation of SAM of *n*-alkanethiolate molecules chemisorbed to a gold surface is shown in Figure 6.6a. The presence of molecules chemically bound to the surface renders modified interfacial properties (wetting, conductivity, adhesion, and chemistry), which are distinctly different from those of the bare substrate and, therefore, SAMs are of prime technological interest.

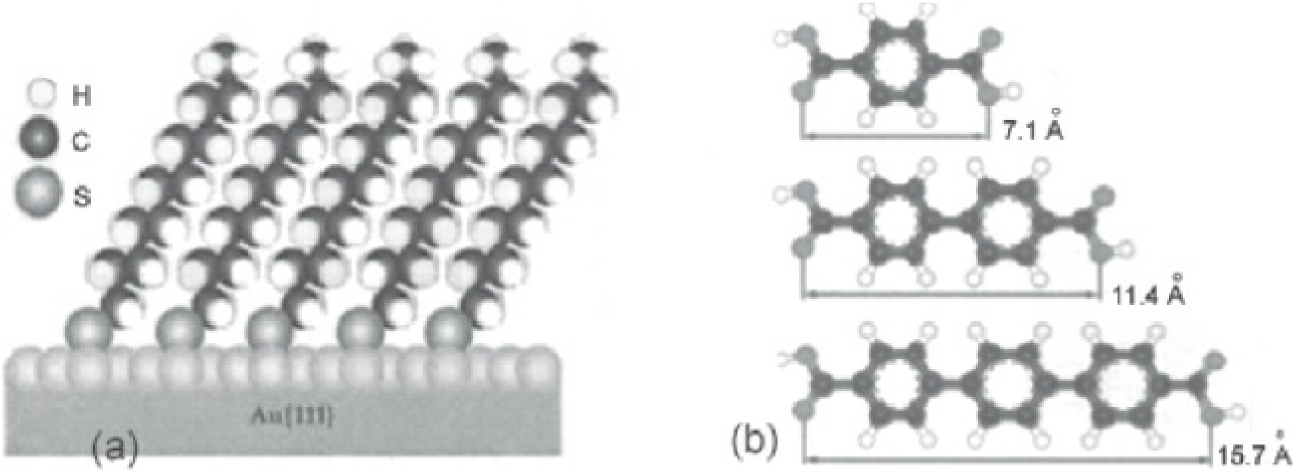

Figure 6.6 Schematic representation of (a) *n*-dodecanethiolate monolayer, self-assembled on an atomically flat gold substrate. Smith et al. [18], © 2004. With permission of Elsevier; (b) dicarboxylic acid derivatives as spacer.

Stepanow et al. [19], © 2006. With permission of ACS.

6.5.3 Metal Ion–Ligand Interactions

Interaction of metal ion centers with organic ligands (Lewis bases) results in stronger, directional, and selective bonding and are widely used for the preparation of coordination polymers and network structures. This methodology provides an excellent way of organizing metal ions on surfaces. Metal ions possess smaller size (<1 nm), and their properties can be tailored by the type and geometrical arrangement of the ligands. The local distribution of electron density around the respective metal ion can form structural and functional base in the design of molecular devices. The inherent properties of the coordinated metal ions such as redox, electronic, or spin states can be used for multistate digital information storage and processing (e.g., spintronics) [19]. Spacing between Fe atoms can be controlled through metal-organic coordination networks with the proper choice of ligands. Dicarboxylic acid derivatives of proper lengths have been used as spacer between iron atoms (Figure 6.6b).

6.6 Biological Self-Assembly

Understanding the folding of proteins is one of the outstanding challenges of science as a whole, and not just biophysics and biochemistry. Although much progress has been made in modeling protein folding, there is no consensus on the best method. Analytical methods have modeled the free energy landscape based on random energy models, the most recent of which analyze the conformational transition in a random heteropolymer by using spin-glass methods. Some structural insights into protein conformational dynamics have emerged from steered molecular dynamics simulations in which Monte Carlo moves are used as well as molecular dynamics trajectories. DNA is an important component of many structures and devices in Nanobiotechnology. DNA computing is an application currently attracting considerable attention. In one approach, single DNA strands are attached to a silicon chip. Computational operations can then be performed in which certain DNA strands couple to added DNA molecules. Multistep computational problems can also be solved. In these systems, the DNA strands encode all possible values of the variables. Complementary DNA strands are then added and attach themselves to any strand that represents a solution to one step of the computation. The remaining single strands are removed. This process is repeated sequentially for each step, and the DNA that is left is read out (via PCR amplification) to provide the solution (represented in binary form, a given binary number corresponding to an eight nucleotide sequence). The DNA-directed assembly of proteins, by using oligonucleotides capped with streptavidin, is another exciting realm of applications. The method can be used to fabricate laterally patterned arrays of many types of biotinylated macromolecules. The charged nature of DNA has been exploited to bind metal ions, for example, silver, which aggregate into nanoparticles; these are then used as seeds for the further deposition of silver to produce nanowires. Positively charged C_{60} fullerene derivatives have also been condensed onto DNA. Similarly, CdS nanoparticles have been template on the charged DNA backbone. Arrays of DNA-functionalized CdS nanoparticles have been assembled layer by layer on a gold electrode by using a set of two populations of DNA-capped CdS nanoparticles and a soluble DNA analytes. The two oligonucleotides bound to CdS nanoparticles are complementary to the ends of the target DNA. The construction of nanoscale geometric objects and frameworks by using three-arm and four-arm synthetic DNA molecules has also been reported. Vesicles formed by lipids (termed liposomes) are model systems for the cell membrane. The incorporation of channel forming is the biotin–streptavidin complex, for which the free energy of binding is comparable to that of a covalent bond. Proteins (porins) into lipid bilayers have been studied for many years, and synthetic structural and functional mimics have been devised. It is straightforward to form vesicles from the lipid bilayers. Block copolymers form vesicles that can be polymerized, which is clearly advantageous in encapsulation applications. The incorporation of channel-forming proteins into planar polymerized triblock copolymer membranes has been reported. This result extends further the delivery/nanoreactor capabilities of the biomimetic structures. Recently, porous core–shell latexes with pH-dependent swelling properties have been developed. These are analogous to the pH-controlled pore opening of the protein shell of Cowpea chlorotic mosaic virus. By appropriate surface functionalization, the recognition properties of bilayers can be enhanced, as required for many drug-delivery applications. A model recognition system is the biotin–streptavidin complex, for which the free energy of binding is comparable to that of a covalent bond.

6.7 Templated (Non-Molecular) Self-Assembly

Self-assembly of molecular or nonmolecular components by noncovalent interactions offers an invaluable tool for the preparation of discrete nanostructures and extended 2D and 3D materials, which are often not accessible by any other fabrication process. Study of biology has identified many processes that use templated self-assembly; these strategies provide stimuli for nonmolecular self-assembly for many years. Biological strategies, however, may be constrained in ways that are not relevant in nonbiological systems; we cannot assume that biology demonstrates all strategies for self-assembly. It seems that templating (i.e., providing constraints whether physical boundaries or sequence in a chain) may be an important way to bring order and asymmetric structure to self-assembled aggregates. The attributes for increased interest of scientific community in the area of strategy for self-assembly are as follows:

i. The nonmolecular systems allow tests of hypotheses about self-assembly that cannot be carried out with molecules and extend our understanding of the fundamental, abstract concepts of self-assembly. The characteristics of atoms determine the interactions between molecules. It is difficult to adjust the potential function between, say, two chlorine atoms to determine the influence of that change on self-assembly; chlorine atoms are what they are. Chemistry has great control over the structure of molecules, but little control over the characteristics of atoms. By contrast, it is possible to choose among a wide range of interactions (van der Waals, ionic, steric, entropic, magnetic, gravitational, electrostatic, and others) when using components larger than molecules, and often it is possible to adjust these interactions over wide ranges of strength, range, and selectivity. Nonmolecular systems are, thus, in many ways more flexible in their design than molecular systems.

ii. Experimental convenience: It is often easier to fabricate nonmolecular components than it is to synthesize molecules, and easier to observe the process and products of self-assembly using these large components.

iii. Self-assembly offers routes to ordered states of matter (e.g., ordered arrays of nanospheres for photonic crystals that probably cannot be generated practically by any other type of process; it thus has specific application in important problems in materials science, condensed matter science, and engineering.

iv. Self-assembly shows every promise of playing a key role in nanoscience and nanotechnology. Assembling nanometer-scale components into ordered arrays probably will be possible only by self-assembly.

v. Self-assembly offers a possible route to the fabrication of 3D microstructures. Photolithography, the technique used most widely to fabricate microstructures, is intrinsically a planar technology, and its extension to 3D structures is limited to the stacking of planar sheets. Self-assembly may offer a more flexible alternative.

vi. A number of problems in manufacturing including problems in robotic assembly may be aided by self-assembly. For macroscopic objects (those sufficiently large that conventional robotic pick-and-place might in some circumstances be practical and economical), self-assembly may offer the opportunity to form structures in regions inaccessible to robotic arms. It may even be an interesting strategy for the assembly of large structures in environments (e.g., the microgravity of space or the ocean) where lateral mobility is relatively unhindered by the effects of gravity and friction.

6.7.1 Self-Assembly Through Capillary Interactions

Currently, microelectronic components are fabricated using primarily 2D fabrication technologies such as photolithography or etching. The 2D components are integrated using strategies based on pick-and-place robots. As smaller sizes and higher speeds become increasingly important, these robots become unfit for the job. Fluidic self-assembly using capillary forces has shown great potential for the manufacture of heterogeneous and 3D microsystems because of its self-aligning and parallel assembly nature [20]. Surface energy minimization drives hydrophobic materials to attract each other in an aqueous environment. The interest in these forces has grown due to their recognized importance for the self-assembly of macroscopic and microscopic (Brownian) particles and even of protein molecules and viruses. Capillary forces responsible for self-assembly can be of two types, namely, normal and lateral. The normal capillary force is directed to the planes of the contact lines on the particle surfaces (Figure 6.7a). It can be attractive or repulsive depending on whether the capillary bridge is concave or convex. Attractive forces of this type lead to 3D aggregation and consolidation of bodies built up from particulates. On the other hand, the overlap of the perturbations (menisci) around two particles gives rise to a *lateral* capillary force between them (Figure 6.7b). This force could be attractive or repulsive depending on whether the overlapping menisci, formed around the two particles, are similar (say, both concave) or dissimilar (one is concave and the other is convex). The attractive lateral capillary forces cause 2D aggregation and ordering in a rather wide scale of particle sizes: from 1 cm down to 1 nm.

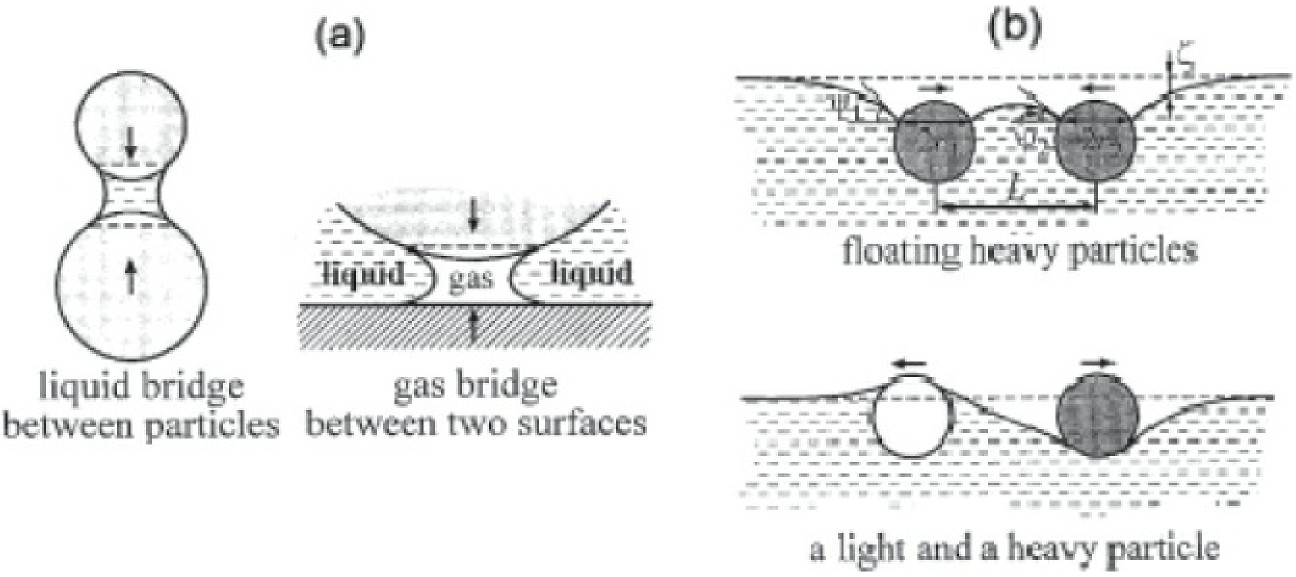

Figure 6.7 (a) Normal capillary bridge forces, (b) lateral capillary forces.

Kralchevsky and Denkov [20], © 2001. With permission of Elsevier.

Many different questions arise regarding accuracy goals for self-assembly in the fluidic phase. The binding site and micro part shape is of crucial significance for the uniqueness of assembling and has been investigated in detail [21]. Moreover, the strengths of the capillary forces and the potential energy shape with respect to the degrees of freedom are crucial for an eventual accurate alignment. To accelerate detection of optimized fluidic system's parameters for self-assembly, it is essential to apply simulations to different configurations in order to reduce extensive experimental effort. Examples of micronized 2D and 3D structures, realized by capillary interactive forces, are illustrated in Figure 6.8: open hexagonal array (a) and hexagonal lattice formed around circular templates (b) self-assembled from poly(dimethylsiloxane) plates floating at the interface between perfluodecalin and water. A spherical structure formed by self-assembly of hexagonal metal plates on the surface of a drop of perfluodecalin in water (c) and a compact 3D structure formed by self-folding of a string of tethered, polymeric polyhedral (d) are some of the examples.

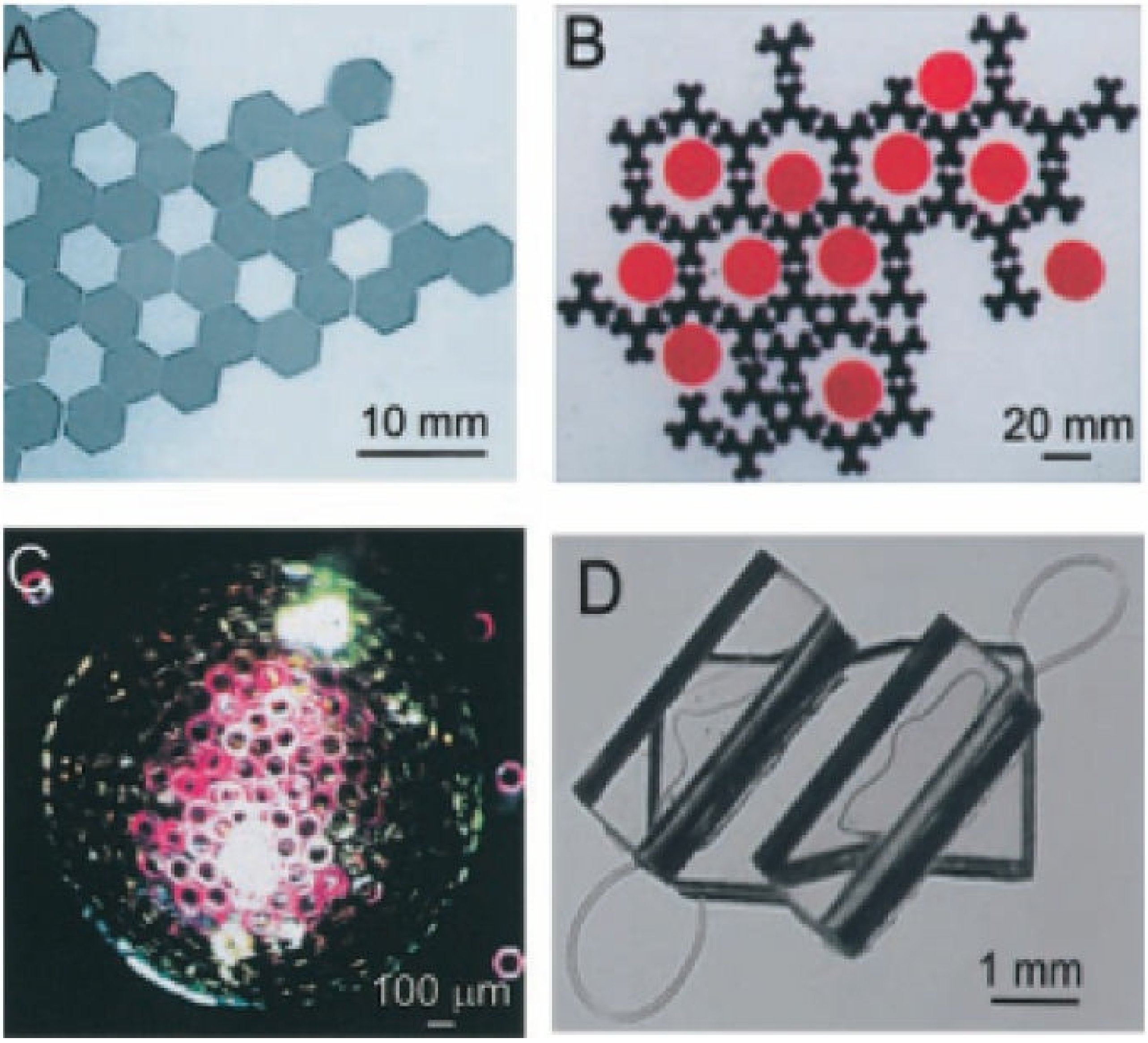

Figure 6.8 Self-assembled 2D (a and b) and 3D (c and d) structures in systems of macroscopic components interacting via capillary interactions.

Vlasov et al.[21], © 2001. With permission of NPG.

6.7.2 Self Assembly Through Lego Chemistry

On the scale of atoms and molecules, everything shakes and bumps around very quickly due to thermal energy: the higher the temperature, the more bumping and shaking. This ambient energy makes individual molecular bonds unstable: they do not last long. Instead of sticking pieces together on every strong chemical bond, nature uses several weak intermolecular bonds in parallel. When the pieces fit properly, all of these bonds work together like many hands joining and make the overall bonding stable [22]. If some bonds are made in the incorrect geometrical arrangement, the pieces are only loosely bound and unstable. This serves as an error-correction mechanism. Geometrical compatibility plays an important role in the self-assembly. The pieces fit together as puzzle pieces: the multiple weak bonds only come together when the pieces fit correctly. For example, proteins are shaped in a very precise way to fit together specifically with other proteins to perform a task or build a structure within the body. Along with the “lock-and-key” compatibility, the protein will have a “code” of sticky spots that will correspond to the similarly sticky spots of the partner protein. The binding event will be stable if the parts fit together in the correct way.

Figure 6.9 shows how the exercise can help to understand basic thermodynamic relations through the use of mechanical model. The Gibbs free energy, *G*, is the parameter that is minimized for a physicochemical system at equilibrium. A process will proceed spontaneously if the change in free energy (*G*) is negative (it proceeds to a lower free energy). ΔG is equal to the change in enthalpy, ΔH , minus the change in entropy, ΔS , multiplied by absolute temperature *T*. In the process of self-assembly (just as in the case of water freezing), the change of enthalpy is negative (ΔH < 0, exothermic) because bond formation releases energy and the change in entropy is negative (ΔS < 0, more order), because the assembled structure is more ordered than the unassembled particles. As the temperature rises, the second term ($T\Delta S$) becomes larger and more negative, and ($-T\Delta S$) becomes more and more positive (because of the negative sign) until ΔG is positive. A positive ΔG means that the process is energetically unfavorable. The pieces will not assemble (or if already assembled at a lower temperature, they will come apart or “melt”). The point at which the green line in the graph crosses the zero energy axis can be thought of as a freezing/melting point, or the point where self-assembly becomes favorable/unfavorable. Note that the process depicted in the figure can be directly related to the formation of complex biomolecules, for bonds (multiple weak bonds) and the lock-and-key strategy to allow several pieces to come together in a unique predetermined way [23].

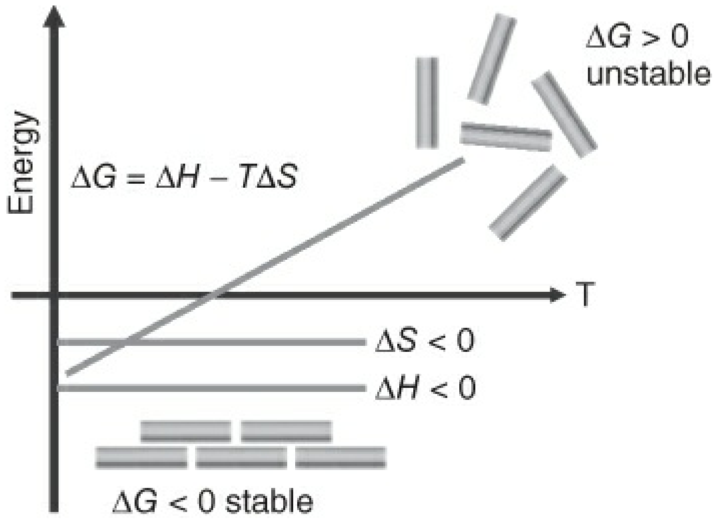

Figure 6.9 Thermodynamics of self-assembly.

Courtesy of G. Jones, National Science Teachers Association.

6.8 Self-Assembled Supramolecular Nanostructures

Within the last few years, there has been a surge of interest in composite materials consisting of a polymer filled with plate-like particles, such as clay particles. Such fillers are extremely effective in modifying the properties of polymers and orders-of-magnitude improvements in transport, mechanical, and thermal properties. Examples of applications include low-permeability packaging for food and electronics, toughened automotive components, and heat- and flame-resistant materials. Polymer–clay nanocomposites have several unique features:

i. Lighter in weight than conventional filled polymers with the same mechanical performance.

ii. Mechanical properties are potentially superior to fiber-reinforced polymers because reinforcement from the inorganic layers occurs in two rather than one dimension.

iii. Exhibit outstanding diffusion-barrier properties without requiring a multipolymer layered design, and thus can be recycled. Self-assembled inorganic nanoparticles are generally synthesized through colloidal chemistry.

6.8.1 Inorganic Colloidal Systems

Clays are colloidal suspensions of plate-like mineral particles, with a large aspect ratio. Typically, the particles are formed from silicate layers combined with layers of octahedrally coordinated aluminum or magnesium atoms. The layer structure leads to a lamellar phase for the clay in water. The aim in applications is to retain this structure in the polymer–clay nanocomposite, possible structures for which are illustrated schematically in Chapter 7 (Figure 7.19). These structures are obtained by the chemical treatment of the clay particles (in particular, adsorption of organic molecules). The intercalated structure leads to enhanced barrier properties, which result from the tortuous path for gas diffusion around the clay platelets.

The colloidal behavior of vanadium pentaoxide (V_2O_5) has been investigated since the 1920s. Under appropriate conditions of pH, ribbon-like chains can be obtained by the condensation of V–OH bonds in a plane [24]. A scanning electron micrograph of dried ribbons is shown in Figure 6.10a suspension of V_2O_5 can be aligned in electric and magnetic fields, similar to the organic nematogens used in liquid-crystal displays. A number of strategies have been adopted to create macroscopic colloidal crystals. A common technique relies on the sedimentation of particles under gravity. However, the resulting samples generally contain polycrystalline domains. Other approaches rely on surfaces to act as templates to induce order. For example, spin coating onto planar substrates can provide well-ordered monolayers. Flow-induced ordering has also been exploited. A method that relies on the so-called convective self-assembly has been used to create ordered crystals upon rapid evaporation of solvent. A related technique is the controlled withdrawal of a substrate from a colloidal solution (similar to Langmuir–Blodgett film deposition), where lateral capillary forces at the meniscus induce crystallization of spheres. If the meniscus is slowly swept across the substrate, well-ordered crystal films can be deposited. Convective flow acts to prevent sedimentation and to continuously supply particles to the moving meniscus. Controlled layer-by-layer growth on template is achieved by the slow sedimentation of the silica spheres. The formation of well-ordered crystal monolayer “rafts” of charged colloid particles on the surface of oppositely charged surfactant vesicles has also been demonstrated. The most promising materials for the matrix seem to be certain wide-band-gap semiconductors, such as CdS and CdSe, because they have a high refractive index and are optically transparent in the visible and near-IR region. The preparation of porous metallic (gold) nanostructures within the interstices of a latex colloidal crystal has been demonstrated. Here, a solution of gold nanoparticles fills the pores between colloidal particles, and the latex is subsequently removed by calcination. A similar method can be used to fabricate inverse opal structures of titanium dioxide. The same idea has been applied to form nanoporous polycrystalline silicon, templated by 855 nm silica spheres deposited by low-pressure chemical vapor deposition (CVD), Figure 6.10b.

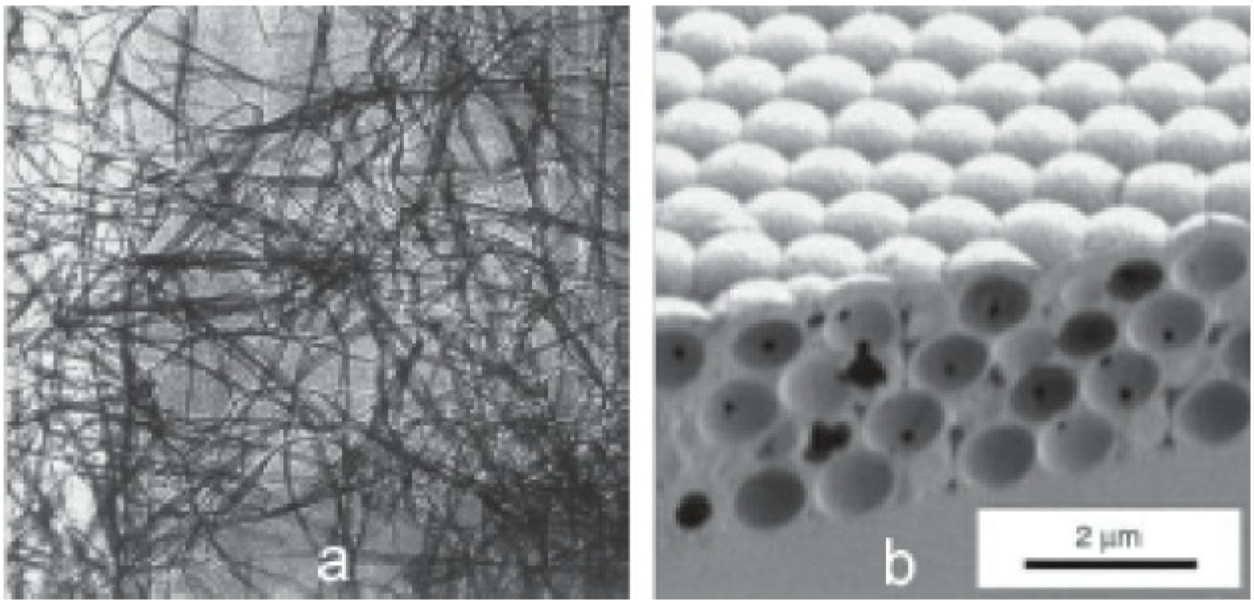

Figure 6.10 Cross-sectional view of SEM image: (a) dried suspension of V_2O_5; (b) polycrystalline silicon templated by 855-nm silica spheres.

Pelletier et al. [24], © 2000. With permission of EDP Sciences, Springer-Verlag, Societa Italiana di Fisica.

In a related approach, silica spheres are coated with gold (to reinforce the colloidal crystal) and then immersed in electroless deposition baths to deposit metal films within the porous template, the silica is then being removed in a HF rinse. These types of approach have been extended to a “lost wax approach” to prepare high-quality arrays of hollow colloidal particles (or filled particles) of various ceramic and polymer materials [25]. Here, a well-ordered silica colloidal crystal is taken and used as a template for polymerization in the interstices. If the pores are interconnected, the polymer forms a continuous porous matrix. By appropriate choice of polymer, either hollow or solid nanoparticles can be grown in it (the former grow from the polymer matrix inwards, the latter form within the voids). In this way, it was possible to prepare colloidal crystals of solid or hollow TiO_2 particles, as well as conducting polymer nanoparticles. An extension of colloidal polymerization techniques can be used to prepare defined waveguides. Crossed laser beams were used to polymerize polymer precursors within particular pores. By scanning the laser beams, a waveguide with a chosen path and shape can be fabricated.

6.8.2 Liquid-Crystalline Structures

Liquid crystals are the material having a new phase intermediate between a solid and a liquid. They flow like liquids and show ordered structures like solids. These materials do not show sharp transition point from solid state to liquid state or vice versa. Depending on the intermolecular arrangement, liquid crystals can be classified into three main categories, namely, nematic, semactic, and cholesteric. Many of the liquid crystals are known to show supramolecular nanostructures.

Liquid-crystal phases formed by mineral moieties have been known for almost as long as organic liquid crystals. Renewed interest in them has arisen because of the ability to combine the properties of liquid crystals, in particular anisotropy and fluidity, with the electronic and structural properties of minerals. They may also be cheaper to produce than conventional liquid crystals, which require organic synthesis. Rod-like mineral systems that form nematic phases have been well studied. Sheet-forming mineral compounds that form smectic (layered) structures in solution are also known. Colloidal smectic phases have been observed for β-FeOOH, which forms “Schiller layers” (German word for iridescent). The rod-like β-FeOOH particles form layers at the bottom of the flask. The spacing between the layers is comparable to the wavelength of light, hence the iridescence [26]. A swollen liquid-crystalline lamellar phase based on extended solid-like sheets (rather than rod-like particles) has been rationally prepared using a solid acid $H_3Sb_3P_2O_{14}$. In contrast, plate-like $Ni(OH)_2$ nanoparticles (91 nm radius, 12 nm thick) and $Al(OH)_3$ nanodisks (radius 200 nm, thickness 14 nm) self-assemble into columnar mesophases. A nematic phase has also been observed for the latter material. The formation of a smectic phase rather than a columnar phase is expected if the polydispersity in particle radius is large enough to prevent the efficient packing of columns. In fact, at very high volume fractions in the $Al(OH)_3$ suspensions, evidence was obtained for a smectic phase, which can accommodate the polydispersity in radius (although a low polydispersity of particle thickness is required). It has been proposed that liquid crystals can be used as switchable birefringent phase shifters. However, as yet, the means to arrange the liquid crystal in nanometer-scale arrays has been lacking. Patterning of liquid crystals in micelles or microemulsion is a promising way to achieve this.

6.8.3 Self-Assembled Structured Nano-Objects in Unusual Shapes

Nanoparticles with shapes other than simple spheres, shells, or tubes have been prepared by soft-material-mediated methods. The photoinduced conversion of silver nanosphere into silver nanoprisms has been reported. Photoinduced fragmentation of silver nanoparticles is believed to produce the single-crystal prism-shaped particles (the faces of which correspond to planes of the crystal lattice). The growth habit of (nano) crystals can be controlled by using organic agents, such as surfactants (as well as through the degree of supersaturation or ionic strength), to produce polyhedra with faces controlled by the growth rate of certain planes in the crystal unit cell. Nanoparticles of CdSe with rod, arrow, teardrop, and tetrapod shapes may be fabricated by using surfactants to selectively control the growth of certain crystal faces. String and other superstructures of spherical nanoparticles may be prepared in the same way. Nature exploits soft materials to template the synthesis of hard nanostructures, which includes examples of the intricate structures made by certain organisms. Self-assembled nanostructures may also be used to template the formation of helical nanoparticles (using peptides in solution) or of string, necklace, or vesicular structures formed by block copolymers in solution. The self-assembly of rod–coil block copolymers can, for example, be used to make mushroom-shaped nano-objects that assemble into lamellar stacks that have polar ordering.

6.9 Self-Folding Nanostructures

The first issue in designing components whose self-assembly will generate functional systems is to understand the trade-offs between ease of fabrication (easier with large components) and function (often higher with small components). The shape of the components is also important for 3D microelectronic devices, for example, self-assembly must probably generate a structure with continuous voids to allow for external cooling. The more complicated the shape, the more difficult it is to fabricate, especially in a form functionalized for self-assembly. Most methods for 3D microfabrication are based on photolithography. A number of techniques (some very clever but none very simple or easily extended to the parallel fabrication of very large numbers of components) have been used to convert 100-µm-scale 2D structures produced by photolithography into 3D structures. The most versatile of these at present seems to be **self-folding**, which is another form of self-assembly. This technique uses conventional lithographic technology to make planar precursors to the 3D microstructures. These structures then fold spontaneously into 3D shapes via capillary forces or electrical activation of conjugated polymers. The processes used in this type of fabrication involve multiple steps of fabrication, however, and the folding processes are early in their development. Hierarchical self-assembly, the self-assembly of simple components such as microspheres into structured aggregates such as triangles or tetrahedra, followed by the self-assembly of those structures into more complex structures is another promising approach.

6.10 Applications

Molecular self-assembly is ubiquitous in chemistry, materials science, and biology and has emerged as a discrete field of study for formulating strategies for synthesis. The formation of molecular crystals, colloids, lipid bilayers, phase-separated polymers, and SAMs are all examples of molecular self-assembly, as are the folding of polypeptide chains into proteins and the folding of nucleic acids into their functional forms occurring in biological systems. Even the association of a ligand with a receptor is a form of self-assembly: the semantic boundaries between self-assembly, molecular recognition, complexation, and other processes such as supramolecules that form more ordered from less ordered assemblies of molecules. Following section briefly outlines the important applications specific to the supramolecules and self-assembled nanostructures [27–29].

6.10.1 Supramolecular Chemistry

Materials Technology

Supramolecular chemistry and molecular self-assembly processes, in particular, have been applied to the development of new materials. Large structures can be readily accessed using up synthesis as they are composed of small molecules requiring fewer steps to synthesize. Thus, most of the bottom-up approaches to nanotechnology are based on supramolecular chemistry.

Catalysis

A major application of supramolecular chemistry is the design and understanding of catalysts and catalysis. Noncovalent interactions are extremely important in catalysis: binding reactants into conformations suitable for reaction and lowering the transition state energy of reaction. Template-directed synthesis is a special case of supramolecular catalysis. Encapsulation systems such as micelles and dendrimers are also used in catalysis to create microenvironments suitable for reactions (or steps in reactions) to progress that is not possible to use on a macroscopic scale.

Medicine

Supramolecular chemistry is also important for the development of new pharmaceutical therapies by understanding the interactions at a drug binding site. The area of drug delivery has also made critical advances as a result of supramolecular chemistry, providing encapsulation and targeted release mechanisms. In addition, supramolecular systems have been designed to disrupt protein–protein interactions that are important to cellular function.

Data Storage and Processing

Supramolecular chemistry has been used to demonstrate computation functions on a molecular scale. In many cases, photonic or chemical signals have been used in these components, but electrical interfacing of these units has also been shown by supramolecular signal transduction devices. Data storage has been accomplished by the use of molecular switches with photochromic and photoisomerizable units, by electrochromic and redox-switchable units, and even by molecular motion. Synthetic molecular logic gates have been demonstrated on a conceptual level. Even full-scale computations have been achieved by semisynthetic DNA computers.

Green Chemistry

Supramolecular chemistry also finds applications in green chemistry where reactions have been developed that proceed in the solid state directed by noncovalent bonding. Such procedures are highly desirable since they reduce the need for solvents during the production of chemicals.

Other Devices and Functions

Supramolecular chemistry is often pursued to develop new functions that cannot appear from a single molecule. These functions also include magnetic properties, light responsiveness, self-healing polymers, synthetic ion channels, and molecular sensors. Supramolecular research has been applied to develop high-technological sensors, processes to treat radioactive waste, and contrast agents for CAT scans.

6.10.2 Self-Assembled Nanomaterials

Biomedical Applications

Very recently, the physical and chemical properties of nanomaterials have inspired scientists to create new devices that are able to interact with biological systems at the nanoscale. While still in its early stages of development, the field of nanotechnology has already made a tremendous impact in medicine and biology in general. In particular, the field of Nanobiotechnology – which refers to the use of biological systems and molecules to build nanoscale materials – is currently leading to promising applications in diagnostics and therapeutics. The most recent advances in the field of diagnostics and sensing using self-assembled nanomaterials include sensors based on optical, magnetic, and electrochemical detection. Nanomaterials for gene and drug delivery, in particular viruses, analogs of viruses, micellar systems, carbon nanotubes, inorganic/organic hybrid nanostructures, and nanomaterials are based on lipids or amphiphiles, and DNA: self-assembled nanomaterials for therapeutic, regenerative medicine, and tissue engineering.

Information Technologies

Information technologies based on optics and electronics play a key role in our modern society. In particular, organic (opto)electronics is a promising field of research with a high potential for the fabrication of new devices with a low cost of production. To implement this field, the bottom-up construction of electroactive nanomaterials is becoming a very popular domain of investigation, thanks to its potential for miniaturizing and improving the material characteristics.

Self-assembled nanomaterials used for organic electronic devices include conducting materials, organic field-effect transistors, organic light-emitting diodes, and organic solar cells. Nanomaterials created for the storage and processing of information including memory devices and Boolean logic circuits are nanofibers, inclusion complexes, coordination complexes, rotaxanes, and so on.

Environmental Sciences

One of the main societal issues of the century concerns environment and in particular how to solve problems related to pollution and wastes. Various approaches ranging from inorganic to polymeric or carbon materials have been envisioned to overcome these issues. While still in their infancy, functional devices made of supramolecular self-assemblies have emerged as promising tools to tackle some of these environmental concerns. Self-assembled structures used to sense chemical analytes ranging from gases to metal ions up to substances present in food or cosmetics. Supramolecular materials that are used to store gases or small molecules are nanoporous molecular crystals and metal-organic frameworks. Supramolecular ion channels as synthetic transport systems. Nanostructured membranes and metal-organic frameworks are useful for the separation and purification of mixtures of gases or chemicals and as catalyst in chemical reactions.

6.10.3 Nanomotors

A key element of any nanomachine is a nanomotor. A variety of approaches to the manufacture of nanomotors is being followed. The crudest is to make miniature versions of motors from the macroscopic world; however, the ability to scale such structures downwards is limited by the energy dissipation from friction. Alternative strategies include attempts to mimic motors in biological systems and the simpler “motors” driven by chemical potential or concentration gradients, for example, in oscillating gels. By considering biological motors [30] as models for artificial motors, two types of nanomotors can be identified. In the first type, proteins such as kinetin, dynein, and myosin behave as linear slides. In the second category are the well-studied rotary motors such as the synthetic ATP complex and bacterial flagella motors. The development of rotary nanomotors is crucial for advancing nanoelectromechanical system technology. Recently, design, assembly, and rotation of ordered arrays of nanomotors have been reported. The nanomotors (Figure 6.11a–e) are assembled from nanoscale building blocks with nanowires as rotors, patterned nanomagnets as bearings, and quadrupole microelectrodes as stators. Arrays of nanomotors rotate with controlled angle, speed (over 18,000 rpm), and chirality by electric fields. It is revealed using analytical modelling that the fundamental electrical, mechanical, and magnetic interactions at the nanoscale level in the nanomotor system excellently agrees with experimental results and provides critical understanding for designing metallic nanoelectromechanical systems. The nanomotors can be continuously rotated for 15 h over 240,000 cycles. They are applied for controlled biochemical release and demonstrate releasing rate of biochemicals on nanoparticles that can be precisely tuned by mechanical rotations. Such innovations derived from concept, design, and actuation to application are relevant to nanoelectromechanical system (NEMs), nanomedicine, microfluidics, and lab-on-a-chip architectures.

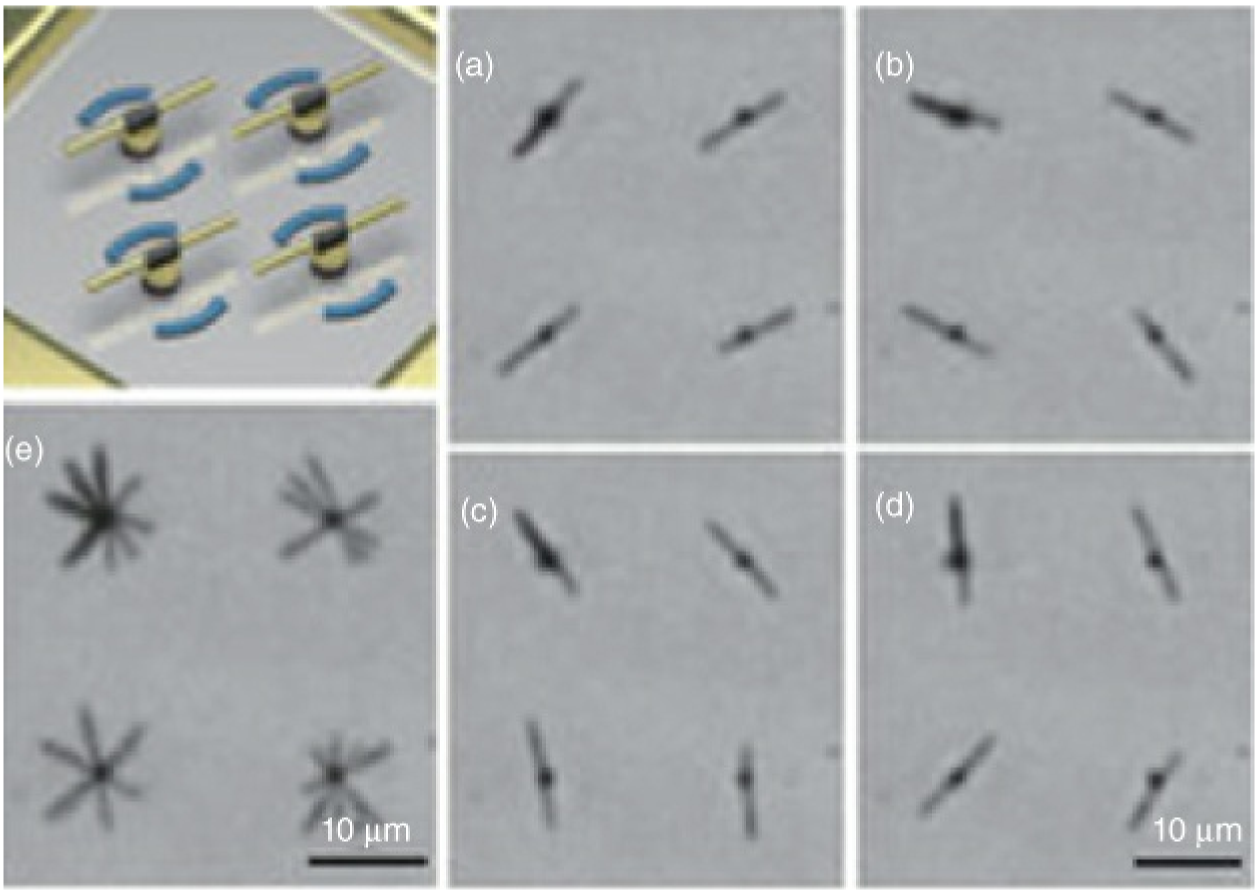

Figure 6.11 Nanomotors assembled in ordered arrays: (a–d) Schematic diagrams and snapshot images of a 2 × 2 nanomotor array rotating; (e) overlapped snapshot image of a 1 × 3 nanomotor array.

Kwanoh et al. [30], © 2014. With permission of NPG.

Review Questions

Q1. Name different interactions involved in supramolecular structures; identify the weakest and the strongest among them.

Q2. Differentiate self-assembled monolayer from supramolecules.

Q3. Define the process of self-assembly and outline its two different modes. How self-assembly differs from molecular recognition.

Q4. What do you understand by template-directed synthesis and outline its advantages.

Q5. Differentiate between metal-organic framework (MOF) and supramolecular organic framework (SOF) structures. Mention significant application areas of SOFs.

Q6. What do you understand by (a) biomimetics, (b) molecular imprinting, (c) molecular machinery.

Q7. Discuss the van der Waals, electrostatic, and magnetic interactions involved in self-assembled structures by giving examples.

Q8. What are the short-range attractive forces? Discuss their implications in self-assembled structures?

Q9. How does entropy of molecules helps in the formation of self-assembled structures?

Q10. Outline the advantages of self-assembly in the synthesis of functional nanomaterials.

Q11. What are soft materials and how does self-assembly help in their existence?

Q12. Explain the term “nanoscale surface chemistry” and its utility in the formation of nanostructured materials of different dimensionalities.

Q13. Name the biomolecules that represent self-assembled structures.

Q14. “Self-assembly is a nature inspired phenomena,” justify the statement.

Q15. Name the polymer–clay nanocomposites formed through the process of self-assembly.

Q16. How self-assembly helps in creating nanoparticles in different structural forms?

Q17. Discuss briefly the nonmolecular self-assembly.

Q18. “Self-folding is another form of self-assembly,” justify the statement.

Q19. Discuss briefly the applications of self-assembled/supramolecular structures in following fields: (a) catalysis, (b) medicine, (c) data storage, (d) green chemistry, and (e) sensors.

Q20. Which biological systems can be referred as nanomotors?

References

1. *Supramolecular Organization and Materials Design*, Eds. W. Jones and C. N. R. Rao, Cambridge University Press, Cambridge, UK, 2002.

2. C. M. Lieber, “Nanoscale Science and Technology: Building a Big Future from Small Things”, *MRS Bull.* **28** (2003) 486–491.

3. G. M. Whitesides and M. Boncheva, “Beyond Molecules: Self-Assembly of Mesoscopic and Macroscopic Components”, *Proc. Natl. Acad. Sci. U. S. A.*, **99** (2002) 4769–4774.

4. M. Albrecht, “Supramolecular Chemistry: General Principles, Selected Examples and Applications”, *Naturewissenschaften*, **94** (2007) 951–966.

5. Y. Lan, “Supramolecular Chemistry: General Principles, Selected Examples and Applications”, http://ak-powell.chemie.uni-karlsruhe.de/.

6. C. J. Pedersen, “The Discovery Of Crown Ethers” Nobel lecture, December 8, 1987. http://www.nobelprize.org/nobel_prizes/chemistry/laureates/1987/pedersen-lecture.pdf.

7. (a) J.-M. Lehn, “Supramolecular Chemistry”, *Science*, **260** (1993) 1762, 1763. (b) J.-M. Lehn, *Supramolecular Chemistry*, Wiley-VCH, 1995.

8. K. Ariga, J. P. Hill, M. V. Lee, A. Vinu, R. Charvet and S. Acharya, “Challenges and Breakthroughs in Recent Research on Self-Assembly”, *Sci. Technol. Adv. Mat.*, **9** (2008) 014109.

9. *Supramolecular Chemistry: From Molecules to Nanomaterials*, Eds. P. A. Gale and J. W. Steed, Wiley, 2012.

10. K.-D. Zhang, J. Tian, D. Hanifi, Y.-B. Zhang, A. C.-H. Sue and T.-Y. Zhou, “Towards a Single-Layer, 2D Honeycomb Supramolecular Organic Frameworks in Water”, *J. Am. Chem. Soc.* **135** (2013) 17913–17918.

11. K. J. M. Bishop, C. E. Wilmer, S. Soh and B. A. Grzybowski, “Nanoscale Forces and Their Uses in Self-Assembly”, *Small*, **5** (2009) 1600–1630.

12. S. A. Harfenist, Z. L. Wang, M. M. Alvarez, I. Vezmar and R. L. Whetten, “Highly Oriented Molecular Ag Nano Crystal Arrays”, *J. Phys. Chem. B*, **100** (1996) 13904–13910.

13. T. K. Sau and C. J. Murphy, “Self-Assembly Patterns Formed Upon Solvent Evaporation of Aqueous Cetyltrimethyl Ammonium Bromide-Coated Gold Nanoparticles of Various Shapes”, *Langmuir*, **21** (2005) 2923–2929.

14. J. R. Thomas, “Preparation and Magnetic Properties of Colloidal Cobalt Particles”, *J. Appl. Phys.*, **37** (1966) 2914–2915.

15. Y. Lalatonne, J. Richardi and M. P. Pileni, “Van der Waals vs Dipolar Forces Controlling Mesoscopic Organizations of Magnetic Nanocrystals”, *Nat. Mater.*, **3** (2004) 121–125.

16. J. V. Barth et al., “Building Supramolecular Nanostructures at Surfaces by Hydrogen Bonding”, *Angew. Chem. Int. Ed.* **39** (2000) 1230–1234.

17. M. Lackinger, S. Griessl et al., “Self-Assembly of Trimesic Acid at the Liquid–Solid Interface: A Study of Solvent –Induced Polymorphism”, *Langmuir*, **21** (2005) 4984–4988.

18. R. K. Smith, P. A. Lewis and P. S. Weiss, “Patterning Self Assembled Monolayers”, *Prog. Surf. Sci.*, **75** (2004) 1–68.

19. S. Stepanow, N. Lin et al., “Surface-Template Assembly of Two-Dimensional Metal–Organic Coordination Networks”, *J. Phys. Chem. B*, **110** (2006) 23472–23477.

20. P.A. Kralchevsky and N. D. Denko, “Capillary Forces and Structuring in Layers of Colloidal Particles”, *Curr. Opin. Coll. Interf. Sci.*, **6** (2001) 283–401.

21. Y. A. Vlasov, X. Z. Bo, J. C. Strum and D. J. Noris, “On-Chip Natural Assembly of Silicon Photonic Bandgap Crystals”, *Nature*, **414** (6861), (2001) 289–292.

22. A. W. Jacksona and D. A. Fulton, “Making Polymeric Nanoparticles Stimuli-Responsive with Dynamic Covalent Bonds”, *Polym. Chem.*, **4** (2013) 31–45.

23. S. Ogi, K. Sugiyasu, S. Manna, S. Samitsu and M. Takeuchi, “Living Supramolecular Polymerization Realized Through a Biomimetic Approach”, *Nat. Chem.*, **6** (2014) 188–195.

24. O. Pelletier, C. Bourgaux, O. Diat, P. Davidson and J. Livage, “A Small Angle X-Ray Scattering Study of the Isotropic and Pneumatic Phases of V_2O_5”, *Eur. Phys. J. E*, **2** (2000) 191–198.

25. S. H. Im, U. Jeong and Y. Xia, “Polymer Hollow Particles with Controllable Holes in their Surfaces”, *Nat. Mater.*, **4** (2005) 671–675.

26. *Liquid Crystals: Materials Design and Self-Assembly*, Ed. C. Tschierske, Springer, Heidelberg, Dordrecht, NY, 2012.

27. S. Bureekaew, S. Shimomura and S. Kitagawa, “Chemistry and Application of Flexible Porous Coordination Polymers”, *Sci. Technol. Adv. Mat.*, **9** (2008) 014108.

28. Y. Cui, Q. Wei, H. Park and C. M. Lieber, “Nanowire Nanosensors for Highly Sensitive and Selective Detection of Biological and Chemical Species”, *Science*, **293** (2001) 1289–1292.

29. N. K. Chaki and K. Vijayamohanan, “Self-Assembled Monolayers as a Tunable platform for Biosensor Applications”, *Biosens. Bioelectron.* **17** (2002) 441–456.

30. K. Kwanoh, X. Xiaobin, G. Jianhe and D. L. Fan, “Ultrahigh-Speed Rotating Nanoelectromechanical System Devices Assembled from Nanoscale Building Blocks”, *Nat. Commun.*, **5** (2014) 4632.

Chapter 7
Nanocomposites

7.1 Introduction

As a general definition, **composites** are solids made from more than one material. Composites are designed so that the properties of the composite utilize and combine the properties of the components.

Conventional composite materials consist of one or more discontinuous phases distributed in one continuous phase. Discontinuous phase is usually harder and with superior mechanical properties than continuous phase; the continuous phase is "*matrix*" and the discontinuous phase is "*reinforcement, or reinforcing material.*" The two materials work together to give a composite with unique properties; however, individual material do not dissolve or blend into each other. The properties of the composite are superior to those of either individual material and depend very much on the chemical composition of its components, microstructure, interfaces/adhesion, and morphology. To achieve the desired properties, a particular reinforcement is chosen for a particular matrix. A **nanocomposite** is a composite material, in which one of the components has at least one dimension in nanoscopic size.

Nature has mastered the synthesis of nanocomposites using natural reagents and polymers such as carbohydrates, lipids, and proteins to create strong composites such as wood (cellulose/lignin), bone (apatite/collagen), nacre (mother-of-pearl) (aragonite/protein), granite (quartz, feldspar), and a myriad of other materials [1]. Wood is a composite made up of long cellulose fibers (a polymer) held together by a much weaker substance called lignin. Cellulose (found in cotton) and lignin, both weak substances, when bind together form a much stronger substance. The bone in our body is also a composite. It is made from a hard but brittle material called hydroxyapatite (mainly calcium phosphate) and a soft and flexible material called collagen (a protein). Collagen is also found in hair and finger nails. Nature's remarkable features are its ability to combine, at the nanoscale, (bio)organic and inorganic components, allowing the construction of smart natural materials with a combination of different properties or functions, namely mechanics, density, permeability, color, and hydrophobia. Such a high level of integration associates several aspects: miniaturization of objects while accommodating a maximum of elementary functions in a small volume; hybridization between inorganic and organic components optimizing complementary possibilities, functions, and hierarchy. Figure 7.1 illustrates an excellent example of nature's wonderful nanocomposites, abalone. Abalone shell is made of thousands of layers of "tiles" of calcium carbonate, about 10 μm across and 500 nm thick. A key to the strength of the abalone shell is a protein adhesive that binds to the top and bottom surfaces of the calcium carbonate tiles. The protein glue is strong enough to hold layers of tiles firmly together, but weak enough to permit the layers to slip apart, absorbing the energy of a heavy blow in the process. The irregular stacks of thin tiles refract light to yield the characteristic luster of mother-of-pearl. They are organized in a highly ordered brick-like structure arranged in the toughest configuration theoretically possible. It is the design that makes the shell almost 3000 times stronger than the materials it is made out of, that is, calcium carbonate (chalk) and protein.

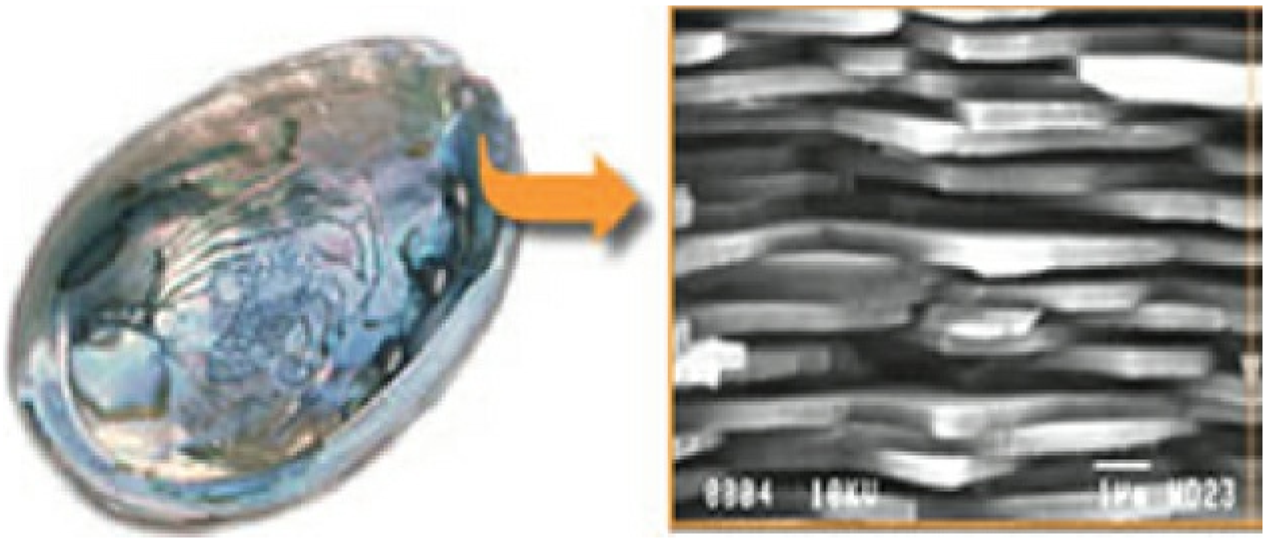

Figure 7.1 Abalone shell and its structure.

7.1.1 Man-Made Ancient Composites

The earliest man-made composite materials are bricks for building construction. By mixing mud and straw together, it is possible to make bricks that are resistant to both squeezing and tearing and make excellent building blocks. Ancient plywood prepared by Mesopotamians gluing wood at different angles was found to give better properties than natural wood. Concert, a mix of aggregate (small stones or gravel), cement, and sand, is another known ancient composite. It has good compressive strength (it resists squashing). The possibility to combine properties of organic and inorganic components for materials design and processing is a very old challenge that has started since ages (Egyptian inks, green bodies of china ceramics, prehistoric frescos, etc.). Maya blue is a remarkable example of quite an old man-made class I hybrid material whose conception was the fruit of an ancient serendipitous discovery [2]. Ancient Maya fresco paintings as shown in Chapter 1 (Figure 1.8b) are characterized by bright blue colors that had been miraculously preserved. The depth of color and resistance to acid and biocorrosion of Maya blue paint is attributed to a nanoparticle mechanism. From the mid-1950s, nanoclays have been used to control the flow of polymer solutions (e.g., as paint viscosifiers) or the constitution of gels (e.g., as a thickening substance in cosmetics). By the 1970s, polymer/clay composites were the topic of textbooks although the term "nanocomposites" was not in common use.

7.1.2 Modern Examples of Composites

Fiberglass is considered to be the first modern composite material. It is still widely used today for boat hulls, sports equipment, building panels, and many car bodies. In it, the matrix is a plastic and the reinforcement is glass fiber that has been made into fine threads and often woven into a sort of cloth. The plastic matrix holds the glass fibers together and also protects them from damage by sharing out the forces acting on them. Some advanced composites are now made using carbon fibers instead of glass. These materials are lighter and stronger than fiberglass but more expensive to produce. They are used in aircraft structures and expensive sports equipment such as golf clubs. Carbon nanotubes have also been used successfully to make new composites. The biggest advantage of modern composite materials is that they are light as well as strong. By choosing an appropriate combination of matrix and reinforcement material, a new composite material can be made to provide design flexibility because many of them can be molded into complex shapes such as aircrafts or aerospace vehicles.

7.1.3 Nanocomposites

Nanocomposites are reported to be the material of the twenty-first century. A nanocomposite is a multiphase solid material where one of the phases has one, two, or three dimensions of less than 100 nm or structures having nanoscale repeat distances between the different phases that make up the material. The general idea behind the addition of the nanoscale second phase is to create a synergy between the various constituents, such that novel properties capable of meeting or exceeding design expectations can be achieved. The properties of nanocomposites rely on a range of variables, particularly the matrix material, which can exhibit nanoscale dimensions, loading, degree of dispersion, size, shape, and orientation of the nanoscale second phase and interactions between the matrix and the second phase [3].

Nanocomposites are either prepared in a host matrix of inorganic materials (glass, metals, porous ceramics, etc.) or by using conventional polymers as one component reinforced by nanoscale particles or nanostructures, which are dispersed through the host matrix. In the broader sense, the definition of nanocomposites may include the porous media, colloids, gels, and copolymers apart from the usual combination of a bulk solid matrix and nanodimensional phase(s). The idea behind nanocomposites is to use building blocks with dimensions in the nanometer range to design and create new materials with unprecedented flexibility and improvements in their physical properties. This concept is exemplified in many naturally occurring materials, such as bone, which is a hierarchical nanocomposite built from ceramic tablets and organic binders. When designing the nanocomposite, one can choose constituents with different structures and composition and hence properties, so that materials built from them can be multifunctional. The mechanical, electrical, thermal, optical, electrochemical, and catalytic properties of the nanocomposites differ markedly from that of the component materials. In mechanical terms, nanocomposites differ from conventional composite material due to the exceptionally high surface-to-volume ratio of the reinforcing phase and/or its exceptionally high aspect ratio. A uniform dispersion of nanoparticles leads to a very large matrix/filler interfacial area, which changes the molecular mobility, the relaxation behavior, and the consequent thermal and mechanical properties of the material. Fillers with a high ratio of the largest to the smallest dimension (i.e., aspect ratio) are particularly interesting because of their high specific surface area, providing better reinforcing effects. In addition to the effects of the nanoreinforcements themselves, an interphase region of altered mobility surrounding each nanoparticle is induced by well-dispersed nanoparticles, resulting in a percolating interphase network in the composite and playing an important role in improving the nanocomposites properties. For a constant filler content, a reduction in particle size increases the number of filler particles, bringing them closer to one another. Thus, the interface layers from adjacent particles overlap, altering the bulk properties significantly. Apart from reinforcing nanoparticles, whose main role is to improve mechanical and barrier properties of the packaging materials, there are several types of nanostructures responsible for other functions, sometimes providing active or "smart" properties to the packaging system such as antimicrobial activity, enzyme immobilization, biosensing, and so on. Some particles can have multiple applications, and sometimes the applications can overlap, such as some immobilized enzymes that can act as antimicrobial components, oxygen scavengers, and/or biosensors.

7.1.4 Structure and Composition of Nanocomposites

7.1.4.1 Matrices

Matrix is the continuous phase of a composite whose function is to transfer stress to other phases and protect phases from environment. There are three main categories of matrices: polymer, metal, and ceramic. Matrices hold and protect the fibers (or other reinforcing material geometries, e.g., particles, platelets, short fibers, or whiskers) from environmental and physical damage. Keeping the fibers separated decreases cracking and redistributes the load equally among all fibers. Thus, the matrix contributes greatly to the properties of the composites. The ability of composites to withstand heat, or to conduct heat or electricity, depends primarily on the matrix properties since this is the continuous phase. Therefore, the matrix selection depends on the desired properties of the composite being constructed. For structural applications, the maximum usable temperature is critical and will often dictate the choice of matrix [4]. Approximate usable temperature ranges for the different matrix materials are as shown in Figure 7.2.

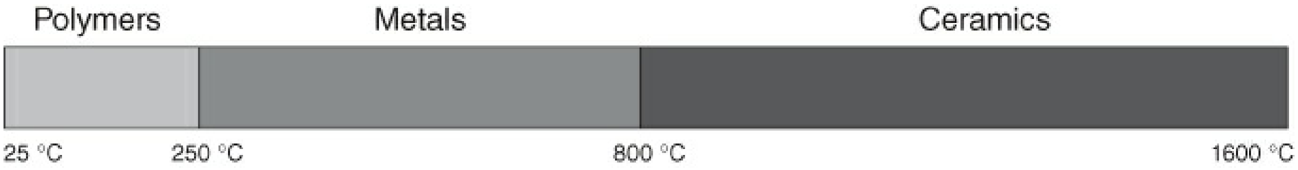

Figure 7.2 Working temperature range for different matrix materials.

Polymers

A polymer is a substance consisting of a large number of atoms bonded together in a long chain. Polymeric matrices are used because they are lightweight and easy to fabricate. Artificial skin, used for severe burn victims, is an example of a composite that contains a polymer matrix. There are two general types of polymer matrices: **thermoset** and **thermoplastic**. Thermoset polymers (e.g., epoxy) cure into an irreversibly hardened material. This is accomplished by "cross-linking," the formation of bonds between polymer chains that fixes the polymer in a 3D array, limiting the motion. Thermoplastic (e.g., polymethylmethacrylate) polymers are capable of being repeatedly softened by the application of heat and hardened by cooling the polymer. For temperature applications of 250 °C or lower, the matrices of choice are polymers.

Metals

Metal matrices have an intermediate working temperature range between 200 and 800 °C. The metals most commonly employed as matrices are lightweight alloys of aluminum, magnesium, and titanium. Metal matrices provide electrical conductivity, ductility, high strength, and high stiffness. These alloys are commonly used when it is necessary to extend the temperature range for a given application. Metal matrices are used in car engines and turbine blades. However, due to their relatively higher density and processing complexity as compared to polymer matrices, they are less commonly used.

Ceramics

Ceramic matrices are used for high-temperature applications. Ceramic matrices are not as commonly used as polymers because they are brittle and difficult to process. Their main constituents are alumina (Al_2O_3), silica (SiO_2), and other inorganic nonmetallic substances that are abundant in nature. Ceramic materials are a combination of a metal (e.g., aluminum) or intermediate metal (silicon) with a nonmetal (e.g., oxygen, nitrogen, or carbon). Their bonding is either ionic or covalent. Generally, ceramics are oxidation resistant, corrosion resistant, hard, strong, and able to withstand very high temperatures. The reinforcing material is usually selected to reduce brittleness. An example is the Al_2O_3/Al composites, where aluminum, a ductile material, serves as the reinforcing phase.

7.1.4.2 Reinforcements

The strength, stiffness, and density of the composite material are dependent on the reinforcing material [5]. The ultimate tensile strength of a composite is a result of the synergy between the reinforcement and the matrix. The main types of reinforcements are continuous fibers, discontinuous fibers (short fibers), whiskers, and particulates (Figure 7.3a–c). The elements selected as reinforcements are usually the lower atomic numbered elements of groups 2 (Be, Mg), 13 (B, Al), 14 (C, Si), 15 (N), and 16 (C) because of the desirable engineering traits of lightweight, high strength, and stiffness. These elements, or compounds of these elements, can be made into various kinds of reinforcements. The stable covalent bonding contributes to the strength and stiffness of the composites.

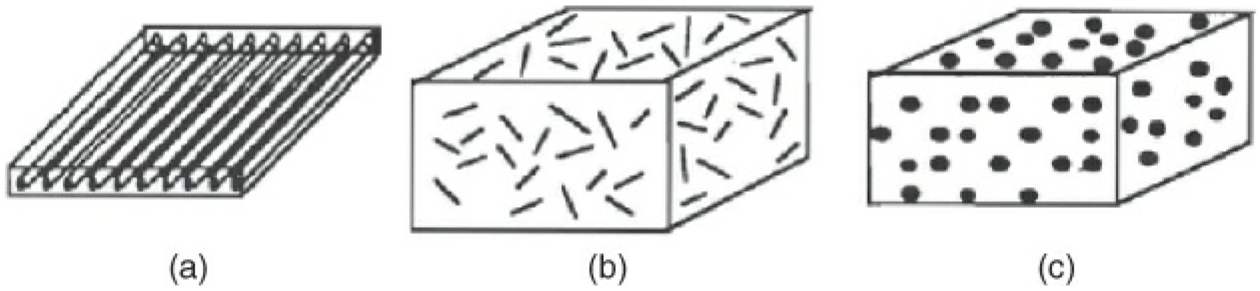

Figure 7.3 Types of reinforcements: (a) continuous fibers; (b) whiskers; (c) particulates.

7.1.5 Properties of Composite Materials

Major factors that determine the properties and performance of composites are as follows:

- Properties of the constituent materials
- The size, shape, quantity, and distribution of the reinforcement
- The effectiveness of the bond between matrix and reinforcement in transferring stress across the interface.

A unidirectional continuous fiber composite is strong and stiff along the fiber axis, but considerably weaker perpendicular to the fiber direction. The choice for the materials of reinforcement fibers depends on their chemical and physical properties that include strong covalent bonding, abundance, thermal stability, and low density. These fibers may be continuous or discontinuous, be aligned within the matrix, or randomly oriented. The threshold size ("critical size") of reinforcement below which the addition of nanoparticles improves various physicochemical properties is given in Table 7.1.

Table 7.1 Critical Size of Reinforcement Applicable to Different Properties

Properties	Critical Reinforcement Size (nm)
Catalytic activity	<5
Softening of hard magnetic materials	<20
Change of refractive index	<50
Superparamagnetism	<100
Strengthening and toughening	<100
Modifying hardness and plasticity	<100

Source: Courtesy of Kamigaito et al. [6], © 1991. With permission of Japan Society of Powder and Powder Metallurgy.

It must be noted that the mechanism responsible for property improvements remains a matter of debate. Strengthening theory based on a continuum approach is not useful because it ignores the influence of particles on micromechanics of deformation, that is, location of particles, grain size, and dislocation density. Several discontinuous approaches have been formulated to include the particle effect. They take into account one or more of the following strengthening mechanisms:

> **Orowan mechanism**: The stress that must be applied to force a dislocation to bypass an obstacle (such as a particle) is at the base of the Orowan strengthening effect, which is really the resistance of closely spaced hard particles to the passing of dislocations. If the particles are coarse (in the microsize range) and the interparticle spacing is large, the Orowan effect is not significant. Instead, when highly dispersed nanosized particles are present in a metal matrix, Orowan strengthening becomes more favorable. Creep resistance and thermal stability are consistently enhanced, even for only a small volume fraction (<1%), due to the fact that bowing is necessary for dislocations to bypass the particles. In addition to this, TEM (transmission electron microscope) observations reveal strong dislocation of bowing and tangling around the particles themselves, further confirming what stated above.
>
> **Thermal mismatch**: Matrix and reinforcement have different coefficients of thermal expansion. Therefore, during the cooling process, plastic deformations are produced in the matrix at the interface. These deformations can cause defect to such dislocations. Due to the increment of interfacial area, the density of dislocation is also increased.
>
> **Load bearing**: The strong bond due to the cohesion between particle and matrix contributes to carry the load applied to the material. When all these factors are taken into account, the increase in mechanical properties with the decrease in size can be estimated.

7.1.6 Classification of Nanocomposites

On the basis of nature of matrix, nanocomposites can be divided into three groups; each group may further be subdivided on the basis of the type of reinforcement, typical examples of these groups are included in Table 7.2 wherein nanocomposites are represented by the molecular formula of matrix/reinforcement.

> **I. Ceramic–matrix nanocomposites (CMNC)**, characterized by an inorganic matrix mainly ceramics, reinforced by nanoscale particles of inorganic (e.g., metal) or organic (e.g., carbon) nature.
>
> **II. Metal–matrix nanocomposites (MMNC)**, characterized by a ductile metal or alloy matrix reinforced by nanoscale rigid ceramics. The reinforcement can be either in the form of particles (e.g., silicon carbide, aluminum oxide), fibers (e.g., silicon oxide, carbon), or a mixture of both, that is, hybrid reinforcement.
>
> **III. Polymer–matrix nanocomposites (PMNC)**, characterized by an organic matrix mainly polymers reinforced by nanoscale particles or nanostructures of inorganic (e.g., clay) or organic nature.

Table 7.2 Classification of Nanocomposites and Typical Examples

Class	Examples
I. **Ceramic–Matrix Nanocomposites**	
• Ceramic–ceramic nanocomposites • Ceramic–metal nanocomposites • Ceramic–carbon nanocomposites	• Al_2O_3/SiC, Al_2O_3/Si_3N_4, Al_2O_3/TiO_2, Al_2O_3/SiO_2 • AI_2O_3/W, MgO/Fe, SiO_2/Ni, Fe/$Al_2O_{3,}$, Fe/SiO_2 • Al_2O/CNT, MWCNT–Si_3N_4, GPL/Si_3N_4

II. Metal–matrix nanocomposites	
• Metal–ceramic nanocomposites • Metal–carbon nanocomposites	• Ni/Al_2O_3, Cu/Al_2O_3, Fe-Cr/Al_2O_3, Al/SiC, Mg/SiC, Al/Al_2O_3, Mg/Al_2O_3, Al/AlN, Fe/MgO • Al/CNT, Mg/CNT
III. Polymer–matrix nanocomposites	
• Polymer–inorganic nanocomposites • Polymer–clay nanocomposites • Polymer–carbon nanocomposites • Polymer–polysaccharide nanocomposites • Polymer–starch nanocomposites • Polymer–chitin nanocomposites	• Polyester/TiO_2, PMMA/γ-Al_2O_3, PANI/V_2O_5, PMMA/Fe, PMMA/CoPt, PPF/WS_2, PPy-PTS/Fe_2O_3 • PET/exfoliated clay, PS/clay, PMMA/Na-MMT • PVA/ SWCNT, PPF/GO, PEO/GO • PVOH/cellulose whiskers, HPMC/MCC • PVOH/SNC • HPMC/ CS–TPP

PMMA, polymethyl methacrylate; PANI, polyaniline; PTS, *para*-toluene sulfonate; PPF, polypropylene fumarate; PPy, polypyrrole; PTS, *para*-toluene sulfonate; PET, poly(ethylene terephthalate); PS, polystyrene; MMT, montmorillonite; PVA, poly(vinyl alcohol); PEO, poly(ethylene oxide); GO, graphene oxide; MCC, microcrystalline cellulose; PVOH, polyvinyl alcohol; HPMC, hydroxy propyl methyl cellulose; MCC, microcrystalline cellulose, SNC, starch nanocrystal; CS–TPP, chitosan-tripolyphosphate.

7.2 Ceramic–Matrix Nanocomposites

Inorganic nanocomposites are mainly based on ceramic matrices. Ceramics, the nonmetallic high-performance chemical compounds derived from oxides, nitrides, borides, carbides, and silicides of metal, sought in many applications, namely highly efficient gas turbines, aerospace materials, automobiles, and so on. Ceramics-based nanocomposites with improved mechanical, tribological, corrosion resistant, and so on are referred to as **structural nanocomposites**, whereas **functional nanocomposites** demonstrate improved optical, electrical, and magnetic properties.

7.2.1 Structural Ceramic Nanocomposites

Presently, even the best processed ceramics pose many unsolved problems such as poor resistance to creep, fatigue, and thermal shock; degradation of mechanical properties at high temperatures; and low fracture toughness and strength. To solve these problems, one approach has been incorporating a second phase such as particulates, platelets, whiskers, and fibers in the micron-sized range at the matrix grain boundaries. However, the results obtained with these methods have been generally disappointing. Recently, the concept of nanocomposites have been considered, where nanometer-sized second-phase dispersions are inserted into ceramic matrices. Large improvements in both the fracture toughness and the strength of a ceramic can often be achieved with nanometer-range particles embedded in a matrix of larger grains at their grain boundaries. These can involve the incorporation of nanoceramic in ceramic, nanometal in ceramic, and carbon nanomaterial in ceramic, with improved structural properties are discussed here.

7.2.1.1 Ceramic–Ceramic Nanocomposites

The incorporation of fine SiC and Si_3N_4 nanoparticles in an alumina matrix (Al_2O_3, a structural ceramic material) first demonstrated the concept of structural nanocomposites. The dispersion of these particles have shown to improve the fracture toughness from 3 to 4.8 MPa $m^{1/2}$ and the strength from 350 to 1050 MPa at only 5 vol% additions of SiC as shown in Figure 7.4a. A further increase in SiC content lowers the strength to a constant value of approximately 800 MPa due to agglomeration problems. Nanocomposites with considerably improved mechanical properties have, to date, only been achieved in hot-pressed materials. The strength depends on relative density and decreased with increasing porosity. The evidence is that Al_2O_3/SiC nanocomposites show an explicit increase in strength accompanied by a modest increase in toughness. Furthermore, grain boundaries are strengthened in nanocomposites as manifested by the transcrystalline fracture mode as well as by the increased resistance to wear and creep.

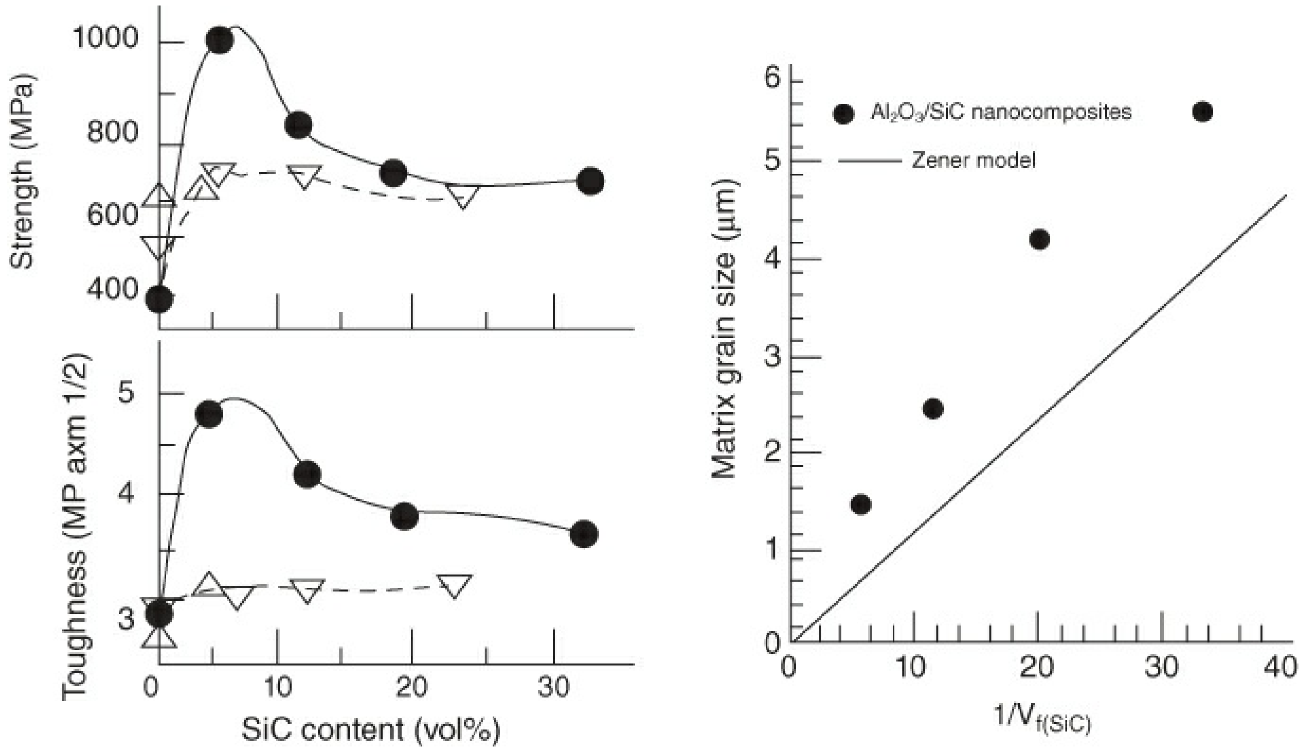

(a) (b)

Figure 7.4 (a) Strength and fracture toughness for various Al_2O_3/SiC nanocomposites as a function of SiC volume fraction. Nanocomposites derived from the classical powder route are represented by solid symbols and nanocomposites fabricated from an amorphous Si–C–N powder by open symbols; (b) average matrix grain size (*R*) as a function of $1/V_f$ of SiC for Al_2O_3/SiC nanocomposites.

Stearns et al. [31], © 1992. With permission of Elsevier.

Strengthening and Toughening Mechanisms

Al_2O_3/SiC nanocomposites show an explicit increase in strength accompanied by a modest increase in toughness. Furthermore, grain boundaries are strengthened nanocomposites as manifested by the transcrystalline fracture mode as well as by the increased resistance to wear and creep. One of the main features of nanocomposites is that matrix becomes refined on adding nanosize SiC, leading to higher strength. Furthermost, abnormal grain growth is reduced in nanocomposites, thus leading to a narrower grain size distribution. The effect of grain boundary pinning by small inclusions is described by Zener model (7.1):

$$\mathbf{R} \cong {}^3\!/\!_4\, r/V_f \tag{7.1}$$

where **R** is the average matrix grain boundary radius of curvature, depending on the radius (r) and the volume fraction (V_f) of spherical inclusions. Equation 7.1 often given in the form (7.2)

$$\mathbf{D} \propto r/V_f \tag{7.2}$$

where **D** is the average matrix grain diameter. In Figure 7.4b, the Zener model ($\mathbf{R} \cong {}^3\!/\!_4\, r/V_f$) is compared with experimental data where R is plotted as a function of $1/V_f$, the radius of SiC nanoparticles, model agrees well with the experimental data.

7.2.1.2 Ceramic–Metal Nanocomposites

Advanced structural ceramics can be fabricated by the dispersion of nanometallic second-phase particles into ceramics, which improves their mechanical properties, such as fracture toughness, and influences other properties including magnetic, electrical, and optical properties. Nanocomposites of this type are Al_2O_3/W or MgO/Fe. In most cases, ceramic–matrix nanocomposites encompass a metal as the second component where ideally both components are finely dispersed in each other in order to elicit the particular nanoscopic properties. The binary phase diagram of the mixture should be considered in designing ceramic–metal nanocomposites and measures must be taken to avoid a chemical reaction between both components especially for the metallic component that may easily react with the ceramic and thereby lose its metallic character. This is not an easily obeyed constraint because the preparation of the ceramic component generally requires high process temperatures. The safest measure thus is to carefully choose immiscible metal and ceramic phases. A good example for such a combination is represented by the ceramic–metal composite of TiO_2 and Cu, the mixtures of which were found immiscible over large areas in the Gibbs' triangle of Cu–O–Ti. The concept of ceramic–matrix nanocomposites was also applied to thin films that are solid layers of a few nanometers to some tens of micrometer thickness deposited upon an underlying substrate and that play an important role in the functionalization of technical surfaces. Gas flow sputtering by the hollow cathode technique turned out as a rather effective technique for the preparation of nanocomposite layers. The process operates as a vacuum-based deposition technique and is associated with high deposition rates up to some micrometers per second and the growth of nanoparticles in the gas phase. Nanocomposite layers in the ceramics range of composition were prepared from TiO_2 and Cu by the hollow cathode technique that showed a high mechanical hardness, small coefficients of friction, and a high resistance to corrosion. Granular films can also be made with a ceramic phase embedded with nanosized metal granules (such as $Fe/Al_2,O_3$, Fe/SiO_2). Such films often show unusual or enhanced transport, optical, and magnetic properties. The inclusion of nanosized metals in a thin ceramic film can transform it from an insulator to a conductive film.

7.2.1.3 Ceramic–CNT Nanocomposites

Nanoscale ceramic powders with carbon nanotubes provide another method for creating dense ceramic–matrix composites with enhanced mechanical properties. For instance, hot-pressed alumina with mixed carbon nanotubes results in lightweight composites with enhanced strength and fracture toughness compared to polycrystalline alumina. The processing conditions greatly influence the properties of this material.

Composites made from nanocrystalline ceramic materials and nanotubes fillers are much less brittle than monolithic ceramic materials. For example, a material made with nanophase alumina particles as the matrix and dispersions of both single- and double-walled carbon nanotubes as fillers exhibited a 25% increase in fracture toughness, without compromising the strength of the ceramic matrix. The characteristics of this proof-of-concept material apply to a wide range of nanophase ceramic oxide materials. The nanotube fillers can be made from other materials, such as boron nitride, silicon nitride, and silicon carbide. The benefits are less brittle than traditional ceramic materials and greater hardness than graphite fiber-reinforced ceramic composites. Ceramic composites effectively reinforced with CNTs are expected to possess greatly improved fracture toughness to complement their high hardness/strength at room and elevated temperatures, resistance to corrosion, and so on. They will be ideal cutting tools and be able to increase ceramics' market share substantially in the multibillion dollar cutting tool industry. Additionally, these novel composites with excellent room/high-temperature mechanical properties combined with the lubricating properties of CNTs will be ideal for the manufacture of parts of high-temperature applications such as heat and gas turbines. Some of the SWNT–ceramic composites show promise as thermoelectric materials with a high degree of thermoelectric efficiency due to high electrical and low thermal conductivities. The MWCNT–Si_3N_4 ceramic composites are likely to be used for manufacturing components for extremely severe mechanical and environmental condition such as ceramic bearings for high speed, high temperature, and corrosive environment and as novel material with high durability and electrical conductivity.

7.2.1.4 Ceramic–Graphene Nanocomposites

Graphene with its combination of large specific surface area, 2D high-aspect-ratio sheet geometry, and outstanding mechanical properties shows great promise as nanofiller in composite materials [6]. The majority of work in graphene nanocomposites has focused on polymer matrices (for details see Section 7.4.3). Ceramics are ideally suited for high-temperature applications but suffer from poor toughness. Recently, graphene fillers have been reported to enhance the toughness of bulk silicon nitride ceramics. Conventional ceramic matrix composites (CMCs) use 1D fibers as the reinforcement phase, such as carbon fibers or carbon nanotubes and ceramic whiskers. A major reason why processing graphene-reinforced bulk ceramic composites has been limited is the thermal stability limitations of graphene at high temperature. Ceramics start to densify and sinter at temperatures >1000 °C, and Si_3N_4 is usually sintered at ~1800 °C, therefore making it challenging to incorporate graphene that has low thermal stability at temperature in excess of ~600 °C. In order to determine the true effect of graphene on the toughness of Si_3N_4 and to eliminate the effect of the β-Si_3N_4, grains on toughening graphene nanofiller were incorporated into Si_3N_4 matrix employing spark plasma sintering (SPS) technique. SPS is a process that reduces the time at temperature from hours to minutes over conventional sintering methods, thus allowing accurate control of the α- to β-Si_3N_4 conversion and also limits thermally induced structural damage to the graphene platelets (GPL) by avoiding long processing times at high temperature.

In order to obtain uniform, densified microstructures of nanocomposites, colloidal processing methods were used to create homogeneously dispersed particle systems in aqueous suspension. Highly dispersed GPL/Si_3N_4 nanocomposite slurries, using 0.02, 0.5, 1.0, and 1.5 vol% graphene, were processed using methods analogous to that of those used for single-walled carbon nanotube (SWNT)–Si_3N_4 ceramic nanocomposites [8]. The platelets comprise an average of approximately three to four graphene sheets with less than 2 nm thickness. CTAB was used to disperse GPLs, assuming a carbon surface chemistry similar to that of the SWNTs. The amount of surfactant used was based on its dry weight and was used at concentration above the critical micelle concentration (1.0 wt%). The advantages of using SPS to densify ceramics are (1) rapid heating rates (up to 600 °C/min) and (2) simultaneous applied pressure (60–120 MPa). SPS simultaneously applies pressure and quickly pulses electric current through a graphite die containing the ceramic powders that are to be densified. The pulsed current assists in densification upon applied pressure and relies on creep and related mechanisms for densification and not the conventional sintering methods that involve diffusion and mass transport of material across the grain boundaries during long periods of time at elevated temperatures. Table 7.3 summarizes the density, theoretical density, hardness, and toughness values for each nanocomposite (0.02, 0.2, 1.0, and 1.5 vol% (Figure 7.5) GPL–Si_3N_4) and the monolith that were all sintered at ~1650 °C (for 2 min).

Table 7.3 Physical and Mechanical Properties of GPL-Si_3N_4 Nanocomposites

Starting Material Composition	Density (g/cm^3)	% Theoretical Density	Hardness (GPa)	Toughness (MPa^3 $m^{1/2}$)
0.00 vol% GPL + 100.00 vol% Si_3N_4	3.223	100.0	22.3 ± 0.84	2.8 ± 0.12
0.02 vol% GPL + 99.98 vol% Si_3N_4	3.204	99.5	21.2± 0.34	2.7 ± 0.14
0.50 vol% GPL + 99.50 vol% Si_3N_4	3.198	99.7	19.3 ± 0.69	5.21 ± 1.00
1.00 vol% GPL + 99.00 vol% Si_3N_4	3.175	99.3	20.4± 0.37	5.8 ± 1.18
1.50 vol% GPL + 98.50 vol% Si_3N_4	3.175	99.6	15.7± 0.61	6.6 ± 1.31

Source: Walker et al. [8], © 2011. With permission of ACS.

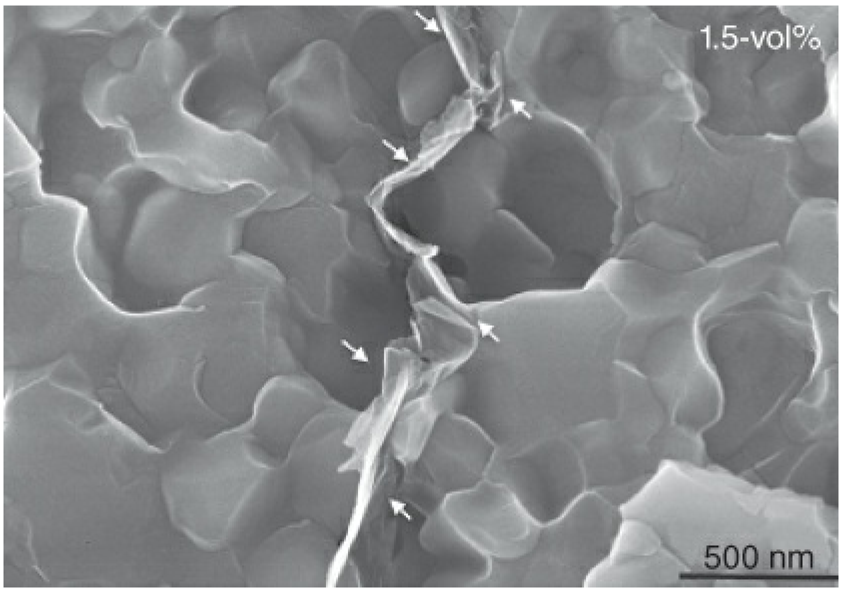

Figure 7.5 High magnification SEM images of the 1.5 vol% GPL-Si_3N_4 nanocomposites (arrows illustrate the location of GPL on the fracture surface).

Walker et al. [8], © 2011. With permission of ACS.

7.2.2 Functional Ceramic Nanocomposites

7.2.2.1 Nanocomposites with Enhanced Magnetic Properties

Materials with outstanding magnetic properties are in high demand as these are employed in nearly all important technical fields, for example, electrical power, mechanical power, high-power electromotors, miniature motors, computer elements, magnetic high-density recording, telecommunications, navigation, aviation and space operations, medicine, sensor techniques, magnetic refrigeration, materials testing, and household applications. Recent developments in the field of magnetic materials have involved materials with a nanocrystalline structure or layers of nanometer thickness. Nanocomposites with improved magnetic properties evolve either by nanostructuring the bulk magnetic materials or by nanosizing the magnetic powders [9]. Nanostructuring of bulk magnetic materials leads to soft as well as hard magnets (permanent magnets) with improved properties. “Finmet” is an excellent example of nanocrystalline soft magnetic alloys, which consist of melt-spun Fe–Si–B alloys containing small amounts of Nb and Cu. When annealed at temperatures above the crystallization temperature, the Fe–Si–B–Nb–Cu amorphous phase transforms to a crystalline solid, Fe–Si–B/Nb–Cu with grain size of about 10 nm. These alloys have excellent magnetic induction and large permeability, and a very small coercive field. In the context of nanostructuring of hard magnets (permanent magnets), the strongest known magnets are made of neodymium (Nd), iron, and boron (e.g., $Nd_2Fe_{14}B$). In these materials, it has been found that the coercive field decreases significantly below 40 nm and the remnant magnetization increases. Another approach to improving the magnetization curve of permanent magnets has been to fabricate nanocomposites made of hard magnetic phases, such as $Fe_{14}B/Nd_2$ and $Fe_{17}N_3/Sm_2$, within soft magnetic matrices (e.g., soft α-phase of iron). The effect of the inclusion of a soft iron mixed in with a hard material is to increase the remnant field.

Nanosized magnetic powders have extreme properties and show no hysteresis at any temperature. These materials are called **superparamagnetic,** and one example is nanosized powders of a Ni–Fe–Co alloy. The grain size of the material also influences the magnetization saturation point. For instance, the magnetization of ferrite increases significantly below a grain size of 20 nm. Thus, reducing the size of the grains in the magnet increases the energy product (which is the product of magnetization and coercivity). The coercivity also increases with decreasing the grain sizes. In the case of nanocomposites magnetic films, this is true if the grains are isolated (no interaction), but when the grains start contacting and exchange interaction kicks in, the coercivity falls rapidly with grain size. The coercivity is thus highest at percolation when the grains just start touching each other. This effect is important in the context of designing thin-film nanocomposites (**magnetic multilayer nanocomposites**), for instance high magnetic density recording. Magnetic multilayer nanocomposites are becoming an essential component of the new-generation data storage devices such as **magnetoresistive random access memory (MRAM**) having immense application in information and computer technology (ICT) sector.

7.3 Metal–Matrix Nanocomposites

The attention is now oriented toward the incorporation of nanoparticles and nanotubes to a ductile metal or alloy matrix resulting in **metal–matrix nanocomposites (MMNCs)** for structural applications because these materials exhibit even greater improvements in the physical, mechanical, and tribological properties compared to MMC with micron-sized reinforcements [10, 11]. Although metal–matrix nanocomposite materials have emerged as a viable alternative to overcome the limitations of metal–matrix composites, nanocomposites are challenging to produce as structural components due to difficulties in attaining a homogeneous distribution of the nanophased particles. Materials produced by this method are particularly useful in the aerospace, automotive, and aircraft industry. The advantage of MMCs is that they combine metallic properties (ductility and toughness) with ceramic characteristics (high strength and modulus), leading to materials having greater strength to shear and compression and to higher working temperature capabilities. The properties of MMCs are controlled by the size and volume fraction of the reinforcements as well as by the nature of the matrix/reinforcement interface.

The characteristics of nanoparticle reinforced metal composites show drastic change of fracture mode from intergranular fracture of monolithic metal to transgranular fracture of nanocomposites, improved strength, toughness, creep resistance, thermal shock resistance, and wear resistance and dimensional stability at high temperatures. The temperature sensitivity of aluminum decreases in the presence of both micro- and nanosized silicon carbide, although the effect of nanosized silicon carbide on dimensional stability is much higher than that of microsized silicon carbide. Reinforcement of SiC nanoparticles (50 nm) to 7075 aluminum alloy increases their wear resistance and high-temperature creep resistance when comparing the same alloy reinforced with 13 μm SiC particles. Furthermore, the volume percentage of nanoparticles needed to achieve this result was considerably smaller than the volume percentage of microparticles. Again, the tensile strength of an aluminum alloy reinforced with 1% volume of Si_3N_4 (10 nm) has been found to be comparable to that of the same alloy reinforced with 15% volume of SiC particle in the microsize range (3.5 μm), with the yield strength of the nanometric composite being significantly higher than that of the micrometric.

7.3.1 Metal–Ceramic Nanocomposites

Metal matrix composites are a hybrid material in which rigid ceramic reinforcements are embedded in a ductile metal–alloy matrix. The reinforcement can be either in the form of particles (e.g., silicon carbide, aluminum oxide), fibers (e.g., silicon oxide, carbon), or a mixture of both (hybrid reinforcement). Nanoparticles have progressively replaced other discontinuous reinforcement structures such as nanofibers, nanowires, or nanoplatelets. SiC, TiC, WC, TaC, TiB_2, AlN, and Al_2O_3 are some of the most common types of nanoparticles. They tailor the best properties of two different materials, such as ductility and toughness of the metallic matrix and the high modulus and strength of ceramic reinforcements. Representative metal–matrix nanocomposite systems and the associated attributes are given in Table 7.4. Boron nitride reinforced metal matrix composite and carbon nitride metal matrix composites are also new research areas of metal–matrix nanocomposites. A hybrid sol–gel with a silica base combined with metal oxides and nanoscale aluminum powder can form “**superthermite materials**.” Their first application can be traced back to the late 1960s, with the development of a steel wire reinforced copper alloy. The aerospace industry was the first one to apply the technology of composite materials to spacecraft components.

Table 7.4 Nanoceramic Metal–Matrix Nanocomposites and Associated Properties

Matrix/Nanoreinforcement	Properties
Al/SiC, Mg/SiC, Al/Al_2O_3, Mg/Al_2O_3	Improved ultimate strength, hardness, and elastic modulus
Al/AlN	Higher compression resistance and low strain rate
Ni/PSZ and Ni/YSZ	Improved hardness and strength
Cu/Al_2O_3	Improved microhardness

High-performance materials are a necessity when the environment is extreme and critical, as experienced in space missions. It is worth mentioning that the International Space Station, during its life, will undergo 175,000 thermal cycles from +125 °C to −125 °C as it moves in and out of the Earth's shadow. During the last four decades, aluminum matrix composites were specifically developed to meet both aerospace and defense needs. Continuous boron fiber-reinforced aluminum was used in the Space Shuttle Orbiter as the frame and rib truss members in the mid-fuselage section; there are other applications such as landing gear drag link yielding 45% weight saving. A Ga/Al composite is the constituent of a high-gain antenna boom for the Hubble Space Telescope. This boom (3.6 m long) offers the desired stiffness to maintain the position of the antenna during space maneuvers. Aluminum metal matrix composites find applications in a variety of other markets such as automotive, electronic packaging, industrial product, and recreational products.

7.3.2 Carbon Nanotubes–Metal Matrix Composites

Carbon nanotubes-metal matrix composites (CNTs-MMC) are emerging as new materials having advantage of the high tensile strength and electrical conductivity of carbon nanotubes [12]. The inorganic nanotubes such as tungsten disulfide nanotubes have proved to be better reinforcing agents as compared to carbon nanotubes.

7.3.2.1 Synthesis

Developments of synthetic techniques for CNTs-MMC are oriented toward an economically viable method, provide a homogeneous dispersion of nanotubes in the metallic matrix, and must lead to a strong interfacial adhesion between the metallic matrix and the carbon nanotubes. Among the variety of processing techniques [13–15], the **powder metallurgy** is the most popular and widely applied technique for preparing MM-CNTs composites. Electrodeposition and electroless deposition are the second most important techniques for deposition of thin coatings of MM-CNT composites as well as for deposition of metals on to the CNTs. For low-melting-point metals such as Mg and bulk metallic glasses, melting and solidification is a viable route. Various processes that have been adopted for synthesis of CNT-reinforced MMCs are discussed briefly:

> ***Powder metallurgy route:*** Most of the studies on Al-CNT and approximately half of the research work on Cu-CNT composites have been carried out using the powder metallurgy method. A few researchers have also prepared CNT composites based on Mg, Ni, Ti, Ag, Sn, and intermetallics through this route. The basic process steps consist of mixing CNTs with metal powder by grinding or mechanical alloying, followed by consolidation by compaction and sintering, cold isostatic pressing, hot isostatic pressing, or SPS. In most of these works, the composite compacts were subjected to postsintering deformation processes such as rolling, equichannel angular processing, extrusion, and so on. Irrespective of the process steps, the main focus was on obtaining good reinforcement by achieving homogeneous dispersion of CNT in the metal matrix and good bonding at the metal/CNT interface.
>
> ***Electrochemical route:*** In terms of the number of publications on MM-CNT composites, electrochemical deposition is the second most popular route after powder metallurgy techniques. The main difference between the two is that the electrochemical method is primarily used for the formation of thin composite coatings with a reported thickness of 20–180 mm, although some of the studies on electrochemical deposition do not report

coating thickness. This technique has also been used for coating CNTs with metals to produce 1D composites, the projected application for which includes, but is not limited to, different types of nanosensors, electrodes, interconnects, and magnetic recorder head in computer applications. Both electrodeposition and electroless deposition have been used for MM-CNT fabrication. Electrodeposition requires the traditional electrochemical cells in which composite film is deposited by the current flow between anode and cathode. The second technique, known as electroless plating, does not require any external energy source. This is basically a chemical process, in which thermochemical decomposition of metallic salts takes place in the bath to release metallic ions that forms composite with CNTs.

Molecular level mixing: Most of the studies reported in this method are related to Cu-CNT composites, except one that deals with Sb and $SnSb_{0.5}$ matrix composites. This method is capable of producing composite particles or 1D nanostructure of CNT coated with metal. The process requires CNTs to be acid treated and functionalized before introducing them into the metal-salt bath, thus aiding the CNT suspension and surface metal deposition on their surface. Subsequently, the bath is sonicated to prepare a CNT-metal ion precursor that goes through drying, calcinations, and a reduction process, in series, to produce metal-CNT composite powder. Figure 7.6 illustrates the process schematically. Reducing agents can also be used directly in the bath to avoid the separate step of reduction.

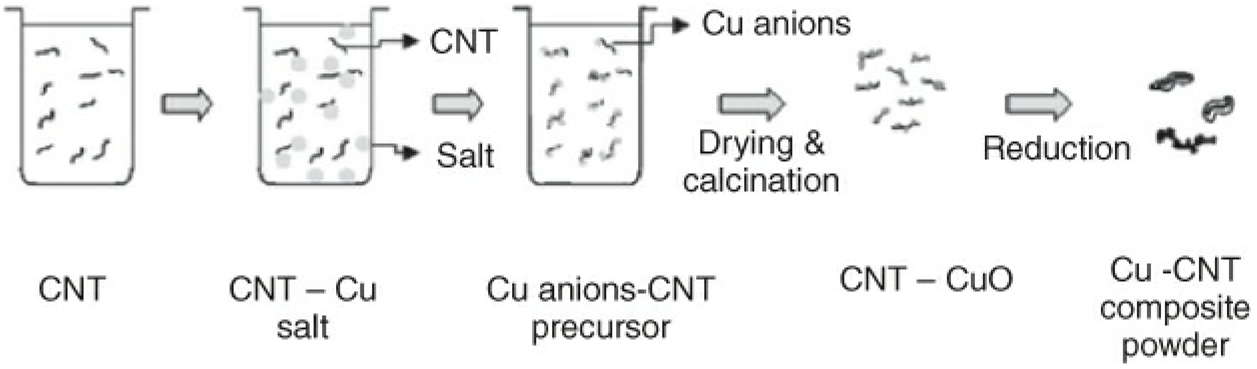

Figure 7.6 Preparation of CNT–metal matrix composites via chemical routes.

Ping et al. [15], © 2006. With permission of Wiley-VCH.

7.3.2.2 Properties

CNTs have a higher stiffness and strength compared to the metal matrix [16]. Therefore, the objective of fibrous reinforcements in the form of CNTs increases the tensile strength and the elastic modulus of the composite. Both of these effects are based on the following properties.

Mechanical: The critical issues in mechanical properties in MM-CNT composites are the homogeneous distribution of CNTs in the metal matrix, and the interfacial reaction and bonding to the matrix, to work as an effective reinforcement. It has been shown that the percentage enhancement in mechanical property of MM-CNT systems is a function of CNT content, which is nonlinear and very much depends on the processing method. The percentage enhancement in the mechanical property of MM-CNT systems takes place as a function of CNT content. The nonlinearity in the trend with CNT content owes to the variance in the microstructural features, defects, flaws, and porosity level caused by processing. The variance is further aggravated by the difficulty in measuring the mechanical properties of CNT-reinforced composites caused by difficulties of preparing mechanical testing samples.

Electrical and electronic properties: Owing to excellent electrical properties, evinced by the current carrying density of ~4×10^9 A/cm^2 (three orders of magnitude higher than Cu or Al), CNTs have been used as reinforcement to metals for the enhancement of electrical properties. Al 12.5 vol% CNT composite prepared by powder metallurgy displayed increased electrical resistivity by 66%. The sharp increase in the electrical property beyond 10 vol% CNT is attributed to the increase in interfacial area and strain in the matrix due to presence of CNT clusters, both of which hinders electron transfer through the composite.

Thermal properties: Carbon nanotubes are known to have very high thermal conductivity of 1812 ± 300 W/(m K) and very low coefficient of thermal expansion (CTE) ~ 0. Hence, MM-CNT composites have a great potential to be used for thermal management. Tang and coworkers reported 63% decrease in CTE with 15 vol% CNT addition to Al matrix. Further increase in CNT content increases CTE, which has been attributed to the agglomeration of CNTs. Deng et al. have obtained 12% reduction in CTE with 1.28 vol% CNT addition in Al, which has been attributed to the larger surface area of CNTs that creates larger interface and thus restricts thermal expansion of the metal matrix.

Wear and friction properties: Wear properties are more critical for coatings, and hence most of the wear studies are on Ni-CNT composite coatings formed by electrodeposition techniques. There are few studies on Cu-CNT and Al-CNT composites. All of these studies have reported a decrease in the coefficient of friction (COF) and increase in the wear resistance with the addition of CNTs to the metal matrix. The decrease in the COF has been attributed to the lubricating nature of the MW-CNTs caused by the easy sliding of their walls, which are attached by weak van der Waals forces. The improved resistance to wear is attributing to the role of CNTs as spacers, preventing the rough surfaces of the matrix from contact with the wear pin.

Corrosion properties: Most of the corrosion studies are performed on electrodeposited Ni-CNT composite coatings with only a single study on Zn-CNT composite coating. Electrodeposited coatings are more prone to corrosion due to the presence of pores and voids. All the studies have shown an increase in the corrosion resistance of the composite coatings with CNT addition due to two reasons. First, the chemical inertness of the CNTs that helps forming a passive layer on the coating surface. Second, CNTs help filling up voids and pores of electrodeposited coatings leaving no place for initiation of localized corrosion.

Hydrogen-storage properties: Hydrogen-storage capacity has been studied for MM-CNT composites by very few researchers. Mg-CNT composites have a better hydrogen-storage capacity and absorption–desorption rate than other hydrogen-storage materials. At higher temperatures, composite with 5 wt% CNT shows better hydrogen-storage capacity than 20 wt% CNT, attributable to the breakage and amorphous carbon content of the CNTs in the latter.

7.3.2.3 Applications

Carbon nanotubes have better strength and stiffness than carbon fibers and hence have the potential in replacing carbon fiber-reinforced MMCs in various applications [17]. Overcoming the challenges in processing, as described in the previous sections, will result in efficient use of the mechanical properties and will result in the strongest MMCs known to mankind. Some of the potential application areas, exploiting their unique properties, are summarized in Table 7.5.

Table 7.5 Potential Application Areas and Unique Properties of CNT-Reinforced Metal Matrix Composites

Application Areas	Unique Properties
Aerospace industry: aircraft brakes, landing gears	Good wear resistance and thermal conductivity; low density and high strength
Space applications: high-gain antenna boom, structural radiators	Low density, high strength, low coefficient of thermal expansion, good electrical conductivity
Sports industry: lightweight bicycles, tennis and badminton rackets	High strength, high elastic modulus
Electronic packaging: heat sinks for thermal management, solders	High thermal conductivity, low coefficient of thermal expansion, increased strength
Energy generation and storage: anodes and anode coatings, hydrogen-storage materials	Large surface area, high current density, increased H_2 adsorption–desorption rate, reduced response times

7.4 Polymer–Matrix Nanocomposites

Nanostructured polymer composites simply referred to as **polymer nanocomposites** (PNCs) form a new generation of materials [18, 19]. PNCs are frequently seen as an attractive route to upgrade and diversify properties of polymers without the need of finding new ones, and with the same (or slightly modified) processing equipment. PNCs are often defined as thermoplastics or thermoset combined with distinctly dissimilar constituents in the form of nanoparticles having at least one dimension less than 100 nm. They can also be classified, depending on their dimensionality of the nanoparticles, into 0D, 1D, and 2D, where 0D refers to spherical (no dimension dominates), 1D refers rod- or tube-like particles (one dimension dominates), and 2D refers to plate-like particles where two dimensions dominate. 1D particles are referred to also as prolates and 2D type as oblates.

The use of nanoscale fillers introduces a series of fabrication challenges. Because of their small size and high surface area, nanoscale fillers such as nanoparticles have a strong tendency to agglomerate rather to disperse homogeneously in a matrix. This leads to particle–matrix mixtures with high viscosities, which can make the processing of those materials quite challenging. The result is that even the most exciting polymer nanocomposites have very low fractions of particle content and relatively weak mechanical properties when compared with those predicted in theory. In the case of particles and fibers, the surface area per unit volume is inversely proportional to the material's diameter (r), thus the smaller the diameter, the greater is the surface area per unit volume [20]; common particle geometries and their respective surface area-to-volume ratios are shown in Figure 7.7. For the fiber and layered material, the surface area/volume is dominated, especially for nanomaterials. Nanoscale fillers include nanoparticles, nanotubes, and layered (or "plate-like") inorganic materials having roughly surface area-to-volume ratio as $3/r$, $2/r$, and $2/t$, respectively, where r is the radius of nanoparticles and nanofibers whereas t is the thickness of the layer. Therefore, logically, a change in particle diameter, fibrous material diameter, or layer thickness from the micrometer to nanometer range will affect the surface area-to-volume ratio by three orders of magnitude.

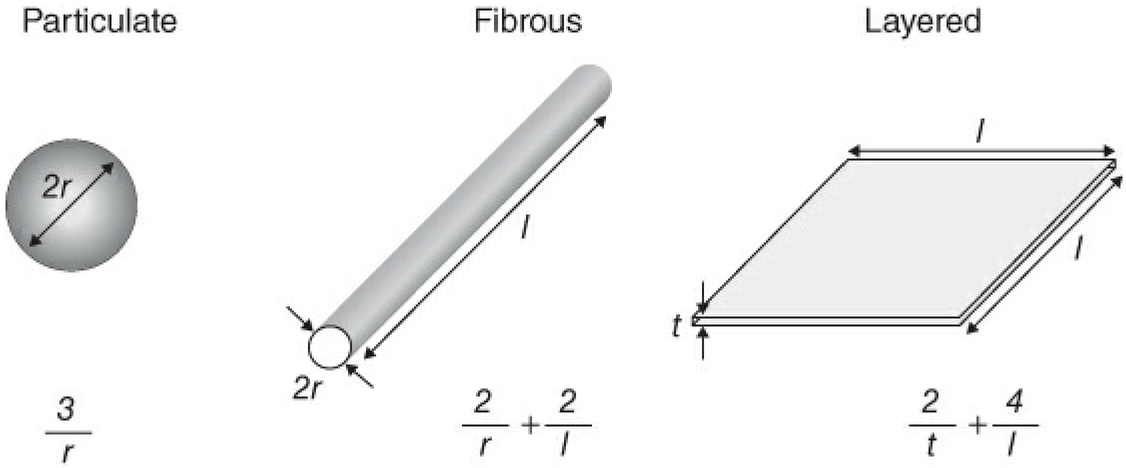

Figure 7.7 Common geometries of reinforcement particle and respective surface-to-volume ratios.

Apart from reinforcing nanoparticles, there are several types of nanostructures responsible for other functions, sometimes providing active or “smart” properties such as antimicrobial activity, enzyme immobilization, biosensing, and so on. Some particles can have multiple applications, and sometimes the applications can overlap, such as some immobilized enzymes, which can act as antimicrobial components, oxygen scavengers, and/or biosensors. A polymer containing even a small amount of nanoparticles may exhibit remarkably improved mechanical properties, when compared with the pristine unfilled polymer, or the same polymer filled with microparticles (conventional composite). Carbon nanotubes, for instance, display the so far highest values of elastic modulus, as high as 1 TPa, and strengths that can be as high as 500 GPa. This could allow for instance the fabrication of polymeric composites with exceptional strength and flexibility. Based on the nature of nanoparticle reinforcement, PNCs can be classified as follows:

i. Polymer–inorganic (metal and semiconductor) nanocomposites (PINC),

ii. Polymer–nanoclay composites,

iii. Polymer–carbon nanocomposites,

iv. Polymer–polysaccharide nanocomposites.

7.4.1 Polymer–Inorganic Nanocomposites (PINCs)

Polymers are considered to be good hosting matrices for composite materials because they can easily be tailored to yield a variety of bulk physical properties. Moreover, organic polymers generally have long-term stability and good processability. Inorganic nanoparticles possess outstanding optical, catalytic, electronic, and magnetic properties, which are significantly different from their bulk states. By combining the attractive functionalities of both components, nanocomposites derived from organic polymers and inorganic nanoparticles are expected to display synergistically improved properties. The potential applications of the resultant nanocomposites are many, for example, automotive, aerospace, optoelectronics, and so on. Here, we review the recent progress in polymer-based inorganic nanoparticle composites. A polymer–Au nanocomposite was probably the first reported PINC. A gold salt was reduced in the presence of Gum arabic, and subsequently a nanocomposite in the form of a purple solid was obtained by the coprecipitation of Gum arabic and gold in ethanol. The as-synthesized composite showed interesting optical properties such as dichroism. After Au was first used as an inorganic nanofiller in PINC for optical applications, other metals such as Ag, Pt, Pd, Rh, Cu, and Hg were also used with natural polymers for similar optical applications. Frequently employed inorganic nanofillers include *metals* and *metal alloys* (e.g., Au, Ag, Cu, Ge, Pt, Fe, CoPt), *semiconductors* (e.g., PbS, CdS, CdSe, CdTe, ZnO), $CaCO_3$, *other oxides* (e.g., TiO_2, SiO_2, ferric oxide, or mixed metal oxides of iron, cobalt, zinc, nickel). The choice of polymer matrix depends on the applications and can be generally divided into industrial plastics (e.g., nylon 6; nylon MXD6; polyimide; polypropylene (PP); conducting polymers, e.g., polypyrrole (PPy), polyaniline (PANI); copolymer of aniline formaldehyde; transparent polymers, e.g., polymethylmethacrylate (PMMA) and polystyrene (PS)).

7.4.1.1 Synthesis

Synthetic strategies for PINCs with a high homogeneity can be classified into two major categories: physical and chemical methods. Physical methods include solvent processing, melt processing, polymer melt intercalation, whereas chemical methods are *in situ* processes. Chemical methods, on the other hand, include *in situ polymerization* and *in situ nanoparticle formation*. Electron irradiation is also reported to be an effective and attractive method to modify the surfaces of inorganic materials and prepare PINCs. The electron irradiation technique was successfully employed to prepare PINCs of anatase and rutile TiO_2 as well as γ-Al_2O_3 nanoparticles with PMMA, where it was suggested that the active species initiating grafting polymerization may form on the nanoparticle surface by electron irradiation. In another report, silica and calcium carbonate nanoparticles were irradiated by ^{60}CO γ-ray in the presence of various monomers including styrene, MMA, butyl acrylate, methyl acrylic acid, and vinyl acetate as grafting monomers. Subsequently, these surface-grafted primary nanoparticles were collected and mixed with melted PP for the formation of PINCs.

Chemical methods based on the *in situ* sol–gel polymerization method allow single-step synthesis of PINCs in the presence of polymer or monomer. This method makes it possible to manipulate the organic/inorganic interfacial interactions at various molecular and nanometer length scales, resulting in homogeneous PINC structures and thus overcoming the problem of nanoparticle agglomeration. A simple method for the synthesis of PINCs is through the hydrolysis or reduction of metal salts in the presence of a polymer. For instance, composite of PANI with a ferromagnetic feature was synthesized by impregnating the polymer with iron salts followed by a treatment with alkali solution to form iron oxide nanoparticles in the polymer matrix. Sol–gel processing of inorganic oxide nanoparticles either in the presence of a preformed polymer or in parallel with the formation of the organic polymer is also proven to be an effective method for the fabrication of PINCs. The process of nanoparticle formation proceeds via hydrolysis and condensation of the organometallic precursor and has been studied extensively. Sol–gel hydrolysis and condensation of a precursor such as tetraethoxysilane (TEOS), tetrabutyl titanate, and aluminum isopropoxide were carried out starting from a preformed functional organic polymer such as polyvinyl acetate, PMMA, polyvinyl alcohol, and several other polymers for the formation of PINCs. A novel route for the synthesis of polymer–metal (mixed metal) oxide nanocomposites in aqueous medium, reported from author's laboratories [[21]], leads to the formation of the polymer matrix and nanosized metal oxide simultaneously on mixing the monomer and soluble metal salts in water followed by treating the reaction mixture with an alkali (Figure 7.8).

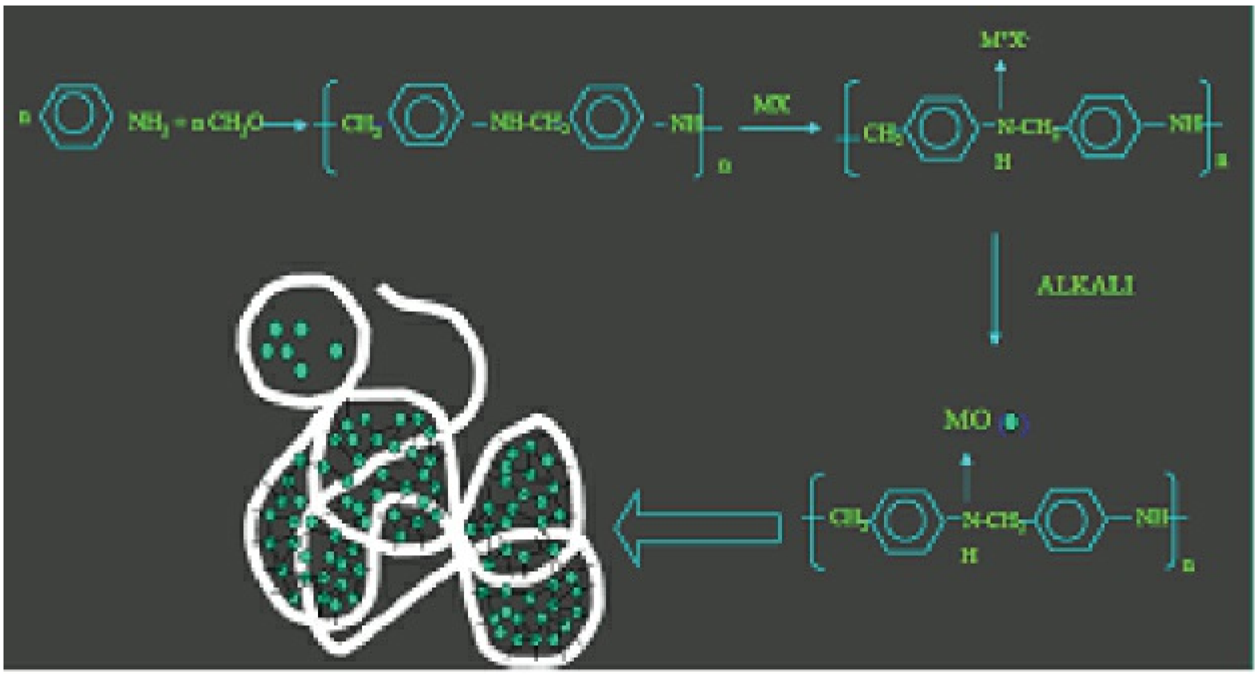

Figure 7.8 A simple route for synthesis of polymer–metal oxide nanocomposites [N. Kumar, Unpublished work].

A new method has been reported for the synthesis of transparent PMMA/ZnO PINCs. Linking inorganic and organic phases is achieved using MEA as a coupling agent between ZnO QD complexes and nonpolar polymer molecules. In the same manner, organic–inorganic hybrid materials are simultaneously synthesized in MMA via free-radical polymerization, which permits covalent bonding with ZnO complexes. The hydroxyl groups in MEA functionalize both polymer molecule moieties and surfaces of inorganic fillers and have the ability to form further cross-links between the immiscible surfaces and covalent bonding. Production of thin films of photosensitive hybrid organic–inorganic glass on silicon was reported using the solution sol–gel method. Preformed ZrO_2 nanoparticles, via hydrolysis and condensation of organometallic precursors, were dispersed in a photopolymerizable silicate monomer matrix containing a photoinitiator, methacryloxypropyltrimethoxysilane (MAPTMS), and methacrylic acid. Controlled hydrolysis of the MAPTMS resulted in highly homogeneous PINC films. Micro emulsions are thermodynamically stable, isotropic liquid mixtures of oil (o), water (w), and surfactant, in which one of the liquids is dispersed in the other; based on their respective distribution, there are two categories as normal (oil in water o/w) and inverse/reverse (water in oil w/o) microemulsions). Several inorganic nanoparticle systems have been synthesized via an inverse microemulsion process. Two or more separate microemulsions can be mixed together for the particle formation via an intermicellar exchange of the reactants. A new way of producing PINCs in a single-step synthesis is the use of a microemulsion system in which the monomer is used as an oil phase, forming a completely polymerizable matrix. Polyaniline/V_2O_5 core–shell nanocomposites have been successfully prepared using hexadecyltrimethylammonium bromide (CTAB) microemulsion. PINCs consisting of PMMA and SiO_2 have been synthesized using a reverse microemulsion process containing water-nonionic surfactant and methyl methacrylate (MMA) monomer as the oil phase. The SiO_2 nanoparticles formed via hydrolysis and condensation of an alkoxide precursor within nanosized microemulsion droplets followed by the polymerization of the microemulsion. Another example is CdS-polyacrylamide nanocomposites prepared by γ-irradiation in w/o microemulsion. An aqueous solution containing the precursor materials for CdS and acrylamide monomers was slowly added to an oil phase containing emulsifiers until a transparent microemulsion was formed. Subsequent γ-irradiation of this emulsion resulted in a CdS–polyacrylamide nanocomposite.

7.4.1.2 Functional Properties

Optical Properties

Optical properties of PINCs were probably the first known functions of PINCs starting from the ancient ages and have attracted attention for centuries. Inorganic nanoparticles, especially metals and semiconductors, have received increasing attention as “transparent nanofillers” for the PINCs during the past two decades. PINCs take advantage of the optical properties of materials that are hard to grow in a single-crystal form or that require protection from the environment, thus giving them the ease of processing. In addition, the inorganic nanoparticles can be used to achieve specific optical properties, and the polymer matrix is used just to hold the particles together and provide processability. Optical applications of PINCs include light absorption including UV and color (visible light absorption), photoluminescence (PL), extreme refractive index (RI), and dichroism. Size of the inorganic nanoparticles as nanofillers is an important factor that affects many optical properties and applications of the PINCs. For example, the PL of polymer–semiconductor quantum dots (QDs) nanocomposites is dependent on the size of QDs; the color and RI of polymer–metal nanocomposites are also dependent on the size of metal particles. In general, the major requirement of inorganic nanoparticles to be used as optically effective additives for transparent polymers is a small size (<40 nm). Rayleigh's law can be used to estimate the intensity loss of light passing through a composite by scattering, as shown in Equation 7.3:

$$I \cdot I_0 = \mathrm{e} - \left[3\varnothing_p x r^3 4\lambda^{4(n_p \cdot n_p - 1)}\right] \quad (7.3)$$

where I is the intensity of the transmitted and I_0 is the incident light, $\varnothing_p$ is the volume fraction of the particles, x is the optical path length, r is the radius of the spherical particles, λ is the wavelength of light, n_p is the RI of the particles, and n_p is the RI of the matrix. It can be clearly seen from Equation 7.4 that the light loss by scattering increases steeply with particle size. Usually, 40 nm is an up limit for nanoparticle diameters to avoid intensity loss of transmitted light due to Rayleigh scattering. The transparency/opacity is also dependent on the difference of RI between nanoparticles and the polymer matrix, and dispersion/agglomeration of nanoparticles into the polymer matrix. When the RI of nanoparticles and the polymer matrix is close, transparency can also be achieved with bigger nanoparticles. Agglomeration of nanoparticles will cause an increase in opacity. The arrangement of nanoparticles into the polymer matrix is another important factor that affects optical properties of PINCs. Random distribution of individually dispersed nanoparticles favors optical transparency, PL, and UV absorption; ordered nanoparticles can introduce iridescence; while uniaxially oriented nanoparticles can cause dichroism.

a. UV absorption*:* A high transparency in the visible range and a steep absorption in the near-UV range (λ<400 nm) are required for most applications on UV absorption. Most promising inorganic materials are nanosized ZnO and TiO_2, which have bulk band gap energies of around 3 eV.

b. Color (visible light absorption): As mentioned earlier, in the nineteenth and early twentieth centuries, it was already discovered that the color of small metallic particles depended on the size and distance between the particles. This can be utilized to make PINCs with a different color just by varying the size of inorganic nanofillers. For example, PVA–Au nanocomposites appeared pink when a particle diameter of Au is 16 nm, purple when 43 nm, and blue when 79 nm. Color of PINCs can depend not only on the size of metallic particles but also on the distance between the particles. This is based on the observation that nanocomposites of gelatin and silver or gold nanoparticles changed their color upon swelling with water. Later, Maxwell Garnett demonstrated it with theoretical analysis. The colors of the PINCs composed of polymer and metallic nanoparticles can be retained over extended periods, which is advantageous when using PINCs for color applications

c. Photoluminescence (PL): High-efficient PL devices with micrometer-sized features are of great interest for photonic applications [22, 23]. Analogous to systems such as dye-doped polymers, PL semiconductor–polymer nanocomposites are also attractive as PL polymeric materials, since various semiconductor nanocrystals show unique tunable light emission properties arising from quantum size effects. Semiconductor nanocrystals, such as QDs (II–VI and III–V), can cover a large range of light emission spectra (from 400 to 1400 nm). Compared to the organic dyes (e.g., Rhodamine 6G), QDs are 20 times brighter, 100 times more stable against photobleaching, and one-third as wide in emission line width. Due to these unique properties of semiconductor nanocrystals and good processability of their dispersions in polymer or monomers, the integration of PL nanoparticles into polymers offers a new range of promising applications in lighting and display devices. Figure 7.9a shows the color fluorescence image of ZnS-coated CdSe QD-poly(lauryl methacrylate) composite rods under a UV lamp. A general concern for PL PINCs is that the PL of semiconductor nanocrystals can be destroyed when incorporated into polymer matrix. Therefore, core–shell structures of PL semiconductor nanocrystals are always employed, and surface modification/engineering of semiconductor nanocrystals is usually needed to protect the PL of semiconductor nanocrystals.

d. Refractive index (RI): Compared to inorganic solids, optical applications of polymers are often limited due to the relatively narrow range of the RI. The RI values of most commercial polymers are typically located between 1.3 and 1.7, while inorganic materials can possess RI far below 1 (e.g., Au) or above 3 (e.g., PbS). Thus, the introduction of inorganic nanoparticles into a polymer matrix can result in polymeric nanocomposites with extreme RI, which finds potential applications in lenses, optical filters, reflectors, optical waveguides, optical adhesives, solar cells, and antireflection films. For high RI PINCs, PbS was the mostly studied inorganic additive. Other inorganic nanofillers to enhanced RI included silicon, ZnS, and iron sulfides. Ultrahigh RI of 2.5–3.2 was achieved on PINCs with additives of PbS, silicon, or iron sulfides. With a ZnS content of 50 wt%, the RI of ZnS/poly(*N*,*N*-dimethylacrylamide) nanocomposite was increased from 1.54 to 1.63. Analogously, the ultralow RI of 1 was also obtained on PINCs by incorporating Au nanoparticles into gelatin, which is the lowest RI known so far for PINCs. The content of Au was as high as 90 wt%. From most studies, the RI of nanocomposites depends linearly on the content of the nanofillers (both increase and decrease). Notably, when quantum confinement has to be considered for semiconductor nanocrystals as additives for PINCs, RI also becomes size-dependent apart from other optical properties such as color and absorption coefficient. For example, a distinct decrease in RI is observed with PbS nanoparticles below 25 nm compared to bulk PbS.

e. Dichroism: Dichroism was found on PINCs comprised of natural polymer (e.g., plant and animal fibrils) and metal particles (e.g., Ag and Au) more than 100 years ago. When metal particles are uniaxially oriented in the polymer matrix, linearly polarized light interacts differently when the angle between the polarization plane of the light and the long axis of the particle arrangement (φ) is 0 and 90°, respectively. As a result, different colors arise at parallel and perpendicular orientation. For example, the PINC comprised of Au and spruce wood fibers turned its color from red to blue green when φ was changed from 0 to 90°. Recently, dichroic PINCs were also produced by the solid-state drawing of isotropic nanocomposites or on stretching of molten nanocomposite films in a controlled uniform extensional flow. PVA, polyethylene, and poly(ethylene-*co*-vinyl alcohol) were employed as the polymer matrix and Au or Ag particles as inorganic additives. The dichroic colors depended on the type of metals as well as the particle diameters. The dichroism was also reflected by UV–vis spectra recorded with polarized light. Anisotropic structures, such as Au nanorods, were also embedded into the polymer matrix, since they have enormous absorption coefficients, tunable peak positions, and high photostability. As shown in Figure 7.9b, different colors of PVA composite films containing oriented Au nanorods have been observed, when placed parallel and perpendicular to the polarization direction induced by a polarizer placed on top. Uniaxially oriented Au nanorods were obtained by drawing/stretching the nanocomposite films, and hence, dichroic PINCs were achieved. Dichroic PINCs are promising materials as optical filters, making them potential candidates for liquid crystal displays.

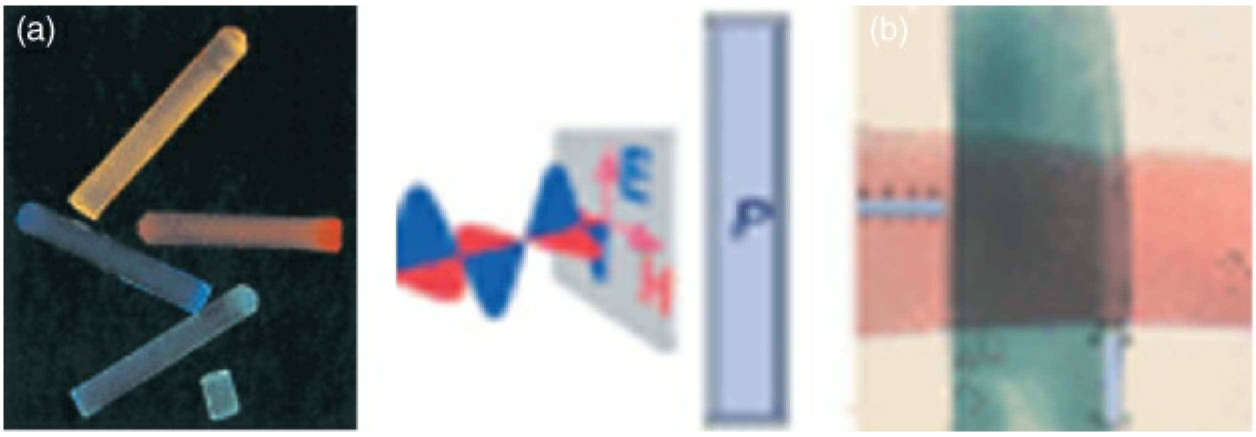

Figure 7.9 Color fluorescence image of (a) QD-poly(lauryl methacrylate) composite rods excited by a UV Hg-lamp (λ_{em} = 365 nm). Lee et al. [22], © 2000. With permission of Wiley-VCH; (b) PVA films containing Au nanorods aligned parallel and perpendicular to the electric field of polarized incoming light (P, represents a polarizer). Pérez-Juste et al. [23], ©2005. With permission of Wiley-VCH.

Superparamagnetic Properties

Nanocomposite materials obtained by dispersing iron oxide or cobalt NPs in polymers have been found to possess magnetic properties, which can be appropriately exploited for fabricating devices with charge storage capabilities, stability during cycling, and dynamics of charge propagation. Novel superparamagnetic nanocomposites have been prepared by the incorporation of magnetic NPs in conducting polymers, such as poly pyrrole (PPy) or poly aniline (PANI) [24]. The obtained materials combine either magnetic or conducting properties of their inorganic and organic components and exhibit modified mechanical and thermal characteristics. Poly(pyrrole) has been modified by the incorporation of Fe_2O_3 NPs in order to increase the electrochemical storage of the electroactive material. The influence on the morphology and electrochemical properties of the nanocomposite material has been studied by modifying synthetic parameters such as composition of iron nanofiller and the type of counter-anion incorporated in the nanohybrid, aiming to the optimization of performances for electrochemical storage applications. In the presence of *para*-toluene sulfonate (PTS) anions, an improvement of charge storage capacity has been observed due to a higher specific surface area attributed to a morphology modification. The incorporation of a high content of PPy-PTS/Fe_2O_3 nanocomposite in an electrode has resulted in improved performances with respect to the bare conductive polymer. Magnetic polymer nanocomposites constituted by methacrylate capped magnetite NPs chemically bounded to both PMMA and PS polymer chains have also been reported. The increasing of T_g of the nanocomposite material has been observed, indicating the positive influence of the NP incorporation and chemical bonding on the mechanical properties of the hybrid nanostructures. Iron NP-modified vinyl ester resin nanocomposites have been recently synthesized by direct binding of NP surface to monomers, which act as stabilizers for preventing NP aggregation and promote copolymerization. The mechanical and magnetic characterizations of the prepared nanocomposites have shown an enhancement of tensile strength and Young's modulus as compared with those of cured pure resin, increased thermal stability, and room temperature ferromagnetic behavior.

Electromagnetic (EM) Wave Absorption

EM wave absorption materials have attracted much attention due to the expanded EM interference problems. The major application for this area is in the military for stealthy aircraft, boats, war ships, and so on. The suggested properties could be tuned by changing the filler materials such as inorganic magnetic particles, metal nanoparticles, and whiskers or nanotubes. Moreover, the final composition, concentration, and crystallinity of the filler also have strong influence on their EM wave absorption properties. The complicated multilayer structures of the layer-by-layer process could enhance their properties. The attenuation mechanism of these materials is mainly based on either dielectric loss or magnetic loss. A proper combination of complex permeability and permittivity is necessary to fabricate the zero-reflection EM wave absorber with an impedance matching [25]. Nanostructured radar absorbing materials (RAMs) have received steadily growing interest because of their fascinating properties and various applications compared with the bulk or microsized counterparts. The increased surface area, number of dangling bond atoms, and unsaturated coordination on surface lead to interface polarization, multiple scatter, and absorbing more microwave. Four types of nanostructured RAMs are concisely introduced as potentials RAMs: nanocrystal RAMs, core–shell nanocomposite RAMs, nanocomposite of MWCNT and inorganic materials RAMs, nanocomposite of nanostructured carbon, and polymer RAMs.

Electromagnetic Interference (EMI) Shielding

EMI, a specific kind of environmental pollution, is drawing more attention recently because of the explosive growth in the utilization of electrical and electronic devices in industrial, commercial, and military applications. Unfortunately, the EM wave emissions from one device could interfere with other devices, causing potential problems including a chronic disease such as damaging brain cells and DNA. To overcome these problems, EM wave absorbers with the capability of shielding unwanted EM fields are required by using proper fillers (inorganic/metallic) and conducting polymer matrix. Generally, a polymer-based nanocomposite containing electrically conductive fillers is widely used for the EMI shielding of electronics. Nanotube–PS foam composite has been suggested as effective EMI shielding materials [26]. Other interesting nanocomposites are bilayer thin films of ferrimagnetic $BaFe_{12}O_{19}$ and ferroelectric $Ba_{0.5}Sr_{0.5}TiO_3$ and Fe-doped ZnO-coated barium ferrite composite particles.

Artificial Dielectric Nanocomposites

Metal-filled polymer composites, known as artificial dielectrics, have the potential to address the needs of emerging dielectric technologies, such as embedded capacitors with high capacitive densities (20–200 nF/cm^2). In an applied field, dipoles form in each of the metal particles, resulting in polarization that simulates a true dielectric. For high-frequency applications, engineered small particles with high electron mobilities are essential since only these properties will enable the rapid field response necessary for high dielectric constant and low loss. These new nanocomposite artificial dielectrics have the potential to have high dielectric constants (>100) at high frequencies and to enable the low temperature processing associated with polymers. This combination of properties is not found in other capacitor materials.

7.4.1.3 Applications

Popular applications of PINCs include optical applications, magnetic applications, mechanical applications, catalysis, electrochemical applications, electrical and thermal applications, and biomedical applications. *Mechanical applications* (e.g., construction material) is an important application area of PINCs where industrial plastics are always chosen as the polymer matrix and clay minerals are the nanofillers. Since smectite clay minerals – especially montmorillonite – are composed of several layers of silicates, this kind of PINCs is also called “polymer-layered silicate nanocomposites,” and the application of this kind of PINCs is called mechanical ‘reinforcement. Recently, with the explosion of CNTs in the material research field, carbon-based materials including multiwalled CNTs, single-walled CNTs, and carbon nanofibers are used instead of clay minerals for the same applications. *Catalytic* and *electrochemical applications*, such as sensors, are other applications of PINCs where metals including Ge, Cu, Pt, and oxides including SiO_2, TiO_2 are selected as inorganic nanofillers. Very recently, PINCs are also used in *electrical and thermal applications*, where nanofillers such as CNTs and carbon nanofibers are used to enhance the electrical/thermal conductivity of the conductive polymer matrix. While Au and iron oxide nanoparticles were frequently used in *biomedical applications*, their polymeric nanocomposites have also recently been used as an intelligent therapeutic system and bioimaging agents. Optical and magnetic applications are two of most important application aspects of PINCs. For *optical applications* of PINCs, inorganic nanoparticles of metals such as Au or Ag and semiconductors such as TiO_2, ZnO, or PbS are commonly used as “optically effective additives,” while transparent micropolymers such as PMMA are used as polymer matrix. For *magnetic applications*, metals and metal alloys such as Fe or CoPt, oxides such as ferric oxide, and ferrite are always used as inorganic nanofillers.

7.4.2 Polymer–Clay Nanocomposites (PCNs)

Clay is referred to a part of soil fraction with the particle size of less than 2 μm. The clay layers have a thickness of about 1 nm, which is in the nanoscale. There are many members of clays as given in Table 7.6 with some difference in their composition, structure, and basal spacing.

Table 7.6 Classification and Examples of Clay Minerals

Structure	Group	Mineral Examples	Ideal Composition	Basal Spacing (Å)
2:l (TOT)	Smectite	Montmorillonie, Hectorie, Saponite	$[(Al_{3.5-2.8}Mg_{0.5-0.2})\ (Si_8)O_{20}(OH)_4]\ Ex_{0.5-0.2}$ $[(Mg_{5.5-4.8}Li_{0.5-1.2})(Si_8)\ O_{20}(OH)_4]\ Ex_{0.5-0.2}$ $[(Mg_6)(Si_{7.5-6.8}Al_{0.5-1.2}O_{20}\ (OH)_4]\ Ex_{0.5-0.2}$	12.4–17.0
2:l (TOT)	Illite	Illite	$[(Al_4)(Si_{7.5-6.8}Al_{0.5-1.2})O_{20}(OH)_4]\ K_{0.5-1.5}$	10.0
2:l (TOT)	Vermiculite	Vermiculite	$[(Al_4)(Si_{8.8-8.2}Al_{1.2-1.8})O_{20}(OH)_4]\ Ex_{1.2-1.8}$	9.3–14.0
1:l (TOT)	Kaolin serpentine	Kaolinite, Dickite, Nacrite	$Al_4Si_4O_{10}(OH)_8$	7.14

Note: The structure of layered silicates consists of tetrahedra (T) and a sheet of edge-sharing octahedra (O), two sheets of tetrahedral with octahedral sheet sandwiched between them is designated as TOT.

Source: Alexandre and Dubois [27], © 2000. With permission of Elsevier.

Those members who are able to be exfoliated by polymer chains or monomers and distributed as individual clay layers within polymer matrix are suitable for the preparation of polymer nanocomposites. The individual clay layers can cause to the dramatic improvements in polymer properties due to their high aspect ratio and high interfacial interactions with polymer matrix. The concept of polymer–clay nanocomposites (PCN) was developed in the late 1980s, and firstly commercialized by Toyota. The interaction between layered silicates and polymer chains may produce different types of ideal nanoscale composites (Figure 7.10a–c). The intercalated nanocomposites result from the penetration of polymers chains into the interlayer region of the clay, resulting in an ordered multilayer structure with alternating polymer/inorganic layers at a repeated distance of a few nanometers. The exfoliated nanocomposites involve extensive polymer penetration, with the clay layers delaminated and randomly dispersed in the polymer matrix. Exfoliated nanocomposites have been reported to exhibit the best properties due to the optimal interaction between clay and polymer.

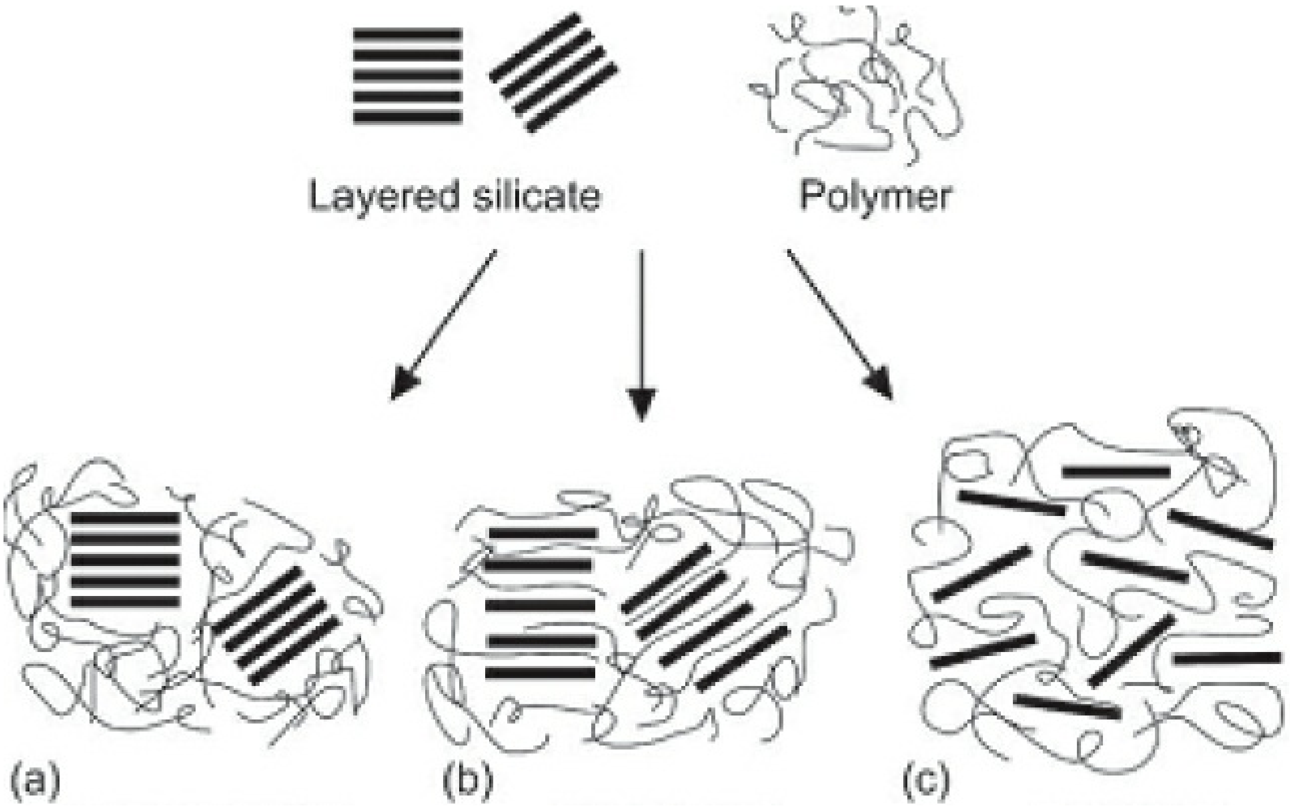

Figure 7.10 Types of composite derived from interaction between clays and polymers: (a) phase-separated microcomposite; (b) intercalated nanocomposite; and (c) exfoliated nanocomposite.

Alexandre and Dubois [27], © 2000. With Permission of Elsevier.

The most widely studied type of clay fillers is montmorillonite (MMT), hydrated alumina-silicate layered clay consisting of an edge-shared octahedral sheet of aluminum hydroxide between two silica tetrahedral layers. The imbalance of the surface negative charges is compensated by exchangeable cations (typically Na^+ and Ca^{2+}). The parallel layers are linked together by weak electrostatic. This type of clay is characterized by a moderate negative surface charge (cation exchange capacity, CEC), which is an important factor to define the equilibrium layer spacing. The charge of the layer is not locally constant as it varies from layer to layer and must rather be considered as an average value over the whole crystal. MMT is effective reinforcement filler due to its high surface area and large aspect ratio (50–1000).

Organic modification of clay is achieved through the exchange of sodium ions with organic alkyl ammonium ions. This modification makes the normally hydrophilic clay hydrophobic and potentially more compatible with the polymer being used in preparation of the polymer–clay nanocomposites. The homogeneous dispersion of organically modified clays in polymer matrices could lead to enhanced thermal, mechanical, gas barrier, dielectric properties, and solvent resistance. Polysaccharide–clay nanocomposites are a class of materials that are important especially for the food industry. These composites make use of naturally occurring polymers, such as starch, mixed with clay to make biopolymer film with enhanced properties, in particular permeability to water vapor.

7.4.2.1 Synthesis

Nanocomposites can, in principle, be formed from clays and organoclays in a number of ways including various *in situ* polymerization methods. The most common methods for the fabrication of polymer–clay nanocomposites include the following:

> ***In situ intercalative polymerization:*** In this method, polymerization occurs in between the intercalated sheets. The process involves swelling of the layered silicate within the liquid monomer and the polymerization can be initiated either by heat or radiation, by the diffusion of a suitable initiator, or by an organic initiator. This is a convenient method for thermoset–clay nanocomposites. One obvious advantage of *in situ* polymerization is the tethering effect, which enables the nanoclay's surface capped with organic chemical, such as 12-aminododecanoic acid (ADA), to link with nylon-6 polymer chains during polymerization [28], as illustrated in Figure 7.11.
>
> ***Exfoliation-Adsorption:*** This is based on a solvent system in which the polymer or pre-polymer is soluble and the silicate layers are swellable. The layered silicates, owing to the weak forces that stack the layers together, can be easily dispersed in adequate quantity of solvent such as water, acetone, chloroform, or toluene. The polymer then adsorbs onto the delaminated sheets and when the solvent is evaporated, the sheets reassemble sandwiching the polymer. This strategy can be used to synthesize epoxy–clay nanocomposites, but removal of solvent is a critical issue.
>
> ***Melt Intercalation:*** In this technique, no solvent is required and the layered silicate is mixed within the polymer matrix in the molten state. A thermoplastic polymer is mechanically mixed by conventional methods such as extrusion and injection molding with organophilic clay at an elevated temperature. The polymer chains are the intercalated or exfoliated to form nanocomposites. This is a popular method for preparing thermoplastic nanocomposites. The polymers, which are not suitable for adsorption or *in situ* polymerization, can be processed using this technique. Surfactants or compatibilzers are required in fabrication of a polymer–clay nanocomposite which requires mixing two components that are intrinsically non-compatible. Surfactants are ionic and thus interact well with the clay, but not with the polymer. An ideal solution is the use of "macrosurfactants" such as block copolymers combining hydrophilic and hydrophobic blocks that can interact with the clay and the polymer, respectively. For instance, poly(ethylene oxide), or PEO, is an excellent intercalation material.

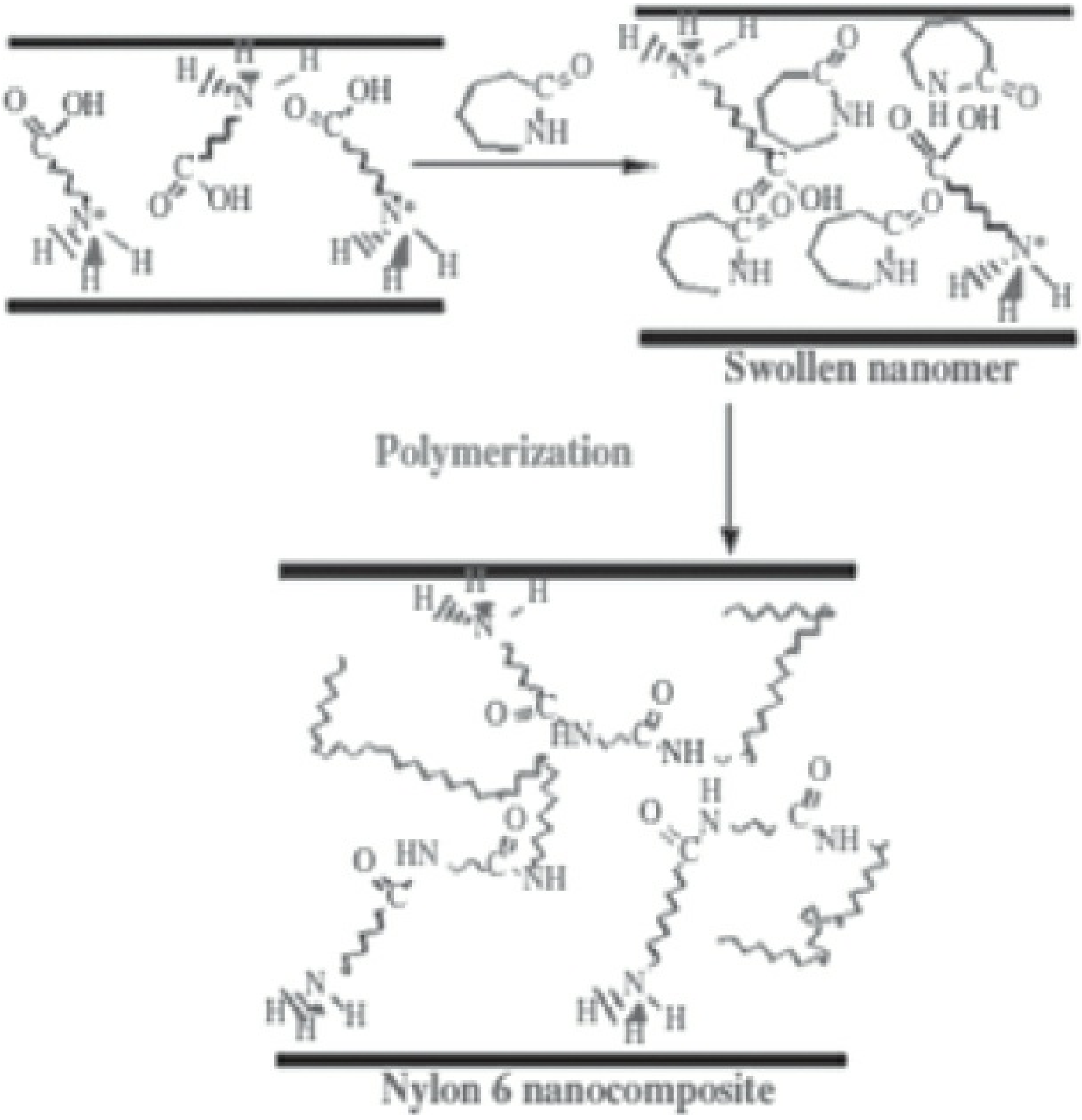

Figure 7.11 Nylon-6 nanocomposite formed through *in situ* polymerization with ADA–MMT.

Kap et al. [28], © 2008. With permission of Soc. Plastic Engineers.

7.4.2.2 Properties

Because of the low price, availability, high aspect ratio as well as desirable nanostructure and interfacial interactions, clays can provide dramatic and adjustable improved properties at very lower loadings. The nature and properties of components as well as preparation methodology and conditions, however, affect the final properties of polymer/clay nanocomposite. The bottom-up assembly of clay/polymer nanocomposite allowed the preparation of a homogeneous, transparent material, where the clay nanosheets have planar orientation. It was found that the stiffness and tensile strength of these multilayer nanocomposites are one order of magnitude greater than those of analogous nanocomposites. Nanoclays are also used as fillers in polymers to increase the thermal stability (i.e., raising the degradation temperature) of polymers. This property was first demonstrated in the late 1960s for montmorillonite/PMMA composites. In addition to thermal stability, the flammability properties of many clay/polymer nanocomposites are also improved. Combining traditional flame retardants with intercalated or, better, exfoliated clays can result in further improvements in flame retardance. Bottom-up assembly of clay/polymer nanocomposite allowed the preparation of a homogeneous, transparent material, where the clay nanosheets have planar orientation. It was found that the stiffness and tensile strength of these multilayer nanocomposites are one order of magnitude greater than those of analogous nanocomposites.. Various improved properties of polymer/clay nanocomposites as well as the mechanism and effective parameters are discussed.

a. ***Mechanical properties:*** Higher aspect ratio clays, polymer–clay interfacial interaction together with chemical nature of clays and polymer matrix, determine the mechanical properties of polymer–clay nanocomposites. Because of the rigid structure of clay layers and their high aspect ratio, they have proven to be very effective in the increasing of modulus and stiffness of the polymer matrix in the well-dispersed condition. In fact due to the higher aspect ratio of nanoclay fillers compared to that of regular fillers such as glass fibers, dramatic improvements in the mechanical properties of nanocomposites are achieved even at very lower nanoclay additions. When polymer chains are strongly adsorbed onto the rigid clay mono layers, it becomes equally a part of rigid material and dramatically exhibits high modulus. Considering the very large interfacial area in well-dispersed nanocomposite structures, significant improvement in the modulus can be expected. However, any enhancement in the polymer–clay interfacial contact leads to the better stress transfer in the nanocomposite. It has been well demonstrated that the enhancement in the interfacial adhesion properties between clay and polymer by surface modification of polymer chains using a suitable polar compatibilzers causes to the increasing in the mechanical properties of nanocomposite.

Generally, addition of organoclays to ductile polymers increases the yield strength; however, for brittle matrices failure strength is typically decreased. Higher loadings of compatibilzers, may however cause to the some degree of plasticization due to their lower molecular weight, negatively affect on the modulus of nanocomposite. The effect of clay fillers on the stress at break values for polymer nanocomposites depends on the interfacial interactions between polymer and clay layers. The stronger interfacial interaction causes to the increasing of stress at break, and the weak interfacial forces may lead to some decreasing of stress at break for nanocomposite. The polymers with more polarity such as nylon and rubber-based polymers have more strong interfacial interactions with polar clay layers, and their nanocomposites represent improved stress at break values compared to that of pure polymer. Polyamide/clay nanocomposites have shown highly improved stress at break values because of their higher degree of exfoliated structures based on the presence of strong ionic bonds between polymer chains and clay layers. The nanocomposites of nonpolar polymers such as polyolefines with clays exhibit weak interfacial interactions and low degree of exfoliation and consequently show decreased or slightly improved stress at break values. However, the modification of polymer chains or clay layers may be causes to improved stress at break characteristics for nonpolar polymers.

b. ***Thermal properties:*** The high thermal expansion coefficients of neat plastics cause dimensional changes during molding and thus the ambient temperature changes that are either undesirable or in some cases unacceptable for certain applications. The latter is a particular concern for automotive parts where plastics must be integrated with metals which have much lower coefficients of thermal expansion (CTE). Fillers are frequently added to plastics to reduce the CTE. For low-aspect-ratio filler particles, the reduction in CTE follows, more or less, a simple additive rule and is not very large; in these cases, the linear CTE changes are similar in all three coordinate directions. However, when high-aspect-ratio fillers, such as fibers or platelets, are added and well oriented, the effects can be much larger; in these cases, the CTE in the three coordinate directions may be very different. The fibers or platelets typically have a higher modulus and a lower CTE than the matrix polymer. As the temperature of the composite changes, the matrix tries to extend or contract in its usual way; however, the fibers or platelets resist this change creating opposing stresses in the two phases. When the filler-to-matrix modulus is large, the restraint to dimensional change can be quite significant within the direction of alignment. Platelets can provide their restraint in two directions, when appropriately oriented, while fibers can only do so in one direction. The CTE in the direction normal to the fibers or the platelet plane can actually increase when such fillers are added. Montmorillonite platelets are particularly effective for reducing CTE of well-exfoliated nylon-6 nanocomposites. MMT is much more efficient at reducing CTE than talc in TPO materials used in automobile industry. Nanocomposites of cyanate esters, prepared by dispersing organically modified layered silicates (OLS) into the resin, inclusion of only 2.5% by weight of OLS, led to a marked improvement in physical and thermal properties (CTE, T_g, and effective thermal stability). PMMA intercalated into the Na-MMT has 40–50 °C higher decomposition temperature, whereas PS/clay nanocomposites have 30–40 °C higher degradation temperature compared to pure PS. In general, it has been reported that the polymer/clay nanocomposites are thermally more stable than pure polymers. The effect of clay layers has been explained as superior insulation and mass transport barrier against the volatile compounds generated during the decomposition of polymer under thermal conditions.

c. ***Flame retardance*****:** Because of the large use of polymers especially in domestic applications, there is need to reduce their potential for ignition or burn in order to make them more safer in applications. Conventionally chemical additives as flame retardants are used to retardant the ignition and control burn. Traditionally, a number of halogen-based as well as phosphorous and some other compounds have the flame retardance effect in polymers without the reducing of their other properties and quality. However, the halogenated compounds suffer from environmental contamination characteristics and have pushed the market trends to halogen-free flame retardants. Some of inorganic candidates require high level of loading that cause to unwanted effects on the costs, process ability, and quality of the product. Investigations on the polymer/clay nanocomposites have demonstrated that clay minerals represent some degree of flame retardance along with the improvement in the physical and mechanical properties for polymers. However, detailed explanations imply that clay materials are beneficial for retarding the flame spread in developing fires and they not improve the ignition retardance or control the fully developed fires. Therefore, the clay minerals are used together with a low fraction of conventional flame retardants. However, the clay minerals and traditional flame retardants have considerable synergistic effect in the reduction of ignitability of polymers, and various reports of organically modified clay nanocomposites combined with halogenated flame retardants and phosphorous flame retardants were presented in the literature. The synergic effect of clays on the flame retardance of halogenated and phosphorous compounds causes to the reduction of their volume fraction needed in the polymer/clay nanocomposite systems.

d. ***Barrier properties:*** The barrier properties of polymers can be significantly altered by the inclusion of inorganic platelets with sufficient aspect ratio that to alter the diffusion path of penetrate molecules. At high aspect ratio that can be achieved (such as with exfoliated clay) in nanocomposites, significant decreases in impermeability are predicted and observed in practice. Exfoliated clay modified poly(ethylene terephthalate)

(PET) is one of the more prevalent nanocomposites investigated by both academic and industrial laboratories for barrier applications. PET-exfoliated clay composites also prepared via *in situ* polymerization using a clay-supported catalyst exhibited a 10- to 15-fold reduction in O_2 permeability with 1–5 wt% exfoliated clay. Modified chlorobutyl rubber showed decreased diffusion for several organic chemicals, suggesting utility for chemical protective gloves/clothing. Exfoliated clay added to polyamide-6/polyolefin (polyethylene or polypropylene) blends yielded an improved barrier to styrene permeation for melt blown films. Polymer blend nanocomposite was a better barrier than the control polyamide nanocomposite.

7.4.3 Polymer–Carbon Nanocomposites

7.4.3.1 Polymer–Carbon Nanotube Composites

Carbon nanotubes have very distinct properties compared to graphite. In the context of nanocomposites, SWNT are the most promising nanotube fillers. Some properties are particularly interesting, in particular their flexibility under mechanical stress, their behavior under high-temperature conditions, and their electrical properties. As with other applications that make use of carbon nanotubes, in composites it has been observed that the processing conditions ultimately affect nanotubes' properties, and as a consequence the composite, as well as the nanotubes' purity. Carbon nanotubes can also be doped, for instance with nitrogen and boron, which changes their surface reactivity. For instance, nitrogen atoms inserted into the lattice of nanotubes make them more dispersed in solution (carbon nanotubes are insoluble in water). Modified nanotubes present different electrical and optical properties and hence their use could lead to composites with novel properties. Inclusion of carbon nanotubes in a polymer does not necessarily improve its mechanical properties. Although in theory the modulus of nanotubes is much higher than any graphite fiber, and hence the composite should have outstanding mechanical properties, it has been demonstrated that a number of variables influence this outcome. For SWNT composites (Figure 7.12), the SWNT are in a bundle; until SWNT are isolated from the bundles or the bundles are cross-linked, the modulus of composites made from these materials will be limited. The structural arrangement of the nanofiller within the polymer is also important: if the nanotubes are not straight when placed in the composite, the modulus of the composite significantly decreases.

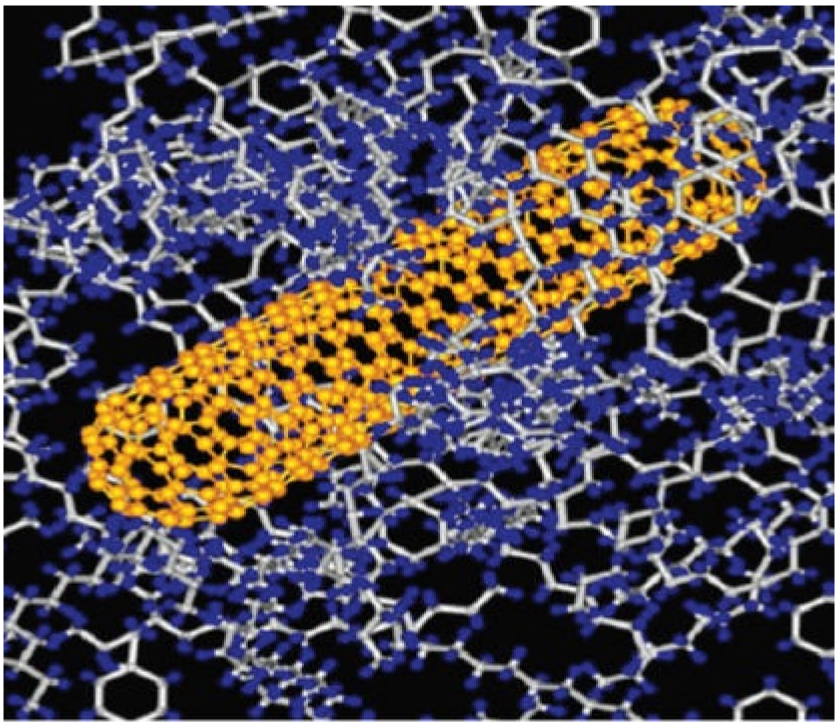

Figure 7.12 Carbon nanotube/polymer matrix nanocomposite.

www.ipt.arc.nasa.gov/cntpolymer.html.

Apart from mechanical enhancement of polymers, nanotubes are also of interest for their electrical properties. Carbon nanotubes are inherently more conductive than graphite. For example, nanotube/PVA and nanotube/PPV composites show a large increase in electrical conductivity compared to simple PVA and PPV, of nearly 4.5 and 8 orders of magnitude, respectively. Finally, nanotube/polymer composites are promising in the context of light-emitting devices. These devices were developed after the discovery of electroluminescence from conjugated polymer materials (such as PPV). The practical advantages of polymer-based LEDs are low cost, low operating voltage, ease of fabrication, and flexibility. Small loadings of nanotubes in these polymer systems are used to tune the color of emitted light from organic LEDs. A recent study comparing the mechanical properties (Young's modulus, compressive yield strength, flexural modulus, and flexural yield strength) suggest that tungsten disulfide nanotubes reinforced polypropylene fumarate (PPF) nanocomposites possess significantly higher mechanical properties, and tungsten disulfide nanotubes are better reinforcing agents than carbon nanotubes. Increases in the mechanical properties can be attributed to a uniform dispersion of inorganic nanotubes in the polymer matrix (compared to carbon nanotubes that exist as micron-sized aggregates) and increased cross-linking density of the polymer in the presence of tungsten disulfide nanotubes (increase in cross-linking density leads to an increase in the mechanical properties). These results suggest that inorganic nanomaterials, in general, may be better reinforcing agents compared to carbon nanotubes.

7.4.3.2 Polymer–Graphene Nanocomposites

Polymer nanocomposites based on carbon black, carbon nanotubes, and layered silicates have been used for improved mechanical, thermal, electrical, and gas barrier properties of polymers. The discovery of graphene with its combination of extraordinary physical properties and ability to be dispersed in various polymer matrices has created a new class of polymer nanocomposites [29]. Graphene is an atomically thick, 2D sheet composed of sp^2 carbon atoms arranged in a honeycomb structure. With Young's modulus of 1 TPa and ultimate strength of 130 GPa, single-layer graphene is the strongest material ever measured. It has a thermal conductivity of 5000 $W/(m^3\ K)$, which corresponds to the upper bound of the highest values reported for SWCNT bundles. Moreover, single-layer graphene has very high electrical conductivity, up to 6000 S/cm, and unlike CNT, chirality is not a factor in its electrical conductivity. These properties in addition to extremely high surface area (theoretical limit: 2630 m^2/g) and gas impermeability indicate graphene's great potential for improving mechanical, electrical, thermal, and gas barrier properties of polymers. The properties of polymer nanocomposites depend strongly on how well they are dispersed. Much of nanocomposite research with carbon nanotubes (CNT) has focused on finding better methods for dispersing nanotubes into polymers. Surface functionalization via fluorination, acid modification, and radical addition improves solubility of CNT in solvents and polymers. However, disentangling the bundles during dispersion into polymers cannot be done easily, and sonication often shortens the tubes. The synthesis of graphene from graphene oxide leaves some epoxide and hydroxyl groups; these greatly facilitate functionalization. However, restacking of the flat sheets, especially after chemical reduction, can significantly reduce their effectiveness. Restacking can be prevented by either use of surfactants that can stabilize the reduced particle suspensions or blending with polymers prior to the chemical reduction. Graphene oxide (GO) readily exfoliates in water or other aprotic solvents via hydrogen bonding interaction. Nanocomposites have been created with GO and water-soluble polymers such as poly(ethylene oxide) (PEO) or poly(vinyl alcohol) (PVA). Nanocomposites have also been produced in aprotic solvents with hydrophobic polymers such as polystyrene (PS), polyurethane (PU), or poly(methyl methacrylate) (PMMA) and GO after chemical modification with isocyanate or amine. Electrical conductivity can be restored via chemical reduction of the graphene oxide. This can also be done *in situ* in the presence of a polymer. For example, sulfonated polystyrene was added to GO and then reduced with hydrazine hydrate. However, depending on polymer type and the reducing agent, the *in situ* reduction technique may result in polymer degradation. Composites of CRG and TRG have been made with a number of polymers via blending with organic solvents followed by solvent removal. Graphene composites can be produced via *in situ* intercalative polymerization of monomers. Successful polymerizations of PVA, PMMA, epoxy, and poly(arylene disulfide) with graphene oxide or silicone foams and PU with thermally reduced graphene (TRG) have been reported. If functional groups on the chemically modified graphene are reactive with the monomer, grafting of polymer chains onto graphene surfaces can occur. Chain grafting has been demonstrated with the polymerization of poly(2-(dimethylamino)ethylmethacrylate) and PVA and with PU formation. The most economically attractive and scalable method for dispersing nanoparticles into polymers is melt blending. However, because of thermal instability of most chemically modified graphene, use of melt blending for graphene has so far been limited to a few studies with the thermally stable TRG. Successful melt compounding of TRG into elastomers and glassy polymers has been reported. Properties of graphene/polymer nanocomposites are discussed as follows.

> **Electrical conductivity**. Graphene sheets can provide percolated pathways for electron transfer, making the composites electrically conductive. Similar benefits can be achieved with other conductive carbon fillers such as carbon black (CB), carbon nanofibers (CNF), and expanded graphite. However, graphene enables the insulator to conductor transition at significantly lower loading, comparable to electrical percolation thresholds for carbon nanotubes (CNT). The lowest electrical percolation threshold was 0.1 vol% reported for PS solvent blended with isocyanate-treated GO (iGO) followed by solution-phase reduction with dimethylhydrazine. Production of electrically conductive polyolefin, vinyl and acrylic polymers, polyester, polyamide, polyurethane, epoxy, natural, and synthetic rubbers with graphene has been reported. These materials can be used, for example, for electromagnetic shielding, antistatic coating, and conductive paints.
>
> **Thermal conductivity**. Superior thermal transport properties of graphene dispersion have potential for thermal management in miniaturized electronic devices, for thermal pastes, and for heat-actuated, shape-memory polymers.
>
> **Mechanical properties**. Defect-free graphene is the stiffest material (E ~1 TPa) ever reported in nature and also has superior intrinsic strength, ~130 GPa. Despite some structural distortion, the measured elastic modulus of CRG sheets is still as high as 0.25 TPa of graphene is believed to have distinct advantages in mechanical reinforcement over existing carbon fillers such as CB, EG, and SWCNT. While modulus increase with graphene dispersion is evident for all polymers, it is more pronounced for elastomeric matrices. This is due to greater stiffness contrast between reinforcement and matrix.
>
> **Thermo calorimetric transitions**. Significant increases in glass transition temperature, T_g, and altered crystallization kinetics of polymers by functionalized graphene dispersion have been observed. TRG increased T_g of oxygen-containing polymers such as PMMA (by 30 °C at 0.05 wt%) and poly(acrylonitrile) (PAN) (by 46 °C at 1 wt%) by hindering segmental motions of polymer chains via mechanical interlocking and hydrogen bonding with surface oxygen functionalities. For graphene oxide sheets esterified with PVA chains, PVA T_g elevation can be attributed to reduced chain mobility by covalent cross-linking. Graphene can nucleate crystallization of polymers. For polycaprolactone (PCL) and PVA, melt crystallization takes place at higher temperature and degree of crystallinity becomes greater after isothermal crystallization in the presence of graphene oxide or TRG. This is suggestive of strong interfacial interaction between polar polymer chains and functionalized graphene surface.
>
> **Gas permeation**. Defect-free graphene sheets are impermeable to all gas molecules. Combining graphene with polymeric hosts makes possible large-scale barrier membranes with mechanical integrity, a significant advantage over 1D SWCNT, MWCNT, or CNF. Especially, incorporation of iGO led to ~90% reduction in nitrogen permeability at 3 wt% loading. Solvent-based processing results in more reduction in permeation than the melt-based due to dispersion of graphene platelets.
>
> **Thermal stability**. Improved thermal stability of host polymers is another benefit expected from graphene-based reinforcements. Thermal degradation temperature, characterized by the maximum weight loss rate in thermogravimetry, shifts up by 10–100 °C at <10 wt% graphene for PS, PVA, PMMA, and silicone foams. Decomposition of graphene composites is substantially slower than neat polymers, which is attributed to restricted chain mobility of polymers near the graphene surface. During combustion, inflammable anisotropic nanoparticles form a jammed network of char layers that retards transport of the decomposition products. This suggests application of graphene/polymer nanocomposites for flame retardation.

Although numerous challenges remain in developing graphene-based polymer composites, these materials have already been explored for a range of applications in different fields such as electronic devices, energy storage, sensors, ESD and EMI shielding, and biomedical applications (Table 7.7).

Table 7.7 Potential Application Areas of Polymer–Graphene Nanocomposites

Area	Examples
Energy storage	Li-ion battery, supercapacitor
Electronic devices	Dye-sensitized solar cells, field emission devices, liquid crystal displays (LCD), organic light-emitting diodes (OLED)
Sensors	pH, temperature, pressure and biosensors
Biomedical	Drug delivery, gene delivery, bioimaging, cancer therapy, artificial muscles

7.4.4 Polymer–Polysaccharide Nanocomposites

7.4.4.1 Polymer–Cellulose Nanocomposites

Cellulose is the building material of long fibrous cells and is a highly strong natural polymer. Cellulose nanofibers are inherently a low cost and widely available material. Moreover, they are environmentally friendly and easy of recycling by combustion, and require low energy consumption in manufacturing. All of this makes cellulose nanofibers an attractive class of nanomaterials for elaboration of low cost, lightweight, and high-strength nanocomposites. Basically two types of nanoreinforcements can be obtained from cellulose–microfibrils and whiskers. In plants or animals, the cellulose chains are synthesized to form microfibrils (or nanofibers), which are bundles of molecule that are elongated and stabilized through hydrogen bonding. The microfibrils have nanosized diameters (2–20 nm, depending on the origin) and lengths in the micrometer range. Each microfibril is formed by the aggregation of elementary fibrils, which are made up of crystalline and amorphous parts. The crystalline parts, which can be isolated by several treatments, are the whiskers, also known as nanocrystals, nanorods, or rod-like cellulose micro crystals, with lengths ranging from 500 nm up to 1–2 μm, and about 8–20 nm or less in diameter, resulting in high aspect ratios. Cellulose whiskers are not yet commercially available, instead microcrystalline cellulose (MCC), a closely related item, is available. MCC is formed by particles of hydrolyzed cellulose consisting of a very large amount of cellulose microcrystals together with amorphous areas. MCC is prepared by removing part of the amorphous regions by acid degradation leaving the less accessible crystalline regions as fine crystals of typically 200–400 nm in length and an aspect ratio of about 10, degree of polymerization (DP) is about 140–400, depending on the cellulose source and treatment procedure [30].

Factors Affecting Performance of Cellulose Nanoreinforcements

The resulting properties of nanocomposites with cellulose fibers have been reported to be strongly related to the dimensions and consequent aspect ratio of the fibers, as well to geometric and mechanical percolation effects. Aspect ratios are related to the origin of the cellulose used and whisker preparation conditions. A MCC with submicron-sized diameters had a much higher effect on tensile strength of hydroxypropyl methylcellulose (HPMC) than that of a micron-sized MCC counterpart; moreover, the negative impact of micron-sized MCC on elongation of the film was much more dramatic than that of its submicron-sized counterpart. The composite produced by using the whiskers with the highest aspect ratio exhibited the highest transparency and best tensile properties. The mean aspect ratio cannot be considered without proper assumptions; one must also consider the orientation distribution of the fillers. When the fillers do not follow asymmetric distribution, the overall mechanical properties obtained by the average aspect ratio of the fillers may be greatly different from those obtained when considering the aspect ratio distribution. The orientation of cellulose fibers can greatly improve the tensile properties of a resulting nanocomposite. For instance, a nanocomposite of polyvinyl alcohol (PVOH) with cellulose whiskers formed under applied magnetic field to orient the whiskers showed an increase in the modulus. Percolation theory predicts a maximum improvement in composite properties when there are just enough fillers to form a continuous structure since they are properly dispersed within the matrix, which means that modulus and strength are expected to be improved if each fiber is in contact with two more others, on average.

Applications and Effects on Polymers Matrices

Cellulose nanoreinforcements have been reported to have a great effect in improving modulus of polymer matrices; such a great effect is ascribed not only to the geometry and stiffness of the whiskers but also to the formation of a fibril network within the polymer matrix, the cellulose fibers being probably linked through hydrogen bonds. Moreover, cellulose fibers have been effective to improve strength and modulus of polymers, especially at temperatures above the glass transition temperature (T_g) of the matrix polymer; on the other hand, they tend to hinder elongation. The modulus seems not to be dependent on such interactions. Moisture barrier of polymer films is improved by cellulose nano reinforcements. The presence of crystalline fibers is thought to increase the tortuosity in the materials leading to slower diffusion processes and, hence, to lower permeability. The barrier properties are enhanced if the filler is less permeable, have good dispersion in the matrix and a high aspect ratio. Nanosized cellulose fibrils have been also reported to improve thermal properties of polymers. The thermal stability of polymers in nanocomposites with cellulose whiskers is improved when compared to those of the corresponding bulk polymers. The presence of whiskers could influence T_g values in two opposite ways, firstly, the solid surface of cellulose whiskers could restrict mobility of polymer chains in the vicinity of the interfacial area, which would result in a global shift of T_g toward higher temperatures. Secondly, the cross-linking density of the polymeric matrix gets decreased in the presence of whiskers, which would indirectly decrease T_g. A variety of surface modifications on cellulose nanoreinforcements can greatly improve their miscibility within hydrophobic matrices. Cellulosic surfaces can be derivatized by several reactions involving the hydroxyl groups, such as esterifications, so as to improve their compatibility with less polar polymers modified cellulose fibers by acylation with fatty acids in order to prepare them for composites with polyethylene (PE). The surface chemical modification of the cellulose fibers resulted in improved interfacial adhesion between the fibers and the matrix, which was evidenced by enhanced mechanical properties and thermal stability. Moreover, the water uptake capacity of the material was decreased. Surfactant addition can also improve the compatibility between cellulose and hydrophobic matrices. The hydrophilic head group of the surfactant adsorbs on the cellulose surface, whereas its hydrophobic tail dissolves in the matrix, avoiding aggregation of cellulose fillers via steric stabilization; the improved performance of the nanocomposite would be explained not only by a better wettability and adhesion between phases, but also by a more uniform distribution of the fillers within the matrix. Grafting between a hydrophobic matrix and hydrophilic fibers can also improve their otherwise poor adhesion. Composites with 1% dicumylperoxide (DCP), a cross-linking agent, which was used to induce grafting between a PE matrix and cellulose fibers from sisal, presented much improved strength than composite with untreated fibers.

7.4.4.2 Polymer–Starch Nanocomposites

Native starch granules can be submitted to an extended-time hydrolysis at temperatures below the gelatinization temperature when the amorphous regions are hydrolyzed allowing separation of crystalline lamellae, which are more resistant to hydrolysis. The starch crystalline particles show platelet morphology with thicknesses of 6–8 nm. Addition of starch nanocrystals (SNC) improved tensile strength and modulus of pullulan films, but decreased their elongation. The T_g values shifted to higher temperatures with increasing SNC content, which was attributed to a restricted mobility of pullulan chains due to the formation of strong interactions between SNC as well as between filler and matrix. The water vapor permeability of pullulan films was decreased by the addition of 20% or more SNC. Addition of SNC to polyvinyl alcohol (PVOH) resulted in different effects, the tensile strength and elongation of PVOH were only slightly improved by the addition of SNC up to 10 wt%, above this content, such properties became lower than that of pure PVOH. The properties of the PVOH composite with SNC, on the other hand, were better than those obtained when native starch was used instead of SNC, suggesting that SNC dispersed more homogeneously and formed stronger interactions with PVOH than native starch granules [31].

7.4.4.3 Polymer–Chitin Nanocomposites

Chitin whiskers can be prepared by acid hydrolysis of chitin. The average dimensions of the whiskers obtained in different laboratories were in the range of 400–500 nm (length) and 30–50 nm (diameter). On addition of chitin whiskers to soy protein isolate (SPI) thermoplastics, whiskers greatly improved not only the tensile properties (tensile strength and elastic modulus) of the matrix but also its water resistance. The addition of chitin whiskers also improves the water resistance of chitosan films. Chitosan nanoparticles can be obtained by ionic gelation, where the positively charged amino groups of chitosan form electrostatic interactions with polyanions employed as cross-linkers, such as tripolyphosphate (TPP). The resulting chitosan–tripolyphosphate (CS–TPP) nanoparticles when incorporated into hydroxypropyl methylcellulose (HPMC) films significantly improved mechanical and barrier properties of the films. Such effects are attributed to the nanoparticles filling discontinuities in the HPMC matrix [32].

7.5 Nanocoatings

Coatings are mainly applied on surfaces for decorative, protective, functional purposes or a combination of these. Apart from their special properties, coatings must often satisfy additional requirements; for example, nonstick, cookware coatings must be resistant to scratching, abrasion, and thermal effects. Typical expectations of coatings include the following:

- durability
- reproducibility
- easy application and cost-effectiveness
- tailored surface morphology
- environmental friendliness

The research issues concerning the production of coatings are one of the more important directions of surface engineering development, ensuring the obtainment of coatings of high utility properties in the scope of mechanical characteristics and wear resistance. Depending on the characteristics of the coating materials (whether inorganic, organic, or ceramic), the coatings may be termed as functional coatings [33]. The term "**functional coatings**" describes systems that possess, apart from the classical properties of a coating (i.e., decoration and protection), an additional functionality. This additional functionality may be diverse and have functions that are innovative and unusual.

Functional nanocoatings may induce changes in properties in a variety of ways; for example, to control friction, lubrication, and wear (tribological coatings); or to change the transmission of visible and IR radiation in glass (responsive nanocoatings); or to introduce new properties such as "self-cleaning" effects.

Nanostructure and particularly nanocomposite coatings, have gained considerable attention due to their unique physical and chemical properties, for example, extremely high indentation hardness (40–80 GPa), corrosion resistance, excellent high-temperature oxidization resistance, as well high abrasion and erosion resistance. The extraordinary interest in nanocomposite materials is mainly due to the vast range of properties that can arise from the combination of the peculiar characteristics of each component; nanoparticles (NPs); and host matrix such as polymers, ceramics, or metals. In addition, nanocomposite coatings can also show original properties, not fully envisioned from the properties of the single components, deriving from the local microstructural arrangements of the nanosized objects in the matrix.

Nanocoatings are a type of nanocomposites. The layer thickness of a nanocoating is usually in the 1–500 nm range. Nanocomposite films include granular homogeneous or multilayer thin films. Nanocomposite coatings synthesized by plasma-assisted deposition processes under highly nonequilibrium conditions have high potential for new applications such as protective and functional coatings in automotive, aerospace, tooling, electronic, or manufacturing industry. Important functionalities along with the associated applications of nanocoatings are briefly discussed in the following sections.

7.5.1 Functional Nanocoating

Functional coatings perform by means of physical, chemical, mechanical, thermal, and properties. Chemically active functional coatings perform their activities either at film–substrate interfaces (anticorrosive coatings), in the bulk of the film (fire-retardant or luminescent coatings), or at air–film interfaces (antibacterial, self-cleaning). Therefore, functional coatings can be classified as several types depending on their matrix as well as functional characteristics.

7.5.1.1 Polymer Nanocoatings

Indeed, the original size-dependent physical and chemical properties of the NPs, joint with the high processability and defined chemical and morphological structure of the polymers, finally result in innovative materials with unique and tunable characteristics that cannot be achieved by traditional materials. In many cases, anisotropy is the basis of physical properties that are distinct from those obtained from isotropic particles, such as nanospheres. Hence, nanorods because of their shape anisotropy are attractive components for creating functional polymer nanocomposites. For example, the shape of gold nanorods makes them ideal candidates for applications involving the manipulation of incident light and sensitive molecular spectroscopy due to enhanced polarizability of the particle. On the other hand, semiconducting nanorods, such as those composed of CdSe, have shown promise in polymer-based photovoltaic devices as sites for electron transport and charge transfer. In this perspective, the fabrication of functional polymer nanocomposites based specifically upon the inclusion of nanorods become important for variety of applications in diverse areas such as sensing, energy harnessing, and mechanical enhancement.

Some of the important applications of the area of polymer nanocomposites coatings are briefly discussed here.

> **a. Photoluminescence:** Recently a novel approach to prepare hybrid organic–inorganic NP have been based on multilayers by using photo cross-linkable polystyrene (PS-N_3) as host matrix and/or thiol functionalized polystyrene (PS-N_3-SH) as ligands of semiconductor and metal NPs (CdSe@ZnS, Au, and Pt). The photo cross-linking layer-by-layer process is efficiently controlled turning out in layers having thickness ranging from few to hundreds of nanometers as a function of the solution concentration and spinning rate. The resulting nanocomposite multilayers exhibit enhanced and prolonged photoluminescent durability, facile color tuning in accord to the layer and number thickness and are used as structural materials for manufacturing nanoscale optical devices.
>
> **b. Antireflection coatings:** Recently, applicative potential of hybrid inorganic NP-modified polymers have been extended for the production of high refractive index materials, for highly reflective and antireflection coatings, and for advanced optoelectronic systems. In particular, optically transparent TiO_2-based nanocomposites with high refractive index are very appealing materials for UV filter and high refractive coatings. Due to their high refractive index and UV absorption, TiO_2 NPs have been incorporated in polymers to improve linear and nonlinear optical properties and to prepare photonic materials. Nevertheless, in order to avoid Rayleigh scattering and intensity loss of the transmitting light, a uniform dispersion and a small size of NCs in the polymer are required. Variation in the titania NP concentration, size, morphology, and surface functionalization, as well as a change in the dielectric constant of the matrix result in the possibility of tuning the optical properties of the materials for practical applications. Sol–gel synthesized TiO_2 NPs embedded in hyper-branched polymers and cured to prepare hard coating or films have also been reported. The optimization of the preparative conditions has led to the improvement of both thermal and mechanical properties of the coatings. In another example, ZnS NPs have been used to prepare polymer nanocomposites with tunable refractive index by varying the nanostructures content in the matrix. 2-Mercaptoethanol (ME)-capped ZnS NPs in polymer matrix has been obtained by free-radical-initiated polymerization. The nanocomposite coatings exhibited optical transparency in the visible range, thermal stability, and good mechanical properties, although at the increasing of the nanofiller content, the plasticizing effect of ME-capped ZnS NPs has resulted in a decrease in T_g values. Fluorescent and highly transparent nanocomposite thin films with high refractive index have been recently prepared by blending *o*-phenylene diamine (*o*-PDA) functionalized ZnS NC solutions with poly(vinylpyrrolidone) (PVP). Compared to the

bare polymer, the ZnS NC polymeric films have exhibited enhanced refractive index, high optical transparency and preservation of the NC band-edge emission. Nanocomposites with highly dispersed ZnS nanophase contents have shown that ZnS NPs and the polymer matrix are linked by covalent-bonds, thus resulting in the enhancement of thermal and mechanical properties. The small size and the homogeneous dispersion of ZnS NPs contribute to the transparency and the linear behavior of the refractive index with the volume fraction of the polymer matrix.

c. Energy conversion: Systems based on semiconductor NCs such as CdSe, ZnO, PbS, or TiO_2 incorporated in conjugated polymers are interested for their potential application in the field of energy conversion. Semiconductor NCs can be coupled with conducting polymers for the fabrication of heterojunctions in which the high surface-to-volume ratio and high conductivity of NPs combine with the flexibility and versatility of the polymeric medium. The resulting hybrid heterojunctions can exhibit high electron mobility or improved spectral coverage and can be therefore exploited for photovoltaic applications. A recently developed hybrid heterojunctions by blending nanocrystalline TiO_2 nanorods and high hole mobility polymer (poly(3-hexylthiophene), P3HT). Anisotropic shaped NCs combined with the polymer properties can reduce the number of interparticle hopping events and therefore improve both electron and hole transport in the nanocomposite, resulting in enhanced performances of the photovoltaic device.

A layer-by-layer (LbL) processing technique has been utilized to obtain nanocomposite film with adjustable thickness as electrochemically active materials suitable for applications in optoelectronic and electrochemical devices. The investigated redox and spectroelectrochemical properties of the prepared thin films have demonstrated an appropriate band alignment for charge separation at the NCs/polymer interface. Preliminary tests of the use of such hybrids inorganic/inorganic photovoltaic cells have been carried out, and morphological studies have pointed out the formation of a quasi-interpenetrating network, which can assist their application in solar cells. Photocarriers can thus be efficiently separated and transported in such hybrid systems, as required for the fabrication of detector, sensor, and solar cells.

d. Superparamagnetic systems: Nanocomposite materials obtained by dispersing iron oxide or cobalt NPs in polymers have been found to possess magnetic properties, which can be appropriately exploited for fabricating devices with charge storage capabilities, stability during cycling, and dynamics of charge propagation.

Novel superparamagnetic nanocomposites have been prepared by the incorporation of magnetic NPs in conducting polymers, such as poly(pyrrole) (PPy) or poly(aniline) (PANI). The obtained materials combine either magnetic or conducting properties of their inorganic and organic components and exhibit modified mechanical and thermal characteristics. Poly(pyrrole) has been modified by the incorporation of Fe_2O_3 NPs, in order to increase the electrochemical storage of the electroactive material. The influence on the morphology and electrochemical properties of the nanocomposite material has been studied by modifying synthetic parameters such as composition of iron nanofillers and type of counter-anion incorporated in the nanohybrid, aiming to the optimization of performances for electrochemical storage applications. In the presence of *para*-toluene sulfonate (PTS) anions an improvement of charge storage capacity has been observed, due to a higher specific surface area attributed to a morphology modification. The incorporation of a high content of PPy-PTS/Fe_2O_3 nanocomposite in an electrode has resulted in improved performances with respect to the bare conductive polymer.

Magnetic polymer nanocomposites constituted by methacrylate capped magnetite NPs chemically bounded to both PMMA and PS polymer chains have also been reported. The increasing of T_g of the nanocomposite material has been observed, indicating the positive influence of the NP incorporation and chemical bonding on the mechanical properties of the hybrid nanostructures. Iron NP-modified vinyl ester resin nanocomposites have been recently synthesized by direct binding NP surface to monomers, which act as stabilizers for preventing NP aggregation and promote copolymerization. The mechanical and magnetic characterization of the prepared nanocomposites have shown an enhancement of tensile strength and Young's modulus as compared with those of cured pure resin, increased thermal stability, and room temperature ferromagnetic behavior.

e. Sensors and electrochromic devices: Recently, a large area of research has focused on the incorporation of nanoscale metals in polymers to design and fabricate advanced optoelectronic and sensor devices. The combination of the thermal-induced tunable absorption properties of gold nanorod with polymers can be exploited to fabricate nanoscale devices for sensing applications. Uniform dispersion of Au NPs in the polymer matrix has been achieved, and the noncovalent Au–S interaction as well as the chemical composition of the polymer has been preserved in the nanocomposite formation. The optical properties based on the plasmon resonance of noble metal NPs are extremely relevant in electrochromic applications. Since surface plasmon absorption depends also on the dielectric properties of the NP host matrix, the incorporation of metal NPs in conducting polymers can be used to fabricate tunable electrochromic devices. Ag and Au NPs have been blended with conducting polymer poly(3,4-ethylenedioxythiophene):poly styrene sulfonate (PEDOT:PSS) to fabricate electrochromic devices. Both the tunable absorption and time response properties exhibited by the prepared nanocomposites make such materials exploitable in the manufacture of full color electrochromic displays. The optical properties and influence of the addition of Ag NPs on thermal properties of PMMA matrix has also been investigated. Spectroscopic measurements of the optical properties have shown that Ag NPs preserve their plasmon absorption when embedded in the polymer matrix. Furthermore, metal NPs have been found to enhance thermo-oxidative stability and glass transition temperature of PMMA matrix.

f. Self-cleaning and biocidal coatings: Another example of functional nanocoating is **photocatalytic coatings** (commercialized as "self-cleaning" glass), which use the catalytic properties of titanium dioxide (TiO_2). Superhydrophobic coatings have surfaces that mimic the surface found in the lotus leaf and are being developed for many applications that require resistance to dirt and ease of cleaning. There is a great interest in the design and development of surfaces that not only are easy to clean and even self-cleaning but also provide biocidal activity. Most of such coatings acquire their biocidal/self-cleaning capacity by incorporating specific nanoparticles: basically silver (Ag) and titanium oxide (TiO_2). Nano-TiO_2 is used for developing anti-UV, antibacterial, and self-cleaning paints. This possesses self-cleaning hydrophobic properties, which causes water droplets to bead-off of a fully cured surface picking up dirt and other surface contaminants along the way.

The self-cleaning action helps to clean and maintain important surfaces and to accelerate drying while leaving the surface with minimal spotting. A recent study utilizes corona treatment technique, inert sol–gel coating, and anatase TiO_2 layer. With the corona treatment, an organic surface was activated to allow a uniform TiO_2 sol–gel coating. Nanoparticles of surface-treated Al_2O_3 molecules help increase hydrophobicity and increase scratch resistance. Microbial evolution on a wide variety of surfaces can cause corrosion, dirt, bad odor and even serious hygiene and health problems. Although no alternatives to the use of biocides are available at present, creation of nanostructured surfaces could offer an innovative and environment-friendly solution to the problem of biofouling. Research has developed new biocidal coating systems that prolong biocidal activity by immobilizing such additives on nanoparticles; the embedded biocides are designed to be released into the environment only when needed, thus extending the lifetime of the biocidal activity.

7.5.1.2 Ceramic Nanocoatings

Nanocomposite coatings are usually formed from ternary or quaternary system with nanocrystalline (nc-) grains of hard transition metal nitrides (e.g., TiN, TiAlN, CrN, BN, VN, ZrN, W_2N) carbides (e.g., TiC, VC, WC), borides (e.g., TiB_2, TiB, CrB_2), oxides(e.g., Al_2O_3, TiO_2, B_2O_3, SiO_2), or silicides (e.g., $TiSi_2$, $CrSi_2$, $ZrSi_2$) surrounded by amorphous (a-) matrices (e.g., Si_3N_4, BN, C). There are many different nanocrystalline grain/amorphous matrix (nc-/a-) systems, such as nc-TiN/a-Si3N4, nc-CrN/a-Si3N4, nc-W2N/a-Si3N4, nc-TiN/a-BN, nc-TiC/a-C, and nc-WC/a-C. The synthesis of such nanocomposite coatings depends on the ability to co-deposit both phases. Nanocoatings for biomedical, **heat dissipation** and **tribological applications** are some of the emerging area of interest.

The composite coatings consisting of CNTs and HA/TiO_2 ceramic particles fabricated by EDP on metallic substrates (e.g., stainless steel, titanium alloy) are suited for biomedical applications, in particular for the attachment and proliferation of cells. The coatings of SWNT-ceramic composites with their anisotropic thermal properties have potential for effective heat dissipation and spreading in a variety of applications, such as in microprocessors and integrated circuit packages (miniature scale devices) and on high-temperature components in turbine engines, reactors, and space vehicles.

Tribology is the science and technology of interacting surfaces in relative motion including friction, lubrication, and wear. Tribological coatings are applied to the surface of a component in order to control its friction and wear. Tribological coatings play a key role in the performance of internal mechanical components of a vehicle, such as the engine and power train. They are also key elements in cutting tools and machinery in general. By reducing wear and friction, these coatings increase the lifetime of the working material while also reducing the dissipation of energy as heat, thus increasing the efficiency of the moving part. When applied to machinery and tools, tribological coatings can reduce (or eliminate) the need for lubricants, increase cutting speed, increase the rate of material removal, reduce maintenance costs, or reduce processing cycle times.

Traditional materials used in coatings for tribological applications are carbides, cemented carbides, metal ceramic oxides, nitrides, and carbon-based coatings. Since the microstructure controls many of the physical properties of the coating, having a nanoscaled microstructure may lead to significant improvements in the coatings' mechanical properties (e.g., hardness), chemical properties (e.g., corrosion resistance), and electrical properties. Thus, nanocomposite coatings are now being investigated as alternatives to the traditional approach of using specific alloying elements in single-phase coating materials to improve, for instance, properties such as hardness. One type of nanocomposite coatings is multilayered thin films made of different layers in the order of nanometers. These films are mostly used for their enhanced hardness and elastic moduli, which is higher in multilayered films than in homogeneous thin films of either component, and for their wear properties. Commercial multilayer coatings made in the nanoscale range, such as WC/C coatings used in the cutting tool industry. Other examples are films of alternating layers of TiN and NbN, or TiAlN/CrN multilayers, which are more efficient than TiAlN films.

7.5.1.3 Metal Matrix Nanocoatings

Metal matrix nanocoatings have also begun to substitute for conventional materials in household appliances, computers, audio and video equipment, as well as in sport appliances. Compressive and tensile strength, as well as the hardness at room, and elevated temperatures, are also increased significantly, resulting in an improvement in the wear resistance of the composite material. However, the addition of the reinforcement particles could significantly alter the corrosion behavior of these materials. In general, the composites are more susceptible to corrosion attack than the matrix alloy. Coating the fiber prior to incorporation in the matrix is a favorable method of inhibiting reaction products (of reinforcement and matrix) growth at the interface while allowing fibers to stiffen the matrix. Selection of an appropriate coating as per filament–matrix interface is important. Organic coatings have been identified as providing excellent corrosion protection for graphite/aluminum MMNCs. These coatings provide only barrier protection, functional graded materials (FGMs) offer an advanced alternative for coatings.

a. Functional graded materials (FGMs): Functional graded materials (FGMs) are a class of composites that possess a gradual and continuous variation composition and microstructure. The idea of Functionally Graded Materials (FGMs) was substantially advanced in the early 1980s in Japan, where this new material concept was proposed to increase adhesion and minimize the thermal stresses in metallic ceramic composites developed for reusable rocket engines. Meanwhile, FGM concepts have triggered worldwide research activity and are applied to metals, ceramics, and organic composites to generate improved components with superior physical properties. Depending on the application and the specific loading conditions, varying approaches can be followed to generate the structure gradients. Consequently, coatings have been deposited by different techniques involving physical vapor deposition (PVD), chemical vapor deposition (CVD), plasma spraying, arc spraying, pulsed laser deposition (PLD), or sol–gel techniques.

Metal matrix composites consisting of SiC monofilaments in Ti-based matrices show great promise for aerospace applications. SiC Sigma monofilaments were coated with a functionally graded (FG) TiC-based coating (SiC_f/C/(Ti,C)/Ti) using closed-field unbalanced magnetron sputtering. The coated fibers were incorporated into Ti matrices using hot isostatic pressing. The interfacial properties of the bulk composites were then evaluated using push out testing of thin composite samples, in order to assess the effect of the graded coating. The test on interfacial properties indicate that the FG coating offers an improvement on composite fracture toughness over the uncoated fibers by approximately 70% before heat treatment, approximately 35% after heat treatment [34].

Coatings made up of single NiCr–WC layers with different concentration of carbide in single and double-layered format, Figure 7.13a and b reveal the microstructure in their SEM image. The graded structure due to the two different carbide concentrations used is clearly distinguished, with a smooth microstructure transition between the two layers. Same features in terms of hardness and phase distribution as those described for the single layers were found under hardness measurement and SEM inspection.

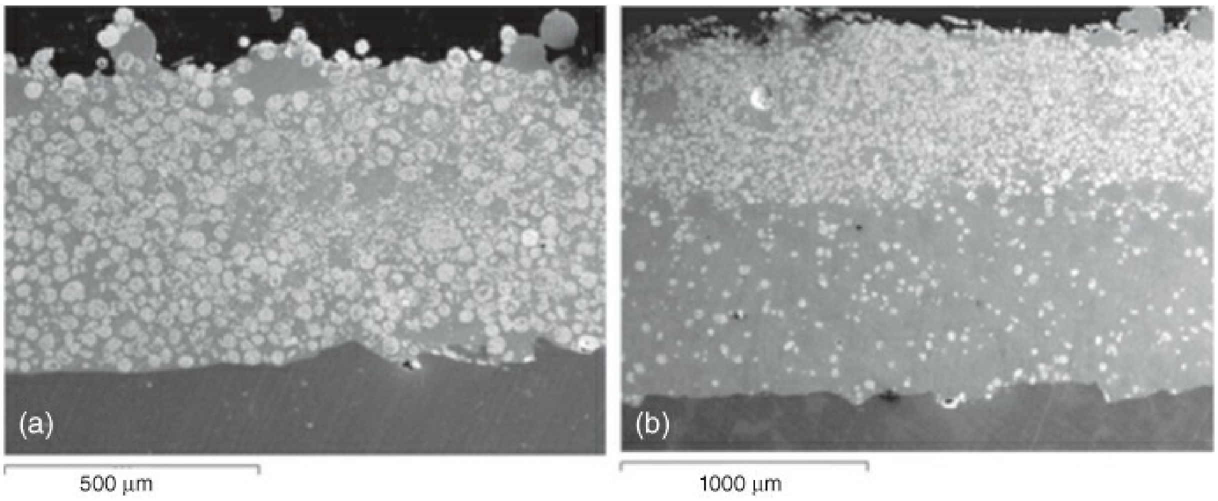

Figure 7.13 SEM micrograph of NiCr–WC coatings with (a) single-layer 60% carbide concentration and (b) double-layer graded coating with outer layer 60% WC over inner layer of 15% WC.

Amado et al. [34], © 2012. With permission of Elsevier.

b. Corrosion Protection: Although ceramic coatings produced by physical vapor deposition demonstrate attractive functional properties of high hardness and chemical inertness, they are not easy to deposit at a thickness adequate to provide satisfactory corrosion protection of a metal substrate. PVD metallic coatings, in general, do not suffer such thickness restrictions. Thick (in excess of 10 μm), lightly stressed coatings, with insignificant porosity can, in principle, be produced at a rate of 10 μm/h or higher. Exploring the possibilities of pairing certain low-miscibility transition metals – for example, titanium/chromium/zirconium with copper/nickel – and the ability, with the selection of appropriate deposition parameters, to preferentially supersaturate the "early" transition metal (i.e., Ti, Cr, Zr) with nitrogen (or other interstitially located elements), thick metallic nanocomposite coatings can be produced. These coatings exhibit excellent wear resistance owing to their high hardness/elastic modulus ratio (H/E) and may also possess many other potentially desirable properties (e.g., toughness and corrosion protection – sacrificial as well as "barrier") inherent to metallic coatings – especially with the addition of aluminum as a base. These nanocomposite coatings that comprise a hard nanocrystalline phase embedded in an amorphous matrix exhibit improved properties over a range of varying conditions with enhanced thermal stability and improved physical and mechanical properties. Such coatings can be deposited on austenitic stainless steel (304), low alloy steel (4145), and silicon wafers using closed-field unbalanced magnetron sputter equipment in reactive (N_2) atmosphere. These coatings can act as alternatives to electroplated cadmium, IVD-aluminum, electroplated hard chromium, electroless nickel, and other 'traditional' coatings used in aerospace, automotive, and other engineering applications – where environmental legislation is restricting the use of toxic processes and materials. These metallic coatings with multifunctional and adaptive properties will suit a range of technically challenging environments.

7.5.2 Smart (Responsive) Nanocoatings

A functional coating is termed as **smart coating** when a system is able to react to a stimulus based on predefined functionalities but providing a smart feedback. In other words, an active coating sensitive to an external stimulus changes its physical or chemical properties, preferably in a reversible way, and is able to work as a sensor and/or actuator. Examples are coatings switching from hydrophilic to hydrophobic according to the environmental humidity or supplying a mechanism of damage prevention, which is activated in response to environmental conditions. Responsive nanocoatings react to the environmental conditions, such as light or heat, either in a **passive** or in an **active** way. These coatings allow changing the properties of some materials, such as glass, by conferring new or improved properties. As an example, the use of glass is very common in modern buildings to allow the construction of transparent and seemingly lightweight structures. However, the relative high transmittance of visible and infrared (IR) light is a major disadvantage, since this leads to a large heat transfer that is particularly undesirable in summer. The problem is reversed in winter, when heat is dispersed through the glass. In order to address these problems, various types of nanocoatings that **modulate light transmission in glass** are under investigation and being commercialized. The aim is to reduce indoor heating in summer, so less air-conditioning is required to keep the atmosphere cool, with consequent energy saving. One type of coating, referred to as "low-e" meaning "low emissivity," is based on a thin silver film, about lonm thick, surrounded by dielectric layers. Metallic layers have been widely used to increase the reflectivity of light (and reduce transmittance) for years, but they have the disadvantage of giving a mirror-like appearance. Silver loses its metallic appearance when scaled to a nanofilm, thus eliminating this problem. **"Low-e" coatings are a type of passive nanocoatings**, since the properties of the layers are unperturbed during its operation. Another class of coatings used in glasses are those often described as dynamic or "**smart coatings**." In this case, the environmental conditions, such as radiation intensity or temperature, induce a change in the properties of the coating (e.g., darkening of windows). When the effect is a change in the color (meaning also transparency) they are called **"chromogenic smart materials**." The change can be induced actively, by pressing a button. This is the case of **electrochromic coatings** where applying a small voltage induces a change in transmittance, and in the case of gas chromic coatings, which change their transmittance in the presence of specific gases. Gas chromic glazing makes use of the properties of tungsten oxide thin films (WO_3) which go from colorless to blue in the presence of hydrogen with a suitable catalyst. Gas chromic windows follow a double-pane model: on one pane a film of WO_3 is deposited with a thin layer of catalysts on top. Hydrogen gas is fed into the gap producing coloration (windows color with 1.1-10 % hydrogen, which is below the flammability concentration). To switch the color of the window back, another gas is purged in (oxygen). Smart coatings can also be passive in the sense of changing their optical properties due to a change of external temperature (**thermochromic)** or light incidence (**photochromic**). Another example of nanotechnology applied to smart coatings is the use of a family of wavelength-selective films for manufacturing "heat mirrors." One of these materials is indium tin oxide (ITO), an infrared absorber. A 300-nm ITO coating on glass provides more than 80% transmission for the wavelengths predominant in sunlight. The transmission properties of the window can be varied by changing the thickness and material composition of the coating, so that a combination of materials could be used to produce smart windows that reflect solar energy in summer but transmit solar energy in winter.

Review Questions

Q1. Define the terms composite, matrix, reinforcement, and nanocomposite. Classify nanocomposites on the basis of matrix material.

Q2. “Nature has mastered the synthesis of nanocomposites” justify the statement giving few examples.

Q3. Discuss critical size of reinforcement below which the addition of particles improves the properties of matrix material.

Q4. What is the plausible mechanism responsible for property improvements of a composite material? Discuss various strengthening mechanisms.

Q5. Describe different types of polymer-based nanocomposites and outline suitable route for their synthesis.

Q6. Describe suitable method of fabrication of CNT–metal matrix composites.

Q7. Explain the improved qualities of structural nanocomposites with suitable example.

Q8. Discuss the significance of nanocomposites reinforced with carbon nanotubes in different matrices.

Q9. Discuss the significance and limitations of graphene-reinforced polymeric and ceramic-based nanocomposites.

Q10. Discuss improvement in properties in metal matrix composites by incorporating CNTs.

Q11. What are ceramics? Give few examples of nanoceramic reinforced metal matrix composites and their properties. Suggest suitable methods for synthesis of ceramic nanocomposites.

Q12. Mention properties of nanoparticles that may contribute to the desirable functional properties in polymer nanocomposites.

Q13. Mention steps involved in chemical route to obtain polymer–inorganic nanocomposites.

Q14. Discuss functional properties and potential applications of polymer–inorganic nanocomposites.

Q15. Discuss the properties of clays which make them suitable as reinforcement for preparing polymer–clay nanocomposites.

Q16. Discuss significant properties and applications of polymer–clay nanocomposites.

Q17. How polymer–graphene nanocomposites useful in energy storage devices?

Q18. What type of reinforcements can be obtained from cellulose for polymer nanocomposites? Give factors affecting performance of cellulose nanoreinforcements.

Q19. How will you obtain nanowhiskers/nanoparticles from polysaccharides such as starch, chitin, and chitosan to incorporation into polymer nanocomposites?

Q20. What do you understand by “functional coatings”? Suggest suitable composition for functional coatings?

References

1. L. A. Polette, N. Ugarte, M. José Yacamán and R. Chianelli, “Discovering Archaeology”, *Sci. Am.*, **283** (1), (2000) 46–53.

2. P. Gómez-Romeroa and C. Sanchezb, “Hybrid Materials. Functional Properties. From Maya Blue to 21st Century Materials”, *New J. Chem.*, **29** (2005) 57–58.

3. P. H. C. Camargo, K. G. Satyanarayana and F. Wypych, “Nanocomposites: Synthesis, Structure, Properties and New Application Opportunities”, *Mater. Res.*, **12** (2009) 1–39.

4. P. M. Ajayan, L. S. Schadler and P. V. Braun, *Nanocomposite Science and Technology*, Wiley, 2003.

5. A. Kelly, *Concise Encyclopedia of Composites Materials*, Elsevier Science Ltd, 1994.

6. O. Kamigaito, “What can be Improved by Nanometer Composites?”, *J. Japan Soc. Powder Metallur.*, **38** (1991) 315–321.

7. L. C. Stearns, J. Zhao, M. P. Harmer, “Processing and Microstructure Development in Al_2O_3-SiC Nanocomposites”, *J. Eur. Ceram. Soc.*, **10** (1992) 473–477.

8. L. S. Walker, V. R. Marotto, M. A. Rafiee, N. Koratkar and E. L. Corral, “Toughening in Graphene Ceramic Composites”, *ACS Nano*, **5** (2011) 3182–3190.

9. F. E. Kruis, H. Fissan and A. Peled, “Synthesis of Nanoparticles in the Gas Phase for Electronic, Optical and Magnetic Applications: A Review”, *J. Aerosol Sci.*, **29** (1998) 511–535.

10. R. Casati and M. Vedani, “Metal Matrix Composites Reinforced by Nano-Particles—A Review”, *Metals*, **4** (2014) 65–83.

11. Sudarshan , M. K. Surappa, D. Ahn and R. Raj, “Nanoceramic–Metal Matrix Composites by *In-Situ* Pyrolysis of Organic Precursors in a Liquid Melt”, *Metallur. Mater. Trans A*, **39** (2008) 3291–3297.

12. S. R. Bakshi, D. Lahiri and A. Agarwal, “Carbon Nanotube Reinforced Metal Matrix Composites: A Review”, *Int. Mater. Rev.*, **55** (2010) 42–64.

13. A. Agarwal, S. R. Bakshi and D. Lahiri, *Carbon Nanotubes Reinforced Metal Matrix Composites*, CRC Press, 2010.

14. C. L. P. Pavithra, B. V. Sarada, K. V. Rajulapati, T. N. Rao and G. Sundararajan, “A New Electrochemical Approach for the Synthesis of Copper-Graphene Nanocomposite Foils with High Hardness”, *Sci. Rep.*, **4** (2014) Article number: 4049.

15. C. Ping, F. Li, Z. Jian and J. Wei, “Preparation of Cu/CNT Composites Particles and Catalytic Performance on Thermal Decoposition of Ammonium Perchlorate”, *Propell. Explos. Pyrotechn.*, **31** (2006) 452–455.

16. J. Liao, M-J. Tan, R. V. Ramanujan and S. Shukla, “Carbon Nanotube Evolution in Aluminum Matrix During Composite Fabrication Process”, *Mater Sci Forum*, **690** (2011) 294–297.

17. P. K. Rohatgi and B. Schultz, “Lightweight Metal Matrix Nanocomposites – Stretching the Boundaries of Metals”, *Mater. Matt.*, **2** (4) (2007) 16–19.

18. D. R. Paul and L. M. Robeson, “Polymer Nanotechnology: Nanocomposites”, *Polymer*, **49** (2008) 3187.

19. F. Hussain, M. Hojjati, M. Okamoto and R. E. Gorga, “Polymer-Matrix Nanocomposites, Processing, Manufacturing, and Application: An Overview”, *J. Compos. Mater.*, **40** (2006) 1511–1575.

20. E. Thostenson, C. Li and T. Chou, “Review Nanocomposites in Context”, *J. Compos. Sci. Technol.*, **65** (2005) 491–516.

21. S. R. Vadera, A. Tuli, N. Kumar, B. B. Sharma, S. R. Gupta, C. Prakash and P. Kishan, “Preparation and Study of Finely Dispersed Magnetic Oxide in Polymer Matrix”, *J. Phys. de. Fr. IV*, **7** (1997) C-1549.

22. J. Lee, V. C. Sundar, J. R. Heine, M. G. Bawendi and K. F. Jensen, “Full Color Emission from II–VI Semiconductor Quantum Dot-Polymer Composites”, *Adv. Mater.* **12** (2000) 1102–1105.

23. J. Pérez-Juste, B. Rodríguez-González, P. Mulvaney, L. M. Liz-Marzán, “Optical Control and Patterning of Gold-Nanorod-Poly(vinylalcohol) Nanocomposite Films”, *Adv. Funct. Mater.* **15** (2005) 1065–1071.

24. K. R. Reddy, W. Park, B. C. Sin, J. Noh and Y. Lee, “Synthesis of Electrically Conductive and Superparamagnetic Monodispersed Iron Oxide-Conjugated Polymer Composite Nanoparticles by In Situ Chemical Oxidative Polymerization”, *J. Colloid Interface Sci.*, **335** (2009) 34–39.

25. Y. Wang, T. Li, L. Zhao, Z. Hu and Y. Gu, “Research Progress on Nanostructured Radar Absorbing Materials”, *Energy Power Eng.*, **3** (2011) 580–584.

26. P. Saini and M. Arora, “Microwave Absorption and EMI Shielding Behavior of Nanocomposites Based on Intrinsically Conducting Polymers”, *Graphene and Carbon Nanotubes*, INTECH, 2012. http://cdn.intechopen.com/pdfs-wm/38964.pdf.

27. M. Alexandre and P. Dubois, “Polymer-layered Silicate Nanocomposites: Preparation, Properties and Uses of a New Class of Materials”, *Mater. Sci. Eng. Rep.*, **28** (2000) 1–63.

28. J. K. Kap, S. L. John, A. P. Arun and K. H. Taek, “Preparation and Characterization of Nylon-6/Organoclay Nanocomposite Filament Fibers”, *Polym. Compos.*, (2008) 265–273.

29. J. R. Potts, D. R. Dreyer, C. W. Bielawski and R. S. Ruoff, “Graphene-Based Polymer Nanocomposites”, *Polymer*, **52** (2011) 5–25.

30. M. A. S. A. Samir, F. Alloin and A. Dufresne, “Review of Recent Research into Cellulosic Whiskers, Their Properties and Their Application in Nanocomposite Field”, *Biomacromolecules*, **6** (2005) 612–626.

31. M. Avella, J. J. De Vlieger, M. E. Errico, S. Fischer, P. Vacca and M. G. Volpe, “Biodegradable Starch/Clay Nanocomposite Films for Food Packaging Applications”, *Food Chem.*, **93** (2005) 467–474.

32. P.-P. Zuo, H.-F. Feng, Z.-Z. Xu, L.-F. Zhang, Y.-L. Zhang, W. Xia and W.-Q. Zhang, “Fabrication of Biocompatible and Mechanically Reinforced Graphene Oxide-Chitosan Nanocomposite Films”, *Chem. Central J.*, **7** (2013) 39–49.

33. S. Abbott and N. MacDermid, *Nanocoatings: Principles and Practice: From Research to Production*, DEStech Publications, Inc., Lancaster, 2013.

34. J. M. Amado, J. Montero, M. J. Tobar and A. Yáñez, “Ni-Based Metal Matrix Composite Functionally Graded Coatings”, *Physics Procedia*, **39** (2012) 362–367.

Chapter 8

Unique Properties

8.1 Introduction

In nanotechnology, a nanoparticle (NP) can be defined as a small elemental ensemble that behaves as a whole unit and presents novel properties not exhibited in the characteristic bulk material. At the nanometer scale, the confinement of electrons, phonons, and photons leads to the appearance of new chemical, physical, and biological properties that makes them new materials in their own right. Relative to microstructural (MSM) metals and alloys, the nanostructural materials (NSM) contain a higher fraction of grain boundary volume (e.g., for a grain size of 10 nm, between 14% and 27% of all atoms reside in a region within 0.5–1.0 nm of a grain boundary); therefore, grain boundaries play a significant role in the properties of the materials. Changes in the grain size result in a high density of incoherent interfaces or other lattice defects such as dislocations, vacancies, and so on. As the grain size d of the solid decreases, the proportion of atoms located at or near grain boundaries relative to those within the interior of a crystalline grain scales as $1/d$. This has important implications for properties in ultrafine-grained materials, which will be principally controlled by interfacial properties rather than those of the bulk. For instance, composites made from particles of nanosize ceramics or metals smaller than 100 nm can suddenly become much stronger than predicted by existing models of materials science while metals with a so-called grain size of around 10 nm are as much as seven times harder and tougher than their ordinary counterparts with grain sizes in the hundreds of nanometers. Moreover, size, morphology, and structure of nanoparticles (NPs) determine not only their properties but also the reactivity as well. Both the thermodynamics and kinetics of reactions are different depending on the size of NPs. The reduction of dimensionality affects to a variety of factors such as melting point (which depends on the coordination number of the participating atoms), optical properties, magnetic properties, reactivity, and conductivity, among others. The causes of these drastic changes stem from the world of quantum physics [1, 2]. The bulk properties of any material are merely the average of all the quantum forces affecting all the atoms. However, as things become smaller and smaller, eventually a point is reached where averaging no longer works.

In general, the unique properties of nanomaterials are attributed to quantum effects, larger surface area, and self-assembly. Q**uantum effects** can begin to dominate the behavior of matter at the nanoscale – particularly at the lower end – affecting the optical, electrical, and magnetic behavior of materials. This is attributed to the fact that matter at nanoscale no longer follows Newtonian physics rather quantum mechanics, which are explained by size effect, quantum confinement, and density of states (DOS). Secondly, nanomaterials have a relatively **larger surface area** when compared to the same mass of material produced in bulk form. The smaller the particle size, the more the proportion of surface atoms, leading to an increased reactivity due to rise in number of the active sites. In some cases, inert materials in their bulk form turn out to be reactive when produced in their nanoscale form. Effect of larger surface area applies to all nanomaterials in different shapes, weather nanocoatings, nanowires, nanotubes or nanoparticles. Thirdly, **self-assembly** is a process that rests on the organization of components producing an ordered pattern or structure. At nanoscale, in particular, it reflects the information encoded in individual molecules such as shape, charge, polarizability, and so on that determine their attractive or repulsive interactions. Molecular self-assembly usually takes advantage of supramolecular interactions (ionic, hydrophobic, van der Waals, hydrogen, and coordination bonds), but can also make use of kinetically labile covalent bonds. This intrinsic mobility leads to ordered nanostructures upon equilibration between aggregated and nonaggregated states, thus providing a number of interesting properties such as error correction, self-healing, and high sensitivity to external stimuli.

8.2 Size Effects

By **Gleiter's definition:** The size effects in microstructures arise when its size *d* is reduced up to a critical value $d - d^*$ when scale length of physical phenomenon (free path length of electrons, phonons, etc.; coherent length, screening length, etc.) becomes to be equal to or compatible with characteristic size (length, thickness, diameter) of building blocks of microstructures.

Basically, the properties of a material are characterized by a specific "length scale," usually on the nanometer dimension. If the physical size of the material is reduced below this length scale, its properties change and become sensitive to size and shape. Size effects constitute a peculiar and fascinating aspect of nanomaterials. The effects determined by size pertain to the evolution of structural, thermodynamic, electronic, spectroscopic, electromagnetic, and chemical features of these finite systems with changing size, which are different from the bulk and their isolated atoms/molecules. Classical laws of physics fail to explain the origin of the novel properties of materials in this size regime. Moreover, nanocrystals possess a high surface area and a large fraction of the atoms in a nanocrystal are on its surface, which in turn depends on the size of the particle (30% for a 1-nm crystal, 15% for a 10-nm crystal), it can give rise to size effects in chemical and physical properties of the nanocrystals [3].

8.2.1 Quantum Confinement

Size effects constitute a peculiar and fascinating aspect of nanomaterials. Nanomaterials are closer in size to single atoms and molecules than to bulk materials, and to explain their behavior it is necessary to use quantum mechanics. Basically, quantum mechanics is a scientific model that was developed for describing the motion and energy of atoms and electrons. The most salient quantum effects together with other physical properties arising at nanoscale are as follows:

- Due to the smallness of nanomaterials, their mass is extremely small and gravitational forces become negligible. Instead electromagnetic forces are dominant in determining the behavior of atoms and molecules.
- Wave-corpuscle duality of matter: For objects of very small mass, such as the electrons, wave-like nature has a more pronounced effect. Thus, electrons exhibit wave behavior and their position is represented by a wave (probability) function.
- One of the consequences is a phenomenon called "tunneling." Classical physics states that a body can pass a barrier (potential barrier) only if it has enough energy to "jump" over it. Therefore, if the object has lower energy than that needed to jump over the energy barrier (the "obstacle"), in classical physics, the probability of finding the object on other side of the barrier is zero. In quantum physics, on the other hand, a particle with energy less than that required to jump the barrier has a finite probability of being found on the other side of the barrier mainly due to the tunneling effect (Figure 8.1).

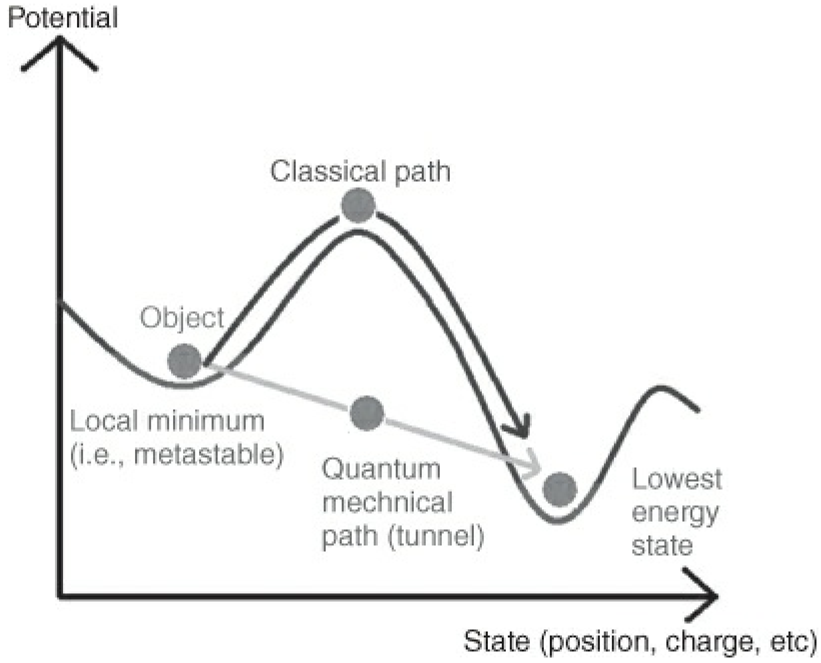

Figure 8.1 Schematic representation of tunneling.

It should be noted that tunneling is the penetration of an electron into an energy region that is classically forbidden. In order to have tunnel effect, the thickness of the barrier (i.e., energy potential) must be comparable to the wavelength of the particle; in other words, electron (or quantum) tunneling is attained when a particle (an electron) with lower kinetic energy is able to exist on the other side of an energy barrier with higher potential energy, thus defying a fundamental law of classical physics [4].Therefore, this effect is observed only at a nanometer level.

The effects determined by size pertain to the evolution of structural, thermodynamic, electronic, spectroscopic, electromagnetic, and chemical features of these finite systems with changing size. The properties of a material depend on the type of motion its electrons can execute, which depends on the space available for them. Thus, the properties of a material are characterized by a specific "length scale," usually on the nanometer dimension. If the physical size of the material is reduced below this length scale, its properties change and become sensitive to size and shape.

Nanoscale materials exhibit many interesting phenomena, which are different from bulk and their constituting elements (e.g., physical, chemical, electronic, and magnetic properties) and are highly dependent on the size and shape of the material. The classical laws of physics fail to explain the behavior of materials at this scale. When one or more dimensions of a crystal are confined to nanoscale and as it approaches the size of an exciton in bulk crystal (often termed as Bohr exciton radius), the electrons experience a confinement of motion in space. This situation can be described in terms of particles in a box; under this condition, quantum mechanics is more suitable to explain their behavior. The boundary conditions play an important role in the confinement of electrons, and the properties of matter at nanoscale are highly dependent on their size and shape. For example, quantum confinement results in discretization of energy levels in Au nanoparticles and they exhibit metallic to semiconducting to insulator transition as their size decreases from 5 to 2 nm.

One of the direct observations of quantum size effect in semiconductor nanocrystals is the blueshift in the absorption and emission spectra with decrease in size. The shape of nanomaterials also has a remarkable effect on its properties: electrons experience different confinement depending on the particle shapes. Depending on the dimensionality of confinement, nanomaterials are classified as 1D, 2D, or OD structures. For 2D nanomaterials, the confinement is imposed only along one axis, and the situation is best explained as in the case of quantum as well. In the case of 1D nanomaterial, the electrons experience confinement along two dimensions. The electrons are free to move only in one dimension and the best example is a nanowire. The material is termed as quantum dot when the particle experience confinement along all the three dimensions. The dimensional confinement of electrons in materials always leads to dramatic modifications in their DOS.

This phenomenon is called quantum confinement, and therefore nanocrystals are also referred to as quantum dots (QDs). In small nanocrystals, the electronic energy levels are not continuous as in the bulk but are discrete (finite DOS) because of the confinement of the electronic wave function to the physical dimensions of the particles.

8.2.2 The Density of States (DOS)

Atoms have their well-known atomic orbital. Depending on the extent of overlap in a solid, they remain mostly unperturbed, as in noble gases, or they combine to extended band structures, as in metals or semiconductors. The core orbital is confined to a relatively small volume and remains localized (atom-like). Each atom contributes with its atomic states to a band so that, although the width of a band increases slightly when more atoms are added, the DOS within a band is basically proportional to the number of atoms (*N*) of an ensemble with an extended band-like state. The bandwidth amounts typically to a few electron volts. Thus, the DOS is on the order of *N* per electron volt, which is very large for a bulk amount of matter (Avogadro's number, NA) but low for small clusters as shown in Figure 8.2.

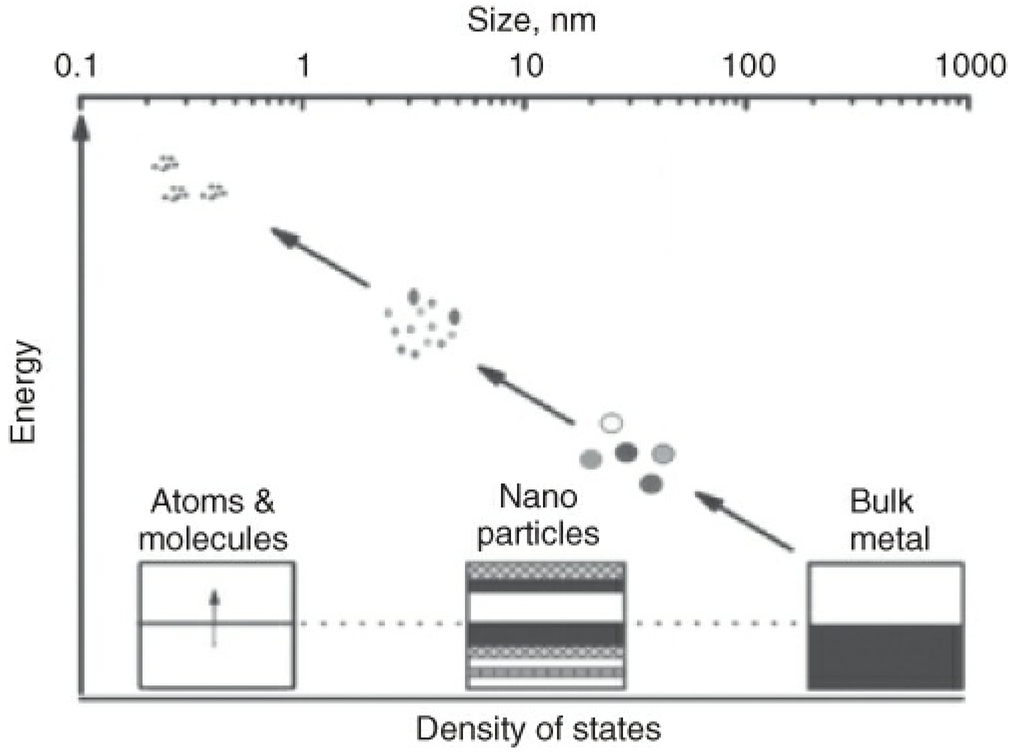

Figure 8.2 Relationship between size, energy, and energy of states of nanoparticles.

White et al. [5], © 2008. With permission of RSC.

The DOS basically scales smoothly with size, but with a scaling law that is different from that found from surface effects. It is described to be a first approximation by the "particle-in-a-box" model in which the size of the box is given by the size of the particle. Discontinuities come in when the states are populated with electrons: for highly symmetric systems there are degenerate states, and when one of these is filled the next electron has to go into the next state of higher energy. These discontinuities are often somewhat blurred since the symmetry is usually lowered when an additional atom is added to a highly symmetric system. Thus, the discontinuities are typically superimposed on a smooth size-dependent slope. An important threshold is reached when the gap between the highest occupied and the lowest unoccupied state (called the Kubo gap, *d*) equals thermal energy [6]. When electrons get thermally excited across the Kubo gap, a low-temperature insulator becomes a semiconductor and at higher temperatures a metal; and also magnetic properties of small clusters can change dramatically. This nonmetal-to-metal transition can take place within a single incompletely filled band, or when two bands begin to overlap because of band broadening. The change of DOS with cluster size is illustrated in Figure 8.3.

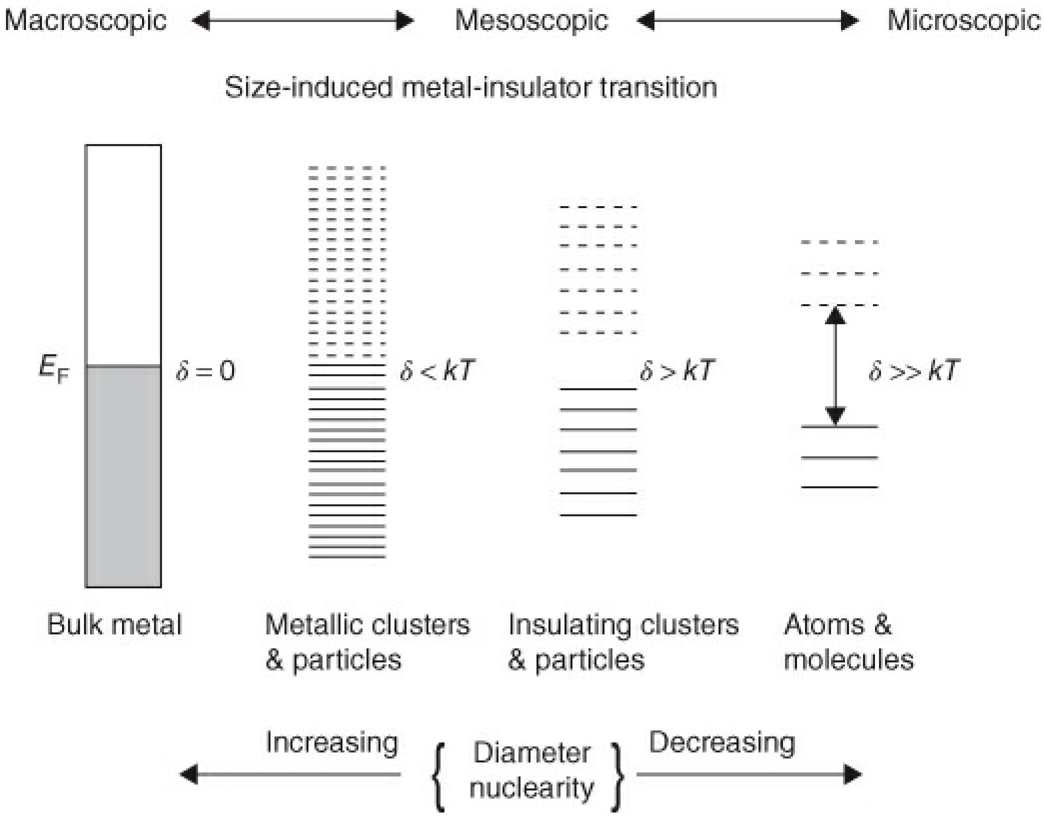

Figure 8.3 Evolution of the band gap and the density of states as the number of atoms in a system increase.

Edwards et al. [6], © 1999. With permission of Wiley, Weinheim.

Chemists may prefer to think of small clusters as molecules. Instead of bands, they talk of delocalized molecular orbitals and the Kubo gap becomes the HOMO–LUMO gap. In such a view, it is obvious that high-cluster symmetry leads to corresponding degenerate molecular orbitals. Incompletely filled degenerate HOMO lead to magnetism, but often also to symmetry lowering by Jahn–Teller distortion.

Two interesting examples representing delocalized systems of high symmetry are those of C_{60} fullerene and Au_{32} gold (Figure 8.4a and b). Both are cage-like hollow clusters. Au_{32} has been predicted from high-level quantum chemical calculations, and its hollow structure was ascribed to the relativistic character of its electrons. For the same reason, AuN_2 clusters up to probably $N = 13$ are planar, in contrast to most other elements that form icosahedral or cuboctahedral minimum energy structures. C_{60} is meanwhile well known from both experiment and theory. As a consequence of its icosahedral symmetry, its HOMO is fivefold degenerate. Since it is fully occupied by 10 electrons, it is not prone to Jahn–Teller distortion [7].

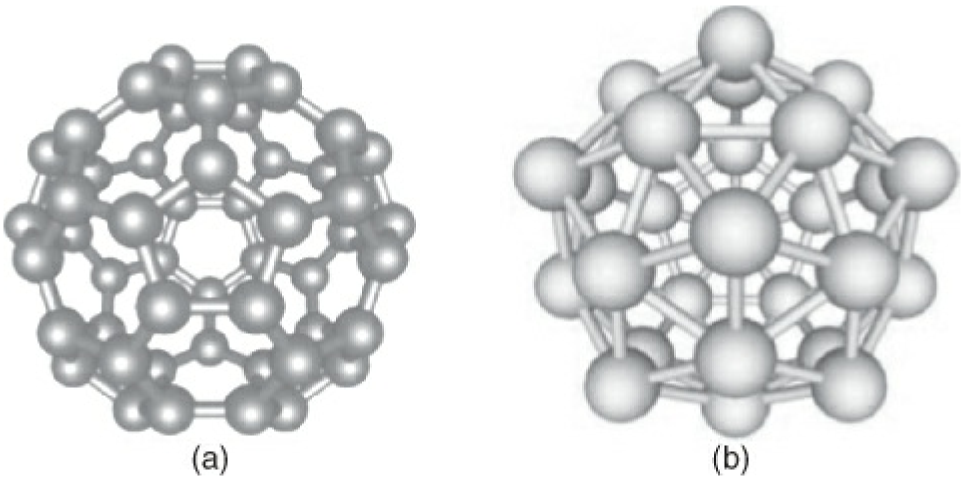

Figure 8.4 Calculated structures of the fullerene C_{60} (a) and of the Au_{32} (b) nanoclusters, which are both hollow.

Johansson et al. [7], © 2004. With permission of Wiley Weinheim.

It should be noted that already at a size of a few nanometers, a system contains several hundred atoms so that discontinuities are no longer observed and the wavelength shift with size appears smooth. It is nevertheless a quantum effect since it is governed by the nature of standing waves of a confined system rather than by the fraction of atoms at the surface. Colloidal gold nanoparticles were already well known in the middle ages. They were used as dyes in stained glass windows of cathedrals and palaces. Particles of 10 nm size absorb green light and thus appear red, smaller ones would even fluoresce. In contrast to the above semiconductor particles, this absorption of metallic particles is due to surface plasmon, a collective excitation of electrons near the surface that represents standing waves on a surface. Their interaction with light is well described by Mie theory. Surface plasmons obey somewhat complex rules, and their wavelength in some cases increases and in others decreases with size.

8.2.3 High Surface Area

Surfaces and interfaces play an increasingly important role for particles or structures as they are made smaller. A variety of physical mechanisms underlie the forces that act at surfaces, but the overall effect is simple; small objects have a very strong tendency to stick together. This stickiness at the nanoscale and the accompanying strong friction that occurs when parts are made to move against each other is an important factor limiting the degree to which microelectronic mechanical systems (MEMS) technologies can be scaled down to the nanoscale. These phenomena also underlie the almost universal tendency of protein molecules to stick to any surface immersed within the body, with important consequences for the design of biomedical nanodevices.

Fraction of Atoms at the Surface

The surface of a sphere scales with the square of its radius r, but its volume scales with r^3. The total number of atoms N in this sphere scales linearly with volume. The fraction F of atoms at the surface is called dispersion, and it scales with surface area divided by volume, that is, with the inverse radius, and thus with $N^{-1/3}$. When the diameter of a specimen reaches the diameter of two atoms, every atom is directly exposed to surface, and $F = 1$ [8]. This is illustrated in Figure 8.5 for the example of cubic crystal with n atoms along an edge and a total of $n = N^{1/3}$ atoms.

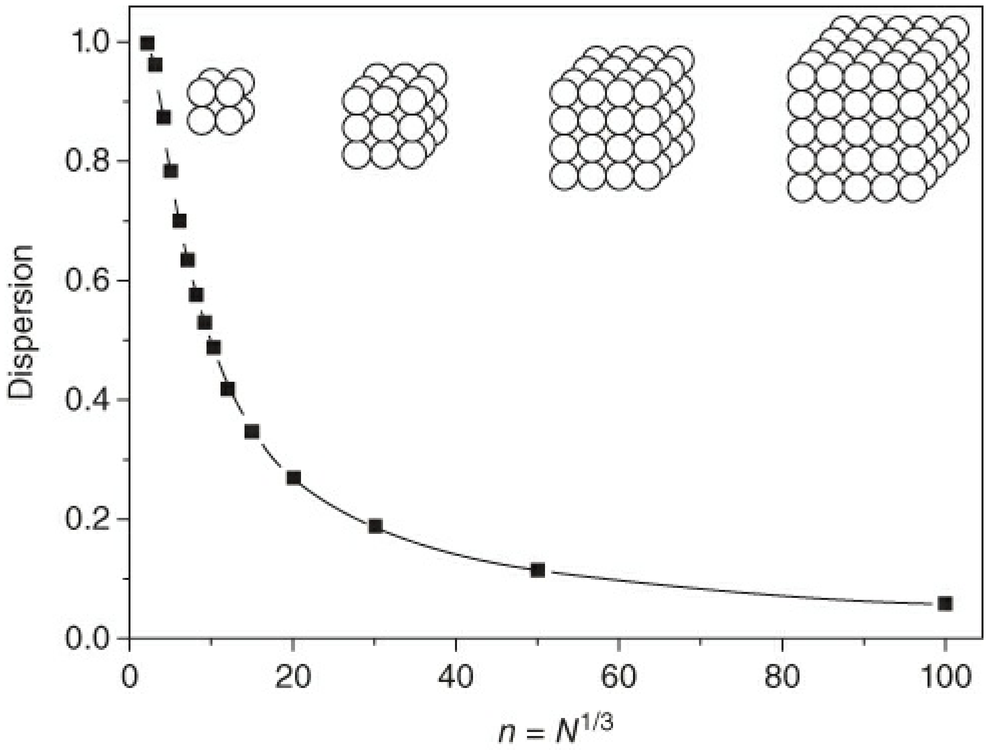

Figure 8.5 Size dependence of the dispersion for cubic particles with $n = N^{1/3}$ atoms along an edge.

Roduner [8], © 2006. With permission of RSC.

The structure of first four clusters is displayed. The atoms are counted and F calculated as follows (8.1):

$$F = \frac{6n^2 - 12n + 8}{n^3} = \frac{6}{N^{\frac{1}{3}}}\left(1 - \frac{2}{N^{\frac{1}{3}}} + \frac{8}{6N^{\frac{2}{3}}}\right) \approx \frac{6}{N^{\frac{1}{3}}} \tag{8.1}$$

All properties that depend on the dispersion of a particle lead to a straight line when plotted against r^{-1}, d^{-1}, or $N^{-1/3}$. Atoms at the surface have fewer direct neighbors than atoms in the bulk. Therefore, particles with a large fraction of atoms at the surface have a low mean coordination number (which is the number of nearest neighbors). In fact, the dispersion and the mean coordination number <NN> obey the same scaling law and are equivalent measures of surface effects [9]. The linearity of a plot of <NN> against $N^{-1/3}$ is shown in Figure 8.6 for small clusters of Mg atoms in various packing symmetries. In the limit of infinitely large clusters, the line extrapolates to <NN> = 12, the coordination number of close-packed spheres in the bulk. Since the dispersion of nanomaterials is high, it is important to understand surface effects and their implications in giving rise to the unique physical, chemical, and biological properties, which radically differ from their bulk counterparts owing to the presence of a large number of atoms with dangling bonds at a surface with low surface energy.

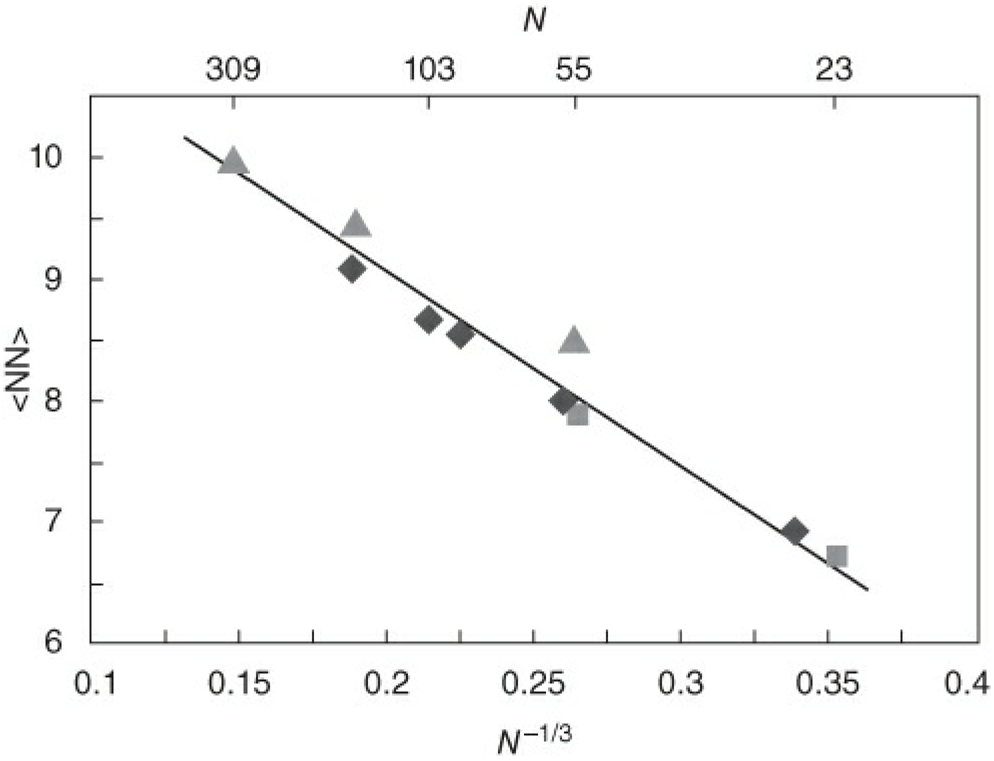

Figure 8.6 Calculated mean coordination number as a function of inverse radius for magnesium clusters of different symmetries (triangles: icosahedra, squares: decahedra, diamonds: hexagonal close packing).

Kohn et al.[9], © 2001. With permission of RSC.

Increased Surface Energy and Tension

Having the extended surface, the nanocrystals have therefore extended external free surface energy (Gibbs energy) and given by Equation 8.2:

$$\Delta G_s = \gamma . S_f \tag{8.2}$$

where γ is a specific surface energy (the energy per surface unit), or a specific work to create the free surface area, or a specific tension. For estimation of γ in accordance with surface dimensionality one need to divide it on any characteristic area. In the physical sense, it is surface area per one atom $S_a \sim 10^{-19}$ m^2. Taking $\Delta H_s \sim 100$ kJ/mol and $N_A = 6 \times 10^{23}$ atoms/mol, Avogadro's number, we obtain Equation 8.3:

$$\gamma \approx \frac{\Delta H_s}{N_A S_a} \approx \frac{100\,\mathrm{kJ/mol}}{6 \times 10^{23}\,1/\mathrm{mol} \times 10^{-19}\,\mathrm{m}^2} \approx 2\frac{\mathrm{J}}{\mathrm{m}^2} \qquad \textbf{8.3}$$

The surface energy causes the surface tension or the surface tangential force, $F = \gamma a$. The tension exists for any surface, including a plane surface. For nanoparticles of radii (*r*), an additional Laplace tension (PL) is arisen or given by Equation 8.4:

$$\mathrm{PL} = 2\gamma/r \qquad \textbf{8.4}$$

It is responsible for capillary phenomena and wetting of liquids. The Laplace tension for solid particles is considered often as Laplace pressure. For instance, for small *r* = 10 nm liquid nanoparticle, the Laplace pressure is very high (Eq. 8.5) and is comparable with the pressure of gun powder gas in a gun barrel.

$$\mathrm{PL} = 2\gamma/r = 2\,\mathrm{J/m}^2/10\,\mathrm{nm} = 200\,\mathrm{MPa} \qquad \textbf{8.5}$$

8.3 Physical Properties

Properties such as color, melting point, ionization potential and electron affinity, electrical conductivity, or magnetism which are not otherwise dependant on size become size dependent when the size of a particle falls, below nanoscale in at least one dimension. On this basis, the properties of matter can be tuned to their desired values by adjusting the size of nanoparticles and the thickness of thin layers or wires. For chemists, this is particularly important in catalysis.

8.3.1 Thermal Properties

Electrons are the primary thermal energy carriers in bulk metals, and their distribution can be altered by nanostructuring, for example, in metallic-type carbon nanotubes, the free electron density is low because of spatial confinement, and phonons dominate their thermal transport behavior. Quantum confinement changes the distribution of carriers by altering the availability of energy states. As a consequence, the carriers tend to be found in narrower energy bands that can be used to enhance or diminish magnitude of thermal properties such as melting point, thermal conductivity, phase transitions, and heat capacity [8].

Melting Point

Melting point T_m of the nanoparticle decreases with the reduction in size d. Its physical origin is the increase in surface energy, the increase in amplitude of atomic vibrations, and the additional surface growth of thermal vibration energy. This effect may be estimated from the dimensionality of the related physical values using the simple Thompson's relation (8.6):

$$T_m(d) = T_m \exp\left[\frac{-P_L\ V_a}{Q}\right] = T_m\left[1 - \frac{2rV_a}{dQ}\right] \tag{8.6}$$

where Q is the fusion heat. For instance, for the bulk silver T_m = 1233 K, γ = 0.9 J/m^2, $V_a = 4\pi r^3{}_a/3 = 13.5 \times 10^{-30}$m^3, Q = 11.3 kJ/mol, then for nanoparticle of d = 10 nm in size from Equation 8.6 one can obtain T_m = 356.5 K, that is, the drop on 87%. In another example, the melting point of 2.5 nm gold particles was reported to be about 930 K, much lower than its bulk value of 1336 K; the melting point of 10 nm CdSe was 700 K compared to the bulk CdSe at 1680 K. The average latent heat of melting shows a size-scaling behavior similar to that of the melting point. It should be noted that also the critical point of pore-confined matter shifts to lower temperatures.

Thermal Conductivity

In the kinetic theory of gases, the thermal conductivity is given by (8.7):

$$k = 1/3Cvl \tag{8.7}$$

where v is the particle velocity, l is the free path length, $C = cn$ is the heat capacity of unit volume, c is the heat capacity of a single particle, and n is the number of particles.

One can apply this simple model for thermal phonons gas in metal if the free path length is the free phonon path, $l = l_{\text{phonon}}$. For bulk solid of big size $d > l_{\text{phonon}}$, the size effect do not arise. However, when the size d become smaller than free path length $d < l_{\text{phonon}}$, there is a cut of phonon spectra and a decrease in k. In particular, for a quarts particle of 10 nm in size at temperature T = 273 K, the size effect is not pronounced. However, at T = 363 K, the l_{phonon} is increased from 4 to 54 nm; therefore k is decreased 0.2 times in spite of the decrease in heat capacity from 2 to 0.55 J/cm^3 K. This phenomenon is used in industry of heat resistance materials, in particular, for the fabrication of the heat resistance coating of turbine blades. By doping and heat treating at high temperatures, the particular phase transition from monoclinic to triclinic structure is forced. The mixed two-phase structure with the triclinic nanoparticles of d = 20–30 nm in size is created and stabilized. In the result, because of $d < l_{\text{phonon}}$, the heat conductivity is increased by several times in couple with the increase in the strength, heat resistance, fracture ductility, and coating adhesion for refractory Ni-based alloy of turbine blade.

Thermodynamics Laws

Phase transitions are collective phenomena. With a lower number of atoms in a cluster a phase transition is less well defined, it is therefore no longer sharp. Small nanosized clusters behave more like molecules than as bulk matter. Rather than of phases, it may be more useful to think of different structural isomers that coexist over a range of temperatures. For example, part of a cluster may look frozen since its atoms do not exchange, while another part exhibits liquid-like dynamic behavior. At a given temperature, the solid-like regime may fluctuate in position and in size. When phases are no longer well defined, the Gibbs phase rule loses its meaning. In narrow pores, the conventional fluid-liquid critical point may shift to very low temperature, it may even vanish. However, new phases may appear that are characterized by discrete chemical potentials and separated by the so-called layering transitions.

A particular phenomenon that can occur with isolated clusters may accompanied by negative heat capacities. This means that the temperature of a cluster drops over a certain range when it is heated. It is understood in the following way: temperature relates to kinetic energy whereas heat capacity is related to total energy; thus temperature drops when a fraction of kinetic energy is converted to potential energy. For example, when more and more energy is deposited on an isolated S_8 ring, this corresponds to heating and is seen by higher amplitudes of vibrational and rotational motion. At some point, sufficient energy may be localized in a single bond so that this bond breaks, converting a hot S_8 ring into a colder linear S_8 chain. This also means that temperature fluctuates at constant energy and is no longer well defined for small isolated species. It may impose a principal limit to certain applications of nanotechnology.

8.3.2 Optical Properties

In general, optical properties of a material are closely related to its electrical and electronic properties. Optical properties refer to the interaction of electromagnetic radiation with matter. The starting point to understand optical properties of a material lie in that when light falls on an object it can be transmitted, absorbed or reflected $(\mathrm{I} = \mathrm{T} + \mathrm{A} + \mathrm{R})$. As the size of the matter is reduced, scattering (S) of light can also contribute to its color or transparency. Reflection (R) occurs when a light strikes a smooth surface and the incident wave is directed back into the original medium. The reflected wave has the same geometrical structure as the incident wave. Absorption (A) is a process that involves energy transformation. The energy levels of a substance determine the wavelengths of light that can be absorbed. It is a molecular phenomenon, dependent on the chemical identity and structure of the substance (not on the size of the molecules or clusters), and involves electronic transitions, vibrations and rotations. Chromophores and fluorophores are examples of organic materials that have specific transitions.

Table 8.1 Color Causing Phenomena in Nanostructured Objects

Nano-objects	Color Causing Phenomena

Butterfly wings (photonic crystal) Liquid crystals (e.g., soap)	Constructive interference of light wavelength with the nanomaterial
Colloids (e.g., milk)	Scattering of light of wavelength matching with particle size
Metal colloids (nanogold and nanosilver)	Surface plasmons. This is a peculiar effect found in metal nanoparticles. Responsible for vivid colors of metal colloids
Semiconductor quantum dots (QDs)	Quantum fluorescence arises due to quantum confinement in nanosized semiconductors, which leads to discrete energy levels from which energy can be emitted (fluorescence) after it has been absorbed by the semiconductor

Transmission (T) is the ability of light to pass through a material; it is complementary to absorption. Transmission of light is what is left after reflection, scattering absorption has occurred. Scattering (S) is the phenomenon that occurs when radiation hits a structure with dimensions comparable to the incident wavelength.

Nanomaterials in general have peculiar optical properties, such as colour, luminescence, non-linear optical properties as a result of the way light interacts with their fine nanostructure. The optical properties in nanomaterials are further governed by ‘plasmon’ (in case of metals) and quantum size confinement (in semiconductor QDs). Some inorganic NPs display interesting optical properties, and the absorption and/or emission wavelength can be controlled by particle size and surface functionalization [10] are discussed here.

Color of Metal Nanoparticles

The color of a material is a function of the interaction between the light and the object. If a material absorbs light of certain wavelength, an observer will not see these colors in the reflected light. For example, leaves appear green because chlorophyll, which is a pigment, absorbs the blue and red colors of the spectrum and reflect the green.

Colloidal suspensions of gold nanoparticles have a deep red color. Furthermore, color of gold colloids varies with the size: >20 nm (purple), 10–20 nm (red), 2–5 nm (yellow); similar is the case with silver nanoparticles: 40 nm (blue), 100 nm (yellow), whereas prism-shaped silver particles exhibit red color. Nanomaterials, in general, have peculiar optical properties as a result of the way light interacts with their fine nanostructure.

Surface Plasmon Resonance in Metal NPs

The surface plasmon resonance (SPR) is an optical phenomenon present in some metal particles and consists of the parallel propagation of surface electromagnetic waves along the metal–dielectric interfaces [11]. Plasmon resonance in metal NPs arises from the collective oscillations of the free conduction band electrons that are induced by the incident electromagnetic radiation (Figure 8.7a).

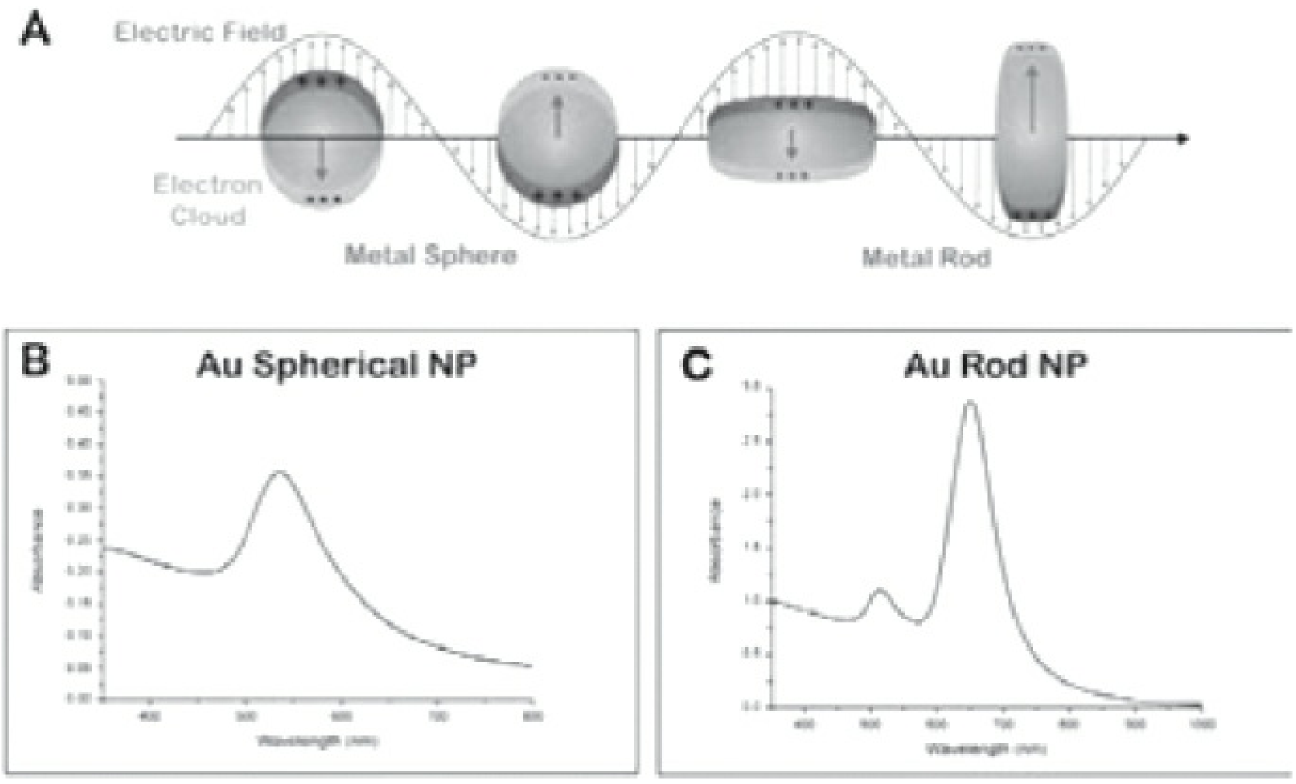

Figure 8.7 (a) Schematic illustration of the excitation of the dipole surface plasmon oscillation. (b) and (c) Characteristic UV–Vis spectra corresponding to the spherical and rod-shaped Au NPs, respectively.

Kelly et al.[11], © 2003. With permission of ACS.

The spherical Au NPs only display one plasmonic band (at 535 nm for this sample), while rod-shaped Au NPs show two plasmonic bands, transverse and longitudinal (at 514 and 650 nm) (Figure 8.7b and c). The surface, the surrounding environment, and the agglomeration state play an important role in the observation of the SPR. As an example, SPR is responsible for the intensive colors of spherical Au NP dispersions, which present strong absorption bands in the ultraviolet–visible (UV–Vis) spectrum (which are not present in the bulk). Instead, nonspherical Au structures generally present more than one plasmonic resonance due to different electron dipolar oscillations in different directions. Moreover, the agglomeration of particles produces a redshift of the resonance peak to a longer wavelength induced by the dipole coupling between the plasmons of neighboring particles, a fact that allow NPs to be used as a sensor.

Quantum Fluorescence

Luminescence in nanometals: Noble metals exhibit extremely weak photoluminescence in the bulk, assigned to recombination of the excited electrons with the holes within the d-band. Whereas at nanoscale the luminescence yield increases by as much as 6 orders of magnitude due to “lightning rod effect” i.e., the incoming (exciting) and outgoing (emitted) electric fields are amplified by the plasmon resonances around the particles (Figure 8.8a and b). Hence, the luminescence energy and efficiency are subjected to the size effect [12].

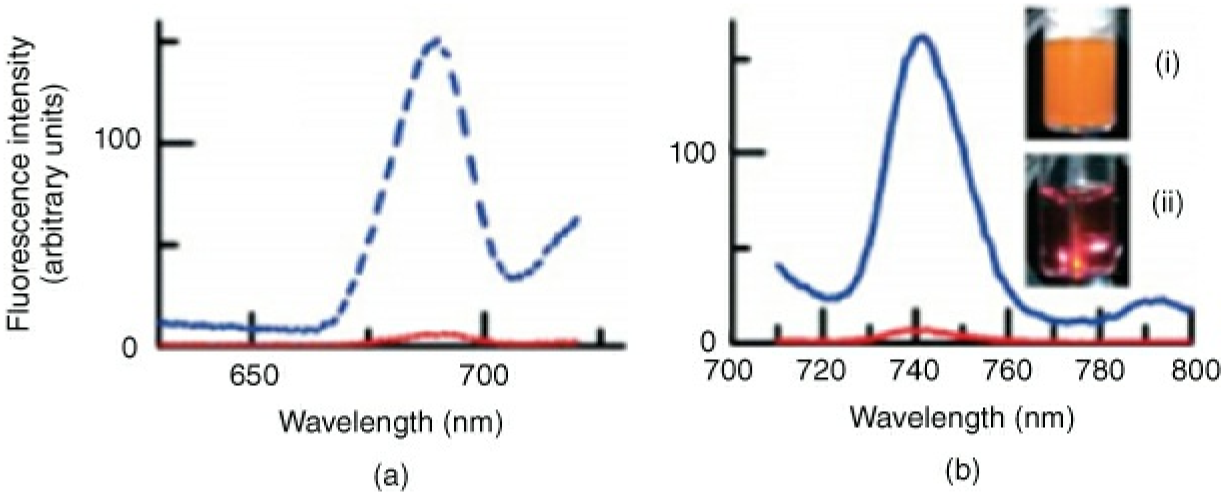

Figure 8.8 Absorption (a) and Fluorescence (b) spectra of longer gold nanorods (230 nm, upper trace) and shorter gold nanorods (30 nm, lower trace) in aqueous solution. Li et al.[12], © 2005. With permission of RSC.

Luminescence in semiconductor nanoparticles: Photoexcitation of a bulk semiconductor results in the transfer of an electron from valence band to conduction band creating an electron–hole pair, called "exciton," bound by a weak columbic interaction. The minimum energy required to generate such an exciton is called the band gap energy E_g. Excitons can be treated as hydrogen-like system and the spatial separation between the charge carrier pair is termed as exciton Bohr radius (α_B), which can be deduced from the Bohr approximation. When the physical dimensions of matter become comparable or lower to the exciton Bohr diameter ($2a_B$), the functional properties of a semiconductor becomes sensitive to the size and shape due to confinement of excitons.

The size dependence of the HOMO–LUMO band gap is best seen in the luminescence properties of semiconductor nanoparticles [13]. Fluorescence in colloidal solution CdSe–CdS core–shell nanoparticles with a diameter of 1.7 nm shows blue fluorescence and particles of size up to 6 nm shows red fluorescence (Figure 8.9), giving an evidence of the scaling of the semiconductor band gap with particle size. Smaller particles have a wider band gap. By adjusting the particle size, the fluorescence can be tuned between blue for particles of 1.7 nm diameter and red at 6 nm. A similar size effect but shifted to higher energy relative to fluorescence applies to the absorbed light. The difference in wavelengths between absorption and fluorescence occurs because after absorption the system relaxes to adapt to the new charge distribution, initiated by the creation of the electron–hole pair that is also called exciton.

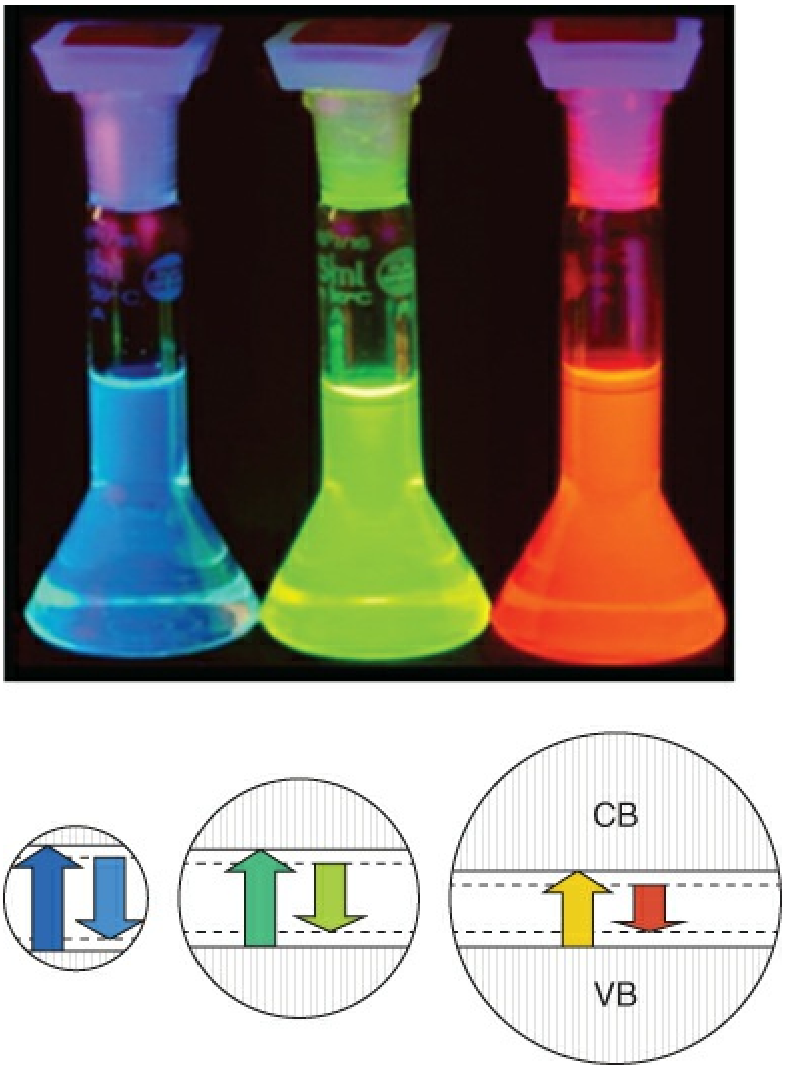

Figure 8.9 Fluorescence in CdSe–CdS core–shell nanoparticles with a diameter of 1.7 nm (blue); 3.7 nm (green) and ~6 nm (red) giving evidence of the scaling of the semiconductor band gap with particle size. Courtesy of H. Weller, University of Hamburg.

In semiconductors, optical excitation causes the promotion of a valence band electron into the conduction band, leaving behind a valence band hole. Once promotion has occurred, the CB electron quickly relaxes into the lowest energy CB state, while the hole moves to the top of the VB (VB electrons cascade down into lower energy valence states). The coupled electron–hole pair is often referred to as a single entity called exciton, since one cannot exist without the other.

Many theoretical models have been reported that correlate the size of quantum dots to their band gap energy, and these models were further compared with the experimentally observed data [13]. The size dependence on the band gap energy of QDs can be quantified as follows:

$$E_g(\mathrm{QD}) = E_g(\mathrm{bulk}) + (2\pi^2/2\mu R^2) - (1.786e^2/\varepsilon R) - 0.248E^*\mathrm{Ry}$$

where “R” is the radius of QD, μ is the reduced mass, “ .” is the permittivity of the vacuum, and E^{*}Ry is the effective Rydberg energy. The first term on the right-hand side represents the band gap of bulk materials, which is the characteristic of the material: for example, 2.53 eV for CdS, 1.74 eV for CdSe, and 1.50 eV for CdTe. The second additive term of the equation represents the additional energy due to quantum confinement having a $1/R^2$ dependence on band gap energy E_g(QD). The third subtractive term stands for the coulombic interaction energy of exciton having $1/R$ dependence, often neglected due to high dielectric constant of the material. The last subtractive term stands for spatial correlation effect (independent of radius) and significant only in case of semiconductor materials with low dielectric constant. The experimental observation of the size dependence in the band gap energy of semiconductor is in good agreement with the theoretical predictions [14]. Variation in the band gap energy of semiconductor with size is directly reflected on their optical responses. The confinement of electrons in semiconductor QDs influences their electronic structure in two ways. The energy gap of semiconductor QDs increases dramatically with a decrease in its radius ($E_g \propto 1/R^2$). Also the continuum observed in the conduction band and valence band in the case of bulk materials is replaced with discrete atomic energy levels as the particle size decreases.

For many applications, it is important to preserve band edge emission. To this aim, the surface of the NP can be passivated by chemically binding a capping agent. Another approach is overcoating a nanocrystal of a given semiconductor with a thin layer of a semiconductor with higher band gap (core–shell particles) as shown in Figure 8.10. All semiconductors undergo absorption processes, but because of selection rules (conservation of momentum) only direct band gap semiconductors (e.g., CdSe) exhibit intense band edge luminescence, with yields close to 100%. Indirect band gap semiconductors (e.g., Si) show luminescence with yields that are 3–4 orders of magnitude smaller than direct band gap materials.

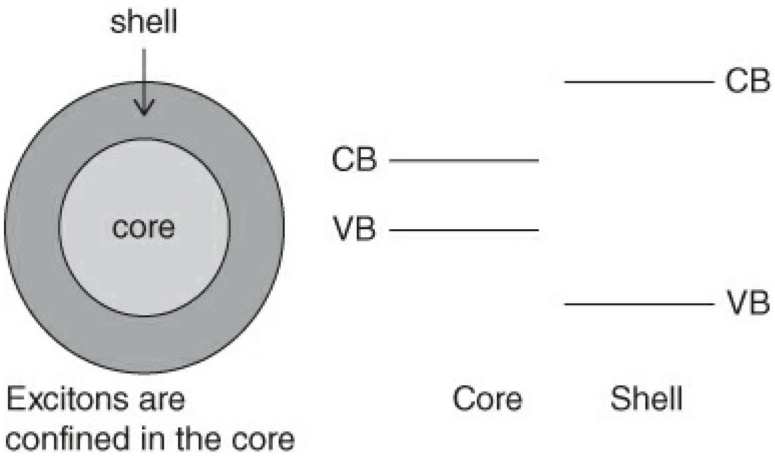

Figure 8.10 The energy levels of valence and conduction bands of core and shell in type I heterostructural QDs.

Courtesy of K. G. Thomas, IISER, India.

8.3.3 Electronic Properties

The changes that occur in electronic properties as the system length scale is reduced are related mainly to the increasing influence of the wave-like property of the electrons (quantum mechanical effects) and the scarcity of scattering centers [15]. The resultant changes in electronic properties at nanoscale are discussed briefly herein.

1. As the size of the system becomes comparable with the de Broglie wavelength of the electrons, the discrete nature of the energy states becomes apparent once again, although a fully discrete energy spectrum is only observed in systems that are confined in all three dimensions.
2. In certain cases, conducting materials become insulators below a critical length scale, as the energy bands cease to overlap. Owing to their intrinsic wave-like nature, electrons can tunnel quantum mechanically between two closely adjacent nanostructures, and if a voltage is applied between two nanostructures that aligns the discrete energy levels in the DOS, resonant tunneling occurs, which abruptly increases the tunneling current.
3. Conduction in highly confined structures, such as quantum dots, is very sensitive to the presence of other charge carriers and hence the charge state of the dot.
4. These Coulomb blockade effects result in conduction processes involving single electrons, and as a result they require only a small amount of energy to operate a switch, transistor, or memory element.
5. All these phenomena can be utilized to produce radically different types of components for electronic, optoelectronic, and information processing applications, such as resonant tunneling transistors and single-electron transistors.

8.3.4 Electrical Properties

There are three categories of materials based on their electrical properties, namely conductors, semiconductors, and insulators. The energy separation between the valence band and the conduction band is called E_g (band gap). The ability to fill the conduction band with electrons and the energy of the band gap determine whether a material is conductor, a semiconductor or an insulator. In conducting materials such as metals the valence band and the conducting band overlap, so that the value of E_g is small: thermal energy is enough to stimulate electrons to move to the conduction band. In semiconductors, the band gap is of few electron volts. If an applied voltage exceeds the band gap energy, electron jump from the valence band to the conduction band, thereby forming electron–hole pairs called excitons. Insulators have large band gaps that require an enormous amount of voltage to overcome the threshold. This is why these materials do not conduct electricity [16].

As the size of a particle is brought down in the nanometer regime, the quantum confinement effect causes the band gap to increase, thus a metal become semiconductors on decreasing its size. Electrical properties of some nanomaterials are related to their unique structures and exhibit electrical properties that are absolutely exceptional. For instance, carbon nanotubes can be conductors or semiconductors depending on their nanostructure.

For the smallest of metallic nanoclusters with dimensions ca. <2 nm, the absorption of surface plasmons disappears. Since so few atoms comprise discrete nanoclusters of this size, the spacing between adjacent energy levels (referred to as the Kubo gap, δ, Eq. 4) becomes comparable to the thermal energy, kT – especially at lower temperatures and smaller nanocluster diameters. This results in a shift in conductive properties of the nanoclusters from metallic to semiconducting and insulating, with decreasing size (Figure 8.11a–c). In band theory, the breadth of a band is directly related to the strength of interactions among nearest neighbors [17]. For atoms/molecules, this interaction is weak, which corresponds to a narrow band. However, as additional atoms are added to the solid, stronger interactions will ensue, resulting in a greater DOS near the Fermi level. Hence, the insulating properties of very small nanoclusters are due to the small number of neighboring atoms, which are held together primarily by nonmetallic interactions (e.g., van der Waal forces). As nanocluster size increases, the atomic s, p, and d orbitals from a large number of constituent atoms will broaden into bands, forming an energy continuum. As the nanocluster size decreases, the energy continuum of the bulk metal is transformed into discrete energy levels, especially at band edges as shown in Figure 8.12. The electrical properties such as electrical conductivity, dielectric constant, electrical strength, voltage endurance, internal charge characteristics etc. changes drastically when materials is in nano regime.

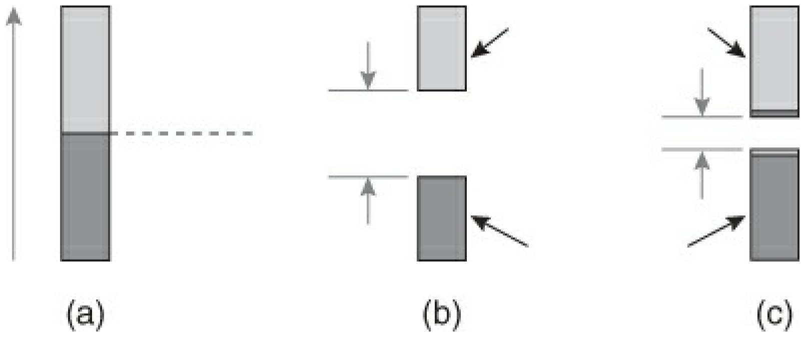

Figure 8.11 Comparative band gap in (a) metals; (b) insulator; (c) semiconductor.

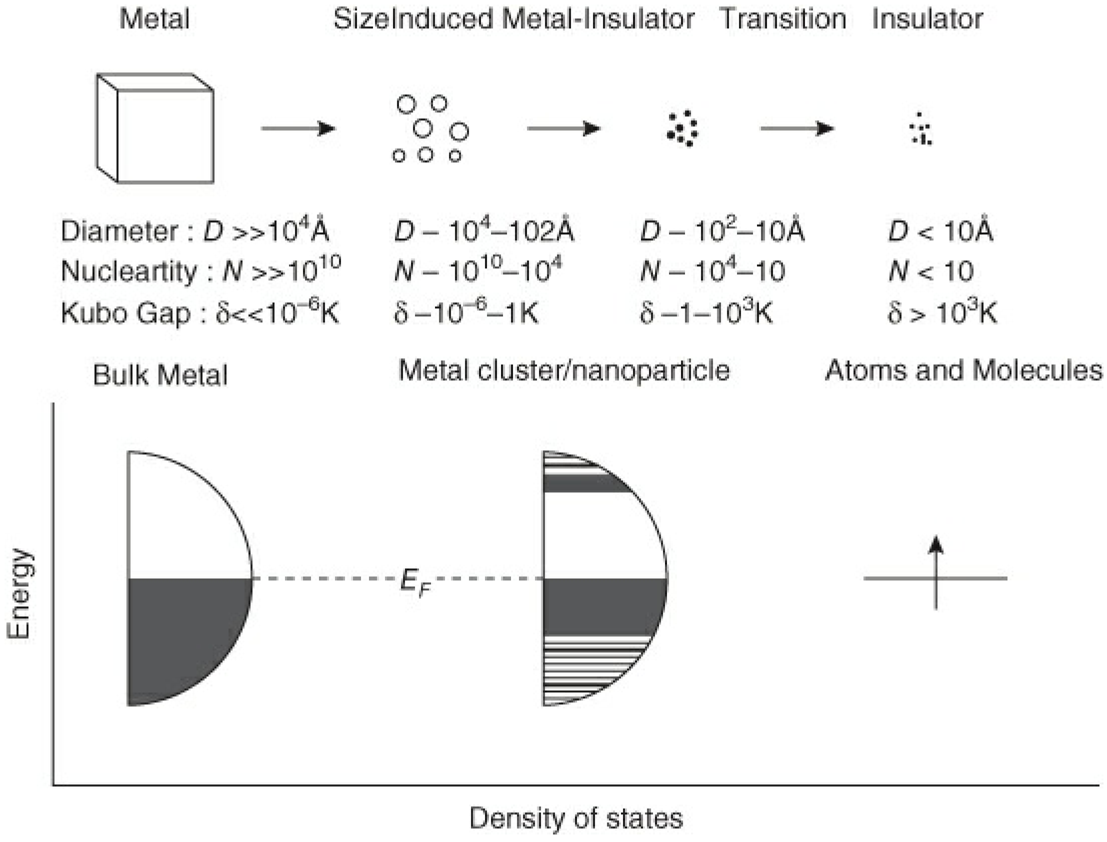

Figure 8.12 Schematic of the density of states exhibited by bulk metal relative to increasingly smaller nanoclusters. The approximate diameter, nuclearity, and Kubo gap for each size regime are indicated.

Rao et al. [17], © 2000. With permission of RSC.

a. *Electrical Conductivity* Some nanomaterials exhibit remarkable electron transport properties, which are strongly dependent on their nanocrystalline structure. In particular, 1D nanomaterials (carbon nanotubes, titania nanotubes, silica nanowires, polymeric nanowires, and nanofibers) are the most attractive materials due to their different electrical conductance, which can be monitored by the change in electrical conductance of the fabricated electrode [18]. Electron transport properties of such nanomaterials are very important for electrical and electronic applications, as well as for understanding the unique 1D carrier transport mechanism. It has been noticed that the wire length and diameter, wire surface condition, crystal structure and its quality, chemical composition, crystallographic orientation along the wire axis, and so on are all important parameters that influence the electron transport mechanism of nanowires. Because of the high surface-to-volume ratio and novel electron transport properties of these nanostructures, their electronic conductance is strongly influenced by minor surface perturbations (such as those associated with the binding of macromolecules). Such 1D material thus offers the prospect of rapid (real-time) and sensitive label-free bioelectronics detection, and massive redundancy in nanosensor arrays. In particular, carbon nanotubes are the most exciting 1D nanomaterial that has generated considerable interest due to their unique structure-dependent electronic and mechanical properties. The direct electron transfer ability of carbon nanotubes is another important factor that has been exploited in the fabrication of efficient electrochemical biosensing devices. Carbon nanotubes enhanced the performance of bioelectronic devices partly due to the high enzyme loading and partly because of the better electrical communication ability of the nanotubes.

b. *Dielectric Constant*

The dielectric constant, the response function of the measured external field (the displacement) to the local electric field, closely relates to the conductivity and optical properties of materials. The dielectric constants of metallic nanoparticles in the microwave frequency range have rarely been reported. Incident electromagnetic (EM) fields of different frequencies cause different responses from ions and electrons. As the size of the metal films or particles declines, the mean free path becomes constrained by surface scattering. The classical size effect, which affects the dielectric constant, occurs as the metal film thickness or the particle size becomes smaller than or similar to the mean free path *l* of the carriers inside the metal. The quantum size effect arises as the particle size decreases further below the Bohr radius where the continuous conduction band becomes discrete [19].

In the simple quantum sphere model (QSM) for small metallic particles embedded in inert gas or air, the quantum-confined electrons can be considered as nearly free electrons but with discrete energy levels. For metallic nanoparticles embedded in an active matrix, the diffusion model is adopted. The conductivity of metallic nanoparticles decreases as the particle size decreases and behaves as nonconducting below a critical size and temperatures. Since the real part of the dielectric constant *E* of metals is negative, the magnitude of the real *E* evidently decreases with the particle size and approaches positive in accord with the material that behaves as an insulator.

The magnitude of the real part of *E* for metallic nanoparticles decreases with a decreasing particle size, suggesting that the particles become less conducting as the particle size decreases. In addition, the microwave absorption depends on the shape and size distribution.

c. ***Electric Strength*** Perhaps the most important property of nanocomposites is the change in electric strength, which is found when the filler particles attain nanometric dimensions. This contrasts with the situation for conventional microparticles where substantial reductions in electric strength are typical as a result of the weak interfaces and defects that are involved. There is a dramatic improvement in electric strength of polyolefin nanocomposites. Enhancement in electric strength can be achieved by the use of appropriate functionalization of the polymer. For example, vinyl silane is one of the effective agent that is known to couple well both to the SiO_2 surface and to the cross-linked polyethylene (XLPE) chain.

d. ***Voltage Endurance*** Analogous to electric strength, voltage endurance under nonuniform field conditions improved dramatically as depicted in Figure 8.13. These endurance curves are plotted in terms of the maximum field at the tip of the point/plane gap and show over 2 orders of magnitude improvement in the voltage endurance in both the epoxy (Figure 8.13a) and XLPE (Figure 8.13b) systems. It is evident that substantial benefit in voltage endurance is obtained from the nanoparticles and additional gains made through changing the interface conditions by the functionalization of polymeric moiety.

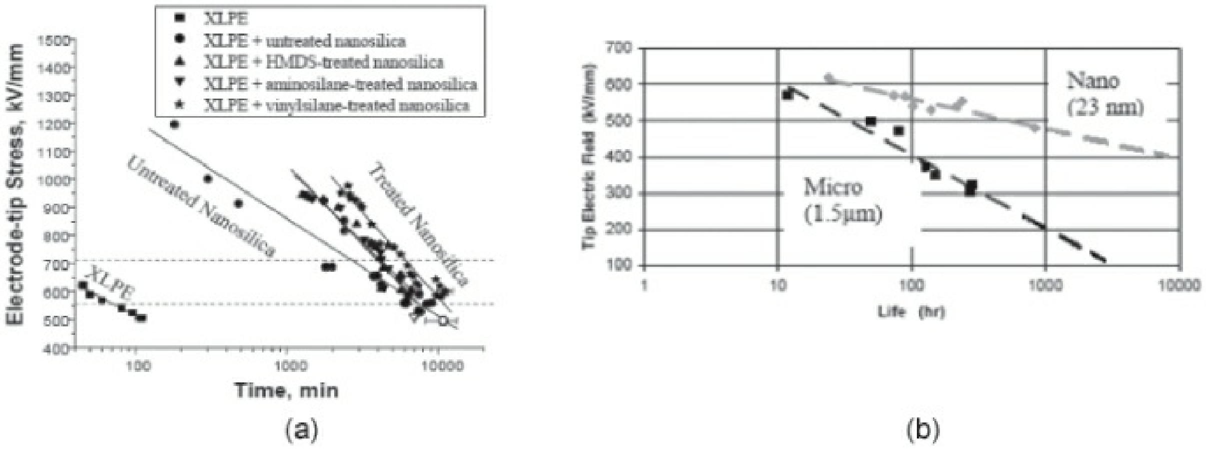

Figure 8.13 Voltage endurance characteristics for nanocomposites using 4 µ tip/plane electrodes. (a) Epoxy-TiO_2, (b) XLPE-SiO_2.

Nelson [20], © 2006. With permission of IEEE.

e. ***Internal Charge Characteristics*** A common feature of many nanodielectric systems is the behavior of the internal space charge build-up. The recent development of systems to measure the internal charge in dielectrics has allowed both the magnitude and dynamics of the internal charge to be assessed, and it appears that there are substantial differences when nanoparticles are incorporated into a polymer matrix. For many nanodielectric systems, three features are usually predominant:

i. The magnitude of the internal charge is much less for nanocomposites

ii. The dynamics of charge decay are much faster for nanocomposites

iii. There is often a very different distribution of charge (and therefore of internal field) with nanocomposites.

8.3.5 Magnetic Properties

In general, the magnetic behavior of a material depends on the structure of the material and on its temperature. In order to feel a magnetic field, a material needs to have nonzero net spin (transition metals). The typical size of classically expected domain is around 1 µm. When the size of a magnetic material is reduced, the number of surface atoms becomes an important fraction of the total number of atoms, surface effects become important, and quantum effects starts to prevail. When the size of these domains reaches the nanoscale, these materials show new properties. The large surface-to-volume ratio results in a substantial proportion of atoms having different magnetic coupling with neighboring atoms leading to differing magnetic properties [21].

1. Bulk gold and platinum are nonmagnetic, but at the nanosize they act as magnetic particles. Au nanoparticles become ferromagnetic when they are capped with the appropriate molecules such as thiol.

2. Giant magnetoresistance (GMR) is a phenomenon observed in nanoscale multilayers consisting of strong ferromagnet (Fe, Co, Ni) and a weaker magnetic or nonmagnetic buffer (Cr, Cu). It is usually employed in data storage and sensing.

3. Magnetic nanoparticles are used in a range of applications such as imaging, bioprocessing, refrigeration, as well as high density magnetic storage media.

Two key issues dominate the magnetic properties of nanoparticles: finite-size effects and surface effects, which give rise to various special features. Finite-size effects result, for example, from the quantum confinement of the electrons, whereas typical surface effects are related to the symmetry breaking of the crystal structure at the boundary of each particle. Because there is no general agreement on the size limits for nanoparticles, in the following we use this term for particles with diameters ranging from 1 to 100 nm.

8.3.5.1 Finite-Size Effects

The two most studied finite-size effects in nanoparticles are the single-domain limit and the superparamagnetic limit. In bulk magnetic particles, it is well known that there is a multidomain structure, where regions of uniform magnetization are separated by domain walls. The formation of the domain walls is a process driven by the balance between the magnetostatic energy (ΔE_{MS}), which increases proportionally to the volume of the materials, and the domain-wall energy (E_{dw}), which increases proportionally to the interfacial area between domains. If the sample size is reduced, there is a critical volume below which it costs more energy to create a domain wall than to support the external magnetostatic energy (stray field) of the single-domain state. This critical diameter typically lies in the range of a few tens of nanometers and depends on the material. It is influenced by the contribution from various anisotropy energy terms.

The critical diameter of a spherical particle (D_c), below which it exists in a single-domain state, is reached when $\Delta E_{MS} = E_{dw}$ (Eq. 8.8)

$$D_c \approx 18\frac{\sqrt{AK_{\text{eff}}}}{\mu_o M^2} \quad (8.8)$$

where A is the exchange constant, K_{eff} is anisotropy constant, μ_o is the vacuum permeability, and M is the saturation magnetization.

Figure 8.14a–f is a simplistic view of some phenomena present in small magnetic particles. In reality, a competition between the various effects will establish the overall magnetic behavior. Here, K_{eff} is the anisotropy constant, μ_o is the vacuum permeability, and M is the saturation magnetization. A single-domain particle is uniformly magnetized with all the spins aligned in the same direction. The magnetization will be reversed by spin rotation since there are no domain walls to move. This is the reason for the very **high coercivity** (H_c) observed in small nanoparticles. Another source for the high coercivity in a system of small particles is the shape anisotropy. The departure from sphericity for single-domain particles is significant and has an influence on the coercivity. For example, the H_c of Fe nanoparticles increases from ~800 Oe for an aspect ratio of 1 to >10,000 Oe for an aspect ratio of 10 [21].

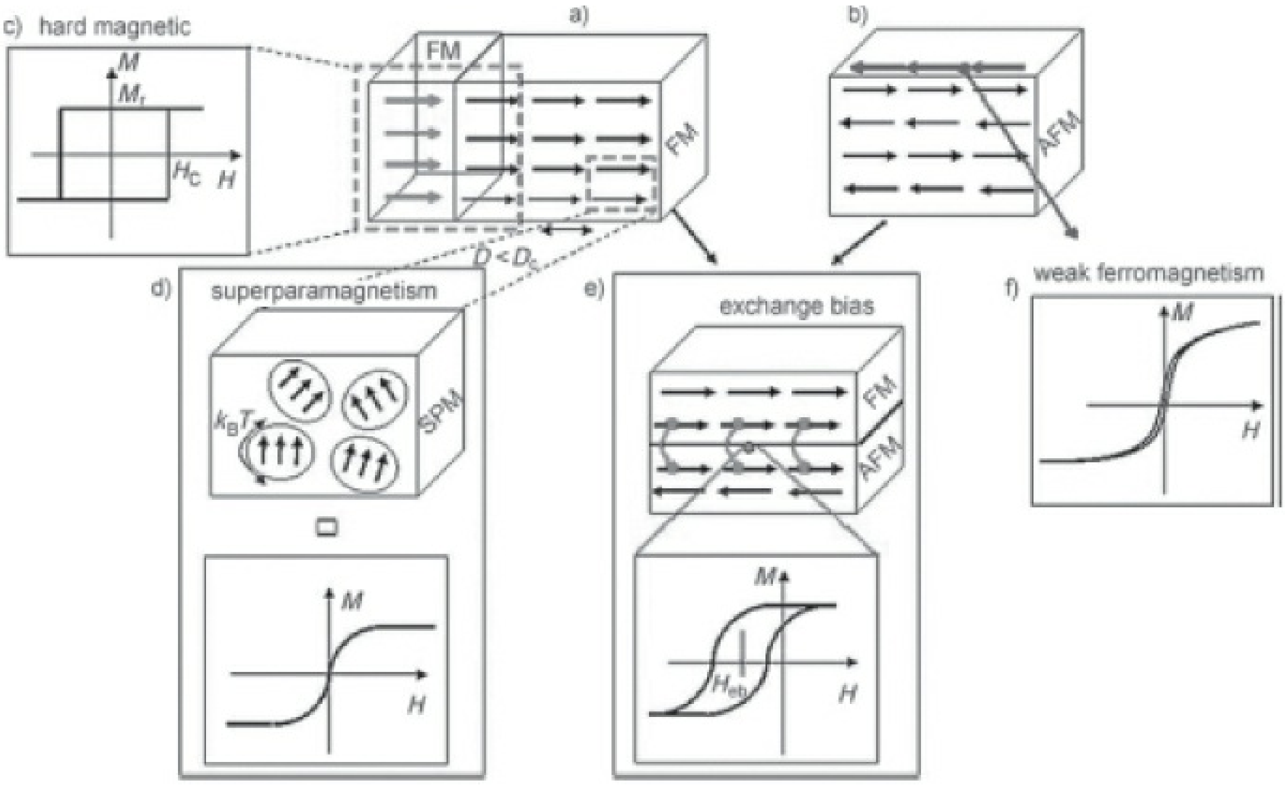

Figure 8.14 The different magnetic effects in magnetic nanoparticles shown through spin arrangement in (a) ferromagnet; (b) antiferromagnet D = diameter, D_c = critical diameter; (c) combination of two different ferromagnetic phases; (d) magnetic moments in a superparamagnet; (e) exchange coupling; and (f) pure antiferromagnetic.

Lu et al. [21], © 2007. With permission of Wiley VCH GmbH.

It must be noted that the estimation of the critical diameter holds only for spherical and noninteracting particles. Particles with large shape anisotropy lead to larger critical diameters.

The second important phenomenon that takes place in nanoscale magnetic particles is the **superparamagnetic** limit. A supermagnet is defined as an assembly of giant magnetic moments, which are not interacting and which can fluctuate when the thermal energy, k_BT, is larger than the anisotropy energy. The superparamagnetism can be understood by considering the behavior of a well-isolated single-domain particle. The magnetic anisotropy energy per particle that is responsible for holding the magnetic moments along a certain direction can be expressed as follows: $E(\theta) = K_{\text{eff}} V \sin^2\theta$, where V is the particle volume, K_{eff} is the anisotropy constant, and θ is the angle between the magnetization and the easy axis.

The energy barrier $K_{\text{eff}}V$ separates the two energetically equivalent easy directions of magnetization. With decreasing particle size, the thermal energy kT exceeds the energy barrier $K_{\text{eff}}V$ and the magnetization is easily flipped. For $k_BT > K_{\text{eff}}V$, the system behaves as a paramagnet, instead of atomic magnetic moments, there is now a giant (super)moment inside each particle (Figure 8.14d). This system is named a superparamagnet. Such a system has no hysteresis, and the data of different temperatures superimpose onto a universal curve of M versus H/T. The relaxation time of the moment of a particle t is given by the Neel–Brown expression (Eq. 8.9), where k_B is the Boltzmann's constant and $t_0 \approx 10^{-9}\,\text{s}$.

$$t = t_o \exp\left(\frac{KV}{kT}\right) \quad (8.9)$$

If the particle magnetic moment reverses at times shorter than the experimental timescales, the system is in a superparamagnetic state, if not, it is in the so-called blocked state.

The temperature, which separates these two regimes, the so-called blocking temperature, T_B, can be calculated by considering the time window of the measurement. For example, the experimental measuring time with a magnetometer (roughly 100 s) gives $T_B = \frac{KV}{k}$.

The blocking temperature depends on the effective anisotropy constant, the size of the particles, the applied magnetic field, and the experimental measuring time.

For example, if the blocking temperature is determined using a technique with a shorter time window, such as ferromagnetic resonance that has $t_0 \approx 10^{-9}\,\text{s}$, a larger value of T_B is obtained than the value obtained from dc magnetization measurements. Moreover, a factor of two in particle diameter can change the reversal time from 100 years to 100 ns. While in the first case the magnetism of the particles is stable, in the latter case the assembly of the particles has no remanence and is superparamagnetic.

The most common techniques used to measure the magnetic properties of an assembly of nanoparticles include SQID magnetometry and vibrating sample magnetometry to measure the net magnetization of the samples. Ferromagnetic resonance (FMR) probes magnetic properties in ground state and provides information about magnetic anisotropy, magnetic moment, relaxation mechanism of magnetization, and g-factor. X-ray absorption magnetic circular dichroism (XMCD) is the method of choice to determine the optical and spin magnetic moments.

8.3.5.2 Surface Effects

As the particles size decreases, a large percentage of all the atoms in a nanoparticle are surface atoms, which implies that surface and interface effects become more important. For example, for face-centered cubic (fcc) cobalt with a diameter of around 1.6 nm, about 60% of the total number of spins are surface spins. Owing to this large surface atoms/bulk atoms ratio, the surface spins make an important contribution to the magnetization. This local breaking of the symmetry might lead to changes in the band structure, lattice constant, or/and atom coordination. Under these conditions, some surface and/or interface-related effects occur, such as surface anisotropy and, under certain conditions, core–surface exchange anisotropy can occur.

Nonmagnetically Inert Surface Coatings

Surface effects can lead to a decrease in the magnetization of small particles, for instance, oxide nanoparticles, with respect to the bulk value. This reduction has been associated with different mechanisms, such as the existence of a magnetically dead layer on the particle's surface, the existence of canted spins, or the existence of a spin-glass-like behavior of the surface spins. On the other hand, for small metallic nanoparticles, for example cobalt, an enhancement of the magnetic moment with decreasing size was reported as well. This result is associated with a high surface-to-volume ratio, however, without more detailed explanation.

Another surface-driven effect is the enhancement of the magnetic anisotropy, K_{eff}, with the decreasing particle size. This anisotropy value can exceed the value obtained from the crystalline and shape anisotropy and is assumed to originate from the surface anisotropy. In a very simple approximation, the anisotropy energy of a spherical particle with diameter *D*, surface area *S*, and volume *V* may be described by one contribution from the bulk and another from the surface: $K_{\text{eff}} = K_V + \frac{6}{D} K_S$, where K_V and K_S are the bulk and surface anisotropy energy constants, respectively. K_{eff} changes when the surfaces are modified or adsorb different molecules, which explains very well the contribution of the surface anisotropy to K_{eff}. For uncoated antiferromagnetic nanoparticles, weak ferromagnetism can occur at low temperatures (Figure 8.14f), which has been attributed to the existence of uncompensated surface spins of the antiferromagnet. Since this situation effectively corresponds to the presence of a ferromagnet in close proximity to an antiferromagnet, additional effects, such as exchange bias, can result.

However, only in some cases can a clear correlation between the surface coating and the magnetic properties be established. For example, a silica coating is used to tune the magnetic properties of nanoparticles, since the extent of dipolar coupling is related to the distance between particles and this in turn depends on the thickness of the inert silica shell. A thin silica layer will separate the particles, thereby preventing a cooperative switching that is desirable in magnetic storage data. In other cases, the effect of the coating is less clear. A precious metal layer around the magnetic nanoparticles will have an influence on the magnetic properties. For example, it was shown that gold-coated cobalt nanoparticles have a lower magnetic anisotropy than uncoated particles, whereas gold coating of iron particles enhances the anisotropy, an effect that was attributed to alloy formation with the gold. Organic ligands, used to stabilize the magnetic nanoparticles, also have an influence on their magnetic properties, that is, ligands can modify the anisotropy and magnetic moment of the metal atoms located at the surface of the particles. For instance, cobalt colloidal particles stabilized with organic ligands show a reduction of the magnetic moment and a large anisotropy. Surface-bonded ligands lead to the quenching of the surface magnetic moments, resulting in the reduction of magnetization. In the case of nickel nanoparticles, donor ligands, such as amines, do not alter the surface magnetism but promote the formation of rods, whereas the use of trioctylphosphine oxide leads to a reduction in the magnetization of the particles. Overall, it must be concluded that the magnetic response of a system to an inert coating is rather complex and system specific.

Magnetic Coatings

A magnetic coating on a magnetic nanoparticle usually has a dramatic influence on the magnetic properties. The combination of two different magnetic phases will lead to new magnetic nanocomposites, with many possible applications. The most striking feature that takes place when two magnetic phases are in close contact is the exchange bias effect. The exchange coupling across the interface between a ferromagnetic core and an antiferromagnetic shell or vice versa causes this effect. Exchange bias is the shift of the hysteresis loop along the field axis in systems with ferromagnetic (FM)–antiferromagnetic (AFM) interfaces. This shift is induced by a unidirectional exchange anisotropy created when the system is cooled below the Neel temperature of the antiferromagnet. This exchange coupling can provide an extra source of anisotropy leading to magnetization stabilization. The exchange bias effect was measured for the first time in cobalt nanoparticles surrounded by an antiferromagnetic CoO layer. There are numerous systems where the exchange bias has been observed, and some of the most investigated systems are ferromagnetic nanoparticles coated with their antiferromagnetic oxides (e.g., Co/CoO, Ni/NiO), nitrides ($Fe–Fe_2N$), and sulfides (Fe–FeS), ferromagnetic–antiferromagnetic (Fe_3O_4–CoO), or ferrimagnetic–ferromagnetic ($TbCo–Fe_{20}Ni_{80}$) nanoparticles.

Recently, single-domain pure antiferromagnetic nanoparticles have shown an exchange bias effect arising from uncompensated spins on the surface. This reveals a complicated surface spin structure that is responsible for the occurrence of a weak ferromagnetism (Figure 8.14f), the exchange bias effect, and the so-called training effect. The training effect represents a reduction of the exchange bias field upon subsequent field cycling.

Metallic particles embedded in a matrix are interesting systems of magnetic-coated particles. The role of the matrix has been demonstrated in establishing the magnetic response of small particles. The magnetic behavior of the isolated 4-nm Co particles with a CoO shell changes dramatically when, instead of being embedded in a paramagnetic matrix, they are embedded in an antiferromagnetic matrix. The blocking temperature of Co particles embedded in an Al_2O_3 or C matrix was around 10 K, but by putting them in a CoO matrix, they remain ferromagnetic up to 290 K. Thus, the coupling of the ferromagnetic particles with an antiferromagnetic matrix is a source of a large additional anisotropy.

Exchange biased nanostructures have found applications in many fields, such as permanent magnets recording media, and spintronics. A new approach to produce high-performance permanent magnets is the combination of a soft magnetic phase (easily magnetized), such as FePt, and a hard magnetic phase (difficult to magnetize and thus having high coercivity), such as Fe_3O_4 that interact through exchange bias effect, and the so-called training effect. The right choice of ferromagnetic and antiferromagnetic components can provide a structure suitable for use as a recording medium. The exchange coupling can supply the extra anisotropy that is needed for magnetization stabilization, thus generating magnetically stable particles. Another interesting aspect related to a magnetic coating is given by the bimagnetic core–shell structure, where both the core and the shell are strongly magnetic (e.g., $FePt/CoFe_2O_4$). These bimagnetic core–shell nanoparticles allow a precise tailoring of the magnetic properties through tuning the dimensions of the core and shell, which selectively controls the anisotropy and the magnetization.

The magnetic behavior of an assembly of nanoparticles is a result of both the intrinsic properties of the particles and the interactions among them. The distributions of the sizes, shapes, surface defects, and phase purity are only a few of the parameters influencing the magnetic properties, which makes the investigation of the magnetism in small particles very complicated. One of the great challenges remains the manufacturing of an assembly of monodisperse particles, with a well-defined shape, a controlled composition, an ideal chemical stability, tunable interparticle separations, and a functionalizable surface. Such particles will tremendously facilitate the discrimination between finite-size effects, interparticle interactions, and surface effects. Thus, the synthesis of magnetic nanoparticles with well-controlled characteristics is a very important task.

Magnetism in Non-magnetic Nanoparticles

Enhanced magnetism in clusters of elements that are ferromagnetic as bulk solids such as iron, cobalt, or nickel is well known and has been demonstrated in Stern–Gerlach deflection experiments. Theoretical studies predicted high spin ground states for clusters of up to 13 atoms even in nonmagnetic elements such as Pd and Pt. Nanoparticles comprising several hundred atoms of Au, Pd, and Pt embedded in a polymer reveals magnetic moments corresponding to several unpaired electron spins per entire particle.

Bulk Pt metal has an incompletely filled d-band corresponding to a $5d^9\ 6\ s^1$ electronic configuration and a Fermi level of 6.10 eV. In the Pt_{13} cluster, the Fermi level rises considerably because of the shorter interatomic distances and concomitant higher orbital overlap. Density functional calculations of the discrete energy level diagram predict near-degenerate frontier orbitals with 8 unpaired electrons. Such studies provide insight into the electronic and magnetic structure of clusters and are fundamental for an understanding of how magnetism develops in nonmagnetic elements. Clusters may have to be regarded as pseudo-atoms, with the important difference that the cluster orbital momentum should be expected to be much larger than for atoms, because it scales with the square of the radius. It is quite likely that the orbital momentum has important implications for the magnetic character of the clusters.

8.3.6 Mechanical Properties

Planar defects, such as dislocations, in the crystalline structure of a solid are extremely important in determining the mechanical properties of a material. It is expected that dislocations would have a less dominant role to play in the description of the properties of nanocrystals than in the description of the properties of microcrystals (MC), owing to the dominance of crystal surfaces and interfaces. The free energy of a dislocation is made up of a number of terms: (1) the core energy (within a radius of about three lattice planes from the dislocation core); (2) the elastic strain energy outside the core and extending to the boundaries of the crystal, and (3) the free energy arising from the entropy contributions. In MC, the first and second terms increase the free energy and are by far the most dominant terms. Hence, dislocations, unlike vacancies, do not exist in thermal equilibrium.

In nanocrystals, the elastic strain energy is reduced. The forces on dislocations due to externally applied stresses are reduced by a factor of about 3 and the interactive forces between dislocations are reduced by a factor of about 10. Hence, recovery rates and the annealing out of dislocations to free surfaces are expected to be reduced as well. Dislocations are positioned closer together and their movement in the net is hindered by interaction between them. Together with the reduced elastic strain energy, this fact results in dislocations that are relatively immobile and the imposed stress necessary to deform a material that increases with the decrease in grain size. Moreover, nanostructures allow alloying of components that are commonly immiscible in the solid and/or molten state.

Mechanical properties of nanoparticles consisting of metallic and ceramic materials is greatly influenced by porosity, grain size, and so on and show exciting mechanical properties such as superplasticity; enhancement of hardness, strength, fracture ductility; and raising of wear resistance [22].

Filling polymers with nanoparticles or nanorods and nanotubes, respectively, leads to significant improvements in their mechanical properties. Such improvements depend heavily on the type of the filler and the way in which the filling is conducted. The latter point is of special importance, as any specific advantages of a nanoparticulate filler may be lost if the filler forms aggregates, thereby mimicking the large particles. Particulate-filled polymer-based nanocomposites exhibit a broad range of failure strengths and strains. This depends on the shape of the filler, particles, or platelets, and on the degree of agglomeration. In this class of material, polymers filled with silicate platelets exhibit the best mechanical properties and are of the greatest economic relevance. The larger the particles of the filler or agglomerates, the poorer are the properties obtained. Although, potentially, the best composites are those filled with nanofibers or nanotubes; however, sometimes such composites have the least ductility. On the other hand, by using carbon nanotubes, it is possible to produce composite fibers with extremely high strength and strain at rupture. Among the most exciting nanocomposites are the polymer–ceramic nanocomposites, where the ceramic phase is platelet-shaped. This type of composite is preferred in nature and is found in the structure of bones, where it consists of crystallized mineral platelets of a few nanometers thickness that are bound together with collagen as the matrix. Composites consisting of a polymer matrix and defoliated phyllosilicates exhibit excellent mechanical and thermal properties.

8.4 Chemical Properties at Nanoscale

Chemical properties of nanomaterials also change at nanoscale. As the percentage of surface atoms in nanoparticles is large compared with bulk objects, the reactivities of nanomaterials are more than bulk materials [23]. The following are some of the reasons responsible for the change in chemical properties at nanoscale:

1. The preponderance of surface is a major reason for the change in behavior of materials at the nanoscale. As up to half of all the atoms in nanoparticles are surface atoms, properties such as electrical transport are no longer determined by solid-state bulk phenomenon.
2. The atoms in nanomaterials have a higher average energy than atoms in their bulk counterparts because of the larger proportion of surface atoms. For example, catalytic materials have a greater chemical activity per atom of exposed surface as the catalyst is reduced in size at the nanoscale.
3. Defects and impurities may be attracted to surfaces and interfaces, and interactions between particles at those small dimensions can depend on the structure and nature of chemical bonding at the surface.
4. Molecular monolayer may be used to change or control surface properties and to mediate the interaction between nanoparticles.

8.4.1 Bonding

It is well established now that a nanomaterial is formed of at least a cluster of atoms, more often a cluster of molecules. It follows that all types of binding that are important in chemistry are also important in nanoscience. They are generally classified as follows:

- Intramolecular bonding (chemical interactions): These are bondings that involve changes in the chemical structure of the molecules. They include covalent bonds and metallic bonds.
- Intermolecular bonding (physical interaction): These are bonding that do not involve changes in the chemical structure of the molecules. They include ion–ion and ion–dipole interactions; van der Waals interactions; hydrogen bonds; hydrophobic interactions; and repulsive forces (such as steric repulsions).

Nanomaterials often arise from a number of molecules held together or large molecules that assume specific 3D structures through intermolecular bonding [24]. Therefore, nanoscience also deals with supramolecular chemistry (i.e., the chemistry that deals with interactions among molecules), which is just a subarea of chemistry. The properties of these supramolecular structures are determined and governed by the nature of the existing intermolecular bonding.

- Intermolecular bondings such as hydrogen bonding and van der Waals bonding are weak interactions, but in a large number they can be quite strong. For example, in DNA (which has a cross section of 2 nm), the two helixes are held together by numerous hydrogen bonds thereby giving it enough strength.
- Intermolecular bondings often hold together macromolecules (such as proteins) in specific 3D structures with which precise biological functions are associated. Any disruption of these interactions in a protein irreversibly affects its 3D structure and leads to a total loss of function together with many diseases.
- One type of intermolecular bonding that is particularly significant in nanoscience is the hydrophobic effect. This is a process that is basically driven by entropy and has a major role in biological materials. In simple words, it is the property by which nonpolar molecules (e.g., oil) tend to form aggregates of like molecules in water.

8.4.2 Surface Properties

Regardless of a material whether it a bulk or nanoscale, its physical and chemical properties depend on a lot of its surface properties. Surfaces perform numerous functions; keep things in or out; allow the flow of material or energy across an interface; initiate or terminate a chemical reaction as in the case of a catalyst. If a bulk material is subdivided into an ensemble of individual nanomaterials, the total volume remains the same, but the collective surface area is greatly increased. Table 8.2 gives an idea as to what extent the total surface increases when a cube of 1 m^3 cut progressively into smaller and smaller cubes until it is formed of 1 nm^3 cubes.

Table 8.2 Change in Surface Area on Size Reduction

Size of the Cube Side	Number of Cubes	Collective Surface Area
1 m	01	6 m^2
0.1 m	10^3	60 m^2
0.01 m (1 cm)	10^6	600 m^2
0.001 m (1 mm)	10^9	6000 m^2
10^{-9} m (1 nm)	10^{27}	$6 \times 10^9 m^2$ = 6000 km^2

Nanomaterials have a significant proportion of atoms existing at the surface. This has a profound effect on reactions that occur at the surface such as catalysis reactions, detection reactions, and reactions that, to be initiated, require the physical adsorption of certain species at the material's surface.

8.4.3 Catalysis

A catalyst is a substance that increases a chemical reaction rate without being consumed or chemically altered. Enzymes, the nature's catalysts, are able to assemble specific end-products, always finding pathways by which reactions takes place with minimum energy consumption [25]. Artificial catalysts are not so energy efficient. They are mostly made of metal particles fixed on a oxide surface, working on hot reactant stream (to reduce a phenomenon called “catalyst poisoning,” which occurs when species dispersed in the atmosphere, such as CO, occupy the active sites of the catalysts). Active surface is one of the most important properties of a catalyst where the reaction takes place. The active surface increases when the size of the catalyst is decreased; the smaller the catalyst particles, the greater the surface-to-volume ratio. The higher is the catalyst's active surface, the greater is the surface reactivity. It has been shown that the spatial organization of the active sites in a catalyst is also important. Both properties, that is, nanoparticle size and molecular structure/distribution, can be controlled using nanotechnology. Hence, this technology has a great potential to expand catalyst design with benefits for the chemical, petroleum, automotive, pharmaceutical, and food industries. The use of nanoparticles that have catalytic properties will allow a drastic reduction of the amount of material used, with resulting economic and environmental benefits.

A good example of how nanoscience can impact the development of catalytic materials is that of gold. Bulk gold is a noble metal; it is stable, nontoxic resistant to oxidation and chemical attack. On the other hand, nanoscale gold particles can catalyze chemical reactions. It has been found that finely dispersed gold nanoparticle on oxide supports are catalytically very active. In many cases, the catalytic activity and selectivity of dispersed gold nanoparticles exceed those of the commonly used transition metal catalysts such as Pt, Rh, and Pd. This is an exciting result because metals such as Pt and Pd (commonly used in catalysis such as automobile catalytic converters) are toxic and are also very rare and expensive.

8.4.4 Detection

The detection of a specific chemical or biological compound within a mixture represents its basis for the operation of numerous devices, such as chemical sensors, biosensors, and microarrays. As with catalysis, a detection reaction occurs at the material interface. The rate, specificity, and accuracy of this reaction can be improved using nanomaterials rather than bulk materials in the detection area. The higher surface-to-volume ratio of nanomaterials increases the surface area available for detection with a positive effect on the rate and on the limit of detection of the reaction. In addition, nanomaterials can be designed to have specific surface properties (chemical or biochemical) tailored at a molecular level. This way, the active sites on the material surface can act as “locks” to detect specific molecules (the “keys”). Scaling down using nanomaterials allows packing more detection sites into the same device, thus allowing the detection of multiple analytes. This scaling down capability, together with the high specificity of the detection sites obtainable using nanomaterials, will allow the fabrication of super-small “multiplex detection devices,” that is, devices that can test and detect more than one analyte at a time.

8.5 The Concept of Pseudo-Atoms

Because of the quantized states of electrons and holes, these nanocrystallites are often called quantum dots, pseudo-atoms, or superatoms. The core–shell structure serves to control the potential that confines the electrons and determines the lifetime of excited states. Applications range from light-emitting diodes (LEDs) and novel solid-state lasers to potential future devices for quantum electronics and quantum information processing (quantum computing) [26].

Experimental and theoretical support for the pseudo-atom character of small metal clusters comes from properties such as ionization potentials and electron affinities, which reveal shell structures akin to those of conventional elements.

An example of a superatom is $AlPb_{12}^+$ where 12 lead atoms are placed in a perfectly icosahedral shell around a core Al atom [27]. The 50 valence electrons occupy molecular orbitals that are delocalized over the cluster and remind very much of conventional hydrogen-like atomic orbitals (Figure 8.15). It may be noted that there is a HOMO–LUMO gap of ca. 3 eV, indicating the large band gap semiconductor nature of this species. The orbitals of this superatom resemble the s-, p-, d-, and higher hydrogen-like orbitals and show basically the energetic sequence that is also obtained from the 3D "particle-in-a-box" model.

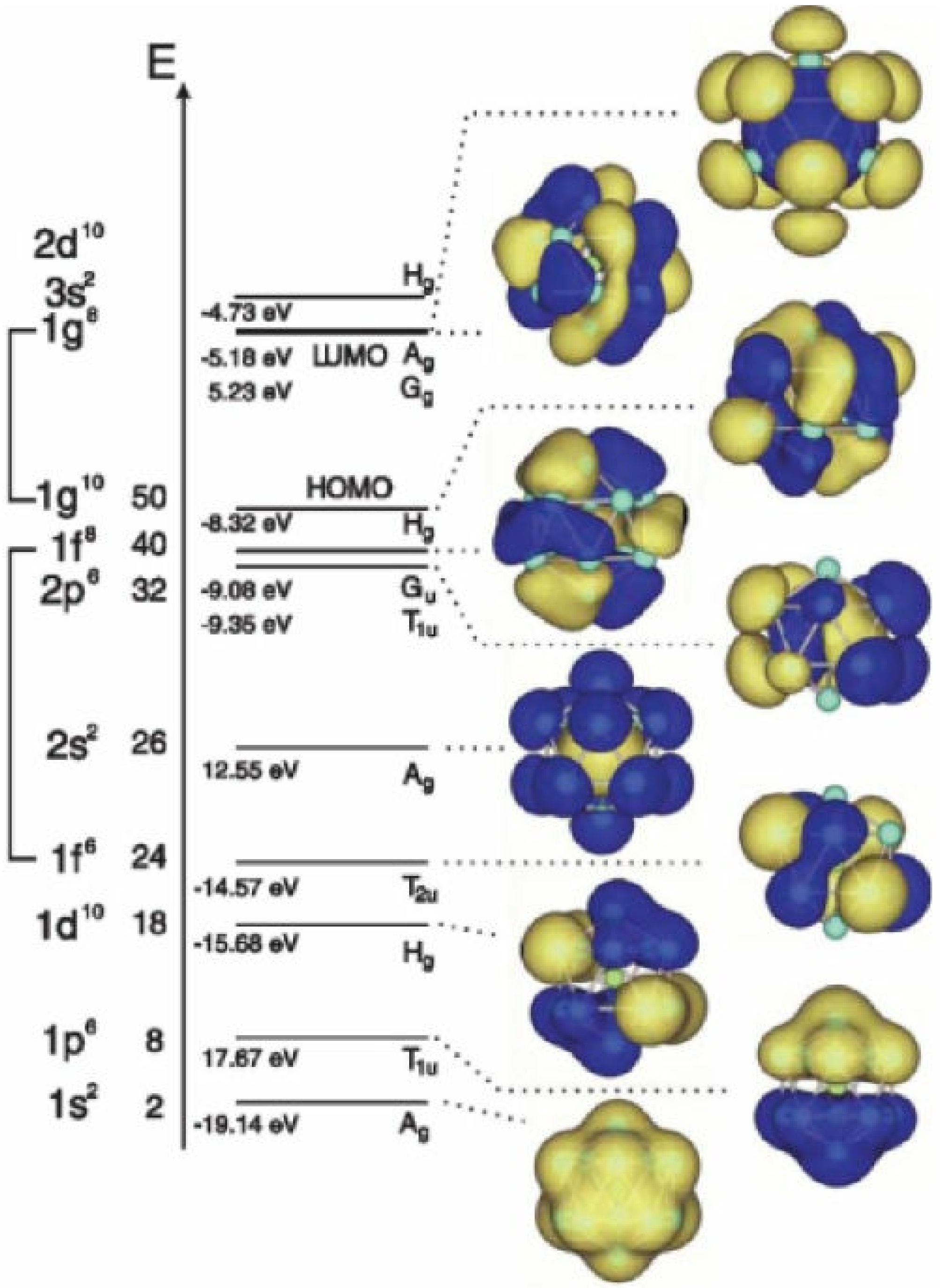

Figure 8.15 Calculated electronic orbitals for the core–shell icosahedral cluster $AlPb_{12}^+$.

Neukermans et al. [27], © 2004. With permission of APS.

An instructive example of a composite superatom is the magic aluminium cluster anion Al_{13}^-, which has 40 valence electrons and forms a closed 2p shell, whereas the neutral Al_{13} open shell cluster has distorted icosahedral structure. The closed shell ground state of the anion is calculated to be of almost perfect icosahedral symmetry. It is a halogen-like superatom and can form a molecular ion with an iodine atom, $Al_{13}I^-$, which has an Al_{13}–I bond dissociation energy of 2.46 eV, and a remarkable finding is that the negative charge remains on the aluminium cluster. It is a fantastic perspective for young scientists to have pseudo-atoms available that are best regarded as new elements, which can be combined with others, leading to completely new chemistry. It is a halogen-like superatom and can form a molecular ion with an iodine atom, Al_{13}, which has an Al_{13}–I bond dissociation energy of 2.46 eV, and the remarkable finding is that the negative charge remains on the aluminum cluster. It is a fantastic perspective for young scientists to have pseudo-atoms available that are best regarded as new elements, which can be combined with others, leading to a completely new chemistry.

Review Questions

Q1. Give factors responsible for novel properties of nanomaterials.

Q2. What do you understand by quantum confinement?

Q3. What is tunneling effect? What are the implications of tunneling effect in nanotechnology?

Q4. What is band gap? How does it differs in conductors, semiconductors, and insulators?

Q5. How does change in band gap with the size of NPs affect the electrical behavior of a material?

Q6. How does size of NPs affect the surface properties of nanomaterials in terms of (a) fraction of atoms at the surface (b) smooth scaling properties?

Q7. How does thermal, optical, and electrical properties of materials are affected when material transforms to nanosize?

Q8. What are the color causing phenomena in nanostructured objects?

Q9. Write short notes on surface plasmon resonance in metal nanoparticles and quantum fluorescence.

Q10. Give a plausible cause for photoluminescence in semiconducting material. Explain with the help of band gap energy model.

Q11. What is dielectric constant? How dielectric constant is measured? How does it affects the conductivity and optical properties of nanomaterial?

Q12. Discuss important dielectric properties of nanomaterials.

Q13. What are the new properties arise when the size of a magnetic material reaches in nanosize regime? Explain the underlying causes giving examples.

Q14. Give characteristic features of superparamagnetic material.

Q15. How superparamagnetism is related to thermal energy (k_BT) and anisotropy constant (K_{eff})?

Q16. What will be the impact of coating of a non-magnetic material over a magnetic nanoparticle?

Q17. Explain why mechanical properties of nanocomposites are better than their constituent materials?

Q18. Does bonding changes when bulk material transform into nanomaterial? Give significance of physical bonding in nanomaterials?

Q19. Discuss the various types of bonding leading to the formation of supramolecular structures. Give some examples of biological supramolecules.

Q20. What features of NPs make them attractive for catalysis and sensor applications? Explain with some examples.

Q21. What do you understand by pseudo-atom, give some of its potential applications?

References

1. C. N. R. Rao, A. Müller and A. K. Cheetham, *Nanomaterials – An Introduction*, Wiley-VCH Verlag GmbH & Co, KGaA, 2005.

2. M. K. Patra, K. Manzoor, S. R. Vadera and N. Kumar, "Functional nanomaterials for sensors and display applications", *Encyclopedia of Nanoscience and Nanotechnology*, Vol. 14 Ed. H. S. Nalwa, American Scientific Publishers, USA, 2011, pp. 385–435.

3. H. Gleiter, "Nanostructured Materials: Basic Concepts and Microstructure", *Acta Mater.*, **48** (2000) 1–29.

4. J. A. Scholl, A. García-Etxarri, A. L. Koh and J. A. Dionne, "Observation of Quantum Tunneling between Two Plasmonic Nanoparticles", *Nano Lett.*, **13** (2013) 564–569.

5. R. J. White, R. Luque, V. L. Budarin, J. H. Clarka and D. J. Macquarriea, "Supported Metal Nanoparticles on Porous Materials. Methods and Applications", *Chem. Soc. Rev.*, **38** (2008) 481–494.

6. P. Edwards, R. L. Johnston and C. N. R. Rao, "On the size-induced metal-insulator transition in clusters and small particles", *Metal Clusters in Chemistry*, Vol. 3, Eds. P. Braunstein, L. A. Oro, P. R. Raithby, Wiley, Weinheim, 1999.

7. M. P. Johansson, D. Sundholm and J. Vaara, "Au_{32}: A 24-Carat Golden Fullerene", *Angew. Chem.*, **116** (2004) 2732–2735.

8. E. Roduner, *Nanoscopic Materials: Size Dependent Phenomena*, RSC Publishing, Cambridge, UK, 2006.

9. A. Kohn, F. Weigend and R. Ahlrichs, "Theoretical Study on Clusters of Magnesium", *Phys. Chem. Chem. Phys.*, **3** (2001) 711.

10. M. Quinten, *Optical Properties of Nanoparticle Systems: Mie and Beyond*, Wiley-VCH Verlag GmbH & Co. KGaA, 2011.

11. K. L. Kelly, E. Coronado, L. L. Zhao and G. C. Schatz, "The Optical Properties of Metal NPs: The Influence of Size, Shape and Dielectric Environment", *J. Phys. Chem. B,* **107** (2003) 668–677.

12. C. Z. Li, K. B. Male, S. Hrapovic and J. H. T. Luong, "Fluorescence Properties of Gold Nanorods and their Application for DNA Biosensing", *Chem. Commun.*, (2005) 3924–3926.

13. E. Roduner, "Size Matters: Why Nanomaterials are Different", *Chem. Soc. Rev.*, **35** (2006) 583–592.

14. K. G. Thomas, Tuning functional properties: from nanoscale building blocks to hybrid nanomaterials, *Currents Trends in Science-Platinum Jubilee Special*, Ed. N. Mukunda, Indian Academy of Science, Bangalore, 2009, pp. 53–66.

15. *Handbook of Nanomaterials Properties*, Ed. B. Bhushan, D. Luo, S. R. Schricker, W. Sigmund, S. Zauscher, Springer, 2014.

16. G. Y. Yurkov, A. S. Fionov and Y. A. Koksharov et al., "Electrical and Magnetic Properties of Nanomaterials Containing Iron or Cobalt Nanoparticles", *Inorg. Mater.*, **43** (2007) 834–844.

17. C. N. R. Rao, G.U. Kulkarni, P.J. Thomas and P. P. Edwards, "Metal Nanoparticles and their Assemblies", *Chem. Soc. Rev.,* **29** (2000) 27.

18. J. T. Lue, Physical properties of nanomaterials, *Encyclopedia of Nanoscience and Nanotechnology*, Vol. X, Ed. H. S. Nalwa, American Scientific Publishers, pp. 1–46.

19. J. K. Nelson and Y. Hu, "Nanocomposite Dielectrics: Properties and Implications", *J. Phys. D (Appl. Phys.)*, **38** (2005) 213–222.

20. J. K. Nelson, The Promise of dielectric nanocomposites, Conference Proceeding, International Symposium on Electrical Insulation, 2006.

21. A.H. Lu, E.L. Salabas and F. Schuth, "Magnetic Nanoparticles: Synthesis, Protection, Functionalization and Applications", *Angew. Chem. Intl. Ed.*, **46** (2007) 1222–1244.

22. M. A. Meyers, A. Mishra, D.J. Benson, "Mechanical Properties of Nanocrystalline Materials", *Prog. Mater. Sci.*, **51** (2006) 427–556.

23. N. G. Bastús, E. Casals, I. Ojea, M. Varon and V. Puntes, "The Reactivity of Colloidal Inorganic Nanoparticles", www.intechopen.com.

24. J. A. Alonso, *Structure and Properties of Atomic Nanoclusters*, Imperials College Press, 2005.

25. D. Astruc, "Transition-metal nanoparticles in catalysis: from historical background to the state-of-the art", *Nanoparticles and Catalysis*, Ed. D. Astruc, WILEY-VCH Verlag GmbH & Co. KGaA, Weinheim, 2008.

26. L. P. Kouwenhoven, D. G. Austing and S. Tarucha, "Few-Electron Quantum Dots", *Rep. Prog. Phys.*, **64** (2001) 701.

27. S. Neukermans, E. Janssens, Z. F. Chen, R. E. Silverans, P. V. R. Schleyer and P. Lievens, "Extremely Stable Metal-Encapsulated and Clusters: Mass-Spectrometric Discovery and Density Functional Theory Study", *Phys. Rev. Lett.*, **92** (2004) 163401.

Chapter 9
Applications of Nanotechnology

9.1 Introduction

The use of nanostructured materials is not a recently discovered phenomenon. It dates back to the fourth century ad when Romans were using nanosized metals to decorate glasses and cups. One of the first known and famous example is Lycurgus cup (refer to Figure 1.7, Chapter 1), fabricated from gold and silver nanoparticles embedded in the glass. The cup depicts King Lycurgus of Thrace, appears green under normal light conditions, however, when illuminated from within, it becomes vibrant red in color. Similarly, metal NPs account for the visual appearance of the famous stained glass windows from the tenth, eleventh, and twelfth centuries.

Nanotechnology is distinguished by its interdisciplinary nature and is a science with huge potential and great expectations. The daily announcements of new discoveries and breakthroughs are going to influence all aspects of human society. After more than 20 years of basic nanoscience research and more than a decade of focused research and development, applications of nanotechnology are growing day by day. Nanotechnology is helping to considerably improve, even revolutionize, many technology and industry sectors: information technology, energy, environmental science, medicine, homeland security, food safety, and transportation [1, 2]. Most benefits of nanotechnology depend on the fact that it is possible to tailor the essential structures of materials at the nanoscale to achieve specific properties, thus greatly extending the well-used toolkits of materials science. Products where the addition of a relatively small amount of functionalized nanoparticles leads to a major change in the properties are going to revolutionize many commercial technologies. Using nanotechnology, materials can effectively be made to be stronger, lighter, more durable, more reactive, more sieve-like, or better electrical conductors, among many other traits. It is well established now that size, shape, and morphological characteristics such as surface charge, area, porosity together with composition and structure of the nanomaterials are solely responsible for their unique properties and their associated applications. More and more consumer products are branded with the buzzword “nano” or nanotechnology. In general, the products claiming to contain nanotechnology do indeed exploit nanoscale effects, primarily interface as well as quantum effects. Interestingly, the products that proudly use the “nano” brand are only a small percentage of the number of consumer products that actually contain nanomaterials, for instance in the microelectronics, cosmetics, pharmaceutical, and food industries. Table 9.1 summarizes some of the present and future applications of nanomaterials.

Table 9.1 Areas of Application of Nanotechnology

Areas	Applications
Medicare and health	Nanodevices for monitoring, repair, construction, and control of human biological system, targeted drug delivery, replacement of damaged parts (cancerous cells, blood vessels, skins, bones, etc.)
Information/computer technologies	Miniaturized computing devices with efficacy improvement by a factor of millions and data storage at multitera-bit level
Environment and energy	Environment: air and water pollution control through light weight, high-strength nanoporous filters, nanofilters for isotope separation, energy storage, and conversion Energy: photovoltaic cells, solar absorbers, high-density rechargeable batteries, hydrogen and hydrocarbon storage devices
Biotech and agro forestry	Molecularly engineered chemicals for nourishing plants and protection against insects, genetic improvement of plants and animals testing technology to identify genomes sustaining salt and drought stresses, processing biomass in sewerage treatment plants food processing and preservation
Metallurgical and chemical technologies	High strength, tough, light-weight corrosion, and heat-resistant structural materials (metals, alloys, ceramic, and polymeric) for aerospace vehicles and automobiles. Design and synthesis of new multifunctional molecules. Energy-saving chemical processes using nanocatalytic systems
Defence	Smart military equipments including clothing, armor and weapons; improved low observability; light-weight and high-strength military platforms; improved chemical/biological sensors; miniaturized detectors for surveillance, and so on.

Source: Patra et al. [2]. With permission of ASP.

9.2 Medicine and Healthcare

The application of nanotechnologies to the medical sector is referred to as nanomedicine. On first sight, nanomedicine is the rather more well-defined application of nanotechnology in the areas of healthcare and disease diagnosis and treatment. Specifically, this area of application uses nanometer-scale materials and nano-enabled techniques to diagnose, monitor, treat, and prevent diseases. These include cardiovascular diseases, cancer, musculoskeletal and inflammatory conditions, neurodegenerative and psychiatric diseases, diabetes, and infectious diseases (bacterial and viral infections, such as HIV). The potential contribution of nanotechnologies in the medical sector is extremely broad and includes new diagnostic tools; imaging agents and methods; drug delivery systems and pharmaceuticals; therapies; implants; and tissue-engineered constructs [3].

Nanomaterials by definition are the materials at a nanoscale level, which, in nanomedicine, often goes beyond 100 nm and up to about 500 nm. This is the size range of biomolecules (e.g., proteins, enzymes, DNA) and molecular complexes such as the ion pump. These natural nanomaterials are the constituents of larger hierarchical structures that regulate the function of the cell. Bacteria are larger (up to a few micrometers), but their functions including toxicity to healthy cells derive from the interactions between the biomolecules and the surrounding cells. Basically, nanotechnologies make it possible to create engineering materials such as drug delivery systems, diagnostic probes, or even tissue-engineered constructs of dimensions of biomolecules which, in turn, is the scale that regulates the functions of cells. In a way, nanotechnologies have the great potential to improve the whole healthcare process that starts from diagnosis to therapy and follow-up monitoring.

9.2.1 Diagnosis

The accurate targeting and quantification of molecules indicative of cellular disorders at the single-molecule level is a demanding task for current high-throughput analysis systems. The combination of nanoparticles with other nanotechnology-based materials has the potential to address this emerging challenge and provide technologies that enable diagnoses at the level of single cells and single molecules. There are already several nanoparticles-based commercialized systems for medical diagnostics. Nevertheless, the possibilities for nanoparticle applications in diagnostics are almost unlimited because nanoparticles enable the selective tagging of a wide range of medically important targets, including bacteria, biomarkers, and individual molecules such as proteins and DNA.

Diagnosis of a suspected disease is one of the most critical steps in healthcare and medicine. Diagnoses are wanted quickly, but must also be reliable, specific, and accurate, and with the minimum risk of “false positives.” Nanomedicine has the potential to greatly improve the entire diagnostic process. Some miniaturized *in vitro* diagnostic devices already exist such as the breath analyzers that the police carry for alcohol screening or the portable glucose test devices used by diabetics. These devices can measure ions, small molecules, or proteins, or can test for specific DNA sequences that are diagnostic for a particular disease or medical condition. In the last years, there has been a trend to make these devices even smaller, able to perform hundreds of tests at the same time, and be easier to use. Nanotechnologies have an important role in this development: nanomaterials, such as nanoparticles or nanotubes, can be integrated into the device. Nanomaterials can be engineered to be very specific, so their use will make the device even more accurate and capable of carrying out even more tests simultaneously. Nanomaterials have the characteristic of exhibiting some peculiar quantum effects that can be used to amplify the signal arising from the detection. Thus, the use of nanomaterials in miniaturized *in vitro* diagnostic devices makes it possible to improve the specificity of the analysis, its throughput (the number of tests that can be done simultaneously), and its read-out. In the future, these types of devices are likely to make it possible to perform “point-of-care diagnostics”: it will be possible to make a diagnostic test anywhere, not just in the hospital. The nature of the sample to be tested may probably be changed and become saliva rather than blood, which is much more convenient and safer to handle. This will allow a large number of patients to be tested, for example, in the event of an epidemic, or a large number of diseases, or the many parameters needed for one specific disease to be considered for the diagnosis of complex medical conditions.

Miniaturized diagnostic devices include biosensors, microarrays, and “lab-on-a-chip” (LOC) devices, also called miniaturized total analysis systems (μTAS). The first two are based on a parallel processing technique, whereas LOC devices are based on a serial processing technique.

9.2.1.1 Biosensors

Generally speaking, a sensor is a device capable of recognizing a specific chemical species and “signaling” the presence, activity, or concentration of that species in solution through some chemical change. A “transducer” converts the chemical signal (such as a catalytic activity of a specific biomolecule) into a quantifiable signal (such as a change in color, resonance, current, intensity) with a defined sensitivity. When the sensing is based on bimolecular recognition, it is called a biosensor. Furthermore, depending on the technique used in signal transduction, biosensors are classified as optical biosensors, electrochemical biosensors, mass-sensitive biosensors, or thermal biosensors. Biosensors work as probes recognizing an analyte or differentiating between analytes of interest. In such applications, some biological molecular species (such as antibodies, antigens [4], receptors [5], enzymes [6], nucleic acids) are attached to the surface of the nanoparticles to recognize the specific target of interest through a lock-and-key mechanism in real time. The probes then signal the presence of the target by a change in color, mass, or other physical change. Nanoparticles used as elements for biosensors include quantum dots (QD), metallic nanoparticles, silica nanoparticles, magnetic beads, and fullerenes. Other biosensors use nanostructured particles as nanosieves through which charged molecules are transported in an electric field. In this case, particles with engineered nanopores are used. Carbon nanotubes and nanowires are also employed for sensing. The latter can be fabricated out of a semiconductor material, and their size is tuned to have a specific conducting property. This, together with the ability to bind a specific analyte on their surface, yields a direct, label-free electrical read-out. These nanowire biosensors allow the detection of a wide range of chemical and biological species, including low concentrations of protein and viruses, and their application ranges from the medical to the environmental sector. Figure 9.1a and b illustrates a silicon nanowire and nano-gold sensor based on biorecognition of antibodies. Nanoscale biosensors have the potential to greatly aid the diagnosis of diseases [4] and in monitoring the therapies. A large number of approaches have been developed in recent years, and their wide application in patient care is foreseen in the next 5–10 years.

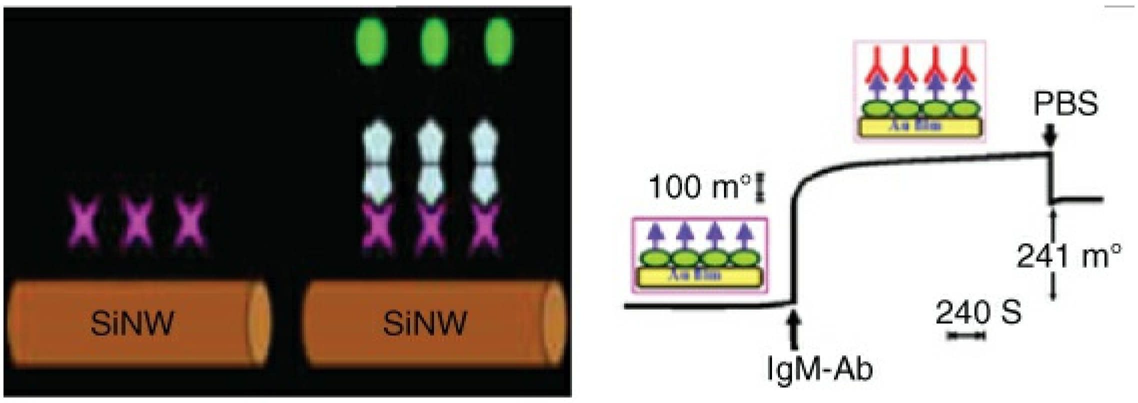

(a) (b)

Figure 9.1 Nanobiosensor. (a) Silicon nanowires surface modified with avidin molecules (purple stars), which selectively bind a streptavidin-functionalized molecule or nanoparticle. Courtesy of Raj Mohanty, Boston University, USA. (b) Nanogold surface immobilized with dengue antigen–BSA conjugate for detection of dengue using SPR technique. Kumbhat et al. [4], ©2010. With permission of Elsevier.

9.2.1.2 Microarrays

Microarrays are platforms made up of hundreds of detection sites that have micron-sized dimensions and allow the specific detection of a biochemical within a mixture or the simultaneous detection of many biochemicals. The detection is related to the chemical functionality on the micron-sized spots in the array, and it leads to a single chemical "yes/no" reaction per spot. Microarrays are used as screening tools for not only diagnostic purposes but also screening new drugs. These devices are used for diagnostic purposes such as DNA analysis (DNA microarray), protein detection (protein microarrays), as well as whole cell analysis. Nanotechnology can impact microarray technology by creating densely packed, smaller, nanosized arrays (nanoarrays) that could allow faster screening of a larger number of (bio)chemicals. There are, however, some problems associated with the handling of ultrasmall quantities of liquid, so nanotechnologies offer the most promising advantages in sample detection on arrays. The conventional method used for detecting the "yes/no" reaction at each spot is fluorescence. This technique uses fluorescent probes made of organic molecules attached to the species to be detected (e.g., a protein or a fragment of DNA): when a reaction occurs, this is attached to the detection spot, which becomes fluorescent in a "color" corresponding to the emission of the fluorescent probe. Fluorescent staining suffers from some disadvantages, mainly fast bleaching of the fluorescent molecules (i.e., loss of "brightness" of the color in time during imaging); a limited number of dye molecules that have distinct "colors" and that can be simultaneously imaged; and limited sensitivity. Nanoparticles in the form of quantum dots (QD) can be used as an alternative to conventional organic dyes, being more stable, sensitive, and monochromatic. A substantial (10-fold) enhancement in sensitivity compared to common fluorescent markers has been accomplished through the use of gold and silver particles of uniform dimensions in the range 40–120 nm. Signal amplification is also obtained using metal nanoparticle labels, such as DNA-modified gold nanoparticles. These nanosized probes have molecules attached to their surface that ensure the selectivity of the detection, while the nanoproperties of the probe are responsible for enhancing the signal. The overall effect is an improvement in the sensitivity and selectivity of microarray technology.

9.2.1.3 Nanobarcodes

The unique properties of nanoparticles, such as the relationship between particle size and color, can also be used to create multiplexed detection systems in the form of nanobarcodes, for example, using quantum dots to create different color-based codes. Alternatively, fragments of DNA on nanospheres can be used to create a "bio-barcode," for example, for protein detection. A bio-barcode has been used to detect small levels of the cancer marker prostate-specific antigen (PSA) in serum. The results showed an increased sensitivity to the PSA protein compared to conventional protein assays, demonstrating the potential of such approaches for detecting cancers at an earlier stage.

9.2.1.4 Lab-on-a-Chip

These devices are "miniaturized integrated laboratories" that allow the separation and analysis of biological samples (e.g., blood) in a single device. They are made up of microfluidic systems, including micropumps and microvalves, integrated with microelectronic components. The devices can also integrate one or more sensors. As with microarray technology, the impact of nanotechnologies in this area is in further miniaturization of these devices, although the handing of ultrasmall volumes of samples would pose a problem. Presently, nanotechnologies are making an impact in improving specific components and functions of LOC devices. For example, analysis is commonly done by dielectrophoresis where nonuniform alternating electrical fields are used to separate and guide small objects through field gradients: this manipulation requires high electrical field strengths that can be obtained using nanosized electrodes. Another example is nanopore-based separation systems that can be integrated into the membranes used in LOC devices, that is, nanopore membranes are proposed for DNA sequencing.

9.2.1.5 Biomarkers for Early Detection of Diseases

A biomarker is an indicator of a biological process or state, such as a disease, or the response to a therapeutic intervention. This can be an altered gene, or a change in protein production, or even a physical feature of a cell. The aim is to detect biomarkers of disease and diagnose illnesses before, or at the onset of, the first symptoms, in this way making *in vivo* imaging a tool for the early detection of a disease. Effective early detection is crucial for planning a therapy with less severe and costly therapeutic demands, especially in diseases such as cancers, where timing is vital for the success of the treatment.

Nanoparticles have been demonstrated for early diagnosis of infectious disease. The nanoparticles attach to molecules in the blood stream indicating the start of an infection. When the sample is scanned for Raman scattering the nanoparticles enhance the Raman signal, allowing detection of the molecules indicating an infectious disease at a very early stage. Silver nanorods in a diagnostic system are being used to separate viruses, bacteria, and other microscopic components of blood samples, allowing clearer Raman spectroscopy signals of the components. This method has been demonstrated to allow identification of viruses and bacteria in less than an hour. Carbon nanotubes and gold nanoparticles are being used in a sensor that detects proteins indicative of oral cancer. A test has shown this sensor to be accurate in detecting oral cancer and provides results in less than an hour. Few other nanomaterial-based technologies for early detection of diseases, which are at an advanced level of development, include the following:

> **Early detection of cancer tumor:** The nanoparticles attached to a cancer tumor release "biomarkers," the specific peptides. The idea is that since each nanoparticle carries several peptides, a high concentration of these biomarkers will occur even at very early stages of cancer, allowing early detection of the disease.
>
> **A test for early detection of kidney damage:** The method uses gold nanorods functionalized to attach to the type of protein generated by damaged kidneys. When protein accumulates on the nanorod, the color of the nanorod shifts. The test is designed to be done quickly and inexpensively for early detection of a problem.

A method for early diagnosis of brain cancer uses magnetic nanoparticles and nuclear magnetic resonance (NMR) technology. The magnetic nanoparticles attach to particles in the blood stream called microvesicles, which originate in brain cancer cells. NMR is then used to detect these microvesicles/magnetic nanoparticle clusters, allowing an early diagnosis.

9.2.1.6 Diagnostic Imaging

Optical imaging techniques, such as fluorescence labeling, are used extensively in clinical diagnosis. However, the organic fluorophores used currently are not photostable and have low intensity. Likewise, fluorescence proteins (i.e., green fluorescence protein) or bioluminescence system (i.e., luciferin/luciferase) applications are limited because they cannot be optimized in multicolor assays. Nanoparticles have helped to overcome these limitations. For example, quantum dots are resistant to photobleaching and photo, chemical, and metabolic degradation. They exhibit high quantum yield and enable the simultaneous identification of multiple markers. Magnetic resonance imaging (MRI) is another important example of a technique that is used commonly in medicine for the 3D examination of biological events. However, MRI applications are limited by their insensitivity to low concentrations of imaging agent. In this regard, superparamagnetic iron oxide nanoparticles have already proven effective in increasing contrast in magnetic imaging.

The second step in the diagnosis of a disease involves *in vivo* imaging, which searches for the symptoms of the disease within the live tissue suspected of being infected without the need to perform surgery. Nanotechnologies are having a very important impact in this area, particularly by developing molecular imaging agents. The latest improvements in the area of imaging deal with the capability of tracking changes at the cellular and molecular level through the analysis of some specific biological markers, and the technique is known as “targeted molecular imaging” or “nano-imaging.” Biomarkers could also be used as early indicators of the success of a treatment, thus reducing treatment time and cost.

Techniques such as X-ray computed tomography (CT), ultrasound (US), MRI, and nuclear medicine (NM) are well-established imaging techniques, widely used in both medicine and biochemical research. Originally, imaging techniques could only detect changes in the appearance of a tissue when the symptoms of the disease were relatively advanced. Later, targeting and contrast agents were introduced to mark the disease site at the tissue level, increasing imaging specificity and resolution. It is in this specific area that nanotechnologies are making their greatest contribution by developing better contrast agents for nearly all imaging techniques. The physiochemical characteristics of the nanoparticles (particle size, surface charge, surface coating, and stability) allow the redirection and concentration of the marker at the site of interest. An example of nanoparticles used in research for imaging is perfluorocarbon nanoparticles employed as contrast agents for nuclear imaging, MRI, and US, with applications in the imaging of blood clots, angiogenesis, cancer metastases, and other pathogenic changes in blood vessels. Gadolium complexes have been incorporated into emulsion nanoparticles for the molecular imaging of thrombi, resulting in a dramatic enhancement of the signal compared to conventional MRI contrast agents. Fullerenes are also used in MRI research, filled with smaller molecules that act as contrast enhancement agents. Metals and silicon nanoparticles are also used to enhance MRI. Silicon particles fabricated into different shapes and coated with conductive layers can have enhanced magnetic resonance interactions with an imaging field

9.3 Drug Development and Drug Delivery System

Advances in the field of pharmacology stem from two main concepts: the drug discovery, the development of new biologically active drugs and the development of new drug delivery systems able to reach the specific site of the disease. Drug delivery systems are in the same form as the "pills" that are frequently taken and that release their active component gradually in time (slowly release drugs) or that dissolve based on some physiological conditions (e.g., acidity of the environment). Drug delivery systems also exist in the form of implants, inserts, or other drug-releasing systems.

9.3.1 Drug Design and Screening

The structure of biological macromolecules defines a 3D nano-environment that mediates specific functions in the cell. The design of new drugs requires a very detailed understanding of this nano-environment. Therefore, gaining insight into the structure of macromolecules on the nanoscale through electron microscopy, NMR spectroscopy, and X-ray crystallography is of fundamental importance to understand biological processes and for the development of new medicines. One of the bottle necks in drug discovery is the necessity to screen thousands of candidate drugs for their efficacy in fighting targeted macromolecules in a disease state. Microtechnologies and, now, nanotechnologies have enabled the development of microarray platforms and new detection methods including label-free to investigate the effects of candidate drugs against disease macromolecules with unprecedented speed. For drugs to be able to maximize the drug's therapeutic action while minimizing side effects do this, the delivery systems need to be miniaturized to much smaller than the target and specific in composition to elicit a certain response. With the use of nanotechnologies, targeted drugs in terms of composition and delivery system are becoming a reality.

9.3.2 Advanced Drug Delivery Systems

Nanoparticle-based drug delivery provides many advantages, such as enhancing drug-therapeutic efficiency and pharmacological characteristics. For example, nanoparticles improve the solubility of poorly water-soluble drugs, modify pharmacokinetics, increase drug half-life by reducing immunogenicity, increase specificity toward the target cell or tissue (thus reducing side effects), improve bioavailability, diminish drug metabolism, and enable a more controllable release of therapeutic compounds and the delivery of two or more drugs simultaneously for combination therapy. Advanced drug delivery systems aim to improve bioavailability and pharmacokinetics of pharmaceuticals and to replace invasive by noninvasive routes of administration. Examples for advanced drug delivery systems are controlled-release formulations or pulmonary dosage forms of proteins such as insulin. Nano-drug delivery systems (NDDS) are a subclass of advanced drug delivery systems that consists of drug carriers with a size of less than 1 μm and mostly less than 200 nm. Examples for NDDS are liposomes, nanosuspensions, polymeric nanoparticles, dendrimers, fullerenes, carbon nanotubes, and inorganic nanoparticles.

Liposome drug delivery systems are nanoscale spheres composed of a lipid layer surrounding the drug. First, liposomal formulations of the anticancer drug doxorubicin were launched at the beginning of the 1990s, such as Doxil®/Caelyx® or Myocet®. By using a liposomal formulation, the cardiac safety of the drug doxorubicin could be improved. There are currently more than 10 liposome-enhanced drugs in the market, and about 30 in clinical trials.

Nanosuspensions are dispersions of pure nanosized drug particles, which are stabilized by surfactants. By reducing the size of drug particles to about 10–100 nm (nanonization), the solubility of the drug can be significantly increased. This technology is of interest for about 40% of drugs in the development pipeline, which is poorly water soluble and therefore cannot be administered. Several drugs formulated with nanosuspension technology are on the market and more in clinical trials.

Furthermore, the so-called polymer therapeutics such as polymer–protein conjugates, polymer–drug conjugates, polymeric micelles, and polymeric drugs also come under the category of NDDS. The systems with currently the highest pharmaceutical and commercial potential are described in the following sections.

9.3.2.1 Polymer Therapeutics

Polymeric nanoparticles are either nanosized solid particles or capsules, which consist of natural or synthetic polymers and to which the drug is attached. They are investigated as drug delivery systems for site-specific targeting of tumors and for the transport of drugs across biological barriers, particularly the blood–brain barrier. Presently, polymeric nanoparticle drug delivery systems are in developing stage. In the anticancer drug Abraxane™, the substance paclitaxel stabilized by albumin is in the market that uses a (bio)polymeric nanoparticle drug delivery system.

9.3.2.2 Polymeric Micelles

Micelles are nanosized, spherical colloidal particles with a hydrophilic exterior (shell) and hydrophobic interior (core). Their main utility is in the preparation of pharmaceutical formulations, particularly agents that are soluble in water. Drugs or contrast agents may be entrapped within the hydrophobic core or linked covalently to the surface of micelles. Their individual particle size is less than 50 nm in diameter, which provides obvious benefits over liposomes. Polymeric micelles may circulate for prolonged periods in the blood, evading host defenses. With their property of continued stability in the blood, they can be used for sustained drug release of drugs and *in vivo* imaging. Polymeric micelles provide a safer alternative for parenteral administration of poorly water-soluble drugs such as amphotericin B, propofol, paclitaxel, and photosensitizers.

Similar to liposomes, polymeric micelles can be modified using piloting ligand molecules for targeted delivery of drugs to specific cells (e.g., cancer cells); pH-sensitive drug-binding linkers can be added for controlled drug release. For this kind of function, micelles are formed from stimuli-responsive amphiphilic block copolymers. Multifunctional polymeric micelles can be designed to facilitate simultaneous drug delivery and imaging.

9.3.2.3 Nanoscale Metal-Organic Frameworks (NMOFs)

Metal-organic frameworks (MOFs), a class of hybrid materials formed by the self-assembly of polydentate bridging ligands and metal-connecting points, have been studied for a variety of applications including the loading and controlled release of several drug molecules. Recently, these materials have been scaled down to nanometer size. The NMOFs possess some potential advantages over the existing nanocarriers (both pure inorganic and organic). First, NMOFs of different compositions, shapes, sizes, and chemical properties can be obtained from MOFs. Second, NMOFs are intrinsically biodegradable as a result of relatively labile metal–ligand bonds, making it possible to rapidly degrade and clear the nanocarriers after the intended task is completed. Recently, the uses of NMOFs in biomedical imaging and drug delivery have been reported. NMOFs have already shown great potential as a new nanocarrier platform for imaging agents for MRI, optical imaging, and X-ray CT together with drug delivery. It is further believed that many imaging and drugs will be incorporated in the future by taking advantage of the totally tunable nature of NMOFs. Particularly, combining both imaging and therapeutic agents in the same platform should greatly facilitate the efficacy of this special class of theranostic particles.

9.3.2.4 Nanoparticles for Gene Delivery

Viruses are particularly efficient gene vectors and are used in more than 70% of gene therapy clinical trials. However, their toxicity and potential for generating a strong immune response are some of the concerns regarding the use of viruses. Nonviral delivery systems can circumvent some of these problems and are emerging as favorable alternatives to viral vectors. Polymeric delivery systems (DNA–polymer complexes) and liposomal delivery systems are used as nanotechnology-based nonviral gene vectors.

9.3.2.5 siRNA Drug Delivery

RNA interference is a natural, fundamental mechanism in gene regulation that occurs in both plants and animals, humans included. Genes carry the genetic material of an individual, the DNA, and are contained in the nucleus of a cell. When genes are expressed (i.e., activated), the genetic information is copied from DNA to messenger molecules, called messenger RNA (mRNA), which then orchestrate the formation of proteins outside the nucleus of the cell. **Small interfering RNA** (siRNA), a new generation of biodrugs, can be utilized for silencing a wide range of target genes to treat a variety of diseases including cancers. However, the delivery of bare siRNA to the appropriate site remains a considerable hurdle owing to rapid enzymatic digestion, limited translocation through cellular membranes, and inefficient release from endosomes. Therefore, one of the main challenges in siRNA therapy is to find a suitable gene delivery carrier, the main features of which, for clinical applications, should be low toxicity and high transfection efficiency. One obvious strategy for RNA/RNA delivery is through viral vectors. However, the issue of immunogenicity, carcinogenicity, and inflammation that are associated with viral vectors makes it necessary to go for the development of nonviral drug delivery systems based on cationic polymers, cell-penetrating peptides (CPPs), and lipids. Among these, cationic polymers are strongly favored for the reasons of being more stable, easier to manipulate, and more economical than CPPs or cationic liposomes. Some cationic polymer-based nanocarriers (both synthetic and naturally occurring) for DNA/RNA drug delivery systems include polyethyleneimine, cetyltrimethylammonium bromide, poly(2-dimethyl-amino)ethyl methacrylate, and chitosan.

9.3.3 Targeted Drug Delivery

In the future, this could lead to targeted therapies and personalized medicine. The aim is to design and deliver drugs in such a way that they can recognize the “bad” cells at a molecular level, penetrate the cell membrane, and act inside the infected cell. This is often crucial for the efficacy of a drug, since most virus replication and other disease conditions take place across the cell membrane and inside the cell. This way, the treatment will be delivered where it is needed and will be specific, eliminating the problem of the drug killing healthy cells. An example of this approach is siRNA drug delivery.

Targeted drugs and targeted DDS could allow the creation of drug formulations with optimal loading, which deliver to the body only the necessary amount of the drugs and reduce side effects for the patients. within addition to the possibility of having nano-DDS that are biodegradable inside the body, this will help to reduce drug toxicity. Drug safety can be further enhanced by the possibility of introducing inside the drug formulation a label that changes color when the drug reaches its expiry date or is no longer functioning. This will allow for the improvement of drug shelf-life and better monitoring of drug safety.

9.3.4 Remotely Triggered Delivery Systems

Systems that release drugs in response to a remote trigger, that is, systems that are actuated by an external stimulus, could offer distinct clinical advantages over those that release drugs passively or are triggered internally, for example, by a chemical stimulus. Drug-release profiles could be tailored to the specific therapy. For example, insulin is most effective when delivered to a diabetic in short bursts, whereas an anesthetic should be delivered in a steady, continuous manner. Most importantly, perhaps, remotely triggered systems would allow the patient or doctor to control the dose, timing, and duration of drug release. Numerous stimuli could be used for drug triggering, including visible or near-infrared (NIR) light, electric or magnetic fields, and US. Some of these techniques, such as US, MRI, and NIR fluorescence microscopy, are already used in the clinic or lab for imaging. Recently, nanofunctional materials have been developed that are sensitive to these stimuli and that have been used to design drug delivery systems.

NIR (~650–900 nm) light is a promising tool for drug delivery because it can penetrate skin and tissue, enabling triggering deep within the body. A variety of nanostructures such as gold nanorods, nanoshells, and nanocages absorb strongly in this range and then convert light energy into heat. Hence, gold nanoparticles can behave as localized heat sources, and they have been used to trigger drug release from temperature-sensitive materials. One temperature-sensitive material that has been used extensively is poly(*N*-isopropyl acrylamide) (pNIPAm), a polymer that abruptly and reversibly collapses when heated beyond a critical temperature.

9.3.5 Therapy

A therapy usually involves a pharmaceutical route (drugs) to treat the disease from the inside of the body or, when a pharmaceutical therapy is not possible or not effective, other routes to fight the disease from the “outside” of the body, such as radiative therapies. In some circumstances, surgery is required, and an organ substitute is inserted into the body in the form of an implant or a donated organ. In all these approaches, which are often used in combination, the aim is always the same: to eliminate selectively the source of the disease in a long-lasting way. Nanotechnologies are making a tremendous impact in this field, with new drugs and new types of treatments under development, some of which have already proven clinically effective and have entered the market. Following are the examples of some of the newly emerging nanotechnology-based treatment.

9.3.5.1 Theranostics

One of the most exciting opportunities that nanotechnologies have brought to the therapeutic field is the possibility of integrating the diagnosis, therapy, and follow-up of a disease. This is referred to as theranostics and could be enabled by nanoparticles incorporated inside a drug that can change some property – such as color – once the drug has reached the target (e.g., quantum dots). Drugs could therefore have a feedback action. In addition to a slow, targeted release system, the nanoparticles could gradually change color during the drug action, thereby informing the progress of a therapy to the doctors. This approach is called “find, fight. and follow” and could become a reality as a result of the parallel progress in the field of molecular imaging. One vision is that, one day, the entire process of diagnosis, pre-imaging, therapy, and post-imaging of a specific disease will be integrated. An example of theranostics is the use of gold nanoshells for imaging and treating cancer cells at the same time.

9.3.5.2 Regenerative Medicine

At times, the only way to treat a disease is the removal of the infected organ or tissue. Such loss can also derive from an injury or a congenital condition (e.g., vision or hearing impairment). To compensate for the lost or impaired body function, an artificial construct is implanted in the body. Depending on the type, site, and extent of the loss, this construct can be in the form of an engineered tissue or an implant. Among all examples of self-assembled nanomaterials, for tissue engineering and regenerative medicine, self-assembled peptide nanofibers are the most common. They are built by the self-assembly of relatively simple peptide building blocks, readily obtained by fast and reliable synthesis, which in turn facilitates the introduction of peptidic or nonpeptidic epitope for specific applications. In addition, their peptidic constitution confers them unique biocompatibility and degradability as they can, in principle, be used as nutrients by cells.

9.3.6 Tissue and Biomaterial Engineering

Tissue engineering deals with the fabrication of artificial scaffolds to support the growth of donor cells, which differentiate and grow into a tissue that mimics the lost natural one. This tissue-engineered construct is then implanted in the patient and, in time, resorbed by the body and fully integrated by the host tissue. Current applications of tissue-engineered constructs include engineering of skin, cartilage, and bone for autologous implantation (i.e., the implantation of a tissue regenerated by seeding cells of the patient).

The "scaffold" that supports cell growth is the core of this technique. In the body, cells are supported in their growth and function by a natural scaffold, called the extracellular matrix (ECM). This is a very complex and intricate "web" of nanofibers that provide the mechanical architecture for cellular growth. Moreover, the ECM is filled with small molecules (e.g., growth factors) and proteins that direct many cell processes, such as adhesion, migration, growth, differentiation, secretion, and gene expression. The 3D spatial organization of these "cues" is critical in controlling the entire life cycle of the cell. Ultimately, this 3D nano-architecture guides the cells to form tissues as complex as those found in the bone, liver, kidney, and heart. The biggest challenge in regenerative medicine is the artificial replication of this "perfect nano-scaffold." The ability to engineer materials having a similar level of complexity is now becoming a reality through nanotechnology.

In recent years, new nanotechnology techniques have enabled studies at higher and higher resolution, revealing the nanoscale detail of the ECM. Analytical tools, such as the AFM, and nanofabrication tools have allowed scientists to fabricate scaffolds with nanoscale features. A great deal of research is now dedicated to engineering scaffolds with tailored material composition and properties, including nanotopography and controlled alignment, to study how these can support and direct cellular growth. The aim is the fabrication of scaffolds that most closely resemble natural ECM. Researchers now have access to techniques that produce macroscale structures with nanometer details. Conventional polymer chemistry combined with new nanofabrication methods is now used to manufacture a wide range of structures, such as nanofibers of different and well-defined diameters and surface properties; nanofibrous and porous scaffolds; nanowires, nanotubes, nanospheres, and nanocomposites.

One of the distinguishing features of nanotechnologies is their ability to create new functional materials. This can be exploited in the fabrication of new biomaterials that have better mechanical properties, for example, to increase the implant stability and reduce fatigue failure in orthopedic implants, and materials that have enhanced electrical properties, for example, needed in neural prostheses. Nanotechnologies can also be used to fabricate implants made of materials that are more resorbable, to increase functionality and durability. For example, nanocoating are being studied which will better integrate synthetic implants with the biological tissue, in order to prevent tissue inflammation and the onset of rejection.

Nanotechnologies are also employed in the fabrication of biomaterials that are responsive to the environment (e.g., responsive to pH or the presence of specific biomolecules) and, for this reason, are called "smart biomaterials." Moreover, research is being conducted to include nanoscale patterns in the biomaterial, which will simulate the natural cues and mimic molecular signaling mechanisms, in order to trigger the desired biological events, such as cell adhesion, differentiation, and spreading. This could facilitate the fabrication of dynamic implants that are not limited to simply replacing a lost organ but truly restore the loss.

9.4 Information and Computer Technologies

Nanotechnology is, in many aspects, already a key player in Information and Communication Technologies (ICT) research and development, both in academia and industry. Computer microprocessors and memory storage devices have followed a path of miniaturization over the last 20 years that has “naturally” brought transistors to have dimensions lower than 100 nm. There are now challenges to continue this miniaturization. Nanotechnology is already in use in many computing, communications, and other electronics applications to provide faster, smaller, and more portable systems that can manage and store a large amount of information [7, 8]. These continuously evolving applications include the following:

- Nanoscale transistors that are faster, more powerful, and increasingly energy efficient; soon your computer's entire memory may be stored on a single tiny chip.
- Magnetic random-access memory (MRAM) enabled by nanometer-scale magnetic tunnel junctions that can quickly and effectively save even encrypted data during a system shutdown or crash, enable resume-play features, and gather vehicle accident data.
- Displays for many new TVs, laptop computers, cell phones, digital cameras, and other devices incorporate nanostructured polymer films known as organic light-emitting diodes, or OLEDs. OLED screens offer brighter images in a flat format, as well as wider viewing angles, lighter weight, better picture density, lower power consumption, and longer lifetimes.
- Other computing and electronic products include Flash memory chips for iPod nanos; ultraresponsive hearing aids; antimicrobial/antibacterial coatings on mouse/keyboard/cell phone casings; conductive inks for printed electronics for RFID/smart cards/smart packaging; more life-like video games; and flexible displays for e-book readers.

9.4.1 Integrated Circuits

As the materials of semiconductors, metals, and insulators are reduced to nanosize, quantum effects start to predominate and determine their properties. Nanotechnology offers the opportunity to exploit, rather than avoid, quantum effects in the development of the next generation of integrated circuits. In the late 1960s, Gordon E. Moore, cofounder of Intel Corporation, made a memorable observation that later became known as Moore's law. He observed that the number of transistors on a chip roughly doubled every 18 months. Originally, this was only an observation but was later adopted as an industry goal. The progression in transistor density on a chip over the last 40 years has, indeed, followed Moore's law. In order to keep up with this law, transistors have become smaller and smaller. The first transistor was about 1 cm high and made of two gold wires of 0.02 in. apart on a germanium crystal. The latest transistors from Intel® (Nehalem microarchitecture) have 45 nm feature sizes and in a quad-core configuration have over 731 million transistors. These numbers give an idea of the enormous miniaturization efforts that have been achieved by the semiconductor industry.

The scale down of transistors has been the driving force for a number of reasons. Transistors are the basic building blocks of the elements in an integrated circuit (microprocessor, mass memory, logic gates). Integrated circuits are the core of the information and memory storage devices that are an essential part of all electronics used: from computers to refrigerators, cars, mobile phones, and so on. As the size of the transistor is reduced, its density on the chip increases, which increases the speed, the amount of memory stored per area, and the number of functions that can be integrated on a single device.

9.4.2 Data Storage

Data storage is a key component of many devices of everyday use such as computers that contain both hard drive and RAM; mobile devices and digital cameras with memory card; and portable media players, for example, iPods, pendrives, and mobile phones that use Flash memory. Data storage technologies include two main groups, **hard disk drives** (having a mechanical component) **and solid-state data storage devices**, which can be further divided in volatile and nonvolatile. “Volatile” means that memory is lost once the power is turned off; “nonvolatile” means that memory is retained when the power of the device is switched off. Volatile memory storage devices today include mainly **static random access memory** (SRAM) and **dynamic random access memory** (DRAM). Nonvolatile memory storage devices, such as **Flash memory**, are used in mobile devices and portable media players. Each type of memory has its advantages and disadvantages: DRAM has a smaller memory cell size than SRAM and can, therefore, store more data but needs to be refreshed periodically, consuming power and lowering speed; SRAM can store less data but is faster; flash memory is nonvolatile, making it ideal for devices where the power is often turned off. Memory storage devices are described by their capacity (amount of data in MB), memory density (a function of the capacity and the size of the memory cell), lifetime (how many read/write cycles it can perform before it degrades), read/write speed, and cost. Microprocessors work by processing information through the passage of an electrical signal. Furthermore, information processing will be done using a state variable other than electric charge, such as spin (spintronics), molecular states (molecular electronics), photons (photonics), mechanical state, resistance, quantum state (including phase), and magnetic flux. These new state variables will require new materials such as nanomaterials to be used (e.g., relying on spin using magnetic materials rather than a semiconductor) and new functional organization of the device (nano-architecture). Some of the technologies and new materials leading to data storage are discussed here.

a. Spintronics: This is a new type of technology that exploits the spin of the electron (rather than only its charge) to store and process information. It requires thin layers of magnetic materials. The giant magnetoresistance effect (GMR) represents the first type of this new technology and is used in the new-generation memory devices such as the Magnetic Random Access Memory or **MRAM** used, for example, in the Apple iPod. Magnetic materials are used in magnetoresistive random access memory (MRAM), in which each memory cell consists of two magnetic thin-film materials separated by an isolating layer. Magnetic multilayer nanocomposites (very thin films made of magnetic materials) display magnetoresistance properties. Magnetoresistance is a phenomenon whereby the application of a DC magnetic field changes the resistance of a material. In metals, this effect occurs only at very high magnetic fields and low temperatures.

b. Photonics: Another possibility is the use of photons (rather than electrons) in the visible or IR range to transmit and process data (optical communication). In this case, semiconductors (e.g., silicon) can no longer be used since they cannot emit and transport light efficiently. Other materials (photonic crystals) engineered at the nanoscale need to be used. A photonic crystal consists of a periodic structure made of dielectric materials that affects the propagation of light. Essentially, photonic crystals contain regularly repeating internal regions of high and low dielectric constants. Photons (behaving as waves) propagate through this structure – or not – depending on their wavelength. The periodicity of the photonic crystal structure has to be of the same length scale as half the wavelength of the electromagnetic waves (i.e., approximately 200 nm (blue) to 350 nm (red) for photonic crystals operating in the visible part of the spectrum. Such crystals have to be artificially fabricated by methods such as electron-beam lithography and X-ray lithography.

c. Quantum electronics: This term means the explicit use of the tunneling effect to transport electrons from the source to the drain of the transistor. One such transistor exists and is called the single-electron transistor (SET). In this type of transistor, three is a quantum dot between the source and the drain: electrons must tunnel through this dot in order to get from the source to the drain. In simple terms, this is like having two electrodes (source and drain) separated by a thin insulating barrier with a third electrode (the quantum dot, or quantum island) in the middle of this insulating gap. The transport of charge from the source to the quantum island and then from the quantum island to the drain occurs via the quantum mechanical process of tunneling.

d. Molecular electronics: Molecules in natural systems (plants, animals) are arranged in macromolecular systems (nanostructures) that perform numerous tasks, which involve the transmission of charges, photons, and so on. These macromolecular systems have developed over millions of years of evolution and are an example of excellence when it comes to efficiency. Examples included the electric flow in nervous signaling, the control of charges in the ionic pump, and the absorption of light and transmission of photons and charge in plant chlorophyll, and many more. Molecular electronics is a branch of nanoscience that aims to make explicit use of molecular assemblies for the transmission and storage of data. The field includes molecular wires, molecular switchers, molecular sensors, and other “hardware” components of electronics.

e. Carbon nanotube transistors: In many ways, carbon nanotubes are considered a “dream material” when it comes to electronics: they can be conductive or insulating depending on their chirality (and when they are conductive, they are extremely good electronic conductors, with little resistance and, consequently, little heat dissipation); they are strong (mechanically) and chemically inert; they are resistant to high temperatures; and they can be functionalized with specific molecules to act as anchoring points. Carbon nanotubes are 1–2 nm in width and they are as narrow as the double-stranded DNA molecule (the molecule that carries our genetic information). So arranging nanotubes into electronic circuitry could allow miniaturization by a factor of about 100 over the current limit.

Each of these technologies is at a different level of maturity, and time will be needed before they can compete with Flash memory.

9.4.3 Displays

Display technology has progressed enormously in the last decade. Until a few years ago, there were bulky televisions with cathode ray tube (CRT) technology, and mobile phones with black and white displays that could only show text. Nowadays, LCD televisions are becoming the norm and mobile phones that can show photos and movies are the norm, many even with touch displays. This progress has been enabled by intense research in the field, driven by a billion-dollar industry and the constant need for more functional devices combining image and video quality, low power consumption, and low cost. Thickness and flexibility are also becoming an important requirement. Display technologies include three broad technology areas: organic LEDs, electronic paper, and other devices intended to show still images and field emission displays (FEDs).

a. Organic light-emitting diodes (OLEDs) and Organic light-emitting transitors (OLETs): OLEDs are full of promise for a range of practical applications. OLED technology is based on the phenomenon that certain organic materials emit light when fed by an electric current, and it is already used in small electronic device displays in mobile phones, MP3 players, digital cameras, and also some TV screens. Areas where nanomaterials and nanofabrication techniques are used in OLED manufacturing are transparent electrodes (where for instance carbon nanotubes of thin films are gaining popularity) and nanoparticles-based coatings for packing the OLEDs to protect them from environmental damages (e.g., water). Nanoparticle-based deposition methods may also overcome OLED fabrication problems where issues such as material damage, yield, and thickness uniformity have not been completely solved yet.

Recently, researchers have even developed brand new concept of **OLEDs** with a few nanometers of graphene as transparent conductor. This paved the way for inexpensive mass production of OLEDs on large-area, low-cost, flexible plastic substrate, which could be rolled up as wallpaper and virtually applied to anywhere you want. Nonetheless, exciton quenching and photon loss processes still limit OLED efficiency and brightness.

OLETs are alternative, planar light sources combining, in the same architecture, the switching mechanism of a thin-film transistor and an electroluminescent device. Thus, OLETs could open a new era in organic optoelectronics and serve as test beds to address general fundamental optoelectronic and photonic issues. OLET is a new light-emission concept, providing planar light sources that can be easily integrated in substrates of different nature – silicon, glass, plastic, paper, and so on – using standard microelectronic techniques.

Quantum dots (QD) are a new class of nanomaterials under investigation in the manufacture of more efficient displays and light sources (QD-LEDs). Quantum dots are nanoscale semiconductor particles characterized by emitting a specific color based on the size of the nanoparticle. A minute change in particle size results in a totally different color being emitted; for instance, a 6-nm-diameter particle would glow red while another of the same material but only 2 nm wide would glow blue. Light emission from a QD is monochromatic; therefore, it is very pure. As a consequence, their use in displays would lead to images of exceptional quality. The most exciting property of QD-LEDs, however, is that they use much less power than the currently used LCDs where light is filtered by numerous polarizers. Similar to OLEDS, QD-LEDs emit light rather than filtering it, so, for this reason, QD-LEDs are expected to be more energy efficient.

b. *Field Emission Displays*

Researchers have turned to carbon nanotubes to create a new class of large-area, high-resolution, low-cost flat panel displays. Some believe FED technology, utilizing carbon nanotubes (CNT) as electron emitter, will be the biggest threat to LCD's dominance in the panel display arena and that FED is the technology of choice for ultrahigh-definition, wide-screen televisions. FEDs, in a sense, are a hybrid of CRT televisions and LCD televisions. They capitalize on the well-established cathode–anode-phosphor technology built into full-sized CRTs using this in combination with the dot matrix cellular construction of LCDs. The electron emitters, arranged in a grid, are individually controlled by “cold” cathodes (unlike in normal CRTs, field emission does not rely on heating the cathode to boil off electrons) to generate colored light.

FED technology makes possible the thin panel of today's liquid crystal displays (LCD), offers a wider field-of-view, provides the high image quality of today's CRT displays, and requires less power than today's CRT displays.

c. *e-Paper Display* e-Paper is a display technology that aims to mimic the appearance of ordinary ink on paper. There are various technologies to create e-paper, among which **electrophoretic paper** is the most established [9]. Unlike conventional flat panel displays, electrophoretic displays rely on reflected ambient light, rather than the emission of light from the display, and can retain text or images without constant refreshing, thereby requiring much less power. This also means that they can be used under sunlight without the image fading. e-Paper display, Figure 9.2, is also very **light** and **flexible**. Some new materials such s transparent carbon nanotubes, photonic crystals, liquid crystals, and other nanomaterials are emerging as elements of e-paper.

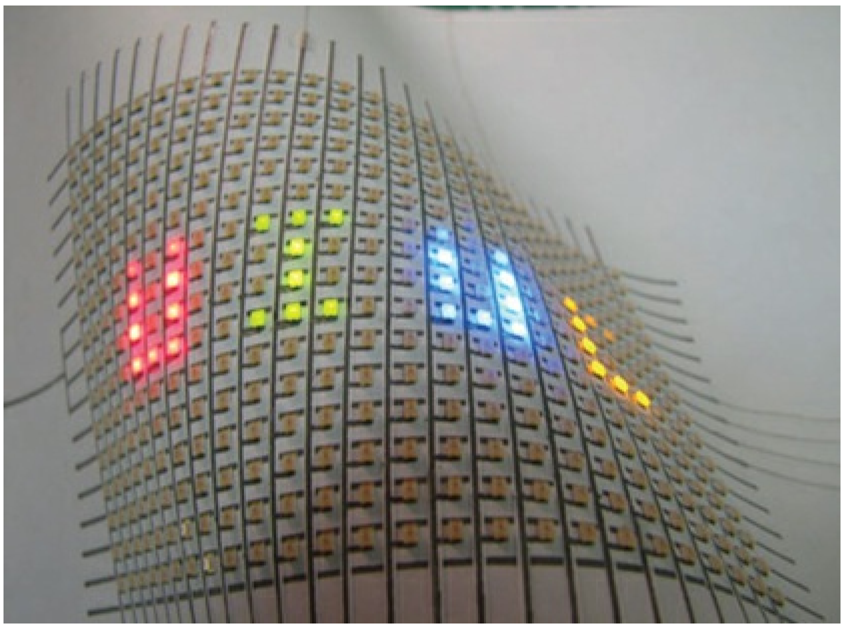

Figure 9.2 Optical image of a flexible paper display containing an LED array (25 × 16). Russo et al. [9], ©2011. With permission of Wiley-VCH Verlag Gmbh and Co.

Electrophoretic displays already are in commercial use, for instance in the Kindle or in the Sony Reader, but so far the displays are mostly black and white. There are still cost and quality issues with color displays. Nanotechnology researchers have shown that organic ink nanoparticles could provide an improved electronic ink fabrication technology resulting in e-paper with high brightness, good contrast ratio, and lower manufacturing cost.

9.5 Nanoelectromechanical Systems (NEMS)

The past decade or so has brought about tremendous growth in the field of microelectromechanical systems (MEMS) devices such as sensors, computers, electronics, and machines at the microscale. The design of these devices utilizes a combination of traditional semiconductor processing and mechanical engineering. Typically, the output of an electromechanical device is the movement of the mechanical component; a transducer is used to convert the mechanical energy into electrical/optical signals, or vice versa. Some current MEMS applications include:

- Automotive (e.g., air flow and tire pressure sensors, “smart” suspension, headlight leveling, navigation, vehicle security, automatic seatbelt restraint)
- Micronozzles for inkjet printers
- Microtweezers
- Aerospace navigational gyroscopes
- Disposable blood pressure transducers
- Portable skin analysis sensors for cosmetics applications

The extension of MEMS to the nanoregime is referred to as nanoelectromechanical systems (NEMS), representing the ultimate in future devices, with benefits such as lower power dissipation and ultrasensitive and localized responses [10]. Furthermore, owing to the size of NEMS, it will be possible to directly incorporate a number of auxiliary functionalities alongside transistors within a single chip. Indeed, the applications for NEMS will span the fields of sensors, electronics, and biotechnology, affecting virtually every aspect of our lives. Though the technology is in place to fabricate NEMS, there are three primary challenges that must be overcome prior to the realization of widespread commercial applications:

- How to communicate signals from the nanoscale to the macroscopic world?
- Understanding and controlling mechanical responses at the nanoscale
- Developing methods for low-cost, high-volume, reproducible nanofabrication

One recent NEMS device is a mass sensor with a resolution at the zeptogram level (1 zg = 10^{-21} g). Thus far, the lowest detection limit for this device is 7 zg, or ca. 30 Xe atoms. Incredibly, it is suggested that this technology may be combined with nanofluidics for the genetic analysis of the DNA present within a single cell. In comparison, current methods utilize PCR amplification, whereby small samples of DNA are repeatedly replicated in order to facilitate detection. Such analyses will be of use for the detection of genetic markers for cancer or other diseases such as HIV. The ability to identify proteins will be essential for future diagnostic and forensics applications.

Another area of NEMS that is receiving tremendous attention is the mimicry of biological systems, aptly referred to as biomimetics, for instance, in the development of linear molecular muscles that undergoes contraction and extension movements.

Initial work in this field utilized transition metal complexes containing **rotaxanes and catenanes** due to the nondestructive redox processes occurring on the metal centers. Though these complexes were actuated by a chemical reaction, the movement was in a noncoherent manner. In order to better mimic skeletal muscle movement, one has to look at the mode of motion within the most efficient molecular machines in our human bodies.

9.6 Nanotechnologies in Tags

Radio-frequency identification (RFID) is a method of remotely storing and retrieving data using devices called RFID tags. RFID tag is a small, wireless integrated-circuit (IC) chip with a radio circuit and an identification code embedded in it (Figure 9.3a and b). The advantages of the RFID tag over other scannable tags, such as the UPC (Universal Product Code) barcodes pasted on most consumer products today are that the RFID tag is small enough to be embedded in the product itself – not just on its package; it can hold much more information, can be scanned at a distance (and through materials, such as boxes or other packaging), and many tags can be scanned at the same time. A "nanobarcode" is an alternative tagging or monitoring device that works more as the UPC code, but on the nanoscale. One type of nanobarcode is a nanoparticle consisting of metallic stripes, where variations in the striping provide the method of encoding information. The length and width of the particles and the number, width, and composition of each stripe can be changed to make billions and billions of variations. RFID tags are already being used in many ways, for example, for livestock tracking (attached to the ear or injected into the animal) or in the latest e-passports. They are used in libraries, schools, transport systems (toll roads), tickets (parking tickets), sports (race timing), and so on. Developers of the technology envision a world where they can "identify any object anywhere automatically." The current size of the RFID chip is about the size of a dust mite, the smallest is about 50 × 50 µm.

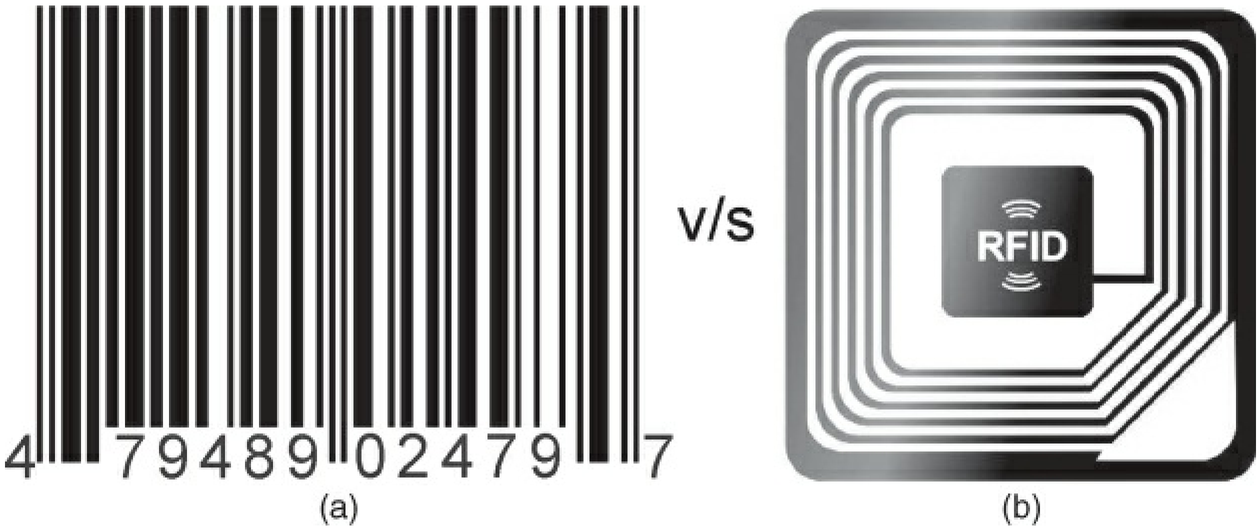

Figure 9.3 Illustration of (a) barcode and (b) the RFID tag.

9.7 Nanotechnology for Environmental Issues

In industrialized nations, the air is filled with numerous pollutants caused by human activity or industrial processes, such as carbon monoxide (CO), chlorofluorocarbons (CFC), heavy metals (arsenic, chromium, lead, cadmium, mercury, zinc), hydrocarbons, nitrogen oxides, organic chemicals (volatile organic compounds, known as VOCs, and dioxins), sulfur dioxide, and particulates. The presence of nitrogen and sulfur oxide in the air generates acid rain that infiltrates and contaminates the soil. The high levels of nitrogen and sulfur oxide in the atmosphere are mainly due to human activities, particularly the burning of oil, coal, and gas. Only a small portion comes from natural processes such as volcanic action and the decay of soil bacteria. Water pollution is caused by numerous factors, including sewage, oil spills, leaking of fertilizers, herbicides and pesticides from land, by-products from manufacturing, and extracted or burned fossil fuels.

Contaminants are most often measured in parts per million (ppm) or parts per billion (ppb) and their toxicity is defined by a "toxic level." The toxic level for arsenic, for instance, is 10 ppm in soil whereas for mercury it is 0.002 ppm in water. Therefore, very low concentrations of a specific contaminant can be toxic. In addition, contaminants are mostly found as mixtures. Consequently, there is a need for technologies that are capable of monitoring, recognizing, and, ideally, treating such small amounts of contaminants in air, water, and soil. In this context, nanotechnologies offer numerous opportunities to prevent, reduce, sense, and treat environment contamination. Nanotechnologies can enhance and enable pre-existing technologies and develop new ones.

What can nanotechnologies do? Nanotechnologies offer the ability to control matter at the nanoscale level to create materials with specific properties that can serve specific functions. This is particularly important in environmental issues where pollution often arises from the presence of a specific contaminant within a mixture of materials in solid, liquid, or gas form. The small size of nanomaterials, together with their high surface-to-volume ratio, can lead to very sensitive detection. These properties allow the development of highly miniaturized, accurate, and sensitive pollution-monitoring devices (nanosensors). Nanomaterials can also be engineered to actively interact with a pollutant and decompose it into less toxic species. Thus, nanotechnology could be used not only to detect contaminated sites but also to treat them. Finally, this technology can be used to reduce the production of harmful wastes in manufacturing processes by reducing the amount of material used and by employing less toxic compounds.

Another application area is the engineering of coatings that are nanostructured in such a way that they resist the attack of pollutants or have self-cleaning properties so that they are easily cleaned by rain water and, therefore, require less detergent to be washed.

9.7.1 Water Purification and Remediation

Only 30% of all freshwater on the planet is not locked up in ice caps or glaciers (not for much longer, though). Of that, some 20% is in areas too remote for humans to access and of the remaining 80% about three-quarters comes at the wrong time and place – in monsoons and floods – and is not always captured for use by people. The remainder is less than 0.08 of 1% of the total water on the planet. The potential impact areas for nanotechnology in water applications are divided into three categories, namely treatment and remediation; sensing and detection; and pollution prevention. Within the category of treatment and remediation, nanotechnology has the potential to contribute to long-term water quality, availability, and viability of water resources, such as through the use of advanced filtration materials that enable greater water reuse, recycling, and desalinization [11]. Within the category of sensing and detection, particular interest is the development of new and enhanced sensors to detect biological and chemical contaminants at very low concentration levels in the environment including water.

Nanotechnology is being fast employed for the fabrication of nanofilters, nano-adsorbents, and nanomembranes with specific properties to be used for decontaminating water and air. As with other applications, it is the ability to manipulate matter at a molecular level that makes nanotechnology so promising in this field, together with the small size and high surface-to-volume ratio of nanomaterials that are employed in the fabrication of these products. In principle, "**nanotraps**" designed for a certain contaminant can be produced, for example, with a specific pore size and surface reactivity. Reactive iron oxide ceramic (ferroxane) membranes are capable of remediating organic waste in water [12].

Filters and membranes can also be engineered to be "active" in the sense of being able not only to trap certain contaminant but also to chemically react with it and convert it to a nontoxic product. For example, a new type of nanofiber has been developed for the removal of microorganisms via filtration that can also kill them on contact. An interesting application of nanomembrane has been developed in the form of a new reverse osmosis (RO) membrane for seawater desalination and wastewater remediation. The membrane is made of a uniquely cross-linked matrix of polymers and engineered nanoparticles designed to draw in water ions but repel contaminants. This is possible due to the nanosize of the holes forming the membrane, which are "tunnels" accessible only to the water molecules. Another distinctive feature of this nanomembrane is its ability to repel organics and bacteria, as a result of the chemical composition of the nanoparticles embedded in the membrane. Compared with conventional RO membrane, these membranes are thus less prone to clogging, which increases the membrane lifetime with an obvious economic benefit.

> **Nanomaterials for water filtration:** Membrane processes are considered key components of advanced water purification and desalination technologies. Nanomaterials such as carbon nanotubes, nanoparticles, and dendrimers are contributing to the development of more efficient and cost-effective water filtration processes. There are two types of nanotechnologically developed membranes: **nanostructured filters**, where either carbon nanotubes or nanocapillary arrays provide the basis for nanofiltration; and **nanoreactive membranes**, where functionalized nanoparticles aid the filtration process. Advances in macromolecular chemistry such as the synthesis of dendritic polymers have provided opportunities to refine, as well as to develop effective filtration processes for purification of water contaminated by different organic solutes and inorganic anions.
>
> **Nanotechnologies for water remediation:** Many areas, especially in developing countries, are seriously contaminated or damaged with consequent impoverishment of natural resources and serious effects on human health. Remediation of contaminated water – the process of removing, reducing, or neutralizing water contaminants that threaten human health and/or ecosystem productivity and integrity – is a field of technology that has attracted much interest recently. In general, remediation technologies can be grouped into categories using thermal, physicochemical, or biological methods. The various techniques usually work well when applied to a specific type of water pollution, though no readily available treatments were discovered that could clean all types of pollutants. Due to the complex nature of many polluted waters, it is frequently necessary to apply several techniques to soil from a particular location to reduce the concentrations of pollutants to acceptable levels. Various nanoparticles and nanomaterials could be used in water remediation: zeolites, carbon nanotubes, self-assembled monolayer on mesoporous supports (SAMMS), biopolymers, single-enzyme nanoparticles, zero-valent iron nanoparticles, bimetallic iron nanoparticles, and nanoscale semiconductor photocatalysts.
>
> **Nanotechnologies for water disinfections:** There is a growing threat of water-borne infectious diseases, especially in the developing world. This threat is rapidly being exacerbated by demographic explosion, a global trend toward urbanization without adequate infrastructure to provide safe drinking water, increased water demand by agriculture that draws more and more of the potable water supply, and emerging pollutants and antibiotic-resistant pathogens that contaminate our water resources. Among the most promising antimicrobial nanomaterials are metallic and metal-oxide nanoparticles, especially silver, and titanium dioxide catalysts for

photocatalytic disinfections.

9.7.2 Nanotechnology for Air Pollution Control

Nanotechnologies offer many innovative strategies to reduce pollution in numerous processes including the reduction of waste in manufacturing processes, a reduction of the use of harmful chemicals, reduced emission of greenhouse-effect gases in fuel combustions, and the use of biodegradable plastics. These are only a few of the many approaches that can be taken to reduce pollution of the environment.

Nanotechnologies are already actively involved in this sector either as a technology producing advanced materials that pollute less or as a method to increase the efficiency of certain industrial processes (e.g., catalytic processes). There are two major ways in which nanotechnology is being used to reduce air pollution [13]: catalysts, which are currently in use and constantly being improved upon; and nanostructured membranes, which are under development.

Catalysts can be used to enable a chemical reaction (which changes one type of molecule to another) at lower temperatures or make the reaction more effective. Nanotechnology can improve the performance and cost of catalysts used to transform vapors escaping from cars or industrial plants into harmless gases. That is because catalysts made from nanoparticles have a greater surface area to interact with the reacting chemicals than catalysts made from larger particles. The larger surface area allows more chemicals to interact with the catalyst simultaneously, which makes the catalyst more effective. **Nanostructured membranes**, on the other hand, are being developed to separate carbon dioxide from industrial plant exhaust streams. The plan is to create a method that can be implemented in any power plant without expensive retrofitting. Table 9.2 lists out some of the commercially available nanomaterials used in reducing air pollution.

Table 9.2 Nanomaterials for Air Pollution Control

Nanomaterials	Application
Manganese oxide nanoparticles	Catalyst to destroy volatile organic compounds (VOCs) in industrial air emissions down to ppb level
Gold nanoparticles embedded in a porous manganese oxide	Room temperature catalyst to break down volatile organic compounds (VOCs) in air
Nanocatalyst containing cobalt and platinum	Remove nitrogen oxide from smoke stacks
Carbon nanotube-based membranes	Removal of carbon dioxide from industrial smoke stacks
Crystals containing nanosized pores	Trapping carbon dioxide emissions
Nano-platinum in catalytic converters	Converting carbon dioxide to methanol; reducing emissions from power plants by converting carbon dioxide into nanotubes
Nanocomposite catalyst for use in automotive catalytic converters	Reduce cost due to lower platinum usage

9.8 Energy

Today, the world's energy demands are satisfied mainly via the combustion of fossil fuels. Of the 210 million barrels of oil equivalent per day used worldwide, about 85 million barrels come from oil; the rest comes from coal (23%), gas (17%), biomass (17%), some fission (5%), a small amount from hydroelectric power (6%), and almost none from renewable resource. It is estimated that by 2050, twice the amount of energy that is burned or consumed today (about 14 TW, terawatts) will be needed.

Because of the limited availability of fossil fuel, the world is presently facing an “energy challenge” and there is an urgent need for alternative energy resources to fossil fuels. Of these, renewable energy sources that are natural solar, wind, geothermal, hydro, and so on are an option. Solar energy is an excellent example. Every day, the Earth is hit by 165,000 TW of solar power; in the words of Nobel Prize winner Richard E. Smalley, every day “we are bathed in energy.” However, the problem is that renewable energy sources such as solar energy are not constant in time and evenly distributed geographically. Therefore, solar energy collection, conversion, storage, and distribution are major challenges. Current solar panels have about 15–20% energy conversion efficiency and they are very expensive. Since solar light is only available during part of the day, suitable storage solutions also need to be found. Another alternative energy carrier is hydrogen, but hydrogen fuel cell technology still faces a number of issues (e.g., hydrogen extraction, hydrogen storage, fuel cell lifetime, and cost) before a hydrogen economy can become a reality. Solving the future energy challenges requires not only advances in the field of energy conversion and storage but also energy savings, considering how much energy is wasted today using conventional incandescent lights. Nanotechnology has the potential to solve many of the issues that the energy sector is facing.

It is in this context that nanoscience and nanotechnology are poised to play a transformative role in providing clean and sustainable energy from secure domestic resources. With control of phenomenon arising out of nanoscale, it is expected to realize new technologies such as low-cost photovoltaics for solar power generation, new classes of batteries for both transportation and grid-connected energy storage, efficient low-cost methods of converting both solar and electrical energies into chemical fuels, new catalysts, and catalyst systems enabling artificial photosynthesis and utilization of CO_2 as a feedstock, ultrahigh surface area materials for energy storage, new membranes for applications such as water and gas purification, and improved thermoelectric and electrocaloric devices for more efficient conversion between heat and electricity [14].

9.8.1 Photovoltaic Technologies for Solar-Energy Harvesting

Solar energy is by far the most abundant exploitable renewable energy resource. More energy is provided to the earth by sunlight irradiation (solar spectrum on earth's surface is illustrated in Figure 9.4a and b) within 1 h than is consumed by human society globally in 1 year. Semiconductor materials that exhibit a photovoltaic (PV) effect can be used to convert solar radiation into electricity through a photovoltaic process. PV technology has been growing and expanding rapidly. The total global energy production by PV processes has reached close to 100 GW (1 GW = 10^9 W). Despite this considerable capacity, however, PV technology only accounts for 0.1% of electricity generation globally, largely as a result of the inability of existing PV technologies to produce electricity with an efficiency that fulfills the grid parity set by conventional power-generation routes.

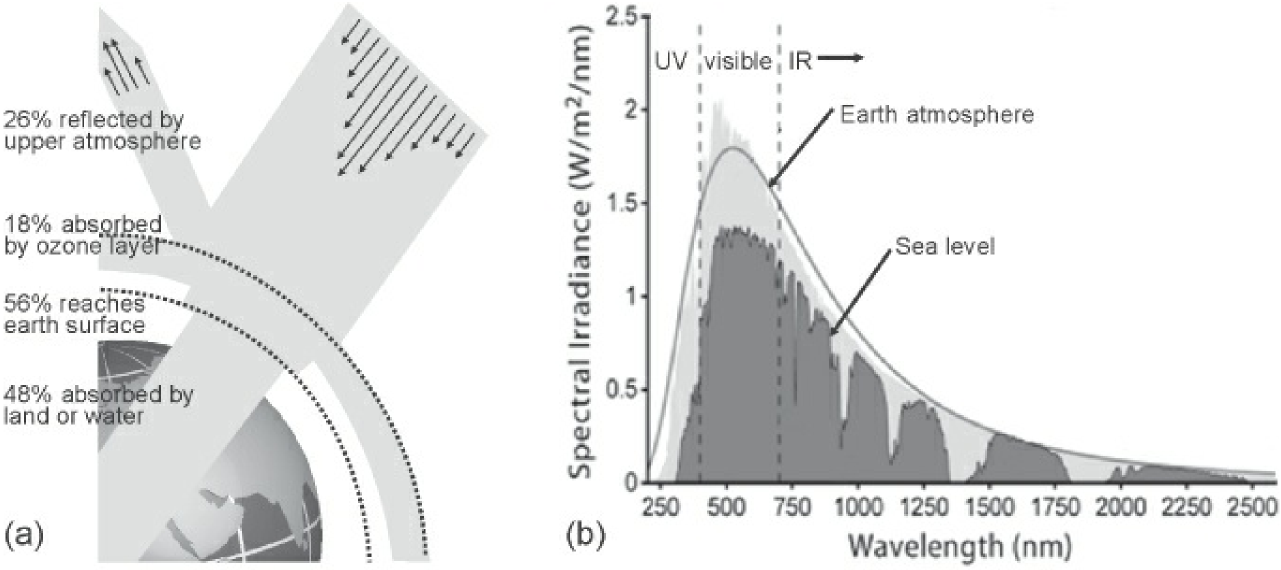

Figure 9.4 (a) Solar radiations reaching to earth surface; (b) solar spectrum.

Practically all PV devices, or solar cells, incorporate a p–n junction. Such junctions occur in various possible configurations. Solar cells containing multiple p–n junctions have recently been investigated intensively for the more efficient absorption of light with different wavelengths with the aim of reducing the inherent sources of energy loss in conventional single-junction cells. A conversion efficiency of 42.3% was achieved by combining multijunction cells and concentrator technology. However, the high efficiency of multijunction cells is offset by their increased complexity and manufacturing cost, which limit their application mainly to aerospace exploration, for which a high power-to-weight ratio is desirable. Some latest developments in PV devices using semiconducting nanomaterials are enumerated [15, 16] here.

9.8.1.1 Dye-Sensitized Solar Cells (DSSC)

Dye-sensitized solar cell is a **thin-film solar cell**, representing a **photoelectrochemical** cell. Modern version of dye-sensitized solar cell (DSSC) is invented by Michael Grtzel and coworkers in 1991. During the past two decades, the efficiency of DSSC could be improved by optimizing the porosity of the electrode prepared from fine oxide powder; however, the instability needs to be addressed.

Dye-sensitized solar cells comprising two electrodes, the photo anode and the counter-electrode, in a sandwich arrangement are shown in (Figure 9.5). The photo anode is a conducting glass covered by a mesoporous and nanocrystalline TiO_2 film, sensitized by the dye sensitizers, which is one of the most important components of this device since it is responsible for the sunlight harvesting and electron injection, the first steps of energy conversion. 2,2-Bipyridine ruthenium salts are used as dye sensitizers. The counter-electrode is a conducting glass covered by a thin film of catalyst, such as platinum or graphite. Between these electrodes is placed a mediator layer, usually a solution of I_3^-/I^- in nitriles. In order to promote the energy conversion, the sunlight is harvested by the dye sensitizers leading to an excited state capable of injecting an electron into the semiconductor conducting band. The oxidized dye is immediately regenerated by the mediator and the injected electron percolates through the semiconductor film, reaches the conducting glass, and flows by the external circuit to the counter-electrode. The counter-electrode is responsible for regenerating the oxidized species of the mediator, reducing it by a catalyzed reaction using electrons from the external circuit. Since there is no permanent chemical change for dye-sensitized solar cells, the estimated lifetime of these devices is 20 years.

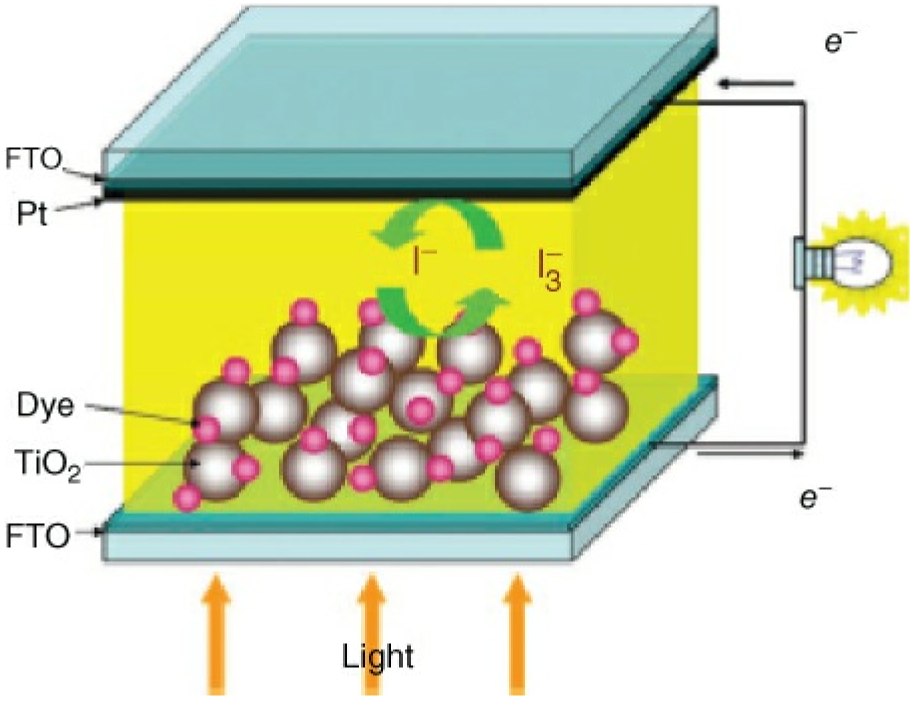

Figure 9.5 Typical sandwich-type dye-sensitized TiO_2 nanocrystal solar cell.

O'Regan and Gratzel [15], © 1991. With permission of NPG.

A 3D network of randomly dispersed TiO_2 nanoparticles has typically been adopted as the photo anode in DSSCs since their first introduction. The disordered network of TiO_2 nanoparticles presents numerous grain boundaries and hence multiple trapping sites. These trapping sites not only promote the increased recombination of electrons but also hinder the collection of the excited electrons and thus compromise the overall conversion efficiency. To overcome these problems, structural configurations with higher degrees of order than the random assemblies of nanoparticles are expected to facilitate the transport/collection of electrons and hence improve the efficiency of solar cells. As an alternative to disordered network of TiO_2 nanoparticles, rapid progress has also been made in the application of ZnO nanomaterials as transparent photo anodes in DSSCs. The coupled piezoelectric, semiconductor, and photo-excitation properties of ZnO together with the straightforward methods available for the synthesis of various ZnO nanostructures at low temperatures could potentially facilitate the wider application of ZnO in DSSCs.

One-dimensional nanostructures have been investigated intensively and utilized in all types of PV devices mentioned earlier. For example, energy-conversion efficiencies of about 10% and 3% have been reported for DSSCs based onTiO_2 NWs and ZnO NWs, respectively. A solar cell based on an array of Si NWs with a projected efficiency of 17.4% and another based on an array of InP nanopillars with an efficiency of 8.1% have also been demonstrated. Moreover, the performance of solar cells based on NW arrays has been improved strategically by enhancing dye adsorption and reducing surface recombination.

Novel strategies, such as the integration of ZnO or TiO_2 nanowires with 3D optical fibers or planar waveguides, have been shown to address issues such as insufficient internal surface area and deficient dye loading, which are shortcomings of DSSCs based on 1D nanostructures. Such strategies offer the potential for the manufacture of DSSCs with high flexibility, adaptability, and enhanced efficiency for concealed applications. DSSCs could be suitable for powering distributed micro-/nanosystems (MNSs) for self-sufficient, maintenance-free applications, since ideally DSSCs convert sunlight into electricity in a self-sustainable manner, without suffering any permanent chemical transformation or consumption of the materials in the system.

9.8.1.2 Semiconductor Quantum Dot-Sensitized Solar Cells (QDSCs)

Because traditional photovoltaic devices (i.e., the p–n junction silicon crystalline solar cells) suffer from high costs of manufacturing and installation, now the focus is on the next generation of solar cells with high efficiency at economically viable costs. As a cost-effective alternative to silicon-based photo-voltaic, semiconductor quantum dot (QD)-sensitized solar cells (QDSCs) have attracted considerable attention recently and have shown promising developments for the next generation of solar cells. QDSCs can be regarded as a derivative of dye-sensitized solar cells (DSCs). In DSCs, the sensitizer commonly uses organic dyes of ruthenium polypyridine complexes. It has always been a challenge to obtain an ideal organic dye as a sensitizer to absorb photons in the full sunlight spectra. For this reason, narrow-band-gap semiconductor QDs, such as CdS , CdSe, PbS, and InAs, have been used as the photosensitizer instead of organic dyes due to their versatile optical and electrical properties, including (1) a tunable band gap depending on the QD size, (2) a larger extinction coefficient, (3) higher stability toward water and oxygen, and (4) multiple exciton generation (MEG) with single-photon absorption. The theoretical photovoltaic conversion efficiency of QDSCs can reach up to 42% in view of the MEG effect of QDs. Such efficiency is much higher than the rate of 31% according to the Schockley–Queisser limit. Figure 9.6a and b shows the cell structure of a QDSC, which consists of a wide-band-gap mesoporous oxide film (a photoelectrode, such as the commonly used TiO_2 or ZnO), QDs (the sensitizer), an electrolyte, and a counter-electrode. During operation, photons are captured by QDs, yielding electron–hole pairs that are rapidly separated into electrons and holes at the interface between the nanocrystalline oxide and QDs. The electrons jump into the oxide film, and the holes are released by redox couples in the electrolyte.

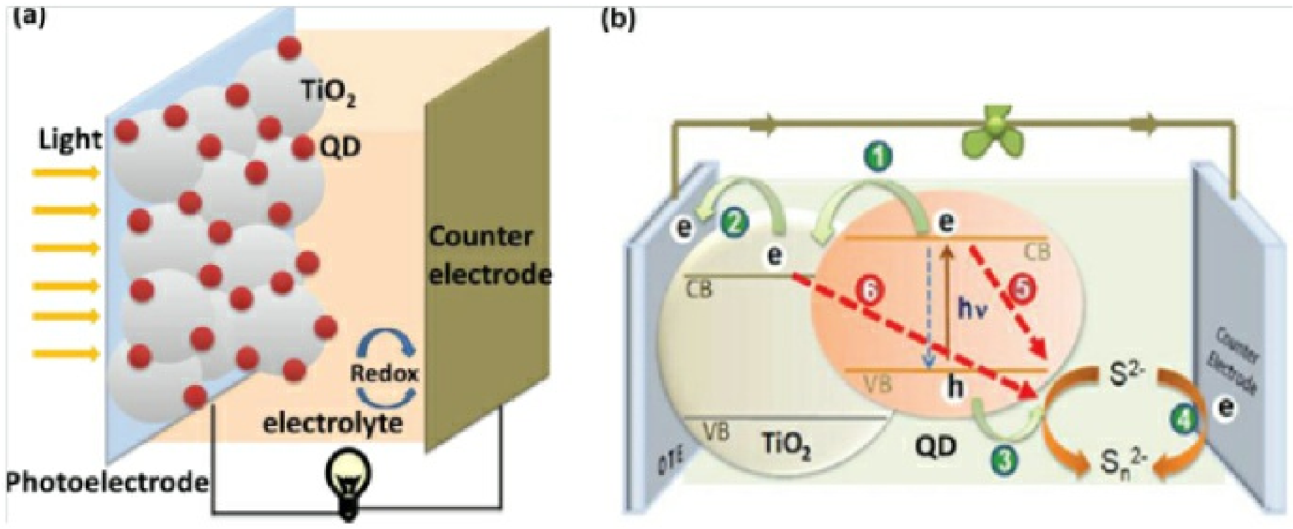

Figure 9.6 Schematic illustration of the structure of (a) quantum dot sensitized solar cell (QDSC) and (b) photoinduced charge transfer processes following a laser pulse excitation. Kamat [16], © 2013. With permission of ACS.

9.8.1.3 Nanostructured Organic–Inorganic Hybrid Solar Cells: Heterojunction Solar Cells

Almost all solar cells installed today are made of crystalline silicon. The production of these cells is growing by approximately 35% each year, and the costs are dropping as the industry matures. Very soon the electricity from solar cells will be cheaper than obtaining it from conventional power plants in certain areas, where sunlight is abundant and electricity is expensive. This is great news for those of us striving to reduce carbon emissions. Nonetheless, it is irresistible to dream of even better technologies, for example, making solar cells in roll-to-roll coating machines similar to those used to make photographic film or newspapers. Such cells would be thin and flexible and could be incorporated directly into roofing shingles in order to reduce packaging and installation costs.

Although considerable progress has been made in improving the PCEs of fully solid-state semiconductor-sensitized solar cells (discussed in the above-mentioned section), these cells still suffer from low performance, mainly because of rapid carrier recombination at the various device interfaces.

Motivated by the goal of fabricating stable, high-efficiency, and cost-effective solid-state solar cells, a number of inorganic–organic heterojunction solar cells have been fabricated and studied for their performance [17]. Notable example among them is the use of inorganic–organic perovskite compounds ($CH_3NH_3PbI_3$) as light harvesters on mesoporous (mp)-TiO_2, and poly-3-hexylthiophene (P3HT), poly-[2,1,3-benzothiadiazole-4,7-diyl[4,4-bis(2-ethylhexyl)-4H-cyclopenta[2,1-b:3,4-b′]dithiophene-2,6-diyl]] (PCPDTBT), (poly-[[9-(1-octylnonyl)-9H-carbazole-2,7-diyl]-2,5-thiophenediyl-2,1,3-benzothiadiazole-4,7-diyl-2,5-thiophenediyl]) (PCDTBT), and poly-triarylamine (PTAA) as organic hole-transport materials (HTMs) or electron-blocking layers.

Because the interfacial charge separation is the critical step in the whole photovoltaic process, the larger the interfaces, the more the opportunity for the excitons to reach the interfaces, and probably the higher the conversion efficiency. Therefore, most of the hybrid photovoltaic materials that have been studied are nanostructured composites. There are many types of nanostructures, including particles, rods, tubes, tetrapods, sheets, needles, and porous network, and the way to mix the components together can be either disordered or ordered as shown in Figure 9.7a–c.

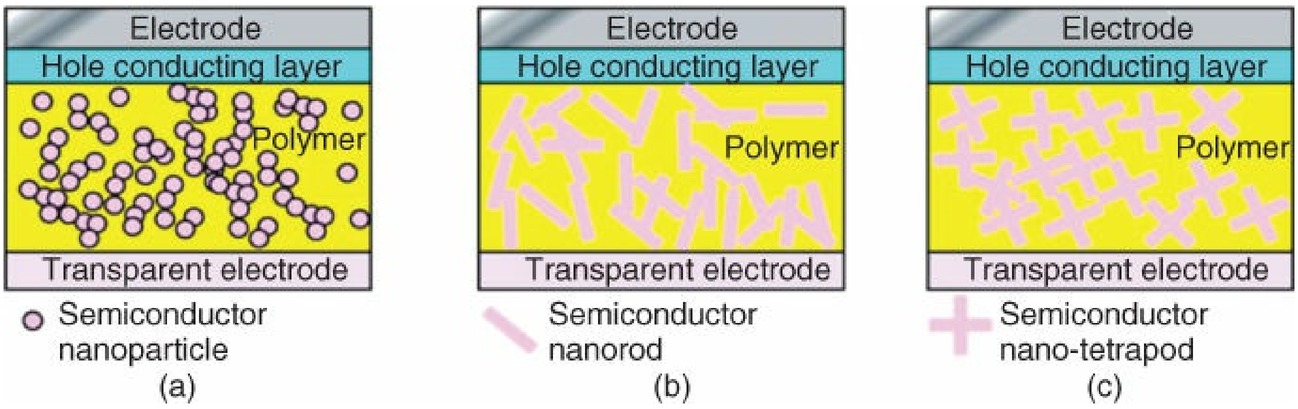

Figure 9.7 Nano-architectures of hybrid solar cell materials. (a) Blend of semiconductor nanoparticles and conducting polymer films; (b) blend of semiconductor nanorods and conducting polymer films; (c) blend of semiconductor nano-tetrapods and conducting polymer films. Courtesy of Liu [17].

9.8.2 Artificial Photosynthesis: Production of Solar Fuel

The conversion of light into stored chemical energy by artificial photosynthesis, a chemical process which replicates natural photosynthesis, has been the focus of much recent attention. Photoelectrolysis, or water splitting, is a form of artificial photosynthesis that converts water into hydrogen and oxygen through the use of sunlight. An artificial photosynthetic system for producing solar fuel typically requires antenna/reaction center complexes for the generation of electrochemical potential from sunlight and appropriate catalysts for the oxidization of water and reduction of precursors to hydrogen. Considerable progress has been made in the design of technologies that mimic natural photosynthesis and the development of efficient water-splitting technology [18]. Efforts have also been focused on the engineering of new materials to optimize processes at both anodes and cathodes and the integration of photoelectrolysis cells with other structures, such as PV cells, which can provide additional voltage to drive the water-splitting reactions and hence increase overall efficiency.

There has been an increasing interest in the use of nanostructured materials as the photo anodes in photosynthesis applications as a result of the benefits offered by the large surface area, short lateral diffusion length, and low reflectivity. The use of structured photo electrodes based on semiconductor NWs with a preferred band gap or an intermediate energy level introduced within the band gap has also been investigated in efforts to improve the water-splitting efficiency through enhanced light absorption in the visible region of interest and enhanced electron-transfer efficiency due to the single-crystalline nature of low-dimensional semiconductor nanostructures. The creation of high-aspect-ratio photo electrode surfaces by engineering the morphology of nanostructures also enables the use of less expensive catalysts with lower catalytic activities. Furthermore, the ability to both modulate the composition of nanomaterials at the atomic scale and synthesize nanostructures of various morphologies in a controlled manner is likely to improve conversion efficiency in artificial photosynthesis applications through more effective management of the light absorption. It is expected that artificial photosynthetic systems will play an important role in providing sustainable and clean energy to MNSs in applications such as environmental monitoring and remote sensing. Thus, the ability of artificial photosynthetic systems to convert harvested solar energy into fuel and store it in the system for later applications will enable the operation of self-powered MNSs.

9.8.3 Thermoelectric Energy

In the current environmental climate, energy needs to be conserved and recycled as much as possible to prevent wastage – every joule saved means less fossil fuel burnt. Harvesting waste energy has become a popular target for researchers and scientists, who are coming up with innovative techniques to achieve this. One of the most promising is nanotechnology-based thermoelectric devices, which look to be a promising approach to save energy [19]. Thermoelectric power generation represents a class of energy conversion technology, which has been used in power supply of aeronautic and astronautic exploring missions, now showing notable advantages to harvest the widely distributed waste heat and convert the abundant solar energy into electricity at lower cost than Si-based photovoltaic technology. Thermoelectric dimensionless figure of merit (**ZT**) plays a key role in the conversion efficiency from thermal to electrical energy. Thermoelectric materials generate a current when placed in a temperature gradient as a consequence of charge carrier diffusion from the hot to the cold side, thus allowing the regeneration of waste heat into electricity.

The direct conversion of heat into electricity, or electricity into heat, is known as **thermoelectricity**. This conversion process is referred to as the **Peltier–Seebeck effect**, named after two physicists – Jean Peltier and Thomas Seebeck. Peltier discovered that current sent into two different electrical conductors that are connected at two junctions will result in heating up of one junction while the other junction cools down. Peltier went on to demonstrate that a drop of water can be made to freeze at a bismuth–antimony (BiSb) junction by just reversing the current. Peltier also discovered that electric current can be made to flow when a temperature difference is placed across a junction of different conductors. Thermoelectric materials generate a current when placed in a temperature gradient as a consequence of charge carrier diffusion from the hot to the cold side, thus allowing the regeneration of waste heat into electricity. Thermoelectricity is an extremely interesting source of electric power because of its ability to convert heat flow directly into electricity. Thermoelectric devices (Figure 9.8) are energy converters that are easily scalable and have no moving parts or liquid fuels, making them applicable in almost any situation where a large quantity of heat tends to go to waste from clothing to large industrial facilities. Although thermoelectric materials have been known and understood for quite sometime, they have so far not been efficient enough to use commercially.

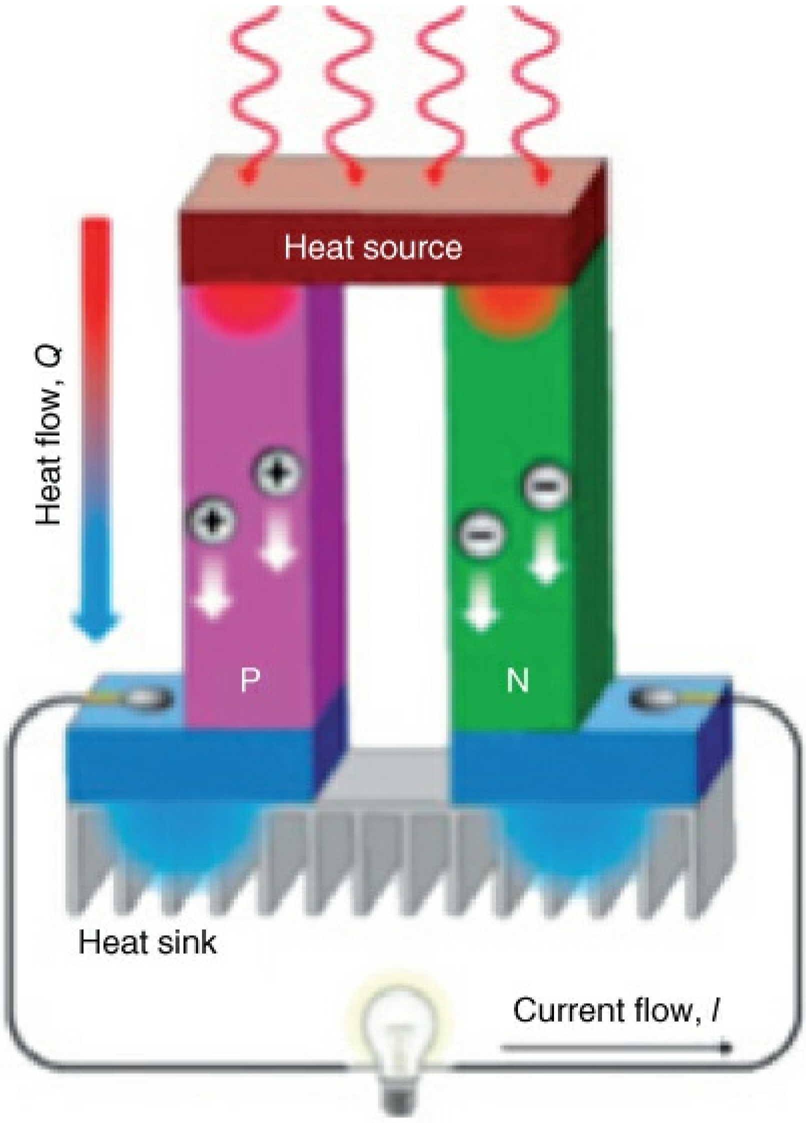

Figure 9.8 Thermoelectric devices.

Li et al. [19], © 2010. With permission of NPG.

A number of research groups have been investing their efforts in finding the perfect material with appropriate properties to create an efficient thermoelectric effect, and nanomaterials seem to fit the bill. Nanostructures used in materials are expected to maintain good electrical conductivity and reduce thermal conductivity of the material thus leading to improvements in ZT. The usage of nanostructures smaller than the wavelength of light enhances the scattering of photons and thus decreases thermal conductivity. Decrease in thermal conductivity seems to be the most vital benefit of nanostructuring for thermoelectric materials. The performance of thermoelectric devices can thus be enhanced with the use of nanotechnology-based materials that have improved thermoelectric properties and good solar energy absorption abilities. Most state-of-the-art thermoelectric materials are characterized with various nanostructures from fine grains, dispersed particles, nanoinclusions to atomic defects, and therefore are referenced as nanocomposite. Recently, remarkable advances have been achieved in various material systems through the introduction of different nanostructures to tune the transport of phonons and electrons.

Thermoelectric (TE) materials based on bismuth telluride are best suited for room temperature applications with ZT (figure of merit) of ~1. Carbon nanotubes, graphene, semiconductor nanowires (NWs), PbTe, $CoSb_3$, Bi_2Te_3, and so on are other nanomaterials showing improved thermoelectric properties. Among these low-dimensional TE materials, silicon NWs with small diameters exhibit interesting and promising TE properties, with a reported ZT value of 0.6 at room temperature and a ZT value approaching those of commercial devices at 200 K. Uniformity in TE conversion and other properties of the as-fabricated nanomaterials remain another practical issue that needs proper attention before these nanomaterials can be implemented in any practical applications for TE energy harvesting.

9.8.4 Piezoelectric Nanomaterials

A nanogenerator is a device that harvests external mechanical energy and converts it into electricity as a result of bending or stretching nanostructured piezoelectric materials such as zinc oxide nanowires [20]. Piezoelectric is a term that comes from pressure and electricity (Figure 9.9). While walking, mechanical force generated is captured or harvested to generate the energy that can be stored in a pill or small watch battery embedded in a shoe sole for further use. The mechanical energy may be provided in a countless number of ways, for example, virtually any body movement, a rolling tire, vibrations, or airflow. Nanogenerators capable of powering commercial liquid-crystal displays or light-emitting diodes have been demonstrated.

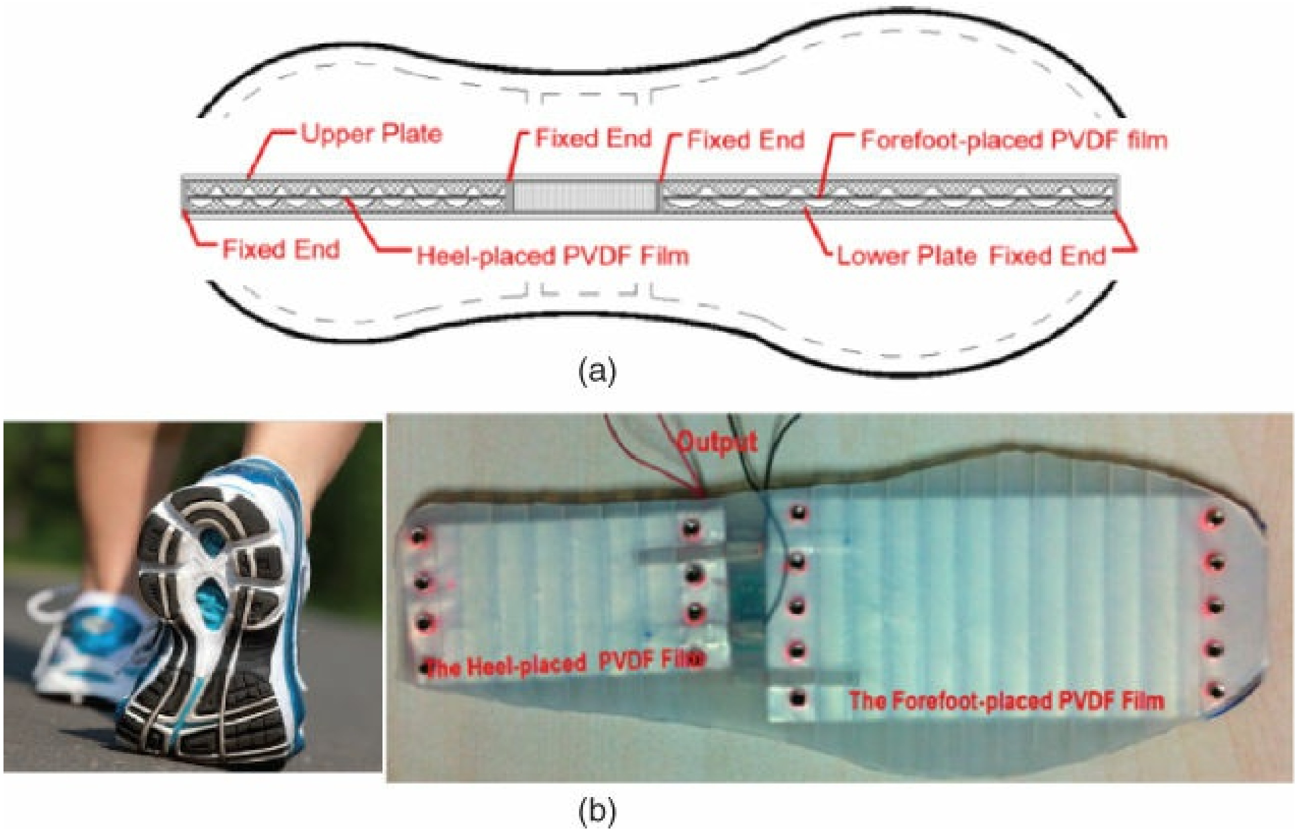

Figure 9.9 (a, b) Nanowires made of piezoelectric materials embedded in shoe sole to generate electricity from mechanical motion such as a human walking or running. http://www.mdpi.com/1424-8220/14/7/12497. Used under CC-BY 3.0. http://creativecommons.org/licenses/by/3.0/.

9.8.5 Hydrogen Generation and Storage

9.8.5.1 Fuel Cell

The idea of a fuel cell was first conceived in 1839 by Sir William Grove who thought that electricity could be produced by reversing the process of electrolysis, in which hydrogen and oxygen are combined to produce electricity, with water and heat as a by-product through an electrochemical reaction. Thus, a fuel cell, which is an electrochemical device, will continue to generate power as long as its fuel, hydrogen and oxygen, is supplied. Hydrogen (H_2) can, in principle, be a future environmentally friendly energy carrier when it is produced from renewable energy. The ideal scheme would be to produce hydrogen by splitting water molecules using solar light. Hydrogen could then be used as an energy carrier to provide electricity in our homes, fuel our cars, and so on. Hydrogen fuel cells, Figure 9.10, use hydrogen and oxygen as fuel to generate electricity. The fuel molecules in the cell must be ionized to react. The ionization must be catalyzed by the electrodes, and an electrolyte must conduct the formed ionic species so that they can react. The subproduct of this reaction is only water, no CO_2 is produced during the conversion of hydrogen to electricity. The result of the electrochemical process is a maximum of 1.2 V and 1 W/cm^2 of power.

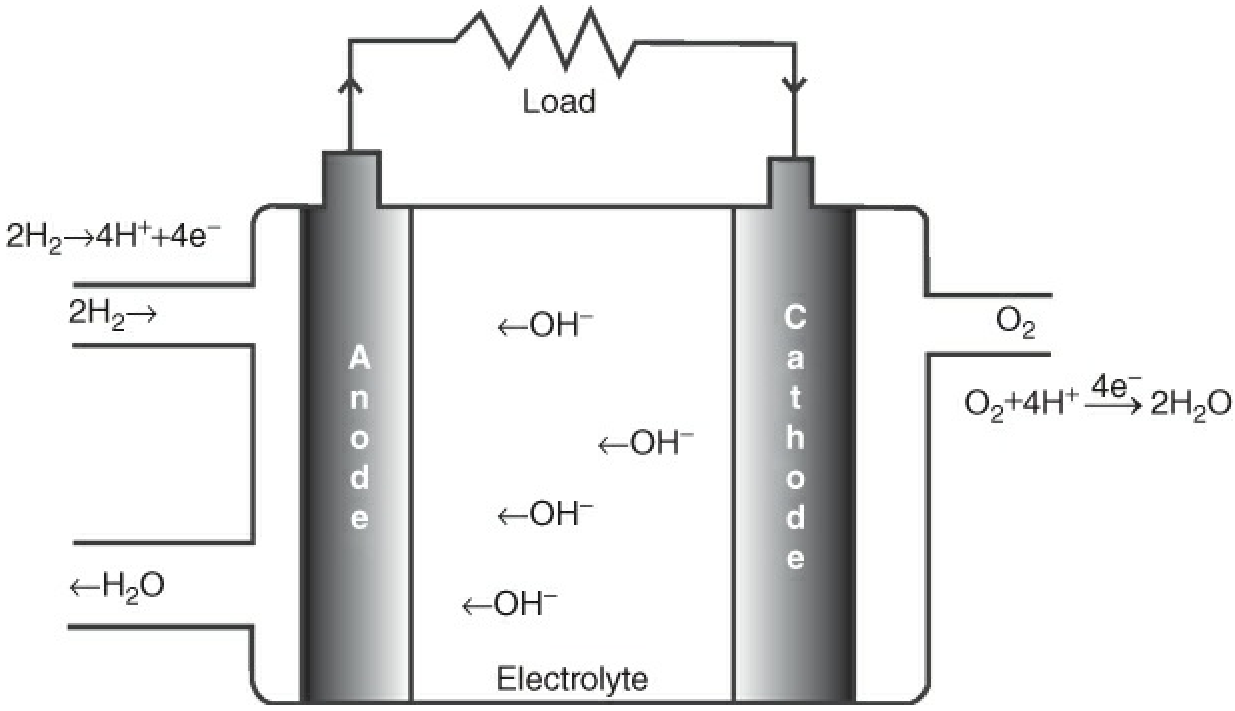

Figure 9.10 Schematic representation of a fuel cell.

http://www.epa.gov/fuelcell/basicinfo.htm.

The three fundamental elements of a hydrogen fuel cell are, therefore, the fuel (H_2 and O_2), the catalyst, and the electrolyte. In order for hydrogen fuel cells to become an economically viable alternative to combustion chambers, two other main problems need to be addressed: the **nature of the catalyst** and that of the **electrolyte** in the cell. Currently, the electrodes in a fuel cell are made of a metal such as platinum (Pt), which is a rare, expensive metal, also sensitive to the CO and sulfur species that are dispersed in the atmosphere. These deactivate the platinum surface (a phenomenon called "poisoning of the catalyst"). Fuel cells operate at high temperatures (>70 °C) since the poisoning agents at these temperatures tend to de-adsorb. Nanotechnology is already actively involved in addressing some of the issues concerning fuel cell catalysts [21]. Improvements in this area through nanotechnology concern (1) increasing the material catalytic activity and (2) reducing the use of rare metals. Since the current generated at an electrode is proportional to the active surface of the catalyst, fuel cells that have higher power density can be formed from nanomaterials, which have a higher surface-to-volume ratio. Properties of electrocatalytic material are also proportional to particle size, so nanoparticles and nanomaterials have increased catalytic activity compared to bulk materials. This characteristic can lead to a reduction in the use of rare metals, for example, by using carbon nanomaterials as a support for the dispersions of nanosized platinum, thereby reducing the weight of platinum needed to produce the same surface area of active Pt catalyst. Carbon nanomaterials are particularly suitable since they act both as a support for the platinum nanomaterials and as a conductor. Suitable carbon nanomaterials are carbon foams containing nanopores, different types of nanotubes and single-walled nanohorns are likely on a large scale.

One of the most promising methods of hydrogen generation is its photochemical extraction from water using sunlight. The idea is to use sunlight to split water into hydrogen and oxygen, but to make it happen artificially is a real challenge. In principle, visible light at wavelengths shorter than 500 nm has enough energy to split water into hydrogen and oxygen. However, water is transparent to this visible range and does not absorb this energy. Therefore, the combination of a light-harvesting system with a water-splitting system is necessary to implement the use of sunlight to split water.

Basically, photovoltaic and photo-induced water splitting implements the same concept of using sunlight to excite electrons but they differ in how the excited electron (e–h pairs) are used: to drive a current (in PVs) or to drive a chemical redox reaction (in photo-induced water splitting). Nanotechnology is leading the way in solving some of the problems associated with solar energy conversion with the introduction of nanostructured materials that have high solar energy absorption rates. Titanium dioxide (TiO_2) nanotube arrays having a modified band gap have been developed for generating hydrogen by splitting water using sunlight. The second problem in photo-induced water splitting is the fast electron–hole recombination, which lowers the efficiency of the process. In simple terms, photocatalysis involves harvesting solar photons in a semiconductor (the TiO_2 surface) and subsequent conversion of these photons to electronic excitations, which then induce the desired water-splitting reaction. The excited electron–hole pair, though, has a high tendency to recombine. Nanostructures offer the opportunity to minimize the distances (and thus the times) over which charges have to survive and be transported after excitation. Deposition of small noble metal islands (<5 nm) or metal nanoparticles enhances the photocatalytic activity of systems that use TiO_2 as the photocatalytic surface. This effect is due to the charge separation across the metal–semiconductor interface. Hydrogen (H_2) can, in principle, be a future environmentally friendly energy carrier when it is produced from renewable energy.

9.8.5.2 Hydrogen Storage

The combustion of hydrogen is straightforward with no detrimental by-products:

$$2H_2 + O_2 \rightarrow 2H_2O$$

However, a problem exists that relates to its storage and transport, which need to be both efficient and safe. The problem is easily seen by comparing the energy-to-volume ratio for gaseous hydrogen (3.0 MJ/l) to that of conventional gasoline (32.0 MJ/l). This means that, given the same volume, the energy produced by hydrogen is about 10 times lower than that from conventional gasoline. This obviously represents a problem for storing hydrogen in a vehicle: a big, heavy tank would be required to store and transport the required amount of hydrogen. Some possible solutions are to use liquid hydrogen (8.5 MJ/l), compressed hydrogen, or to store hydrogen in a solid metallic support such as metal complexes (hydrides).

The use of compressed hydrogen implies using liquid tanks that must be made of a very strong yet lightweight material. This material should also have outstanding insulating and pressurization properties in order to avoid hydrogen leakage. This problem can potentially be solved using nanotechnology to develop new materials with exceptional properties in terms of strength and density. Nanotechnology can contribute in this field by developing new molecules that allow high hydrogen-loading capacity and acceptable regeneration kinetics. Researchers aim to develop nanomaterials that are light in weight and low in volume, have high loading capacities and good regeneration kinetics, and are low in cost.

Two candidate materials are complex metal hydrides, such as $LiBH_4$, $NaBH_4$, $LiAlH_4$, and $NaAlH_4$, which have an intermediate bonding of hydrogen and nanostructured carbon-based materials, such as carbon nanotubes, and graphene [22]. Figure 9.11 shows the schematic representation of Facile Cycling of Ti-doped lithium aluminum hydride ($LiAlH_4$).

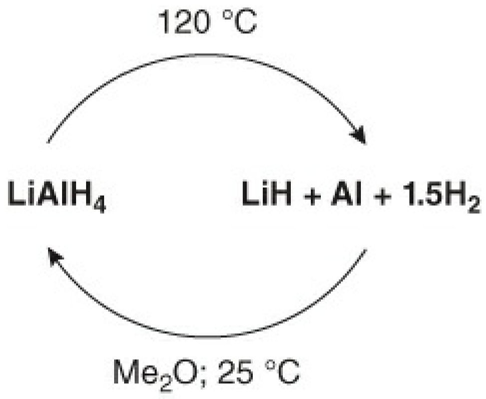

Figure 9.11 Schematic representation of facile cycling of Ti-doped $LiAlH_4$ for high-performance hydrogen storage.

9.8.6 Batteries

A battery is a device that covert chemical energy into electrical energy. There are two types of batteries, namely primary and secondary (rechargeable). In simple terms, a battery is an electrochemical device that generates direct current through a coupled set of reduction–oxidation (redox) reactions. The positive electrode is reduced (captures electrons) and the negative electrode is oxidized (releases electrons). The battery consists of a positive electrode facing a negative electrode divided by a porous separator, which prevents the electrodes from touching, and an ionic electrolyte, which is a conducting medium that ensures movement of the ions from one electrode to the other. Nanotechnology may offer the following benefits in the manufacture of batteries, which are as follows:

- Reducing the possibility of batteries catching fire by providing less flammable electrode material.
- Increasing the available power from a battery and decreasing the time required to recharge a battery. These benefits are achieved by coating the surface of an electrode with nanoparticles. This increases the surface area of the electrode, thereby allowing more current to flow between the electrode and the chemicals inside the battery. This technique could increase the efficiency of hybrid vehicles by significantly reducing the weight of the batteries needed to provide adequate power.
- Increasing the shelf-life of a battery by using nanomaterials to separate liquids in the battery from the solid electrodes when there is no draw on the battery. This separation prevents the low-level discharge that occurs in a conventional battery, which increases the shelf-life of the battery dramatically.

Applications of batteries range from mobile phones and personal computers, to electronic vehicles, hybrid vehicles, power tools and backup power systems. In all the cases, high power and light weight are important. Some of commercially available batteries based on nanotechnology are given in Table 9.3.

Table 9.3 Nanomaterials Based Commercially Available Batteries

Product	Advantages
Battery with chemicals isolated from electrode by "nanograss" when the battery is not in use	Very long shelf-life
Silver–zinc battery using nanoparticles in the silver cathode	Higher power density, low combustibility
Lithium-ion battery with the cathode made from a nanoporous phosphate structure	Higher power, quicker recharge, less combustible than standard lithium-ion batteries
Lithium-ion battery with the anode composed of lithium titanate spindle nanoparticles	Higher power, quicker recharge, less combustible than standard lithium-ion batteries

9.8.6.1 Lithium-Ion Batteries

Intercalation-based batteries using the small lithium (Li^+) ion are the most used electrode material. These batteries have at least one redox-active electrode with an open crystal structure with holes capable of intercalating Li^+. Graphite has been the preferred anode material for Li-ion batteries due to its relatively high capacity, good cyclability, and low redox potential versus lithium metal. Intercalation/deintercalation of Li^+ in and out of the graphite upon charge/discharge forms the basis of graphite as the anode of the battery (Figure 9.12). The thermodynamic equilibrium saturation concentration of the graphite is LiC_6 corresponding to a theoretical capacity of 372 mA h/g. To achieve higher energy density for advanced Li-ion batteries, new anode materials with higher capacity are needed. In addition, the graphite anode limits the recharge rates of Li-ion batteries. CNTs are attractive host anode materials for Li^+ intercalation.

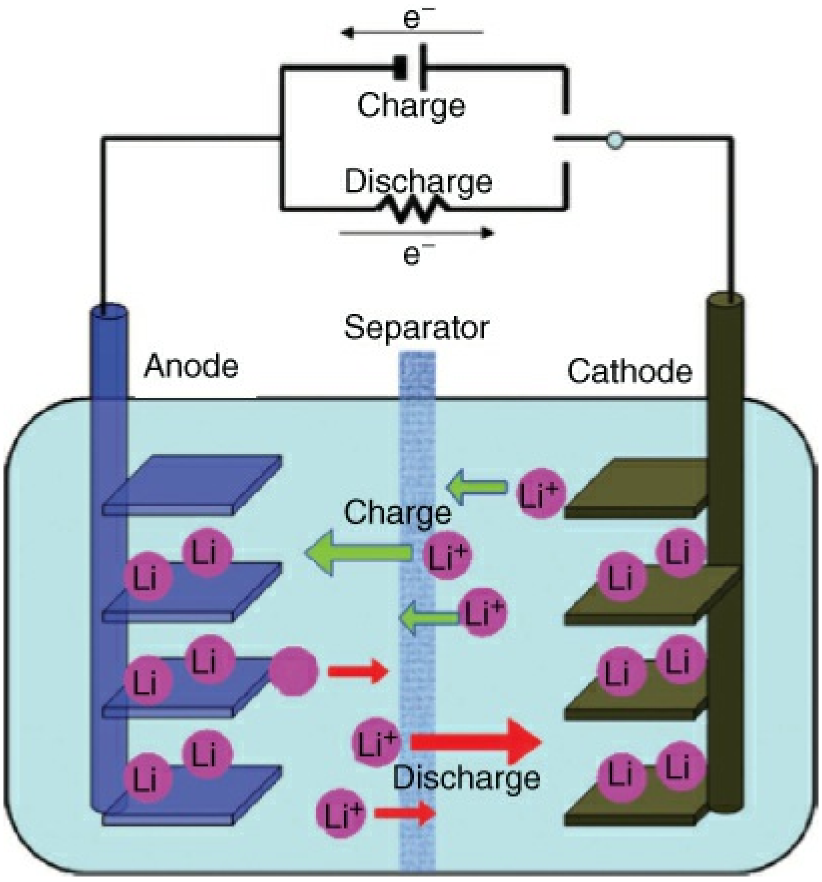

Figure 9.12 Schematic representation of a lithium-ion battery.

Dai et al. [22], © 2012. With permission of Wiley VCH Verlag.

For example, oxidation of cobalt in $LiCoO_2$ expels Li^+, which is taken up in a graphite electrode. When the battery is charged, the Li^+ moves from the positive electrode to the negative electrode via the electrolyte. On discharge, the opposite occurs, releasing energy in the process. Ideally, the structure of the redox-active crystal should be capable of reversibly intercalating the small Li^+ ion. Current problems with lithium rechargeable batteries involve a number of issues, the first being the energy capacity of the battery: in order to allow ions and electrons to move quickly into and out of the active material (allowing fast charging and discharging), the material must be deposited as a thin film. This limits the amount of active material that can be incorporated into the battery (energy capacity). For high-capacity batteries, thickness is increased in order to provide more energy storage but with the drawback of slower charging. The second issue concerns the battery power: an important attribute of large format batteries is their capability to deliver power quickly. Power is restricted by the ion removal capability in lithium batteries, which depends on the electrochemical properties of the battery. Then there is the problem of charge rate: batteries need to be recharged, and recharging times are now in the order of hours. The time of charge is restricted by the incorporation rate capabilities of Li^+ inside the graphite electrode. Lifetime of lithium battery also needs to be improved: in current batteries, every time Li^+ enters/exits the graphite electrode, the pores of the electrode need to expand or shrink. This repeated expansion and shrinkage fatigues the graphite particles, which break apart as a result, reducing battery performance.

9.8.6.2 Current Developments in Lithium Ion Batteries

Various types of nanomaterials as catalyst and anode/cathode materials have been studied to improve the characteristics of lithium-ion batteries, some of which are discussed here.

Catalyst made from nitrogen-doped carbon nanotubes: This type of catalyst could be used in lithium-air batteries, which can store up to 10 times more energy as compared to lithium-ion batteries containing platinum as a catalyst.

Silicon nanoparticles: The use of silicon nanoparticles, rather than solid silicon as anode of a lithium battery, prevents the cracking of the electrode and fast recharge within 10 min.

Silicon-coated carbon nanotubes for anodes: The use of silicon can increase the capacity of Li-ion batteries by up to 10 times by depositing silicon on nanotubes aligned parallel to each other to prevent damage to the anode when the silicon expands.

Carbon nanotubes grown on graphene have demonstrated as very promising electrode material with high surface area and low electrical resistance. The base of each nanotube is bonded, atom to atom, to the graphene sheet; the nanotube–graphene structure is essentially one large molecule with a huge surface area.

Silicon nanowires on a stainless steel substrate: These anodes could have up to 10 times the power density of conventional lithium-ion batteries. Silicon nanowires swell as lithium ions are absorbed during discharge of the battery and contract as the lithium ions leave during recharge of the battery; the nanowires do not crack, unlike anodes that used bulk silicon.

Carbon nanofibers as electrodes: Such electrodes show four times the storage capacity of current lithium-ion batteries. Lithium–sulfur batteries (the cathode-containing sulfur) have the capability of storing several times the energy of lithium-ion batteries. Such batteries are being developed using cathodes made up of carbon nanofibers encapsulating the sulfur cathodes made up of mesoporous carbon nanoparticles, with the sulfur inside the nanopores.

Aligned carbon nanotubes on a substrate as the anode/cathode: The carbon nanotubes attached to organic molecules help the nanotubes to align on the electrode substrate as well as provide many oxygen atoms as centers for the attachment of lithium ions to the electrode. This could increase the power density of lithium-ion batteries significantly.

Nanocomposite-based cathodes have increased the energy density of Li-ion batteries.

Lithium-ion batteries with electrodes made from **nanostructured lithium titanate** have significantly improved the charge/discharge capability at subfreezing temperatures, increasing the upper temperature limit at which the battery remains safe from thermal runaway. These batteries are small enough to be implanted in the eye to power the artificial retina. Long shelf-life battery uses “nanograss” to separate liquid electrolytes from the solid electrode until power is needed. Lithium-ion batteries with nanoparticle (Nanophosphate™) electrodes meet the safety requirements for **electric cars** while improving the performance.

9.9 Nanotechnology in Enhancing the Fuel Efficiency

Nanotechnology can address the shortage of fossil fuels such as diesel and gasoline by the following:

- Making the production of fuels from low-grade raw materials economical
- Increasing the mileage of engines
- Making the production of fuels from normal raw materials more efficient

Nanotechnology can do all this by increasing the effectiveness of catalysts [23]. Catalysts can reduce the temperature required to convert raw materials into fuels or increase the percentage of fuel burned at a given temperature. Catalysts made from nanoparticles have a greater surface area to interact with the reacting chemicals than catalysts made from larger particles. The larger surface area allows more chemicals to interact with the catalyst simultaneously, which makes the catalyst more effective. This increased effectiveness can make a process such as the production of diesel fuel from coal more economical and enable the production of fuel from currently unusable raw materials such as low-grade crude oil.

Nanotechnology, in the form of genetic engineering, can also improve the performance of enzymes used in the conversion of cellulose into ethanol in high yield. Currently, ethanol added to gasoline is made from corn, molasses, and so on. It can allow materials that often become waste, such as wood chips, grass, and other waste biomass, to be turned into ethanol.

Research and development efforts are being focused on the development of nanosphere-based catalysts that reduces the cost of producing biodiesel (i.e., diesel from vegetable oil), modifying crops to allow cellulose material such as stalks to produce enzymes that are triggered at elevated temperatures to convert the cellulose to sugar, and modifying bacteria to cause the production of enzymes to convert cellulosic material to ethanol in one step. Use of cerium oxide NPs and tungsten oxide NPs as a nanocatalyst makes the process of refining gasoline more efficient.

9.10 Chemical and Biosensors Using Nanomaterials (NMs)

A chemical sensor is a self-contained analytical device that can provide information about the specific chemical composition of its environment. The information is provided in the form of a measurable physical signal that is correlated with the concentration of a certain chemical species. Nanotechnology can enable sensors to detect very small amounts of chemical vapors. Two main steps are involved in the functioning of a chemical sensor, namely, recognition and transduction. In the recognition step, analyte molecules interact selectively with receptor molecules or sites included in the structure of the recognition element of the sensor. Consequently, a characteristic physical parameter varies, and this variation is reported by means of an integrated **transducer** that generates the output signal. A sensor based on biological recognition element such as protein (enzymes, antibodies, antigen), cells, nucleic acid, and even biomimetic polymers falls into the category of **biosensor**.

Various types of detecting elements, such as carbon nanotubes, zinc oxide nanowires, or palladium nanoparticles, can be used in nanotechnology-based sensors [24]. These detecting elements change their electrical characteristics, such as resistance or capacitance, when they absorb a gas molecule. Because of the small size of nanotubes, nanowires, or nanoparticles, a few gas molecules are sufficient to change the electrical properties of the sensing elements. This allows the detection of a very low concentration of chemical vapors. Table 9.4 includes some of examples of sensors making use of nanomaterials.

Table 9.4 Chemical Sensors and Biosensors Based on Nanomaterials

Analytes	NM Used	Measurable Parameter
Hydrogen	Pd NPs	Resistance
Nerve gas	MoS_2	Resistance
Ammonia	Graphene foam sheets	Resistance
Chemical vapors	CNT and ZnO_2 nanowires	Resistance
Volatile organic compounds	Gold NPs on polymer films	Resistance
Biological molecules such as viruses	Nanocantilever coated with antibodies	Resonance Frequency
Chemical gas leak or release of toxins	Nanoporous silicon incorporated in cell phones	Dielectric properties

These sensors can also be useful in industrial plants that use chemicals in manufacturing to detect the release of chemical vapors. When hydrogen fuel cells come into use in cars or in other applications, a sensor that detects escaped hydrogen could be very useful in warning of a leak. This technology should also make possible inexpensive networks of air quality monitoring stations to improve the tracking of air pollution sources. The goal is to have small, inexpensive sensors that can sniff out chemicals just as dogs are used in airports to smell the vapors given off by explosives or drugs.

9.10.1 Artificial Nose as Chemical/Biosensor

An artificial nose sensor is a device that mimics the ability of some mammals, such as dogs, to detect explosives and drugs through their olfactory system. Recent research has shown that this fine capacity in dogs may also be used to detect molecules that, if present, are early indicators of various diseases such as cancer. The application of such types of biosensor ranges from medicine, early disease detection [4, 5], and security (explosives detection) to the food industry [24]. This type of biosensor is an electrochemical sensor that mimics the natural mammal olfactory system. The nose biosensor, as our own noses, is composed of three main parts: a biomolecule receptor, an electrode, and a transducer. When the detector finds the target, a chemical reaction occurs between the detector and the receptor biomolecules for odor. The chemical reaction between the receptor and the substance we smell emits a chemical signal. The electrode translates this chemical signal into electrical signals and transports them to the brain or, in the case of the nose biosensor, they are transported to a transducer. In mammals, the equivalent of the electrodes would be neurons. The transducer (the brain in mammals) receives the electrical signal and translates it into analytical information on a screen. Nanotechnology has inspired a revolution in sensor technology. With respect to chemical and biological warfare scenario, nanomaterials might permit more sensitive sensors for chemical or biological warfare agents. Nanomaterials with high active surface areas could be used to bind and neutralize agents, or they could be used in protective equipment and for decontamination of affected areas.

9.11 Nanotechnology in Agro Forestry

Agriculture is the backbone of most developing countries, with more than 60% of the population reliant on it for their livelihood. In addition to the development in the improved systems for monitoring environmental conditions and delivering nutrients or pesticides as appropriate, nanotechnology can improve our understanding of the biology of different crops and thus potentially enhance yields or nutritional values. Moreover, it can offer routes to added value crops or environmental remediation. Nanotechnology has the potential to revolutionize the agricultural and food industry with new tools for the molecular treatment of diseases, rapid disease detection, enhancing the ability of plants to absorb nutrients, and so on [25]. Smart sensors and smart delivery systems will help the agricultural industry combat viruses and other crop pathogens. In the near future, nanostructured catalysts will be available that will increase the efficiency of pesticides and herbicides, allowing lower doses to be used.

9.11.1 Precision Farming

Precision farming has been a long-desired goal to maximize output, that is, crop yields, while autonomous sensors linked into a GPS system for real-time monitoring. These nanosensors could be distributed throughout the field where they can monitor soil conditions and crop minimizing input (i.e., fertilizers, pesticides, herbicides) through monitoring environmental variables and applying targeted action. Precision farming makes use of computers, global satellite positioning systems, and remote sensing devices to measure highly localized environmental conditions, thus determining whether crops are growing at maximum efficiency or precisely identifying the nature and location of problems. By using centralized data to determine soil conditions and plant development, seeding, fertilizer, chemical, and water use can be fine-tuned to lower production costs and potentially increase production – all benefiting the farmer. Precision farming can also help to reduce agricultural waste and thus keep environmental pollution to a minimum. Although not fully implemented yet, tiny sensors and monitoring systems enabled by nanotechnology will have a large impact on future precision farming methodologies. Ultimately, precision farming, with the help of smart sensors, will allow enhanced productivity in agriculture by providing accurate information, thus helping farmers to make better decisions.

The following examples shows that the integration of biotechnology and nanotechnology in sensors creates an equipment of increased sensitivity, allowing an earlier response to environmental changes.

- Nanosensors utilizing carbon nanotubes or nanocantilevers are small enough to trap and measure the individual proteins or even small molecules.
- Nanoparticles or nanosurfaces can be engineered to trigger an electrical or chemical signal in the presence of a contaminant such as bacteria.
- Nanosensors based on triggering an enzymatic reaction or by using nanoengineered branched molecules (dendrimers) as probes to bind to the target chemicals and proteins.

9.11.2 Smart Delivery Systems

The use of pesticides increased in the second half of the twentieth century, with DDT becoming one of the most effective and widespread pesticide throughout the world. However, many of these pesticides, including DDT were later found to be highly toxic, affecting human and animal health and as a result the whole ecosystem. To maintain crop yields, integrated pest management systems, which mix traditional methods of crop rotation with biological pest control methods, are becoming popular and implemented in many countries, such as Tunisia and India.

In the future, nanoscale devices with novel properties could be used to make agricultural systems “smart.” For example, devices could be used to identify plant health issues before these become visible to the farmer. Such devices may be capable of responding to different situations by taking appropriate remedial action. If not, they will alert the farmer to the problem. In this way, smart devices will act as both a preventive and an early warning system. Such devices could be used to deliver chemicals in a controlled and targeted manner in the same way as nanomedicine has implications for drug delivery in humans.

Technologies such as encapsulation and controlled release methods have revolutionized the use of pesticides and herbicides. Many companies make formulations that contain nanoparticles within the 100–250 nm size range that are able to dissolve in water more effectively than existing ones (thus increasing their activity). Other companies employ suspensions of nanoscale particles (nanoemulsion), which can be either water or oil-based and contain uniform suspensions of pesticidal or herbicidal nanoparticles in the range of 200–400 nm. These can be easily incorporated into various media such as gels, creams, and liquids and have multiple applications for preventative measures, treatment, or preservation of the harvested product.

9.12 Defense Applications

The lesson from history is that the better equipped an army is, the more likely their chances of winning in battle. Militaries of advanced nations, therefore, have been quicker than most to appreciate the potential of nanotechnology. The idea that nanotechnology could lead to lighter weight, smarter devices for soldiers in the field, uniforms that offer ballistic and other protection, and more deadly weapons has proved irresistible. Nanotechnology opens a broad spectrum of possible military uses that both expand and extend existing systems and define radical new applications [25].

9.12.1 Light Military Platforms

The new nanomaterials such as nanocomposites that are lighter and stronger than their conventional counterparts are able to create low-weight materials and structures such as maneuverable aircraft and missiles with extended ranges, while not compromising on strength and ruggedness. With the addition of new nanocoatings that enhance "stealth" capabilities, the latest aircraft and missiles can now travel further while reducing the likelihood of detection by an enemy. Nanostructured ceramic coatings exhibit much greater toughness than conventional wear-resistant coatings for machine parts. In 2000, the US Navy qualified such a coating for use on gears of air-conditioning units for its ships, saving $20 million in maintenance costs over 10 years. Such coatings can extend the lifetimes of moving parts in everything from power tools to industrial machinery.

9.12.2 Nanotechnology for Camouflage/Stealth

Apart from designer nanoparticles to enhance the performance of coatings, which can make surfaces harder, smoother, and less liable to corrode, nanotechnologies offer the potential for both "stealth" coatings that minimize the likelihood of radar detection and coatings that can change color in order to maintain camouflage in different environments. Surfaces with locally variable color, for example, through the use of mobile pigment particles can be used for camouflage [26]. Surfaces with tailored absorption properties for electromagnetic radiation can reduce radar and infrared signatures. It is likely that camouflage paint schemes of the near future, applied on vehicles as "smart" coatings, could be altered with an electrical impulse as simply as changing pixel colors on a screen.

The idea of "invisibility cloaks" has been much publicized through the Harry Potter stories. Far from mere fantasy, these "cloaks" can be created relatively simply by projecting what is behind a military target onto its surface to all intents and purposes, thus making it effectively camouflaged as illustrated in Figure 9.13. Materials used are termed as "metamaterials," which are basically artificially engineered materials having negative refractive index [27–30]. Light is neither absorbed nor reflected by the metamaterial, but rather passes "like water flowing around a rock." As a result, only the light from behind the object can be seen. Applications are still very limited at this stage, as the metamaterial can only be produced in small quantities.

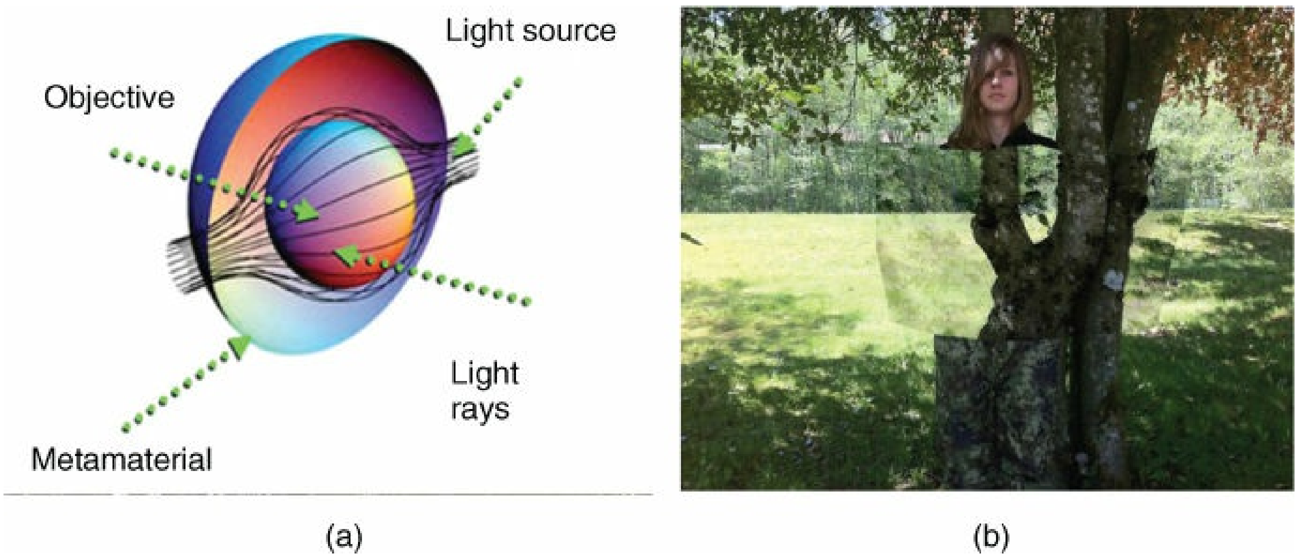

Figure 9.13 The complete invisibility system based on metamaterials: (a) Schematic representation of metamaterial showing bending of light. http://www.physics.org. (b) Quantum stealth mock-up using metamaterial. Courtesy of G. Cramer, Hyper Stealth Biotechnology Corp. [27].

9.12.2.1 Soldier Protection

A military uniform today needs to perform a variety of tasks, such as providing ballistic protection: the ability to autonomously gather and transmit information, assist in the healing process if a soldier is wounded, and protect its wearer from extreme environments such as heat and cold and the threat of biological warfare. It needs to be lightweight yet strong and, of course, cheap to produce. Nanofiber-based garments can provide better protection against projectiles.

Critical to many of these textile applications are carbon nanotubes, a new "supermaterial," possessing some extraordinary properties. For example, carbon nanotubes have a similar tensile modulus to the current best carbon fibers, but are nearly 20 times stronger! Similarly, remarkable properties are true for their electrical and thermal conductivities.

Another important phenomenon about nanoparticles is that below the diffraction limit of light, they are invisible to the naked eye. Carbon nanotubes can therefore impart properties to their host matrix, unseen, whether it is an increase in strength or in electrical and thermal conductivities.

New ways of sensing can also be achieved with networks of nanotubes embedded within a polymer matrix that can also form part of battle fatigues. These networks can be distorted by external stimuli, thus creating flexible sensors. Since most polymers are insulators, any distortion of the conductive network of the nanotubes will cause an increase in electrical resistance. Thus, the carbon nanotube network becomes an integrated analog switch, whose on/off characteristics will be a function of the host polymer. For example, a stimulus could be swelling of the polymer in the presence of water, a solvent or gas, or mechanical strain. In this way, nanotube networks enable the creation of smart, responsive textiles when incorporated in a polymer fiber.

9.12.2.2 Knowledge Building

The military has always been fascinated by the idea of undetectable surveillance. In the past, the phone tapping and miniature cameras were the technologies of the day. Now, listening, imaging, and information processing devices are tinier and more efficient than could ever have been imagined in the past. Nanotechnology is enabling new forms of almost "invisible" surveillance through the incorporation and integration of different technologies with IT, otherwise called ubiquitous computing, including radio-frequency identification chips (RFIDs), integrated circuits, quantum dot tags, minute (bio)sensors, intelligent fabrics, films, and smart surfaces. Because surveillance techniques can be miniaturized so effectively, the idea of using live insects ("spy" bees) or creating tiny-winged robots that emulate insects to be flown into an enemy situation to record data has formed the basis of intensive research.

9.12.3 Affordable Energy

Lighter energy-storage and conversion systems, such as fuel cells using nanoparticle-based membranes or hydrogen tanks based on nanotubes or fullerenes, could make all-electric military vehicles practical including electromagnetic guns. For small systems, contracting molecules or deforming materials offer the potential of muscle-like motion. Soldier-worn systems could sense the state of health of the wearer and react by releasing drugs or, using smart materials, by compressing wounds. Energy for communication could be generated by normal body movements.

9.12.4 Deadly Weapons

Employing advances in materials and explosives, conventional guns can shoot to larger ranges at reduced mass, and with nanotechnology-based guidance systems, targeting accuracy has increased many folds. The same holds true for missiles. With respect to penetrating projectiles, it is unclear whether nanotechnology-designed materials and structures will transcend the properties of tungsten or uranium. Whether nanotechnology-based armor will prevail over nanotechnology penetrators, or vice versa, is an open question?

With nanotechnology, the size of autonomous minirobots and microrobots could decrease, principally down to far below 0.1 mm. These could move in all media: on the ground, in water, and in air, using propulsion principles known from larger technical systems (wheel, track, propeller, wing, jet, rotor) or biomimetic ones (using legs, wriggling like a snake, hopping, using flapping wings, flagella). Mini-/microrobots could be designed for a wide variety of purposes, such as reconnaissance, communication, target designation for larger weapons, actuation on a small scale, or as weapons. Capabilities for sensing, communication, and actuation would decrease with shrinking size. Such limitations, however, could be compensated for by close range or mass use. One possible scenario would involve entering into a target object or subject and approaching a central node: there the robot could eavesdrop, manipulate, or destroy.

Another possibility would be acting in high numbers, choking air intakes, blocking windows, putting abrasives into mechanics, and so on. Biological–technical hybrids, such as insects or small mammals controlled by nerve/brain electrodes, could fulfill similar purposes. Thus, they should be classed with mini-/microrobots.

For military uses of outer space, nanotechnology will provide many possibilities for markedly smaller *satellites* together with smaller launch vehicles. Small satellites could be used in swarms for radar, communication, or intelligence. Owing to the large effective antenna size of such a system, the target resolution would be high; however, the total antenna and solar-cell area would determine the strength of received or transmitted signals. Small satellites could damage or destroy other satellites – either by a direct hit with high relative velocity or through manipulations after rendezvous and docking. Nanotechnology-enabled electromagnetic acceleration could also be used for kinetic-energy space weapons.

9.13 Nanotechnology *in Space*

Nanotechnology may hold the key to making space flight more practical. Advancements in nanomaterials make lightweight solar sails and a cable for the space elevator possible. By significantly reducing the amount of rocket fuel required, these advances could lower the cost of reaching orbit and traveling in space. In addition, new materials combined with nanosensor and nanorobots could improve the performance of spaceships, spacesuits, and the equipment used to explore planets and moons, making nanotechnology an important part of the “final frontier” [31].

9.13.1 Space Flight and Nanotechnology: Applications Under Development

Researchers are looking into the following applications of nanotechnology in space flight to make faster, lighter, cheaper, and better (Figure 9.14):

- Employing materials made from carbon nanotubes to reduce the weight of spaceships like the one shown below while retaining or even increasing the structural strength.
- Using carbon nanotubes to make the cable needed for the space elevator, a system which could significantly reduce the cost of sending material into orbit.
- Including layers of bio-nanorobots in spacesuits. The outer layer of bio-nanorobots would respond to damages to the spacesuit, for example, to seal up punctures. An inner layer of bio-nanorobots could respond if the astronaut was in trouble, for example, by providing drugs in a medical emergency.
- Deploying a network of nanosensors to search large areas of planets such as Mars for traces of water or other chemicals.
- Satellites are being used for both defense and civilian applications. These satellites utilize thruster rockets to remain in or change their orbits due to a variety of factors including the influence of gravitational forces exerted by the earth. In fact, more than one-third of the fuel carried aboard by the satellites is wasted by these repositioning thrusters due to incomplete and inefficient combustion of the fuel such as hydrazine. The reason for the incomplete and inefficient combustion is that the onboard ignitors wear out quickly and cease to perform effectively. Nanomaterials, such as nanocrystalline tungsten–titanium diboride–copper composite, are potential candidates for enhancing these ignitors' life and performance characteristics.
- Using carbon nanotubes to build lightweight solar sails that use the pressure of light from the sun reflecting on the mirror-like solar cell to propel a spacecraft. This solves the problem of having to lift enough fuel into orbit to power spacecraft during interplanetary missions.
- Working with nanosensors to monitor the levels of trace chemicals in spacecraft to monitor the performance of life support systems.

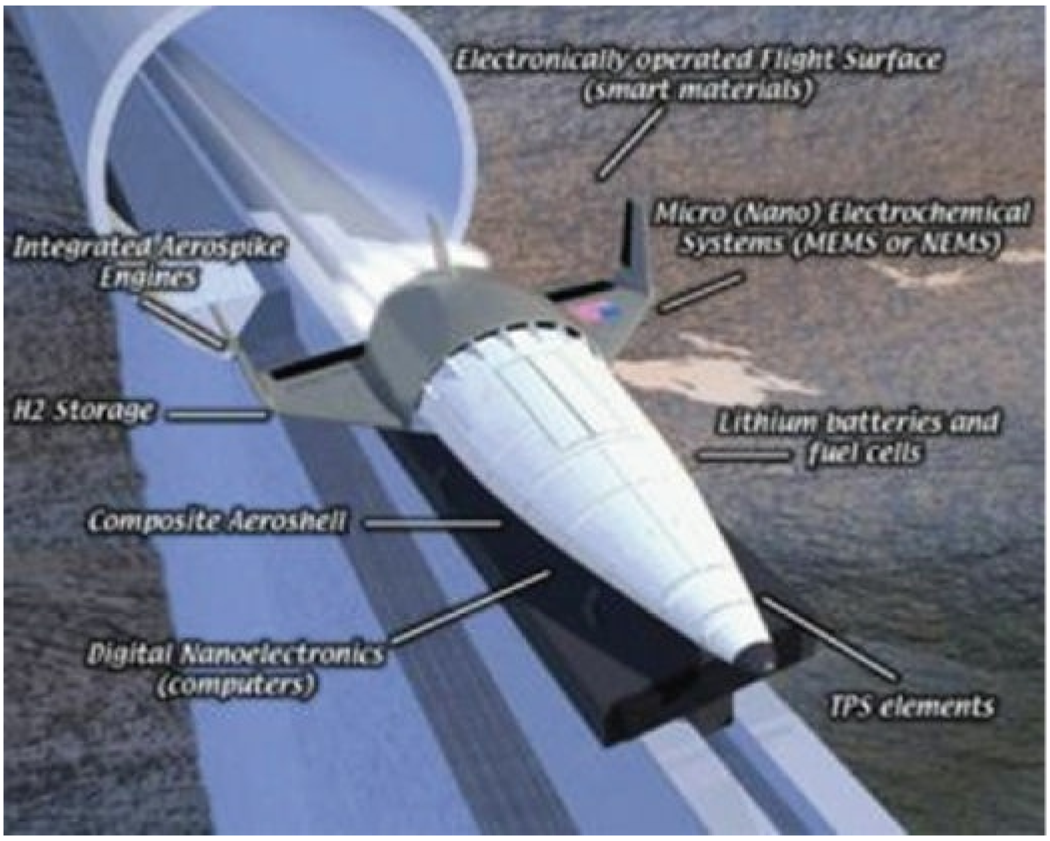
Electronically operated Flight Surface (smart materials)
Micro (Nano) Electrochemical Systems (MEMS or NEMS)
Integrated Aerospike Engines
H2 Storage
Lithium batteries and fuel cells
Composite Aeroshell
Digital Nanoelectronics (computers)
TPS elements

Figure 9.14 Space transportation with nanotubes: faster, better, cheaper. [http://www.ipt.arc.nasa.gov/spacetransport.html.]

9.14 Consumer Goods

Nanotechnology is already impacting the field of consumer goods, providing products with novel functions ranging from easy-to-clean to scratch-resistant. Different nanoparticle-improved products are already in use [32, 33]. Modern textiles are wrinkle resistant and stain-repellent; clothes will become “smart,” through embedded “wearable electronics”; novel products of cosmetics have a promising potential as well.

9.14.1 Nanotextiles

The properties imparted to the textiles using nanotechnology include water repellence, soil resistance, wrinkle resistance, antibacteria, antistatic and UV protection, flame retardation, improvement of dye ability, and so on. Making composite fabric with nanosized particles or fibers allows improvement of fabric properties without a significant increase in weight, thickness, or stiffness as might have been the case with previously used techniques. For example,

- Nanowhiskers that cause water to bead up, making the fabric water- and stain-resistant.
- Silver nanoparticles in fabric that kills bacteria making clothing odor-resistant.
- Nanopores providing superior insulation for shoe inserts in cold weather.
- Nanoparticles that provide a “lotus plant” effect for fabric used as awnings and other material left out in the weather, causing dirt to rinse off in the rain.

9.14.2 Self-Cleaning

Lotus effect: Investigations into the surface using reflection electron microscopy (REM) have shown that the surface of the lotus leaf is not especially even but has instead a special, characteristic roughness (Figure 1.2, Chapter 1): systematically arranged, water-repellent, nanosized wax crystals form 3D structures, similar to small nipples, which are no greater than a few nanometers or micrometer in size. When combined with the waxes' water-repellent chemical properties, these structures make the lotus leaf extremely nonwettable, a state called ultrahydrophobia or superhydrophobia, and they give it its self-cleaning properties. Dirt particles only sit on the tip of the wax crystals, and as a result only a very small surface area comes into contact with the plant's surface. If water falls onto a leaf surface like this, the interplay of the surface tension and the low attraction force between the surfaces and the water produce a spherical water drop that only sits on the tips of the wax structures. If the leaf tips in the slightest, the water drop immediately rolls off, taking the dirt particles with it. As the gravitational pull between the dirt and the leaf's surface is very slight, that is, it is smaller than that between the water and the dirt, even lipophilic impurities, such as soot for example, can be washed away. In this case, the coating is not a uniform layer with a specific chemical functionality (as in the case of photocatalytic coating), but a surface with an engineered topography at the nanoscale level. This leads to a surface that is superhydrophobic (extremely water repellent). Water droplets roll off the surface, and in doing so collect and remove dirt deposited on the surface.

The lotus effect has been an inspiration for several innovative materials, such as coatings and textiles. The realization that certain surface properties can induce water repellence is important in numerous applications. Numerous types of materials are being engineered now to render them superhydrophobic.

Composite materials made up of nanoparticles in a coating matrix make it possible to manufacture the surface structure required for the “Lotus-Effect.” These polyester fabrics are of particular interest in the manufacture of dresses, parasols, sails, and tents. Manufacturing surfaces that feature a “Lotus-Effect” is technically challenging and still poses certain problems. To date, there are only a few low-cost processes that can produce the surface structures on a large scale. There are still only a handful of practical applications available on the market that has the “Lotus-Effect.” Nevertheless, there are already several products with dirt-repellent and water-repellent properties on sale, which, the manufacturers claim, are based on nanotechnology or contain nanoparticles. These include, for example, ceramic sanitary facilities, spectacle lenses, or textiles.

Photocatalytic effect: To date, photocatalytic self-cleaning is probably the most widespread application ascribed to nanotechnology in the construction industry. There are already a great number of buildings worldwide that have been treated with it. Titanium dioxide (TiO_2), the most studied photocatalytic material [34], is hydrophilic due to its high surface energy; hence, water does not form drops on a surface coated with it, but a sealed water film instead. A coating of this kind hence behaves in exactly the opposite manner to a surface whose self-cleaning properties are based on the “Lotus-Effect.” It is also transparent and can therefore also be used on glass. In addition, TiO_2 is photocatalytic; in other words, in the presence of water, oxygen radicals are produced under UV light irradiation that in turn can decompose organic materials such as fats, oils, soot, or plant materials. TiO_2 is especially reactive in nanoform. It is not expended during catalysis, with the result that the effect is lasting. On self-cleaning surfaces of this type, organic dirt is dissolved in the water film, decomposed, and the residue is removed by the next heavy shower of rain.

Photocatalytic self-cleaning only works in outdoor use because it requires UV light and water to remove the residue. Ways of modifying the properties of TiO_2 are currently being researched so that it becomes photocatalytic by irradiation with visible light. This is achieved by doping them with metal atoms such as chromium, vanadium, tungsten, or carbon. The results of earlier research have already been implemented in commercial products such as photocatalytically active interior paints that reduce gaseous pollutants in the air, for example, to improve the air quality. The above-mentioned applications are examples of cases where the superhydrophobic properties of an engineered material, such as a textile or a coating, can reduce cleaning needs, with a consequent reduction in water usage and obvious environmental benefit.

9.14.3 Antimicrobial Coatings on Textiles and Other Products

Antimicrobial coatings are needed in many applications, for example, to protect medical surfaces and tools, or to reduce microbial attack on the hulls of boats. Sprays and coatings for this use already exist, but improvement in this area is needed as many microbes are becoming resistant to the antibiotic treatments that have been used so far. To prevent bacteria attachment, surfaces with nanocoatings with specific functionalities and topographies are under investigation. Antifouling surfaces are being investigated for use in the coating of medical utensils and instruments and household appliances, as well as for coating boats. A nanomaterial that is becoming widely used is silver nanoparticles.

Silver is a metal with a long history used for its antibacterial properties – even the Romans used it to dress wounds. This property explains why silver has been used to produce the highest-quality cutlery (silverware) or to store water in vessels in antiquity (even by the Phoenicians). In medicine, 1% silver nitrate was used in the past as an eye solution to prevent infections in newborn children, and until antibiotics were discovered, silver nitrate was added to germicides and antiseptics as a disinfectant.

The **antibacterial properties** of silver are due to the **silver ions ($Ag+$)** released by the bulk metal once this is oxidized [35]. In fact, silver tableware or dishware has antimicrobial activity only if oxidized species are present on their surface. Silver ions induce the oxidative stress of the bacteria cell wall, where many cellular functions are performed, affecting the bacteria's ability to respire and to maintain an intracellular environment suitable for life. Silver ions inhibit bacteria growth; suppress respiration and metabolism; and basically induce cell death, preventing them from multiplying.

Silver ionizes when in contact with water to form Ag+, which has a strong interaction with biological molecules containing thiols, including enzymes and bacterial cell membranes. This strong interaction denatures enzymes and causes cellular damage, ultimately leading to cell death. The Ag+ ion further bonds to bacterial cell DNA, preventing the cell from replicating. A new approach for fabricating robust, regenerable antimicrobial coatings containing an ionic liquid phase incorporating silver nanoparticles (AgNPs) as a reservoir for Ag^0/Ag^+ species within sol–gel-derived nanocomposite films integrating organosilicate nanoparticles; Figure 9.15a is a schematic representation of this concept. Silver toxicity has been shown toward many strains of bacteria, both gram-negative and gram-positive, and to fungi but less toward viruses. Nanosilver-impregnated textiles find applications in varied fields that require aseptic environment including aprons (Figure 9.15b), masks, dressings, socks, and so on. Table 9.5 includes few enhanced properties of textiles fibers with inclusion nanostructure.

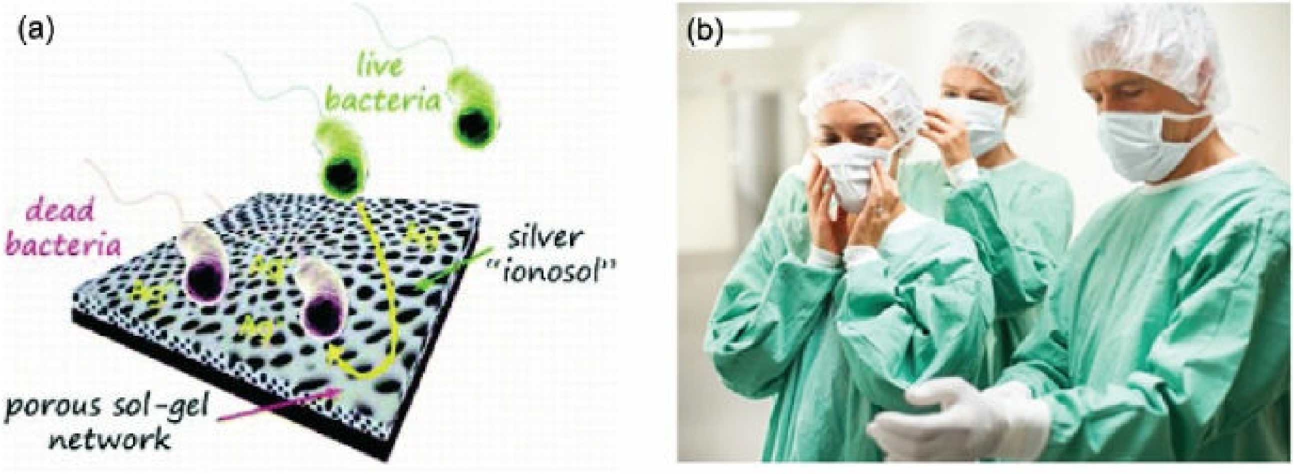

Figure 9.15 Antibacterial textiles: (a) interaction between bacteria and coating of AgNPs within sol–gel-based silicate material. Hamm et al. [35], © 2012. With permission of ACS; (b) doctor's sterile suit containing nanosilver. http://www.ecouterre.com/.

Table 9.5 Enhanced Properties of Textile Fibers with Inclusion Nanostructure

Nanostructures	Enhanced Properties
Nanowhiskers	Water and stain resistant
Nanopores	Insulates against heat or chill
Nanoparticles	Self-cleaning
Silver nanoparticles	Antibacterial and reduces odors

9.14.4 Cosmetics

The applications of nanotechnology and nanomaterials can be found in many cosmetic products including moisturizers, hair care products, make up, and sunscreen. In cosmetics, there are currently two main uses for nanotechnology. The first of these is the use of nanoparticles as UV filters. Titanium dioxide (TiO_2) and zinc oxide (ZnO) are the main compounds used in these applications. They are efficient, photostable UV filters that absorb UV-B and UV-A radiation and re-emit it as less damaging UV-A through visible fluorescence or heat. Formulations that utilize TiO_2 or ZnO as the only active sunscreen agents provide photoprotective properties and reduced risk of irritation compared to other sunscreen ingredients; avobenzone, for example, offers protection against UV-A rays but it can also be a skin irritant. An ideal sunscreen formulation must efficiently block UV-A/UV-B radiation, be nontoxic, and be esthetically appealing. Uncoated TiO_2 absorbs photons of light and emits an excited electron, which can be transferred to free radicals and absorbed into dermal layers, resulting in oxidative damage. To stop the formation of reactive oxygen species (ROS) and prevent the agglomeration of particles, TiO_2 and ZnO are generally coated with aluminum oxide, silicon dioxide, or silicon oils. Organic alternatives to these have also been developed.

The second use is nanotechnology for delivery. Liposomes and isomers are used in the cosmetic industry as delivery vehicles. Newer structures such as solid–lipid nanoparticles (SLN) and nanostructured lipid carriers (NLC) have been found to be better performers than liposomes. In particular, NLCs have been identified as a potential next-generation cosmetic delivery agent that can provide enhanced skin hydration, bioavailability, stability of the agent, and controlled occlusion. Encapsulation techniques have been proposed for carrying cosmetic actives. Nanocrystals and nanoemulsions are also being investigated for cosmetic applications. Other novel materials, such as fullerene, have also appeared in a few beauty products. Nanoparticles in cosmetic preparations are found to improve the stability of various cosmetic ingredients such as unsaturated fatty acids, vitamins, or antioxidants by encapsulating them; increase the efficacy and tolerance of UV filters on the skin surface; make the product more esthetically pleasing; and enhance the penetration of certain active ingredients to the epidermis. This article reviews various forms of nanoparticles used in the cosmetics industry and discusses their properties, mechanisms of action, and possible health effects.

9.15 Sport Goods

The degree of competitiveness in sports has been remarkably impacted by nanotechnology similar to any other innovative idea in materials science. Within the niche of sport equipments, nanotechnology offers a number of advantages and immense potential to improve sporting equipments making athletes safer, comfortable, and more agile than ever. Baseball bats, tennis and badminton racquets, hockey sticks, racing bicycles, golf balls/clubs, skis, fly-fishing rods, archery arrows, and so on are some of the sporting equipments, whose performance and durability are being improved with the help of nanotechnology [36]. Nanomaterials such as carbon nanotubes (CNTs), silica nanoparticles (SNPs), nanoclays, and fullerenes are being incorporated into various sports equipment to improve the performance of athletes as well as equipments (Figure 9.16). Each of these nanomaterials is responsible for an added advantage such as high strength and stiffness, durability, reduced weight, and abrasion resistance in sporting equipments as listed in Table 9.6.

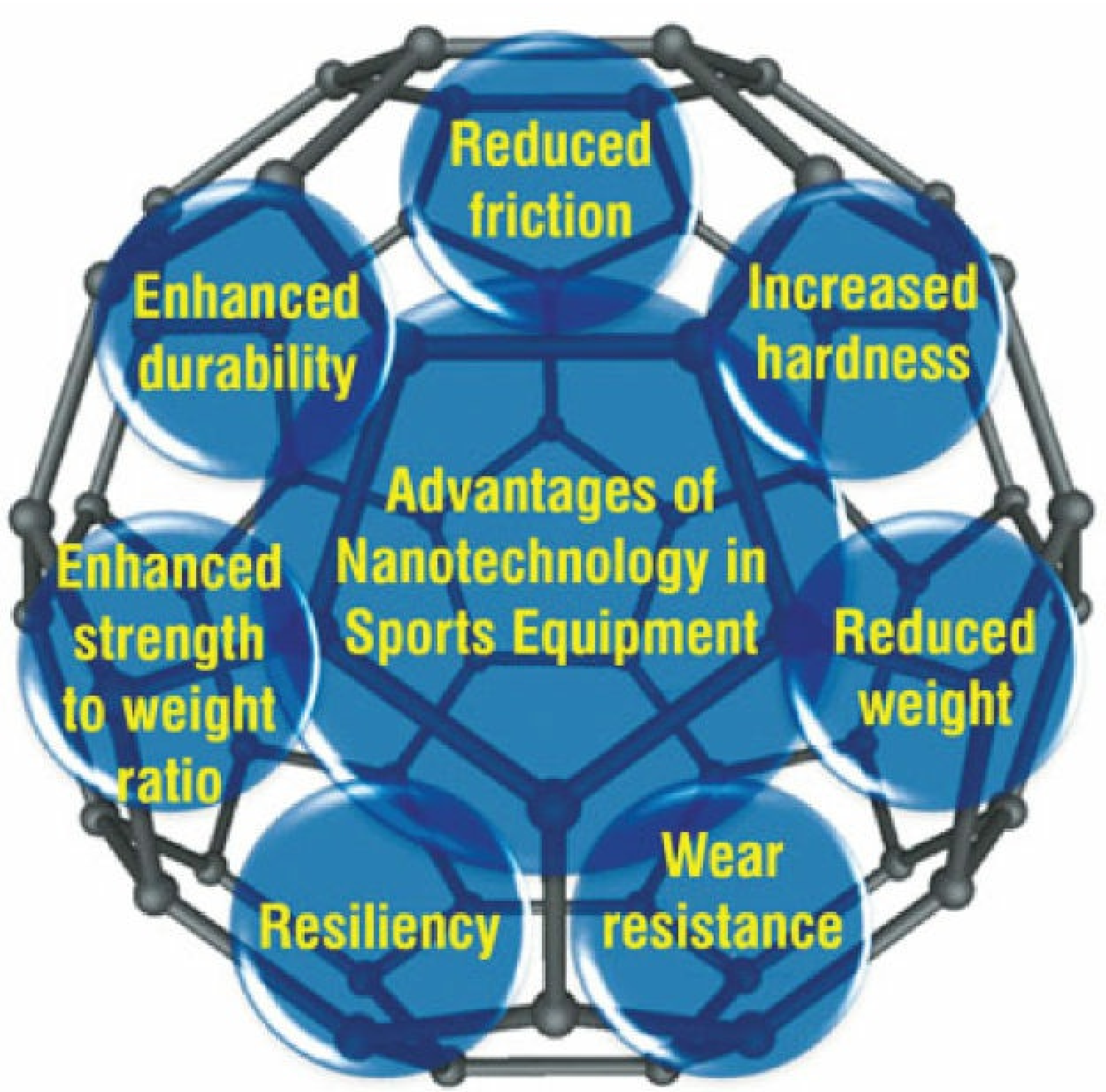

Figure 9.16 Specific advantages of nanotechnology in sports equipment.

Courtesy of CKMNT, India [36].

Table 9.6 Attributes Nanomaterials in Sports Equipments and Its Associated Benefits

Nanomaterials	Sports	Attribute
Silica nanoparticles	Tennis/badminton	Increase stability, power, and durability of racquets
	Skiing	Decrease torsion index and facilitate transition in skis
	Fly-fishing	Enhance hoops and flex strength of rods
Nano-titanium	Tennis/badminton	Resist deformation of racquets
		Increase strength and durability of racquets
		Transmit more power to shuttle cock/ball
		More accurate shots
Nano-nickel	Golf	Increase moment of inertia and stability of clubs
Carbon nanotubes	Tennis/badminton	Improved stiffness, consistency, durability, resiliency, impact, repulsion power, and vibration control racquets
	Golf	Reduced weight, lower torque/spin of clubs
	Kayaking	Enhanced abrasion/crack resistance
		Easy peddling
	Archery	Better vibration control in arrows
	Kayaking	Enhanced abrasion/crack resistance
		Easy peddling
Fullerenes	Tennis/badminton	Reduce weight and twisting of racquet frames

	Golf	Facilitate flexible club whipping
	Bowling	Reduce chipping and cracking of balls
Carbon nanofibers	Cycling	Reduce weight
		Increase stiffness
Carbon nanoparticles	Motor Racing	Decrease rolling resistance of tires
		Increase grip and mileage of tires
Nanoclays	Tennis/Golf	Increase resiliency and bounce of balls
	Watercraft	Reduce weight
		Enhance speed of water-boats

Source: Courtesy of CKMNT, India [36].

Equipments such as footballs/tennis balls with nanoclay lining as a barrier material uphold reassure for a longer game-play. Incorporation of nanomaterials (e.g., fullerene) lightens the golf clubs by lowering the center of gravity, which increases the power and accuracy during the game-play. Graphene oxide and buckypaper (sheet of CNTs) are incorporated into canoes or race-boat hulls/masts to increase glide while making them stronger and much lighter. In ice-skating, ultrahard nanoceramics make the edges of skates supersharp, whereas self-assembling bionic nanoparticles are used in land speed cars to improve the fuel economy and speed even with 50% less nitromethane fuel mixture. Among various nanomaterials, CNTs are the most prominent nanomaterial being used in nano-enhanced sporting equipments such as golf shafts, rackets, skis, and snowboards.

Review Questions

Q1. What is so special about the Lycurgus cup and medieval stained glass windows of churches? How will you explain on this feature on the basis of nanotechnology?

Q2. Name the consumer products in the field of sports that are already being made using nanotechnology? Mention the nanocomponent introduced and resultant unique feature.

Q3. How nanotechnology has been successful in introducing following properties in consumer goods of everyday use:

- **i.** Antimicrobial action
- **ii.** Self-cleaning effect
- **iii.** Adhesive mimicking Gecko's feet
- **iv.** UV protection

Q4. How nanotechnology has improved the diagnosis for better healthcare?

Q5. What do you understand by nanodrug delivery systems (NDDS)? Give the mechanism of targeted drug delivery.

Q6. Explain how nanotechnology is contributing in developing targeted drugs in terms of composition and delivery system.

Q7. What do you understand by small interfering RNAs (siRNA)? Give plausible role of siRNA in controlling diseases.

Q8. What is the impact of nanotechnology in the field of "therapy"?

Q9. What is Moor's law? Give example on how nanotechnology is helping to prove.

Q10. Define and describe importance of following concepts: i. Theranostics; ii. Spintronics; iii. Photonics; iv. Quantum electronics.

Q12. Write a note on "Impact of nanotechnology in the evolution displays"?

Q13. Give some future application of nanotechnology.

Q14. How nanotechnology has contributed in improving the Universal Product Code system?

Q15. Discuss briefly the impact of nanoscience in the water purification and remediation technologies.

Q16. Discuss the impact of nanoscience in improving the following technologies related to energy sector:

- **i.** Dye-sensitized solar cells
- **ii.** Semiconductor quantum dot-sensitized solar cell
- **iii.** Heterojunction solar cells
- **iv.** Fuel cells
- **v.** Batteries

Q17. What do you understand by **Peltier–Seebeck effect**? How nanoscience has brought renaissance to thermoelectric power generation.

Q18. How a chemical sensor is different from a biosensor? Give examples of specific nanomaterials used in chemical sensors.

Q19. Discuss the impact of nanotechnology following field related to defense and security:

- **i.** Camouflage
- **ii.** Stealth
- **iii.** Night vision
- **iv.** Light military platforms

Q20. How nanotechnology is making its mark in missile and space technology?

References

1. http://www.nano.gov/you/nanotechnology-benefits.

2. M. K. Patra, K. Mazoor, S.R. Vadera and N. Kumar, Functional nanomaterials for sensors and display applications, *Encyclopedia of Nanoscience and Nanotechnology*, Vol. 14, Ed. H.S. Nalwa, American Scientific Publishers, USA, 2011, 385–435.

3. N. Kumar and R. Kumar, *Nanotechnology and Nanomaterials in the Treatment of Life Threatening Diseases*, Elsevier, 2014.

4. S. Kumbhat, K. Sharma, R. Gehlot, A. Solanki and V. Joshi, "Surface Plasmon Resonance Based Immunosensor for Serological Diagnosis of Dengue", *J. Pharm. Biomed. Anal.*, **52** (2), 2010 255–259.

5. S. Kumbhat, D.R. Shankaran, S.J. Kim, K.V. Gobi, V. Joshi and N. Miura, "Surface Plasmon Resonance Biosensor for Dopamine using D3 Dopamine Receptor as a Biorecognition Molecule", *Biosens. Bioelectron.*, **23** (2007) 421–427.

6. R. Gehlot, K. Sharma, M. Mathew and S. Kumbhat, "Surface Plasmon Resonance Based Biosensor for Label Free Detection of Cholesterol", *Indian J. Chem.* **47A** (2008) 1804–1808.

7. Commercial Applications of Nanotechnology in Computing and Information Technology, http://www.azonano.com/article.aspx?ArticleID=1057.

8. R. Waser (Ed.) *Nanotechnology: Volume 3: Information Technology I*, Wiley, 2008.

9. A. Russo, B. Y. Ahn, J. J. Adams, E. B. Duolls, J. T. Bernhard and J. A. Lewis, *Adv. Mater.*, **23** (2011) 1–5.

10. M. L. Roukes, "Nanoelectromechanical Systems", Technical Digest of the 2000 Solid-State Sensor and Actuator Workshop, Hilton Head Isl., SC, 6/4-8/2000 (ISBN 0-9640024-3-4), 2000.

11. N. Kumar, "Nanotechnology for Remediation and Purification of Water", *Nanotech Insights*, **6** (1), (2015) 29–39.

12. M. R. Wiesner, H. Lecoanet and M. Cortalezzi, "Nanomaterials, Sustainability, and Risk Minimization", www.mindfully.org.

13. I. S. Yunus, Harwin, A. Kurniawan, D. Adityawarman and A. Indarto, "Nanotechnologies in Water and Air Pollution Treatment", *Environ. Technol. Rev.*, **1** (2012) 136–148.

14. D. Elcock, Potential Impacts of Nanotechnology on Energy Transmission Applications, Agronne National Laboratory (2007). http://www.osti.gov/bridge.

15. B. O'Regan and M. Gratzel, "A Low-Cost, High-Efficiency Solar-Cell Based on Dye Sensitized Colloidal TiO2 Films", *Nature*, **353** (6346), (1991) 737–740.

16. P. V. Kamat, "Quantum Dot Solar Cells: The Next Big Thing in Photovoltaics", *J. Phys. Chem. Lett.* **4** (2013) 908–918.

17. R. Liu, "Hybrid Organic/Inorganic Nanocomposites for Photovoltaic Cells", *Materials*, **7** (2014) 2747–2771.

18. Solar Fuels and Artificial Photosynthesis: Science and Innovation to Change our Future Energy Options, A Report, (2012) www.rsc.org/sustainable-energy.

19. J. F. Li, W.S. Liu, L.D. Zhao and M. Zhou, "High-Performance Nanostructured Thermoelectric Materials", *NPG Asia Mater.* **2** (2010) 152–158.

20. Power generation technology based on piezoelectric nanocomposite materials, Posted on May 7, 2012, http://phys.org/news/2012-05-power-technology-based-piezoelectric-nanocomposite.html.

21. S. S. Mao , S. Shena and L. Guob, "Nanomaterials for Renewable Hydrogen Production, Storage and Utilization", *Prog. Nat. Sci.*, **22** (2012) 522–534.

22. L. Dai, D. W. Chang , J. B. Baek and W. Lu "Carbon Nanomaterials for Advanced Energy Conversion and Storage", *Small*, **8** (2012) 1130–1166.

23. A. Dalai (Ed.), *Nanocatalysis for Fuels and Chemicals*, ACS Symposium Series 1092, Oxford University Press, USA, 2012.

24. K. C. Honeychurch (Ed.), *Nanosensors for Chemical and Biological Applications: Sensing with Nanotubes, Nanowires and Nanoparticles*, Woodhead Publishing Limited, 2014.

25. N. Kumar, "Nanotechnology for Rural Development in India", Nano Digest September 2014.

26. M. C. DeRosa, C. Monreal, M. Schnitzer, R. Walsh and Y. Sultan, "Nanotechnology in Fertilizer", *Nat. Nanotechnol.* **5** (2010) 91.

27. G. Cramer, "Quantum Stealth; The Invisible Military Becomes A Reality", Hyper Stealth Biotechnology Corp., Canada, 2012.

28. F. Simonis and S. Schilthuizen, "Nanotechnology Innovation Opportunities for Tomorrow's Defence", TNO Science & Industry, (2006).

29. S. R. Vadera and N. Kumar, "Nanotechnology and Nanomaterial for Camouflage and Stealth Application", *Nanotech. Insight.*, **5**(3&4) (2014) 16–30.

30. D. R. Smith, J. B. Pendry and M. C. K. Wiltshire, "Metamaterials and Negative Refractive Index", *Science*, **305** (2004) 788–792.

31. Nanotechnology in Space, http://www.nanowerk.com/nanotechnology-in-space.php.

32. S. Coyle, Y. Wu, K.T. Lau, D.D. Rossi, G. Wallace and D. Diamond, "Smart Nanotextiles: A *Review of Materials and Applications*". *MRS Bull.* **32** (2007) 434–442.

33. J. W. Wiechers and N. Musee, Engineered Inorganic Nanoparticles and Cosmetics: Facts, Issues, Knowledge Gaps and Challenges, *J. Biomed. Nanotechnol.*, **6** (2010) 408–431.

34. Z. Michalcik, M. Horakova, P. Spatenka, S. Klementova, M. Zlamal and N. Martin, "Photocatalytic Activity of Nanostructured Titanium Dioxide Thin Films", *Int. J. Photoenergy*, **2012** (2012), Article ID 689154, 8 pages.

35. S. C. Hamm, R. Shankaran and V. Korampally, et al. “Sputter-Deposition of Silver Nanoparticles into Ionic Liquid as a Sacrificial Reservoir in Antimicrobial Organosilicate Nanocomposite Coatings,” *ACS Appl. Mater. Interfaces* **4** (2012) 178–184.

36. *Nanotechnology in Sports Equipment: The Game Changer*, Nanotech Insight, (ed. Y.K. Mahajan) 2013.

Chapter 10
Toxicity and Environmental Issues

10.1 Introduction

As an important future technology, nanotechnology presents an opportunity for positively influencing economic development in the long term through intensive research and the effective translation of the research results into innovative products. Nanotechnology describes the production; investigation; and application of structures, molecular materials, and inner boundary surfaces having at least one critical dimension below 100 nm. The low end of the nanometer range borders on the molecule size range, which has long been shaped by targeted chemical reactions. The upper nanometer range encompasses microtechnology, which is also undergoing a dynamic development through, for example, computer technology (integrated circuits). Nanotechnology closes a gap here and is increasingly in the public eye. It is expected that the importance of nanotechnology will continue to grow and that workers, consumers, and the environment will be increasingly exposed. Hence, there is the need to monitor the development of the new technology and to weigh up the opportunities and risks in a transparent process and to compare them with the opportunities and risks associated with established technologies. Nanoparticles can potentially cause adverse effects on organ, tissue, cellular, subcellular, and protein levels due to their unusual physicochemical properties, for example, small size, high surface-to-volume ratio, chemical composition, crystallinity, electronic properties, surface structure reactivity and functional groups, inorganic or organic coatings, solubility, shape, and aggregation behavior [1–4].

Every person has been exposed to nanometer-sized foreign particles: we inhale them with every breath and consume them with every drink. In truth, every organism on Earth continuously encounters nanometer-sized entities. The vast majority causes little ill effect and goes unnoticed, but occasionally an intruder will cause appreciable harm to the organism. The most advanced of the toxic intruders are viruses, which are composed of structures based on nucleic acids that allow them to not only interfere with biological systems but also parasitically exploit cellular processes to replicate themselves. Among the more benign viruses are the ones causing the familiar human symptoms of the common cold or flu, which are the evident manifestations of biochemical battles occurring between these foreign intruders and our immune systems, whose nanometer-sized constituents (chemicals and proteins) usually destroy and remove the viral invaders. A growing number of recent studies show, however, that nano- and microorganisms may play a role in many chronic diseases where infectious pathogens have not been suspected, diseases that were previously attributed only to genetic factors and lifestyle [5, 6]. Only NPs translocate into the circulatory system and subsequently accumulate in the secondary organs and tissues of the body. Translocated NP fractions are rather, low but they depend strongly on the physicochemical and surface properties of NPs. Growing evidence indicate that the binding and conjugation of proteins to NPs play an essential role in translocation across cellular membranes and organ barrier. It appears that adverse effects are caused by NPs accumulated in secondary organs only after chronic exposure over extended time period. One is tempted to think that nanoparticles (such as dust, or ash particles), while similar in size to viruses, would be more benign, as these materials lack the viruses' ability to replicate. Nevertheless, while nonreplicating bodily intruders do not directly take control of cellular processes, some have been shown to sufficiently interfere with cellular function to influence basic process of cells, such as proliferation, metabolism, and death. Many diseases can be associated with dysfunction of these basic processes, the most notable being cancer (uncontrolled cells proliferation) and neurodegenerative diseases (premature cell death). In addition, several diseases with unknown cause, including autoimmune diseases, Crohn's, Alzheimer's, and Parkinson's diseases, appear to be correlated with nanoparticles exposure. Conversely, the toxic properties of some nanoparticles can be beneficial, as they are thereby able to fight disease at a cellular level and could be used as a medical treatment, by targeting and destroying cancerous cells.

Nanometer-sized particles are created in countless physical processes from erosion to combustion, with health risks ranging from lethal to benign. Industrial nanoparticle materials today constitute a tiny but significant pollution source that is, so far, literally buried beneath much larger natural sources and nanoparticle pollution incidental to other human activities, particularly automobile exhaust soot.

The misapprehension of nanotoxicity may create a general fear that all nanomaterials are toxic. While uncontained/free-flowing nanoparticles clearly represent a serious health threat, fixed/templated nanostructured materials, such as thin-film coatings, microchip electronics, and many other existing nanoengineered materials, are known to be virtually benign. Many synthetic nanoparticulate materials produce positive health effects, for example, functionalized fullerene chemicals that act as antioxidants. The use of nanoparticles in medical diagnostics and treatment is driven by their safety as well as utility [7].

Nanotoxicology was proposed as a new branch of toxicology to address the adverse health effects caused by nanoparticles [3]. Despite suggestions that nanotoxicology should only address the toxic effects of engineered nanoparticles and structures, it is recommended that nanotoxicology should also encompass the toxic effects of atmospheric particles, as well as the fundamentals of virology and bacteriology. While significant differences exist between the health effects of nonbiological particles and viruses and bacteria, there are significant common aspects of intrusion and translocation.

10.1.1 Toxicity of Nanoparticles

Human skin, lungs, and the gastrointestinal tract are in constant contact with the environment. While the skin is generally an effective barrier to foreign substances, the lungs and gastrointestinal tract are more vulnerable. These three ways are the most likely points of entry for natural or anthropogenic nanoparticles. Injections and implants are other possible routes of exposure, primarily limited to engineered materials. Due to their small size, nanoparticles can translocate from these entry portals into the circulatory and lymphatic systems, and ultimately to body tissues and organs. Some nanoparticles, depending on their composition and size, can produce irreversible damage to cells by oxidative stress or/and organelle injury [5]. Figure 10.1 summarizes the possible pathways of exposure of nanoparticles to human body and the associated health effects. Point to be noted that not all nanoparticles produce these adverse health effects, the toxicity of nanoparticles depends on various factors, including size, aggregation, composition, crystallinity, surface functionalization, and so on. In addition, the toxicity of any nanoparticle to an organism is determined by the individual's genetic complement, which provides the biochemical toolbox by which it can adapt to and fight toxic substances.

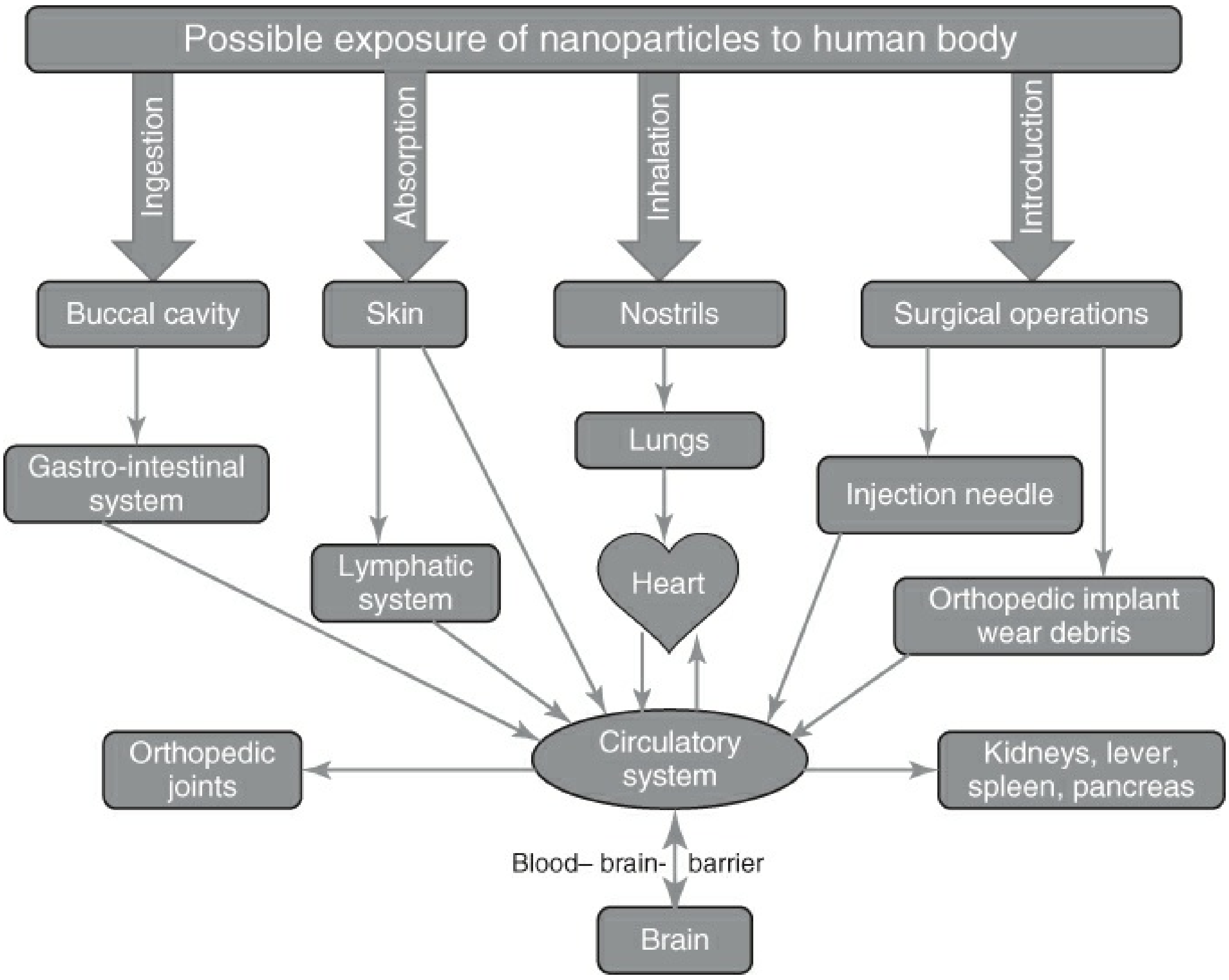

Figure 10.1 Possible pathways of exposure of nanoparticles to human body.

The most extreme adverse health effects produced by nanoparticles in order to immediately increase the awareness of potential toxicity of some nanoparticles. Diseases associated with inhaled nanoparticles are asthma, bronchitis, emphysema, lung cancer, and neurodegenerative diseases, such as Parkinson's and Alzheimer's diseases. Figure 10.2 shows pathways of relocation of inhaled NPs after deposition on the alveolar epithelium of a rodent lungs and transport into the interstitial spaces for long-term retention [6]. Nanoparticles in the gastrointestinal tract have been linked to Crohn's disease and colon cancer. Nanoparticles that enter the circulatory system are related to the occurrence of arteriosclerosis, and blood clots, arrhythmia, heart diseases, and ultimately cardiac death. Translocation to other organs, such as liver and spleen, may lead to diseases of these organs. Exposure to some nanoparticles is associated with the occurrence of autoimmune diseases, such as systemic lupus erythematous, scleroderma, and rheumatoid arthritis [8].

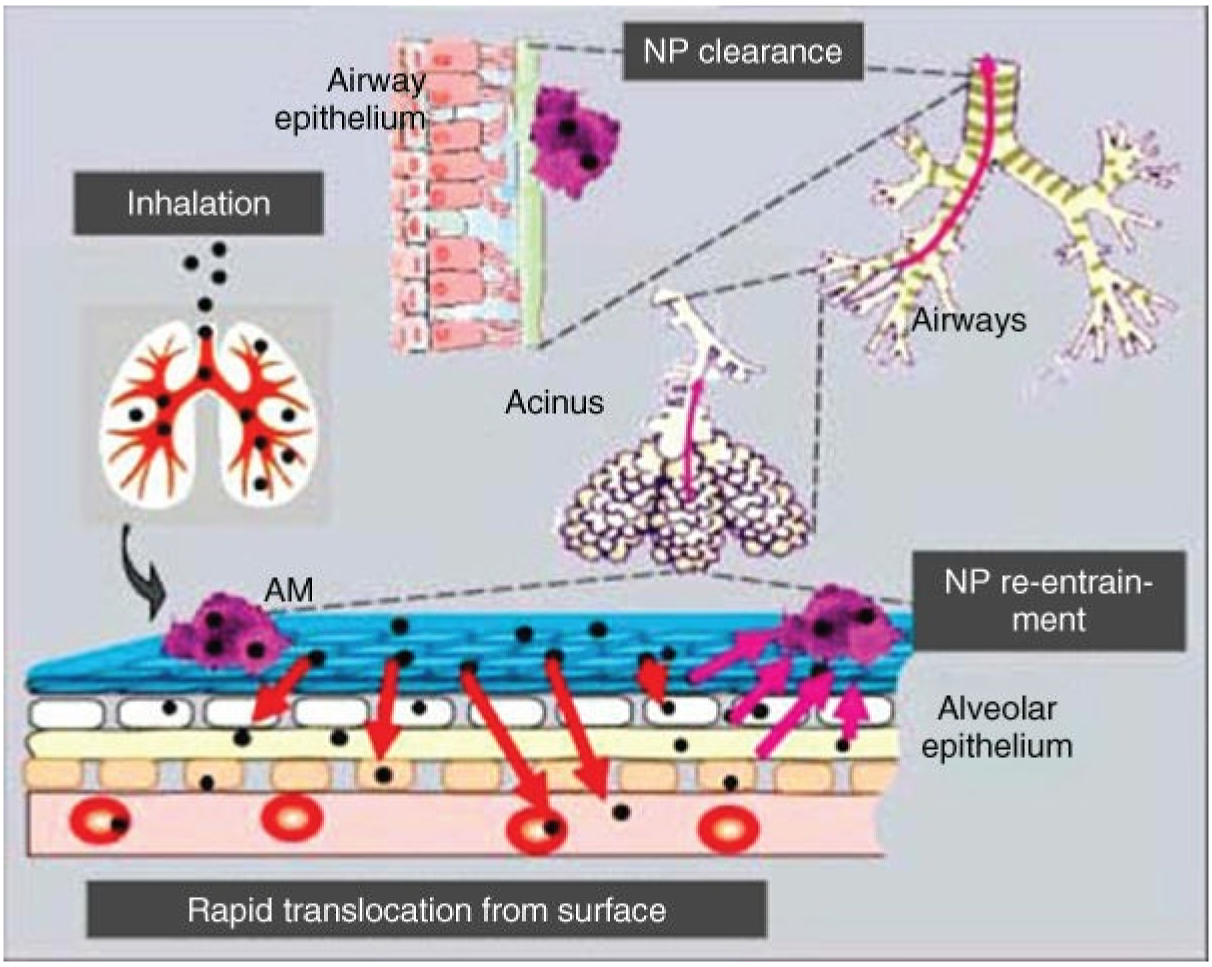

Figure 10.2 Relocation of inhaled NPs after deposition on the alveolar epithelium. Kreyling et al. [6], © 2013. With permission of ACS.

10.2 Sources of Nanoparticles and Their Health Effects

Nanoparticles, occurring naturally as well as generated through human activity, are abundantly available in the environment. Various types of natural and engineered nanoparticles and their sources are illustrated in Figure 10.3 and are discussed in the following sections.

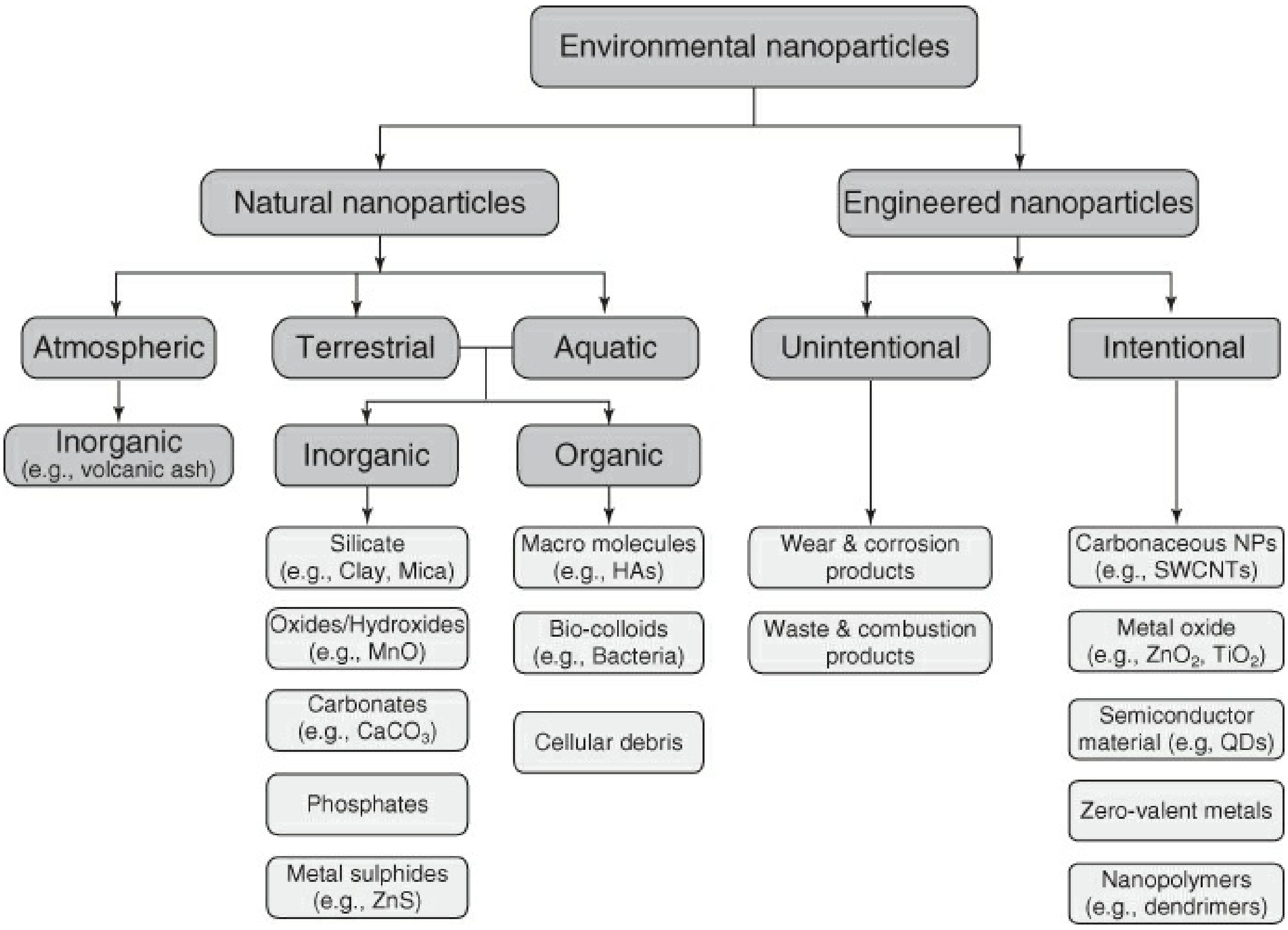
Environmental nanoparticles
Natural nanoparticles
Engineered nanoparticles
Atmospheric
Terrestrial
Aquatic
Unintentional
Intentional
Inorganic (e.g., volcanic ash)
Inorganic
Organic
Silicate (e.g., Clay, Mica)
Oxides/Hydroxides (e.g., MnO)
Carbonates (e.g., $CaCO_3$)
Phosphates
Metal sulphides (e.g., ZnS)
Macro molecules (e.g., HAs)
Bio-colloids (e.g., Bacteria)
Cellular debris
Wear & corrosion products
Waste & combustion products
Carbonaceous NPs (e.g., SWCNTs)
Metal oxide (e.g., ZnO_2, TiO_2)
Semiconductor material (e.g, QDs)
Zero-valent metals
Nanopolymers (e.g., dendrimers)

Figure 10.3 Classification of natural and engineered nanoparticles existing in the environments.

Bhatt and Tripathi [9], © 2011. With permission of Elsevier.

10.2.1 Natural Sources of Nanoparticles

Nanoparticles are abundant in nature, as they are produced in many natural processes, including photochemical reactions, volcanic eruptions, forest fires, dust storms, soil erosion, and by plants and animals, for example, shed skin and hair. Human activities, such as cars, industry, and charcoal burning, and natural events, such as volcanic eruptions and forest fires, can produce such vast quantities of nanoparticulate matter that they profoundly affect air quality worldwide. The aerosols generated by human activities are estimated to be only about 10% of the total, the remaining 90% having a natural origin. These large-scale phenomena are visible from satellites and produce particulate matter and airborne particles of dust and soot ranging from the micro- to nanoscale. Small particles suspended in the atmosphere, often known as aerosols, affect the entire planet's energy balance because they both absorb radiation from the sun and scatter it back to space. It has been estimated that the most significant components of total global atmospheric aerosols are, in decreasing mass abundance [10]: mineral aerosols primarily from soil deflation (wind erosion) with a minor component (<1%) from volcanoes (16.8 Tg), sea salt (3.6 Tg), natural and anthropogenic sulfates (3.3 Tg), products of biomass burning excluding soot (1.8 Tg), and of industrial sources including soot (1.4 Tg), natural and anthropogenic nonmethane hydrocarbons (1.3 Tg), natural and anthropogenic nitrates (0.6 Tg), and biological debris (0.5 Tg); Tg denotes terragram, equal to 10^{12} g.

i. Dust

Terrestrial dust storms: Dust storms appear to be the largest single source of environmental nanoparticles [11]. Long-range migration of both mineral dust and anthropogenic pollutants from the major continents has recently been the subject of intense investigation. Approximately 50% of troposphere atmospheric aerosol particles are minerals originating from the deserts. The size of particles produced during a dust storm varies from 100 nm to several microns, with one-third to a half of the dust mass being smaller than 2.5 µ. Particles in the range 100–200 nm can reach concentrations of 1500 particles/cm^3.

Meteorological observations and modeling have identified 10 main sources of global dust events: (1) the Salton Sea, (2) Patagonia, (3) the Altiplano, (4) the Sahel region, (5) the Sahara Desert, (6) the Namibian desert lands, (7) the Indus Valley, (8) the Taklimakan Desert, (9) the Gobi Desert, and (10) the Lake Eyre basin. Satellite imagery has revealed the dynamics of large-scale dust migration across continents and demonstrated that nanoparticles generated by major environmental events in one part of the world can affect regions thousands of kilometers away.

Extraterrestrial dust: Nanoparticles exist widely in extraterrestrial space. The extraterrestrial dust poses major environmental problems for astronauts as well as for equipment. Lunar dust is very fine grained compared to typical terrestrial dust, with more than 50% of particles found to be in the micron range or smaller. The lunar dust contains a considerable amount of magnetic nanoparticles, clinging to electrostatically charged surfaces such as the astronauts space suits rendering it nearly impossible to remove [12]. On Mars, dust accumulating on the solar panels of the exploration robots has limited the power available to them for locomotion, sensing, and communication.

Terrestrial airborne dust particles can lead to a number of health problems, especially in subjects with asthma and emphysema. The composition of dusts is important, as iron or other metals rich-dust can generate reactive oxygen species (ROS) on the lung surface that can scar the lung tissue. In addition, viruses, bacteria, fungi, or chemical contaminants hitchhiking dust particles may adversely affect health and the environment. Studies on rats have found that intratracheal administration of small amounts of lunar material resulted in pneumoconiosis with fibrosis formation (lung disease and abnormal tissue growth) [13].

ii. Forest Fires

Forest fires and grass fires have long been a part of Earth's natural history and are primarily caused by lightning strikes or by human activity. Major fires can spread ash and smoke over thousands of square miles and lead to an increase in particulate matter (including nanoparticles) exceeding ambient air quality standards. Around 75% of fire-related deaths are due to respiratory problems related to smoke inhalation and not necessarily burns [14].

iii. Volcanoes

When a volcano erupts, ash and gases containing particulate matter ranging from the nanoscale to microns are propelled high into the atmosphere, sometimes reaching heights over 18,000 m. The quantity of particles released into the atmosphere is enormous; a single volcanic eruption can eject up to 30 million tons of ash [10]. Volcanic ash that reaches the upper troposphere and the stratosphere (the two lowest layers of the atmosphere) can spread worldwide and affect all areas of the Earth for years. A primary effect of upper atmospheric particulate debris is the blocking and scattering of radiation from the sun. One particularly harmful volcanic product is particles composed of heavy metals, as these are known to be toxic to humans. While some effects are seen worldwide, the highest levels of particulate matter are found in areas within tens of kilometers from the volcano.

Short-term effects of ash on health include respiratory effects (nose and throat irritation, bronchitis symptoms) and eye and skin irritation. Long-term exposure, on the other hand, leads to the diseases of lympho-endothelial origin, such as Podoconiosis and Kaposi's sarcoma [14, 15].

iv. Ocean and water evaporation

A large amount of sea salt aerosols are emitted from seas and oceans around the world.

These aerosols are formed by water evaporation and when wave-produced water drops are ejected into the atmosphere. Their size ranges from 100 nm to several microns. Nanoparticles can also form in bodies of water through precipitation, as a result of temperature changes and evaporation.

No adverse health effects have been associated to sea salt aerosols. On the contrary, beneficial health effects have been suggested from the use of salt aerosols in the restoration of the mucociliary clearance in patients with respiratory diseases.

v. Biological species

Many biological species are smaller than a few microns, including viruses (10–400 nm) and bacteria (30–700 nm). However, a clear distinction needs to be understood between nanoparticles and nano-organisms or their components (including bacteria, viruses, cells, and their organelles). Cells, bacteria, and viruses are self-organizing, self-replicating, dissipative structures, with a short-lived structure than inorganic solids. Nano-organisms generally dissipate when their supply of energy is exhausted. In contrast, nanoparticles are typically inorganic solids that require no supply of energy to remain in a stable form. They interact, dissipate, or transform via chemical reactions with their environment.

Many organisms, both unicellular and multicellular, produce nanoparticulate inorganic materials through intracellular and extracellular processes [16]. For example, magnetite nanoparticles are synthesized by magnetotactic bacteria and used for navigation relative to the earth's magnetic field, siliceous materials are produced by diatoms, or calcium carbonate layers are produced by S-layer bacteria. Magnetotactic bacteria orient and migrate along the geomagnetic field toward favorable habitats using nanometer-sized magnetic particles inside the cell. These bacteria are aquatic microorganisms inhabiting freshwater and marine environments. Diatoms are unicellular algae with cell walls made of silica. They are abundant in plankton communities and sediments in marine and freshwater ecosystems, where they are an important food source for other marine organisms. Some may even be found in moist soils. Diatoms are used in forensic science to confirm drowning as a cause of death and localize the site of drowning based on the observation of diatoms in the lungs, blood, bone marrow, and organs. Nanobacterium is a nano-organism that synthesizes a shell of calcium phosphate to cover itself and resembles an inorganic particle. The shell ranges in size between 20 and 300 nm, and due to its porous nature it allows the flow of a slimy substance. This slime (presumably together with electrical charge) promotes the adhesion to biological tissues and the formation of colonies.

Among bio-nanoparticles, diatoms might pose a health risk to workers of diatomaceous earth mining and processing; biogenic magnetite is associated with neurodegenerative diseases; and nanobacteria shells were found in humans and animals [17]. Nanobacteria are very resilient, being temperature resistant and gamma radiation resistant. Nanobacteria are ubiquitous within living organisms, humans, and animals, being identified in the blood, serum, and organs. These very small bacteria are suspected of being the cause (at least in part) for many diseases involving calcifications, such as artery plaque, aortic aneurysm, heart valves, renal stone formation, chronic prostatitis, ovarian, and breast tumors. They may also be the cause of rapid kidney stone formation in astronauts on space travels, according to a NASA study [18], probably due to the fact that their multiplication rate in a microgravity environment increases fourfold compared to the rate under normal condition of gravity (of only about 3 days for doubling rate). Definitive mechanisms relating nanobacteria to these above-mentioned diseases are unknown.

10.2.2 Anthropogenic Nanomaterials

Nanomaterials in huge quantities are generated since time immemorial as by-products of various human activities such as simple fuel combustion, cooking, chemical manufacturing, welding, ore refining, smelting, combustion in vehicle and airplane engines, combustion of treated pulverized sewage sludge, and combustion of coal and fuel oil for power generation [6]. Although engineered nanoparticles have been on the market for sometime and are commonly used in cosmetics, sporting goods, tires, stain-resistant clothing, sunscreens, toothpaste, and food additives, these nanomaterials and new more deliberately fabricated nanoparticles, such as carbon nanotubes (CNTs), constitute a small minority of environmental nanomaterials. The quantity of artificial nanoparticles ranges from well-established multiton per year production of carbon black (for car tires) to microgram quantities of fluorescent quantum dots (markers in biological imaging).

i. Diesel and engine

Diesel and automobile exhaust are the primary source of atmospheric nano- and microparticle in urban areas. Most particles from vehicle exhaust are in the size range 20–130 nm for diesel engines and 20–60 nm for gasoline engines, and are typically approximately spherical in shape. Carbon nanotubes and fibers, already a focus of ongoing toxicological studies, were recently found to be present in engine exhaust as a by-product of diesel combustion and also in the environment near gas-combustion sources [19]. The aspect ratio of these fibers is comparable to those of lung-retained asbestos, suggesting that strong carcinogens may exist in exhaust. Nanoparticles constitute 20% of the particles mass but more than 90% of the number of diesel-generated particles. Owing to recent health concerns, particle size and number distribution studies were conducted in various cities across different continents. A high number concentration of nanoparticles can be located near freeways on scales of hundreds of meters, showing that vehicular pollution is a major source of local contaminant particulate matter that includes nanoparticles. These daily profile of nanoparticles matches that of local vehicles usage. High pollution episodes or proximity to high-traffic roads can increase the mass concentration of nanoparticles by several times from typically low background levels of approximately 0.5–2 μg/m.

Research has shown some heterogeneity in the magnitude of adverse health effects of engine exhaust at different places, probably due to the complexity and composition of the exhaust particle. Atmospheric particle pollution from automobile exhaust seems to have a major influence on mortality, with a strong association between increased cardiopulmonary mortality among population living near major roads [20]. The findings of this epidemiological study are in concordance with measurements of nanoparticle concentration near highways, the concentration decreasing exponentially over several hundred meters from the traffic.

ii. Indoor pollution

Indoor air can be 10 times more polluted than outdoor air, according to the Environmental Protection Agency (EPA). Humans and their activities generate considerable amounts of particulate matter indoors. Nanoparticles are generated through common indoor activities, such as cooking, smoking, cleaning, and combustion (e.g., candles, fireplaces). Examples of indoor nanoparticles are textile fibers, skin particles, spores, dust mites droppings, chemicals, smoke from candles, cooking, and cigarettes. A quantitative determination of nanoparticle emissions from selected indoor sources is given in Table 10.1.

Table 10.1 Measured Concentrations of Nanoparticles Resulting from Various Common Indoor Household Activities

Nanoparticle Source	Concentration (Nanoparticles/cm^3)	Estimated Source Strength (Particles/min × 10^{11})
Pure wax candle	241,500	3.65
Radiator	218,400	8.84
Cigarette	213,300	3.76
Frying meat	150,900	8.27
Heater	116,800	3.89
Gas stove	79,600	1.3
Scented candles	69,600	0.88
Vacuum cleaner	38,300	0.38
Air freshener spray	29,900	2.34
Ironing a cotton sheet	7,200	0.007

Source: Afshari et al. [21]. With permission of Wiley.

Particles have also been shown to enter buildings from outdoors through ventilation systems. As humans generally spend much of their time indoors (more than 80%), indoor pollution directly affects our health.

Health effects: Long-term exposure to indoor cooking emissions may pose adverse health effects due to particulate matter inhalation [22]. During cooking, the level of particulate matter increases more than 10-fold compared to noncooking hours (Figure 10.4). In many regions, especially of Africa and Asia, the indoor smoke of solid fuels using biomass (wood, crop residue, dung, coal) in a poorly ventilated stove poses health hazards. Word Health Organization estimates that more than 50% of the world population uses solid fuels for cooking and heating, including biomass fuels. Wood burning is often disregarded as a source of nanoparticles and assumed to be benign to the environment simply because wood is a renewable source.

Figure 10.4 Indoor air pollution from cooking.

iii. Cosmetics and other consumer products

The use of nanomaterials in cosmetics is not new. Black soot and mineral powders have been used as cosmetics since thousands of years ago in ancient Egypt, and some of them continue to be used today. Due to the recent development of nanotechnology, engineered nanomaterials have been embraced by the cosmetics industry (refer Chapter 9), which includes, personal care products (deodorants, soap, toothpaste, shampoo, hair conditioner), sunscreen, cosmetics (cream, foundation, face powder, lipstick, blush, eye shadow, nail polish, perfume, and after-shave lotion). Everything labeled “nanoparticle” is considered dangerous to some in the absence of lack of regulations for testing of cosmetic products before they are sold to the public. Similar to pharmaceutical products, cosmetics using nanoparticles are required to undergo testing and calibration protocols before declaring them safe for use.

Many other consumer products incorporate nano or microparticles. Titanium dioxide (TiO_2) particles with diameter larger than 100 nm are considered biologically inert in both humans and animals. Based on this understanding, titanium dioxide nanoparticles have been widely used in many products, such as white pigment, food colorant, sunscreens, and cosmetic creams. However, adverse effects of titanium dioxide nanoparticles have recently been uncovered [23].

Silver nanoparticles are used as antibacterial/antifungal agents in a diverse range of applications: air sanitizer sprays, socks, pillows, slippers, face masks, wet wipes, detergent, soap, shampoo, toothpaste, air filters, coatings of refrigerators, vacuum cleaners, washing machines, food storage containers, cellular phones, and even in liquid condoms.

Coatings of nanoparticles are widely used for modifying fabrics to create stain and wrinkle-free properties. In addition, one can find clothes with built-in sunscreen and moisture management technology. Fabric containing bamboo–charcoal nanoparticles claims antibacterial antifungal properties. They are intended for use as face cloth masks, shoes insoles. Nanocoatings are applied to wetsuits for higher performance of athletes or self-cleaning surfaces. Textiles with 30-nm embedded nanoparticles help prevent pollen from entering gaps in the fabric. Nanoparticles or nanofibers are starting to be used in water-repellent, stain-resistant plush toys, stain-repellent mattresses. Nanosealant sprays for fabrics or leather, and hydrophobic nanoparticle solutions adhering to concrete, wood, glass, cloth, and so on allow the surfaces to deflect water. The most peculiar applications of nanofibers and nanoparticle are nanofibers that hide hair loss and liquid condoms.

Health effects: All the health effects of the gamut of nanoparticles used in consumer products are not yet known, although nanotoxicology has revealed adverse health effects of materials previously considered safe. For example, silver, widely used as an antibacterial agent, proves to be toxic to humans or animal cells because when it is in nanoparticle form, its cytotoxicity is higher than that of asbestos [24]. Inhalation of silver nanoparticles leads to their migration to the olfactory bulb, where they locate in the mitochondria, as well as translocation to the circulatory system, liver, kidney, and heart. Silver nanoparticles have been found in the blood of patients with blood diseases and in the colon of patients with colon cancer.

A controversial subject is the association between the uptake of aluminum and Alzheimer's disease [25]. Epidemiological studies to find the connection between aluminum in antiperspirants, antacids, or drinking water and Alzheimer's disease are conflicting, some finding positive associations and others none. Due to their latent evolving nature and multipart etiology, these neurological diseases are difficult to associate with specific factors. Along with the beneficial antioxidant properties of some nanomaterials, long-term effect needs to be studied. Number of questions needs to be addressed before taking them into use such as the following:

- Are nanoparticles biocompatible?
- Do the nanoparticles enter the lymphatic and circulatory systems? If not, do they accumulate in the skin and what are the long-term effects of accumulation?
- Do nanoparticles produce inflammation?
- If nanoparticles enter the lymphatic and circulatory system, is the amount significant?
- What are the long-term effects of nanoparticles uptake?
- What is the long-term fate of nanoparticles?
- Are nanoparticles stored in the skin?
- Do nanoparticles enter circulation?
- What happens when the nanoparticles undergo chemical reactions and lose their antioxidant properties?

iv. Engineered nanomaterials

A critical fact to consider with engineered nanomaterials is that they can be synthesized in almost any shape and size. Nanostructured materials which are firmly attached to a substrate and do not pose a health risk as long as they do not detach from the substrate. Nanostructured materials where nanostructures are free and can become airborne, consequently pose a potential health risk (Table 10.2). Some artificial nanoparticles engineered by glancing angle deposition are more or less similar in size to microorganisms, such as bacteria and viruses.

Table 10.2 Expected Toxicological Effects of Engineered Nanoparticles

Toxicological Effect	Example of Study
Nanoparticles may be toxic to cells *in vitro*	Cadmium–selenium quantum dots toxic to monkey and human cell lines causing cell death
Cytotoxicity may be modified or reduced by coatings or substituent groups	Cd–Se quantum dots coated with ZnS or polyethylene glycol do not cause cell death during 2-week incubation in liver hepatocytes
Nanoparticles may be more toxic than micron-sized particles in short-term animal tests	Nanosized titanium dioxide (20 nm) produced 43-fold more inflammation than 250 nm size particles in short-term tests of pulmonary toxicity in rats
Nanoparticles may translocate to other organs in body	Radioactive carbon particles found in liver after 6-h inhalation exposure in rats
Nanoparticles may enter brain through nasal epithelium olfactory neurons	Radioactive carbon reached olfactory bulb, cerebellum, and cerebrum via olfactory neurons in rats
Nanoparticles may cause pulmonary inflammation, granulomas, and fibrosis in short-term animal tests	CNTs cause inflammation, granulomas, and fibrosis after single dose instillation in mice. Also decreased breathing rate and bacterial clearance
Nanoparticle may penetrate skin in isolated skin assays	Quantum dots penetrate to living dermis in isolated pig skin bioassay

Source: Hallock et al. [26]. With permission of Division of Chemical Health and Safety of the ACS, Elsevier Inc.

10.3 Toxicology of Engineered Nanoparticles

10.3.1 Respiratory Tract Uptake and Clearance

After inhalation, nanoparticles deposit throughout the entire respiratory tract, starting from the nose and the pharynx, down to the lungs. Lungs consist of airways that transport air in and out and alveoli, which are gas exchange surfaces. Human lungs have an internal surface area between 75 and 140 m^2 and about 300 million alveoli. Due to their large surface area, the lung is the primary entry portal for inhaled particles.

i. Nanoparticle size-dependent inhalation

Spherically shaped solid material with particle diameters smaller than 10 μm can reach the gas exchange surfaces. Larger diameter particles tend to be deposited further up in the respiratory tract as a result of gravitational settling, impaction, and interception. Many larger diameter fibers are deposited at “saddle points” in the branching respiratory tree. Smaller diameter particles are more affected by diffusion, and these can collect in the smaller airways and alveoli. Fibers having a small diameter may penetrate deep into the lung though very long-aspect-ratio fibers will remain in the upper airways. As shown in Figure 10.5, the nasopharyngeal region captures mainly microparticles and nanoparticles smaller than 10 nm, while the lungs will receive mainly nanoparticles with a diameter between 10 and 20 nm [27].

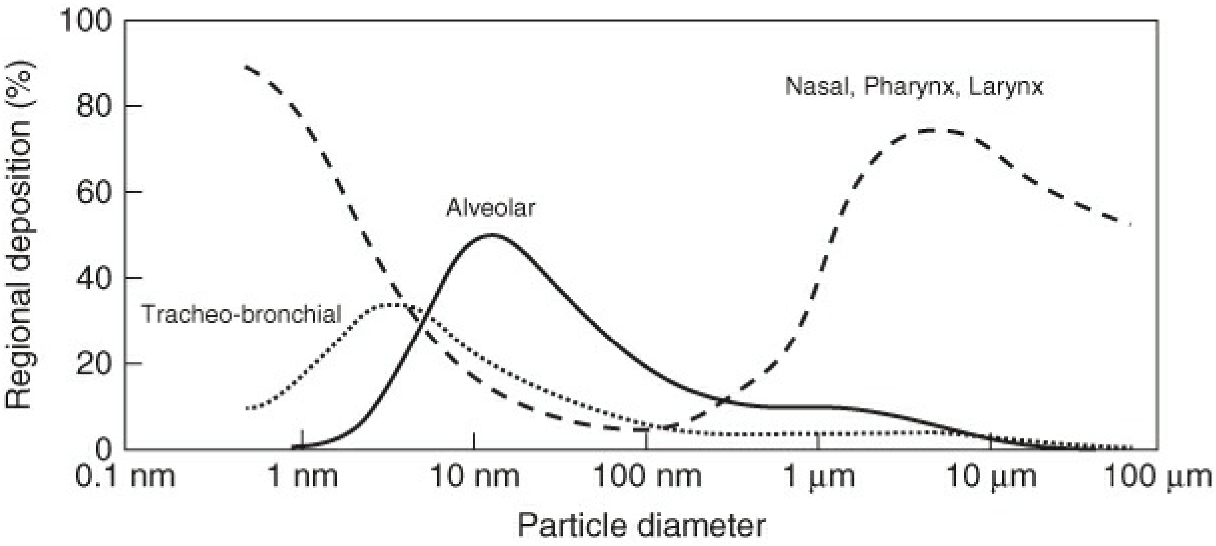

Figure 10.5 Deposition of inhaled particles in the human respiratory tract versus particle diameter.

Oberdorster [27], © 2001. With permission of Springer.

ii. Nanoparticle size-dependent phagocytosis

Human alveolar macrophages measure between 14 and 21 μm, while rat alveolar macrophages measure between 10 and 13 μm. Macrophages can engulf particles of a size comparable to their own dimensions, but are significantly less effective with particles that are much larger or smaller. Experimental data show that, compared with larger particles, nanoparticles smaller than 100–200 nm are more capable of evading alveolar macrophage phagocytosis, entering pulmonary interstitial sites, and interacting with epithelial cells to get access to the circulatory and lymphatic systems. There are contradictory reports related to the phagocytosis of nanoparticles smaller than 100 nm. *In vitro* studies show that nanoparticles activate and are phagocytized by alveolar macrophages that are not efficiently phagocytized in comparison with particles between 1 and 3 μm. A 12-week inhalation study in rats showed that 20 nm nanoparticles of titanium dioxide are characterized by longer retention time in the lungs and increased translocation to interstitial sites than larger nanoparticles (250 nm) of the same material. Small nanoparticles that evade the alveolar macrophages penetrate the alveolar epithelium, resulting in a slower clearance rate from the lung and possibly later translocation to the circulatory and lymphatic system [28].

iii. Concentration-dependent phagocytosis

At high concentrations, nanoparticles tend to cluster, forming aggregates often larger than 100 nm. Larger nanoparticles (>100 nm) can be readily phagocytized by alveolar macrophages. Results of studies involving inhalation or intratracheal instillation of high concentrations of nanoparticle (silver, iron, India ink, or titanium dioxide) smaller than 100 nm, which aggregate in larger particles, suggest that most nanoparticles are indeed stopped by alveolar macrophages. Rat studies based on the inhalation of low concentrations of 15-nm-diameter silver nanoparticles showed that soon after inhalation (30 min), nanoparticles are distributed in the blood and brain, and subsequently to organs, such as the heart, kidney, while the lungs rapidly cleared of the nanoparticles. Hence, minute concentrations of nanoparticles with size smaller than 100 nm can have a higher probability of translocating to the circulatory system and organs (and produce damage) than high concentrations of the same particles, which are likely to form aggregates, and which will be stopped from translocation by macrophage phagocytosis [24].

iv. Lung burden

The adverse effect of inhaled nanoparticles on the lungs depends on the lung burden (determined by the rate of particle deposition and clearance) and on the residence time of the nanoparticles in the lung. For example, carbon nanotubes are not eliminated from the lungs or very slowly eliminated (81% found in rat lungs after 60 days). The persistent presence within the alveoli of inhaled particles, especially those with mutagenic potential, increases the risk of lung cancer [29].

v. Translocation and clearance of inhaled nanoparticles

Inhaled nanoparticles are shown to reach the nervous system via the olfactory nerves and/or blood–brain barrier. Nanoparticles that reach the lung are predominantly cleared via mucociliary escalator into the gastrointestinal tract (and then eliminated in the feces), lymphatic system, and circulatory systems. From the lymphatic and circulatory systems, nanoparticles may be distributed to organs, including kidneys from where partial or total clearance may occur [30].

vi. Adverse health effects in the respiratory tract

Recent research has led to changes in terminology and brought about the realization that no particles are completely inert, and that even low concentrations of particles have negative health effects. The adverse health effects of nanoparticles depend on the residence time in the respiratory tract. Smaller particles have a higher toxicity than larger particles of the same composition and crystalline structure, and they generate a consistently higher inflammatory reaction in the lungs. Smaller nanoparticles are correlated with adverse reactions such as: impaired macrophage clearance, inflammation, accumulation of particles, and epithelial cell proliferation, followed by fibrosis, emphysema, and the appearance of tumors. Particle uptake and potential health effects may be dependent on genetic susceptibility and health status. Recent studies have demonstrated that inhalation of nanoparticles can affect the immune system defense ability to combat infections. Nanoparticles of various compositions are able to modulate the intrinsic defensive function of macrophages, affecting their reactivity to infections. It is reported that several types of nanoparticles (such as ZrO_2) enhance the expression of some viral receptors, making macrophages exposed to nanoparticles hyper-reactive to viral infections and leading to excessive inflammation [31]. On the other hand, exposure to other nanoparticles (SiO_2, TiO_2) leads to a decrease in the expression of some other viral and bacterial receptors, leading to lower resistance to some viruses or bacteria.

Adaptability: Organisms are capable of adapting to specific environmental stresses. Recent studies suggest that pre-exposure to low concentrations of nanoparticles stimulates the phagocytic activity of cells, while high concentration of nanoparticles impairs this activity. At the same time, genotype is an important factor in adaptability.

Treatment: Treatments for nanoparticles inhalation include those that act to enhance mucociliary clearance, and those that reduce the effects of oxidation and inflammation. Mucociliary clearance can be enhanced twofold by the inhalation of increasing concentrations of saline solutions. The saline solution acts as an osmotic agent increasing the volume of airway surface liquid. Anti-inflammatory medicine (sodium cromoglycate) was found to strongly reduce airway inflammation caused by diesel exhaust nanoparticles. Sodium cromoglycate works by reducing allergic responses (inhibits the release of mediators from mast cells – cells responsible for the symptoms of allergy). Antioxidant vitamins (particularly vitamin C), rosmarinic acid, and a high intake of fresh fruit and some vegetables have a protective effect against lung diseases.

10.3.2 Cellular Interaction with Nanoparticles

Due to proximity in the size of living cells with those of nanoparticles, there is a high probability of their interaction that may cause adverse health effects. In the following, the mechanism of such interaction and the resulting health effects are discussed.

i. Cellular uptake

Like nano-organisms (viruses), nanoparticles are able to enter cells and interact with subcellular structures. Cellular uptake, subcellular localization, and ability to catalyze oxidative products depend on chemistry, size, and shape of the nanoparticles. The mechanism by which nanoparticles penetrate cells without specific receptors on their outer surface is assumed to be a passive uptake or adhesive interaction. This uptake may be initiated by van der Waals forces, electrostatic charges, steric interactions, or interfacial tension effects, and does not result in the formation of vesicles. (Steric interactions occur when nanoparticles have molecules with size, geometries, bonding, and charges optimized for the interaction with the receptors.) After this type of uptake, the nanoparticles are not necessarily located within a phagosome (which offers some protection to the rest of the cellular organelles from the chemical interaction with the nanoparticle). For example, C_{60} molecules enter cells and can be found along the nuclear membrane and within the nucleus. This type of uptake and free movement within the cell makes them very dangerous by having direct access to cytoplasm proteins and organelles. Upon nonphagocytic uptake, nanoparticles can be found in various locations inside cell, such as the outer-cell membrane, cytoplasm, mitochondria, lipid vesicles, along the nuclear membrane, or within the nucleus [32]. Depending on their localization inside the cell, the nanoparticles can damage organelles or DNA, or ultimately cause cell death. Nanoparticles are internalized not only by professional phagocytes such as alveolar macrophages but by various types of cells, including endothelial cells, pulmonary epithelium, gastrointestinal epithelium, red blood cells, platelets, and nerve cells. Particle internalization location, however, depends on nanoparticle size. Very small nanoparticles, such as C_{60} molecules with a diameter of 0.7 nm, are able to penetrate cells via a different mechanism than phagocytosis, probably through ion channels or via pores in the cell membrane.

ii. Oxidative stress, inflammation, and genotoxicity

Although the exact mechanism whereby nanoparticles induce pro-inflammatory effects is not known, it has been suggested that they create ROS and thereby modulate intracellular calcium concentrations, activate transcription factors, and induce cytokine production. Nanoparticles have been shown to generate more free radicals and ROS than larger particles, likely due to their higher surface area. The current understanding of these very complex cellular mechanisms is described as follows.

Oxidative stress generation: Both *in vivo* and *in vitro* studies have shown that nanoparticles of various compositions (fullerenes, carbon nanotubes, quantum dots, and automobile exhaust) create ROS that have been shown to damage cells by peroxidizing lipids, altering proteins, disrupting DNA, interfering with signaling functions, and modulating gene transcription [30]. Oxidative stress is a response to cell injury and can also occur as an effect of cell respiration, metabolism, ischemia/reperfusion, inflammation, and metabolism of foreign compounds [33, 34]. The oxidative stress induced by nanoparticles may have several sources:

- ROS can be generated directly from the surface of particles when both oxidants and free radicals are present on the surface of the particles. Many compounds hitchhiking on the surface of nanoparticles (usually present in ambient air) are capable of inducing oxidative damage, including ozone (O_3) and NO_2.
- Transition metal (iron, copper, chromium, vanadium, etc.) nanoparticles can generate ROS acting as catalysts in Fenton-type reactions. For example, the reduction of hydrogen peroxide H_2O_2 with ferrous iron (Fe^{2+}) results in the formation of hydroxyl radical ($^{\cdot}OH$) that is extremely reactive, attacking biological molecules situated within diffusion range.
- Altered functions of mitochondrion. As shown in several studies, small nanoparticles are able to enter mitochondria and produce physical damage, contributing to oxidative stress.
- Activation of inflammatory cells, such as alveolar macrophages and neutrophils, which can be induced by phagocytosis of nanoparticles, can lead to the generation of ROS and reactive nitrogen species. Alveolar macrophages participate in the initiation of inflammation in the lung.

Inflammation: Inflammation is the normal response of the body to injury. When generated in moderation, inflammation stimulates the regeneration of healthy tissue, however when in excess, it can lead to disease. *In vitro* and *in vivo* experiments demonstrate that exposure to small nanoparticles is associated with inflammation, with particle size and composition being the most important factors. Inflammation is controlled by a complex series of intracellular and extracellular events. The oxidative stress results in the release of pro-inflammatory mediators or cytokines – intercellular chemical messengers alerting the immune system when an infection is present. Some nanoparticles can produce cell death via mitochondrial damage without inflammation.

Antioxidants: The oxidative stress also results in the release of antioxidants – proteins that act to remove the oxidative stress. In addition to the antioxidants released as a response to the oxidative process, nanoparticles may interact with metal-sequestering proteins and antioxidants (from body fluids and intracellularly), which will likely modify the surface properties of the nanoparticle to some extent, rendering them less toxic.

DNA damage: Generation of ROS to the point that they overwhelm the antioxidant defense system (shifting the redox balance of the cell) can result in oxidation, and therefore destruction, of cellular biomolecules, such as DNA, leading to heritable mutations. For example, the chemical modification of histones (or binding proteins that support the supercoiled structure of DNA) opens the coiled DNA and allows its alteration. Epidemiological *in vitro* and *in vivo* studies show that nanoparticles of various materials (diesel, carbon black, welding fumes, transition metals) are genotoxic in humans or rats. In summary, nanoparticles can directly generate ROS on their surfaces or by activation of macrophages. Overall, the generation of oxidative species leads to increased inflammation and increased antioxidant production. The activation of macrophages leads to modulation in intracellular calcium concentration that, in turn, activates further the ROS production, which in turn enhances further calcium signaling by the oxidation of calcium pumps in the endoplasmic reticulum, leading to calcium depletion. Intracellular calcium modulation results in impaired motility and reduced macrophage phagocytosis. Nonphagocytized nanoparticles are likely to access and interact with epithelial cells, thus enhancing inflammation. Ultimately, the interaction of nanoparticles with cells may lead to DNA modifications, cell injury, and disease.

Adverse health effects

Nanoparticles, due to their small size, can influence basic cellular processes, such as proliferation, metabolism, and death. Many diseases can be associated with dysfunction of these basic processes. For example, cancer results from uncontrolled cell proliferation, while neurodegenerative diseases are caused in part by premature cell death. Oxidative stress has been implicated in many diseases, including cardiovascular and neurological disease, pancreatitis, and cancer [34]. Severe inflammation is assumed to be the initiating step in the appearance of autoimmune diseases (systemic lupus erythematosus, scleroderma, and rheumatoid arthritis) associated with exposure to some nanoparticles, such as silica and asbestos.

Regarding the treatment of adverse health effects caused by nanoparticles cytotoxicity, antioxidants, anti-inflammatory drugs, and metal chelators show promising effects. Antioxidant therapy has been found to protect against the development of hypertension, arteriosclerosis, cardiomyopathies, and coronary heart disease, providing further evidence of the link between the oxidative stress response and cardiovascular effects. The adverse health effects of transition metals can be diminished by metal-chelating ligands [33].

10.3.3 Nervous System Uptake of Nanoparticles

The nervous system comprises brain, spinal cord, and nerves that connect the brain and spinal cord to the rest of the body. In addition to the uptake of nanoparticle due to inhalation, the nervous system uptake may also occur via other pathways. Uptake via olfactory bulb and the blood–brain barrier are the most studied pathways.

Adverse health effects: Experimental evidence suggests that the initiation and promotion of neurodegenerative diseases, such as Alzheimer's disease, Parkinson's disease, Pick's disease, are associated with oxidative stress and accumulation of high concentrations of metals (such as copper, aluminum, zinc, but especially iron) in brain regions associated with function loss and cell damage. Iron is necessary in many cellular functions, especially in the brain, where it participates in many neuronal processes. In excess, however, iron is toxic to cells. The brain continuously accumulates iron, resulting in increased stored iron amounts with the age. In order to prevent its toxicity, organisms developed a way to store excess iron in proteins called ferritin (Ft). Dysfunction of ferritin resulting from excessive accumulation of iron may cause oxidative stress and myelin (the electrically insulating coatings of axons) breakdown [30].

Both metal homeostasis imbalance and neuronal loss are present in neurodegenerative diseases. (Homeostasis is a dynamic equilibrium balancing act necessary for a proper function of a living system.) It is not known if the presence of metals in brain of subjects with neurodegenerative diseases is due to nanoparticles themselves translocating to the brain or their soluble compounds.

Despite the fact that the etiology of neurodegenerative diseases is unknown, environmental factors are believed to play a crucial factor in their progress, being able to trigger pro-inflammatory responses in the brain tissue. Recent studies on DNA damage in nasal and brain tissues of canines exposed to air pollutants show evidence of chronic brain inflammation, neuronal dysfunction, and similar pathological findings with those of early stages of Alzheimer's disease. Autopsy reports on humans suggest similar results. Significant oxidative damage was found in the brain of a largemouth bass after exposure to C_{60}.

Treatment: Antioxidants and metal chelators are treatment options for the adverse health effects caused by the neuronal uptake of nanoparticles. In the therapy of neurodegenerative diseases, metal chelators transported across the blood–brain barrier seem to be a very promising approach [35]. Functionalized fullerenes and nanoparticles made of compounds holding oxygen vacancies show great antioxidant properties. Fullerols, or polyhydroxylated fullerenes, are excellent antioxidants with high solubility and ability to cross the blood–brain barrier, showing promising results as neuroprotective agents. CeO_2 and Y_2O_3 nanoparticles have strong antioxidant properties on rodent nervous system cells. Cerium oxide tends to be nonstoichiometric, Ce atoms having a dual oxidation state, +3 or +4, leading to oxygen vacancies.

10.3.4 Nanoparticles Translocation to the Lymphatic Systems

Translocation of nanoparticles to lymph nodes is a topic of intense investigation today for drug delivery and tumor imaging. Progression of many cancers (lung, esophageal, mesothelioma, etc.) is seen in the spread of tumor cells to local lymph nodes. The detection and targeted drug delivery to these sites are the steps involved in the therapeutic treatment of cancer. Several studies show that interstitially injected particles pass preferentially through the lymphatic system and not the circulatory system, probably due to permeability differences. After entering the lymphatic system, they locate in the lymph nodes [36]. The free nanoparticles reaching the lymph nodes are ingested by resident macrophages. Nanoparticles that are able to enter the circulatory system can also gain access to the interstitium, and from there they are drained through the lymphatic system to the lymph nodes as free nanoparticles and/or inside macrophages.

10.3.5 Nanoparticles Translocation to the Circulatory System

Inhalation or instillation studies in healthy animals show that metallic nanoparticle with size smaller than 30 nm pass rapidly into the circulatory system, while nonmetallic nanoparticles with size between 4 and 200 nm pass very little or not at all [37]. In contrast, the subjects suffering from respiratory and circulatory diseases have higher capillary permeability, allowing fast translocation of metallic or nonmetallic nanoparticle into circulation.

i. Long-term translocation

Nanoparticles, unlike larger particles, are able to translocate across the respiratory epithelium after being deposited in the lungs. Once they have crossed the respiratory epithelium, they may persist in the interstitium for years, or they may enter the lymphatic system and circulatory system. From the circulatory system, long-term translocation to organs (such as the liver, heart, spleen, bladder, kidney, bone marrow) is possible, depending on the duration of exposure. Smaller particles (20 nm) are cleared faster from the lung than larger particles (100 nm) probably because small nanoparticles are not efficiently phagocytized by macrophages and are able to enter more rapidly into the circulatory and/or lymphatic systems [24].

ii. Short-Term Translocation

Evidence of rapid translocation of metal nanoparticles from lungs into the circulation and to organs has been provided by animal studies [30], which shows the location of nanoparticles (Ag, Au, TiO_2) with size ranging from 10 to 30 nm in the blood, liver, kidney, spleen, brain, and heart. These studies suggest that nanoparticles in particular size range may induce aggregation of platelets, leading to the formation of blood clots. There is no conclusive evidence showing fast translocation of carbon-based nanomaterials into systemic circulation. Short-term translocation of radiolabeled nanoparticles from the lungs to the organs is currently the subject of debate as a significant fraction of radioactive labels detaches from their labeled nanoparticles, so radioactivity observed throughout the body may not indicate the actual translocation of nanoparticles, but of radiolabels. Technetium's short-lived isotope ^{99m}Tc, with an atomic diameter of about 0.37 nm, is used in labeling nanoparticles that are subsequently injected or inhaled by subjects. In many cases, the radiolabel can separate from the nanoparticles and follow a different translocation route. In the presence of oxygen, the radioactive label can transform into pertechnetate (^{99m}TcO) having a slightly larger diameter of roughly 0.5 nm. Most studies show very little or no translocation of radiolabeled polystyrene nanoparticles with diameters of 56 and 200 nm, or carbon nanoparticles with diameters of 5, 4–20, 35, and 100 nm, while others show a rapid and substantial translocation into circulation for particles sized 5–10 and 20–30 nm [38].

While the short-term extra-pulmonary translocation into circulation in healthy subjects is still under debate, there seems to be an agreement on the fact that nanoparticle fast translocation into circulation may be enhanced by pulmonary inflammation and increased microvascular permeability. Subjects suffering from respiratory or blood diseases may have an increased susceptibility of nanoparticles translocation from the lungs to circulation and organs.

iii. Nanoparticles uptake and interaction with blood cells

There are three main types of cells in the blood: red cells in charge of oxygen transport; white cells responsible for fighting infections; and platelets that help prevent bleeding by forming blood clots. The uptake of nanoparticles by each type of blood cells is essentially different [39].

Nanoparticle uptake by red blood cells (that do not have phagocytic abilities due to the lack of phagocytic receptors) is entirely dictated by size, while the nanoparticle charge or material type plays little importance. In contrast, nanoparticle charge plays an essential role in their uptake by platelets and their influence on blood clot formation. Uncharged polystyrene particles do not have an effect on blood clots formation. Negatively charged nanoparticles significantly inhibit thrombi formation, while positively charge nanoparticles enhance platelet aggregation and thrombosis.

Microscopic and energy-dispersive spectrometry (EDS) analysis of blood clots from patients with blood disorders revealed the presence of foreign nanoparticles. Most notably, patients with the same type of blood disorder show fibrous tissue clots embedding nanoparticle with different composition: gold, silver, cobalt, titanium, antimony, tungsten, nickel, zinc, mercury, barium, iron, chromium, nickel, silicon, glass, talc, and stainless steel. The common denominator of the particles is their size, ranging from tens of nanometers to few microns.

Adverse health effects

Thrombosis: Translocation of nanoparticles into the circulatory system was correlated with the appearance of thrombi (or blood clots). The time frame of this process is very short, thrombosis occurring during the first hour after exposure. Hamster studies of tracheally or intravenously instilled nanoparticles of charged polystyrene (60 nm) and diesel exhaust particles (20–50 nm) significantly increased arterial or venous thrombus formation during the first hour after administration. There is a clear dose-dependent response correlating the quantity of pollutant administered and the observed thrombus sizes [20]. Prothrombotic effects persisted 24 h after instillation. If inhaled nanoparticles were to be found in red blood cells located in pulmonary capillaries, one would expect adverse health effects as blood-related diseases, such as anemia, due to reduced oxygen transport capacity of the red blood cells.

Cardiovascular malfunction: It is clear from clinical and experimental evidence that inhalation of nano- and microparticles can cause cardiovascular effects. Despite the fact that there is an intuitive relationship between inhaled nanoparticles and adverse respiratory effects, the causal link between particles in the lung and cardiovascular effects is not entirely understood. It was thought that the pulmonary inflammation caused by the particles triggers a systemic release of cytokines, resulting in adverse cardiovascular effects. However, recent studies on animals [24] and humans [40] have shown that nanoparticles diffuse from the lungs into the systemic circulation, and then are transported to the organs, demonstrating that cardiovascular effects of instilled or inhaled nanoparticles can arise directly from the presence of nanoparticles within the organism.

10.3.6 Liver, Spleen, Kidneys Uptake of Nanoparticles

Micro- and nanoparticle debris was detected by scanning electron microscopy in the organs and blood of patients with orthopedic implants, drug addiction, worn dental prostheses, blood diseases, colon cancer, Crohn's disease, ulcerative colitis, and with diseases of unknown etiology [41]. Coal workers autopsies reveal an increased amount of particles in the liver and spleen compared to non-coal workers. The workers with pronounced lung diseases have more nanoparticles in their organs than healthier nanoparticles. The pathway of exposure most likely involves the translocation from lungs to circulation of the inhaled nanoparticles, followed by uptake by the organs.

Present knowledge on the effect of nanoparticles on organs such as liver, kidneys, spleen is not conclusive, however, one can speculate that as long as there is translocation to and accumulation of nanoparticles in these organs, potentially adverse reactions and cytotoxicity may lead to diseases [42]. Dental prosthesis debris internalized by intestinal absorption can lead to severe health conditions, including fever, enlarged spleen and liver, suppression of bile flow, and acute renal failure about a year after the application.

10.3.7 Gastrointestinal Tract Uptake and Clearance of Nanoparticles

Endogenous sources of nanoparticles in the gastrointestinal tract are derived from intestinal calcium and phosphate secretion. Exogenous sources are particles such as titanium oxide from food (colorants), pharmaceuticals, water, toothpaste, cosmetics (lipstick), dental prosthesis debris, and inhaled particles [24]. The dietary consumption of nanoparticles in developed countries is estimated around 10^{12} particles/person per day [43]. They consist mainly of TiO_2 and mixed silicates. The use of specific products, such as salad dressing containing a nanoparticle TiO_2 whitening agent, can lead to an increase by more than 40-fold of the daily average intake. These nanoparticles do not degrade in time and accumulate in macrophages. A portion of the particles cleared by the mucociliary escalator can be subsequently ingested into the gastrointestinal tract. Also, a small fraction of inhaled nanoparticles was found to pass into the gastrointestinal tract.

i. Size and charge-dependent uptake

The gastrointestinal tract is a complex barrier-exchange system and is the most important route for macromolecules to enter the body. The epithelium of the small and large intestines is in close contact with ingested material, which is absorbed by the villi. The extent of particles absorption in the gastrointestinal tract is affected by size, surface chemistry and charge, length of administration, and dose. The absorption of particles in the gastrointestinal tract depends on their size, the uptake diminishing for larger particles. A study of polystyrene particles with size between 50 nm and 3 µm indicated that the uptake decreases with increasing particle size from 6.6% for 50 nm, 5.8% for 100 nm nanoparticles, 0.8% for 1 µm, to 0% for 3 µm particles. The time required for nanoparticles to cross the colonic mucus layer depends on the particle size, with smaller particles crossing faster than larger particles: 14-nm-diameter latex nanoparticles cross within 2 min, 415 nm within 30 min, and 1000 nm particles do not pass this barrier [44]. Particles that penetrate the mucus reach the enterocytes and are able to translocate further. Enterocytes are a type of epithelial cell of the superficial layer of the small and large intestine tissue, which aid in the absorption of nutrients. When in contact with the submucosal tissue, nanoparticles can enter the lymphatic system and capillaries and then are able to reach various organs.

ii. Translocation

Varying the characteristics of nanoparticles, such as size, surface charge, attachment of ligands, or surfactant coatings, offers the possibility for site-specific targeting of different regions of the gastrointestinal tract. The fast transit of material through the intestinal tract (on the order of hours), together with the continuous renewal of epithelium, led to the hypothesis that nanomaterials will not remain there for indefinite periods. Most of the studies of ingested nanoparticles have shown that they are eliminated rapidly: 98% in the feces within 48 h and most of the remainder via urine [30]. However, other studies indicate that certain nanoparticles can translocate to the blood, spleen, liver, bone marrow, lymph nodes, kidneys, lungs, and brain, and can also be found in the stomach and small intestine. Oral uptake of polystyrene spheres of various sizes (50 nm–3 µm) by rats resulted in a systemic distribution to liver, spleen, blood, and bone marrow.

Adverse health effects

Crohn's disease, ulcerative colitis, cancer: Nanoparticles have been constantly found in colon tissue of subjects affected by cancer, Crohn's disease, and ulcerative colitis, while in healthy subjects nanoparticles were absent. The nanoparticles present in diseased subjects had various chemical compositions and are not considered toxic in bulk form. Microscopic and energy-dispersive spectroscopy analysis of colon mucosa indicated the presence of carbon, ceramic filosilicates, gypsum, sulfur, calcium, silicon, stainless steel, silver, and zirconium [45]. The size of debris varied from 50 nm to 100 µm, the smaller the particle the further is able to penetrate. The particles were found at the interface between healthy and cancerous tissue. Based on these findings it was suggested that the gastrointestinal barrier is not efficient for particles smaller than 20 µm. Recently, it was suggested that there is an association between high levels of dietary nanoparticles (100 nm–1 µm) and Crohn's disease. Exogenous nanoparticles were found in macrophages accumulated in lymphoid tissue of the human gut, the lymphoid aggregates being the earliest sign of lesions in Crohn's disease. Microscopy studies showed that macrophages located in lymphoid tissue uptake nanoparticles of spherical anatase (TiO_2) with size ranging between 100 and 200 nm from food additives; flaky-like aluminosilicates 100–400 nm typical of natural clay; and environmental silicates 100–700 nm with various morphologies. A diet low in exogenous particles seems to alleviate the symptoms of Crohn's disease [41].

10.3.8 Dermal Uptake of Nanoparticles

The skin is composed of three layers – epidermis, dermis, and subcutaneous. The outer portion of the epidermis called *stratum corneum* is a 10-µm-thick keratinized layer of dead cells and is difficult to pass for ionic compounds and water-soluble molecules [44]. The surface of epidermis is highly microstructured, having a scaly appearance as well as pores for sweat, sebaceous glands, and hair follicle sites. As with many subjects involving nanoparticles, dermal penetration is still controversial.

Several studies show that nanoparticles are able to penetrate the stratum corneum [46]. Nanoparticle penetration through the skin typically occurs at hair follicles, and flexed and broken skin. Intracellular nanoparticles penetration is also possible, as demonstrated by cell culture experiments. Multiwalled carbon nanotubes (MWCNTs) are internalized by human epidermal keratinocytes (the major cell type of the epidermis) in cytoplasmic vacuoles and induce the release of pro-inflammatory mediators. Spherical particles with diameter between 750 nm and 6 µm selectively penetrate the skin at hair follicles with a maximum penetration depth of more than 2400 µm (2.4 mm). Broken skin facilitates the entry of a wide range of larger particles (500 nm–7 µm). While stationary unbroken skin has been shown to be impervious to penetration, nanoparticles have been observed to penetrate when the skin is flexed. Thus, mechanical deformation is capable of transporting particles through the stratum corneum and into the epidermis and dermis. It is still a debating issue whether or not nanoparticles of TiO_2 found in commercially available sunscreens penetrate the skin. For example, the application of a sunscreen containing 8% nanoparticles (10–15 nm) onto the skin of humans showed no penetration, while oil-in-water emulsions showed penetration, higher penetration being present in hairy skin at the hair follicles site UV radiation, however, which in aqueous media leads to the production of reactive oxygen species, including superoxide anion radicals, hydrogen peroxide, free hydroxyl radicals, and singlet oxygen. These ROS can cause substantial damage to DNA. Titanium dioxide particles under UV light irradiation have been shown to suppress tumor growth in cultured human bladder cancer cells via reactive oxygen species. Sun-illuminated titanium dioxide particles in sunscreen were observed to catalyze DNA damage both *in vitro* and *in vivo*.

It is known that silver has a beneficial antibacterial effect when used as a wound dressing, reducing inflammation and facilitating healing in the early phases [47]. However, there are contradictory studies on silver nanoparticles and ions cytotoxicity from laboratories around the world. Silver is known to have a lethal effect on bacteria, but the same property that makes it antibacterial may render it toxic to human cells. Concentrations of silver that are lethal for bacteria are also lethal for both keratinocytes and fibroblasts.

10.3.9 Nanoparticles Uptake via Injection

Injection is the administration of a fluid into the subcutaneous tissue, muscle, blood vessels, or body cavities. Injection of nanoparticles has been studied in drug delivery. The translocation of nanoparticles following injection depends on the site of injection: intravenously injected nanoparticles quickly spread throughout the circulatory system, with subsequent translocation to organs; intradermal injection leads to lymph nodes uptake; while intramuscular injection is followed by neuronal and lymphatic system uptake. For example, the injection of magnetic nanoparticles smaller than 100 nm into the tongues and facial muscles of mice resulted in synaptic uptake [30].

Nanoparticles injected intravenously are retained longer in the body than ingested ones. For example, 90% of injected functionalized fullerenes are retained after 1 week of exposure.

Intravenously injected nanoparticles (quantum dots, fullerenes, polystyrene, plant virus) with size ranging from 10 to 240 nm show localization in different organs such as liver, spleen, bone marrow, lymph nodes, small intestine, brain, and lungs. Talc particles introduced by injection are found in the liver of intravenous drug users. The distribution of particles in the body is a function of their surface characteristics and their size. Coating nanoparticles with various types and concentrations of surfactants before injection significantly affects their distribution in the body. For example, coating with polyethylene glycol or other substances almost completely prevents hepatic and splenic localization. Another example is the modification of nanoparticles surface with cationic compounds that facilitate arterial uptake by up to 10-fold. The adverse health effects of injected nanoparticles are a function of particle chemistry and charge. A common side effect of injecting nanoparticles intravenously is hypersensitivity, a reaction that occurs in a large number of recipients and is probably due to the complement activation.

10.3.10 Nanoparticles Generation by Implants

Nanoparticle debris produced by wear and corrosion of implants is transported to the region beyond the implant [42]. Implants release metal ions and wear particles and, after several years of wear, in some cases the concentration of metals in the blood exceeds the biological exposure indices recommended for occupational exposure. Materials considered chemically inert in bulk form (such as ceramic porcelain and alumina), or in other terms biocompatible, are used for implants and prostheses. However, nanoparticles with the same composition have been observed in the liver and kidneys of diseased patients with implants and prostheses. It was suggested that the concept of biocompatibility should be revised in view of these findings. Patients with orthopedic implants have a statistically significant rise in the incidence of autoimmune diseases, perhaps due to the particulate wear-debris generated by the implant, which is associated with electrochemical processes that may activate the immune system. Immunological responses and aseptic inflammation in patients with total hip replacement are a response to wear particles. Exposure to orthopedic wear-debris leads to inflammatory-initiated bone resorption, implant failure, dermatitis, urticaria, and vacuities.

10.4 Positive Health Effects of Nanoparticles

It is prudent to say that the positive impact of nanoparticles on healthcare surpasses their negative health impact, to an extent that a new discipline called “Nanomedicine” has emerged where nanomaterials showing unique applications in terms of diagnosis, drug delivery, therapy, and so on to early detection and treat many life-threatening diseases. Some of the common examples are cited herein.

10.4.1 Nanoparticles as Antioxidants

Fullerene derivatives and nanoparticles made of compounds holding oxygen vacancies (CeO_2 and Y_2O_3) have demonstrated neuroprotective properties and anti-apoptotic activity. Fullerene derivatives have been shown to prevent apoptosis in hepatic, kidney, and neuronal cells, a fact attributed to their antioxidant properties [48]. The use of fullerenes as radical sponges (or scavengers) has been shown to decrease neuronal death. Functionalized fullerenes can react with oxygen species that attack lipids, proteins, and DNA, conferring neuroprotective properties. In particular, polyhydroxylated fullerenes (fullerols) [C_{60} (OH)n] are excellent antioxidants and offer exceptional neuroprotective properties, having high solubility and ability to cross the blood–brain barrier.

10.4.2 Antimicrobial Activity

Several types of nanoparticles are known to have an antimicrobial effect, such as silver, titanium dioxide, fullerenes, zinc oxide, and magnesium oxide. Silver nanoparticles and ions are the broad spectrum antimicrobial agents. Their antibacterial action results from destabilization of the outer membrane of bacteria and depletion of the levels of adenosine triphosphate, a molecule that is the principal form of energy immediately usable by the cell. Fullerenes have also been shown to have an anti-HIV activity, probably due to a good geometrical fit of a C_{60} sphere into the active site (diameter of about 1 nm) on the fundamental enzyme (HIV protease) necessary for HIV virus survival, leading to strong van der Waals interactions between the enzyme and fullerene [48]. It has been demonstrated that silver nanoparticles undergo a size-dependent interaction with HIV-1 virus, with nanoparticles exclusively in the range of 1–10 nm attached to the virus. Due to this interaction, silver nanoparticles inhibit the virus from binding to host cells, as demonstrated *in vitro* [49].

10.5 Environmental Sustainability

The use of nanoparticles for improved *in situ* environmental remediation of polluted soils and ground water is held up as one of the most promising areas for nanotechnology to offer for environmental benefits. Nanoparticles are being used for *in situ* environmental remediation on more than 60 sites across North America, Europe, and Asia. Currently, the use of zerovalent iron and bimetallic nanoparticles (e.g., incorporating manganese, nickel, palladium, and zinc) predominates, although the potential of nanoscale zeolites, enzymes, metal oxides, and carbon nanotubes are also all being explored. The benefits of using nanoscale particles for remediation include the possibility to degrade a larger range of contaminants, reduce degradation times, and create less toxic intermediate products. While the benefits seem clear, the potential risks associated with these technologies have not been substantively researched and remain poorly understood.

The preliminary studies on the toxicology of nanoparticles used for remediation do indicate a potential for undesirable impacts. Notable observations include cytotoxic effects from oxidative stress, a physical disruption of cell membranes, and ecological impacts such as altered microbial population dynamics. The main challenges facing efforts to use nanoparticles for environmental remediation include rapid oxidation decreasing the reactivity of the particles, a tendency for nanoparticles to aggregate and agglomerate, and limited distribution of injected particles due to agglomeration. Interestingly, strategies being pursued to overcome these challenges (such as surface coatings and multiple treatment injections) result in exactly the types of characteristics that might be undesirable from the perspective of ecotoxicology, that is, increased mobility, exposure, persistence, and reactivity.

A nanomaterial life cycle assessment [50, 51], including manufacturing, transport, product use, recycling, and disposal into the waste stream, as illustrated in Figure 10.6, is necessary to understand to evolve various statutory and regulatory systems. Full life cycle environmental, health and safety effects must be assessed prior to commercialization. Once loose in nature, manufactured nanomaterials represent an unprecedented class of manufactured pollutants. Potentially damaging environmental impacts can be expected to stem from the novel nature of manufactured nanomaterials, including mobility and persistence in soil, water, and air, bioaccumulation, and unanticipated interactions with chemical and biological materials.

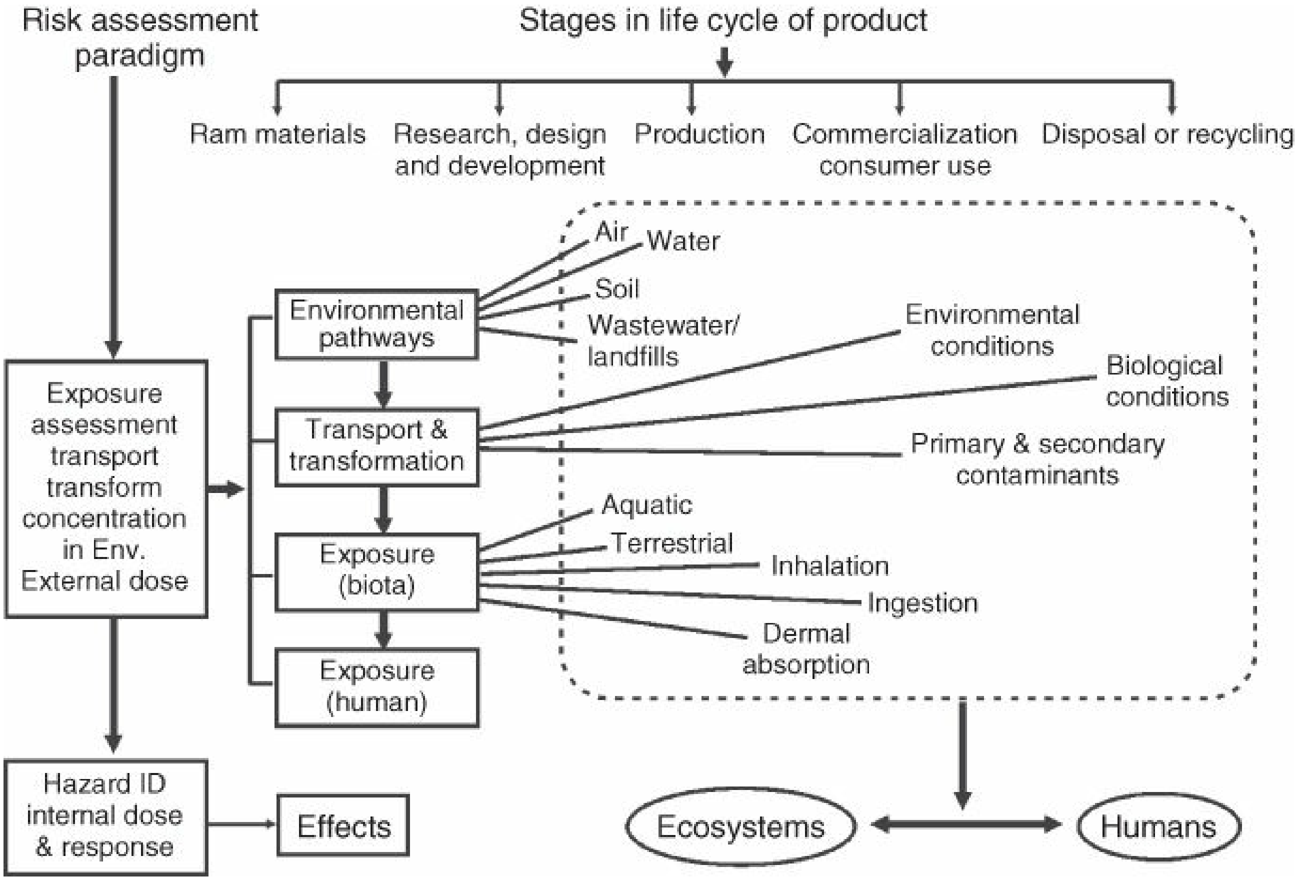

Figure 10.6 The risk assessment paradigm integrated with life cycle stages of nanomaterials.

The limited number of existing studies has raised red flags, such as exposure to high levels of nanoscale aluminum stunting root growth in five commercial crop species, by-products associated with the manufacture of single-walled carbon nanotubes causing increased mortality and delayed development of a small estuarine crustacean, and damage to beneficial microorganisms from nanosilver. The U.K. Royal Society has recommended that, “the release of nanoparticles and nanotubes in the environment should be avoided as far as possible” and that, “factories and research laboratories treat manufactured nanoparticles and nanotubes as hazardous, and devise methodologies to reduce or remove them from waste streams.”

Nanomaterials create immense difficulties for the application of existing environmental protection regimes. Agencies lack cost-effective tools and mechanisms to detect, monitor, measure, and control manufactured nanomaterials, let alone the means to remove them from the environment. Industry shields even the scant data provided to government from public view by claims of confidential business information. The risk assessments, oversight triggers, toxicity parameters, and threshold minimums used by environmental laws in many countries, including the United States and the European Union, are designed for bulk (non-nano) material toxicity parameters. The metrics used in existing laws, such as a relationship between mass and exposure, are insufficient for nanomaterials. Internationally, existing laws lack life cycle analyses and fail to address existing regulatory gaps. Environmentally sustainable management of nanomaterials must address and remedy these failings.

10.6 Safe Working with Nanomaterials

The preliminary conclusions to be drawn from the toxicology studies to date are that some types of nanomaterials can be toxic, if they are not bound in a substrate and they are available to the body. Multiple government organizations are working to fund and assemble toxicology information on these materials. In the interim, researchers must use procedures developed under their Chemical Hygiene Plan that prevent inhalation and dermal exposures because at this time nanotoxicology information is limited. In promulgating the Laboratory Safety Standard, the **Occupational Safety and Health Administration** (OSHA), USA, have recognized that many research materials and newly synthesized chemicals have limited or no toxicity information. Using stringent precaution is, therefore warranted for these materials.

Based on particle physics and studies of fine atmospheric pollutants, nanoparticles are in size range that remains suspended for days to weeks if released into air. Nanoparticles can be inhaled and will be collected in all regions of the respiratory tract; about 35% will deposit in the deep alveolar region of the lungs. Based on existing data for nanometer-sized particles and collection efficiency curves, National Institute of Occupational Safety and Health (NIOSH) has stated that high-efficiency particulate arrestance (HEPA) filters are expected to capture nanoparticles.

10.6.1 Safe Laboratory Practices in Handling Nanomaterials

In the last several years, a number of universities and research laboratories have posted specialized guides for working with nanomaterials on their websites. There is a convergence of ideas in these documents regarding interim best practices until more is known about the toxicity of these materials. Working safely with nanomaterials involves following standard procedures that would be followed for any particulate material with known or uncertain toxicity: preventing inhalation, dermal, and ingestion exposure.

Many nanoparticles are synthesized in enclosed reactors or glove boxes. The enclosures are under vacuum or exhaust ventilation, which prevent exposure during the actual synthesis. Inhalation exposure can occur during additional processing of materials removed from reactors, and this processing should be done in fume hoods, glove boxes, or biosafety cabinets. Manipulation of nanomaterials as free particles or on the lab bench should be avoided. For equipment or processes too large to be enclosed in a fume hood, specialized local exhaust ventilation can be used to capture particles at potential emission points. Material removed from reactor should be in sealed container for transport. In addition, maintenance on reactor parts that may release residual particles in the air should be done in fume hoods or other exhausted enclosures. The synthesis of particles such as quantum dots using sol–gel chemistry should be carried out in ventilated fume hoods or glove boxes. A sol–gel process is a wet chemical technique in which chemical solutions react to produce colloidal particles. Contamination of lab surfaces should be prevented. Fume hood surfaces should be wet wiped after each use or at the end of the day. Alternative use of bench liners would also prevent contamination. In case of spills outside enclosures, wet wiping would be acceptable for small spills. Large spills can be cleaned using a vacuum cleaner fitted with a HEPA filter on the exhaust.

Since the ability of nanoparticles to penetrate the skin is uncertain at this point, gloves should be worn when handling particulate and solutions containing particles. A glove having good chemical resistance to any solution the particles are suspended in should be used. If working with dry particulate, a sturdy glove with good integrity should be used. Disposable nitrile gloves commonly used in many labs would provide good protection from nanoparticles for most procedures that do not involve extensive skin contact. Two pairs of gloves can be worn if extensive skin contact is anticipated, as well as gloves with gauntlets or extended sleeve nitrile gloves, to prevent contamination of lab coats or clothing.

One potential safety concern with nanoparticles is fires and explosions if large quantities of dust are generated during reactions or production. This is expected to become more of a concern when reactions are scaled up to pilot plant or production levels. Both carbonaceous and metal dusts can burn and explode if an oxidant such as air and an ignition source are present. Nanodusts can be anticipated to have a greater potential for explosivity than larger particles. Determination of lower flammability limits using standard test bomb protocols is being planned in Europe.

10.6.2 Exposure Monitoring

Based on the unique characteristics of nanoparticles, many believe that mass is not the appropriate measure of exposure. There also exists a background of nanoparticles in air, in the range of 3000–10,000 particles per cc, due to artificial emissions from vehicles and combustion sources and also from natural sources. Groups performing monitoring currently use a suite of instruments to measure particle concentration and size distribution and to characterize particle type. Both **NIOSH** (National Institute of Occupational Safety and Health) and the Department of Energy (**DOE**) have outlined air sampling approaches using direct-reading instrumentation for particle number and active and passive sampling for electron microscopy analysis (particle characterization). Scanning Mobility Particle Sizer (SMPS) and Fast Mobility Particle Sizer (FMPS) are very useful for particle size distribution measurements. Further number of instruments is being reported to characterize nanomaterial exposures as well as to mitigate their adverse health effects.

The British Standards Institute has published benchmark exposure levels for four categories of nanomaterials: fibrous nanomaterials, insoluble nanomaterials, soluble nanomaterials, and nanomaterials for which the bulk materials are carcinogenic, mutagenic, asthmagenic, or a reproductive toxin. When occupational health standards are eventually developed, they may take the form of “control bands” for different physical categories of nanomaterials, that is, different types of exposure controls would be required for different categories.

10.7 Nanomaterial Waste Management

As nanotechnology emerges and evolves, potential environmental applications and human health and environmental implications are under consideration by the EPA and local regulators. EPA has a number of different offices coordinating their review of this rapidly evolving technology. The EPA is currently trying a voluntary approach to testing and developing a stewardship program addressing the disposal of waste nanomaterials. British Standard Institute has also issued guidelines for safe handling and disposal of manufactured nanomaterials [52]. MIT and other universities are taking cautious approach to nanowaste management, and recommended practices are included in Table 10.3.

Table 10.3 Best Practices for a Nanotechnology Laboratory

Exposure	Best Practices for Prevention of Exposure
Inhalation	Use of fume hood, biosafety cabinet, or other exhausted enclosure. Synthesis in furnace or reactor: exhaust reactor gases, purge before opening, provide local exhaust ventilation for emission points, perform part maintenance in fume hood. Eliminate use on open lab bench. Transport within lab in sealed containers
Dermal	Use of sturdy gloves for dry particulate. Use of gloves, resistant to solvent if nanoparticles are in suspension. If skin contamination is likely, use double gloves or gloves with gauntlets or extended sleeves. Use lab coats, preferably disposable. Use appropriate eye protection
Laboratory contamination	Wet wipe hood and other lab surfaces after use or at end of day; never sweep or use compressed air for cleaning. Use bench liners or HEPA vacuum cleaners as alternatives
Spills	Have spill kit on hand: wet wipe for dry spills, use appropriate absorbent for spills of suspensions. Use HEPA vacuum cleaner for larger spills.
	Use respirator (disposable P100 or elastomeric half-mask with P100 cartridges) if inhalation exposure possible
Nanomaterial waste	Dispose of nanomaterials and nanomaterial-contaminated lab materials as hazardous waste until specific regulations are developed. Label waste as nanoscale

Source: Hallock et al. [26]. With permission of Division of Chemical Health and Safety of the ACS, Elsevier.

In order to better understand the characteristics of these waste streams, all waste materials potentially contaminated with nanomaterials are identified and evaluated or collected for special waste disposal. On the label content sections, the researchers are asked to indicate that it contains nanosized particles and indicate base materials and carrier liquids.

The following waste management guidance applies to the nanomaterial bearing waste streams consisting of the following:

- Pure nanomaterials (e.g., carbon nanotubes)
- Items contaminated with nanomaterials (e.g., wipes/PPE)
- Liquid suspensions containing nanomaterials
- Solid matrixes with nanomaterials that are friable or have a nanostructure loosely attached to the surface such that they can reasonably be expected to break free or leach out when in contact with air or water, or when subjected to reasonably foreseeable mechanical forces.

The guidance does not apply to nanomaterials embedded in a solid matrix that cannot reasonably be expected to break free or leach out when they contact air or water, but would apply to dusts and fines generated when cutting or milling such materials. Researchers are told to never put material from nanomaterial – bearing waste streams into the regular trash or down the drain. Paper, wipes, PPE, and other items with loose contamination are collected in a plastic bag or other sealing container stored in the laboratory hood. When the bag is full, close it, it is taken out of the hood, sealed, and placed it into a second plastic bag or other sealing container. The outer bag is labeled with the laboratory's proper waste label. The content section of the label must indicate that it contains nanosized particles and specify type.

Currently, the disposal requirements for the base materials are considered first when characterizing these materials. If the base material is toxic, such as silver or cadmium, or the carrier is a hazardous waste, such as a flammable solvent or acid, clearly they should carry those identifiers. Many nanoparticles may also be otherwise joined with toxic metals or chemicals. Bulk carbon is considered a flammable solid, so even carbon-based nanomaterials should be collected for the determination as hazardous waste characteristics.

10.8 Gaps in Knowledge about Health Effects of Engineered Nanoparticles

While ultrafine particle studies, along with earlier toxicological and clinical investigations, have laid the foundation for the nascent field of nanotoxicology, there are some fundamental yet unresolved questions about the impact of engineered nanoparticles on human health [53].

Basic questions still needs to be addressed includes the following:

- Can human exposures to engineered nanomaterials be prevented? If not, what is a safe threshold for exposure and what are the likely exposure levels that might be encountered by workers, researchers, and consumers?
- How are engineered nanoparticles taken up by the human body and how are they metabolized? Do they reach organs and tissues that larger, less reactive particles are not able to reach? Do they interfere with cellular signaling in consequential ways? Does the immune system treat materials on that scale differently?
- Are there chronic (long-term) health effects associated with exposure to engineered nanoparticles that cannot be evaluated with acute (short-term) and subacute (medium-term) studies? How can long-term effects be assessed without allowing people to be exposed to uncertain risks?
- Are there meaningful differences between the health effects of *engineered* nanoscale materials and those of *naturally occurring* or *incidental* materials with similar chemical composition?

If there are different risks posed by engineered nanomaterials, then these materials must be evaluated separately without relying on toxicity values and mechanisms identified for naturally occurring materials in the light of following factors.

1. The role played by physical, chemical, and electrostatic forces to alter the transport dynamics, physical separation, and surface charge of these materials after they are released during processing or manufacturing.
2. The experimental conditions need to be defined and controlled so that health effects studies are measuring exposure to discrete nanoscale materials rather than larger clumps of material likely to form over time.
3. To assess the probability (or risk) that a given individual will experience adverse health effects after being exposed to engineered nanoparticles for a limited period of time.
4. To study the latent (or delayed) health risks that might emerge years after the exposure has ended.

10.9 Government Standards and Materials Safety Data Sheets

In 2011, NIOSH issued a **recommended exposure limit** (REL) for ultrafine (nano) titanium dioxide and a draft REL for carbon nanotubes and carbon nanofibers [26]. They recommend 0.1 mg/m^3 for nanosized TiO_2 (<100 nm) and 1.5 mg of controls would be different for the following forms of nanomaterials (from least to most control): solid materials with embedded nanostructures, solid materials with nanostructure bound to the surface, liquid suspension of nanoparticles, free nanoparticles (dry, dispersible single particles, or agglomerates). One should also be aware that **Material Safety Data Sheets** (MSDSs) may not have accurate information at this point. For example, the MSDSs that accompany some commercially available carbon nanotubes refer to the graphite **Permissible Exposure Limit** (PEL) as a relevant exposure standard. Both graphite and carbon nanotubes are composed of carbon arranged in a honeycomb pattern. However, CNTs have very different tensile and conductive properties than graphite. Additionally, CNTs are much more toxic in the short-term animal tests that have been performed to date. Consequently, the graphite PEL and toxicity information is not appropriate for MSDSs of CNTs. If not bound in a substrate, CNTs should be treated as potentially toxic fibers and should be handled with appropriate controls.

The lack of regulatory standards and formal recommendations for many nanomaterials make it is difficult to determine or even estimate a safe exposure level. Although the toxicity of many nanomaterials is unknown, but initial research indicates that there may be health concerns related to occupational exposures. Due to the potential for health effects, it is important to control the exposures to the best possible extent. Based on the current knowledge, following are the recommendations for reducing the potential risks for employee exposures during nanomanufacturing processes.

1. Hazards involved in processing and manufacturing nanomaterials should be managed as part of a comprehensive occupational safety and health management plan. **Preliminary hazard assessments** (PHAs) should be conducted to determine the need for control measures during the planning stage. Hazard assessments should be done during the operation of a facility and regularly updated when any processes change.

2. The concept of **Prevention through Design** (PtD) is to design out or minimize hazards early in the design process. When PtD is implemented, the control hierarchy is applied by designing safety into the work environment to prevent work-related injuries and illnesses.

10.9.1 Control Banding

Control banding is a potentially useful concept in the risk management of nanomaterials. Control banding is not intended to be a substitute for Occupational Exposure Limits (OELs) and does not alleviate the need for environmental monitoring or industrial hygiene expertise.

10.9.2 Hierarchy of Controls

The hierarchy of controls should be followed when controlling potential occupational hazards from nanoparticles. Elimination and substitution are at the top of the hierarchy. However, eliminating nanomaterials may not be possible as the nanomaterials were likely chosen because of their unique properties. The manner in which these materials are handled and processed can largely affect the overall safety of the process. The substitution of less hazardous materials for those that are a higher hazard should be considered to reduce the risk to workers. Substitution also applies to the form of the product used; for example, slurry with less exposure potential could be used to replace a dry powder.

10.9.3 Engineering Controls

If elimination and substitution are not feasible to reduce hazards, engineering controls should be implemented. These could include local exhaust ventilation, isolation measures, and application of water or other material for dust suppression. Engineering controls are likely the most effective control strategy for nanomaterials.

Common controls used in the nanotechnology industry include fume hoods, biological safety cabinets, glove box isolators, glove bags, bag dump stations, and directional laminar flow booths. Each of these controls should be carefully designed and operated properly to be effective.

Preventative maintenance schedules should be developed to ensure that engineering controls are operating at design conditions.

Nonventilation engineering controls cover a range of controls (e.g., guards and barricades, material treatment, or additives). These controls should be used in conjunction with ventilation measures to provide an enhanced level of protection for workers. Many devices developed for the pharmaceutical industry, including isolation containment systems, may be suitable for the nanotechnology industry.

a. The continuous liner system allows filling product containers while enclosing the material in a polypropylene bag. This system should be considered for off-loading materials when the powders are to be packed into drums.

b. Water sprays may reduce respirable dust concentrations generated from processes such as machining (e.g., cutting, grinding). Machines and tooling, as well as the material being cut or formed, must be compatible with water. If a fluid other than water is used, attention should be given to the fluid being applied to avoid creating a health hazard to workers.

10.9.4 Administrative Controls

Administrative controls and PPE are frequently used with existing processes where hazards cannot be effectively controlled solely with engineering controls. This could occur when control measures are not feasible or do not reduce exposures to an acceptable level. Administrative controls and PPE programs may be less expensive to establish but, over the long term, can be very costly to sustain. These methods for protecting workers have proven to be less effective than other measures and require significant efforts by the affected workers. A program that addresses the hazards present; employee training; and PPE selection, use, and maintenance should be in place when PPE is used. Administrative controls and PPE can also be useful for redundancy, especially in high-hazard situations. While engineering controls serve as primary controls, the administrative and PPE controls provide backup. Employers should implement the following work practices to control worker exposure to nanomaterials:

- Educate workers on the safe handling of engineered nanomaterials to minimize the likelihood of inhalation exposure and skin contact.
- Provide information to workers on the hazardous properties of the nanomaterials being produced or handled with instruction on how to prevent exposure.
- Obtain the MSDSs when using nanomaterials from an outside source and review the information with employees who may come in contact with the materials. Given the lack of complete health information of many nanomaterials, the MSDSs may not provide adequate guidance and should be assessed by the health and safety office.
- To reduce the potential for release of nanomaterials, consider transferring powdered materials to slurry, where

possible.

- Clean-up spills of nanomaterials immediately and in accordance with written procedures. Appropriate PPE should be donned while performing clean-up tasks.
- Provide additional control measures (e.g., a buffer area, decontamination facilities located by the hazard) to ensure that engineered nanomaterials are not transported outside the work area. Place a sticky mat at the exits of production areas to reduce the likelihood of spreading nanomaterials.
- Encourage workers to use hand-washing facilities before eating, smoking, or leaving the worksite.
- Provide facilities for showering and changing clothes to prevent the inadvertent contamination of other areas (including take-home) caused by the transfer of nanomaterials on clothing and skin.
- Prohibit the consumption of food or beverages in work areas where nanomaterials are handled.
- Ensure work areas and equipment, for example, balance, are cleaned at the end of each work shift, at a minimum, using either a HEPA-filtered vacuum cleaner or wet wiping methods. Dry sweeping or compressed air should not be used to clean work areas. Cleanup should be conducted in a manner that prevents worker contact with wastes. Disposal of all waste material should comply with all applicable federal, state, and local regulations.
- Store nanomaterials, whether suspended in liquids or in a dry particle form, in closed (tightly sealed) containers whenever possible.
- Conduct routine industrial hygiene and medical monitoring to ensure that work practices and engineering controls are effective.

10.9.5 Personal Protective Equipment

Because nanoparticles have been found to penetrate the skin, items such as gloves, gauntlets, and laboratory clothing or coats should be worn when working with nanoparticles. Good hygiene practices for wearing the protective equipment should be followed.

- Gloves made of neoprene, nitrile, or other chemical-resistant gloves should be used and changed frequently or whenever they are visibly worn, torn, or contaminated.
- Respiratory protection should be used to reduce worker exposures to acceptable levels in the absence of effective engineering controls, during the installation or maintenance of engineering controls, for short-duration tasks that make engineering controls impractical, and during emergencies.
- Respirators in the workplace should be used as part of a comprehensive respiratory protection program. The program should include written standard operating procedures; workplace monitoring; hazard-based selection; fit-testing and training of the user; procedures for cleaning, disinfection, maintenance, and storage of reusable respirators; respirator inspection and program evaluation; medical qualification of the user; and the use of NIOSH-certified respirators.

10.10 Risk Management

At present, regulatory agencies, industry groups, and health organizations at the state, national, and international levels are considering how to regulate or monitor possible health risks from engineered nanoscale materials using a full life cycle (cradle-to-grave) assessment approach. It becomes a great practical challenge to establish an evidence-based risk management framework for the safe production, manipulation, and disposal of engineered nanoscale materials give a large number of questions that remain unresolved.

It is worth noting that regulatory agencies, manufacturers, and academic institutions in the United States and Europe have already taken the lead in incorporating a precautionary approach (avoidance of exposure) into a risk management framework to manage persistent uncertainties associated with many nanomaterials. Several creative frameworks have been developed that balance existing technical knowledge, expert judgment, and the use of precautionary policies in the face of larger gaps in knowledge. A responsible framework for managing risk in the face of basic uncertainties must balance the value of the enterprise or research against the cost of taking protective precautionary measures that meet the standards of the company or institution and the community.

The speed with which nanotechnologies have moved from research laboratories to markets has taken some observers and regulators by surprise. No reliable database exists that tracks commercial developments, but the **Project on Emerging Nanotechnologies** (PEN) has shown some light into the market by creating an Internet-based inventory that over 1000 nanoproducts are commercially available in sectors as wide-ranging as food, cosmetics, electronics, automotive, appliances, and children's products. Since the PEN inventory relies on the work of a small team conducting online research, it may well underestimate the true state of nanotechnology commercialization.

As more and more nanoproducts are being marketed, scientists and regulatory experts have voiced growing concerns about the safety of some nanomaterials. These concerns are focused on the miniscule size of nanomaterials and their unique physicochemical characteristics. For example, some nanomaterials may enter the human body through mucous membranes or the skin and migrate via the bloodstream to vital organs including the brain. Some nanomaterials can also enter cells, interact with their molecular structure, and have cytotoxic or genotoxic effects. Traditional protective equipment such as gloves or masks may not provide sufficient protection against accidental inhalation or absorption through the skin.

Changes to the physicochemical properties, especially when they lead to increased toxicity, may produce unexpected negative effects in the human body or the environment, particularly so as nanomaterials may change as a consequence of their interaction with living systems.

Considerable uncertainty exists with regard to the specific environmental and health threats that some nanomaterials pose along the path from production to use and disposal. Laboratory experiments have shown that the inhalation of certain insoluble ultrafine nanotubes may cause pulmonary inflammation, tissue damage and lung tumors. In particular, recent studies indicate that MWCNTs of a certain shape can cause mesothelioma in the linings of the lungs if they are inhaled, similar to the toxicological effects of asbestos. Nanosilver, which is used in textiles, washing machines, food supplements, and surface coatings, has also been the focus of recent studies and NGO campaigns, for example, overconcerns that if released into wastewater it could adversely affect aquatic organisms, including those that are needed in sewage treatment plants. No conclusive evidence exists of nanomaterials having caused actual health damage or deaths.

Although research is ongoing, there are a few important observations about engineered nanomaterials that can be found in the existing toxicological literature:

> **1.** There is emerging evidence that biological effects observed in some studies are tied to various properties, including size, surface area, shape, surface chemistry, and electric charge of nanoscale particles. Some nanoscale particles that do not have special surface charges or reactive sites have been found to elicit inflammation at lower concentrations than would be expected with similar materials produced in larger dimensions (e.g., bulk graphite vs. carbon nanotubes). This has led to the observation that total surface area can sometimes be a better predictor of toxicity with certain classes of nanomaterials than mass concentration.
>
> **2.** Some nanoscale materials appear to be associated with cellular oxidative stress (free radical mechanisms) once inside a cell. This process results in the release of unstable forms of charged molecules and is tied to genetic damage and cellular dysfunction. While this insight may become important in understanding the precise molecular mechanism of harm, it will not help scientists predict the likelihood of these materials finding their way from the place of initial contact into the bloodstream and then inside certain cells.
>
> **3.** Important questions remain about the ability of inhaled nanoscale materials to be transported into the bloodstream and then to specific organs, or for nanoscale materials to penetrate the skin directly. Specific concerns have been raised about the possibility that engineered nanoparticles, like other nanosized particles such as viruses, welding fumes, and diesel exhaust particulates, may be able to *translocate* directly into the bloodstream from the surface of the skin or along the olfactory nerve into the brain. There is only limited evidence that these uptake routes may be of potential significance for humans, and some evidence that direct translocation through the skin is not taking place.
>
> **4.** It is essential not to presume that effects exhibited by “parent” materials (large-scale) can be extrapolated to the effects of the derived nanoscale equivalent (e.g., engineered nanogold vs simple gold dust). Efforts to predict nanoscale effects from existing toxicology data have been found to be less than useful in many cases.

The manipulation of matter at the scale of atoms, “nanotechnology,” is creating many new materials with characteristics not always easily predicted from current knowledge. Within the near-limitless diversity of these materials, some happen to be toxic to biological systems; others are relatively benign, while others confer health benefits. “Nanoparticles and ultrafine particles” are considered as the most important emerging risk in the area of occupational safety. It is particularly important to launch coordinated and effective research aimed at creating a sound and comprehensive knowledge base for toxicological and ecotoxicological risk assessments, which have to satisfy the demands imposed by the regulatory framework, and the resultant recommendations.

Review Questions

Q1. Which are the routine human activities leading to the formation of nanoparticles? Give examples and their health hazards if any.

Q2. In which form nanoparticles causes health risks?

Q3. Describe environmental activities producing nanoparticles and their possible health effects.

Q4. In what manner NPs and microorganisms are comparable with respect to human health?

Q5. State the factors determining toxicity of NPs.

Q6. Name diseases associated with inhalation, ingestion, and contact of nanoparticles.

Q7. What do you understand by anthropogenic nanomaterials and its impact on human health and ecosystem.

Q8. How do NPs affect the respiratory system?

Q9. Explain the cellular interaction with nanoparticles.

Q10. Explain nanoparticles translocation to the lymphatic systems, their health effects, and possible treatment.

Q11. Give mechanism of size-dependent translocation of NPs into the circulatory system of living beings.

Q12. Do NPs affect blood cells? What is the basic difference in uptake of NPs by WBCs and RBCs?

Q13. Discuss bioaccumulation of NPs in liver and kidneys.

Q14. Which nanomaterial is useful for implants for human body? What are the adverse effects of their erosion over a period of time?

Q15. Name some diseases caused by gastrointestinal tract uptake of NPs.

Q16. Name nanoparticles having positive health effects.

Q17. How are NPs helpful in environmental remediation? Explain with suitable examples?

Q18. Illustrate some safe laboratory practices in handling nanomaterials.

Q19. What are the proposed strategies worked out for management of nanomaterial waste?

Q20. How natural and man-made NPs are going to affect ecosystem?

References

1. V. L. Colvin, “The Potential Environmental Impacts of Engineered Nanoparticles”, *Nat. Biotechnol.*, **21** (10), (2003) 1166–1170.

2. K. Dreher, “Heath and Environmental Impact of Nanotechnology: Toxicological Assessment of Manufactured Nanoparticles”, *Toxicol. Sci.*, 77 (1), (2004) 3–5.

3. A. E. Nel, T. Xia, L. Medler and N. Li, “Toxic Potential of Materials at the Nano Level”, *Science*, **311** (2006) 622–627.

4. A. M. Schrand, M. F. Rahman, S. M. Hussain, J. J. Schlager, D. A. Smith and A. F. Syed, “Metal-Based Nanoparticles and their Toxicity Assessment”, *Adv. Rev.*, **2** (2010) 544–568.

5. C. Buzea, I. I. P. Blandino and K. Robbie, “Nanomaterials and Nanoparticles: Sources and Toxicity”, *Biointerphases*, **2** (4), (2007) MR17–MR71.

6. W. G. Kreyling, M. Semmler-Behnke, S. Takenaka and W. Moller, “Differences in the Biokinetics of Inhaled Nano- vs Micrometer Sized Particles”, *Acc. Chem. Res.*, **46** (3), (2013) 714–722.

7. N. Kumar and R. Kumar, *Nanotechnology and Nanomaterials in Treatment of Life Threatening Diseases*, Elsevier, USA, (2014).

8. M. Semmler-Behnke, S. Takenaka, S. Fertsch, A. Wenk, J. Seitz, P. Mayer, G. Oberdorster and W. G. Kreyling, “Efficient Elimination of Inhaled Nanoparticles from the Alveolar Region: Evidence for Interstitial Uptake and Subsequent Reentrainment onto Airways Epithelium”, *Environ. Health Perspect.* **115** (2007) 728–733.

9. I. Bhatt and B. N. Tripathi, “Interaction of Engineered Nanoparticles with Various Components of the Environment and Possible Strategies for their Risk Assessment,” *Chemosphere*, **82** (2011) 308–317.

10. P. R. Buseck and M. Pósfai, “Airborne Minerals and Related Aerosol Particles: Effects on Climate and the Environment”, *Proc. Natl. Acad. Sci. U. S. A.*, **96** (1999) 3372–3379.

11. D. A. Taylor, “Dust in the Wind”, *Environ. Health Perspect.* **110** (2002) A80–A87.

12. L. A. Taylor, H. H. Schmitt, W. D. Carrier and M. Nakagawa, “The lunar dust problem: from liability to asset”, First Space Exploration Conference: *Continuing the Voyage of Discovery*, Orlando, Florida, 2005.

13. I. D. Batsura, G. G. Kruglikov and V. D. Arutiunov, “Morphology of Experimental Pneumoconiosis Developing after Exposure to Lunar Soil”, *Bull. Eksp. Exp. Biol. Med.* **92** (1981) 376–379.

14. J. A. Mott, P. Meyer, D. Mannino, S. C. Redd, E. M. Smith, C. Gotway-Crawford and E. Chase, “Wildland Forest Fire Smoke: Health Effects and Intervention Evaluation, Hoopa, California, 1999”, *West. J. Med.,* **176** (2002) 157–162.

15. M. Corachan, J. M. Tura, E. Campo, M. Soley and A. Traveria, “Podoconiosis in Equatorial Guinea. Report of Two Cases from Different Geological Environments”, *Trop. Geogr. Med.* **40** (1988) 359–364.

16. A. Ahmad, S. Senapati, M. I. Khan, R. Kumar and M. Sastry, “Extra-/Intracellular Biosynthesis of Gold Nanoparticles by an Alkalotolerant Fungus, Trichothecium sp.”, *J. Biomed. Technol.* **1** (2005) 47–53.

17. E. O. Kajander, “Nanobacteria – Propagating Calcifying Nanoparticles”, *Lett. Appl. Microbiol.* **42** (2006) 549–552.

18. H. M. Wood and D. A. Shoskes, “The Role of Nanobacteria in Urologic Disease”, *World J. Urol.* **24** (2006) 51–54.

19. A. Evelyn, S. Mannick and P. A. Sermon, “Unusual Carbon-Based Nanofibers and Chains Among Diesel Emitted Particles”, *Nano Lett.* **3** (2003) 63–64.

20. J. Vermylen, A. Nemmar, B. Nemery and F. Hoylaerts, “Ambient Air Pollution and Acute Myocardial Infarction”, *J. Thromb. Haemost.* **3** (2005) 1955–1961.

21. A. Afshari, U. Matson and L. E. Ekberg, “Characterization of Indoor Sources of Fine and Ultrafine Particles: A Study Conducted in a Full-Scale Chamber” *Indoor Air* **15** (2005) 141–150.

22. World Health Organization. http://www.who.int/heli/risks/indoorair/indoorair/en/index.html.

23. N. Serpone, A. Salinaro and A. Emeline, “Deleterious Effects of Sunscreen Titanium Dioxide Nanoparticles on DNA: Efforts to Limit DNA Damage by Particle Surface Modification”, *Proc. SPIE* **4258** (2001) 86–98.

24. S. Takenaka, E. Karg, C. Roth, H. Schulz, A. Ziesenis, U. Heinzmann, P. Schramel and J. Heyder, “Pulmonary and Systemic Distribution of Inhaled Ultrafine Silver Particles in Rats”, *Environ. Health Persp.* **109** (Suppl. 4) (2001) 547–551.

25. J. M. Antonini, A. B. Santamaria, N. T. Jenkins, E. Albini and R. Lucchini, “Fate of Manganese Associated with the Inhalation of Welding Fumes: Potential Neurological Effects”, *Neurotoxicology* **27** (2006) 304–310.

26. M. F. Hallock, P. Greenley, L. Di Berardinis and D. Kallin, “Potential Risks of Nanomaterials and How to Safely Handle Materials of Uncertain Toxicity”, *J. Chem. Health Safety*, **16** (2009) 16–23.

27. G. Oberdorster, “Pulmonary Effects of Inhaled Ultrafine Particles”*, Int. Arch. Occup. Environ. Health,* **74** (2001) 1–8.

28. A. Aderem and D. M. Underhill, “Mechanisms of Phagocytosis in Macrophages”*, Annu. Rev. Immunol.* **17** (1999) 593–623.

29. J. Muller, F. Huaux, N. Moreau, P. Misson, J. F. Heiliea, M. Delos, M. Arras, A. Fonseca, J. B. Nagyb and D. Lison, “Respiratory Toxicity of Multi-Wall Carbon Nanotubes”, *Toxicol. Appl. Pharmacol.,* **207** (2005) 221–231.

30. G. Oberdörster, E. Oberdörster and J. Oberdörster, “Nanotoxicology: An Emerging Discipline Evolving from Studies of Ultrafine Particles”, *Environ. Health Perspect.* **113** (2005) 823–839.

31. M. Lucarelli, A. M. Gatti, G. Savarino, P. Quatronni, L. Martinelli, E. Monari and D. Boraschi, “Innate Defence Functions of Macrophages can be Biased by Nano-Sized Ceramics Metallic Particles”, *Eur. Cytokine Netw.* **15** (2004) 339–346.

32. E. Garcia-Garcia, K. Andrieux, S. Gil, H. R. Kima, T. Le Doana, D. Desmaele, J. d'Angelo, F. Taran, D. Georgin

and P. Couvreur “A Methodology to Study Intracellular Distribution of Nanoparticles in Brain Endothelial Cells”, *Int. J. Pharm.* **298** (2005) 310–314.

33. D. M. Brown, K. Donaldson, P. J. Borm, R. P. Schins, M. Dehnhardt, P. Gilmour, L. A. Jimenez and V. Stone, “Calcium and ROS-Mediated Activation of Transcription Factors and TNF-α Cytokine Gene Expression in Macrophages Exposed to Ultrafine Particles”, *Am. J. Physiol. Lung Cell. Mol. Physiol.* **286** (2004) L344–L353.

34. L. Risom, P. Moller and S. Loft, “Oxidative Stress-Induced DNA Damage by Particulate Air Pollution”, *Mutat. Res.* **592** (2005) 119–137.

35. G. Liu, P. Mena, P. R. L. Harris, R. K. Rolston, G. Perry and M. A. Smith, “Nanoparticle Iron Chelators: A New Therapeutic Approach in Alzheimer Disease and Other Neurologic Disorders Associated with Trace Metal Imbalance”, *Neurosci. Lett.* **406** (2006) 189–193.

36. J. Liu, H. L. Wong, J. Moselhy, B. Bowen, X. Y. Wu and M. R. Johnston, “Targeting Colloidal Particulates to Thoracic Lymph Nodes”, *Lung Cancer* **51** (2006) 377–386.

37. P. Wiebert, A. Sanchez-Crespo, R. Falk, K. Philipson, A. Lundin, S. Larsson, M. Mooler, G. Kreyling and M. Svartengren, “No Significant Translocation of Inhaled 35-nm Carbon Particles to the Circulation in Humans”, *Inhal. Toxicol.* **18** (2006) 741–747.

38. G. Oberdörster, Z. Sharp, V. Atudorei, A. Elder, R. Gelein and A. Lunts, “Extra Pulmonary Translocation of Ultrafine Carbon Particles Following Whole-Body Inhalation Exposure of Rats”, *J. Toxicol. Environ. Health A*, **65** (2002) 1531–1543.

39. A. Nemmar, M. F. Hoylaerts, P. H. M. Hoet, D. Dinsdale, T. Smith, H. Xu, J. Vermylen and B. Nemery, “Ultrafine Particles Affect Experimental Thrombosis in an vivo Hamster Model”, *Am. J. Respir. Crit. Care Med.* **166** (2002) 998–1004.

40. A. Nemmar, P. H. Hoet, B. Vanquickenborne, D. Dinsdale, M. Thomeer, M. F. Hoylaerts, H. Vanbilloen, L. Mortelmans and B. Nemery, “Passage of Inhaled Particles into the Blood Circulation in Humans”, *Circulation* **105** (2002) 411–414.

41. A. M. Gatti, S. Montanari, E. Monari, A. Gambarelli, F. Capitani and B. Parisini, “Detection of Micro- and Nano-Sized Biocompatible Particles in the Blood”, *J. Mater. Sci. Mater. Med.* **15** (2004) 469–472.

42. A. M. Gatti and F. Rivasi, “Biocompatibility of Micro- and Nanoparticles. Part I: In Liver and Kidney”, *Biomaterials*, **23** (2002) 2381–2387.

43. E. Oberdörster, “Manufactured Nanomaterials (Fullerenes, C60) Induce Oxidative Stress in the Brain of Juvenile Largemouth Bass”, *Environ. Health Persp.* **112** (2004) 1058–1062.

44. P. H. M. Hoet, I. Bruske-Hohlfeld and O. V. Salata, “Nanoparticles – Known and Unknown Health Risks”, *J. Nanobiotechnol.* **2** (2004) 12–27.

45. A. M. Gatti, “Biocompatibility of Micro- and Nano-Particles in the Colon. Part II”, *Biomaterials* **25** (2004) 385–392.

46. J. S. Tsuji, A. D. Maynard, P. C. Howard, J. T. James, C. W. Lam, D. B. Warheit and A. B. Santamaria, “Research Strategies for Safety Evaluation of Nanomaterials, Part IV: Risk Assessment of Nanoparticles,” *Toxicol. Sci.* **89** (2006) 42–50.

47. V. K. Poon and A. Burd, “In Vitro Cytotoxicity of Silver: Implication for Clinical Wound Care”, *Burns* **30** (2004) 140–147.

48. S. Bosi, T. da Ros, Spalluto G and M. Prato, “Fullerene Derivatives: An Attractive Tool for Biological Applications”, *Eur. J. Med. Chem.* **38** (2003) 913–923.

49. J. L. Elechiguerra, J. L. Burt, J. R. Morones, A. Camacho-Bragado, X. Gao, H. H. Lara and M. J. Yacaman, “Interaction of Silver Nanoparticles with HIV-1”*, J. Nanobiotechnol.*, **3** (2005) 6.

50. L. Reijnder, “Cleaner Nanotechnology and Hazard Reduction of Manufactured Nanoparticles”, *J. Clean. Prod.* **14** (2006) 124–133.

51. http://www.nano.gov/you/environmental-health-safety.

52. British Standards Institute. Nanotechnologies – Part 2: Guide to safe handling and disposal of manufactured nanomaterials. PD 6699–2:2007, 2007.

53. A. Kumar, P. Kumar, A. Anandan, T. F. Fernandes, G. A. Ayoko and G. Biskos, “Engineered Nanomaterials: Knowledge Gaps in Fate, Exposure, Toxicity, and Future Directions”, *J. Nanomater.*, **2014** (2014) 1–16.

Index

Absorption
Acid rain
Actinomycetes
Activated carbon (AC)
    metal– organic framework (MOF)
Administrative controls
Advanced composites
Aerosol based techniques
Affordable energy
Aluminum oxide
Aluminum-Oxo hydroxides
    hematite
    magnetite
Anisotropy constant
Anisotropy energy
Anthropogenic nanomaterials
    consumer products
    cosmetics
    engineered nanomaterials
    engine exhaust
    indoor pollution
Artificial dielectric nanocomposites
Artificial nose
Artificial photosynthesis
Atomic force microscopy (AFM)
Auger electron spectroscopy
Auger process

Bacteria
Band broadening
Bimagnetic core– shell structure
Biological nanomaterials
    carbohydrates
    lipids
    nucleic acids
    proteins
    small molecules and
Biomimetic
Biomimetic approaches
Bionanocomposites
Blocking temperature
Bohr approximation
Bohr radius
Bovine serum albumin (BSA)
Bragg's law
Brillouin zone
Brunauer– Emmett– Teller (BET) technique

Cancer nanomedicine
Capillary interactions
Carbon black
Carbon nanofibers
Carbon nano-onions (CNOs)
Carbon nano tube (CNT)-ceramic nanocomposites
Carbon nanotubes (CNTs)
    chiral SWCNTs
    functionalization
    multiwalled carbon nanotubes (MWCNT)
    properties
    purification

  - single walled carbon nanotubes (SWNTs)
  - synthesis
  - zigzag SWCNTs
- Carbon nanotube transistors
- Cardiovascular diseases, nanomedicine
- Catalysis
- Cellular dysfunction
- Cellular interaction with nanoparticles
- Ceramic-matrix nanocomposites (CMNC)
- Ceramic membranes
- Cerium dioxide
- Chemical and biosensors
- Chemical properties at nanoscale
- Chemical reduction
- Chemical vapor condensation (CVC)
- Chemical vapor deposition (CVD)
- Chemisorption
- China ceramics
- Chitin-polymer nanocomposites
- Chromogenic smart materials
  - photochromic
  - thermochromic
- Chromophores
- Coefficients of thermal expansion (CTE)
  - coefficient of friction (COF)
- Coercivity
- Coherent anti-Stokes Raman spectroscopy (CARS)
- Colloidal lithography
- Color causing phenomena
- Color of metal NPs
- Commercial applications
- Composites
  - advanced composites
  - ancient composites
  - nanocomposite
- Computer technologies
- Conducting polymers
  - poly aniline (PANI)
  - poly pyrrole (PPy)
- Conduction band
- Conductor
- Confocal Raman imaging
- Conservation of momentum
- Constructive interference of light
- Control banding
- Core– surface exchange anisotropy
- Crohn's disease
- Cross linking interactions
- Current carrying density

- Data storage
- Debye-Scherrer relation
- Delocalized clusters
- Dendrimers
- Density of states (DOS)
- Diabetes, nanomedicine
- Diagnosis
  - biomarkers
  - biosensors
  - diagnostic imaging
  - DNA analysis
  - in-vivo imaging

  - lab-on-a-chip
  - magnetic resonance imaging (MRI)
  - microarrays
  - nanobarcodes
  - NIR fluorescence microscopy
  - ultrasound
- Diamond
- Diamondoid
- Diatoms
- Dichroism
- Dicumylperoxide (DCP)
- Dielectric constant
- Differential scanning calorimetry (DSC)
- Dipole coupling
- Dip-pen lithography
- Dirac equation
- Discontinuities
- Discrete energy levels
- Dislocations
- Dispersion
- Displays
  - cathode ray tube (CTR)
  - e-paper displays
  - field emission displays
  - flexible displays
  - liquid crystal displays (LCD)
  - organic light-emitting diodes (LEDs)
- DNA
- DNA base-pair interactions
- DNA damage
- Drug delivery system
  - drug design and screening
  - gene delivery
  - liposome drug delivery
  - nanoscale metal-organic frameworks (NMOFs)
  - remotely triggered delivery systems
  - siRNA drug delivery
  - targeted drug delivery
- Drug development
- Dynamic light scattering (DLS)
- Dynamic random access memory (DRAM)

- Electrical conductivity
- Electric arc-discharge
- Electric strength
- Electrochromic devices
- Electro-explosion
- Electromagnetic (EM) fields
- Electromagnetic interference (EMI) shielding
- Electromagnetic lenses
- Electromagnetic radiations
- Electromagnetic (EM) wave absorption
- Electron
  - fundamental properties
  - optics
- Electron-beam lithography
- Electron density
- Electron gun
  - field emission
  - thermionic
- Electron-hole pairs
- Electron spectroscopy for chemical analysis (ESCA)

Electron transport
Electron tunneling
Electrophoretic light scattering (ELS)
Electrospinning
Electrospray deposition
Energy
Energy conversion
Energy dispersive X-ray analysis (EDX)
Engineering controls
Environmental risks
Environmental science
Environmental sustainability
Etching
Evolution of nanoscience and nanotechnology,\hb
Exchange bias effect
    single-domain
Exchange reaction
Exciton

Face-centered cubic (fcc)
Failure strengths
Fermi level
Ferromagnetic
Ferromagnetic resonance (FMR)
Field emission transistor (FET)
Finite-size effects
Flash memory chips
Fluorophores
Focused ion-beam lithography
Food safety
Fourier transform infrared spectroscopy (FTIR)
Free phonon path
Fuel cell
Fullerenes (C_{60})
    endohedral fullerenes
    higher fullerenes
Functional graded materials (FGMs)
Fungi
Futuristic out-look

Geckos technology
Genotoxicity
Giant magnetoresistance (GMR)
Gibbs energy
Glancing angle deposition (GLAD)
Gleiter's definition
Graphene
    band structure
    electronic structure
    properties
    surface modification
    synthesis
Graphene oxide (GO)
Graphene– ceramic nanocomposites
Graphite

Hard disk drives
Hard magnetic phase
Health hazards
Heat dissipation
Hierarchy of controls
High performance liquid chromatography (HPLC)

High resolution transmission electron microscopy (HRTEM)
High surface area
Homeland security
HOMO– LUMO
Hummer's method
Hybridization
Hydrogen-storage capacity
    elastic modulus
Hydrothermal/solvothermal synthesis
Hydroxypropyl methylcellulose (HPMC)

Indentation hardness
Indium tin oxide (ITO)
Infectious diseases, nanomedicine
Inflammation
Inflammatory conditions, nanomedicine
Information technology
Inhalation of nanoparticles
Insulator
Integrated circuits
Interfacial area
Interlocked molecular architectures
Intermolecular bonding
Internal charge
Intramolecular bonding
Intrinsic properties

Jahn– Teller distortion

Knowledge building

Lab-on-a-chip architectures
Landau level spectrum
Langmuir– Blodgett (LB) film
Laser ablation
Laser Doppler electrophoresis
Laser scanning confocal microscopy (LSCM)
Layer-by-layer (LbL) processing
Lego chemistry
Light military platforms
Lightning rod effect
Liquid crystals
    birefringent phase
    cholesteric
    nematic
    sematic
Lithium ion batteries
Lithography
Load bearing
    wear resistance
Localized surface plasmon resonance (LSPR),\hb
Lotus effect
Luminescence
    nanometals
    semiconductor nano particles
Lycurgus cup

Maghemite
Magnetic anisotropy
Magnetic coupling
Magnetic interaction
Magnetic moments

Magnetic phases
Magnetic random access memory (MRAM)
Magnetism in nonmagnetic nanoparticles
Magnetoresistive random access memory (MRAM)
Magnetostatic energy
Magnetotactic bacteria
Material safety data sheets (MSDS)
Matrix
    ceramic
    metal
    polymer
Maya blue
Mechanical milling
Mechanochemical processing (MCP)
Medicine
Melting point
Metal ion-ligand interactions
Metal-matrix nanocomposites (MMNC)
    carbon nanotubes-metal matrix composites
    ceramic-metal matrix nanocomposites
Metastable organometallic compounds
Microcrystalline cellulose (MCC)
Microelectronic mechanical systems (MEMS)
Microfluidics
Microscopy
    characteristic features
    electron microscopy
    optical microscopy
    scanning electron microscopy (SEM)
    scanning probe microscopy (SPM)
Micro structural material (MSM)
Microwave absorption
Modes of STM
Modulation of light transmission
Molecular beam epitaxy
Molecular-dipole interactions
Molecular electronics
Molecular imprinting
Molecular machines
Molecular recognition
Molecular self-assembly
Musculoskeletal, nanomedicine

Nanobarcode
Nanobelts
Nanocellulose
Nanoclusters
    magic numbers
    properties
Nanocoatings
    anticorrosive coatings
    antimicrobial coatings
    antireflection coatings
    biocidal coatings
    ceramic nanocoatings
    functional coatings
    low-e coatings
    metal matrix nanocoatings
    self-cleaning
    smart coating
    tribological nanocoatings
Nanocomposite

  - functional
  - structural
- Nanocontact printing
- Nanodiamond
- Nanodielectric
- Nanoelectromechanical system (NEMs)
- Nanofibers
- Nanoimprint lithography (NIL)
- Nanomagnets
- Nanomaterials
  - alloys
  - carbon
  - colloidal systems
  - colloidal vanadium penta oxide (V_2O_5)
  - configurations
  - hydrosols
  - inorganic
  - interface induced effect
  - metal colloids
  - metals
  - organic
  - organo sols
  - piezoelectric nanomaterials
  - polymeric
  - properties
  - size and shape related attributes
  - size effect
  - surface effect
- Nanomedicine
- Nanomotors
- Nano-object
  - agglomerate
  - aggregate
  - nanoparticle
- Nanoparticles (NPs)
  - biodegradable polymer
  - characterization
  - exposure
  - functionalization
  - stabilization
  - surface charge
  - toxicity
- Nanoparticles generation
- Nanoporous materials
  - classification of pores
- Nanorice
- Nanorods
- Nanoscale
  - comparison
  - size
  - uniqueness
- Nanoscale surface chemistry
- Nanoscale transistors
- Nanoscience
  - biological world
  - definition
  - historical perspective
  - significance
- Nanoscience in nature
  - clays
  - colloids
  - erosion

  - mineralized materials
  - volcanic activity
- Nanosphere lithography
- Nanostructural materials (NSM)
- Nanostructures
  - nanocoatings
  - nanocrystallite
  - nanolayers
  - nanoporous
  - nanowires and nanotubes
  - quantum dot
  - quantum well
  - quantum wire
- Nanotechnology
  - agro forestry
  - air pollution control
  - batteries
  - camouflage/stealth
  - consumer goods
  - cosmetics
  - defense
  - definition
  - electrical and electronic goods
  - energy
  - enhancing the fuel efficiency
  - food industry
  - hydrogen generation and storage
  - medicine and healthcare
  - space
  - sport goods
  - textiles
  - water disinfections
  - water filtration
  - water remediation
- Nanotoxicology
- Nanotraps
- Nanotubes
  - synthesis
- Nanowires
- Natural sources of nanoparticles
  - biological species
  - dust storms
  - forest fires
  - ocean
  - volcanoes
- Neel– Brown expression
- Net spin
- Neurodegenerative, nanomedicine
- Nonmagnetically inert surface

- Olfactory nerve
- One-dimensional carrier transport mechanism
- Optical excitation
- Orbital momentum
- Organic light-emitting transistors (OLETs)
- Orowan mechanism
- Oxidative stress

- Paramagnet
- Particle-in-a-box model
- Particle size analyzer
- Patterned organic monolayers

- Peltier-Seebeck effect
- Peptides
- Permissible exposure limit (PEL)
- Personal protective equipment
- Phagocytosis
- Phase transition
- Photocatalytic effect
- Photoexcitation
- Photo lithography
- Photoluminescence (PL)
- Photonic crystal
- Photonics
- Photovoltaic technologies
  - dye-sensitized solar cells (DSSC)
  - organic– inorganic hybrid solar cells
  - photoelectrochemical cell
  - semiconductor quantum dot-sensitized solar cells (QDSCs)
- Physical adsorption
- Physiosorption
- Planar defects
- Plants
- Plasma arching
- Plasma enhanced CVD
- Plasmon resonance light scattering
- Polymeric nanofilms
- Polymer– matrix nanocomposites (PMNC)
  - polymer– carbon nanocomposites
    - carbon nanotubes-polymer matrix nanocomposites
    - graphene– polymer matrix nanocomposites
  - polymer– clay nanocomposites (PCN)
    - cation exchange capacity (CEC)
    - exfoliation-adsorption
    - intercalative polymerization
    - modification of clay
  - polymer– inorganic nano composites (PINC)
  - polymer– polysaccharide nanocomposites
- Polymer therapeutics
  - sustained drug release
- Positive health effects of nanoparticles
- Preliminary hazard assessments (PHAs)
- Preparation of nanomaterials
  - carbon nano-onions (CNOs)
  - chalcogenides
  - colloidal gold
  - copper nanopowder
  - $Fe_{40}Co_{60}$ alloy
  - gold NPs
  - hierarchical TiO_2nanostructure
  - iron– cobalt NPs
  - iron NPs
  - iron oxide Nps
  - metals
  - palladium alloy
  - platinum alloy
  - polyacrylonitrile (PAN) nanoparticles
  - polysilicon
  - pyrogenic (fumed) silica
  - silicon carbide
  - silicon dioxide (SiO_2)
  - silicon nitride
  - silver NPs
  - synthetic silica gels

  - zinc oxide (ZnO)
- Prevention through design (PtD)
- Protective groups
- Protein glue
- Pseudo-atoms
- Psychiatric diseases, nanomedicine

- Quadrupole microelectrodes
- Quantum confinement
- Quantum dots (QDs)
  - alloyed
  - core– shell
  - core– type
  - semiconductor nanocrystals
- Quantum effects
- Quantum electronics
- Quantum fluorescence
- Quantum forces
- Quantum mechanical effects
- Quantum mechanical properties
- Quantum physics
- Quantum size effect
- Quantum sphere model (QSM)
- Quantum tunneling

- Radar absorbing materials (RAMs)
- Radio-frequency identification (RFID)
- Raman effect
- Raman spectroscopy (RS)
- Rayleigh's law
- Reactive oxygen species (ROS)
- Recommended exposure limit (REL)
- Redshift
- Reducing agents
- Reflection (R)
- Refractive index (RI)
- Reinforcement
  - continuous fibers
  - particulate
  - short fibers
  - whiskers
- Reverse micelle method
- Reverse osmosis (RO) membrane
- Richard Feynman
- Risk management

- Safe laboratory practices
  - exposure monitoring
  - waste management
- Safe working with nanomaterials
- Saturation magnetization
- Scaling law
- Scanning lithography
- Scanning probe lithography
- Scanning transmission electron microscopy (STEM)
- Scanning tunneling microscopy (STM)
- Scattering
- Scattering techniques
- Secondary ion mass spectrometry (SIMS)
  - dynamic SIMS
  - static SIMS
- Self-assembly

    advantages
    biological
    challenges
    definition
    dynamic self-assembly
    entropic effects
    molecular self-assembly
    soft materials
    solvent effect
    static self-assembly
    templated (nonmolecular)
    unusual shapes
Self-cleaning
Self-folding nanostructures
Semiconductor
Sensors
Soft lithography
Soft magnetic phase
Solar panels
Soldier protection
Sol-gel
Solid-state data storage devices
Sonochemical synthesis
Spectrocscopy
    fourier transform infrared spectroscopy
    Raman spectroscopy
    vibrational spectroscopies
Sphericity
Spintronics
Sputtered plasma processing
Sputtering
SQID magnetometry
Starch-polymer nanocomposites (SPNC)
Static random access memory (SRAM)
Superatom
Super hydrophobicity
Superparamagnetic
Superparamagnetism
Supramolecular chemistry
    dipole– dipole interactions
    electrostatic interactions
    hydrogen bonding
    hydrophilic interactions
    hydrophobic interactions
    intermolecular forces
    non-covalent interactions
    π– π stacking
    supramolecular interactions
Supramolecular organic frameworks (SOFs)
Surface anisotropy
Surface area
Surface area to volume ratio
Surface charge
Surface effects
Surface-enhanced Raman spectroscopy (SERS)
Surface plasmon resonance (SPR)
Surface porosity
Surface properties
Surface scattering
Surface spins
Synthesis of nanomaterials
    bottom– up29

- strategies
- top– down

Synthetic carbon allotropes (SCAs)

Therapy
- regenerative medicine
- theranostics

Thermal conductivity
Thermal CVD
Thermal mismatch
Thermodynamics laws
Thermoelectric energy
Tip enhanced Raman spectroscopy (TERS)
Tissue and biomaterial engineering
Training effect
Translocation of nanoparticles
Transmission
Transmission electron microscopy (TEM)
Transportation

Ulcerative colitis
Ultrananocrystalline diamonds (UNCD)
Ultraresponsive hearing aids
Ultrasonic spray pyrolysis
Unique properties
- bio-inspired

Universal Product Code (UPC)
Uptake of nanoparticles
UV filter
UV-Visible

Vacuum permeability
Valence band
Van der Waals forces
Vibrating sample magnetometry
Volatile organic compounds (VOCs)
Voltage endurance

Wave-like property
- de Broglie wavelength

Weapons
Wear and corrosion protection

X-ray diffraction
- small-angle X-ray scattering (SAXS)
- wide angle X-ray diffraction (XRD)

X-Ray photoelectron spectroscopy (XPS)
XRD spectra

Zener model
- grain boundary

Zeolite
Zeta potential analysis
Zirconium dioxide

WILEY END USER LICENSE AGREEMENT

Go to www.wiley.com/go/eula to access Wiley's ebook EULA.